AN INVESTIGATION
INTO
THE SCALE EFFECTS ON CAVITATION INCEPTION AND NOISE IN MARINE PROPELLERS

Emin Korkut

A Thesis submitted for the degree of
Doctor of Philosophy
in the
Department of Marine Technology
at the
University of Newcastle upon Tyne

May, 1999

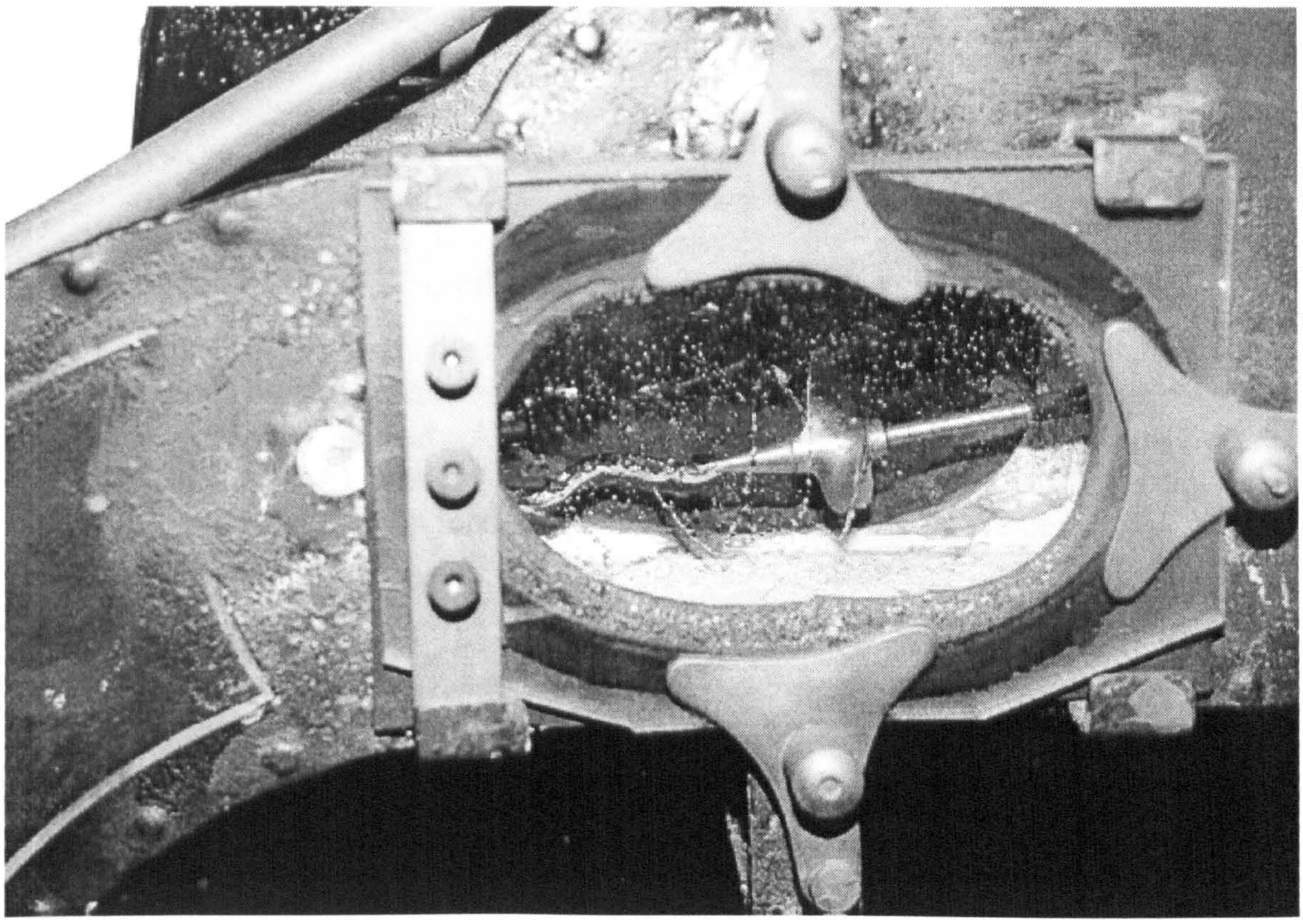

(*Photograph by courtesy of Dr. M. Atlar)*

A view from Parsons' Cavitation Tunnel (the world's first cavitation tunnel established in 1895) displaying typical tip and hub vortex cavitation.

"The phenomena of cavitation and associated scale effects are still major problems for naval architects and researchers after 104 years. It is hoped that this thesis will shed some light on these complex phenomena."

Abstract

This thesis presents an investigation into the phenomena of scale effects on cavitation inception and noise of marine propellers. The overall aim is to extend the understanding of these phenomena and improve predicting methods. The investigations, which are largely experimental in nature, are restricted to the tip vortex and sheet types of cavitation.

Chapter 1 includes a state-of-the-art review of the scale effect studies based on published papers to form the basis for the main objectives and structure of thesis. The objectives require systematic tests in a cavitation tunnel to explore the viscous scale effects contributing to the phenomena, particularly for the effect of the free-stream turbulence, and to include this effect in extrapolation procedures.

Chapter 2 is concerned with the background flow measurements in the cavitation tunnel under the effect of systematically varying levels of the free-stream turbulence generated by using wire meshes. This background information is obtained using a Laser Doppler Anemometry; measurements made with the latter provide a systematic basis on which the analyses of the cavitation inception and noise experiments can be performed.

In Chapter 3, a set of cavitation inception tests is described with a NACA66 rectangular foil whose cross-section represents a typical blade section of a marine propeller. The inception measurements for systematically varying levels of the free-stream turbulence and that of the leading edge roughness are presented for different angles of attack and the results are discussed.

Chapter 4 includes another set of cavitation inception experiments with a 5-bladed of model propeller of the Meridian Series. The measurements are taken for varying levels of the free-stream turbulence, blade roughness and dissolved gas contents. The results are analysed and discussed with a specific emphasis on the similarities between the effects of the free-stream turbulence and blade roughness.

Chapter 5 presents a set of systematic noise measurements, with the same test propeller under the similar effects of the free-stream turbulence, blade roughness and dissolved gas content, using a single external hydrophone. The analyses of these measurements, in terms of the tunnel background noise and net propeller noise, are presented and discussed for two operating conditions representing a typical non-cavitating and cavitating noise spectrum.

In Chapter 6, a semi-empirical tool is developed to predict the inception of cavitation including the effect of the free-stream turbulence based on Lighthill's Leading Edge Correction factor (Lighthill, 1951). This tool is correlated with the inception tests results of the model propeller and its potential to be used as an extrapolator for the full-scale prediction is discussed. An attempt is made to establish a correspondence between the level of the free-stream turbulence and that of the blade roughness and its impact on the

current test procedures is discussed. This chapter also includes an analysis of the similarity criteria to incorporate the effect of the free-stream turbulence in the inception of cavitation using the Dimensional Analysis procedure.

In Chapter 7, a general review of the study together with the main conclusions from the thesis are presented and some recommendations for future work are made.

Contents

Notations and Symbols

Upper Case:

A	: Foil planform area
A_0	: Disc area of propeller
A_E	: Expanded blade surface area of propeller
A_{fm}	: Full mesh area
A_{net}	: Net mesh area after subtracting the area covering mesh thickness and length from the full mesh area
AR	: Aspect ratio
B	: Breadth
BAR	: Blade area ratio
BRF	: Blade rate frequency of a propeller
C	: Constant in Equation (1.16)
C_L	: Lift coefficient
C_p	: Local pressure coefficient of a foil or propeller
$\overline{C}_p$	: Mean value of pressure coefficient
C_{pmin}	: Minimum pressure coefficient
C(x)	: Camber line of foil or propeller blade section
D	: Diameter of propeller or wire
F	: A function in Equation (1.15)
F_r	: Froude Number
F(x)	: Fairing line of symmetrical foil section or propeller blade section

G	: Power spectrum
H	: Height
H(ω)	: Transfer function as a function of angular frequency
Hz	: Hertz, unit of frequency, equal to one cycle per second
J	: Advance coefficient of propeller
K	: Gas constant in Equation (1.10)
K	: Effects of bubble dynamics in Equation (1.20)
K_T	: Propeller thrust coefficient
L	: Characteristic length in Equation (1.29)
LDA	: Laser Doppler Anemometry
L.E.	: Leading edge
N	: Rotational speed of propeller
N	: Number of nuclei per unit volume or nuclei density
N	: Number of grid points in LDA measurements
N/m^2	: Newton per square metre (Pascal)
NACA	: National Advisory Committee for Aeronautics
NMAR	: Net mesh area ratio
P	: Pitch of propeller
P	: Local pressure at a reference point
P	: Pressure measured at a point in Equation (1.28)
P_0	: Reference pressure in Equation (1.28)
P_1	: Critical pressure
Pa	: Pascal (N/m^2)
P_{crit}	: Critical pressure or inception pressure
P/D	: Pitch to diameter ratio

P_L : Pressure surrounding a bubble (external pressure)

P_m : Mean pitch of propeller

P_{min} : Minimum local pressure

$\overline{P}_{min}$: Mean minimum local pressure

P_{st} : Static pressure at a reference point

P_v : Vapour pressure of water

P_{xr} : Pitch of propeller at radius of x_r

Q : Gas factor

R : Radius of propeller

R : Radial distance from vortex core

R : Bubble radius in Equation (1.10)

R_0 : Initial bubble radius

R_1 : Characteristic vortex core radius

R_e : Reynolds number

R_{ec} : Reynolds number based on foil chord length

R_{ek} : Reynolds number based on roughness height

R_{en} : Reynolds number based on rotational speed of propeller

$R_{e\Lambda}$: Reynolds number based on integral length scale

S : Surface tension

SPL : Sound pressure level or reduced sound pressure level

SPL_B : Background sound pressure level

SPL_m : Measured sound pressure level in bandwidth

SPL_N : Net sound pressure level

SPL_T : Total (propeller + background) sound pressure level

T : Tensile strength or tension of fluid

T_c : Collapse time of bubble

T.E. : Trailing edge

TI : Relative intensity or turbulence number or turbulence level or turbulence intensity of the flow

TI_{rm} : Mean value of resultant turbulence intensities

TI_u : Axial component of turbulence intensity

TI_{ui} : Axial component of turbulence intensity at each grid point

TI_{um} : Mean value of axial component of turbulence intensities

TI_v : Transverse component of turbulence intensity

TI_{vi} : Transverse component of turbulence intensity at each grid point

TI_{vm} : Mean value of transverse component of turbulence intensities

U : Instantaneous free-stream axial velocity

U : Characteristic velocity

$\overline{U}$: Mean velocity component of free-stream axial velocity

U_l : Instantaneous local velocity

$\overline{U}_l$: Mean value of local velocity

U_A : Instantaneous advance velocity of propeller

$\overline{U}_A$: Mean value of advance velocity of propeller

U_k : Local velocity at the position of roughness height

U_{pitot} : Tunnel inflow velocity or free-stream velocity measured by pitot tubes

$\overline{U}_{unweighted}$: Averaged velocity based on unweighted arithmetic mean

V : Reference velocity

V : Tip velocity of propeller blade

V_0 : Resultant velocity without the effects of induced velocities

V_{xr} : Resultant velocity at x_rR

V_R : Resultant or relative velocity of propeller

V_R : Resultant velocity including the effects of induced velocities

W : Power measured at a point in Equation (1.27)

W_e : Weber number

W_0 : Reference power in Equation (1.27)

Z : Number of blades of propeller

Lower Case:

a : NACA mean line designation

a(t) : Vibration as a function of time

a, b : End points of mesh in the transverse direction

b : Span length of foil

c : Chord length of foil or propeller blade section

c_{max} : Maximum chord length of foil or propeller blade section

dB : Decibel, a unit (one-tenth of a bel) used in the comparison of two power levels relating to electrical signals or sound intensities

dBA : A-weighting scale of dB

f : Frequency

f_0 : Blade rate frequency of propeller ($f_0 = N.Z$)

f_b : Occurrence frequency of bubble

f_c : Collapse frequency of bubble

f_D : Doppler frequency shift

f_I : Frequency of incident light

f_{max} : Maximum camber of foil

f_S : Frequency of scattered light

f_t : Transition frequency of bubble

g : Acceleration due to gravity

g(y) : Correlation of lateral velocity fluctuations in transverse direction

k : Roughness height

k : kilo

knot : Unit of a ship or aircraft equivalent to one nautical mile (1852 m) per hour

kW : kilo-watt, unit of a power

k_2 : Constant in Equation (6.45)

k_f : Factor involving the interaction of the bubble dynamics and fluctuation pressure

k_R : Reference roughness height

m : Model

m : Number of all parameters in the list of dimensional analysis

m : Metre

m/s : Metre per second

mm : Millimetre

m_{0u} : Variance of axial component of velocity

m_{0v} : Variance of transverse component of velocity

n : Reynolds number exponent in Equation (1.14)

n : Number of validated data at each grid point in LDA tests

n : Number of parameters in non-dimensional form

n(t) : Waterborne noise as a function of time

$p^{'}$: Pressure fluctuations

q : Velocity distribution on foil surface or propeller blade section

r : Distance from centre of a cavity to an observer

r : Number of dimensions concerned in dimensional analysis

r_L : Leading edge radius of foil or propeller section

rpm : Revolutions per minute

rps : Revolutions per second

s : Ship

s : Second

s(t) : Hydrophone output as a function of time

s_u : Standard deviation of u component of velocity

s_v : Standard deviation of v component of velocity

t : Time

t : Angle of attack component in Equation (1.14)

t_{max} : Maximum thickness of foil

u : Axial velocity component in LDA measurements

u_f : Fluctuation component of velocity in axial direction

u_f' : Root-mean-square of fluctuations of velocity

u_f' : Root-mean-square of fluctuations of velocity in axial direction

u_{fl} : Fluctuation component of local velocity

u_{fl}' : Root-mean-square of fluctuations of local velocity

u_{fe} : Effective fluctuation in Equation (6.45)

u_{ia} : Axial component of induced velocity of propeller

u_{it} : Tangential component of induced velocity of propeller

u_{ldai} : Measured axial velocity by LDA at each grid point

u_{mlda} : Mean value of axial component of velocity, u_{ldai} measured by LDA

u_x : Velocity component of a particle in LDA system

$\bar{u}$: Mean value of u component of velocity at each grid point

$\overline{u_f^2}$: Mean value of square of fluctuating component of velocity in axial direction

v : Transverse component of velocity in LDA measurement

v_f : Fluctuation component of velocity in transverse direction

v_f' : Root-mean-square of fluctuations of velocity in transverse direction

v_{ldai} : Measured transverse velocity by LDA at each grid point

v_{mlda} : Mean value of transverse component of velocity, v_{ldai} measured by LDA

$\bar{v}$: Mean value of v component of velocity at each grid point

$\overline{v_f^2}$: Mean value of square of fluctuating component of velocity in transverse direction

w_f : Fluctuation component of velocity in vertical direction

w_m : Mean wake fraction at radius of x_r due to ship hull

$\overline{w_f^2}$: Mean value of square of fluctuating component of velocity in vertical direction

x : Distance from leading edge of foil or propeller blade section

x_1 : Variable in Equation (6.21)

x_m : Position of minimum pressure from leading edge of foil or propeller blade section

x_{lower} : Abscissa of foil from leading edge on face side

x_r : Non-dimensional radius of propeller

x_{upper} : Abscissa of foil from leading edge on back side

x,y,z : Co-ordinate system

$y_{lower(face)}$: Ordinate of foil on face side

$y_{upper(back)}$: Ordinate of foil on back side

Greek Symbols:

α : Angle of attack

$\bar{\alpha}$: Mean value of angle of attack

α_D : Dissolved gas content of a fluid at static pressure

α_D/α_S : Dissolved gas content ratio

α_E : Effective angle of attack

α_F : Free or dissolved gas content of a fluid at static pressure

α_G : Geometric angle of attack

α_i : Ideal angle of attack

α_S : Dissolved gas content of saturated water at 760 mmHg

α_T : Total gas content of a fluid

β : Advance angle of propeller

$\bar{\beta}$: Mean value of advance angle of propeller

β_i : Hydrodynamic pitch angle of propeller

$\delta\alpha$: Fluctuating component of angle of attack due to free-stream turbulence

$\overline{(\delta\alpha)^2}$: Mean of squares of fluctuations of angle of attack

$\delta\alpha'$: Root-mean-square of fluctuations of angle of attack

$\delta\beta$: Fluctuating component of advance angle of propeller due to free-stream turbulence

$\overline{(\delta\beta)^2}$: Mean of squares of fluctuations of advance angle of propeller

$\delta\beta'$: Root-mean-square of fluctuations of advance angle of propeller

ΔC_p : Fluctuating component of pressure coefficient due to free-stream turbulence

ΔC_{pmin} : Fluctuating component of minimum pressure coefficient due to free-stream turbulence

$\Delta C_{pmincorresp}$: Corresponding fluctuating component of minimum pressure coefficient in cases of roughness to cases of free-stream turbulence

ΔC_{pminR} : Fluctuating component of reference minimum pressure coefficient

Δf : Filter bandwidth

Δk : Roughness height relative to reference roughness height

ΔP : Characteristic pressure in Equation (1.29) or pressure difference between free-stream and critical pressure

ΔSPL : Difference between levels of full-scale and model scale sound pressure

$\Delta \Lambda_g$: Integral length scale relative to reference integral length scale

$\Delta \sigma_i$: Effects of viscosity and nuclei on cavitation inception

$\Delta \sigma_T$: Effect of free-stream turbulence on cavitation inception

$\Delta u(\%)$: Variation of axial mean velocity deviation in percentage with U_{pitot}

ε : Small parameter defining size of disturbance in Ligthill's leading edge correction

γ : Ratio of specific heats of permanent gas

λ : Ship to model length scale

λ : Laser beam wavelength

Λ_g : Integral length scale of flow

Λ_{gR} : Reference integral length scale

μ : Dynamic coefficient of viscosity of flow

ν : Kinematic viscosity of flow

θ : Geometric pitch angle of propeller

θ : Intersection angle of laser beams

ρ : Density of water

σ : Cavitation number

σ_{calc} : Predicted (calculated) cavitation number

σ_i : Cavitation inception number

σ_i : Cavitation inception number of unattached tip vortex cavitation

σ_{iR} : Reference inception number corresponding to an assumed or known level of reference free-stream turbulence and roughness, and distribution of nuclei (in terms of size, content and number) in flow

σ_{ist} : Cavitation inception number measured in strong water without an adequate amount of nuclei in water

σ_{iw} : Cavitation inception number measured in weak water with an adequate amount of nuclei in water

σ_n : Cavitation number based on rotational speed of propeller

σ_{res} : Residual cavitation index contributed by effects of bubble dynamics

σ_{SC} : Cavitation number of sheet cavitation

σ_{TV1B} : Cavitation number of tip vortex cavitation attached to one blade only

σ_{TVAB} : Cavitation number of tip vortex cavitation fully attached to all blades

σ_u : Cavitation number based on tunnel axial (free-stream) velocity

ω : Angular frequency

List of Figures

List of Pictures

List of Tables

Acknowledgements

I would like to acknowledge the help, support and encouragement of several people, who have made this study possible and valuable.

I am extremely grateful to Dr. Mehmet Atlar for giving me the opportunity to work with him, and for his supervision, encouragement and guidance during my Ph.D. study. I believe that his contribution to the study and to my way of thinking in research has been invaluable.

My thanks should also go to Professor A. Yücel Odabaşı of the Technical University of İstanbul for his experience, guidance and comments on the essential stages of the work. This study would not be the same without his contribution.

I am deeply grateful to Prof. George R. Snaith for his kindness, help and comments on the final stage of the thesis.

I also owe special thanks to Mr. Ian Paterson, who is the supervisor of the Emerson Cavitation Tunnel, for his support, help and technical advice during the tests. My thanks are also extended to the staff of the Department of Marine Technology for their kindness, tremendous help and friendship during the whole period of the study.

I feel deeply indebted to my wife, Şenay Vural Korkut, for her support and concern throughout my Ph.D. whenever I needed.

I must also give my deep gratitude to my parents for their support, encouragement and love in all my life.

Finally, I would like to thank the Technical University of İstanbul, especially the Faculty of Naval Architecture and Ocean Engineering, for their financial support in the period of this study.

CHAPTER 1 INTRODUCTION

Cavitation is an important fluid mechanics phenomenon for metal surfaces, such as pumps, turbines, propellers, bearings, and even for the human body, e.g., heart and knee joints, which affects their lives, efficiencies, noise and vibration levels that are excited. Increasing demand for design of silent propellers especially for naval vessels but also to improve the quality of comfort on board commercial ships have led to the cavitation of propellers and foils being investigated very extensively. This is the subject of this thesis.

The term **"Cavitation"** denotes the formation of vapour or gas-filled bubbles within a fluid as a result of local pressure reductions around a body. Due to the local pressure in the fluid, the mean distance between liquid particles exceeds a critical value, which causes the liquid to break down and change its phase. This initial break-down is the beginning of cavitation and it is called **"Inception of Cavitation"**. In principle when the local pressure around the body becomes nearly equal to the vapour pressure of the fluid then the phenomenon of cavitation occurs. In reality, however, the local pressure at inception is usually different from the vapour pressure and the pressure at which cavitation occurs, is called **"Inception or Critical Pressure"**. On the other hand, in small scale model testing of ship propellers in cavitation testing facilities, the results of cavitation measurements vary with different flow conditions and differing qualities of the fluid as well as the size of the facility used. These discrepancies are the so-called **"Scale Effects"** on cavitation; these are generally understood to be due to three main causes:

- the **"viscous nature"** of the flow
- the **"dynamics of bubbles"**
- the **"effects of gravity"**

The development of cavitation bubbles consists of three stages, namely the inception, growth and collapse of bubbles. The inception stage is initiated by the reductions in the pressure of the liquid surrounding each bubble; initially the bubble grows only slightly, this indicates the existence of an equilibrium condition when the difference between the

inner and outer pressures of the bubble balances the surface tension force. The surface tension force attempts to hold the bubble against the force caused by pressure differential between the internal and external pressures, which attempts to pull the bubble apart. This equilibrium condition disappears below a certain critical pressure, and then the bubble grows rapidly. This is the onset of cavitation. After a short time, the external pressure around the bubble starts to increase, the difference between the pressures will decrease, and this causes the bubble to collapse suddenly. This collapse creates shock waves hence noise. As the development of these cavitation bubbles in this way is one of the principal factors that contribute to the creation of noise, it is intuitively obvious that the scale effects associated with the inception of cavitation are also expected to affect the noise levels that are created.

During the last two decades (Rood, 1991) research on the scale effects of cavitation has been concentrated on the effects of viscosity and bubble dynamics. In the late 1970's, the viscous effects, such as laminar separation and turbulence were found to be major factors affecting the scale effect phenomena of cavitation. These effects were examined closely and were demonstrated to be more complex than previously assumed in the early 1980's. Thus, effect of free-stream turbulence was left aside, but the roughness effect, which causes boundary layer tripping, was investigated extensively. In the late 1980's the effects of bubble dynamics were found to play an important role in the development of cavitation. In the 1990's the effects of size, distribution and contents of nuclei in the flow were recognised to be important and with the use of modern cavitation tunnel testing facilities and measuring equipment their effects were systematically explored. One of the main results of the investigations associated with those effects is that, although the effect of the free stream turbulence has been left aside, two separate factors in the inception of cavitation, i.e. the effects of the flow structure of the turbulence and nuclei cannot be separated and should be investigated together.

At the outset of the research study presented in this thesis, the aim of the research was specified to make further contribution to overall understanding of the scale effect phenomena on the inception of cavitation of marine propellers. Although the main emphasis of the study was expected to be on the inception of cavitation, the inherent interdependency between the cavitation and the resulting noise generated implied that

the investigation be extended to include the noise aspects if there was available resources, time and experimental facilities.

Bearing in mind the above aim and its extension, the following sections of this chapter review the state-of-the-art in the understanding of certain aspects of the phenomena of cavitation scale effects and noise and it is likely relevance to marine propellers. The review concentrates on the definition of the scale effects, main factors contributing to the scale effects, particularly its viscous nature plus investigations carried out so far to identify the contribution of these factors and methods to include these effects in the predictions of the inception of cavitation and noise. It was expected that the conclusions obtained from the review work within the limits of the above aim would lead to a set of specific objectives for the research study which would be reflected in the structure of this thesis.

Therefore, the main objectives and layout of the thesis as well as the re-statement of its aim are given in Section 1.3 of this chapter.

1.1 LITERATURE REVIEW

1.1.1 THE INCEPTION OF CAVITATION ON MARINE PROPELLER BLADES

The cavitation number, σ, at a reference point in a flow on the surface of a propeller blade is defined as:

$$\sigma = \frac{P_{st} - P_v}{\frac{1}{2}\rho V^2} \tag{1.1}$$

where:

- P_{st} is the static pressure at the reference point
- P_v is vapour pressure of water
- ρ is density of the water
- V is the reference velocity.

The reference point can be anywhere on a propeller blade, V can be based on the axial free-stream velocity, U, or the rotational velocity, N, or the resultant velocity V_R as the vector sum of these velocity components, U and N.

Alternatively, a local pressure coefficient at a point on or around the propeller can be defined as:

$$C_p = \frac{P - P_{st}}{\frac{1}{2}\rho V^2} \tag{1.2}$$

where:

- P is the local pressure at the point considered.

By definition it is assumed that cavitation will occur when the local pressure P is reduced to a minimum value P_{min} which is equal to the vapour pressure of the water, i.e.

$$P_{min} = P_v \tag{1.3}$$

and hence

$$\sigma_i = -C_{pmin} \tag{1.4}$$

where

- σ_i is called the **"Inception Number of Cavitation"**

It is well-known that as the minimum pressure is usually different from the vapour pressure and that the prediction of the inception of cavitation based on model tests will suffer from scale effects. Most of the fundamental problems in predicting inception are related to scaling from model to full-scale, scale effect corrections and understanding of the various phenomena involved in the scale effect phenomena.

Holl and Wislicenus (1961) defined the phenomena such that the scale effects include not only the effects of changes in linear dimension, but also those of changes in flow velocity or pressure and other fluid properties.

According to Billet and Holl (1979), the scale effects associated with the inception of cavitation can, in general, be sorted into two groups of factors:

- The first group of factors influence the flow outside the cavitation bubbles and the free-stream pressure.
- While the second group of factors influence the growth process of the bubbles.

The first group of factors are mainly caused by:

- changes in the flow field due to variations in Reynolds number, Froude number and Mach number as well as the fluctuations in turbulence pressure,
- deviations from exact geometrical similarity such as those due to surface roughness.

While the second group and their change over time are those associated with the effects of:

- surface tension
- cavitation nuclei
- transport of non-condensable gases
- heat transfer

The formal classification of the scale effect phenomena within the context of ship hydrodynamics was specified at the 18th International Towing Tank Conference (ITTC, 1987) when its Cavitation Committee proposed that the scale effects can be associated with:

- viscous nature of the flow
- dynamics of bubbles
- gravity.

Because it is not possible in a conventional cavitation tunnel to satisfy simultaneously both conditions of identical Reynolds and Froude numbers, the latter is ignored thus the effect of gravity is usually not taken into account. Therefore, this review is restricted to the scale effects associated with the viscous nature of the flow and dynamics of bubble involved in the inception of cavitation and the associated noise that is generated.

1.1.1.1 Viscous Scale Effects

When cavitation tests with small-scale models of propellers are carried out the similarity law based on the relevant Reynolds numbers cannot be satisfied due to the speed and size limitations in a cavitation tunnel. Because of these factors the propeller in model scale operates at much lower Reynolds number than the full-scale propeller. This difference causes **"Viscous Scale Effects"** mainly due to there being insufficient turbulence in the model tests.

These viscous scale effects are closely associated with the level of turbulence in the free-stream and the level of surface roughness of the propeller blades. As explained earlier (Section 1.1.1), the inception of cavitation occurs when the local pressure is close to but not necessarily equal to the vapour pressure of the fluid. By definition, the local pressure or more precisely local instantaneous pressure can be defined as the sum of the local mean pressure and the local fluctuation pressure. These pressure fluctuations are caused by the turbulence level in the incoming free-stream flow and the conditions of the boundary layer near the propeller surface (Kuiper, 1978). In the light of these considerations the viscous effects can be classified as those are associated with **"Free-Stream Turbulence"** and **"Roughness"**; these are described in the following Sections (1.1.1.1.1 and 1.1.1.1.2).

1.1.1.1.1 *Effects of Free-Stream Turbulence*

The effect of turbulence on the inception of cavitation is one of the principal contributions to the viscous scale effects. Although the turbulence level of water in full-scale is usually higher than the turbulence level in model scale, every cavitation tunnel test facility has a different turbulence level. It is also expected that different turbulence levels result in different inception numbers of cavitation for the same propellers and foils. In view of this the effects of free-stream turbulence on the inception of cavitation should be investigated closely especially by developing a basic understanding of turbulence.

Hinze (1975) describes turbulence as an irregular condition of flow in which the various quantities show a random variation with time and space co-ordinates, so that statistically distinct average values can be obtained. Therefore, an instantaneous value of the velocity, U, at a point is given by:

$$U = \overline{U} + u_f \tag{1.5}$$

where:

- over bar denotes the mean value
- $\overline{U}$ is the mean value of the velocity
- u_f is the fluctuating component of the velocity.

The turbulence level (i.e. the intensity) of a fluid is expressed as the ratio of the root-mean-square of the velocity fluctuations, u_f', to the mean velocity of the free-stream, $\overline{U}$:

$$TI = \frac{u_f'}{\overline{U}} = \frac{\sqrt{\overline{u_f^2} + \overline{v_f^2} + \overline{w_f^2}}}{\overline{U}} \tag{1.6}$$

where:

- u_f, v_f and w_f are the fluctuations of the velocity components in axial, transverse and vertical directions respectively
- $\overline{u_f^2}, \overline{v_f^2}$ and $\overline{w_f^2}$ are the mean values of the squares of fluctuations in the corresponding directions.

In the literature, TI is variously called **"relative intensity", "turbulence number", "turbulence level"** as well as simply **"Turbulence Intensity"**.

The scale effects that are viscous in nature can be minimised by imposing flow conditions with high Reynolds number based on the resultant velocity in model scale. However, as the boundary layer can be laminar over a considerable region of the propeller blade in model scale, as shown in Figure 1.1, while the boundary layer is almost totally turbulent in full scale; the high Reynolds number conditions created in model scale do not really move the transition region nearer to the leading edge of the blade (Kuiper, 1981).

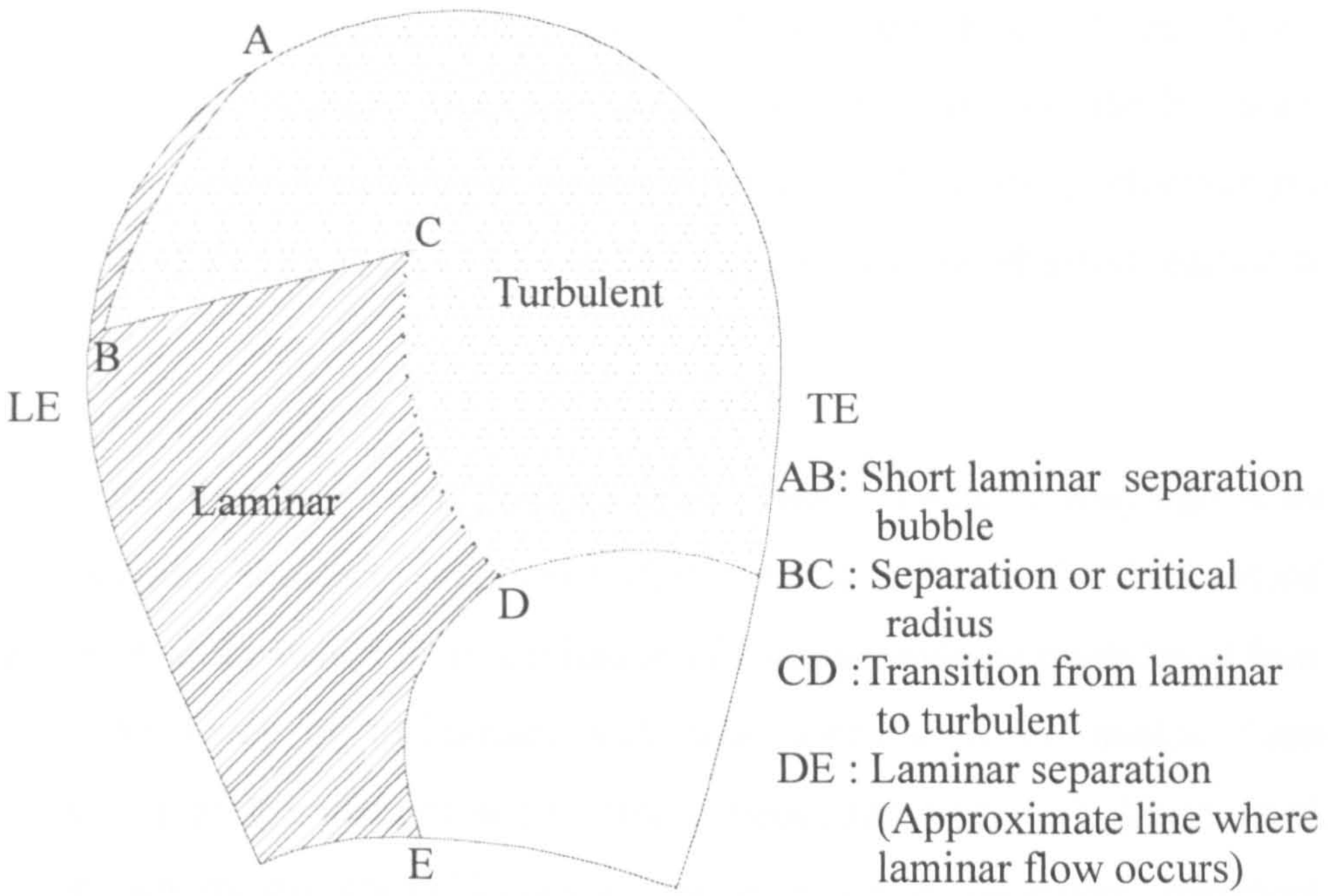

Figure 1.1 Schematic representation of the general shape and extent of the boundary layer on the suction side of a model propeller (Kuiper, 1981)

Huang (1986) argues that as a high turbulence level is known to cause early boundary layer transition which in turn can lead to the complete elimination of laminar separation, it is expected that the effect of the turbulence on the inception of cavitation becomes important when the turbulence level can cause significant change in transition and/or laminar separation.

Arndt and George (1979) reviewed the turbulent pressure fields and cavitation and the role of viscous effects in the cavitation process. They found that the viscous effects associated with the laminar separation and the transition of the boundary layer from laminar to turbulent can have a major impact on the cavitation process.

ITTC cavitation inception experiments on a modified ellipsoidal head form resulted in widely different inception values, whereby the σ value for the inception of cavitation differed by up to 300% (Gates and Acosta, 1979). The differences in inception of cavitation of the same body in various cavitation tunnels were explained by different turbulence levels by Gates and Acosta (1979). They carried out some experiments on

three axisymmetric bodies in varying free-stream turbulence levels by using turbulence generating grids with varying sizes. They showed that if the level of free-stream turbulence is increased the laminar separation point moves forward and the boundary layer becomes fully turbulent. Furthermore, the contribution of fluctuating velocities and hence the levels of free-stream turbulence may be more critical in affecting earlier or delay of inception.

Keller (1979) indicated that the level of free-stream turbulence could be responsible for variations in the inception results of identical bodies tested in different facilities. Murai et al. (1979) showed that the inception of cavitation of foils depends on qualities of free-stream, such as the level of turbulence and size distribution of nuclei. Later Keller (1992) stated that the viscous scale effects associated with turbulence level, boundary layer, etc. are mostly not held constant, or are not even measured, therefore, are left unconsidered during the measurements of cavitation inception. Odabasi (1987) has also emphasised the importance of the level of free-stream turbulence on the inception of cavitation. Later he (Odabasi, 1995) claimed that studies on the effect of the free-stream turbulence should also be focused as well as on the effects of blade roughness and bubble dynamics. Brennen (1995) has also indicated that increased level of the free-stream turbulence can cause an increase in the inception values of the body tested.

The level of the free-stream turbulence also affects the nucleus-forming mechanisms. Franklin et al. (1984) showed that the formation mechanism of cavities is related to free-stream turbulence as well as other effects (pressure history of the tunnel, dissolved gas content, etc.). The 18th ITTC (1987) stated that in different cavitation tunnels, the mechanisms causing the formation of nuclei are somehow different and are essentially governed by the test conditions, such as pressure history, free-stream turbulence, dissolved gas content, etc.

Rood (1991) reviewed the published work about the inception of cavitation and concluded that two separate topics of the inception of cavitation, such as the effects of nuclei and turbulent flow structures, cannot be separable. Pauchet (1998) has shown that a theoretical model to predict the inception of cavitation should be associated with the

fine description of physical phenomena, such as instantaneous flow and pressure field, modelling of turbulent diffusion and modelling of interaction between the turbulence and nuclei spectra.

The level of turbulence in model scale is usually varied by using either wire mesh screens, grids, rods, honeycombs or combinations of them. They are usually positioned at the upstream of a foil or a propeller or a body tested by choosing a suitable base frame supporting them. These alternative arrangements are referred to in the following papers.

Daily and Johnson (1956) used a series of screens at the upstream of the test section to reduce the level of free-stream turbulence in the Hydrodynamics Laboratory of Massachusetts Institute of Technology.

Keller (1979) placed a turbulence grid at the upstream of the location of an axisymmetric body in order to change the level of turbulence of the flow in the test section.

Gates and Acosta (1979) also used turbulence generating grids with varying sizes in the Low Turbulence Water Tunnel of California Institute of Technology.

Muari et al. (1979) performed tests with some rods of different diameters at the High Sped Water Tunnel of University of Tohoku in Japan.

Hoffman (1991) also used a set of monoplane rods to generate free-stream turbulence in the Subsonic Wind Tunnel of California Polytechnic for the measurements of an airfoil.

Bandyopadhyay et al. (1991) generated free-stream turbulence by using screens and grids to investigate the organised nature of a turbulent vortex of a NACA 0012 foil in the Low-Speed Boundary-Layer Channel of the NASA Lagley Research Center.

Farell and Youssef (1996) have recently used some screens and honeycombs for the management of turbulence in a plexiglas pipe.

The methods mentioned above are still in use to control the level of turbulence in model scale at various experimental facilities depending upon their size, test requirements and experiences.

1.1.1.1.2 *Effects of Roughness*

The scale effects of the viscous nature are also associated with Reynolds number dependent boundary layer phenomena, which include laminar and turbulent flows, transition from the laminar to turbulent flows and separation of the laminar and turbulent flows. Many researchers have reported their observations and findings on the close relationship between the inception of cavitation and the characteristics of the flow past the body.

Pan et al. (1981) stated that the inception of cavitation does not necessarily occur in the vicinity of the lowest mean pressure on the body, but rather occurs in the region of natural boundary layer transition.

Ling (1984) reported that turbulent transition near the leading edge was found to cause an increase in the inception of cavitation of propellers from the case where the boundary layer of the model propeller remains laminar.

Stinebring et al. (1991) have also shown that roughness applied to the tip of a 3-D foil increased the cavitation extent by modifying the local boundary layer at the point of separation. Therefore, boundary layer characteristics can directly influence the inception of cavitation.

Since the high Reynolds number conditions do not move the transition region to the leading edge of a blade in model scale and as the boundary layer is almost fully turbulent in full-scale, the scale effect associated with the viscosity will always be present. The other reason to have different inception numbers of cavitation in model and full-scale related to the viscous scale effects is that surface irregularities of the model propeller blades are different from those of ship propeller blades. Therefore, some researchers have used artificial stimulators, such as sand roughness, trip wire, etc. to trip the boundary layer into being turbulent.

Holl (1960a), Kuiper (1981), Van der Meulen and Pei (1982), Shen (1985), Huang (1986), Holl and Billet (1986), Johnsson and Rutgersson (1991), Ye at al. (1992), Kim et al. (1995) and Pichon et al. (1995) have shown that the use of a roughness element at the leading edge may be a useful technique to move the transition region to the leading edge. Pichon et al. (1997) have recently indicated that the boundary layer tripping by thin strips of cyanoacrilate glue or aluminium foil on both sides of a foil appeared to be a good technique when studying the scale effect on the inception of cavitation. Thus, as the roughness element can increase the inception numbers of cavitation, but the size and location of roughness element are very critical and the stimulator itself may create the phenomenon of **"Premature Cavitation"** (Holl and Billet, 1986).

The roughness basically stimulates the transition of the boundary layer from laminar to turbulence. There have been two types of roughness applied to propeller blades in model scale to stimulate the flow that is fully turbulent, these are called the:

- **"distributed"**
- **"isolated"** types.

Roughness that is applied and distributed equally is called the distributed roughness whilst the type applied in the form of studs, such as triangle, arc etc., is called the isolated roughness.

Distributed roughness has been found more effective than isolated roughness in stimulating turbulence. However, since the location of minimum pressure, where cavitation occurs, is not known precisely and its location can be covered up by using the distributed roughening rather than the isolated roughening (ITTC, 1990). When the roughness is large enough to move the transition region to the leading edge the size or height of the roughness, at which the transition to turbulence takes place, can be expressed non-dimensionally by the roughness Reynolds number,

$$R_{ek} = \frac{U_k k}{\nu} \tag{1.7}$$

where:

- U_k is the local velocity at the position of the roughness height
- k is roughness height
- ν is kinematic viscosity of the liquid.

Although a minimum value for the roughness Reynolds number has been recommended in the open literature to trip the boundary layer from laminar to turbulence, there is no recommended maximum value for the roughness Reynolds number. A roughness Reynolds number of 600 has been found to have an effect on the inception numbers of sheet cavitation of axisymmetric headforms and foils (Van der Meulen and Pei, 1982) and (Shen, 1985). Huang (1986) has also found that the value of 600 stimulated the transition region to the turbulence for axisymmetric head forms. Also, a minimum value of 600 was recommended for propellers by the 18th ITTC (1987) to move the transition region to the leading edge of a propeller blade.

The boundary layer developing over the roughened surface is thin and the height, at which the boundary layer velocity goes to zero, is somewhere between the top of the roughened and the smooth surface. This position is virtual wall and the distributed roughness displaces the surface of the blade section so that this displacement effect changes the pressure distribution outside the boundary layer. It is required that this effect should be minimised and therefore, it is important to estimate the minimum and maximum size of the distributed roughness to generate micro-cavitation and avoid unnecessary changes in the pressure distribution. However, there is no recommendation for the upper limit of distributed roughness height in the literature yet although some guidance on the minimum roughness sizes is available. In general, roughness sizes ranging from 20 μm to 100 μm have been reported to be the most frequently applied in the investigations of propeller and foils (ITTC, 1987).

The location, where roughness is to be applied, is also important. Kuiper (1981) applied roughness with a length of 3 per cent of the maximum chord length from the leading

edge in his investigation on the inception of cavitation. The 19th ITTC (1990) recommended that the roughness should be applied between about 5 per cent of the maximum chord length and the leading edge on both sides of the blade. Kim et al. (1995) have also covered 5 per cent of the maximum chord length from the leading edge.

The application of the roughness on the leading edge of both propellers and foils is a practical problem. The glue used to stick roughness element to blades should be watery with a low surface tension to that a thin layer of glue is used.

If a tape is used to apply roughness at the leading edge which guides the boundary of the area to be glued this may create a sharp edge at the boundary of the glued area which may cause premature cavitation. However, tape is used in the following manner at the Admiralty Research Establishment (ARE), Haslar in the UK. Blades are first taped, then the tape is removed before the glue dried and before the roughness particles are applied. This method produced a suitable transition between the roughened surface and the smooth surface. The ARE procedure has been accepted one of the most appropriate roughness gluing method applied to propeller blades to date (ITTC, 1990).

1.1.1.2 Effects of Bubble Dynamics

Perhaps the most complex factor contributing to the scale effect phenomena is the bubble dynamics, which is closely associated with the distribution, size and contents of nuclei contained in the fluid. The term nuclei includes holes, bubbles, solid particles and any combination of them or simply air bubbles in a fluid. The cavitation is a multiphase flow phenomenon consisting of a mixture of solid, liquid and gas phases. In the context of bubble dynamics, the inception of cavitation is defined to occur when nuclei in a fluid reach a critical size and grow explosively, due to the reduced pressure around a body. Therefore, the presence, size, contents and distribution of the nuclei have an important role in the development of the cavitation.

Although the pressure change around the body is assumed to cause cavitation when the local pressure is equal to the vapour pressure of the fluid, in reality, cavitation occurs when the minimum pressure falls below a critical value, P_{crit}. The vapour pressure is defined as the equilibrium pressure of the liquid's vapour without vaporisation, which is in contact with an existing free surface at a specific temperature. The value of difference between the vapour pressure, P_v, and the critical pressure, P_{crit}, is called **"Tensile Strength"** or simply **"Tension"** of the fluid such that (Brennen, 1995):

$$T = P_v - P_{crit} \tag{1.8}$$

and hence

$$P_{min} = P_{crit} = P_v - T \tag{1.9}$$

Tension of a fluid depends upon the number, size, distribution and content of nuclei in the fluid. When the size and number of nuclei are suppressed, relatively large values of tension can be sustained (Arndt and Maines, 1998). Therefore, if the fluid does not have enough nuclei it can resist up to very low pressure or high tensile strength without the cavitation occurring.

The process of cavitation depends on the inception, growth and collapse stages of bubbles in the flow. The dynamic growth of a bubble was initially described by

Rayleigh (1917). This description was modified by Plesset (1949). For this reason, the equation, which describes the dynamic growth of a cavitation bubble, is known as **"Rayleigh-Plesset"** equation:

$$\rho R\ddot{R}+\frac{3}{2}\rho\dot{R}^2 = P_v - P_L - \frac{2S}{R}+\frac{K}{R^3} \tag{1.10}$$

where:

- R is the bubble radius
- P_L is the pressure surrounding the bubble (external pressure)
- S is surface tension
- K is a gas constant
- $\dot{R}$ and $\ddot{R}$ are the time derivatives of R.

Initially, a gas bubble of radius, R_0, already exists in water and its initial radius can be found from the equilibrium condition when the difference between the inner and outer pressures in the bubble balances the surface tension force, thus:

$$P_v - P_L = \frac{2S}{R_0} - \frac{K}{R_0^3} \tag{1.11}$$

The rate of growth of a bubble is small when the condition of equilibrium exists, this implies that the bubble is in a stable condition. Below a certain critical pressure, this equilibrium is destroyed thus the bubble grows rapidly - this is the onset of cavitation. This dynamic growth of these cavitation bubbles is affected by the size, number, contents and distribution of nuclei.

The investigation of the effect of nuclei was started by Daily and Johnson (1956). They showed that the occurrence of cavitation at or near the vapour pressure on mechanical equipment and engineering structures was explained by the presence of relatively large gas nuclei in the fluid. Keller (1974) indicated that the inception number of cavitation became lower when the test water contained less nuclei. Later Keller (1984) and (1994)

showed that cavitation tests without consideration of the water quality may result in enormous deviations from the cavitation behaviour of prototype. Meyer et al. (1989) also found that larger free-stream bubbles were necessary to generate large cavitation bubbles for a Schiebe headform.

Since there are few nuclei in model scale tests, two artificial nuclei techniques are used in the model testing facilities to simulate the nuclei conditions of full-scale. These techniques are called **"Electrolysis Technique"** and **"Nuclei Seeding"**.

Kuiper (1978), and Suhrbier and Lecoffre (1987) used the electrolysis technique to generate some nuclei in model scale. The description of this technique is detailed in (Kuiper, 1978). The technique generates oxygen and hydrogen atoms – mostly the latter. Because of the greater number of hydrogen atoms created this technique is also known as **"Hydrogen Bubble Technique"**. Although this technique is relatively easy to use in depressurised towing tanks, its use in cavitation tunnels is restricted due to long exposure times of bubbles and requirement for high currents to generate bubbles (Kuiper, 1981).

In the nuclei seeding technique, micro bubbles are injected into a cavitation tunnel usually in the vertical upstream leg. The bubbles are produced by gas released through very small orifices. The added micro bubbles must be larger, but not too much larger than the critical bubble size required to initiate the inception of cavitation. It was recommended by the 18th ITTC (1987) that the radii of the added micro bubbles must be in the range of 20 μm and 50 μm. Plesset and Gilmore (1950), Isay and Lederer (1977) and Lecoffre and Bonnin (1979) suggested that, in order to obtain the same cavitation patterns on model and full-scale, the nuclei density in the model testing cavitation tunnel should be a factor of λ^3 times greater than the nuclei density in the operating fluid of the full-scale:

$$\frac{N_m}{N_s} = \lambda^3 \text{ and } N(P) = \frac{N(P_1 + P_2)}{2} \tag{1.12}$$

where:

- N is the number of nuclei per unit volume, whose critical pressure is between P_1 and P_2
- λ is the length scale of ship to model
- subscripts "**m**" and "**s**" correspond to model and full-scale, respectively.

However, Latorre and Ligneul (1995) have claimed that such heavy amount of nuclei seeding can change the characteristics of the quality of the water used in the cavitation tunnel, and thus alter the test results significantly. This was also discussed by the 18th ITTC(1987) and it was recommended that it is not necessary to simulate the complete full-scale nuclei spectrum for scaling of the inception of cavitation.

Apart from the mechanism to generate the nuclei in model scale, other difficulties associated with the nuclei simulator in model scale are to decide what parameters (tension-tensile strength- of water, contents, size and distribution of nuclei, etc.) are more important and how they are to be measured. There are some well-established methods to measure nuclei in the water; these can be grouped into two categories.

The first category characterises the nuclei by tension of water measured by the following methods:

- venturi
- ultrasonic

The second category describes the nuclei by their size measured by the following methods:

- holography
- light-scattering

- Phase Doppler Anemometry, PDA (ITTC, 1987).

The venturi and ultrasonic methods, which were described and evaluated by Oldenziel (1982), are the direct methods. The second category are mainly optical methods, and were explained by Kodama et al. (1981).

The venturi methods use a venturi tube to measure cavitation event rates as a function of the throat pressure of the venturi tube or liquid tension. This technique is known as the Cavitation Susceptibility Meter, CSM. It was first proposed by Oldenziel (1982) and later developed by d'Agostina and Acosta (1991). A description of the latest type of the CSM can be found in Pham et al. (1995) and Pham et al. (1997).

The ultrasonic methods detect bubbles acoustically using their very sharp resonance frequency of radial volume oscillations. Schiebe and Killer (1971) used the acoustic tone burst attenuation technique and tried to measure the size distributions of bubbles in water. A review of acoustic detection methods can be found in Scarton and McDonald (1977). The problem with these methods is that in relatively small structures reflection causes a great amount of noise in the detected signal.

The second group of methods based on the optical techniques provide information on the contents, size and distribution of nuclei particles. A detailed description of the holography technique was given in Gates and Bacon (1978) and Billet and Gates (1981) while the information on PDA and light-scattering techniques can be found in e.g. Tanger and Weitendorf (1989) and Gowing and Ling (1980) respectively. The holography technique offers or records not only the number and size distribution of nuclei accurately, but also the nature of the nuclei (Gates and Bacon, 1978). At present, holography is the best method to discriminate micro bubbles and solid particles although it is limited to bubble size with diameter of 10 μm. The PDA technique can also measure bubble sizes less than 10 μm.

There are some significant differences between the optical and the CSM systems. The optical systems can only give information about the contents and size distributions of particles, however, the use of the CSM is the direct determination of tensile strength of

water in a tunnel. The disadvantage of the CSM is that it only gives the tensile strength of the weakest impurities. It is also not possible to measure all the nuclei, since at a certain number of bubble explosions per unit of time, the throat of the venturi starts to choke (Oldenziel, 1982).

All fluids contain some dissolved and undissolved gases. The gas contents of the fluid affect its tensile strength, hence the scale effects are associated with bubble dynamics. As water in various grades is the operating environment of propellers and foils in model and full-scale, the focus will be on the water as a fluid.

The total gas content of a fluid can be written as:

$$\alpha_T = \alpha_D + \alpha_F \tag{1.13}$$

where:

- α_D is the dissolved gas content of the fluid
- α_F is the free or undissolved gas content of the fluid (Holl, 1970) and (Rood, 1991).

The dissolved gas content of the water consists of oxygen, nitrogen, argon, etc. Free (undissolved) gas content can act as cavitation nuclei while the dissolved gas content affects the size and growth of the nuclei. Therefore, both forms of gas contents play important roles in the development of the number, size and distribution of the bubbles and their effects on the pressure field of the fluid flow.

Holl (1960b) showed that the difference among the inception numbers obtained in varying dissolved gas content of a NACA16012 and 0.5 caliber foils is directly proportional to the dissolved gas content. It has also been shown that relatively small quantity of low air content of water resulted in lower inception values (Arndt and Keller, 1991). Contrary to this, Gowing et al. (1995) have recently shown that the dissolved gas content had a small influence on the inception value without nuclei seeding also that

there was no difference between 80% and 30% of dissolved gas content and small nuclei injection for attached cavitation.

Friesch and Johannsen (1995) indicated that inception numbers of cavitation of propellers are strongly influenced by gas content of the fluid. de Chizelle et al. (1995) also found that the values of the inception of cavitation of axisymmetric headforms were increased with an increase in the dissolved gas content of the water.

Gindroz et al. (1996) found that when the dissolved gas content is changed during cavitation tests, then the inception of cavitation of the propeller tested could be altered. Baur et al (1998) demonstrated that the principal parameter that is significant to increase the growth of bubbles is the diffusion process, i.e. dissolved gas content in the flow, can influence the inception of cavitation.

Tanibayashi et al (1998) also indicated that the inception of cavitation of a cylinder decreases with decreasing the dissolved gas content in water. Therefore, the size distribution and growth process of bubbles, which are affected by the dissolved and free gas contents of the water, have an influence on the inception of cavitation.

The effects of bubble dynamics have also been discussed by Holl and Wislicenus (1961), Arndt (1974), Weitendorf (1979), Ooi (1985), Parkin and Baker (1986), Gowing et al. (1995), Gindroz and Billet (1993), Pauchet and Woillez (1995) and the 21st ITTC (1996). A number of review studies on the subject can be found in ITTC (1990), ITTC (1993) and Matsumoto (1998). Although the mechanisms of bubble dynamics are not yet fully understood, nevertheless the influence of the nuclei content on the conditions of cavitation occurrence is well established.

1.1.1.3 Predicting the Inception of Cavitation

Amongst various types of cavitation, tip vortex is the first type of cavitation observed on marine propellers and foils; this is responsible for increased level of noise and to a certain extent vibration, and may develop progressively into sheet cavitation. The accurate prediction of the inception of each type of cavitation is crucial to the design of silent propellers and to avoid the damage due to the cavitation. Predicting of the inception is usually derived from small scale model experiments in cavitation tunnels, this, of course, requires scaling the prediction to apply to the full-scale propeller.

The methods used to predict the inception of these two types of cavitation can be categorised as:

- **"semi-empirical"**
- **"numerical"**

As the effect of the tip vortex cavitation on the performance of marine propellers has long been recognised, most prediction methods are associated with this type of cavitation. Thus, the semi-empirical methods usually deal with the prediction of the tip vortex cavitation while these based on numerical methods are used to predict both types of cavitation.

In the above context, the semi-empirical methods consist of two different approaches to predict the inception of the tip vortex cavitation, these are based respectively on:

- Reynolds number
- water quality

The use of numerical methods are mainly based on:

- lifting surface
- boundary element (panel)

- Computational Fluid Dynamics (CFD) methods.

In general, the first two methods have been used to predict sheet cavitation and the CFD methods have been used in the prediction of the tip vortex cavitation. In the following section a brief review of these methods is given.

1.1.1.3.1 *Semi-Empirical Methods*

There are two main types of scaling issues for the tip vortex cavitation based on model tests: Reynolds number and water quality based methods.

Methods Based on the Reynolds Numbers:

The methods associated with the Reynolds number are based on the approach by McCormick (1962), who developed a semi-empirical scaling relationship for the tip vortex inception of cavitation on foils by modelling a typical wing and trailing vortex system, as shown in Figure 1.2.

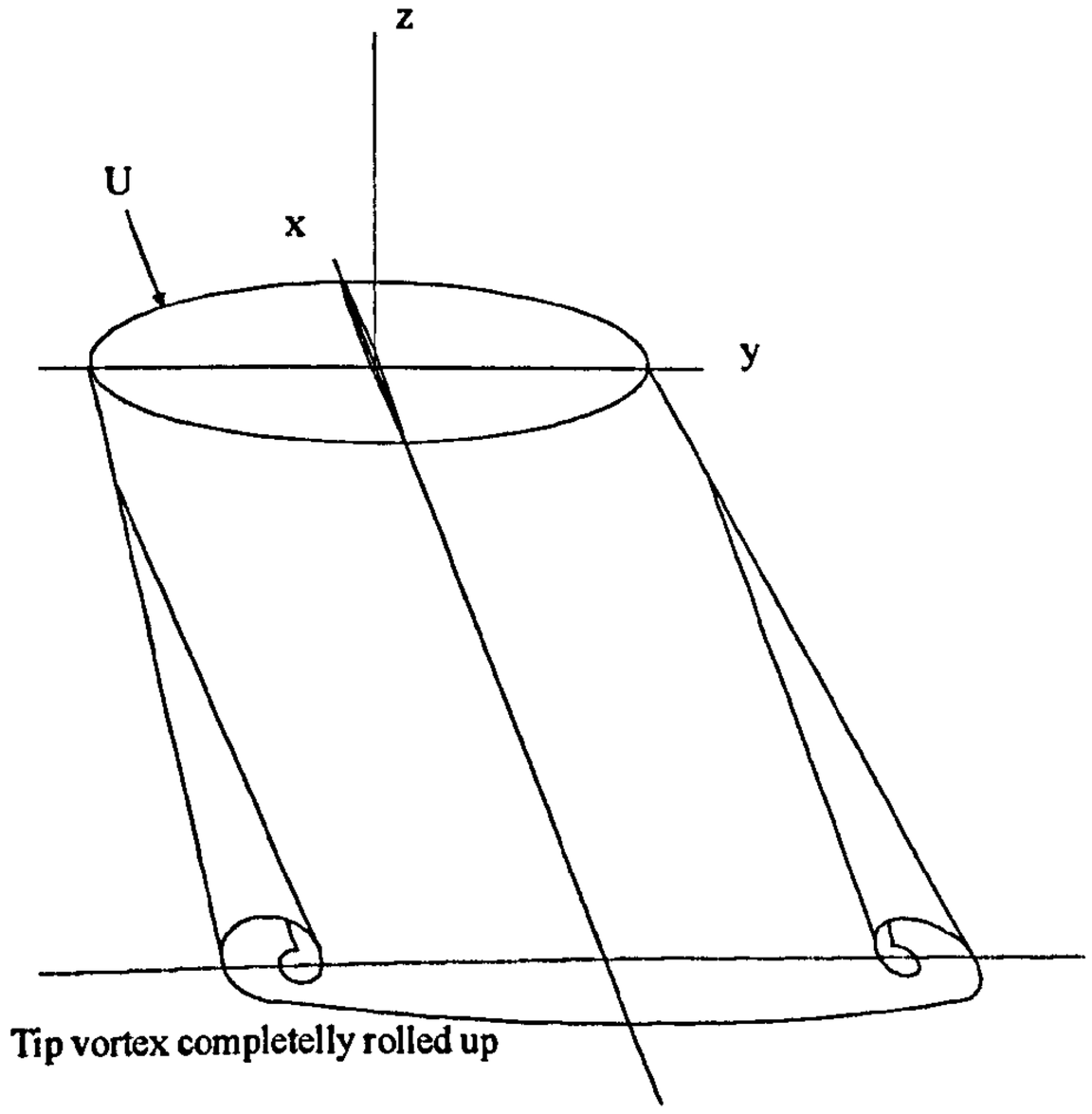

Figure 1.2 A typical wing and trailing-vortex system (McCormick, 1962)

Mathematical modelling of the vortex system is very important in predicting the inception of tip vortex cavitation because it is assumed to take place when the minimum pressure at the vortex core is near the vapour pressure. This minimum pressure occurs at

the centre of the vortex core, where the viscosity plays an important role (e.g. McCormick, 1962 and Kuiper, 1981). Due to the pressure difference between the suction and pressure sides of a lifting foil (Figure 1.2), initially chord-wise stream flow near tip region of foil or propeller blade on the pressure side sweeps outward towards the tip, then passes around the tip, and is gathered into the rolling-up the tip vortex. Based upon this definition, McCormick assumed the tip vortex to be fully rolled up at the tip of foil. The foil was idealised by representing it as a horseshoe vortex. The latter has a combined Rankine vortex structure with a tip circulation Γ_V and a characteristic vortex core radius R_1. The Rankine vortex is irrotational outside the core and rotational inside the core. Based on the above analysis McCormick (1962) developed the following semi-empirical relationship for the inception of tip vortex cavitation of a foil:

$$\sigma_i = R_{ec}^n \alpha^t \tag{1.14}$$

where:

- α is the angle of attack of the foil
- R_{ec} is the Reynolds number ($R_{ec} = \frac{Vc}{\nu}$)
- V is the tip velocity
- c is the foil chord
- n and t are the constants obtained from experiments

The exponent (n) of the Reynolds number was found to vary in the range of 0.35-0.38 while the exponent (t) of the angle of attack was 1.29 for an elliptical wing and 1.44 for a rectangular wing (McCormick, 1962).

Following McCormick's approach Chandrashekhara (1976) later introduced the notation of a residual cavitation index, σ_{res}, to reflect the effects of bubble dynamics on the inception of the tip vortex cavitation. He proposed the inception of cavitation for foils as:

$$\sigma_i = \frac{1}{8\pi^2}\left[\frac{C_L A}{R^2}\right] F\left(\frac{R}{R_1}\right) + \sigma_{res} \tag{1.15}$$

where:

- C_L is the lift coefficient of the foil
- A is the planform area of the foil
- R is a radial distance from the vortex core
- F is a function of the R and vortex core radius R_1

Chandrashekhara (1976) also extended this analysis to the tip vortex cavitation of propellers by using the velocity diagram of a propeller blade section. He developed the following semi-empirical formula for the inception of cavitation of the propellers tested as:

$$\sigma_i = C\left(\frac{P}{D} - J\right)^2 + \sigma_{res} \tag{1.16}$$

where:

- C is a constant
- P is the pitch of the propeller at the desired radius
- D is the diameter of the propeller
- J is the advance coefficient of the propeller, which is defined as:

$$J = \frac{U_A}{ND} \tag{1.17}$$

where:

- U_A is the advance velocity of the propeller
- N is the rotational speed of the propeller.

Noordzij (1977) examined the McCormick's analysis and showed that the inception of the tip vortex cavitation for foils depends on the angle of attack and Reynolds number.

Kuiper (1981) re-examined McCormick's analysis in combination with Chandrashekhara's approach and developed a scaling relationship in terms of propeller pitch-to-diameter ratio and the tip speed. He successfully correlated his formula with the experimental results for lightly loaded propellers to give:

$$\sigma_i = \left(\frac{P}{D} - J\right)^{1.4} R_{en}^{0.35} \tag{1.18}$$

where:

- R_{en} is the Reynolds number based on the rotational speed of the propeller, N, $\left(R_{en} = \frac{ND^2}{\nu}\right)$ at 0.9R radius.
- $\frac{P}{D}$ is the pitch-to-diameter ratio set at 0.9 propeller radius

Hsu (1991) also carried out a scaling analysis of the trailing tip vortex flow generated by a lifting surface by using the model for roll-up of vortex sheet developed by Betz (1933). His solution for the inception numbers of cavitation for a planar hydrofoil wing has the form:

$$\sigma_i \propto C_L^2 R_{ec}^n \tag{1.19}$$

where:

- n was found between 0.50 and 0.56 depending upon the type of hydrofoil wing (i.e. elliptical or rectangular).

He also concluded that the Rankine vortex does not provide a realistic model for the tip vortex flow. Later Hsu's Equation (1.19) was used as a universal scaling procedure for foils by Maines and Arndt (1997).

While the direct use of the scaling formula for propellers has limitations for arbitrary propeller blade geometries, the ratio of the expressions for ship to model leads to a familiar form of Reynolds number scaling for the results of model scale inception of cavitation:

$$\frac{\sigma_{is}}{\sigma_{im}} = K\left(\frac{R_{ens}}{R_{enm}}\right)^{n} \tag{1.20}$$

where:

- subscripts s and m refer to ship and model
- K represents the effects of bubble dynamics

The use of the form of Equation (1.20) in the ITTC community is widespread. It is necessary for each testing facility to develop its own database for the parameters K and n. The typical values for the exponent, n, range from 0.35 to 0.4 (ITTC, 1993).

Methods Based on the Effect of Water Quality:

The other type of scaling of tip vortex cavitation is based on the effect of water quality in particular to reflect the effects of bubble dynamics and the turbulence of the flow. Within this context, the bubble dynamics is represented by the tensile strength of the water, T and the effect of the turbulence is represented by the pressure fluctuations, p'. It has been suggested by Higuchi et al. (1989) that when the minimum pressure, P_{min}, is below a certain critical value, P_{crit}, the inception of cavitation occurs and the inception number can be expressed in terms of tensile strength of water, T, and the pressure fluctuations, p', as:

$$\sigma_i = -C_{p\,min} + k_f \frac{p'}{\frac{1}{2}\rho U^2} - \frac{T}{\frac{1}{2}\rho U^2} \tag{1.21}$$

where:

$$\sigma_i = \frac{P_{st} - P_v}{\frac{1}{2}\rho U^2} \text{ and } C_{pmin} = \frac{P_{min} - P_{st}}{\frac{1}{2}\rho U^2} \tag{1.22}$$

In this formulation, the instantaneous minimum pressure, P_{min}, can be less than the mean minimum pressure, $\overline{P}_{min}$, due to the pressure fluctuations such that:

$$P_{min} = \overline{P}_{min} - k_f p' \tag{1.23}$$

where k_f is a correlation factor, which reflects the interaction of the complex bubble dynamics and the fluctuation pressure.

Arndt and Keller (1991) proposed some ideas of how to quantify the tensile strength of water and the term k_f associated with the pressure fluctuations. If the inception of cavitation is measured in weak water with an adequate quantity of nuclei (σ_{iw}) and in strong water without an adequate quantity of nuclei (σ_{ist}), and if the weak water results

σ_{iw} can be corrected to zero tensile strength then the third term in Equation (1.21) is shown to be:

$$T = \frac{1}{2}\rho U^2(\sigma_{iw} - \sigma_{ist}) \tag{1.24}$$

In order to quantify the second term in Equation (1.21), on the basis that the accurate value of C_{pmin} is obtained then the contribution due to the fluctuating pressure can be estimated by:

$$k_f \frac{p'}{\frac{1}{2}\rho U^2} = \sigma_{iw} - C_{pmin} \tag{1.25}$$

Similar approach has also been used by Gindroz (1995). In this case, the relationship between the tip vortex cavitation and water quality involves the tensile strength and nuclei content.

The procedures for scaling water quality effects are qualitative because the tension and turbulence factor k_f are both highly influenced by the nuclei content in the flow (ITTC, 1993). In view of this it is necessary to try and establish reliable quantitative values of k_f so that the effects of tension and turbulence can be adequately reflected when using Equation (1.21) to predict the inception of tip vortex cavitation.

1.1.1.3.2 *Numerical Methods*

Computation of cavitation on marine lifting surfaces can be performed by using a lifting surface theory, surface panel methods and Computational Fluid Dynamics (CFD) methods. The existing theoretical models, such as thin aerofoil theory or other boundary element methods give singular solutions near the leading edge region and they are not suitable to predict the tip vortex cavitation although they are widely used in the design stage of propellers (ITTC, 1996). Therefore, the lifting surface theory and panel methods are generally used to predict sheet cavitation while the CFD methods have recently started to use in predicting of the tip vortex cavitation. In this respect, the numerical methods are grouped into the predicting of sheet and tip vortex cavitation.

Sheet Cavitation:

The lifting surface methods have been used to predict sheet cavitation on marine propellers in the design stage. In these methods, blade sections of propellers (or foil section) are represented by infinitely thin bound vortex sheet, which lies on the mean line of each blade section. The section thickness geometry is represented by source-sink distributions in order to estimate more accurately the distributions of the surface pressure to predict cavitation (e.g. Carlton, 1994). This method is also known as **"Linear Theory"** because the cavity thickness is assumed to be small relative to its length and the ignorance of the thickness of blade section.

The main problem with these methods is the singularity of the pressure distribution at the leading edge of the blade section calculated by the methods. This singularity can be modified by using Lighthill's leading edge correction (1951).

Kinnas (1992) applied the Lighthill's leading edge correction to the lifting surface method for a cavitating 3-D foil and propeller. It was found that the leading edge correction improved the prediction of the sheet cavitation for both bodies compared to the results of the lifting surface method without the leading edge correction. However,

the accuracy of the method was expected to deteriorate in the case of extreme (high skew and /or twist) propeller geometries (Kinnas, 1992).

Brewer and Kinnas (1997) performed an experimental and numerical computation of sheet cavitation of a foil. They used the lifting surface method in combination with a boundary layer solver and found that in cavitating conditions, the predictions correlated well with the experiments.

Boundary element methods, which are also known as **"Panel Methods"**, are based on the approach developed by Hess and Smith (1967). In these methods, the surfaces of propeller blades and hub or foil surface are discretised by a number of small quadrilateral panels having constant source and doublet distributions. The trailing vortex sheet is also represented by similar quadrilateral panels having constant doublet distributions. The strengths of the source and doublet distributions are determined by solving the boundary value problems at each of the control points, which are located on each panel (e.g. Carlton, 1994). They are inherently **"Non-linear"** with either the thickness or the angle of attack, since they make no assumption about the magnitude of these quantities. On the other hand, the panel methods become very expensive, in terms of computing time, in the case of three-dimensional geometries (marine propellers) as the number of panels are increased tremendously compared to the 2-D foils (Kinnas, 1990).

Although it was claimed that these methods are especially efficient to predict sheet cavitation (Szantyr, 1994), a new model of the inception of cavitation should be developed and incorporated with the panel methods.

Kinnas (1998) has recently applied the panel method to the sheet cavitation of three-dimensional bodies (3-D foil and propeller) with the effects of viscosity on cavity detachment and cavity wake. He pointed out that there are still many unresolved issues; the modelling of tip vortex cavitation and its interaction with the sheet type, viscous effects, etc.

Based upon the above frame, since both lifting surface and panel method are based on potential theory, a boundary layer calculation should be included to take into account the viscous effects of the flow for the better prediction of this type of cavitation. The Lighthill's leading edge correction is an important factor to solve the singularity presented by especially the lifting surface methods.

Tip Vortex Cavitation:

The use of CFD methods to predict the inception of the tip vortex cavitation has recently become more available due to tremendous improvement in computer processor speed. In the early numerical simulations, the assumptions were made usually to simplify the well-known Navier-Stokes equations to the Parabolised Navier-Stokes equations (PNS) (Shramroth and Briley, 1979) or to the Thin-Layer Navier-Stokes equations (TNS) (Mansour, 1984). Previous studies using PNS or TNS were unable to determine the tip vortex formation adequately due to the simplifications of the Navier-Stokes equations.

Recently, Dacles-Mariani et al. (1993) carried out a full Navier-Stokes simulation with the one-equation Baldwin-Barth turbulence model (1990), which was derived from a simplified form of the standard k-ε equation, and the inflow and outflow boundary conditions were applied from the experimental data. The particular tip vortex studies were conducted on a rectangular planform with a NACA0012 section. Although they showed an improvement over numerical results obtained by previous researchers, the tip vortex strength was still unpredicted. The difference between the computations and experiments was referred to the insufficient grid density near the tip vortex and the transition/turbulence modelling (Dacles-Mariani et al., 1993).

More recently, Hsiao and Pauley (1998a) have solved a 3-D incompressible Navier-Stokes equation for a steady state tip vortex flow over a rectangular foil with the Baldwin-Barth one-equation turbulence model. In order to obtain an appropriate grid distribution and sufficient grid density for the near-field wake region and the tip vortex core, a combination of algebraic and elliptic grid generation techniques was implemented. Comparison with the available experimental data showed that the method

favourably predicted the tip vortex flow on the foil and near-field wake region. However, over-diffusive error and excessive dissipation were found at the downstream of the tip vortex. Since the flow around the tip vortex is highly non-isotropic turbulent, current eddy viscosity models were not able to accurately model this free-shear layer turbulence. It has been suggested that non-isotropic turbulence models, such as Reynolds-stress model or Large Eddy Simulation may be required to resolve accurately the tip vortex downstream (Hsiao and Pauley, 1998a).

Feng et al. (1998) have proposed a CFD modelling of tip vortex of open marine propellers. In their model, a numerical approach based on solving the Reynolds-averaged Navier-Stokes equations with the standard k-ε turbulence model was presented to model the tip vortex flow. The comparison of numerical results with the experimental results showed that local grid refinement was needed in the near tip region of blade to improve the predictions.

Hsiao and Pauley (1998b) have also extended their application to solve the uniform flow past a marine propeller, but in their application they solved the incompressible Reynolds-averaged Navier-Stokes equations with again the one-equation turbulence model developed by Baldwin-Barth. They compared the predictions with the experimental data measured by Chesnakas and Jessup (1998) and found that the general characteristics of the propeller flow including the blade-to-blade flow, wake and tip vortex were well predicted. However, the numerical result slightly under predicted the tip vortex strength. Hsiao and Pauley (1998b) have also modified the turbulence model and improved the predictions.

Although the CFD methods have been applied to the propeller flow, the modelling of turbulence, grid dependency and excessive computing time are still practical problems to be solved properly before applications of these methods to the design stage of propellers with such confidence.

1.1.1.4 Traditional Similarity Criteria for Cavitation Tests

Traditionally, four similarity criteria, which are obtained from the method of Dimensional Analysis, are satisfied during a cavitation test in model scale (i.e. Newton, 1961 and Kuiper, 1979) and they are given in the following:

$$\begin{aligned} &\text{Froude number,} && F_r = \frac{U}{\sqrt{gD}} \\ &\text{Reynolds number,} && R_e = \frac{UD}{\nu} \\ &\text{Cavitation number,} && \sigma = \frac{P_{st} - P_v}{\frac{1}{2}\rho V_R^2} \\ &\text{Advance coefficient,} && J = \frac{U_A}{ND} \end{aligned} \tag{1.26}$$

where:

- g is acceleration due to the gravity.

As far as the above parameters are concerned, the advance coefficient should be similar for the model and full-scale propeller to ensure the same operational conditions in terms of the same proportionality of the advance and rotational velocities acting on the propeller. The similarities of the Froude and Reynolds numbers of the model and ship cannot be satisfied simultaneously requiring impractical solution. In this case, for cavitation tunnels with free surface or depressurised towing tanks, the similarity of Froude number is kept while the Reynolds numbers restriction is relaxed.

In the case that tunnels with no free surface, the Froude number will be meaningless and therefore this similarity condition can be omitted too. On the other hand, the cavitation number involving the effect of the pressures acting on the blade, which is most dominant parameter in the cavitation phenomenon, should be similar for the model and full-scale propeller, ensuring the same operational conditions.

However, in addition to the above fundamental parameters, there are other parameters, which control the inception phenomena (e.g. free-stream turbulence, roughness, bubble

dynamics in terms of nuclei content, distribution etc.). Therefore, one should attempt to include these parameters in the present similarity criteria for more sound simulation of the flow similarity between the model and full-scale.

1.1.2 NOISE

Sound is defined as mechanical disturbance, which is propagated in an elastic medium, of such character as to be capable of exciting the sensation of hearing (BSRA, 1982). It is generated whenever there is a relative motion between two fluids or between the fluids and a surface. Whereas noise is described as unwanted sound and interferes with the normal functioning of a system.

The noise generated from a ship system can be grouped into two main categories:

- self noise from all shipboard sources generated by vessel, personnel and equipment
- radiated noise generated by the ship and experienced at some point far away from the ship.

Considerable part of noise generated by the ship system is underwater noise and three major sources of the underwater noise are defined by Ross (1976), which are related to the:

- machinery
- propeller
- flow noise.

Amongst these sources the propeller noise is the most important one, as shown in Figure 1.3, and generated by the following mechanisms in water (Carlton, 1994):

- water displacement by propeller blades
- pressure difference between suction and pressure sides of the blade
- sudden collapse of a cavity bubble or vortex
- the periodic fluctuations of the cavity volumes

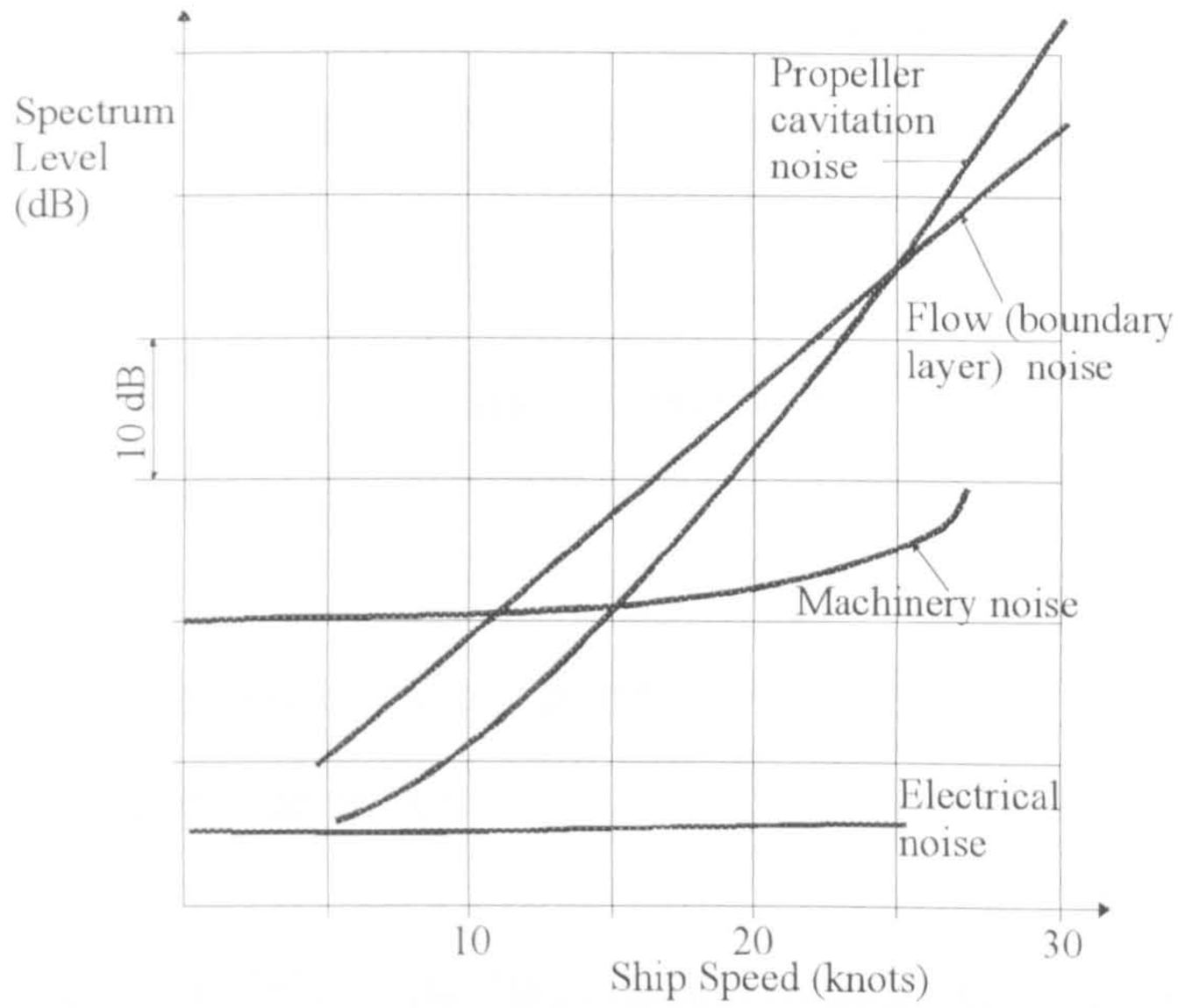

Figure 1.3 Relative influence of underwater noise sources for a surface ship (Carlton, 1994)

If one considers each blade as a lifting surface moving through an unsteady flow, beside the unsteadiness to be caused by the presence of the hull wake, the effect of the free-stream turbulence, boundary layer turbulence generated on the blade surface and flow separation and vortex shedding in the slipstream or wake of the blade will contribute to the sound pressures.

By considering the above mechanisms, the first two mechanisms are associated with a propeller in non-cavitating state, the latter two cases are associated with a propeller in cavitating state. Therefore, a typical propeller noise usually has:

- a non-cavitating
- a cavitating part and the associated noise spectrum is heavily influenced by cavitation (Garen and Vartdal, 1994).

In order to quantify the propeller noise spectrum, acoustic measurements are performed. Acoustic measurements or noise levels are expressed in decibel scale, which is defined by a logarithmic power ratio as:

$$dB = 10 \log(W/W_0) \tag{1.27}$$

where:

- W is the power measured at a point
- W_0 is the reference power.

The sound pressure level (SPL) is the fundamental measure of sound pressure, which is expressed as a pressure ratio by:

$$SPL = 20 \log(P/P_0)\ dB \tag{1.28}$$

where:

- P is the pressure measured at a point
- P_0 is the reference pressure set normally 20 μPa in air and 1 μPa in water and other media.

Since human ear does not respond equally to all frequencies within the audible noise range, a weighting scale was devised by the industry to correct the actual physical levels to those interpreted by the ear. This weighted scale is generally known as the A-weighting scale and shown as dBA. Maximum noise levels permitted on a ship according to the 1981 International Maritime Organisation (IMO) code are between 60 and 110 dBA (IMO, 1981).

In general, acoustic measurements are made in the third-octave and octave filters to show and define noise spectra. The third-octave filter is the ratio of the upper and lower pass band limits that is equal to $2^{1/3}$. In the octave filter, this ratio is equal to 2 and normally centred. The normal range of noise spectrum for a surface ship with well-

developed cavitation may be 5 Hz to 100 kHz, depending upon the type of cavitation (Ross, 1976) and (Carlton, 1994).

It is a standard assumption to consider the issues of cavitating and non-cavitating noise separately. More specifically non-cavitating propeller noise comprises:

- blade rate noise
- inlet turbulence noise
- trailing edge noise.

The blade noise is that the velocity relative to the propeller blade oscillates in amplitude and incidence because of the circumferential variation of velocity into the propeller disc. Therefore, the flow is steady and the unsteadiness is the result of the circumferential variation of the inflow velocity. If turbulence is present in the inlet flow, the flow is unsteady. When the flow is uncorrelated between blades, each blade becomes randomly forced by the inflow and this generates noise (Jenkins, 1988).

Trailing edge noise is generated as a result of the flow around the trailing edge of the propeller blade sections. Thus, viscosity within the boundary layer is a crucial parameter in estimating the level of noise.

Cavitation noise may be generated by various types of cavitation:

- travelling bubbles
- sheet cavitation
- tip vortex cavitation, etc.

When the external pressure around a cavitation bubble starts to increase, after a short time, the pressure gradient between the outer and inner pressure will decrease, and then the bubble will enter its collapse stage. The cavitation bubble in the collapse stage creates shock waves, hence noise. On the other hand, the inception stage of cavitation

also affects the noise level. Wills (1989) showed that a significant increase in noise level occurred with the inception of cavitation on a propeller.

Noise radiation by cavitation was assumed to depend on the behaviour of a single cavitation bubble, theoretically (Fitzpatrick, 1958). According to this approach, spectral power density of a set of bubbles becomes the product of the number of bubbles per unit time and spectral energy density due to the growth and collapse of a single bubble. However, the single bubble approach fails at very high bubble densities. Van der Kooij (1986), Arakeri and Shanmuganathan (1985) and Yu et al. (1995) have supported this conclusion.

It is also more difficult to predict noise generated by cavitation theoretically than for a non-cavitating propeller due to the complex behaviour of the bubbles. Therefore, most predictions are based on model propellers operating in a cavitation tunnel, which have the difficulties in taking into account of the detailed boundary layer and the dynamics of cavitation.

Ideally, identical cavitation numbers should yield identical cavitation patterns in model scale and in full-scale. However, the model cavitation number is often set lower than full-scale cavitation number to obtain equal cavitation patterns, hence noise spectrum.

Bark (1992) proposed cavitation number ratio, σ_s/σ_m, in the scaling for frequencies and sound pressures, where **"s"** denotes full-scale and **"m"** denotes model scale, based on the scaling formula to predict noise developed by Strasberg (1977), Bjorheden and Astrom (1977) and Blake and Sevik (1982). The ratio, σ_s/σ_m, may vary from the inception of cavitation to well-developed cavitation, therefore, different mechanisms could make different cavitation noise scaling. He found that σ_s/σ_m for the inception varies between 1.5 and 3.0.

It is usual to make the following assumptions with regard to bubble size and kinematics for a steady potential flow passing geometrically similar bodies at a constant cavitation number:

- the cavity size is scaled with a characteristic length L
- the non-dimensional cavity radius is only a function of the non-dimensional time $\frac{fL}{U}$ where f is the frequency and U is a characteristic velocity
- the rate of the cavitation events complies with the inverse of the characteristics time of the flow.

According to the above assumptions, Levkovskii (1968) showed the power spectrum scaling as follow:

$$\frac{G_s(f_s)}{G_m(f_m)} = \left(\frac{r_m L_s}{r_s L_m}\right)^2 \left(\frac{\rho_s}{\rho_m}\right)^{0.5} \left(\frac{\Delta P_s}{\Delta P_m}\right)^{1.5} \left(\frac{L_s}{L_m}\right) \left(\frac{\sigma_m}{\sigma_s}\right)^{1.5} \tag{1.29}$$

where:

- G is the power spectrum
- r is the distance from the centre of cavity to the observer
- ρ is the density of water
- ΔP is the characteristic pressure and defined as $\Delta P = P_{st} - P_v$.

The frequency scales as:

$$\frac{f_s}{f_m} = \left(\frac{\rho_m}{\rho_s}\right)^{0.5} \left(\frac{\Delta P_s}{\Delta P_m}\right)^{0.5} \left(\frac{L_m}{L_s}\right) \left(\frac{\sigma_m}{\sigma_s}\right)^{0.5} \tag{1.30}$$

If the diameter of the propeller, **"D"** and **"ND"** are introduced as the characteristic length and velocity, respectively, where N is the rotational speed of the propeller, the frequency scaling will be given by:

$$\frac{f_s}{f_m} = \frac{N_s}{N_m} \tag{1.31}$$

However, in the above approaches, the effects of the viscosity, surface tension and non-condensable gas contained in the bubbles are neglected. Therefore, these approaches have been recommended to be suitable for the scaling of the fully developed cavitation (ITTC, 1987).

Furthermore, the use of the same scaling equations for the entire range of the frequencies in the spectrum has been questioned by Lovik (1981). He proposed different scaling rules in different frequency regions as shown in Figure 1.4. displaying typical noise spectrum of a propeller in cavitating state.

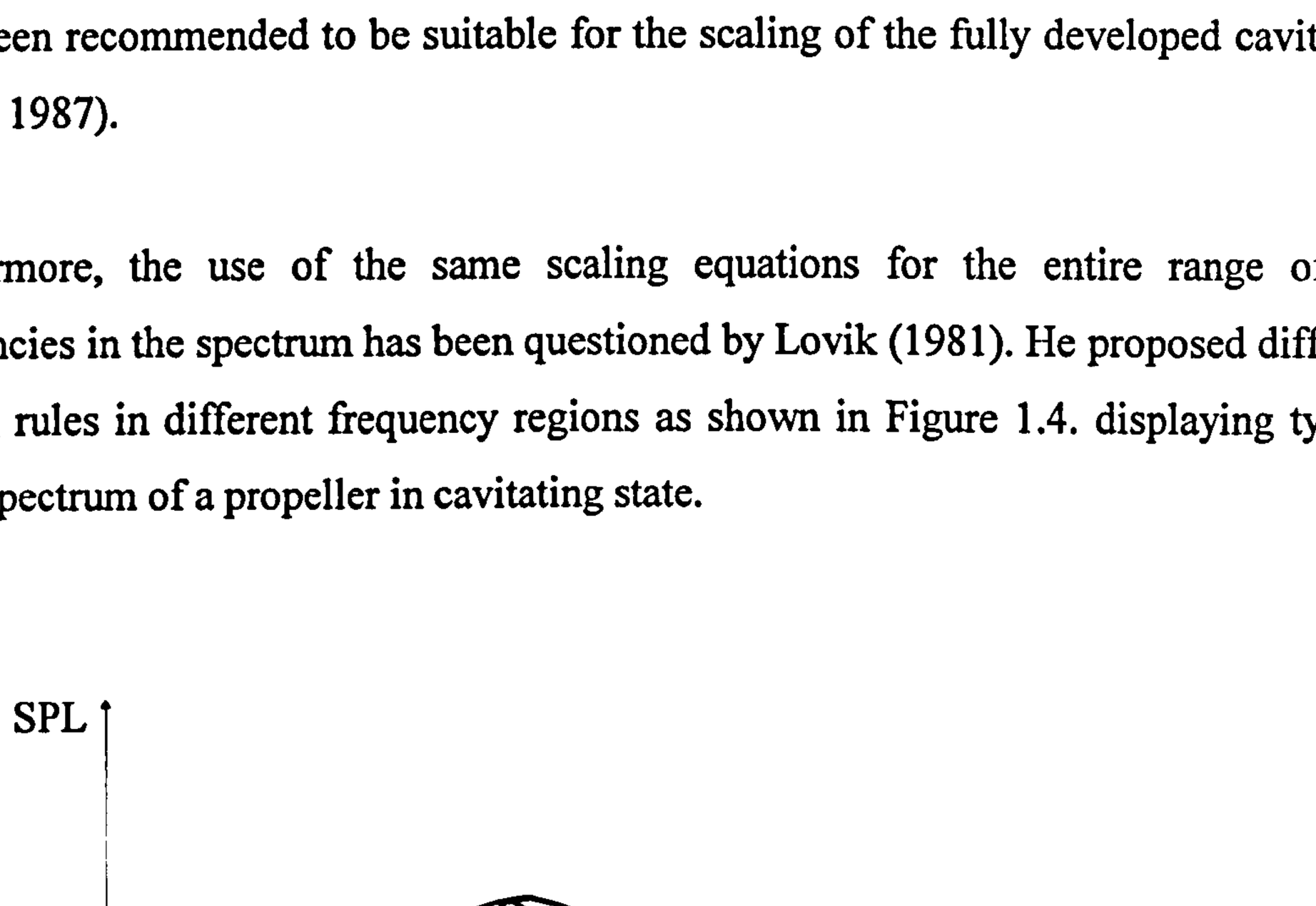

Figure 1.4 Typical noise spectrum of a propeller in cavitating state (Lovik, 1981)

Lovik referring to Fitzpatrick and Strasberg (1956) specified the four distinct regions of the frequency in a typical noise spectrum as follows:

I. Low frequency region containing blade frequency, f_0, and its harmonics where the mean sound pressure level, SPL, increases with the frequency f^4
II. This region starts at the occurrence of bubble frequency, f_b, and the mean sound pressure level decreases as $f^{2.5}$
III. An intermediate region contains elements of both low and high frequency parts of the spectrum, and it starts at the transition frequency, f_t.
IV. High frequency region starts at the collapse frequency of bubble, $f_c = 2\pi/T_c$ and the mean sound pressure level decreases as f^2. Where T_c is a collapse time.

Lovik then applied Equations (1.29) and (1.30) for scaling of continuous spectrum at blade frequency (region I) and in region II by introducing a gas factor into the scaling procedure. At the angular collapse frequency and in region IV, the equations below should be applied due to gas content having a very pronounced influence on the noise at higher frequencies.

$$\frac{G_s^*(f_s)}{G_m^*(f_m)} = \frac{G_s(f_s)}{G_m(f_m)}\left(\frac{Q_s}{Q_m}\right)^{0.5(\gamma-1)} \tag{1.32}$$

$$\frac{f_s^*}{f_m^*} = \frac{f_s}{f_m}\frac{Q_s(Q_m+1)}{Q_m(Q_s+1)} \tag{1.33}$$

where:

- * denotes the modified scaling law
- γ is the ratio of specific heats of permanent gas
- Q is the gas factor proportional to the dynamic pressure divided by the minimum pressure in the cavity at maximum bubble radius.

Kamiirisa (1998) has supported this approach and shown that the gas pressure inside a bubble is more effective than other parameters, such as viscosity, surface tension and the

liquid compressibility is also essential for treating the cavitation noise theoretically due to the significant influence of the gas pressure on the bubble motion.

Although the above scaling procedures are applied, predictions of noise of marine propellers based on model tests usually give higher levels of noise than the full-scale measurements. For the correlation of cavitation noise measurements in model scale with those in full-scale, the difference between full-scale and model scale sound pressure level can be expressed as:

$$\Delta SPL(p) = 20\log\left[\left(\frac{L_s}{L_m}\right)^z\left(\frac{r_m}{r_s}\right)^x\left(\frac{\sigma_s}{\sigma_m}\right)^{y/2}\left(\frac{U_s}{U_m}\right)^y\left(\frac{\rho_s}{\rho_m}\right)^{y/2}\right]$$

or

$$\Delta SPL(p) = 20\log\left[\left(\frac{D_s}{D_m}\right)^z\left(\frac{r_m}{r_s}\right)^x\left(\frac{\sigma_s}{\sigma_m}\right)^{y/2}\left(\frac{N_sD_s}{N_mD_m}\right)^y\left(\frac{\rho_s}{\rho_m}\right)^{y/2}\right] \quad (1.34)$$

where

- x=1, y=1 to 3 and z=1 to 1.5 (Levkovskii, 1968), (Bark, 1982), and (Sasajima and Tanibayashi, 1984).

The difference between the predictions and full-scale measurements was explained by the Cavitation Committee of the 18th ITTC (1987) that model noise tests are usually carried out in a highly reverberant environment (high level of background noise due to the dynamometer, impeller, etc.), this causes the difficulty in interpreting the genuine propeller noise as well as other factors (i.e., dissolved gas content, viscosity, etc.).

Blake et al. (1977) showed that the viscous effects on cavitation of an N112 foil were responsible for varying observed cavitation dynamics and for varying noise characteristics. When the laminar separation was eliminated using a wire placed near the leading edge of the foil to trip the boundary layer into turbulence, the magnitude of noise was generally greater than that produced with untripped boundary layer.

Brennen and Ceccio (1989) concentrated on several aspects of the cavitation and noise and they found that only supercritical nuclei show the sudden collapse of cavitation

contributing to the noise. The critical bubble size or supercritical nuclei population depends not only on the cavitation number, but also on the Weber number ($W_e = \frac{\rho V^2 D}{S}$). The critical bubble radius decreases with increasing velocity and increases with increasing the number of nuclei (Hamilton, et al., 1982).

Bark (1985) showed that the effect of dissolved gas content on the noise level of a propeller. He found that if the dissolved gas content ratio is too high the cavitation noise at high frequencies will be damped by the gas bubbles, and if it is too low the cavitation will be increasingly intermittent which will cause difficulties in the analysis of the noise levels.

Wills (1989) also found that increased total gas content increased the sound pressure level of a propeller at low frequencies but reduced it at high frequencies, indicating the cushioning effect of bubble in the collapse stage. Pollman (1995) have shown that predictions of noise level of a 5 bladed propeller based on model tests were highly dependent on both dissolved and free gas contents of the water.

1.2 CONCLUSIONS

Within the framework of the aim of the thesis and in order to define a clean set of objectives for this research study, a literature survey was carried out into the scale effects on the inception of cavitation and noise of marine propellers in this chapter. Based upon this survey, the following conclusions are drawn:

- Due to complex nature of the physical phenomena involved most of the investigations carried out on the scale effect phenomena of the inception of cavitation and noise of marine propellers rely heavily on the physical model testing methods in cavitation tunnels and rarely in depressurised towing tanks.

- Model propellers, which usually operate at low Reynolds numbers, can have large laminar boundary layer region and a strong tendency to the laminar separation. This is in contrast to full-scale propellers, which operate at high Reynolds numbers hence at almost fully turbulent conditions.

- In general, high turbulence levels cause early transition of the boundary layer from laminar to turbulent and hence complete elimination of the laminar separation. Based on the limited amount of experimental investigation with differing simple test bodies (i.e. axisymmetrical head, small scale of foil etc.), it has been reported the clear effect of the free-stream turbulence on the inception of cavitation. The increase in the levels of turbulence in the free-stream flow moves the line separating the laminar and turbulent regions towards the leading edge and thus causing the boundary layer to become almost turbulent.

- Testing the same object in different testing facilities has indicated different values of the inception numbers of cavitation; this is related to different levels of the free-stream turbulence experienced in these facilities. This evidence further supports the view that the effect of the free-stream turbulence has a pronounced effect on the inception of cavitation.

- As the level of the free-stream turbulence affects the nucleus-forming mechanism then the combined effect of these parameters on the inception of cavitation needs to be investigated.

- There are various types of turbulence generators used to manage (i.e. establish and control) the level of turbulence of the free-stream flows in testing facilities. These generators are wire meshes, honey combs, grids and roads or combinations of them depending upon the type, size, test requirements and experiences of using each testing facility.

- The inception of cavitation does not necessarily occur in the vicinity of the lowest mean pressure on the surface of a body, but occurs in the region of natural boundary layer transition. When the turbulence level is too low as usually occurs at model scale, a change in the boundary layer structure using various roughness techniques applied at the leading edge clearly affects the inception of cavitation.

- Although the leading edge roughness technique has been used in some testing facilities, proper size, location and its application procedure appear to be very critical causing some concern about the reliability of the test results. In view of this there is a little confidence in the use of this technique.

- The effect of the bubble dynamics is reported as being the most complex factor contributing to the scale effect phenomena especially in terms of the distribution, size and characteristics of the fluid.

- In general, the lack of nuclei content in the model testing facilities requires the use of various techniques and equipments to generate the necessary quantity of nuclei. The techniques of Electrolysis (i.e. Hydrogen Bubble Generation) and Nuclei Seeding are two well-known procedures. While the electrolysis technique is relatively easy to implement in depressurised tanks its use in cavitation tunnels is not recommended due to the requirements for long exposure times and high

electrical currents. The implementations of the nuclei seeding procedures are preferred in cavitation tunnels although they are technically complex and costly.

- The total gas content of the flow medium is assumed to consist of dissolved and undissolved (free) gas components. The free gas content which acts as nuclei can be measured by e.g. a van Slyke mechanism. The dissolved gas content which appears to effect the size and growth of the nuclei can be measured by e.g. an oxygen meter. Both of these components are reported to have an important effect on the inception of cavitation and noise.

- In generating nuclei, the important parameters are reported to be the number, size distribution and nature of the nuclei. By considering the two available techniques used to analyse the nuclei, namely the venturi based Cavitation Susceptibility Meter (CSM) and optical methods (including Phase Doppler Anemometry (PDA), etc.), the latter is considered to be the best choice.

- Most methods of predicting the inception of cavitation are associated with the tip vortex cavitation since it is the first type of cavitation usually observed on marine propellers. These methods can be categorised as semi-empirical and numerical. The semi-empirical methods are mainly based on the parameters associated with Reynolds number and water quality and these methods are used widely in testing facilities. Although the application of the CFD methods are available, the modelling of turbulence, grid dependency and excessive computing time are still practical problems before proper applications of these methods to the design stage of propellers can be made with sufficient confidence.

- Mechanisms contributing to the propeller noise can be classified as **"non-cavitating"** and **"cavitating"** type in nature. The noise spectrum of a typical cavitating propeller is heavily influenced by the cavitation.

- When noise is generated in the absence of any cavitation it depends on the effect of free-stream turbulence, boundary layer turbulence on the blades and flow separation and vortex shedding effect at the trailing edge.

- When noise is generated in the presence of cavitation it is the type of cavitation that determines the level of the propeller noise. The mechanism of the noise radiation by cavitation can be adequately represented by the mechanism of a single cavitation bubble although this representation is not satisfactory where there are high bubble densities. Based on this approach both the inception and collapse stages of cavitation affect the noise levels.

- Prediction of the noise spectrum is quite a complex task and such methods currently in use are based on model test measurements combined with appropriate scaling equations. Various scaling equations have been developed based on differing ratios of the cavitation number in model and full-scale to represent the stages of the cavitation from the inception to the well-developed phase.

- In early scaling procedures for the power spectrum and frequencies, the effects of viscosity, surface tension and non-condensable gas content on the bubble were neglected and the scaling equations were applied over the entire frequency range of the spectrum. These procedures have been somewhat modified by applying different scaling rules in different frequency regions as well as introducing a suitable factor for the gas content. However, the effect of the viscosity has still been left out although its effect on the cavitation dynamics as well as on the noise has been reported in limited investigations.

- The effects of the gas content, in terms of its free and dissolved nature, have both been found to influence the noise characteristics of a propeller.

- As model tests are usually carried out in a highly reverberant environment this complicates the prediction of noise. This undesirable phenomenon also contributes

to the differences in the prediction and full-scale measurements of the noise and hence to the scale effect phenomena.

1.3 THE AIM, OBJECTIVES AND LAYOUT OF THESIS

1.3.1 AIM OF THESIS

The aim of this research study was to

- contribute to the state-of-the-art understanding of the physical mechanisms that affect the scale effect phenomena on the inception of cavitation and the consequential noise of marine propellers
- use this as a better basis for establishing mathematical modelling based on semi-empirical methods to predict the inception of cavitation of full-scale marine propellers.

1.3.2 OBJECTIVES OF THESIS

As an introduction into defining the objectives it is useful to discuss some of the key aspects as described below.

Bearing in mind the above aim and conclusions drawn from the state-of-the-art literature survey, it is clear that the nature of the research will be mainly experimental supported by theoretical investigation wherever this is appropriate or possible.

As the experimental investigations were to be carried out in the existing Emerson Cavitation Tunnel (ECT), thus an introduction to the testing procedures in this tunnel involving propeller cavitation and noise is essential.

In general, the ECT has been recognised as a reverberant environment and not specifically designed for acoustic research. The current acoustic measurement equipment uses an external mini-hydrophone. Because of the extremely complex nature

of the propeller noise generated, it is sensible at this stage in the development of predicting methods to be somewhat conservative on the noise investigation and put more emphasis on the research into the mechanisms directly affecting the inception of cavitation and predicting the inception of tip vortex and sheet cavitation.

As concluded in the literature review (Section 1.2) the effects of viscosity and bubble dynamics dominate the inception of cavitation and noise in model scale and hence require separate scaling procedures to full-scale. As far as the viscous effects are concerned, although the effect of the free-stream turbulence has been reported in various studies on a limited number of test bodies, there has always been a limited number of thorough systematic investigations with marine propellers and to understand its nature and quantify its contribution to the inception of cavitation and noise are scarce. Therefore, by taking advantage of the large measuring section of the Emerson Cavitation Tunnel a systematic investigation into this effect with a relatively large foil section, whose cross-section represents a typical propeller blade section, and a propeller will provide a suitable basis for a more detailed study of these phenomena.

In Section 1.2, it has been concluded that although the leading edge roughness technique has been used in some testing facilities, there is little confidence in the use of this technique. Provided that the generation of free-stream turbulence may induce similar effects on the blade section, it will be more interesting to systematically investigate the effects of both the roughness and free-stream turbulence parameters and look for any correspondence between these in terms of their characteristic values.

The important effect of the bubble dynamics on the inception of cavitation and noise is recognised to be complex. Therefore, any investigation into the scale effect should include the effect of bubble dynamics in combination with the viscosity. A thorough research into the effect of the bubble dynamics will require sophisticated nuclei seeding mechanisms and optical devices to control the detailed particulars of the seeding process. From this point of view, the Emerson Cavitation Tunnel does not have such a mechanism and sophisticated measuring equipment. The effect of the bubble dynamics can be based on measurement of the dissolved gas content of the tunnel water. In view of these circumstances it will be justified not to emphasis on the dynamic effects of

bubbles directly, but to introduce this effect in terms of the dissolved gas content parameter.

There are various theoretical and semi-empirical approaches to predict the inception of cavitation and noise in model and full-scale that are corrected by various scaling procedures. As the effect of the free-stream turbulence has to be identified and quantified, it will be appropriate to attempt to devise a theoretical or semi-empirical procedure for the inception of cavitation particularly of the simple attached tip vortex cavitation.

Finally, it would be worth re-considering the traditional similarity criteria used to scale the inception of cavitation and look for rationally based amendment to include the viscous effect.

In essence the main objectives of the thesis are specified by taking into account the above discussions and time limitations of the study as follows:

- To carry out a set of introductory tests in the Emerson Cavitation Tunnel with model propeller and dummy hull involving wake simulations, cavitation observations and measurements of the hull pressure and noise to get familiarised with the testing facility and measurement technique used in the cavitation tunnel.

- To carry out systematic measurements of the inception of cavitation and noise of a simple foil section and a propeller for varying levels of
    1. free-stream turbulence
    2. surface roughness and
    3. dissolved gas content

  in order to identify the trend in resulting new parameters affecting the phenomena for the scale effects associated with these parameters.

- To establish a semi-empirical method of predicting the inception of both the tip vortex and sheet cavitation of a propeller; this is to include the viscous effects in particular with the free-stream turbulence

- To investigate if there is a similarity between the effects of the free-stream turbulence and roughness for the same cavitation number to improve the current cavitation testing procedures.

- To derive new similarity parameters which represent the effect of the free-stream turbulence between the full-scale and model propeller. This is to be based on the method of dimensional analysis to be used as the basis for establishing more rational extrapolation procedure to predict the inception of cavitation of a full-scale propeller based on the cavitation test procedures of small-scale propellers.

1.3.3 LAYOUT OF THESIS

In order to set the objectives of the research work, Chapter 1 contains descriptions of:

- the phenomena of cavitation and especially the inception and noise as experienced by ships' propellers
- the Author's findings of a comprehensive critical review of all relevant papers published in the open literature and ITTC Cavitation Committee reports
- the use of these findings to define the basic aims and specific objectives of the Author's research for this thesis; the principal focus of which is into the various scale effects such as blade surface roughness, turbulence, dissolved gas content, etc.

Based upon the conclusions of the literature survey, the aim, objectives and layout of the thesis are presented at the end of this chapter (Section 1.3).

Since the nature of the research study has required a set of experimental investigations, Chapters 2, 3, 4 and 5 of the thesis are dedicated to the entire physical tests, which were carried out at the Emerson Cavitation Tunnel, their analyses, presentations of the results and discussions.

Chapter 2 describes

- an essential programme of flow tests and measurements to establish the characteristics of the flow in way of the test section of the tunnel corresponding to controlled changes in the turbulence of the upstream of flow.
- the experimental set-up included:
    - a set of wire mesh screens to generate specific measured turbulence in the free-stream flow upstream of the measurement section of the tunnel
    - a 2-dimensional Laser Doppler Anemometry used to map the flow characteristics at the measuring section of the tunnel.
- The information obtained from the background flow measurements was used as a basis for the measurements of the cavitation inception with a simple rectangular foil section (NACA), which represents a typical propeller blade section, and the measurements of cavitation inception and noise with a 5 bladed model propeller.

Chapter 3 records and analyses the measurements of the inception of the sheet cavitation for varying levels of the free-stream turbulence and roughness of a rectangular foil having a NACA cross-section.

Chapter 4 records and analyses the measurements of the inception of the tip vortex and sheet cavitation with a model-scale ship's propeller.

The range of experimental conditions were

- varying levels of the free-stream turbulence
- different blade roughness
- two values of the dissolved gas content.

Chapter 5 presents the measurements of noise with the same model propeller and experimental conditions used in the tests described in Chapter 4.

Chapter 6 describes how a semi-empirical method was developed to predict the inception of the tip vortex and sheet types of cavitation. This method takes into account of the turbulence present in the upstream flow.

The method uses a modification of Lighthill's Leading Edge Correction. Using this semi-empirical approach predictions are made for all the experimental conditions reported in Chapter 4 and compared with the experimental results. The author describes how a useful relationship is established between the effects of levels of turbulence in the free-stream and roughness of propeller blades and how this leads to improvements in the current cavitation test procedures.

The author also describes the use of dimensional analysis to propose new similarity parameters to be used when scaling predictions based on model-scale test results to full-scale propellers.

Finally, Chapter 7 contains a general overview of the study, conclusions and recommendations for future work.

CHAPTER 2 BACKGROUND FLOW MEASUREMENTS

2.1 INTRODUCTION

The literature survey given in Chapter 1 has shown that investigations into the scale effects on the inception of cavitation and noise have mostly been carried out experimentally due to the complexity of the phenomena involved. As this was the main objective why an experimental investigation was needed, the other objective was the requirement for systematic tests, in terms of the free-stream turbulence, roughness and dissolved gas content of the flow, which have been identified to be the main parameters contributing into the scale effect phenomena.

In order to satisfy above objectives, an experimental programme has been set up, which was composed of the following phases:

- Introductory tests
- Tunnel background flow measurements
- Measurements of the inception of cavitation with a rectangular blade section (NACA) for various parameters involved in the scale effect phenomena
- Measurements of the inception of cavitation with a model propeller based on the similar parameters associated with the scale effect phenomena
- Measurements of the noise with the same model propeller based on the similar parameters associated with the scale effect phenomena

The introductory tests consisted of the noise measurements with two model propellers in uniform flow, the wake simulation and the measurements of hull pressure with one of these model propellers behind a dummy hull fitted with a wake screen to simulate the target wake. The idea behind these tests was to get the author familiarised with the cavitation tunnel, testing facility and the measurement techniques used for noise, wake

simulation and hull pressure in the Emerson Cavitation Tunnel (ECT). The details of these tests and results have been reported in the technical reports (Korkut, 1995a) for the noise measurements, (Korkut, 1995b) for the wake simulation and in the paper (Wang et al, 1995) for the hull pressure measurements.

One of the main parameters contributing to the scale effect phenomena is conjectured to be the influence of the free-stream turbulence. Therefore, there is a requirement for systematic measurements of inflow, preferably in a cavitation tunnel, with various levels of turbulence. In order to generate systematically varying flow conditions with different levels of turbulence in a tunnel, it is customary to use wire meshes with different sizes. The flow condition behind the mesh can be measured by various types of flow devices preferably by a Laser Doppler Anemometry system.

This chapter presents the details of such systematic background flow measurements carried out at the Emerson Cavitation Tunnel by using a specially designed wire mesh frame fitted with differing size of meshes and 2-D Dantec Laser Doppler Anemometry. The main objective of the these measurements was to obtain the flow map of the tunnel cross-section, in terms of the flow velocity and turbulence generated by differing size of the wire mesh over a set of tunnel inflow velocities. The information to be obtained from the background flow measurements would provide a basis for the analysis of the measurements of the inception of cavitation and noise tests, which were carried out later on. In this chapter, relevant sections of the background flow measurements and analysis are provided. The details of the tests and measuring equipment can be found in (Korkut, 1997a).

2.2 TEST CONDITIONS AND EXPERIMENTAL SET-UP

Experiments were carried out through five different inflow conditions at the Emerson Cavitation Tunnel (ECT) of the University of Newcastle upon Tyne, which has a large rectangular test section with the section size of 1.22 m by 0.81 m (BxH). The details of the tunnel and the test section are given in Appendix I for further information.

In order to generate varying levels of the free-stream turbulence in the tunnel, a base frame and 3 different sizes of wire meshes were used. During the measurements of the turbulence, the frame shown in Figure 2.1 was placed at a distance of 0.827 m at the upstream of the model propeller plane or the position of foil leading edge to mount the wire mesh screens. The mesh area covered the entire propeller working area or the reference line on the foil described in Chapter 3, with a comfortable margin, it was 0.350 m by 0.380 m (BxH). The cell sizes of meshes used are given in Table 2.1.

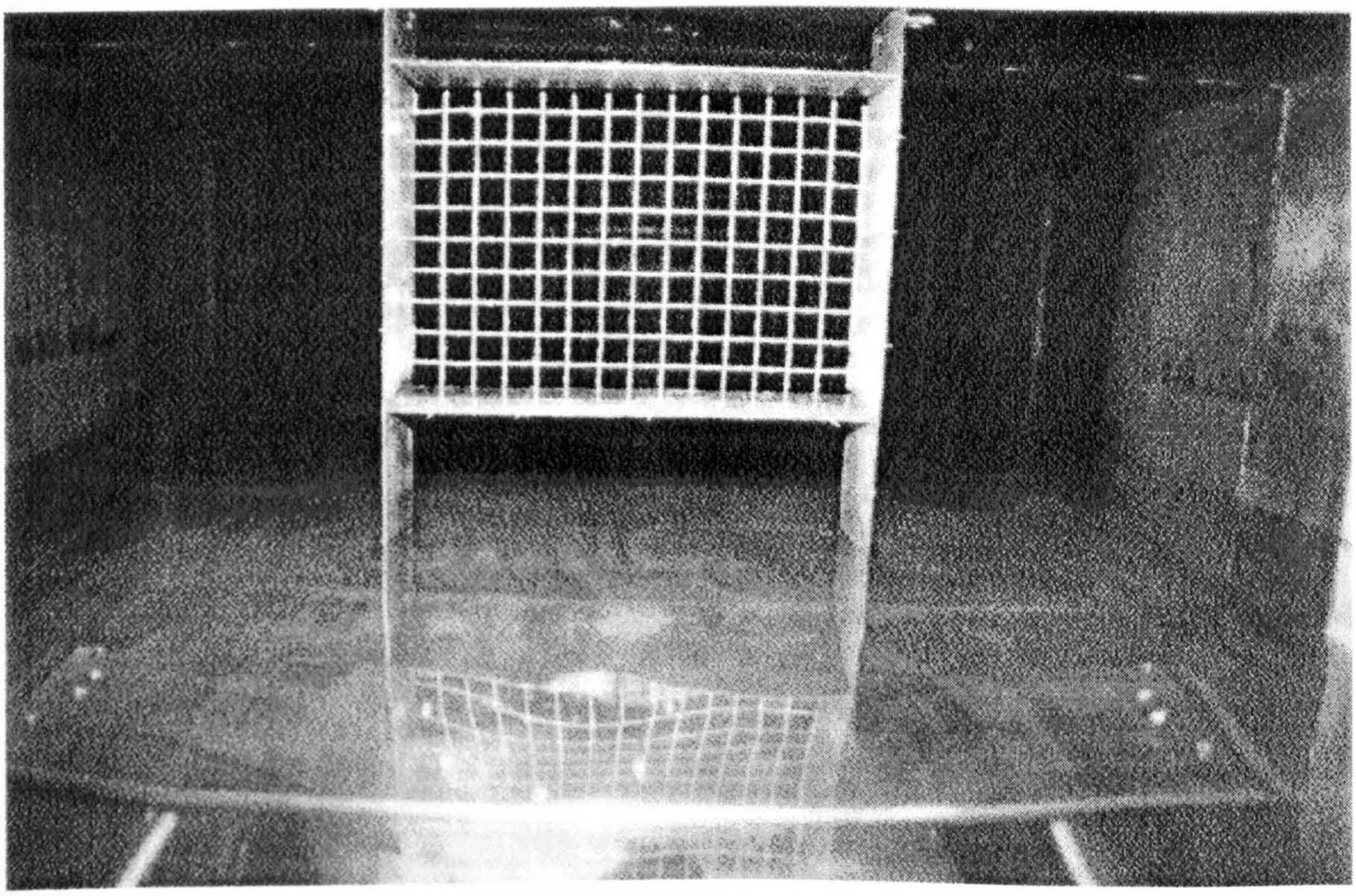

Figure 2.1 Base Frame with medium sized mesh inside the cavitation tunnel (looking from the opposite direction to where flow approaches)

Table 2.1 Mesh sizes used in tests

Mesh type	Cell size (BxHxD) in mm
Largest-sized mesh	25.4 x 25.4 x 1.0
Medium-sized mesh	12.7 x 12.7 x 1.0
Finest-sized mesh	6.36 x 6.36 x 1.0

It must be noted that the medium-sized was the available mesh in the tunnel and the finest-sized mesh was then built by putting two medium-sized meshes crossing each other. The largest-sized mesh was built by cutting and enlarging the medium-sized mesh.

The background flow measurements in the tunnel were performed over the range of inflow velocity given in Table 2.2 by using the back-scatter Laser Doppler Anemometry (LDA) facility. The velocity distributions at the cross section were measured in the axial direction, which is parallel to the incoming flow, and in the transverse direction by using 2-D DANTEC, argon-iron, water-cooled, type 2016 LDA system. A brief detail of the LDA system is given in Appendix II.

Table 2.2 Inflow velocities used for measurements

Velocity, U_{pitot}, in m/s	1	2	3	4	5	6	7

The five different flow conditions are given in Table 2.3

Table 2.3 Flow conditions in experiments

Test No	Flow Condition Details
1	No base frame and wire mesh present in the tunnel
2	Only the base frame present in the tunnel
3	The base frame and the wire mesh with the largest-sized present in the tunnel
4	The base frame and the wire mesh with medium-sized present in the tunnel
5	The base frame and the wire mesh with the finest-sized present in the tunnel

The position of the cross-section where the measurements were taken was at a distance of 0.980 m from the front end of the test section, which has 3.1 m length, and 0.827 m from the base frame. The position of the cross section was very close to the location where a model propeller is usually situated during uniform flow tests or a foil is mounted in the measurements of the inception of cavitation.

Prior to the LDA measurements, the observation windows of the tunnel at the bottom, left and right of the tunnel test section were replaced with the new windows since the original windows, which had been used for a long time under the effect of vacuum, had a considerable curvature on them. During the preliminary tests with the LDA equipment, it was noticed that this curvature had an undesirable polarisation effect on the laser beams, which influenced the quality of the data.

The measurement (grid) area was chosen as 550 mm by 600 mm for the background flow measurements in the presence of no base frame and wire mesh in the tunnel, as shown in Figure 2.2. The measurements were taken from the bottom window because of the fact that the maximum grid area could be covered by the laser beams and by a 2-D traversing mechanism through this window. The limit of 550 mm in the transverse direction was the maximum breadth along which the traversing system could operate. The limit of 600 mm in the vertical direction was the maximum distance where the laser beams from 600 mm focal length of the laser probe could reach. The intervals between the grid points in the transverse and vertical directions were 50 mm and 66.5 mm respectively and this provided 120 individual points for the data collection. Bearing in mind the above limitation due to the particulars of the laser probe and the traversing mechanism, the blockage effect of the steel frames around the windows and usual location of the test objects at the central part of the measuring section played an important role in the selection of the grid at the above specified location.

As sketched in Figure 2.2 and shown in Figure II.6 of Appendix II, the traversing mechanism holding the laser probe was mounted to a bench and the probe scanned the grid area through the window at the bottom over a period of 20 sec. The data rate was varied between 50 and 6000 Hz depending on the positions of grid. The minimum distance between the bottom window and the laser probe was 25 mm where the laser

beams reached the maximum distance of 600 mm in the vertical direction. The blue beams of the laser in the axial plane gave the axial component of velocity, u, and green beams in the transverse plane gave the transverse component of velocity, v.

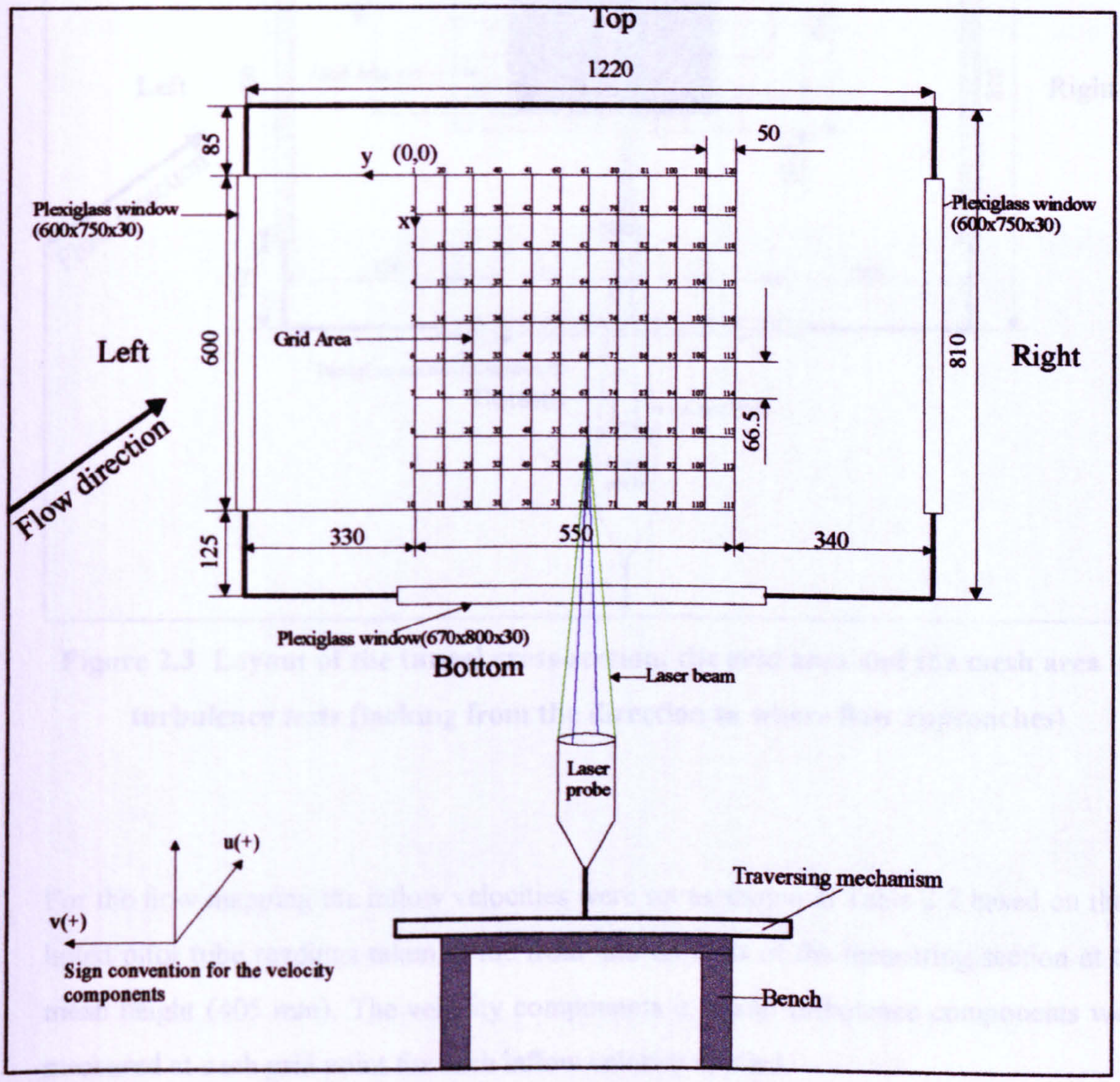

Figure 2.2 Layout of the tunnel cross-section and the grid area (looking from the direction to where flow approaches)

The measurement (grid) area for the background flow measurements in the presence of the base frame and wire meshes was reduced to 550 mm by 400 mm to save time spent in the experiments, as shown in Figure 2.3. The mesh area is also illustrated in Figure 2.3.

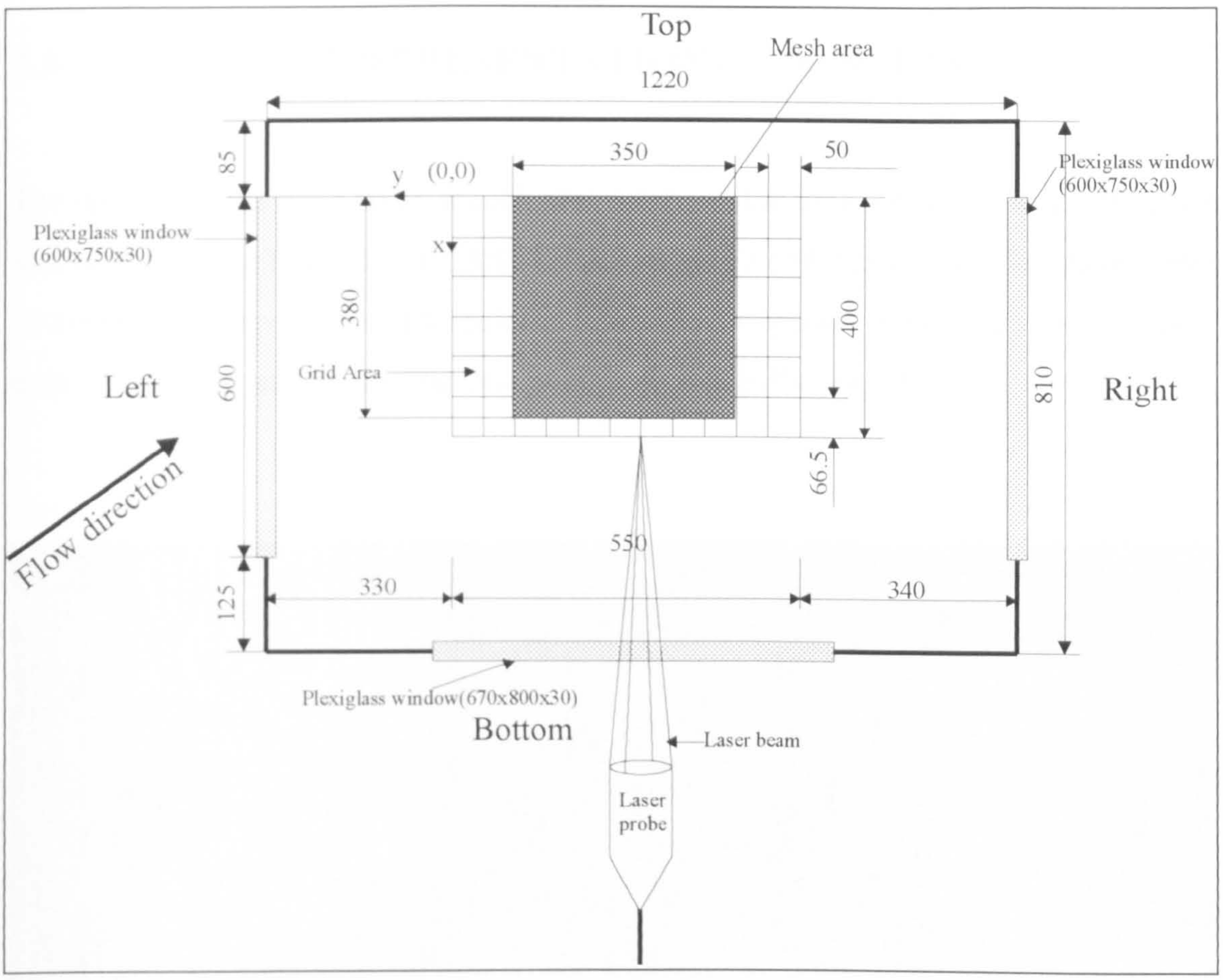

Figure 2.3 Layout of the tunnel cross-section, the grid area and the mesh area in turbulence tests (looking from the direction to where flow approaches)

For the flow mapping the inflow velocities were set as shown in Table 2.2 based on the 2 holed pitot tube readings taken at the front and aft ends of the measuring section at the mean height (405 mm). The velocity components u, v and turbulence components were measured at each grid point for each inflow velocity applied.

2.3 ANALYSIS AND PRESENTATION OF RESULTS

The measurements were taken at each grid point and the time history of data was further analysed by using DANTEC BURSTWARE software (1996) to obtain the mean values of the velocities and levels of turbulence intensities. A typical time history of a validated data, i.e. velocity at a measuring data point is shown in Figure 2.4.

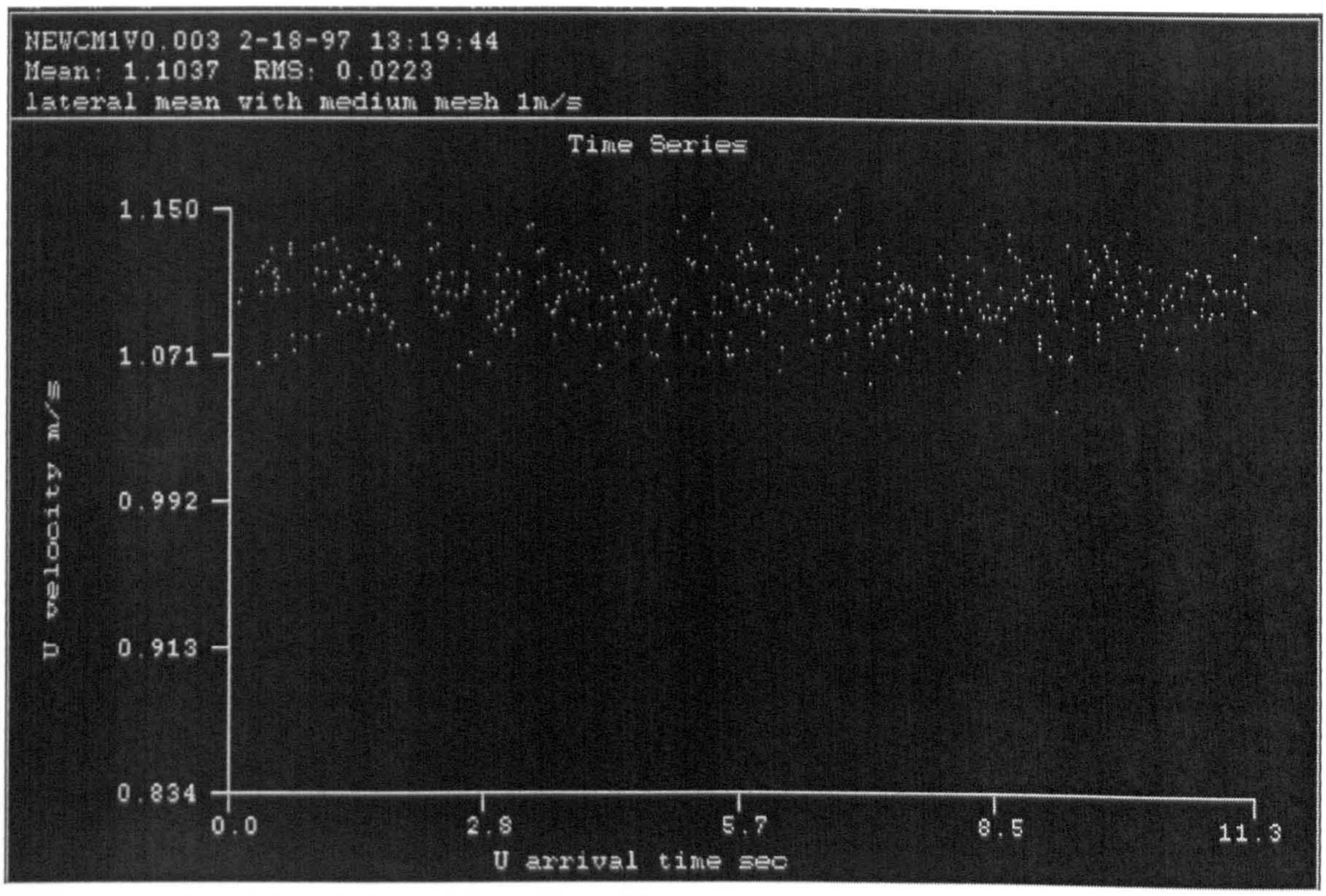

Figure 2.4 Time history of a validated data at a measuring point.

The analysed results of the inflow velocity characteristics in the presence of no base frame and wire mesh in the tunnel are presented in the following categories:

- Plots of distributions and contours of the inflow velocity components, u and v in Figures 2.5 through 2.8
- Plots of the mean deviations in Figures 2.9 through 2.12

- Plots of the mean turbulence intensities in Figure 2.13 through 2.16

While the plots of turbulence intensities are presented in those categories:

- Contour plots of u components of turbulence intensity in Figures 2.17 through 2.21
- Contour plots of v components of turbulence intensity in Figures 2.22 through 2.26.
- Plots of comparisons of turbulence intensities and integral length scale in Figures 2.27 through 2.30

In these figures, when there was no frame and wire mesh the analysis and calculations were performed at the earlier specified grid area. However, when the base fame and meshes were present the measurements and analysis were performed at the mesh area specified. The following legends are also used:

u_{mlda} denotes the mean value of the axial component of the velocity, u_{ldai}, measured, which is defined as:

$$u_{mlda} = \frac{\sum_{i=1}^{N} u_{ldai}}{N} \tag{2.1}$$

where:

- N is the number of the grid points.

v_{mlda} denotes the mean value of the transverse component of the velocity, v_{ldai}, measured, which is defined as:

$$v_{mlda} = \frac{\sum_{i=1}^{N} v_{ldai}}{N} \tag{2.2}$$

$\Delta u(\%)$ represents the variation of the axial mean velocity deviation in percentage with U_{pitot}, where Δu is defined as:

$$\Delta u(\%) = \left[\frac{u_{lda} - U_{pitot}}{U_{pitot}}\right]100 \tag{2.3}$$

The axial component of the turbulence intensity, TI_u is defined as:

$$TI_u(\%) = \frac{u_f'}{\overline{U}}100 = \frac{\sqrt{\overline{u_f^2}}}{\overline{U}}100 \tag{2.4}$$

where:

- u_f' is the root-mean-square of the fluctuations of u component at the measuring point
- $\overline{U}$ is the mean velocity at that point which is equal to u_{lda}.

The transverse component of the turbulence intensity, TI_v is defined as:

$$TI_v(\%) = \frac{v_f'}{\overline{U}}100 = \frac{\sqrt{\overline{v_f^2}}}{\overline{U}}100 \tag{2.5}$$

where:

- v_f' is the root-mean-square of the fluctuations of v component at the measuring point.

Figure 2.13 shows the variation of the tunnel axial velocity, U_{pitot}, measured at the centreline of the tunnel with the mean value of axial components of turbulence intensity, TI_u, measured at the grid area, which is defined as:

$$TI_{um}(\%) = \frac{\sum_{i=1}^{N} TI_{ui}}{N}100 \tag{2.6}$$

Figure 2.14 shows the variation of the tunnel axial velocity, U_{pitot}, with the mean values of transverse components of turbulence intensity, TI_v, measured at the grid area, which is defined as:

$$TI_{vm}(\%) = \frac{\sum_{i=1}^{N} TI_{vi}}{N} 100 \tag{2.7}$$

The mean value of the resultant turbulence intensities, TI_{rm}, is defined as:

$$TI_{rm}(\%) = \left(\sqrt{TI_{um}^2 + TI_{vm}^2}\right) 100 \tag{2.8}$$

By definition the integral length scale, Λ_g, is a measure of the longest connection, or correlation distance, between fluctuation velocities at two points of the flow field. This parameter, which is a function of the turbulence intensity, characterises the large eddy structure of the turbulence and can be defined as (Hinze, 1975):

$$\Lambda_g = \int_0^\infty g(y)dy \tag{2.9}$$

where:

- g is the lateral velocity correlation of fluctuations in the transverse direction, y, and is defined for isotropic turbulence as:

$$g(y) = \frac{\overline{u_f(y_1)u_f(y_2)}}{u_f'^2} \tag{2.10}$$

where:

- over bar denotes the mean value of the product of fluctuations
- y_1 and y_2 are two points in the transverse direction.

Since integral length scale of the flow characterises the eddy structure of the turbulence, which is going to be used in the theoretical analysis in Chapter 6, the mean value of the integral length scale, Λ_g, in the mesh area is defined as:

$$\Lambda_g = \int_a^b g(y)dy \tag{2.11}$$

where:

- a and b are the end positions of the mesh area in the transverse direction.

On the other hand, in order to represent each wire mesh, in terms of their sizes, net mesh area ratio is defined as:

$$NMAR = \frac{A_{net}}{A_{fm}} \tag{2.12}$$

where:

- A_{net} is the net area after subtracting the area covering mesh thickness and length from the full mesh area
- A_{fm} is the full mesh area in the case of without anything in the tunnel such that $350x380 = 133000\ mm^2$.

The ratio of net mesh area for each case is given in Table 2.4.

Table 2.4 Net mesh area ratio

Turbulence generator type	Net mesh area
Base frame	0.945
Largest-sized mesh	0.866
Medium-sized mesh	0.832
Finest-sized mesh	0.748

The variance and standard deviation ranges for the components of the velocity at the grid points are given in Table 2.5 for the axial velocity of 4m/s. The variance of the u component, m_{0u}, and the variance of the v component, m_{0v}, at each grid point are defined as:

$$m_{0u} = \frac{\sum_{i=1}^{n}\left(u_{ldai} - \bar{u}\right)^2}{n} \quad \text{and} \quad m_{0v} = \frac{\sum_{i=1}^{n}\left(v_{ldai} - \bar{v}\right)^2}{n} \tag{2.13}$$

where:

- n is the number of validated data at each grid point
- and $\bar{u}$ and $\bar{v}$ are the mean values of the velocity components at each grid point.

While the standard deviations of the u component, s_u, and the v component, s_v, in percentage are defined as:

$$s_u(\%) = \frac{m_{0u}^{1/2}}{\bar{u}}100 \quad \text{and} \quad s_v(\%) = \frac{m_{0v}^{1/2}}{\bar{v}}100 \tag{2.14}$$

Table 2.5 Variance and standard deviation ranges of velocity components at U_{pitot}=4m/s

Turbulence generator type	Range of m_{0u} $(m/s)^2$	Range of m_{0v} $(m/s)^2$	Range of s_u (%)	Range of s_v (%)
Base frame	0.00308-0.0199	0.00352-0.1267	1.309-3.487	1.400-7.980
Largest-sized mesh	0.00297-0.0216	0.00436-0.1978	1.273-3.729	1.538-9.935
Medium-sized mesh	0.00314-0.0222	0.00316-0.0410	1.293-4.221	1.296-4.494
Finest-sized mesh	0.00286-0.0331	0.00381-0.1837	1.224-4.609	1.420-9.464

Sign convention for the co-ordinates of the grid and mesh points and the velocity components, u and v, are shown in Figure 2.2.

In the figures, all the axes are given in mm while the axial velocity component, u, and the transverse velocity component, v, are given in m/s. The axial component of turbulence intensity, TI_u, and the transverse component of turbulence intensity, TI_v, are given as non-dimensional in percentage.

2.4 DISCUSSION OF RESULTS

As stated in Section 2.2, to establish the flow map of the tunnel, the measurements were taken over a range of the tunnel inflow velocity varying 1-7 m/s. In the presentation of results, a typical inflow velocity of 4 m/s is used. However, entire presentation of the flow can be found in (Atlar and Korkut, 1997) and (Korkut, 1997a).

Figures 2.5 through 2.8 show the distributions and contour plots of the axial, u, and transverse, v, components of the tunnel inflow velocity at U_{pitot} = 4 m/s when there was no base frame and wire mesh present in the tunnel.

It can be seen in these figures that the distribution of the axial velocity component, u, has more even distribution over the cross-section area compared to the transverse velocity component, v. However, there is an increase in the magnitude of the u component from the bottom of the tunnel to the top, indicating a vertical cross-flow, while the v component increases from the right of the tunnel to the left side, also indicating a lateral cross-flow. Therefore, the flow in the tunnel is not perfect in terms of its uniformity, as one would expect.

In Figures 2.9 through 2.12, the mean deviations of the velocity components from the tunnel speed, U_{pitot}, in the presence of no base frame and wire mesh are shown.

The axial mean laser based component, u_{mlda}, coincides well with the tunnel speed measured by the pitot tubes, U_{pitot}, shown in Figure 2.9. At the maximum tunnel velocity, u_{mlda} can be 3% less than the U_{pitot}, indicating a very good correlation with the results obtained from the tunnel's existing pitot measurement facility.

The mean deviations of the axial component, Δu, from U_{pitot}, shown in Figure 2.11, vary between 1.25% and -3% of the tunnel speed, displaying small discrepancies in the low velocities and high discrepancies in the high velocities. The deviation of the transverse velocities, shown in Figures 2.10 and 2.11, also indicated a very slight cross-flow across the tunnel reaching to a maximum value of about 2.25% of the axial velocity

component. Therefore, bearing in mind the accuracy of the pitot tube measurements, the current flow correctors (i.e. guide vanes and honeycomb at the contraction section of the tunnel) appear to be effective although the flow is not perfect.

Figures 2.13 through 2.16 show the variations of the mean axial, u, transverse, v, and resultant turbulence intensities in the presence of no base frame and wire mesh.

The mean u component of the turbulence intensity, TI_{um}, across the grid area fluctuates about the magnitude of 1.75% of the axial velocity component, as shown in Figure 2.13, while the mean v component, TI_{vm}, demonstrates a more steady behaviour as the tunnel speed is increased to high values, as shown in Figure 2.14. One can see in Figure 2.15 that the resultant turbulence intensities, TI_{rm}, across the grid area display nearly constant level of turbulence as the tunnel speed is increased, indicating the mean level of the turbulence in the tunnel is about 2.75%. It can be seen in Figure 2.16 that the magnitude of the v component, TI_{vm}, is slightly higher than the magnitude of u component, TI_{um}, displaying that the tunnel has a considerable cross-flow turbulence characteristic, which makes the transverse components of the turbulence intensity dominant in the tunnel.

As far as the effects of the base frame and wire mesh on the levels of the components of the turbulence intensities are concerned, Figures 2.17 through 2.21 show the contour plots of u component of turbulence intensity for the tunnel speed of 4 m/s.

It can be seen in the figures that as soon as the base frame and wire mesh are introduced the magnitudes of u component of the turbulence intensities increase in the positions of the base frame and wire meshes. It is also observed that there are always some peaks at the position of the base frame, and this position including the mesh area can easily be determined from these figures. On the other hand, the vertical cross-flow observed in the presence of no base frame and wire mesh is disturbed by the base frame and wire meshes. Therefore, both meshes and the base frame influence the characteristics of the u component of the turbulence in the mesh area, indicating an increase in the level of the u component of the turbulence.

For the v components of the turbulence intensities shown in Figures 2.22 through 2.26, as one moves away from the centre part of the grid area to the left and right extremes the magnitude of v component increases and reaches its highest values at the top. The positions of the base frame and the mesh area are not as much as clear as those in the u components. The magnitudes of v component of the turbulence intensity are usually higher compared to the magnitudes of u component of turbulence intensity. Therefore, the v component of the turbulence contributes to the level of resultant turbulence as well as the u component of the turbulence.

Figures 2.27 through 2.30 show the effects of the wire meshes on the level of the turbulence based on the net mesh area. If one investigates the behaviour of the individual component of the turbulence intensities, TI_{um} and TI_{vm}, the trend between the net mesh area and turbulence intensity appears to be more linear for the u component than the trend for the v component. It is also apparent that the magnitude of the level of the turbulence intensity for the u component is smaller than that of the v component. This also affects the mean resultant turbulence level, as shown in Figure 2.29. If one fits a linear line in the experimental results it can be seen that the v component of the turbulence intensity has also larger deviations from the fitted line compared to the u component of the turbulence intensity. Therefore, the cross-flow existing in the tunnel combined with the effect of meshes influences the v component significantly and the transverse component of turbulence cannot be ignored. It is also necessary to take into account the vertical component of the turbulence intensities, w, to obtain more realistic level of the resultant turbulence intensity in the tunnel. Because of the 2-D LDA facility used in these experiments, this has been left for the future work.

Further point to note is that, although there is an abnormality in one of the mesh cases, in general, as the net mesh area ratio is decreased, which means as the mesh size getting smaller, the level of turbulence increases, displaying the effectiveness of the wire meshes to create different levels of the turbulence intensity. This trend is also observed for the mean integral length scale of the flow against the net mesh area ratio.

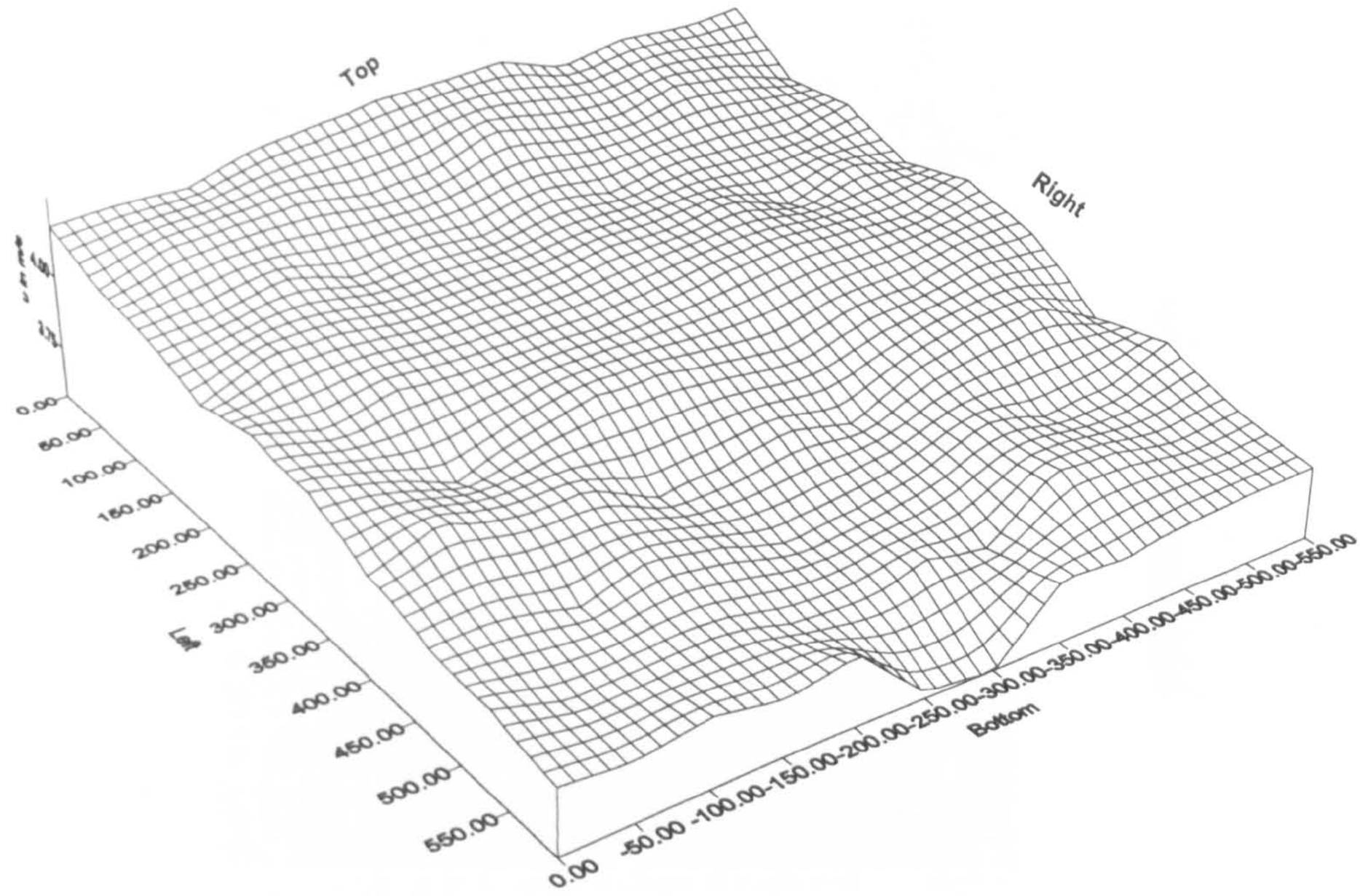

Figure 2.5 Distribution of u component of tunnel inflow velocity across grid (550x600) in the presence of no base frame and wire mesh at U_{pitot}= 4 m/s

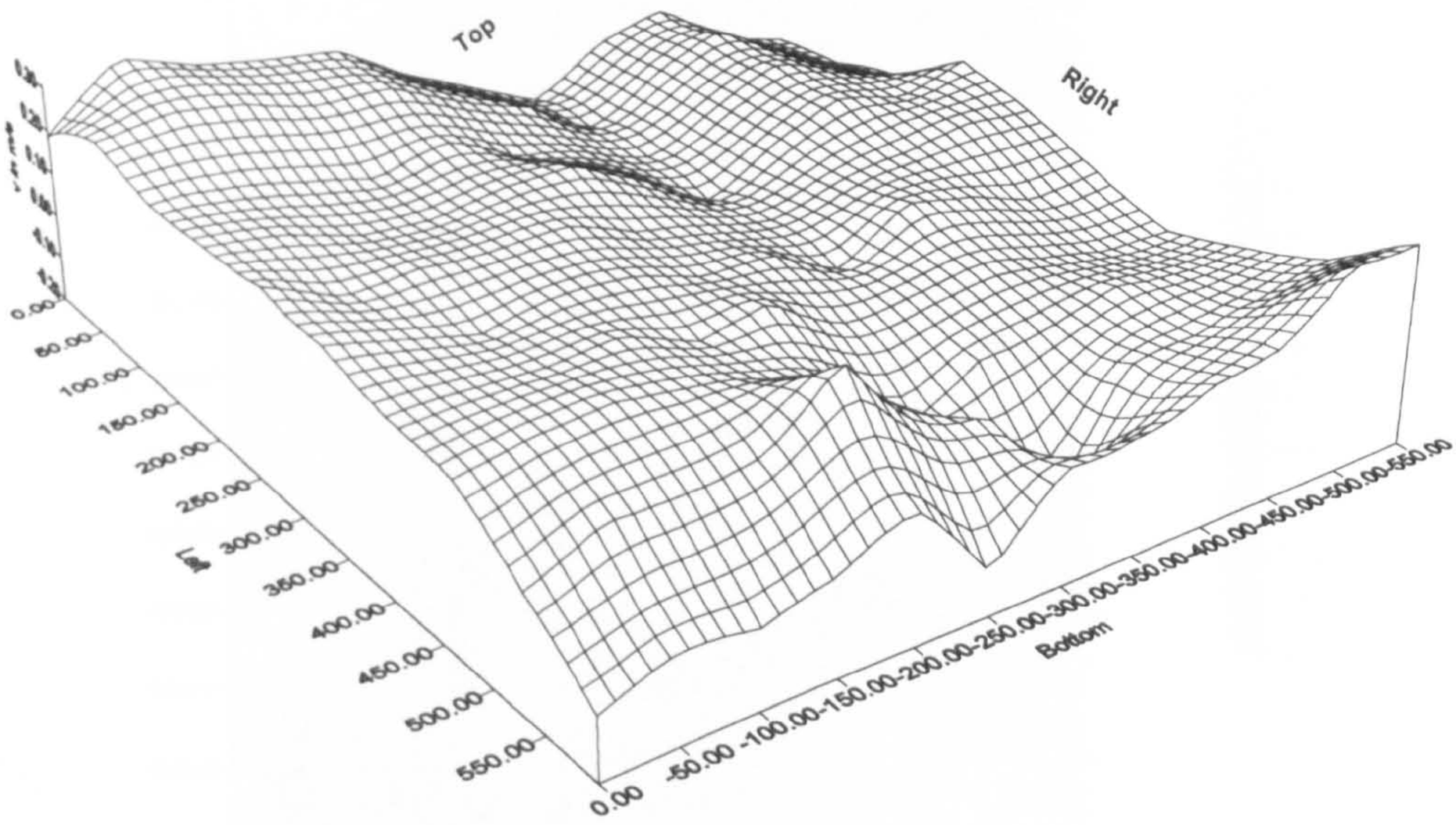

Figure 2.6 Distribution of v component of tunnel inflow velocity across grid (550x600) in the presence of no base frame and wire mesh at U_{pitot}= 4 m/s

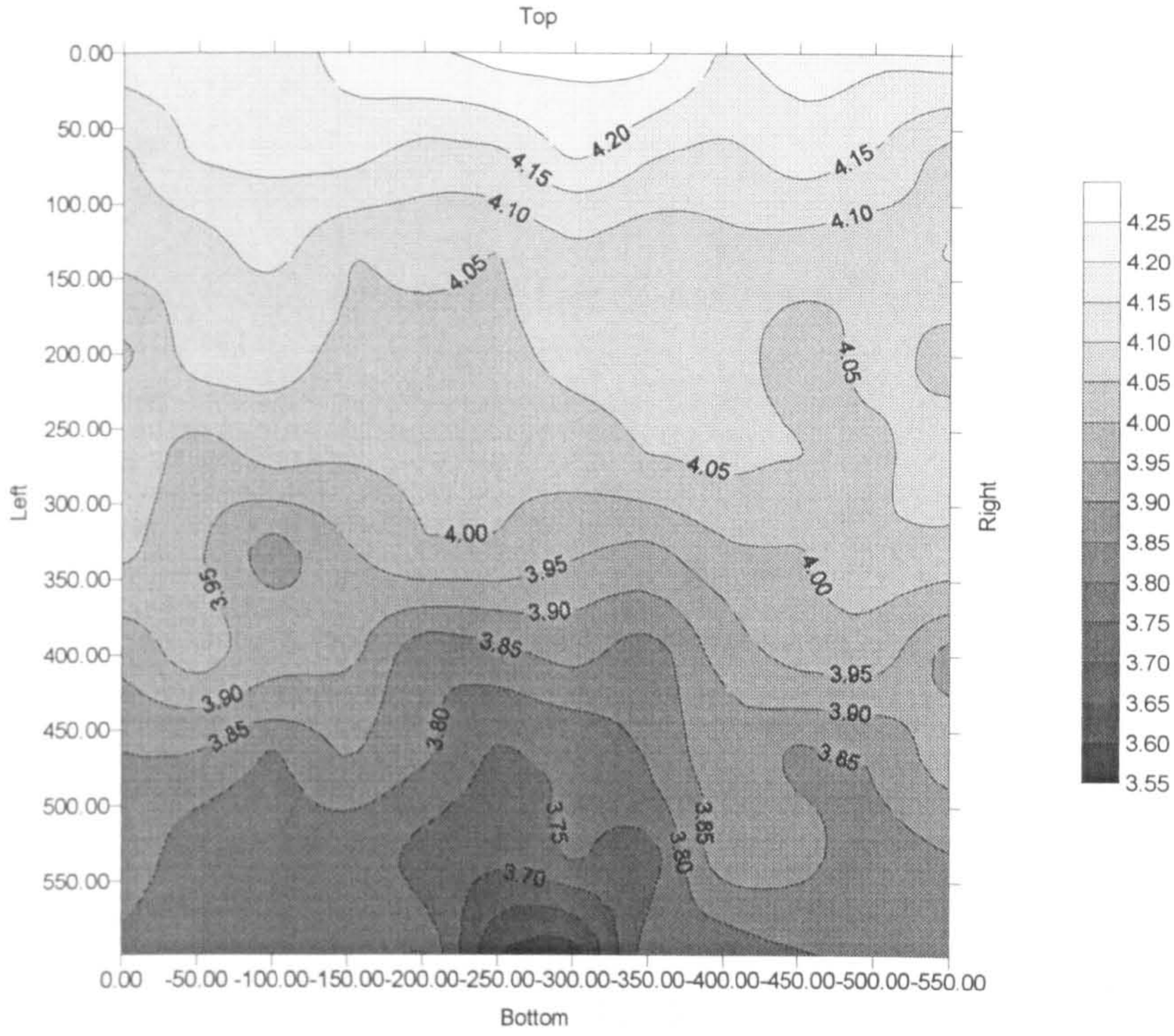

Figure 2.7 Contour plot of u component of tunnel inflow velocity across grid (550x600) in the presence of no base frame and wire mesh at U_{pitot}= 4 m/s

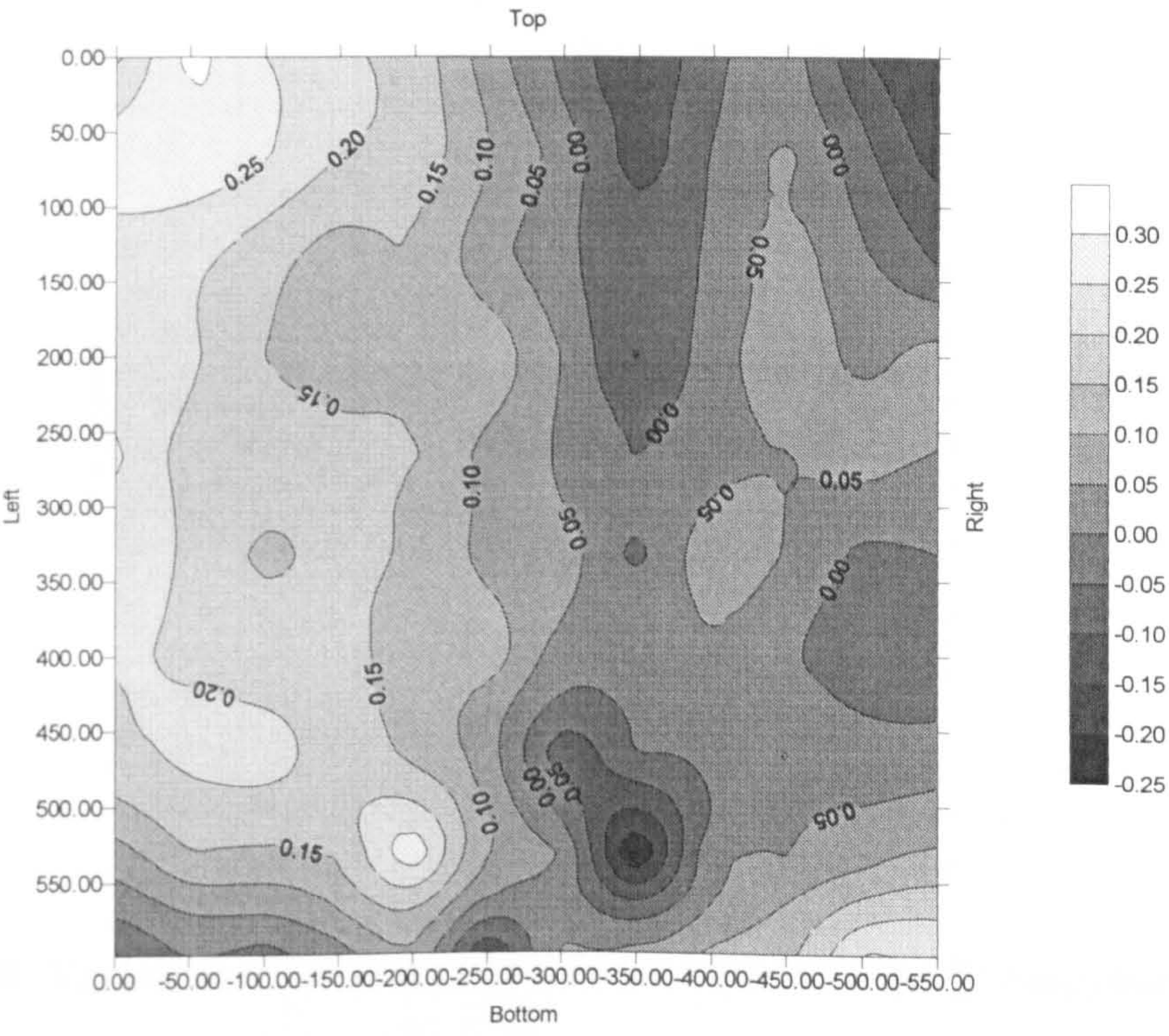

Figure 2.8 Contour plot of v component of tunnel inflow velocity across grid (550x600) in the presence of no base frame and wire mesh at U_{pitot}= 4 m/s

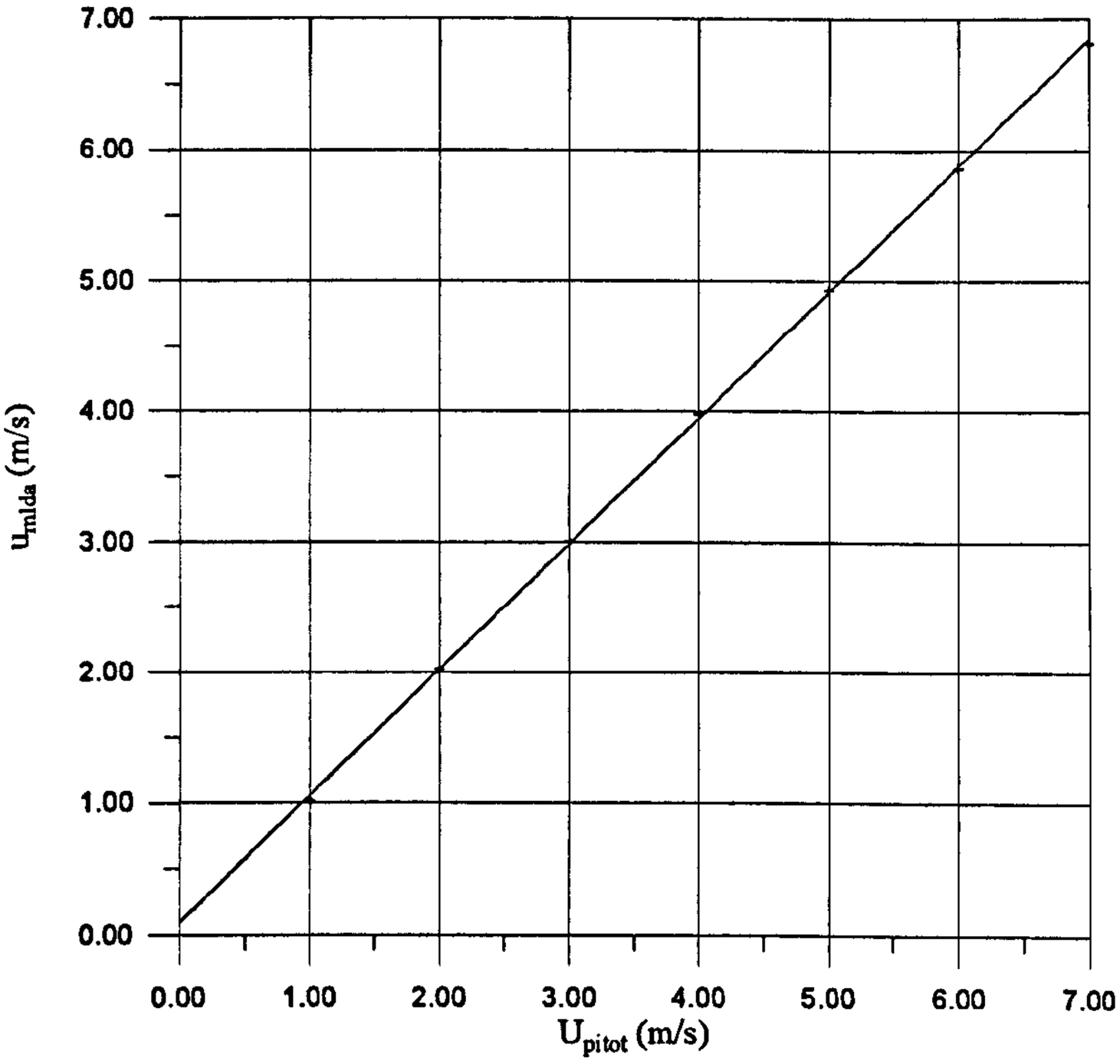

Figure 2.9 Variation of axial mean laser based velocity components, u_{mlda}, across grid (550x600) with tunnel speed, U_{pitot} in the presence of no base frame and wire mesh

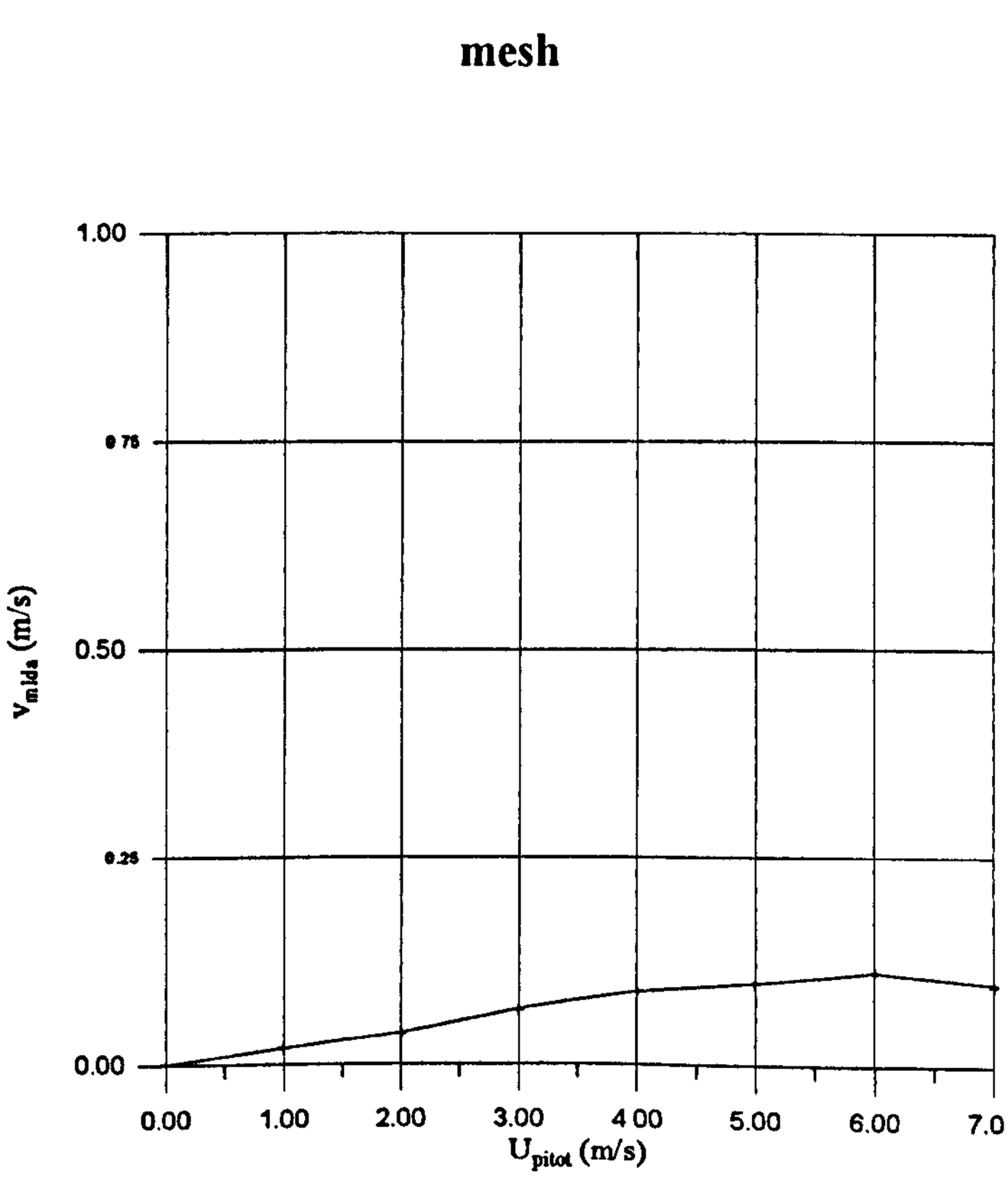

Figure 2.10 Variation of transverse mean laser based velocity components, v_{mlda}, across grid (550x600) with tunnel speed, U_{pitot}, in the presence of no base frame and wire mesh

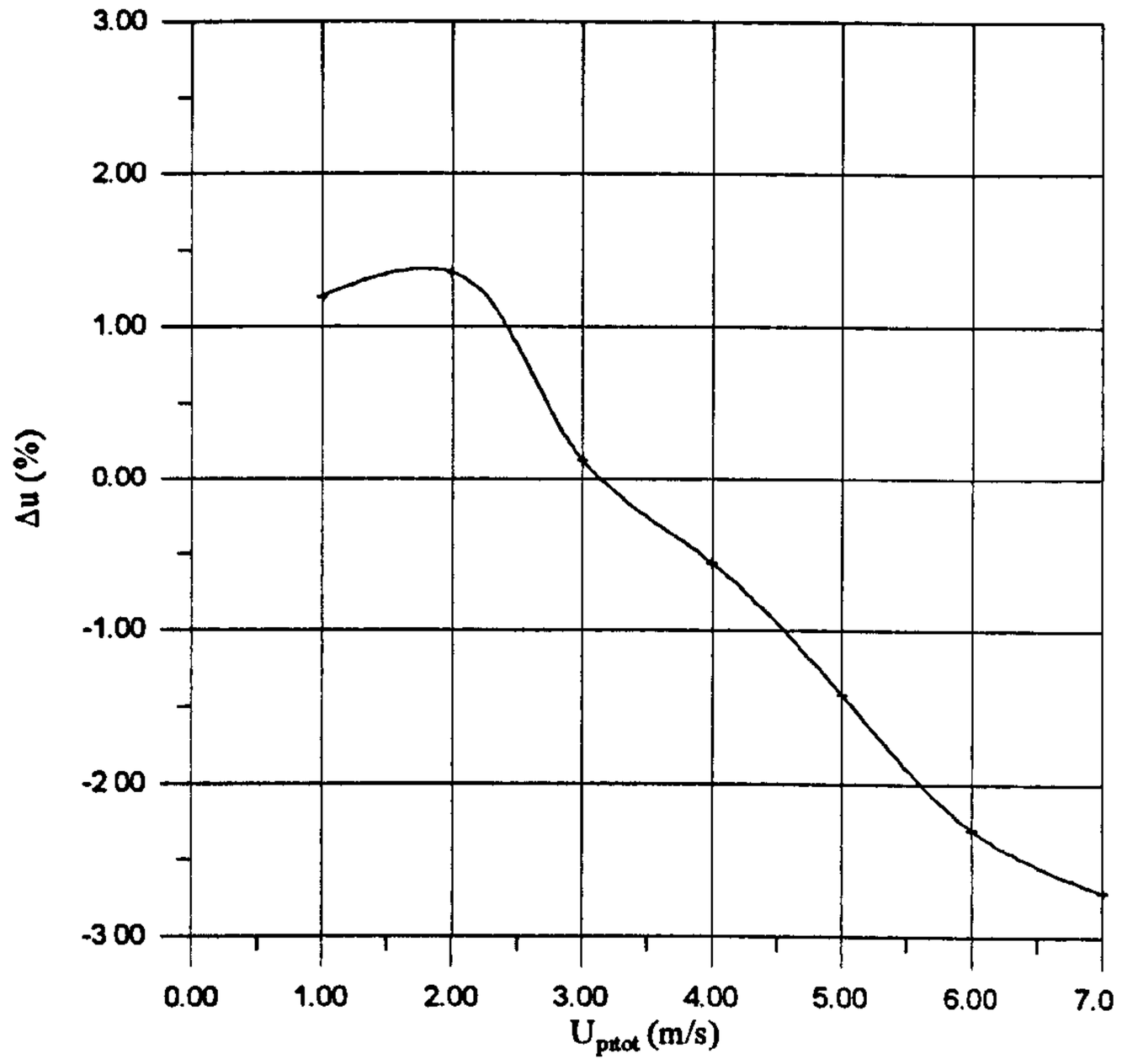

Figure 2.11 Variation of axial mean deviations, Δu, across grid (550x600) from U_{pitot}, in the presence of no base frame and wire mesh

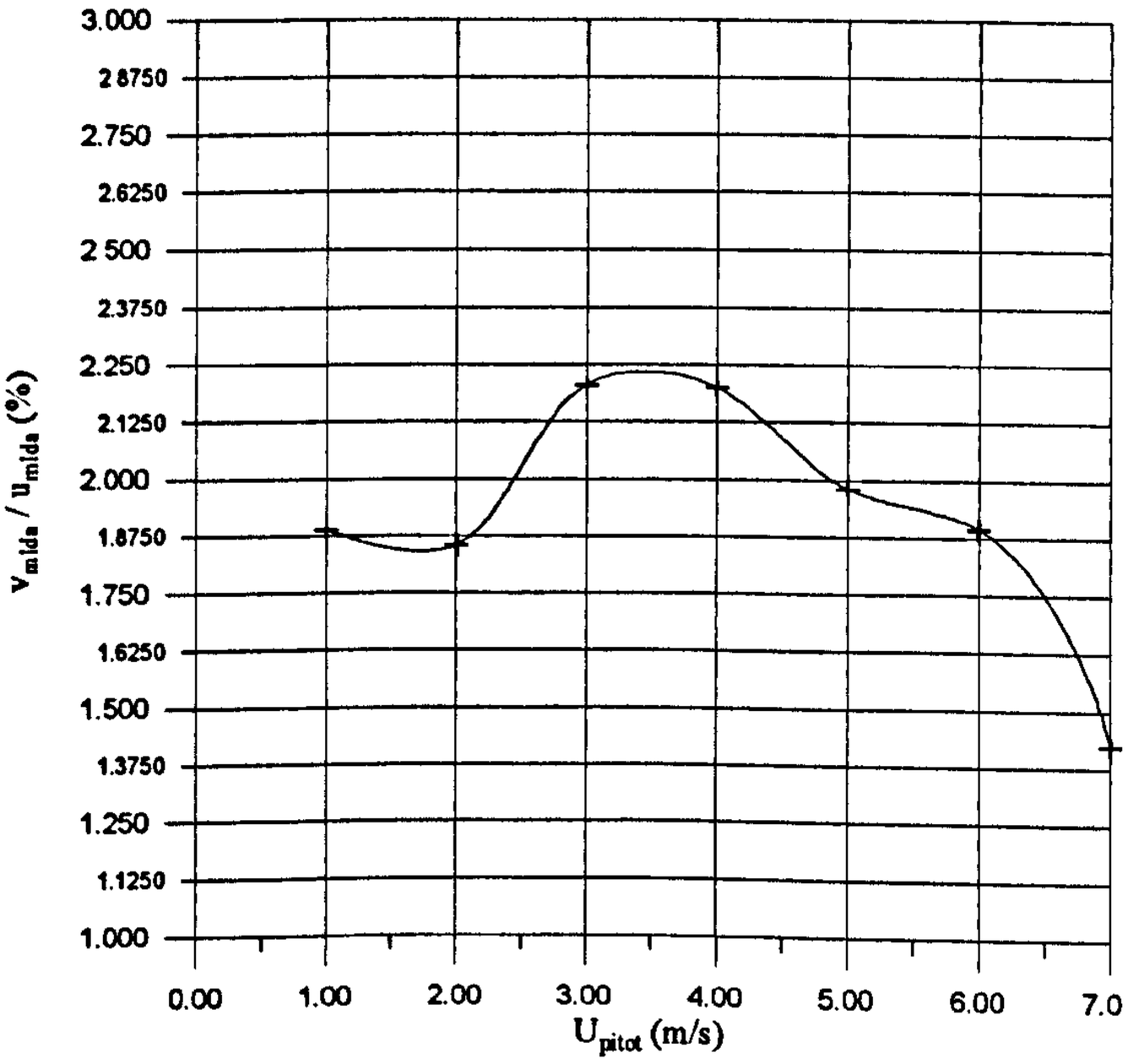

Figure 2.12 Variation of ratio of velocity components, v_{mlda}/u_{mlda}, across grid (550x600) with tunnel speed, U_{pitot}, in the presence of no base frame and wire mesh

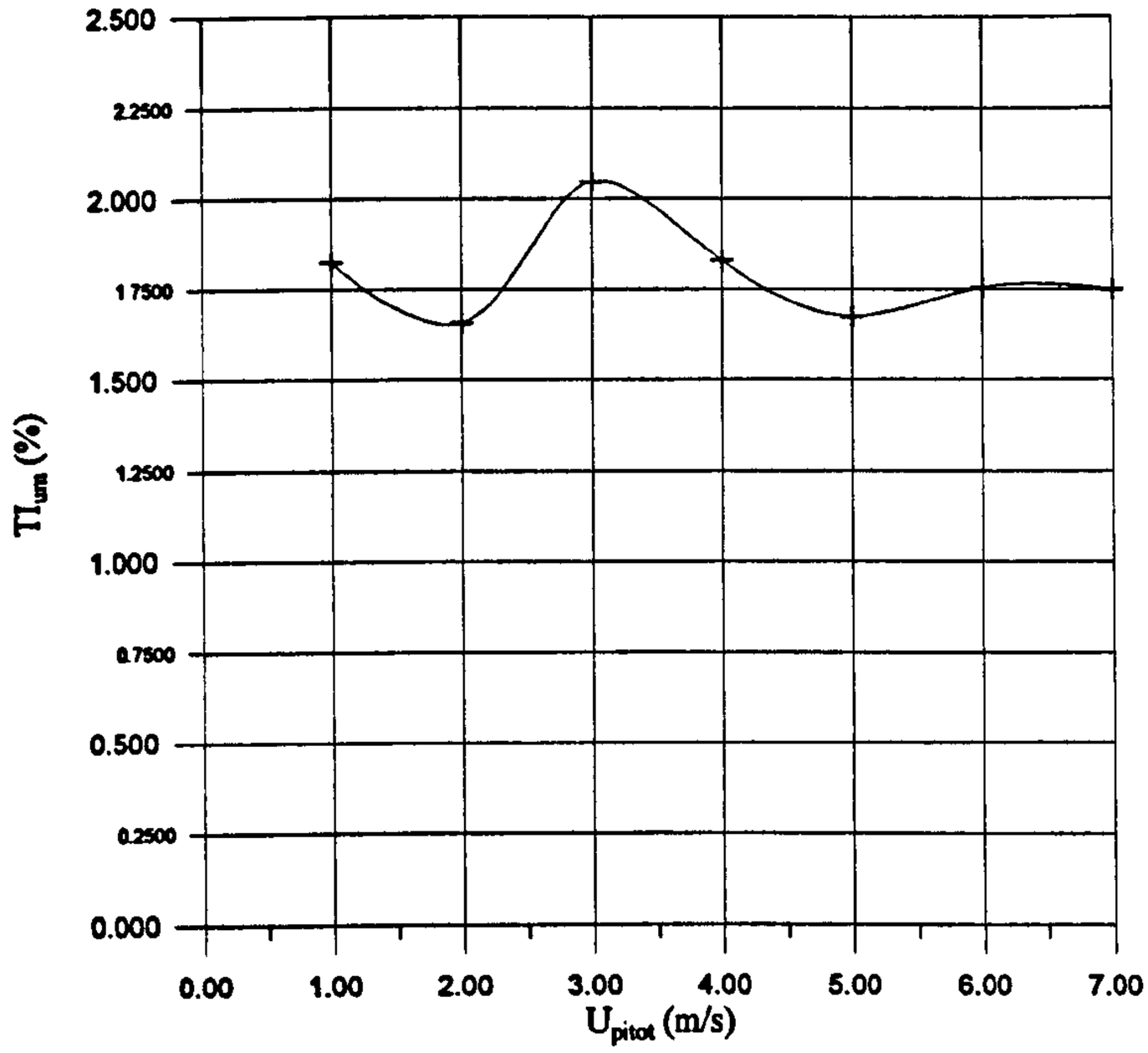

Figure 2.13 Variation of mean u component of turbulence intensity, TI_{um}, across grid (550x600) against tunnel speed, U_{pitot}, in the presence of no base frame and wire mesh

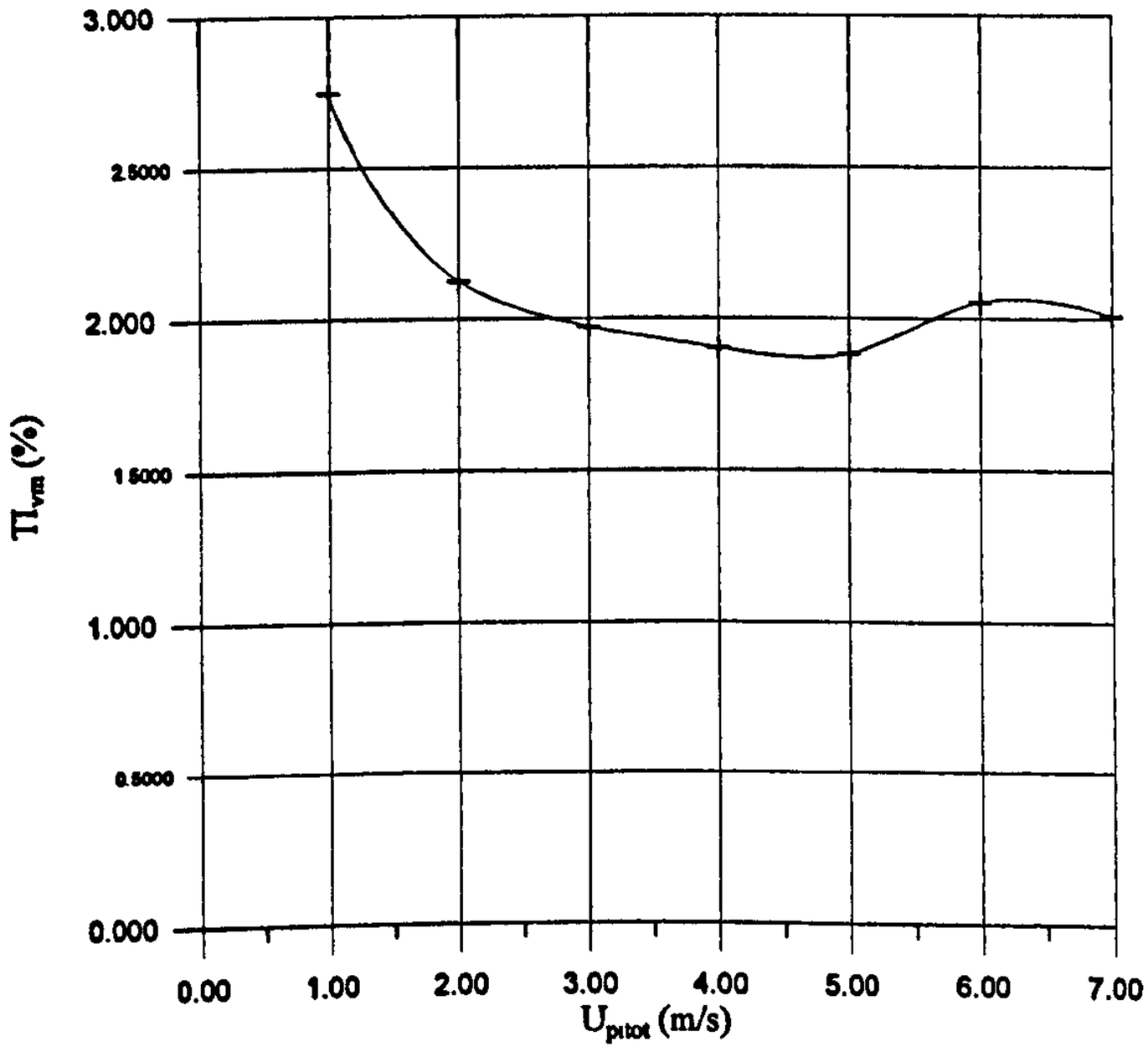

Figure 2.14 Variation of mean v component of turbulence intensity, TI_{vm}, across grid (550x600) against tunnel speed, U_{pitot}, in the presence of no base frame and wire mesh

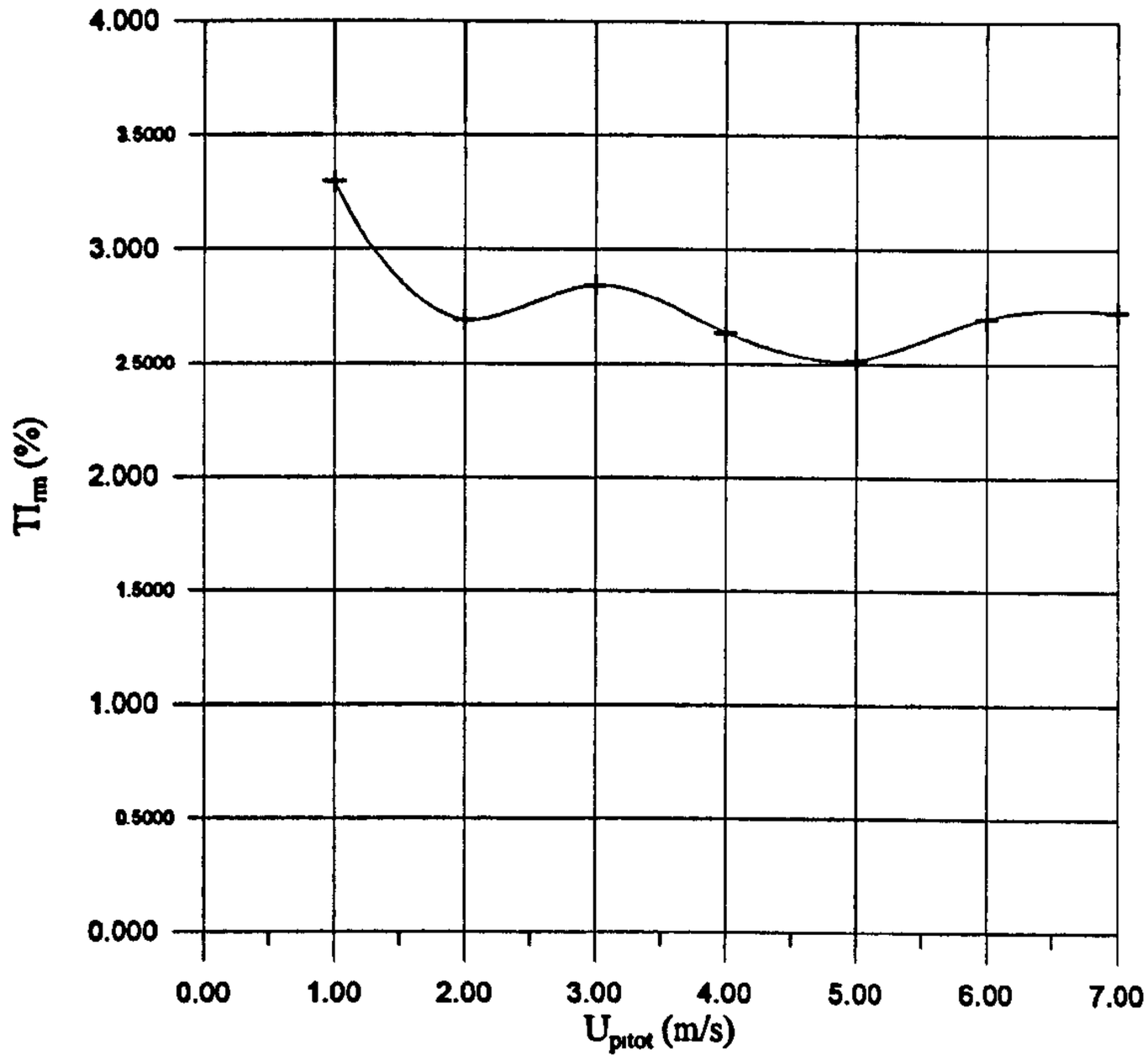

Figure 2.15 Variation of mean resultant turbulence intensities, TI_{rm}, across grid (550x600) against tunnel speed, U_{pitot}, in the presence of no base frame and wire mesh

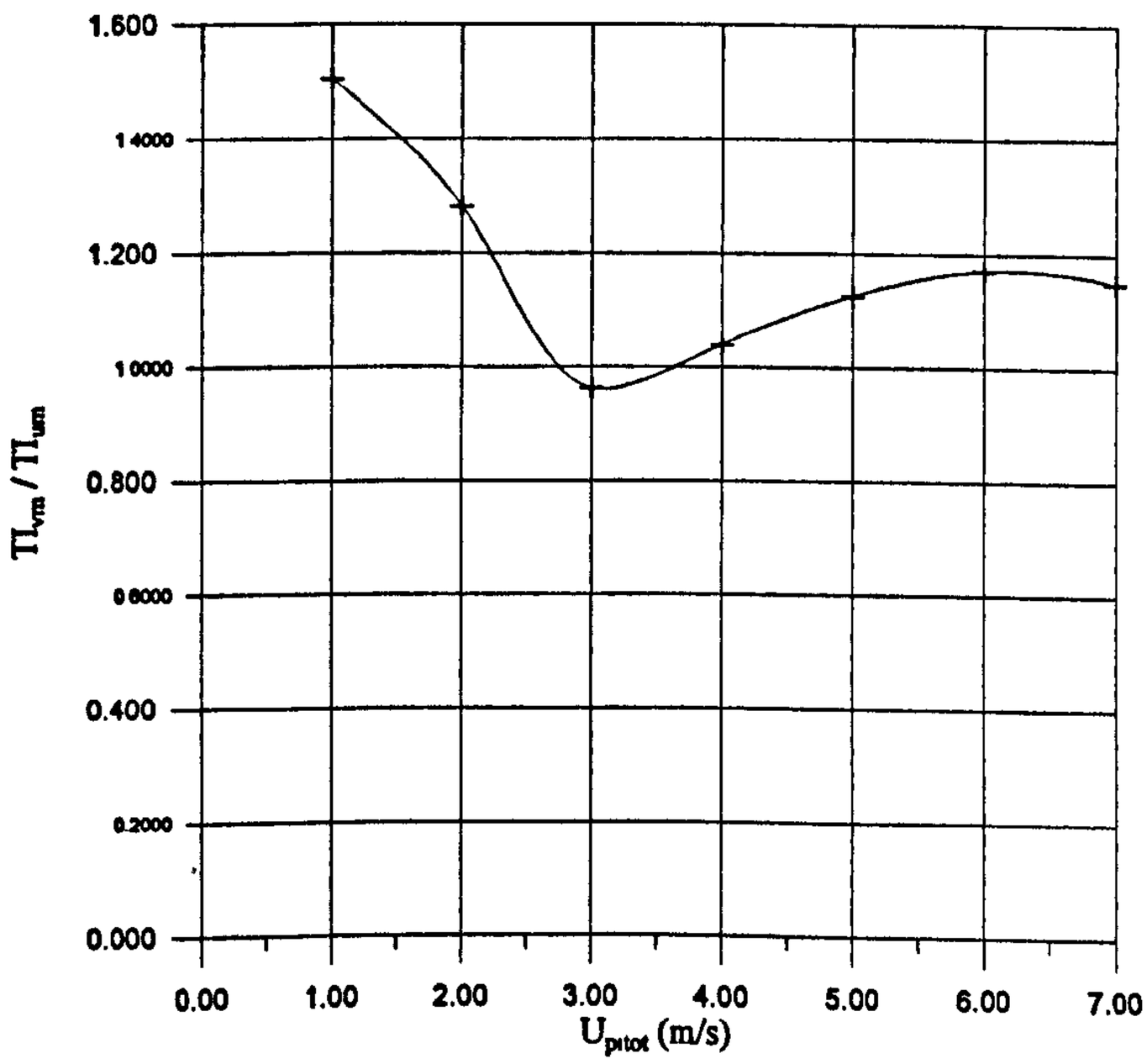

Figure 2.16 Variation of ratio of mean v component of turbulence intensity to mean u component of turbulence intensity, TI_{vm}/TI_{um}, across grid (550x600) against tunnel speed, U_{pitot}, in the presence of no base frame and wire mesh

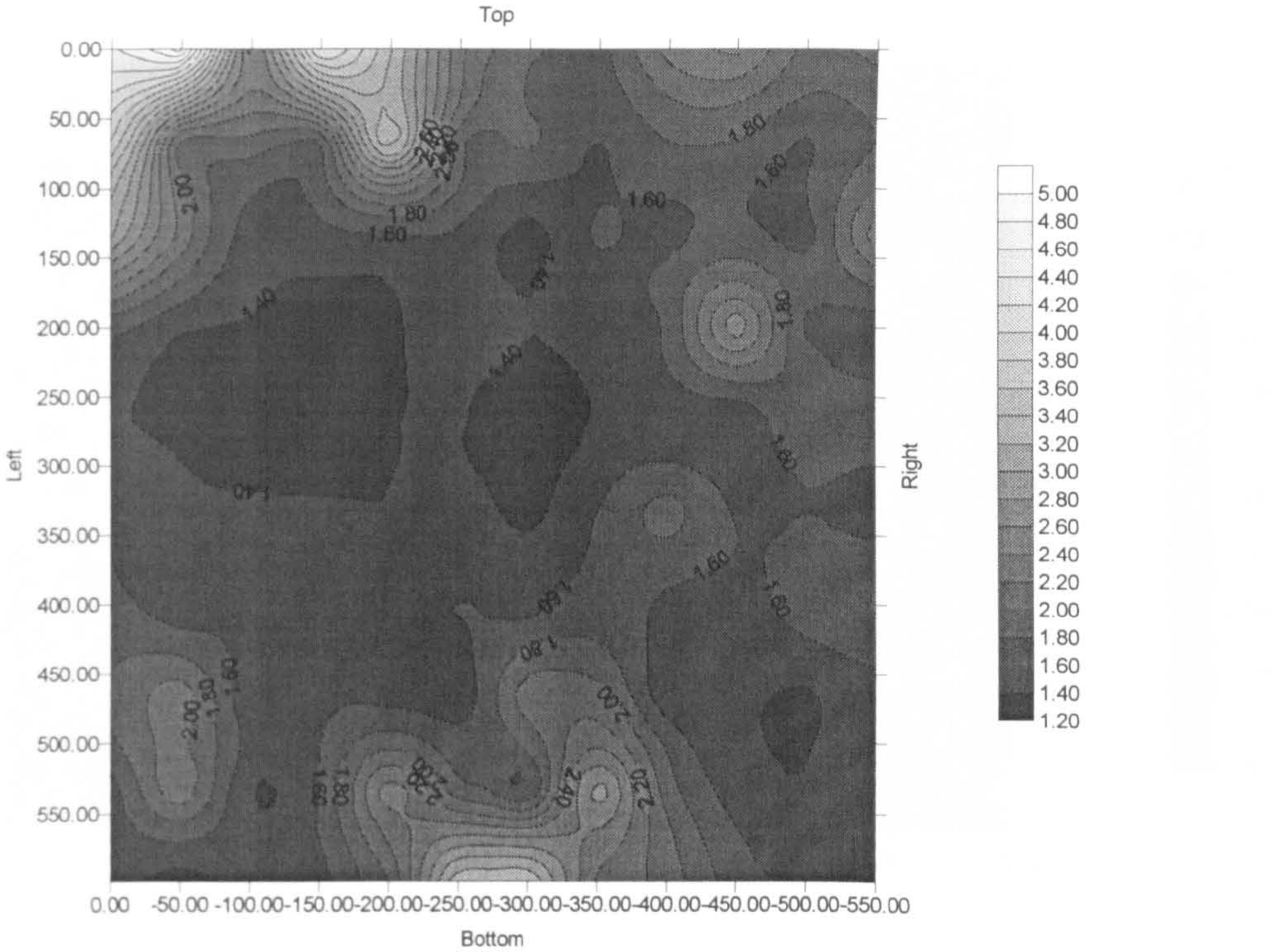

Figure 2.17 Contour plot of u component of turbulence intensity across grid (550x600) in the presence of no base frame and wire mesh in tunnel at U_{pitot}= 4 m/s

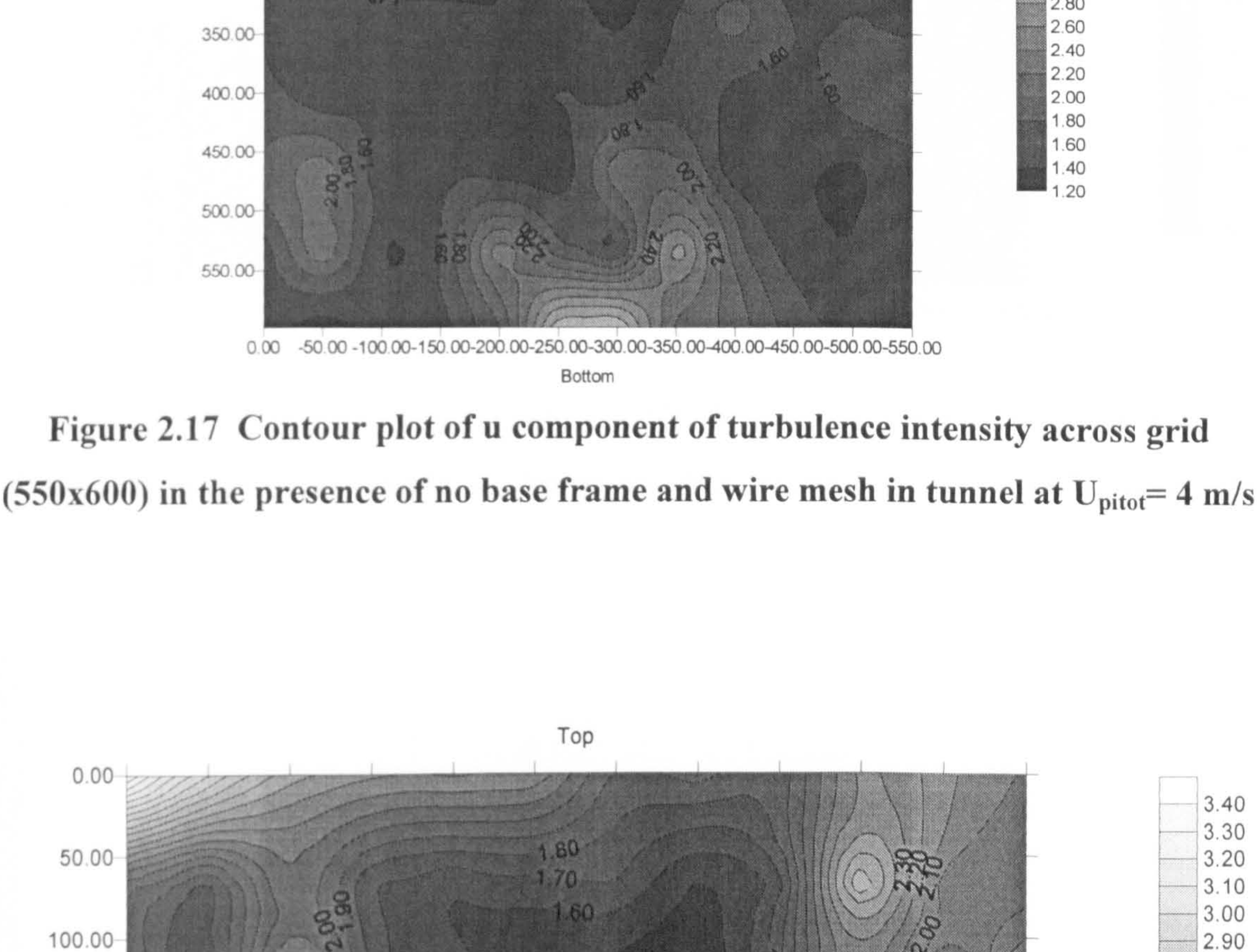

Figure 2.18 Contour plot of u component of turbulence intensity across grid (550x400) in the presence of base frame only in tunnel at U_{pitot}= 4 m/s

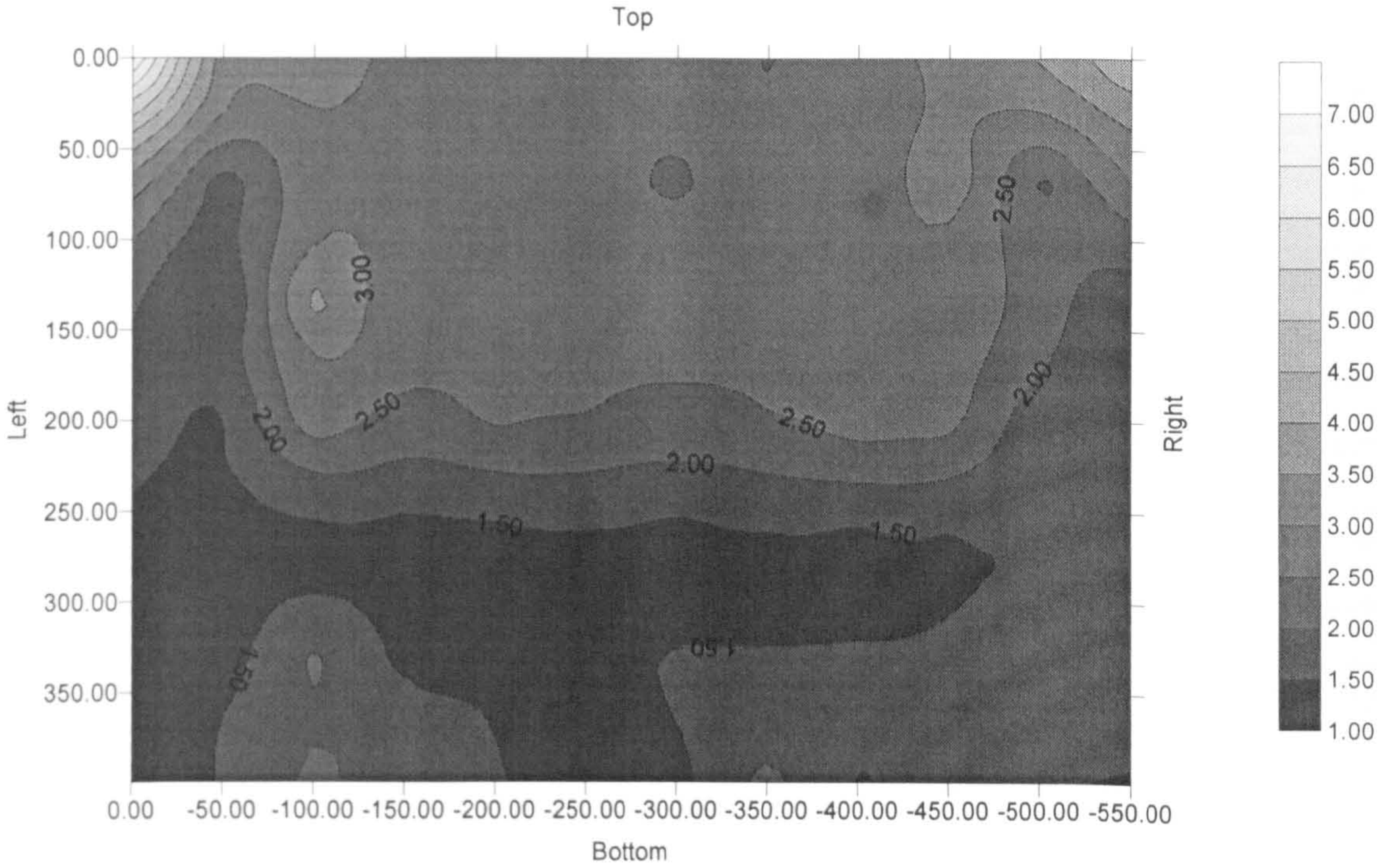

Figure 2.19 Contour plot of u component of turbulence intensity across grid (550x400) in the presence of base frame and largest mesh in tunnel at U_{pitot}= 4 m/s

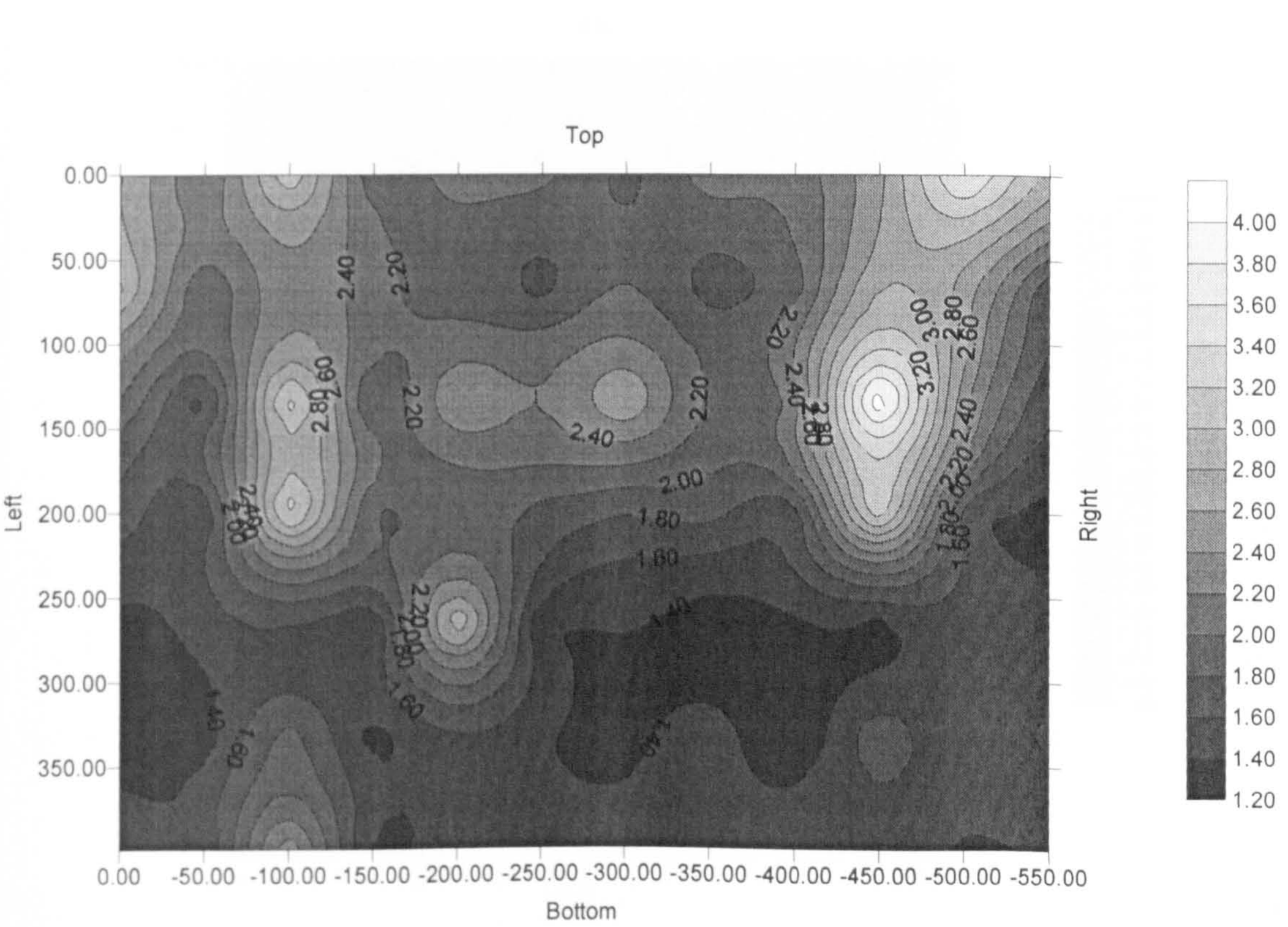

Figure 2.20 Contour plot of u component of turbulence intensity across grid (550x400) in the presence of base frame and medium mesh in tunnel at U_{pitot}= 4 m/s

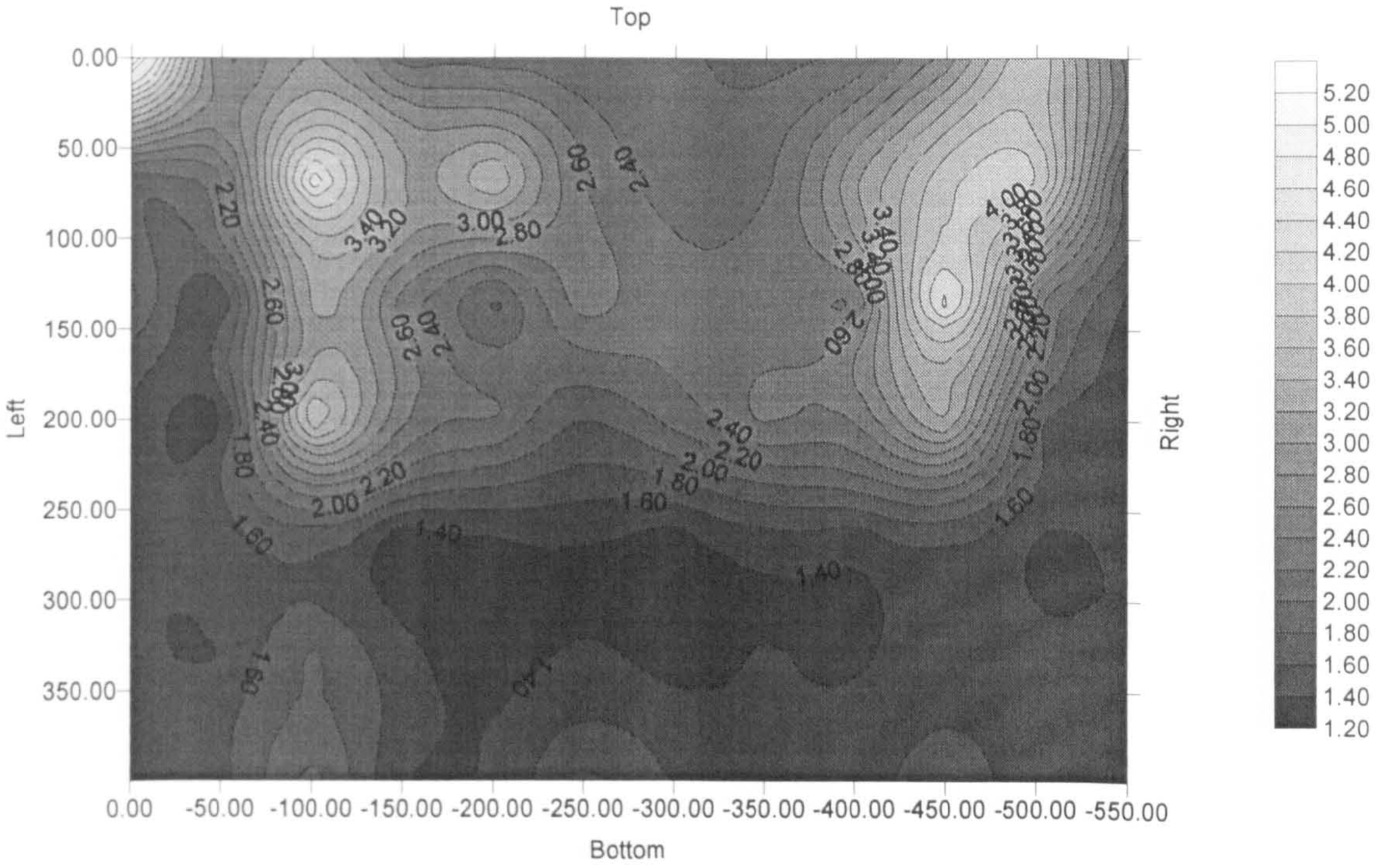

Figure 2.21 Contour plot of u component of turbulence intensity across grid (550x400) in the presence of base frame and finest mesh in tunnel at U_{pitot}= 4 m/s

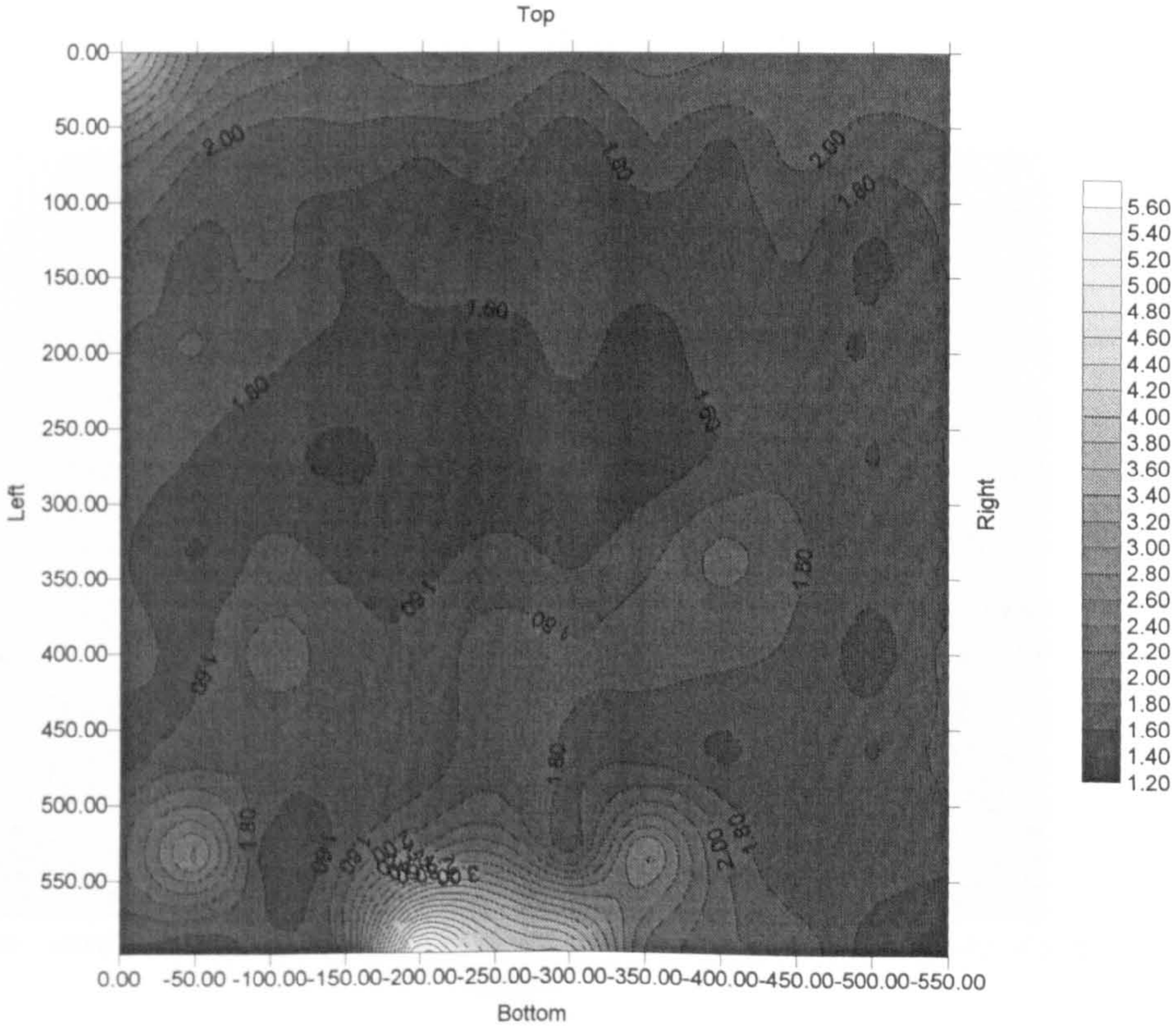

Figure 2.22 Contour plot of v component of turbulence intensity across grid (550x600) in the presence of no base frame and wire mesh in tunnel at U_{pitot}= 4 m/s

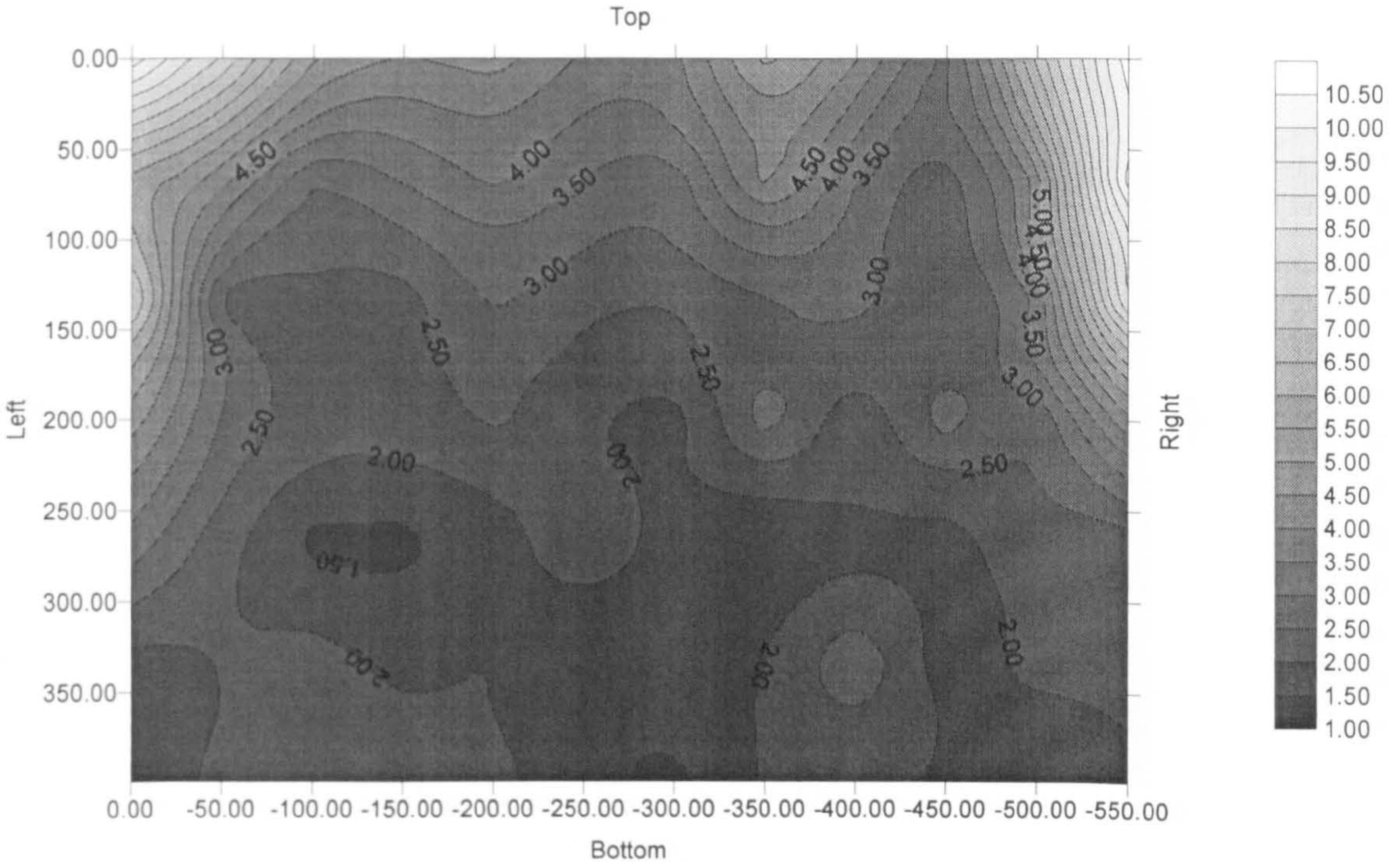

Figure 2.23 Contour plot of v component of turbulence intensity across grid (550x400) in the presence of base frame only in tunnel at U_{pitot}= 4 m/s

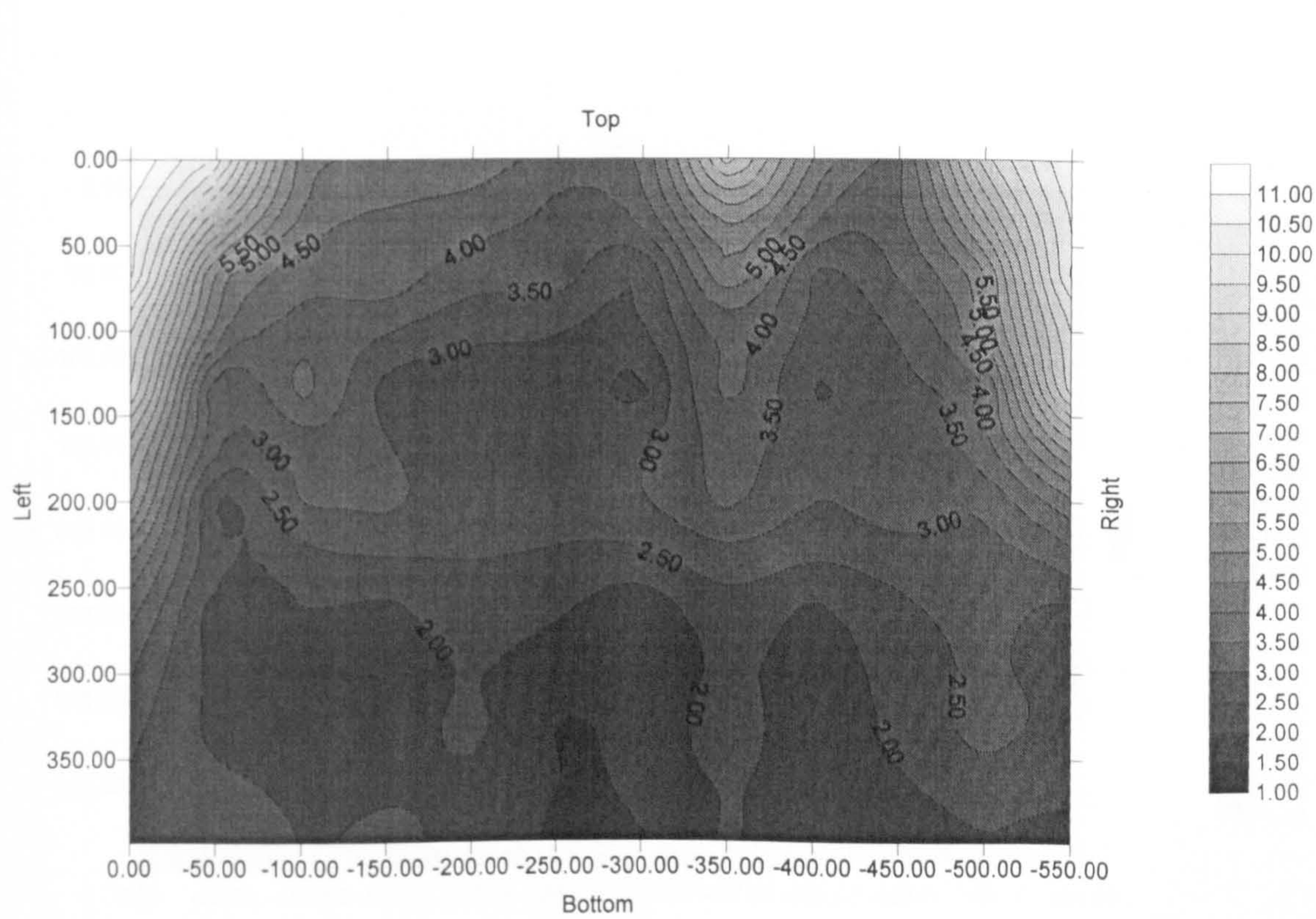

Figure 2.24 Contour plot of v component of turbulence intensity across grid (550x400) in the presence of base frame and largest mesh in tunnel at U_{pitot}= 4 m/s

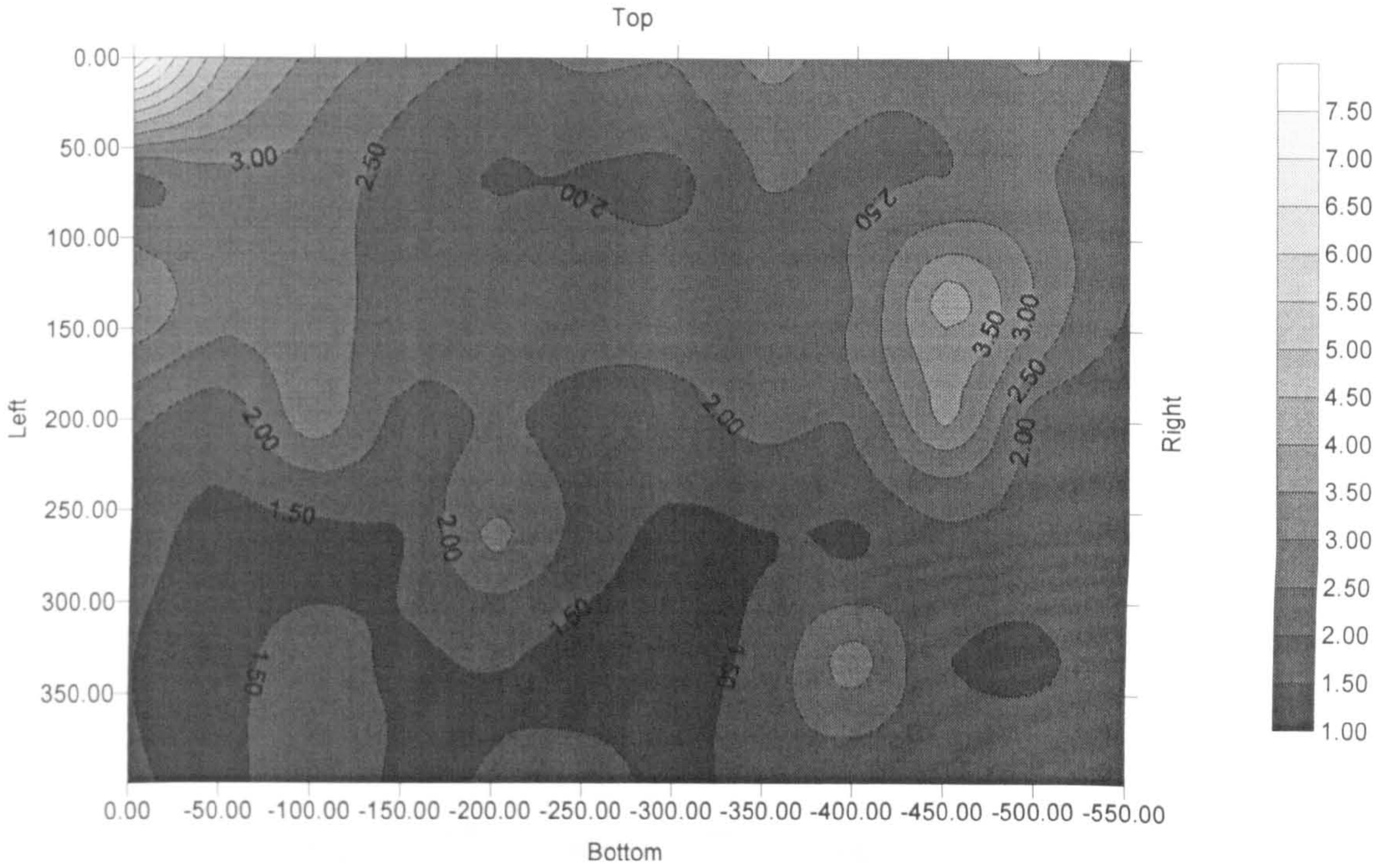

Figure 2.25 Contour plot of v component of turbulence intensity across grid (550x400) in the presence of base frame and medium mesh in tunnel at U_{pitot}= 4 m/s

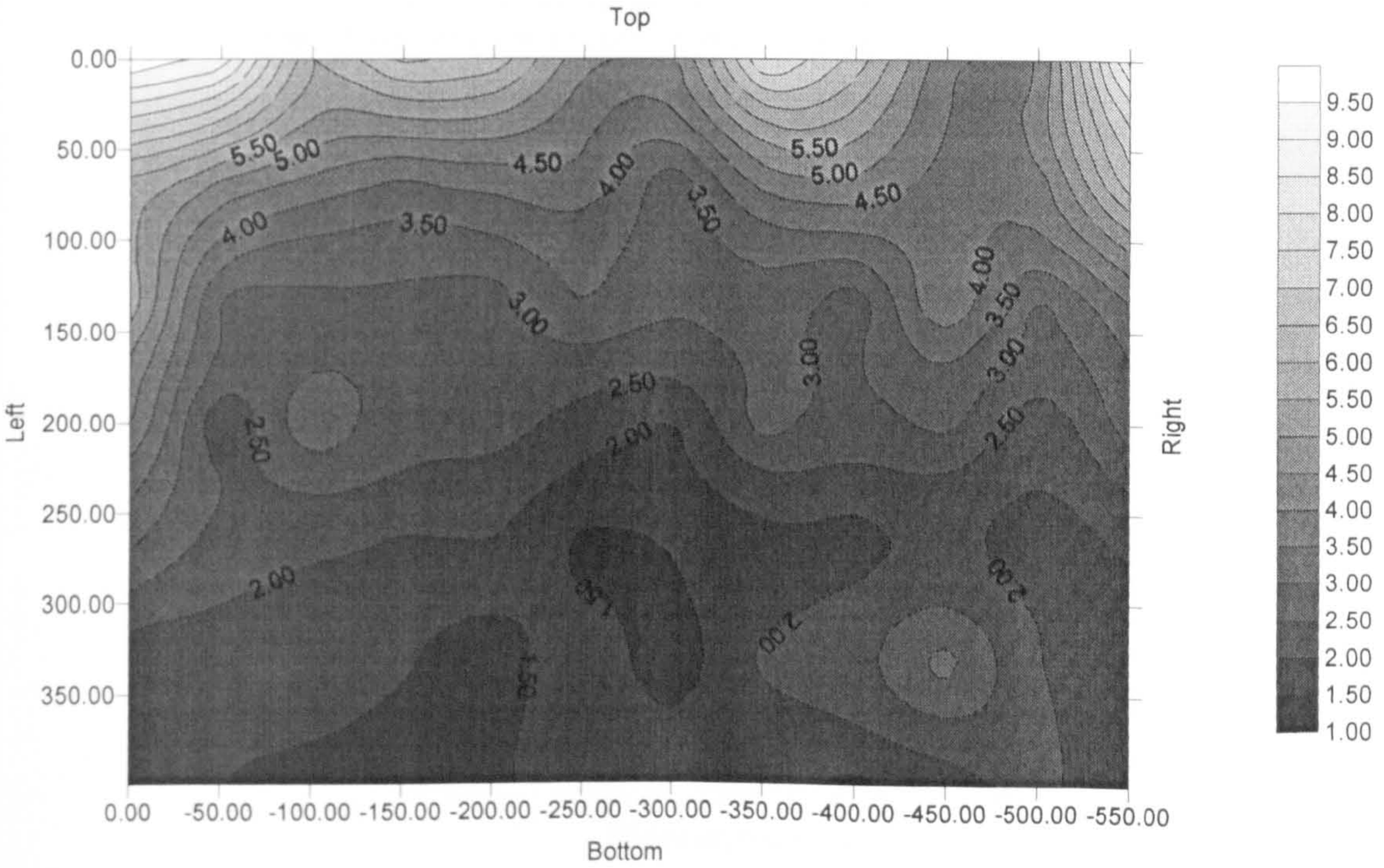

Figure 2.26 Contour plot of v component of turbulence intensity across grid (550x400) in the presence of base frame and finest mesh in tunnel at U_{pitot}= 4 m/s

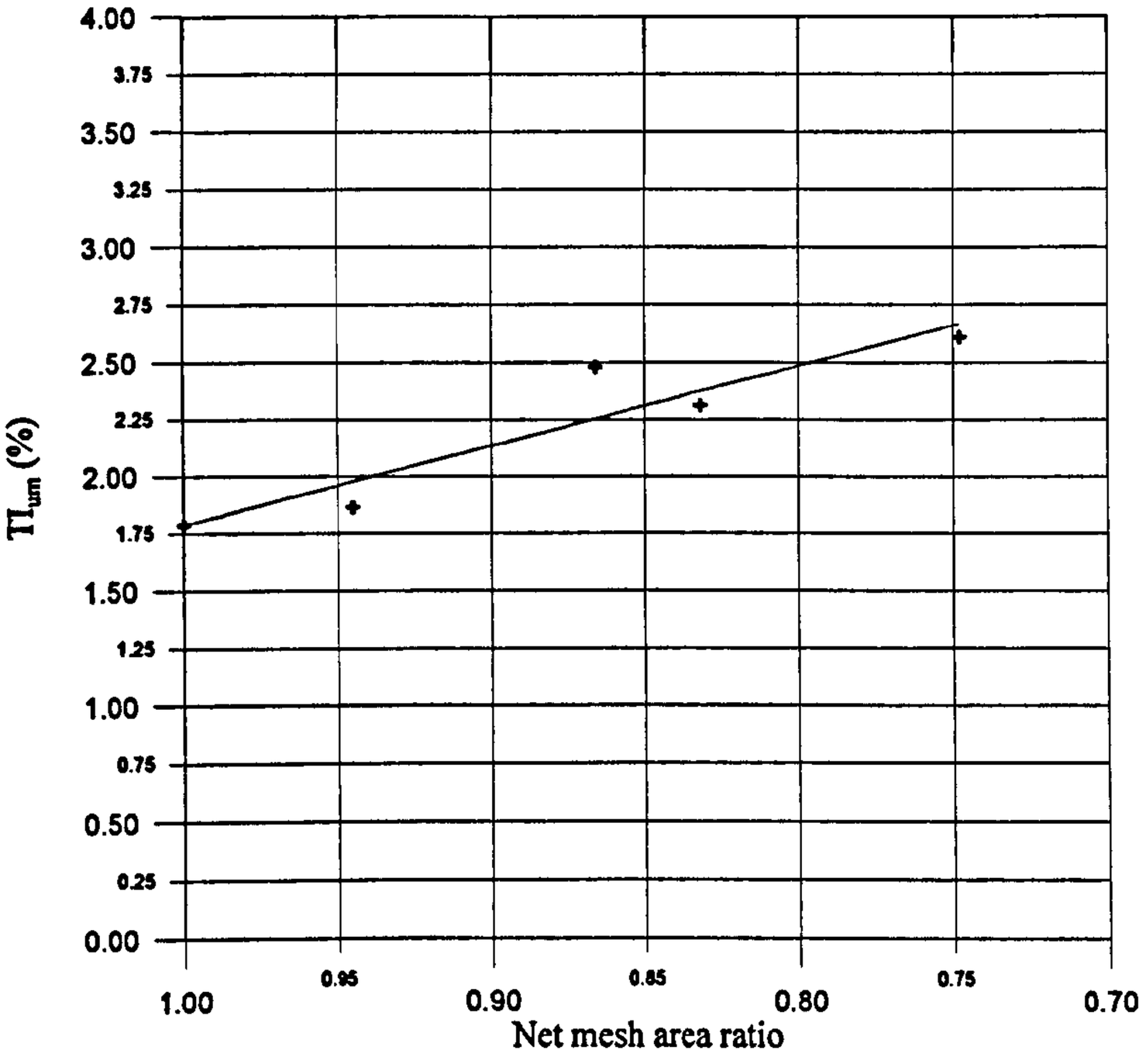

Figure 2.27 Comparison of mean u component of turbulence intensities, TI_{um}, in mesh area (350x380) at U_{pitot}= 4 m/s

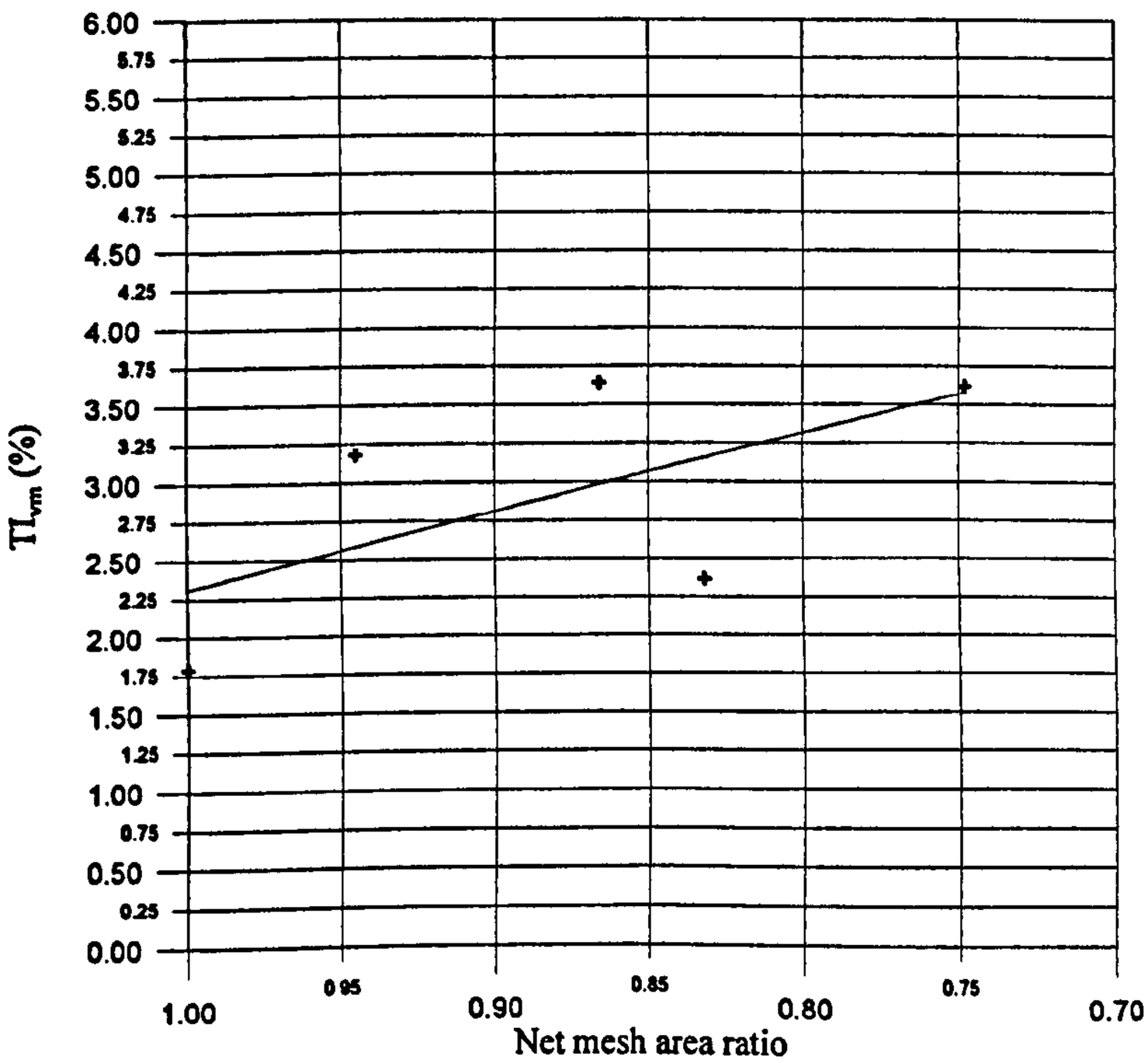

Figure 2.28 Comparison of mean v component of turbulence intensities, TI_{vm}, in mesh area (350x380) at U_{pitot}= 4 m/s

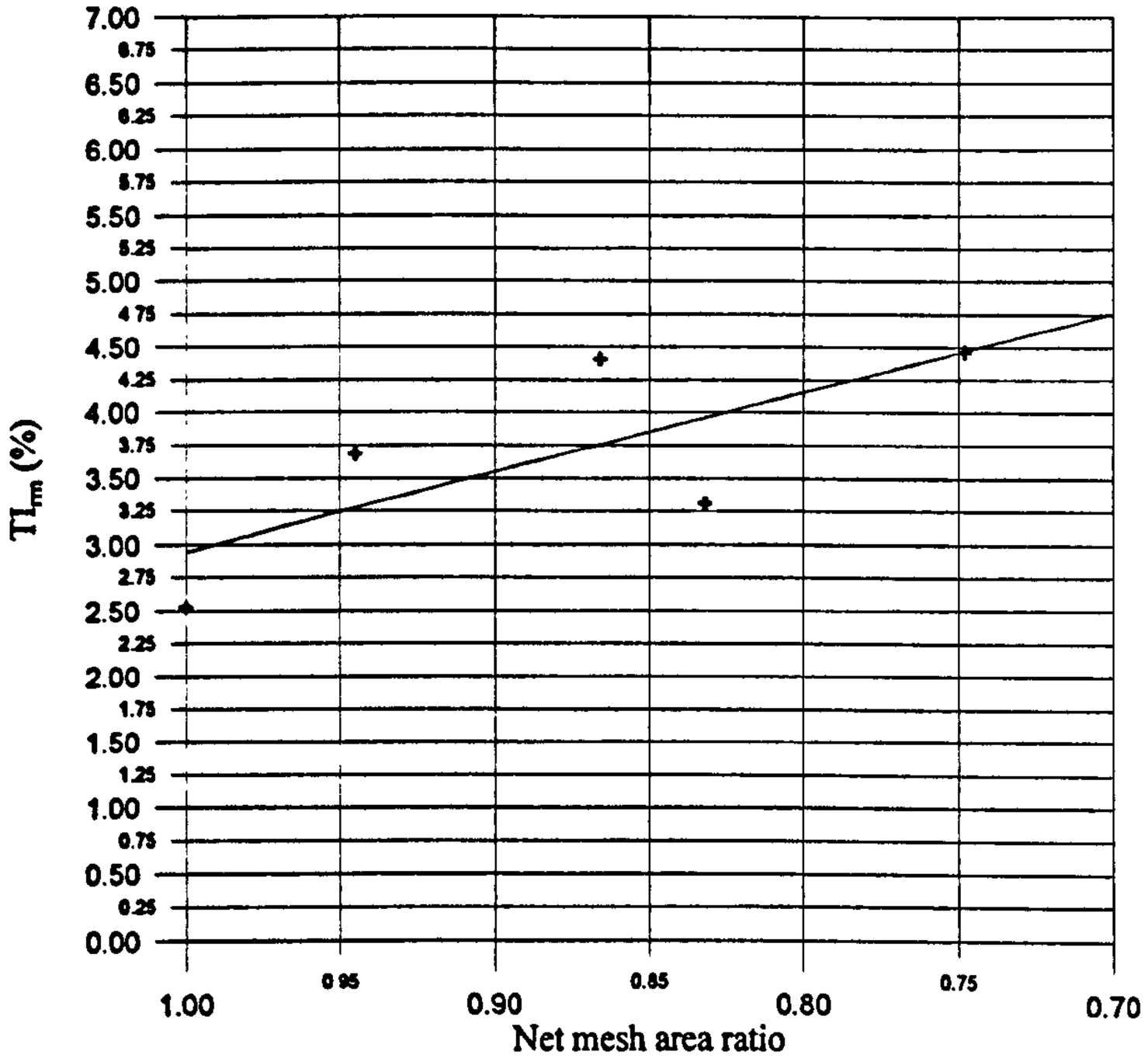

Figure 2.29 Comparison of mean resultant turbulence intensities, TI_{rm}, in mesh area (350x380) at U_{pitot}= 4 m/s

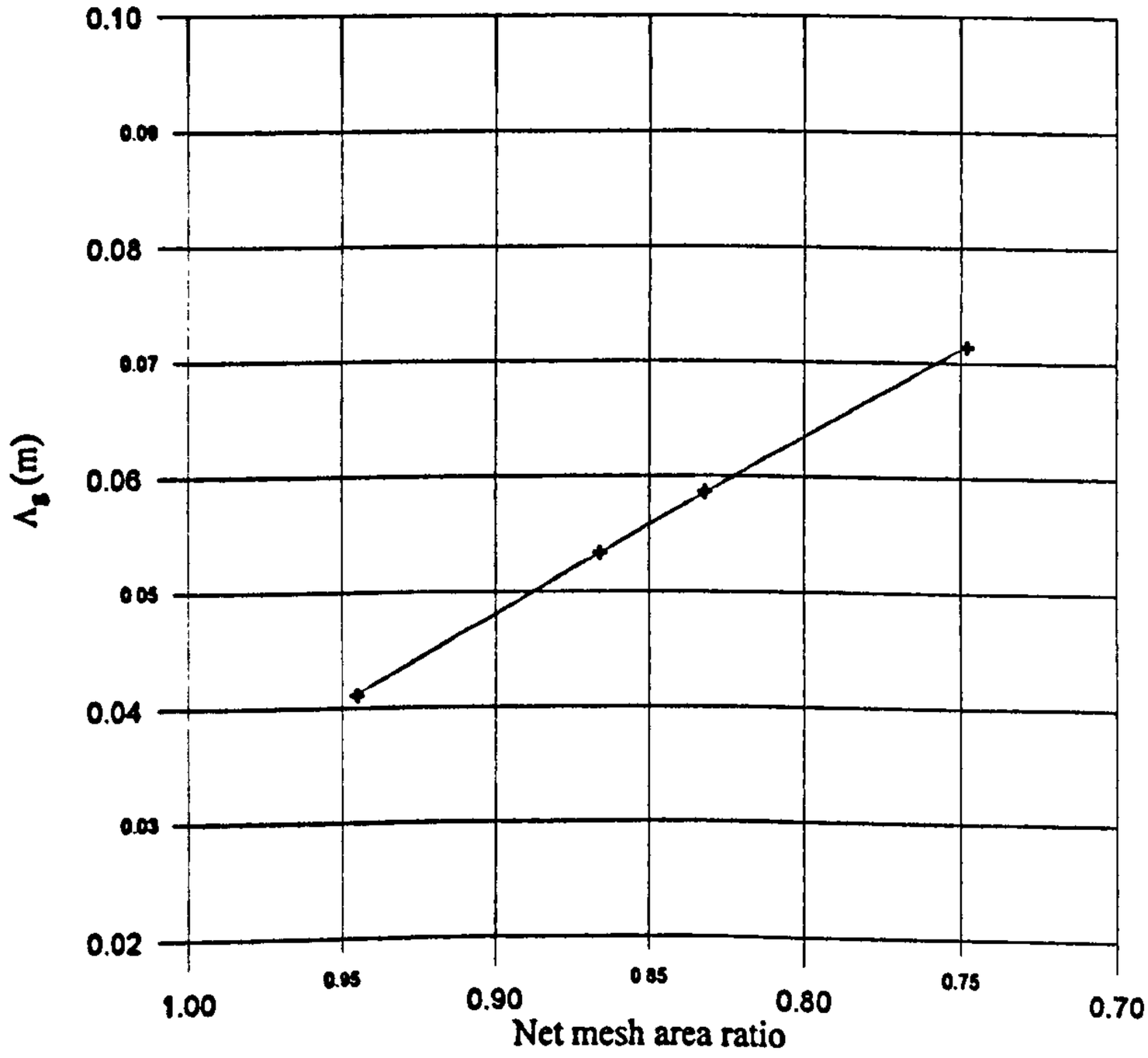

Figure 2.30 Comparison of mean integral length scale, Λ_g, in mesh area (350x380) at U_{pitot} = 4 m/s

2.5 CONCLUSIONS

In order to investigate the effect of free-stream turbulence on the inception of cavitation and noise, a turbulence generator, which involves a base frame and varying size of wire mesh system, has been designed and installed in the ECT. Using a 2-D LDA system the inflow characteristics of the ECT in terms of the velocity and turbulence intensity were measured and analysed. The analysis of the results indicates that:

- The mean axial velocity component of the inflow (u_{mlda}) measured by the LDA and averaged over the grid area across the tunnel correlated well with the pitot tube measurement (U_{pitot}), which is the current measuring system in the cavitation tunnel.

- However, if one investigates the flow map there is a slight cross-flow, which increases with increasing the inflow velocity. At the maximum tunnel velocity, u_{mlda} can be 3% less than U_{pitot}.

- Both magnitudes of the mean axial and transverse velocity components were increased linearly with the increasing tunnel inflow velocity. Although it fluctuated on average, the magnitude of the mean transverse velocity was approximately 2.25% of the axial inflow velocity.

- In the presence of no turbulence generator, the flow map across the grid area indicated more evenly distributed axial component (u) of the flow velocity compared to the transverse velocity component (v), indicating more cross-flow effect in the transverse direction.

- Introduction of the turbulence generator effectively altered the inflow turbulence characteristics in the area covering the base frame and wire mesh. The levels of the axial and transverse components of the turbulence intensities were both increased with decreasing the size of the wire meshes.

- Decreased size of the wire meshes in terms of the net mesh area ratio encouraged the level of the turbulence in the tunnel. The trend between the level of the turbulence and the net mesh area ratio appeared to be linear although there was an abnormality in one of the mesh cases.

- The magnitudes of v component of the turbulence intensity were higher than those of u component in the tunnel, displaying the importance of the transverse component and perhaps the vertical component of the turbulence intensity, which has been neglected in this investigation due to the 2-D configuration of the laser equipment. It will be extremely worthwhile to use 3-D LDA facility and measure all 3 components of the velocities.

CHAPTER 3 MEASUREMENTS OF THE INCEPTION OF CAVITATION WITH NACA66-004, a=0.8 (MODIFIED) MEAN LINE FOIL

3.1 INTRODUCTION

Although the main objective of this study was systematically to investigate the scale effect phenomena on the inception of cavitation and noise in marine propellers, it was thought that it would be sensible to start on the investigation with a simple rectangular foil, whose cross-section represents typical cross-section of a propeller blade, before engaging with the complex three-dimensional propeller flow. Therefore, a group of the experiments of the cavitation inception based on the parameters related to the scale effect phenomena with a rectangular foil having a cross-section of NACA66-004, a=0.8(modified) mean line was performed.

The main objective of these measurements was systematically to explore the effects of the free-stream turbulence on the inception of cavitation of the foil to form a basis for more complex propeller flow.

The measurements of the inception of cavitation with the foil section were performed for sheet type of cavitation at varying levels of the free-stream turbulence, roughness and combination of the former two. It was first thought that the foil experiments would include the investigations of the tip vortex and sheet cavitation as well as of the noise. Because of the physical obstructions encountered in the cavitation tunnel, these tests had to be restricted to the inception measurements of the sheet cavitation only as explained later in this chapter (Section 3.3).

Therefore,

- The first group of the experiments involved the inception measurements in the free flow for the sheet cavitation to be developed on the foil at various angles of attack.
- The second group of tests was the same measurements with the foil behind the turbulence generator with varying mesh sizes.
- The third group was similar to the first group of tests, but the foil had different levels of roughness at its leading edge.
- The fourth and final group of tests involved the inception measurements with the foil, which had differing levels of roughness, behind the turbulence generator to explore the simultaneous effect of the roughness and the free-stream turbulence on the inception of cavitation in combination.

3.2 BLADE SECTION DESIGN AND MANUFACTURE OF FOIL

The foil used for the inception of cavitation measurements was a rectangular planform of foil, which had a cross-section of NACA66-004, a=0.8(modified) mean line. The maximum thickness of the foil was at the mid-chord of the foil. Although the foil had a constant cross-section across its span and hence, one can consider as 2-D, strictly speaking, it can not be treated as a 2-D foil. The main characteristics of the foil are given in Table 3.1 while the offset data of the foil is given in Table 3.2. The profile of the foil section and the nose of the foil are also shown in Figures 3.1 and 3.2 respectively.

Table 3.1 Main particulars of foil

Main particulars	
Chord length, c, (mm)	250
Span length, b, (mm)	300
Aspect ratio, AR	1.2
Maximum thickness, t_{max}, (mm)	10
Maximum camber, f_{max}, (mm)	5
Location of maximum thickness from the leading edge (%)	50
Location of maximum camber from the leading edge (%)	50
Maximum thickness to chord length ratio, t_{max}/c	0.04
Maximum camber to chord length ratio, f_{max}/c	0.02

Based upon the simple beam theory and stressing procedure, the foil stock was determined as 25.4 mm in diameter. The foil was, then, manufactured from Nikalium alloy material by using an NC machine in the MMME Department of Newcastle upon Tyne University. A general view of the foil is shown in Figure 3.3 and Picture 3.1.

Although the foil was manufactured up to a high standard, in terms of its offset and surface finish, special care was paid to the leading edge as well as to other parts of the foil, which were finished by hand.

The foil had two sections as shown in Figure 3.3. The measuring section manufactured precisely had a span length of 250 mm from the bottom of the foil with a constant cross-section. The rest of the span had a varying cross-section with double thickness of the constant cross-section at the top.

A shown in Figure 3.4, because of the observation windows at the bottom and sides of the tunnel measuring section, the foil had to be mounted to a particularly made lid at the top of the tunnel section. It must be mentioned that a support foil was also manufactured in the case of failure and excessive vibration of the test foil due to fluid loading. The support foil had a symmetrical cross-section with the same chord length and thickness of the test foil and was kept at zero angle of attack. As shown in Figure 3.4, the support foil was spanned between the test foil and a stout beam across the bottom observation window and provided the test foil with an extra rigidity as well as avoiding possible vibration.

Following the preliminary tests, it was observed that the test foil without the support foil was rigid enough and free of vibration and the support foil also caused the observation difficulties from the bottom window. Therefore, it was decided that the experiments should be performed without the support foil.

Table 3.2 The abscissas and ordinates of NACA66-004, a=0.8(modified) mean line foil section

x_{upper} in mm	$y_{upper(back)}$ in mm	x_{lower} in mm	$y_{lower(face)}$ in mm
0.00000	0.052597	0.00000	0.052597
0.00351	0.101852	0.00351	0.000000
0.00435	0.22543	0.00435	-0.1235800
0.07500	0.26790	0.08351	-0.1838600
0.15000	0.36300	0.16351	-0.2569900
0.30000	0.50000	0.24351	-0.2979500
0.45000	0.60000	0.28351	-0.3150000
0.60000	0.70000	0.40350	-0.3550000
0.75000	0.78900	0.56350	-0.4000000
1.05000	0.92860	0.68350	-0.4300000
1.20000	1.00000	0.80350	-0.4550000
1.75736	1.21305	0.88350	-0.4725000
2.99213	1.60024	1.00350	-0.4975000
6.10051	2.31545	1.12350	-0.5200000
10.003370	3.02860	1.36222	-0.5493546
12.332870	3.44349	1.99960	-0.6176549
18.575130	4.36204	3.26480	-0.6936097
24.822470	5.15542	6.40634	-0.7292253
30.003090	5.71400	10.003370	-0.7343000
37.327490	6.46145	12.673800	-0.7326182
43.002910	6.94286	18.931360	-0.7054509
49.841070	7.49486	25.183850	-0.6733881
56.002720	7.91429	30.003090	-0.6457000
62.360050	8.31304	37.678480	-0.5931587
68.002560	8.61429	43.002910	-0.5571400
74.882660	8.95176	50.164540	-0.5019300
80.002390	9.15714	56.002720	-0.4571400
87.407890	9.43156	62.645220	-0.4089658
93.002200	9.58600	68.002560	-0.3714300
99.935010	9.75801	75.122250	-0.3184747
106.0020000	9.85714	80.002390	-0.2857140
112.4634000	9.93971	87.596670	-0.2299319
118.0019000	9.96286	93.002200	-0.1942900
124.9927000	9.97499	100.0692000	-0.1444161
130.0017000	9.94286	106.0020000	-0.1028570
137.5222000	9.85992	112.5404000	-0.0599941
144.0015000	9.74286	118.0019000	-0.0171000
150.0513000	9.58390	125.0109000	0.025008
156.0013000	9.36571	130.0017000	0.071429
162.5782000	9.06757	137.4810000	0.110008
169.0011000	8.70000	144.0015000	0.148570
175.1010000	8.30390	149.9515000	0.201096
181.0010000	7.85714	156.0013000	0.271430
187.6189000	7.31315	162.4242000	0.365599
194.0008000	6.71429	169.0011000	0.471430
200.1400000	6.08090	174.9012000	0.586489
205.0006000	5.55700	181.001000	0.700000
212.6302000	4.60206	187.382900	0.807429
220.0004000	3.75000	194.000800	0.902857
225.0818000	3.14866	199.861400	0.945112
230.0003000	2.56400	205.000600	0.914286
237.532300	1.63215	212.370800	0.821184
245.000100	0.81400	220.000400	0.650000
250.000000	0.30000	224.918900	0.537999
		230.000300	0.407000
		237.468100	0.211182
		245.000100	-0.0857000
		250.000000	-0.3000000

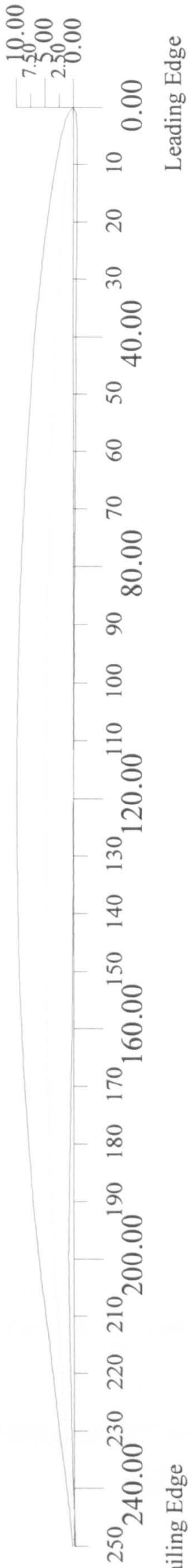

Figure 3.1 Cross-section of NACA66-004, a=0.8(modified) mean line foil

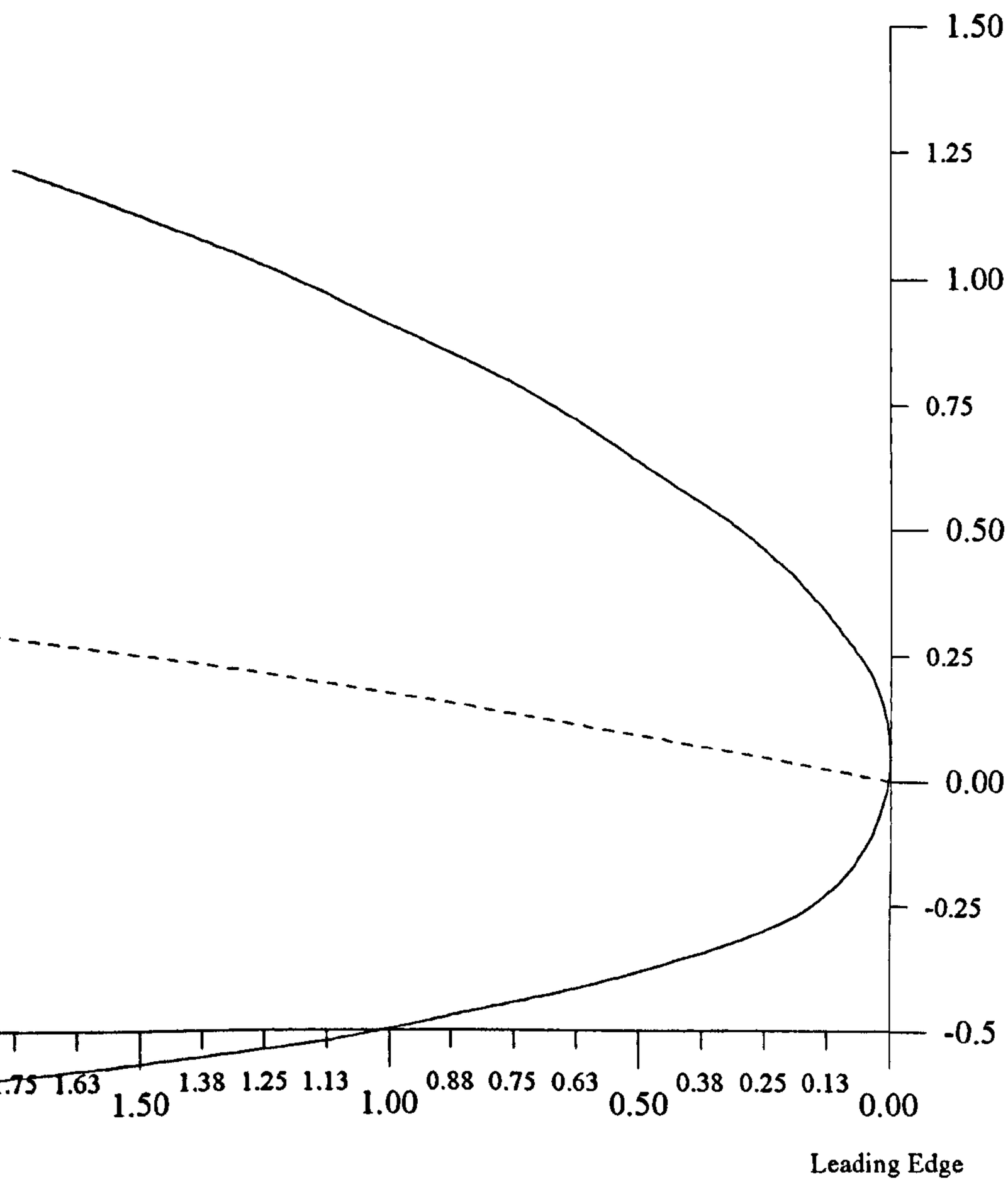

Figure 3.2 Enlarged view of the nose of NACA66-004, a=0.8 (modified) mean line foil

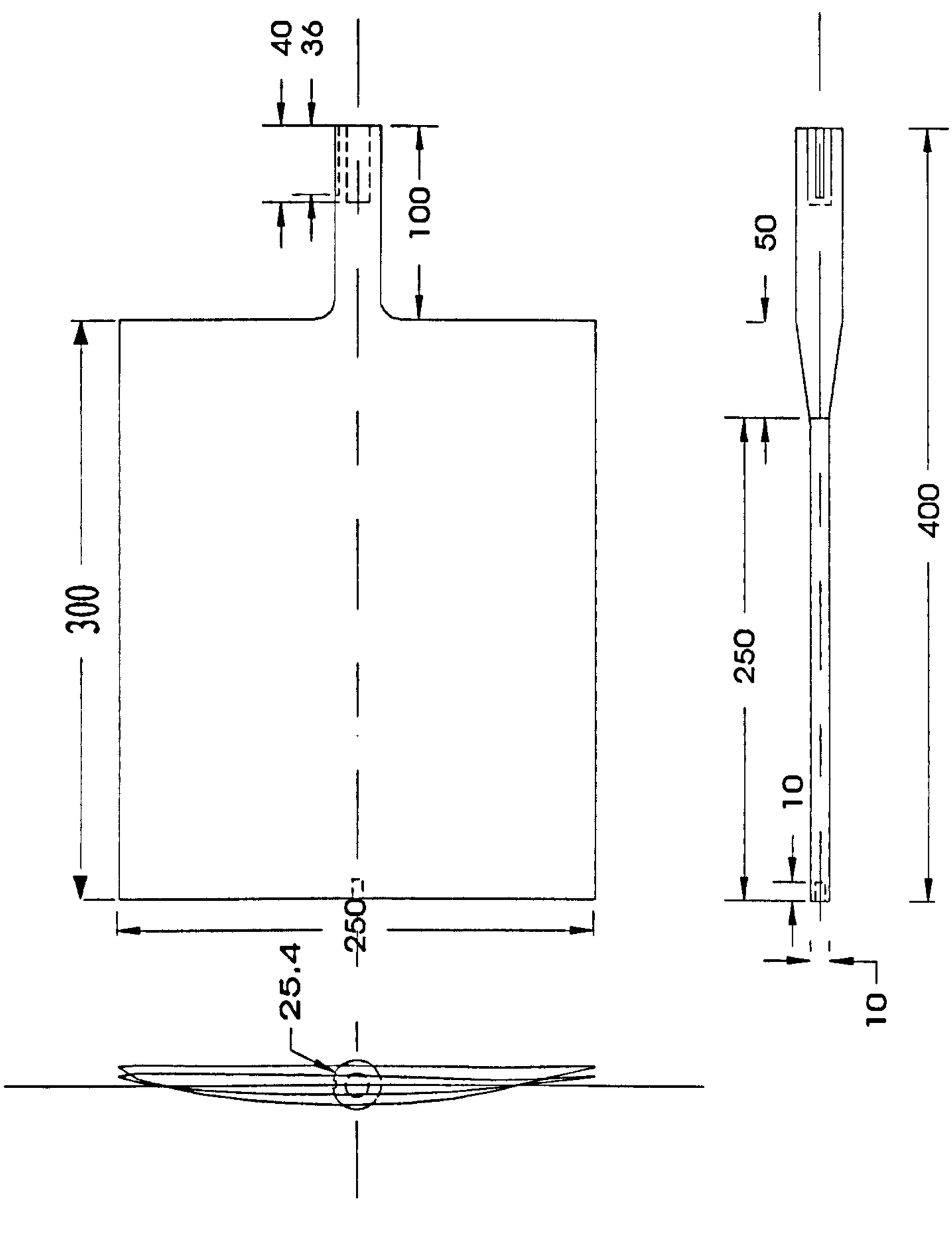

Figure 3.3 Illustration of general view of the rectangular planform foil

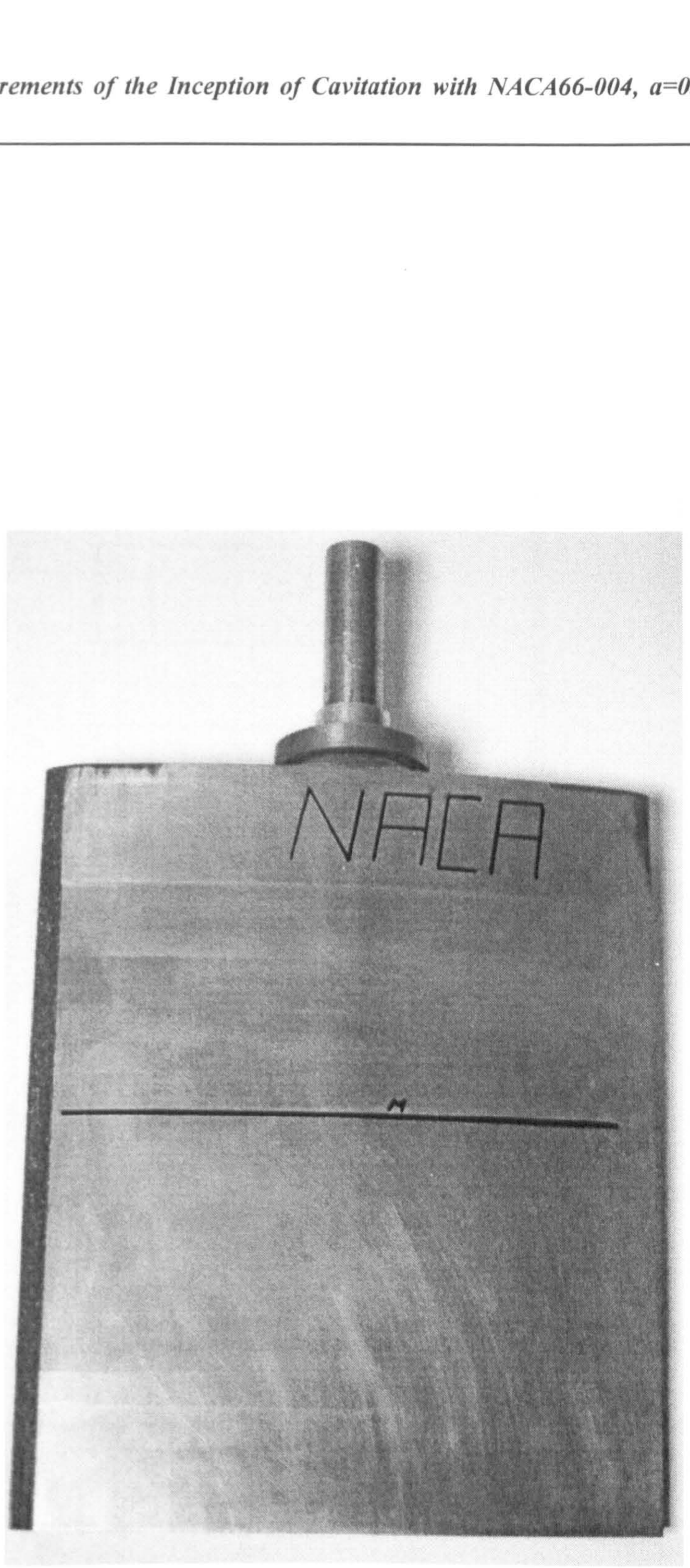

Picture 3.1 General view of the rectangular planform foil with roughness

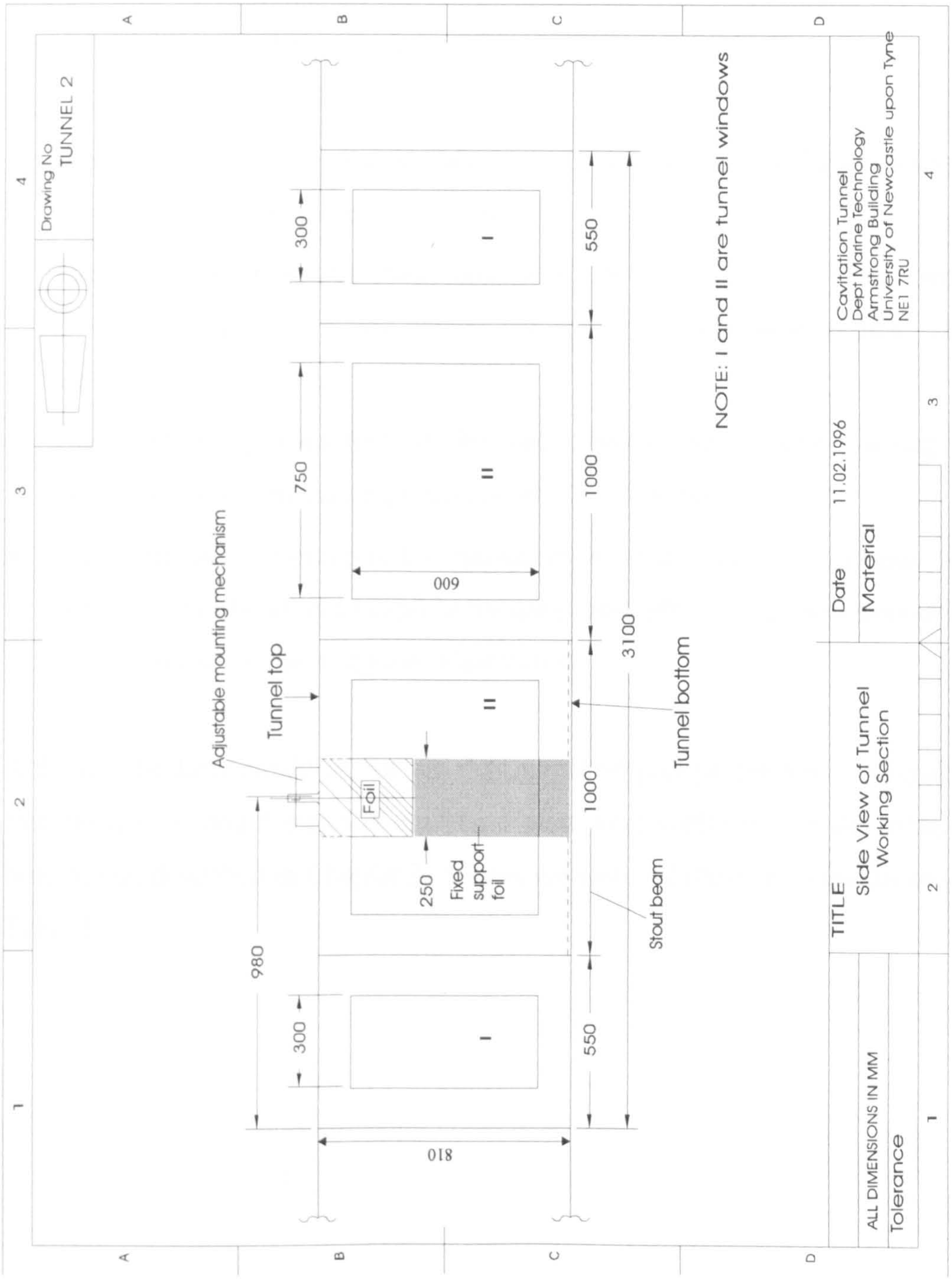

Figure 3.4 Side view of tunnel test section where foil is mounted

3.3 TEST CONDITIONS AND EXPERIMENTAL SET-UP

Experiments were carried out in four groups for the measurements of the inception of cavitation with the foil section in the Emerson Cavitation Tunnel.

- The first group was the measurements of the inception of cavitation with the foil at varying angles of attack in the free flow.
- The second group was the measurements of the inception of cavitation with the foil at varying angles of attack behind the turbulence generator, which was already described in Chapter 2.
- The third group consisted of the same measurements with varying levels of roughness as well as varying angles of attack in the free flow.
- The fourth and last group of the measurements was involved the former two groups of tests in combination to explore the combined effect of the free-stream turbulence and roughness on the inception of cavitation.

Although the flow condition for the first and third groups has been categorised as the free flow, one should mention that these tests were performed in the presence of the base frame, described in Chapter 2. A brief summary of these test conditions is given in Table 3.3.

Table 3.3 Foil test conditions

Test No	Test Condition	Test Condition Details
1	In the free flow	Test with base frame only for 5 different angles of attack
2	In the presence of turbulence generator	Test with base frame and largest-sized mesh for 5 different angles of attack
3		Test with base frame and medium-sized mesh for 5 different angles of attack
4		Test with base frame and finest-sized mesh for 5 different angles of attack
5	In the presence of blade roughness	Test with base frame and 35 μm roughness for 5 different angles of attack
6		Test with base frame and 60 μm roughness for 5 different angles of attack
7		Test with base frame and 100 μm roughness for 5 different angles of attack
8	In the presence of turbulence generator and blade roughness	Test with base frame, 35 μm roughness and largest-sized mesh for 5 different angles of attack
9		Test with base frame, 35 μm roughness and medium-sized mesh for 5 different angles of attack
10		Test with base frame, 35 μm roughness and finest-sized mesh for 5 different angles of attack
11		Test with base frame, 60 μm roughness and largest-sized mesh for 5 different angles of attack
12		Test with base frame, 60 μm roughness and medium-sized mesh for 5 different angles of attack
13		Test with base frame, 60 μm roughness and finest-sized mesh for 5 different angles of attack
14		Test with base frame, 100 μm roughness and largest-sized mesh for 5 different angles of attack
15		Test with base frame, 100 μm roughness and medium-sized mesh for 5 different angles of attack
16		Test with base frame, 100 μm roughness and finest-sized mesh for 5 different angles of attack

The current set up of the ECT, which has observation windows at the bottom and sides of the measuring section, allowed the foil to be mounted to the tunnel lid hanging vertically. The lid was equipped with specially designed adjustable mechanism to hold the foil stock and provide the necessary angle of attack to be set during the tests.

The base frame of the turbulence generator was located at a distance of 0.827 m, which was 3.3 times the foil chord, at the upstream of the leading edge of the foil. The wire meshes attached to the base frame had an area of 0.35 m x 0.38 m (BxH) to generate turbulence which would cover the cavitation observation area on the foil with a comfortable margin as shown in Figure 3.5.

Prior to the tests, it was expected that with the above set up one could observe the tip vortex and sheet cavitation as well as measuring the associated noise by using the available hydrophone facility. Unfortunately, the expectations were not fully materialised, in terms of the measurements of the inception of the tip vortex cavitation and noise while it was possible to measure the inception of the sheet cavitation. This was because that the section of foil near the foil stock had a larger fillet area compared to the rest of the cross-section area of the foil due to the strength considerations. This triggered early inception of the cavitation, which was further complicated by the combined boundary layer of the tunnel lid and the foil. As a result, it was not possible to observe a clean development of the tip vortex at the leading edge of the foil and hence to record proper noise signals corresponding to the tip vortex cavitation.

Under the above circumstances, it was only possible to observe the inception of the sheet cavitation at a suitable reference line on the foil section outside the fillet section. Therefore, as shown in Figure 3.5, a thin reference line was marked with a permanent marker pen at a distance of 140 mm from the top of the foil. Since the cavitation always developed from the top of the foil, the progress of the cavitation was allowed to this reference line. As soon as the extent of cavitation reached the reference line the corresponding condition was recorded as the inception point at that level.

Of course, the above cumbersome situation could be avoided in ideal circumstances by mounting the foil across the tunnel width or between the two side walls. However, this would require a major modification to the tunnel measuring section and complex fitting mechanism, which could not be fitted into the time and budget of this research study and left as a future work.

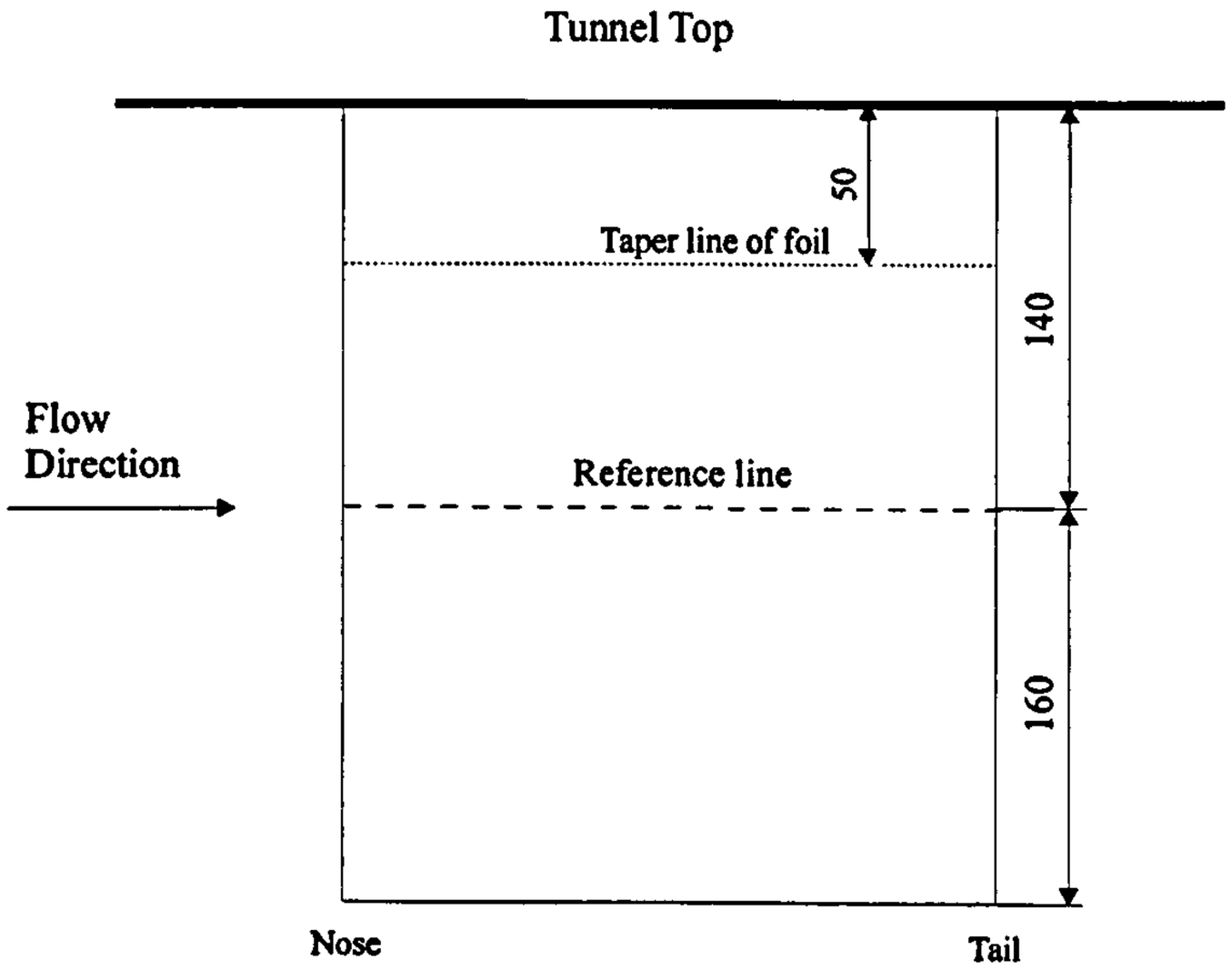

Figure 3.5 Position of reference line on foil

In order to investigate the roughness effect, carborundum was used as a roughness element. The roughness was glued to 4 per cent of the chord length from the leading edge in the whole span length on both face and back sides of the foil by a polyurethane varnish. The foil was first taped and one thin layer of varnish was applied. The tape was immediately removed to avoid sharp edges, which might have been created by the glue, as stated by 19th ITTC (1990) and then, the roughness element was applied. It was left for about 3 hours to dry. The last very thin layer of varnish was applied again. It was left overnight to become completely dried. The sizes of roughness heights applied are given in Table 3.4.

Table 3.4 Roughness heights applied in tests

Roughness height, k (μm)	35	60	100

All the inception points were recorded by the eye observations, which were carried out from the suitable windows of the tunnel. The procedure for collecting a valid inception point was such that initially the tunnel static pressure was adjusted at a constant value and the tunnel speed was increased until the inception was reached and passed the

marked reference line by a reasonable amount. The tunnel speed was then decreased until the inception was steadily just reaching the reference line. The point was, then, accepted as the valid inception point for the sheet cavitation. Three readings for each inception point were taken and averaged to improve the accuracy of the inception results. The foil was illuminated by two stroboscope lights, one from the bottom and the other from the side of the tunnel for accurate readings.

Due to the physical limitations of the Emerson Cavitation Tunnel in terms of the speed (Maximum speed = 7.0 m/s) and the absolute minimum pressure (Minimum pressure = 7600 Pa), there were difficulties to observe an inception point at very small angles of attack where the applied vacuum had to be very high as well as the flow speed. In these conditions, the observations were difficult due to trapped air in the tunnel water as well as darkening colour of the tunnel water generated by the extreme stirring motion at the high velocities. Therefore, 5 angles of attack were investigated where the observations were more reliable, as given in Table 3.5. The definition of the positive and negative angles of attack is shown in Figure 3.6.

Table 3.5 Angles of attack used for measurements

Angle of attack, α, (degrees)	-4	-3	-2	5	6

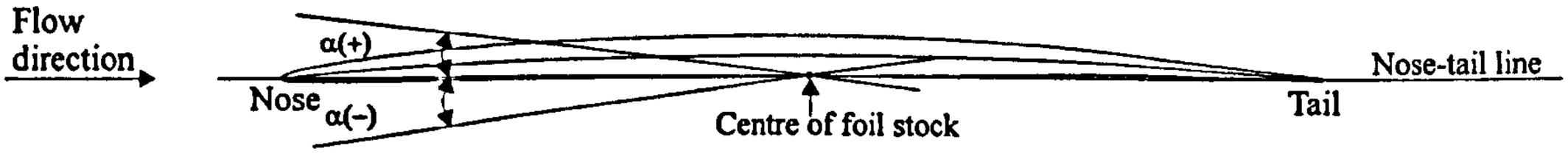

Figure 3.6 Definition of positive and negative angles of attack

During the experiments, the dissolved gas content of water was measured by using a Jenway DO_2 meter 9071 apparatus. It was tried to keep about 35%. Reynolds number range based on the chord length was 0.558×10^6 to 1.328×10^6.

3.4 PRESENTATION AND DISCUSSION OF RESULTS

As mentioned in Section 2.2 of Chapter 2, the turbulence characteristics of the tunnel flow in the presence of the turbulence generator with varying mesh sizes were measured across the tunnel inflow velocity range (U_{pitot}= 1 m/s to 7 m/s). Table 3.6 presents typical values at U_{pitot} = 4 m/s for information. This background flow data was essential to analyse the inception measurements carried out in this chapter since each inception point had a particular inception speed corresponding to a particular turbulence intensity that can be obtained from the background flow data.

Table 3.6 Results of free-stream turbulence measurement at U_{pitot} = 4 m/s

Turbulence generator type	Free-stream turbulence intensity (%)
Base frame	3.273
Largest-sized mesh	3.752
Medium-sized mesh	3.958
Finest-sized mesh	4.466

The inception number of cavitation shown in the following Figures 3.7 through 3.20 was calculated based on the free-stream velocity, U or U_{pitot}, such that:

$$\sigma_i = \frac{P_{st} - P_v}{\frac{1}{2}\rho U^2} \tag{3.1}$$

The results of the measurements of the inception of cavitation with the NACA foil section are presented:

- in Figure 3.7 for the effect of free-stream turbulence.
- in Figures 3.8 and 3.9 for the effect of roughness
- Figures 3.10 through 3.20 for the combined case.

In these figures,

- x-axis presents the levels of free-stream turbulence intensity (TI) in percentage or roughness height (k) in μm or angle of attack (α) in degrees
- y-axis presents the inception numbers of cavitation (σ_i).

Figure 3.7 presents the inception values taken at the sheet cavitation reference line against the levels of the free-stream turbulence intensity for each angle of attack imposed. As one can see in this figure that the inception number (σ_i) clearly increases with increasing the level of free-stream turbulence intensity (TI). This appears to be true for all the angles of attack tested except for -4°.

As far as the effect of the angle of attack is concerned, whether it is positive or negative (i.e. back or face cavitation respectively), the cavitation number also clearly increases with increasing the angle of attack, indicating that at large angles of attack the foil will cavitate earlier than at smaller angles of attack.

Similarly, Figure 3.8 presents the inception values taken at the reference line against varying roughness levels applied at the foil leading edge for each angle of attack imposed. As shown in Figure 3.8, there is a clear increase in the cavitation numbers with increasing roughness level up to 60 μm while there is a clear decrease beyond this level. This trend is somehow different from the trend observed in Figure 3.7, indicating the differences between the two mechanisms to generate inception. On the other hand, in Figure 3.9, the effect of the angle of attack appears to have the same trend as for the varying free-stream turbulence cases: such that increasing angle of attack in positive or negative increases the risk of the sheet cavitation at the corresponding side of the foil.

In order to identify the effect of free-stream turbulence and roughness in combination, the measured values of the inception of cavitation at the fourth group of tests were plotted for varying levels of the roughness against the varying levels of the free-stream turbulence in Figures 3.10 through 3.14 at each angle of attack. These figures also indicate that the increased level of the free-stream turbulence generally causes an

increase in the inception numbers for each level of roughness. The similar trend with different slopes is observed for all the angles of attack.

Figures 3.15 through 3.19 show the same inception results, which were obtained in the fourth group of tests, plotted against the roughness levels for varying level of the free-stream turbulence at each angle of attack. The trend in these curves is similar to the trend observed in the isolated case, i.e. without the turbulence generator. This means that the inception values increase with increasing roughness up to 60 μm, beyond which they decrease with increasing roughness level. The presence of the turbulence in combination with the roughness effect does not change this trend. Although the magnitude of the inception values increases with increasing the level of the free-stream turbulence as observed in the previous sets of plotting.

As far as the effect of the angle of attack is concerned, it is observed in Figure 3.20 that as the angle of attack is increased from -2° to -4° and from 5° to 6° the cavitation number also increases, displaying the well-known fact that the development of cavitation is encouraged with increasing the angle of attack. This trend seems to be unaffected by the varying levels of free-stream turbulence as well as the varying levels of roughness.

From the discussion of the analyses of the results, it can be concluded that the use of turbulence generator and roughness both affected the characteristics of the inception of sheet cavitation of the foil. It is interesting to note that trend in the results of the inception caused by these two different mechanisms is somehow different. Although a systematic increase in the level of turbulence would increase the risk of cavitation, this trend may not be so beyond a certain level of roughness if the roughness technique is used. The change in the trend is so dominant even if the two techniques are combined together. Perhaps one can suggest that the roughness size up to 60 μm stimulates the laminar boundary layer region to the turbulent by moving the transition region to the leading edge of the foil.

During the experiments, it was difficult to take tests photographs due to the visibility problem generated by high vacuum in the tunnel. Therefore, the observations are only

illustrated by sketches for each angle of attack tested, as shown in Figure 3.21. The usual appearance of the cavitation observed was at the face side of the foil for the negative angles of attack (-2°, -3° and -4°) while the cavitation was observed at the back side of the foil for the positive angles of attack (5° and 6°).

In Figure 3.21, when the angle of attack was negative the cavitation was developed at the face of the foil. For the angle of attack of -4°, the inception was sudden and like a flash. The pattern of sheet cavitation was some streak lines along the span of the foil, which did not attached to the foil, and the inception point was really difficult to decide. For the angle of attack of -3°, very thin sheet cavitation was observed which suddenly occurred until the reference line on the foil. The observations were easier compared to those at -4°. The similar character of sheet cavitation also occurred at the angle of attack of -2°.

On the other hand, it was observed that at positive angles of attack the cavitation at the back usually started from the leading edge of the foil towards the reference line, like a wedge shape as sketched at $\alpha = 5°$ and $\alpha = 6°$ of Figure 3.21. The cavitation patterns observed were sheet and streak types of cavitation developed from the nose of the foil towards mid-chord region.

It must also be noted that the observations on the back side of the foil were much easier than those on the face side of the foil due to the cavitation pattern occurred. All the observations showed that as the cell size of meshes was reduced the visibility of cavitation would be worse because the meshes at the upstream of the foil made the visibility harder.

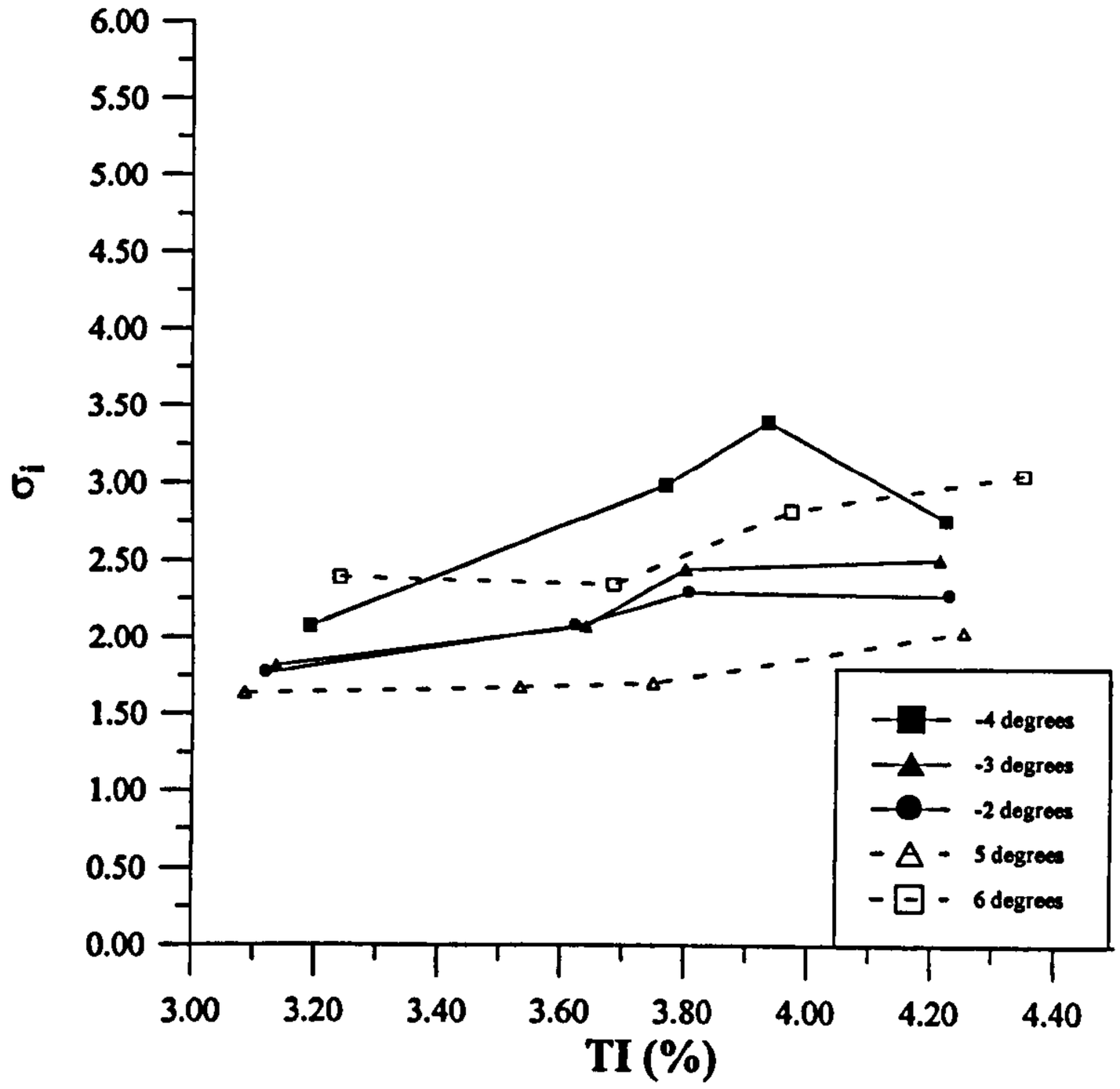

Figure 3.7 Comparison of the inception numbers of cavitation against varying level of free-stream turbulence for varying angle of attack of NACA foil

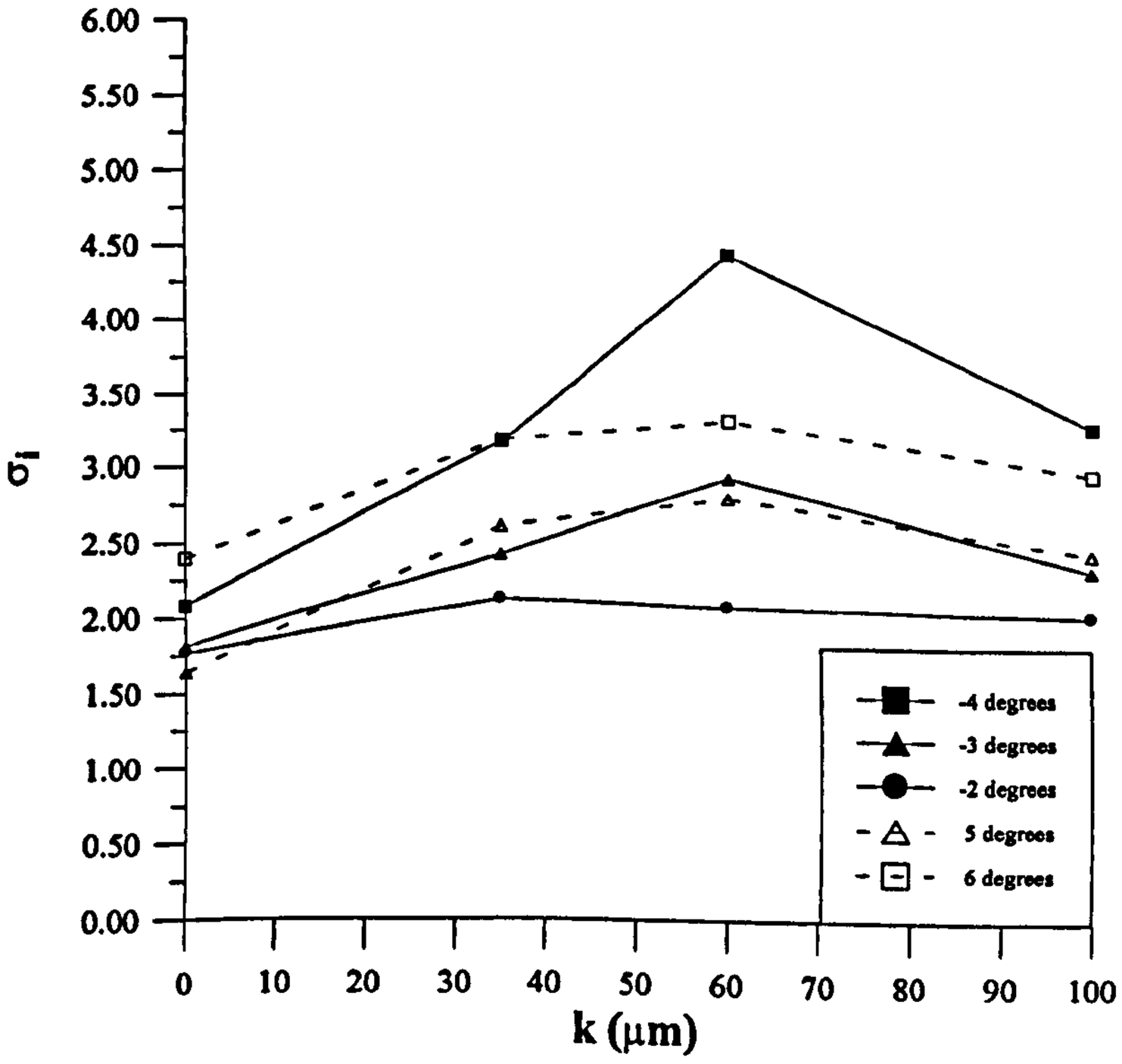

Figure 3.8 Comparison of the inception numbers of cavitation against varying level of roughness height for varying angle of attack of NACA foil

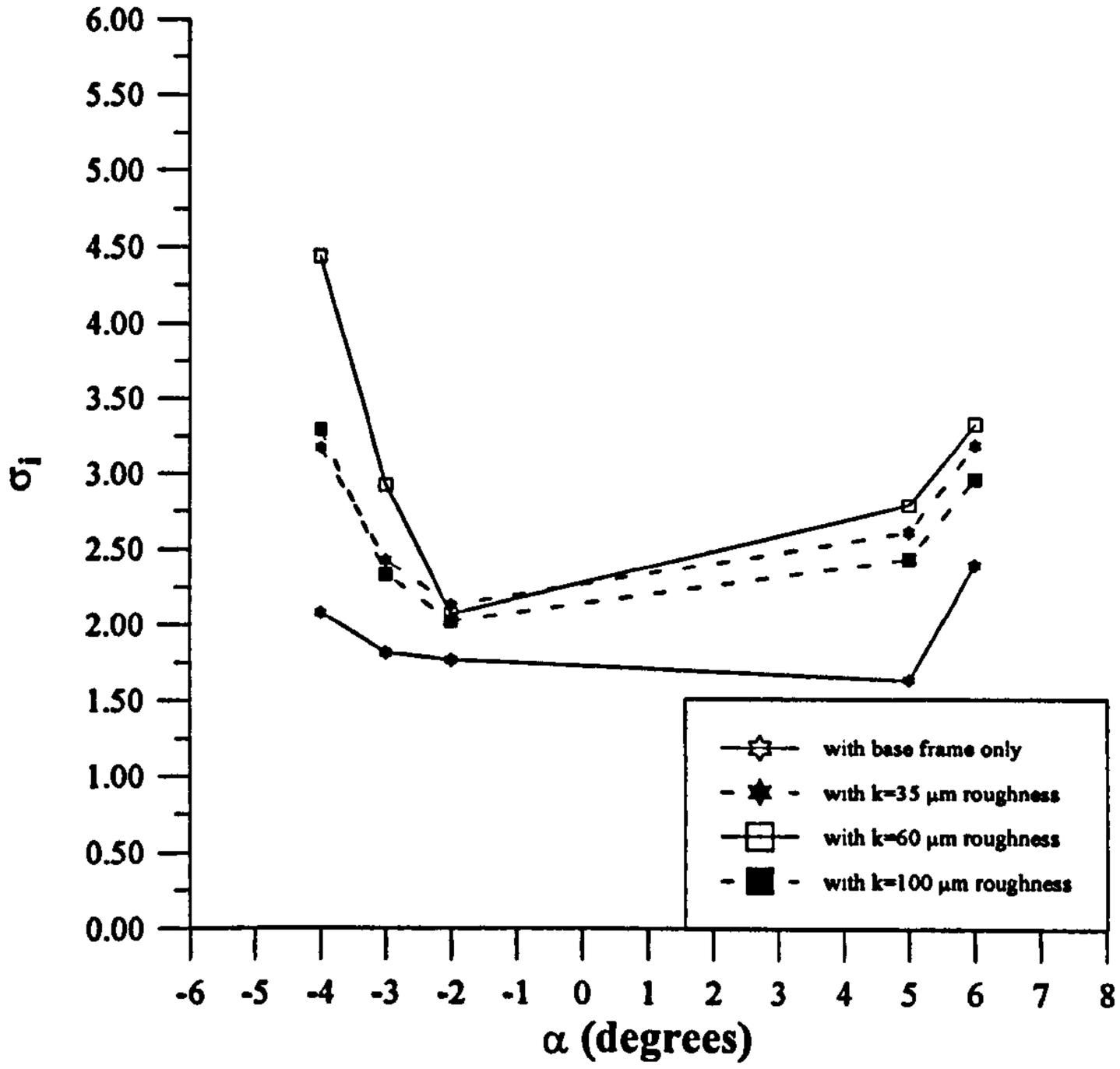

Figure 3.9 Comparison of the inception numbers of cavitation against varying angle of attack for varying level of roughness height

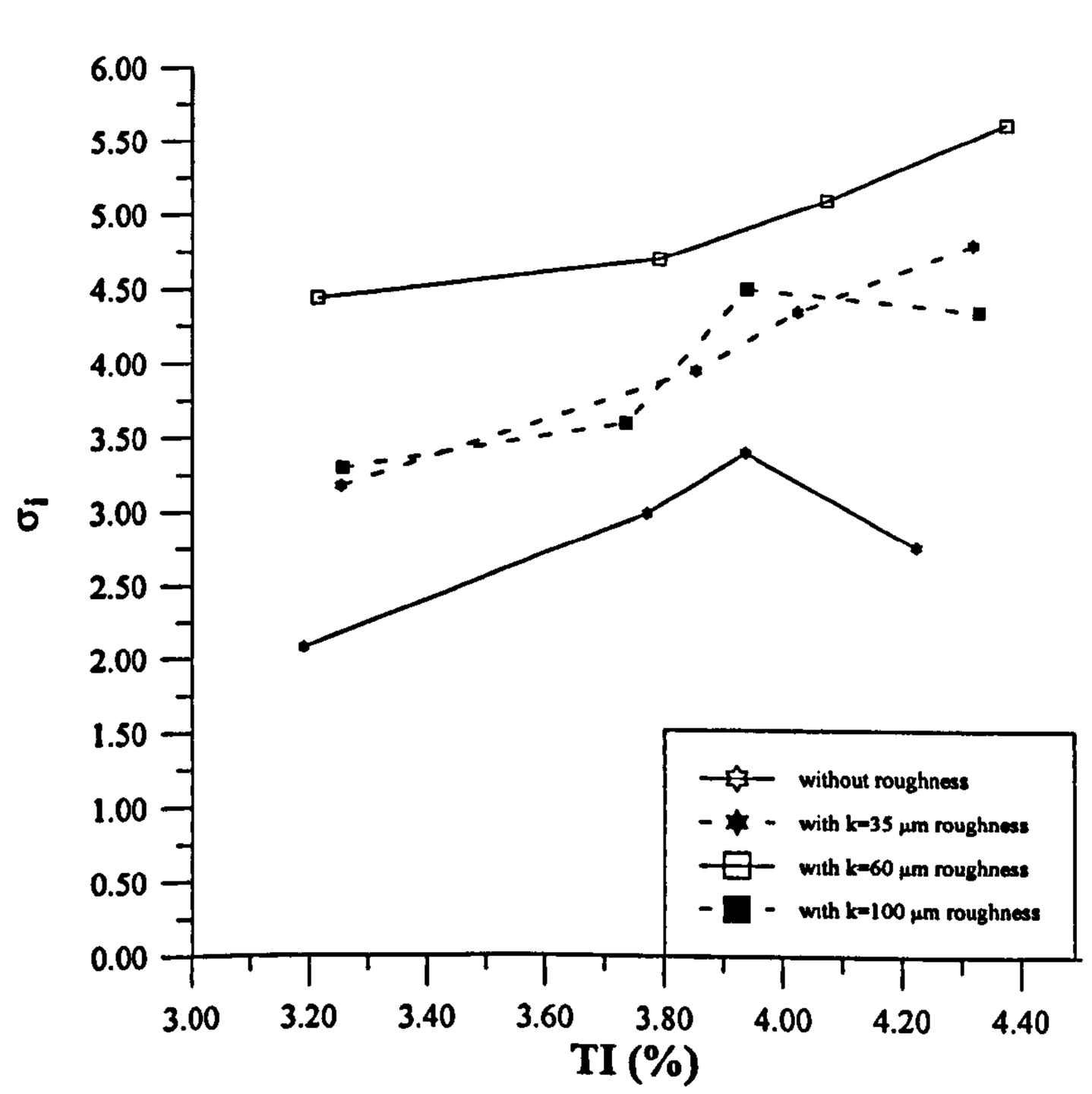

Figure 3.10 Comparison of the inception numbers of cavitation against varying level of free-stream turbulence for varying level of roughness of NACA foil at $\alpha = -4°$

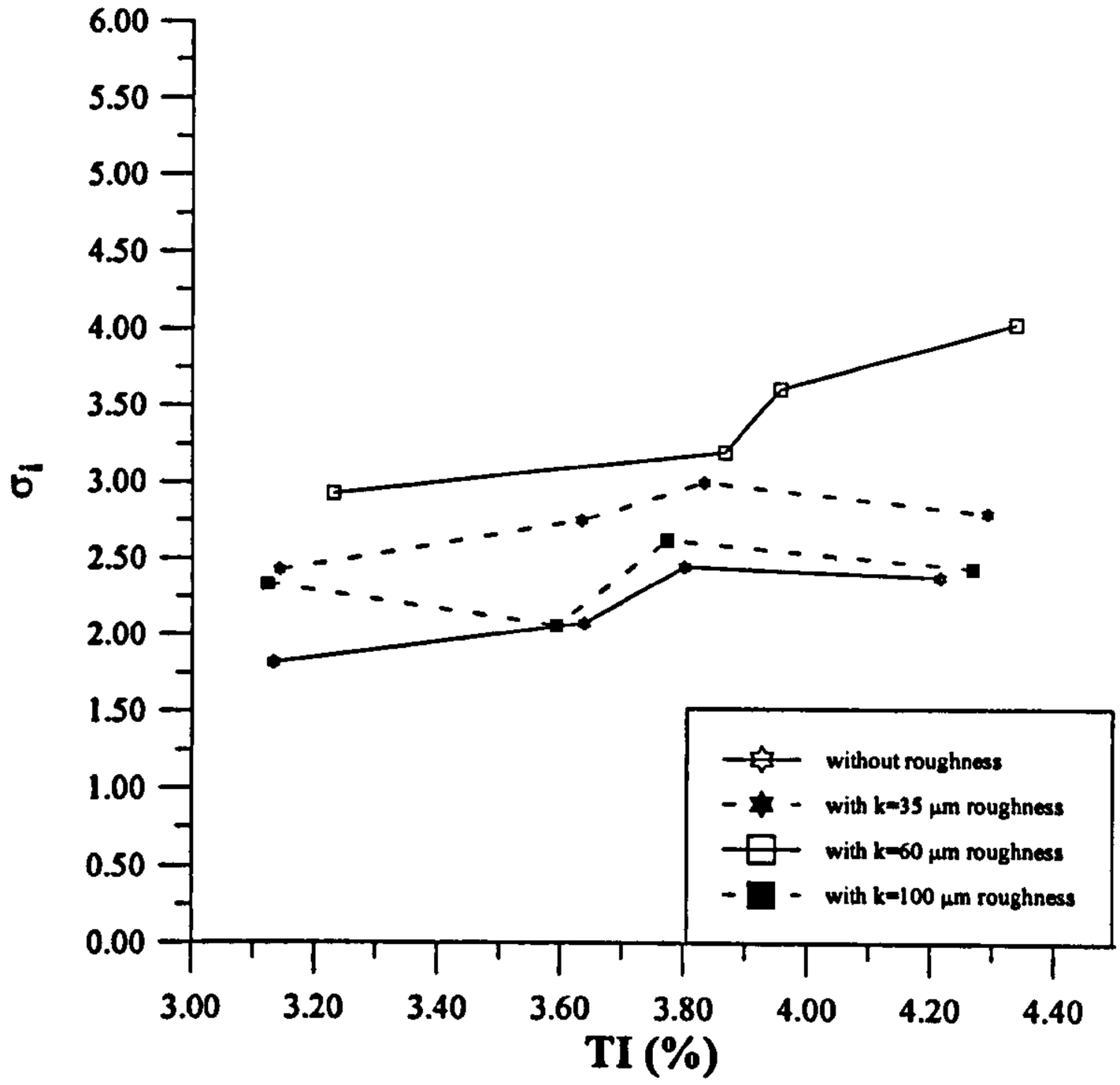

Figure 3.11 Comparison of the inception numbers of cavitation against varying level of free-stream turbulence for varying level of roughness of NACA foil at $\alpha = -3°$

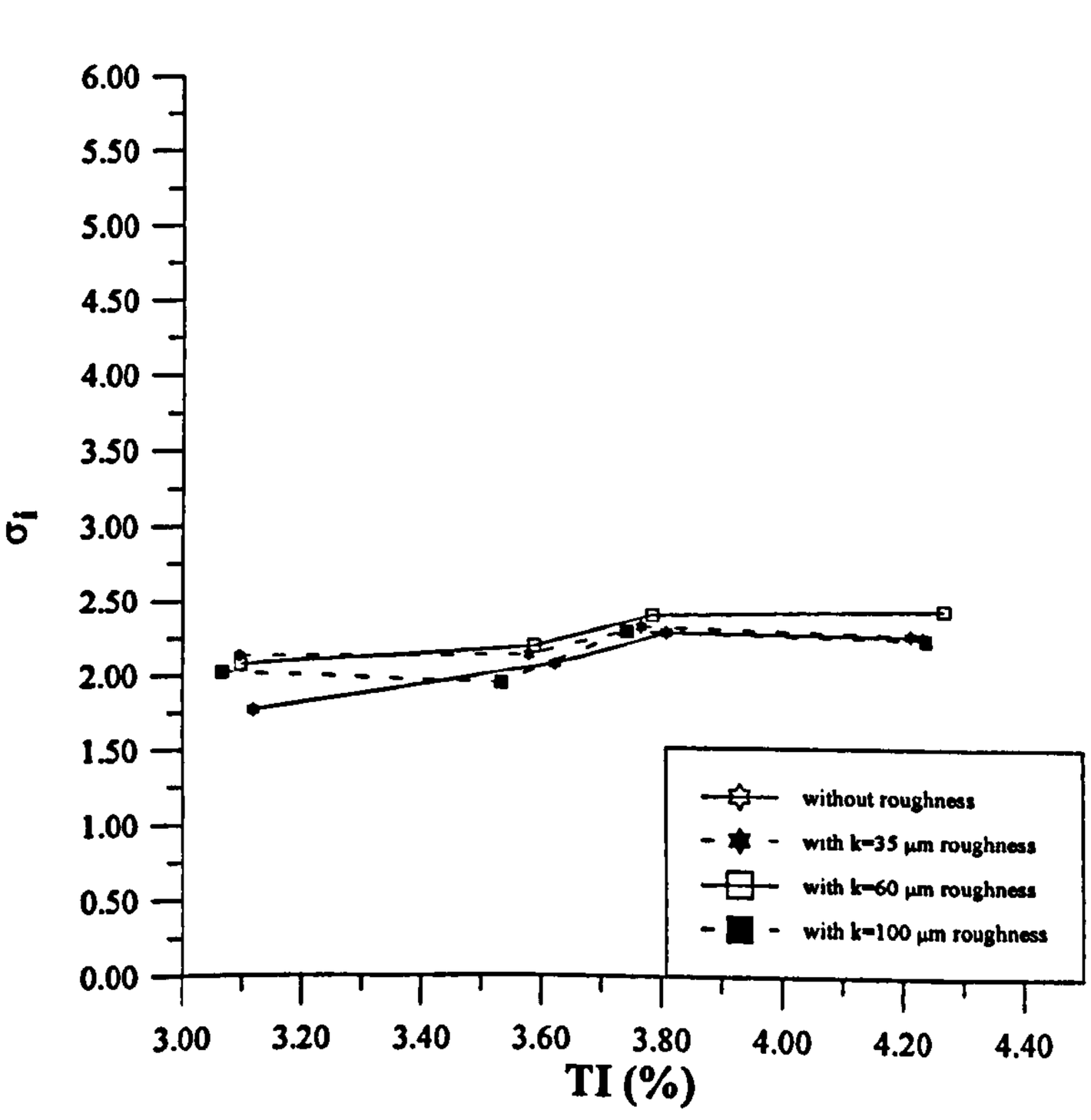

Figure 3.12 Comparison of the inception numbers of cavitation against varying level of free-stream turbulence for varying level of roughness of NACA foil at $\alpha = -2°$

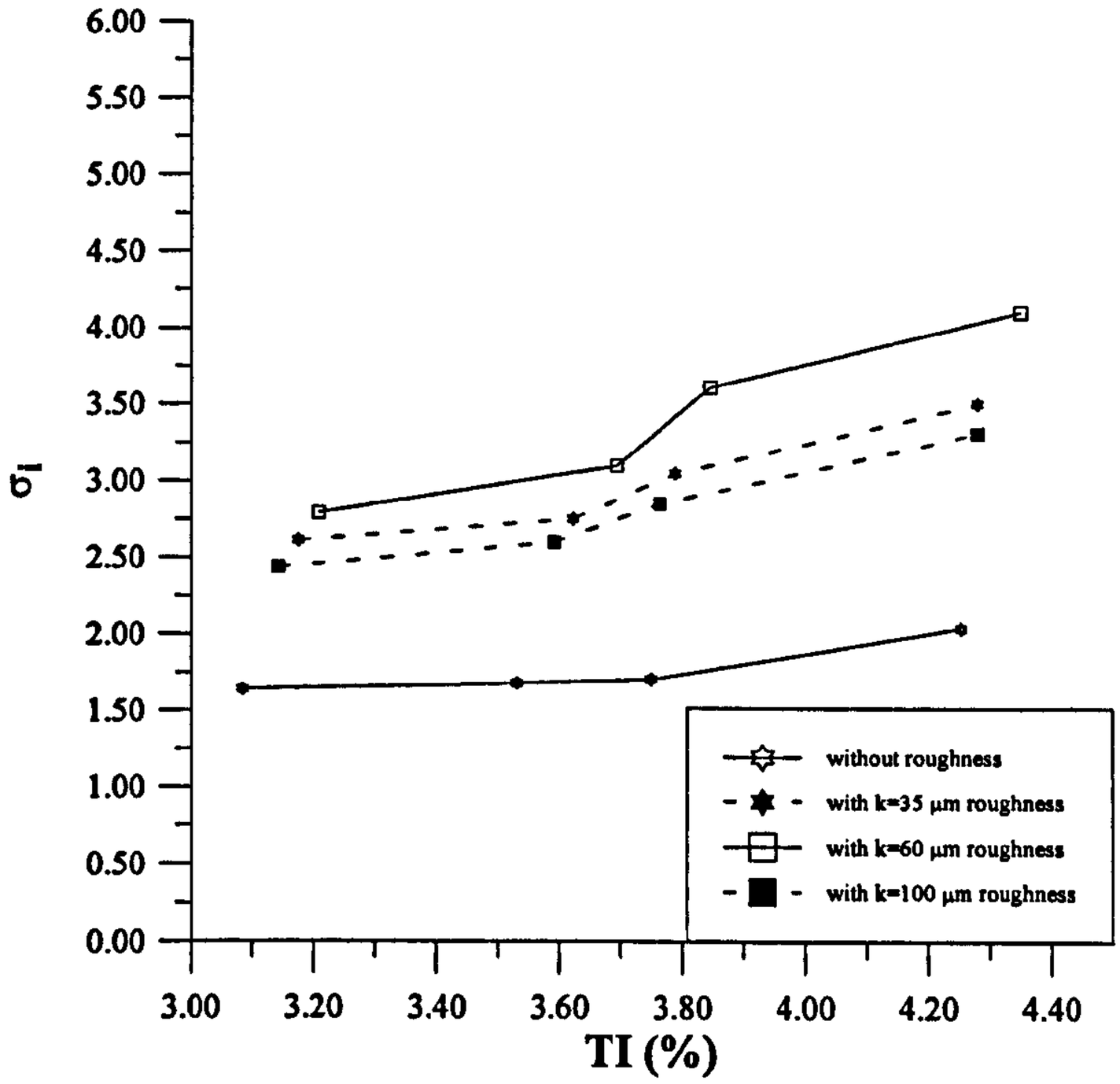

Figure 3.13 Comparison of the inception numbers of cavitation against varying level of free-stream turbulence for varying level of roughness of NACA foil at $\alpha = 5°$

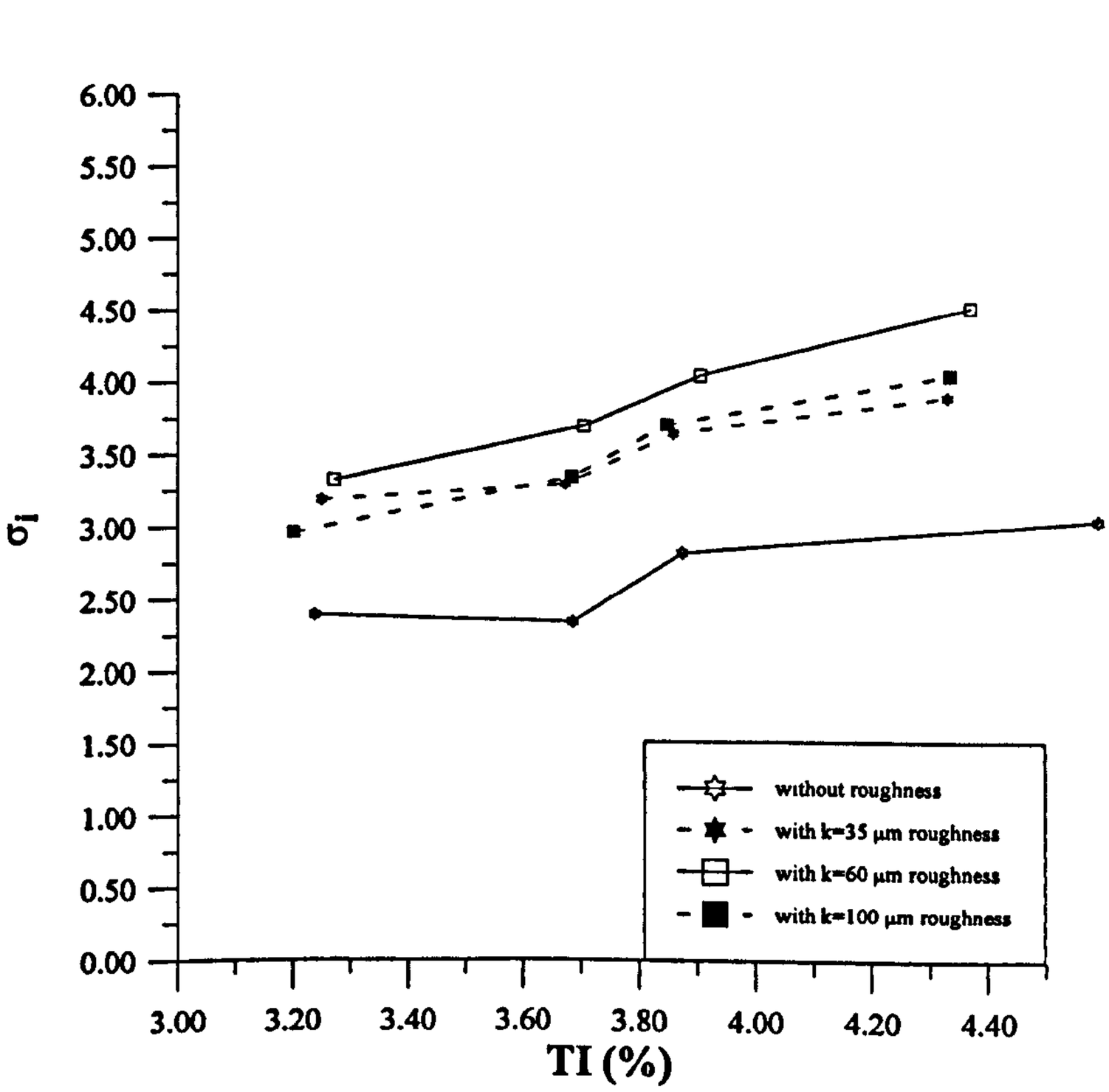

Figure 3.14 Comparison of the inception numbers of cavitation against varying level of free-stream turbulence for varying level of roughness of NACA foil at $\alpha = 6°$

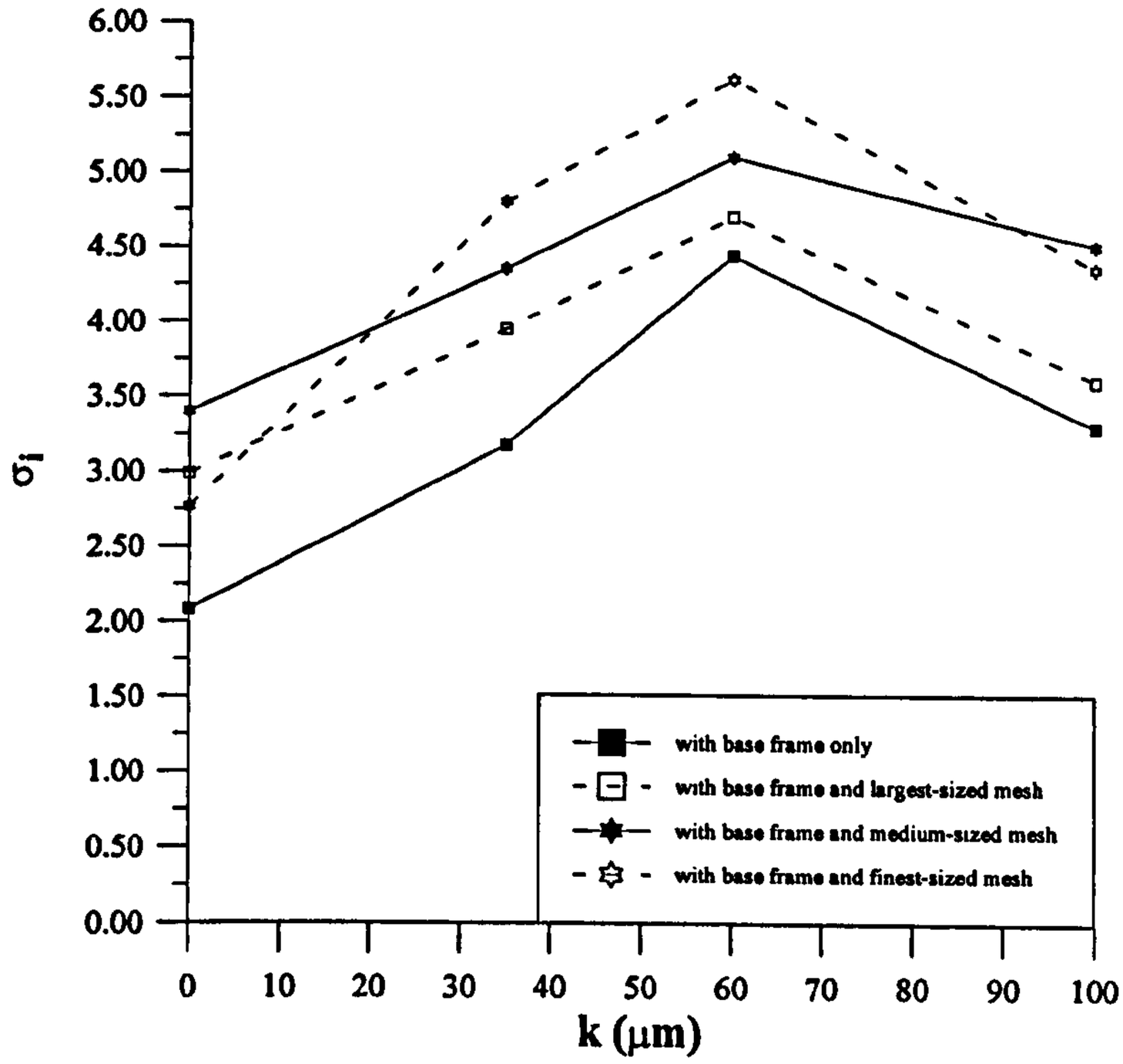

Figure 3.15 Comparison of the inception numbers of cavitation against varying level of roughness of NACA foil for varying level of free-stream turbulence at $\alpha = -4°$

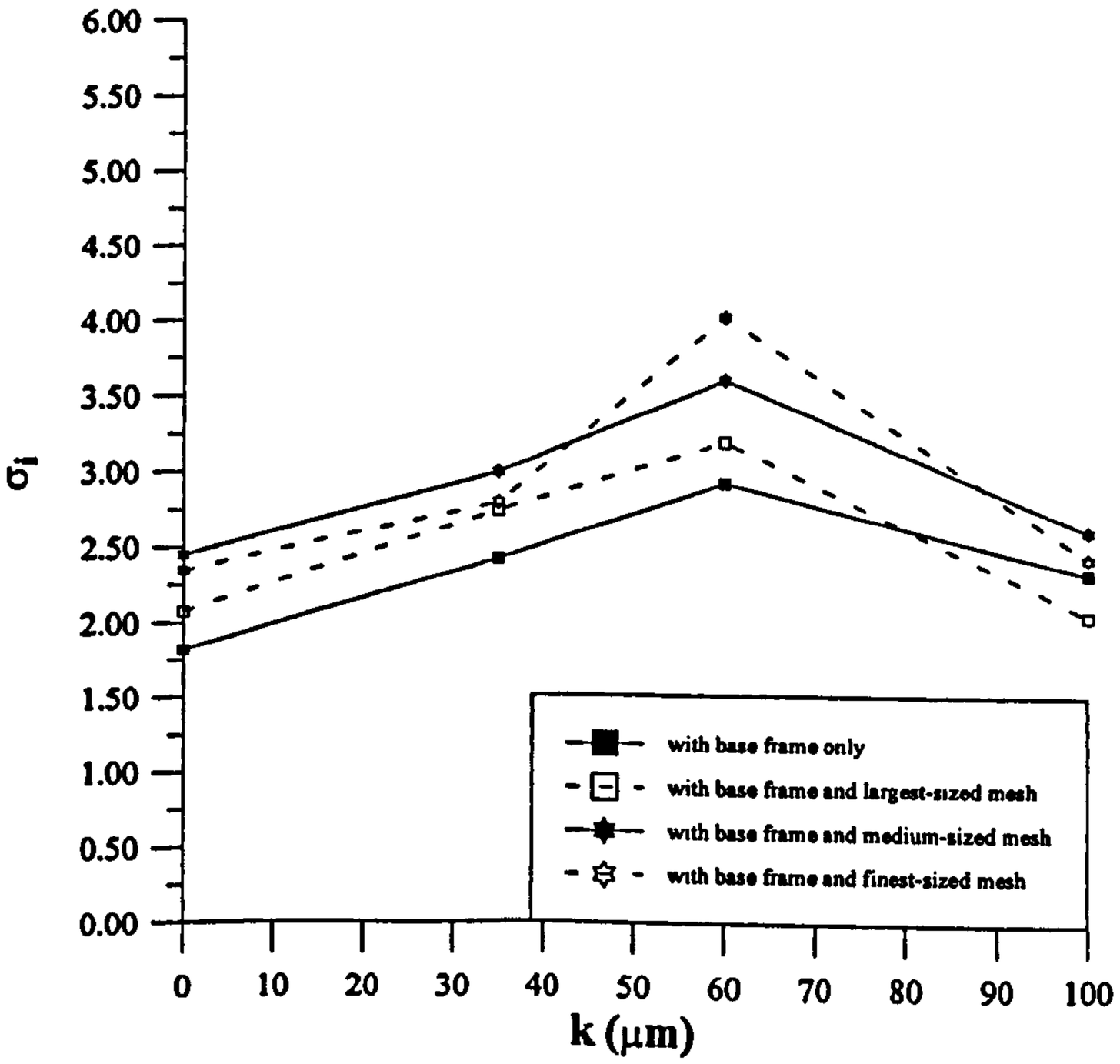

Figure 3.16 Comparison of the inception numbers of cavitation against varying level of roughness of NACA foil for varying level of free-stream turbulence at $\alpha = -3°$

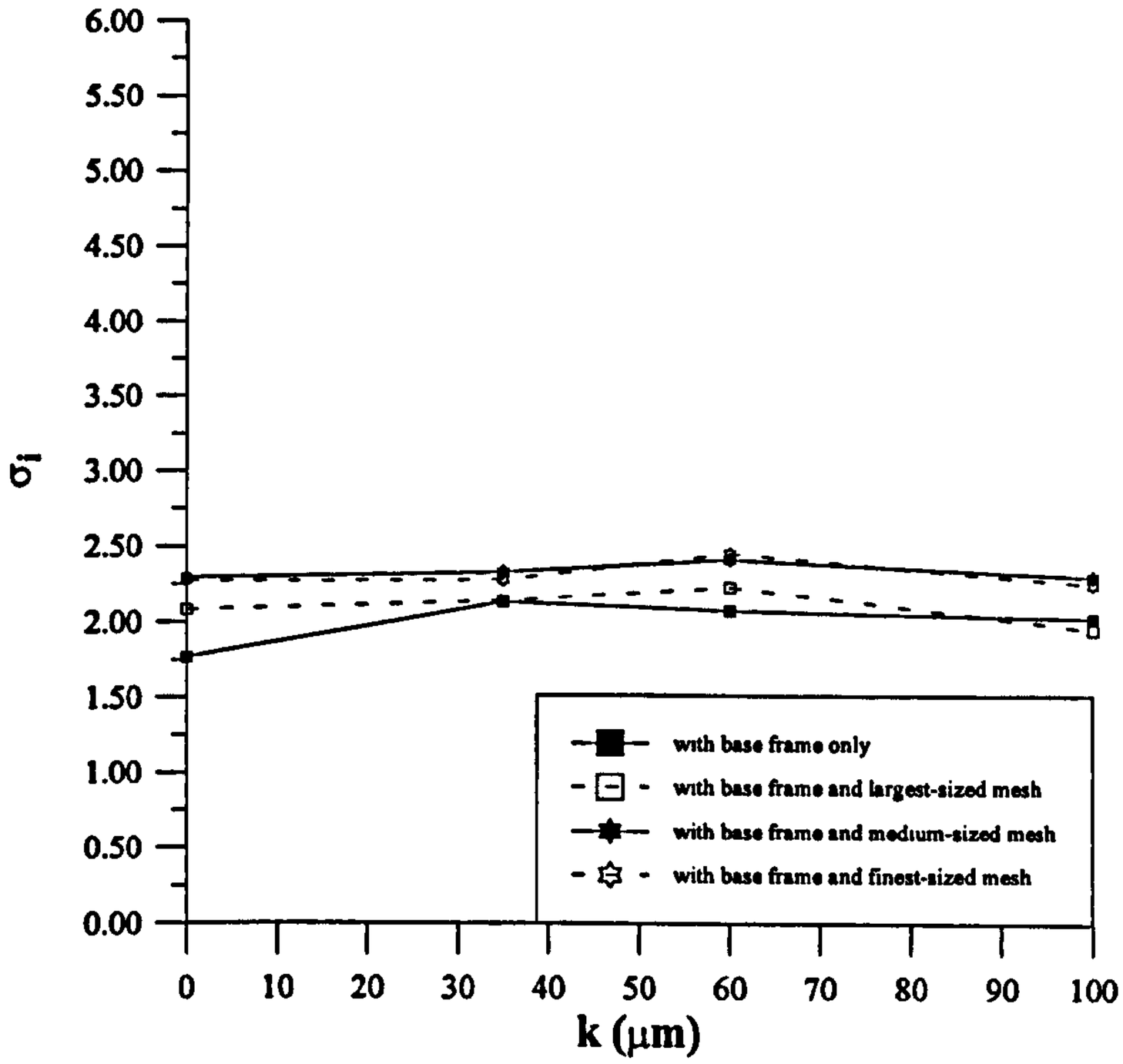

Figure 3.17 Comparison of the inception numbers of cavitation against varying level of roughness of NACA foil for varying level of free-stream turbulence at $\alpha = -2°$

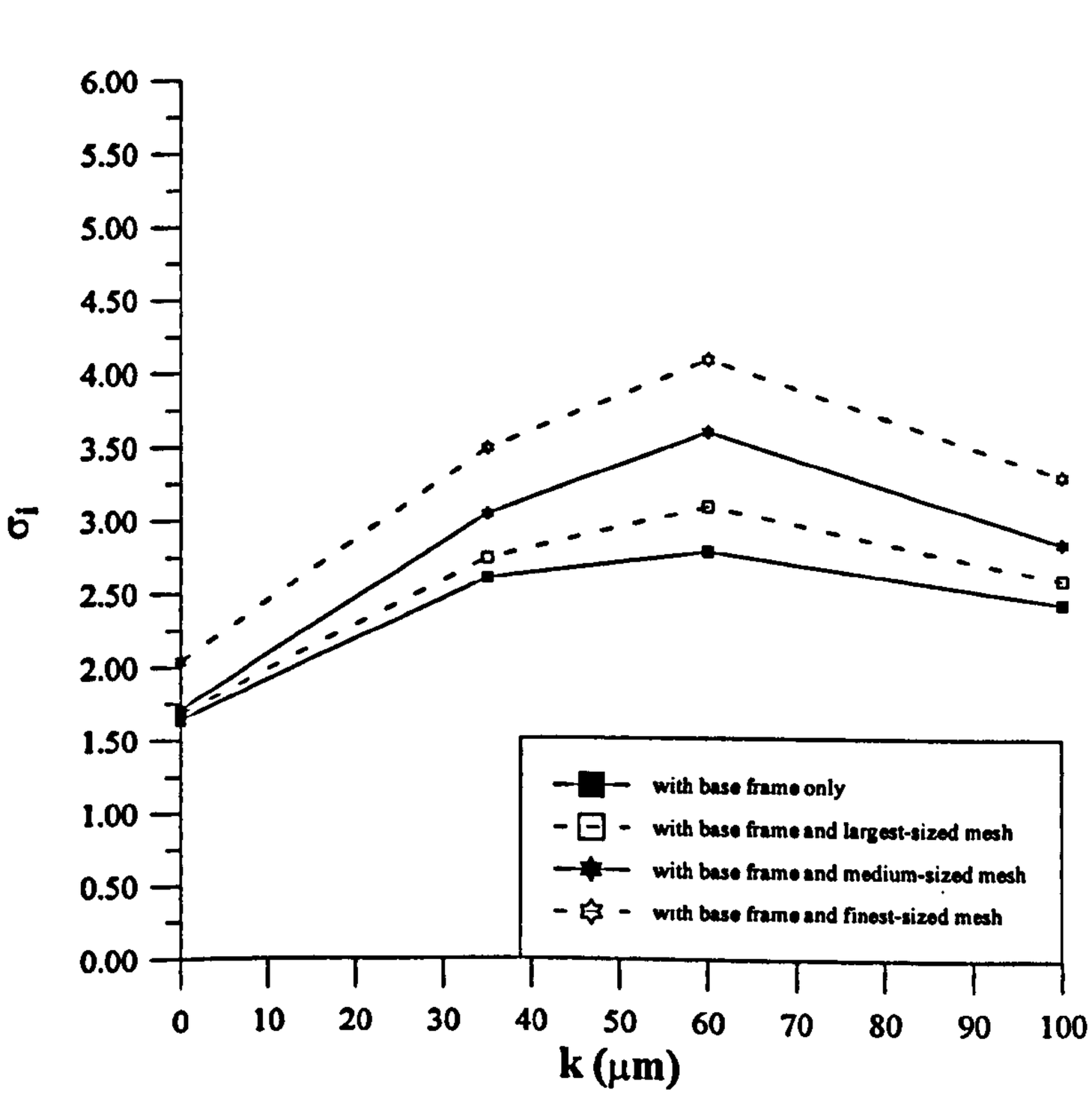

Figure 3.18 Comparison of the inception numbers of cavitation against varying level of roughness of NACA foil for varying level of free-stream turbulence at $\alpha = 5°$

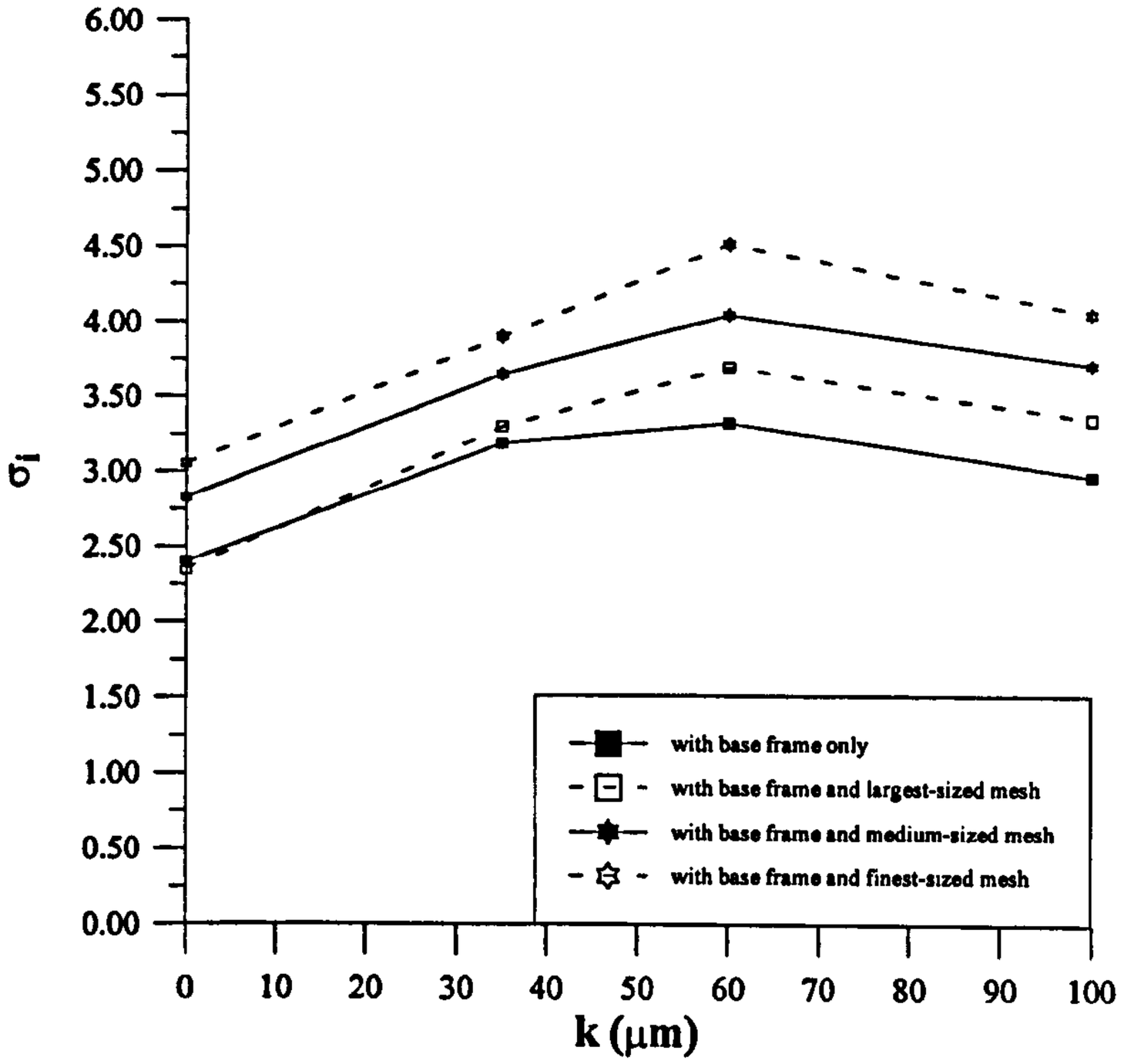

Figure 3.19 Comparison of the inception numbers of cavitation against varying level of roughness of NACA foil for varying level of free-stream turbulence at $\alpha = 6°$

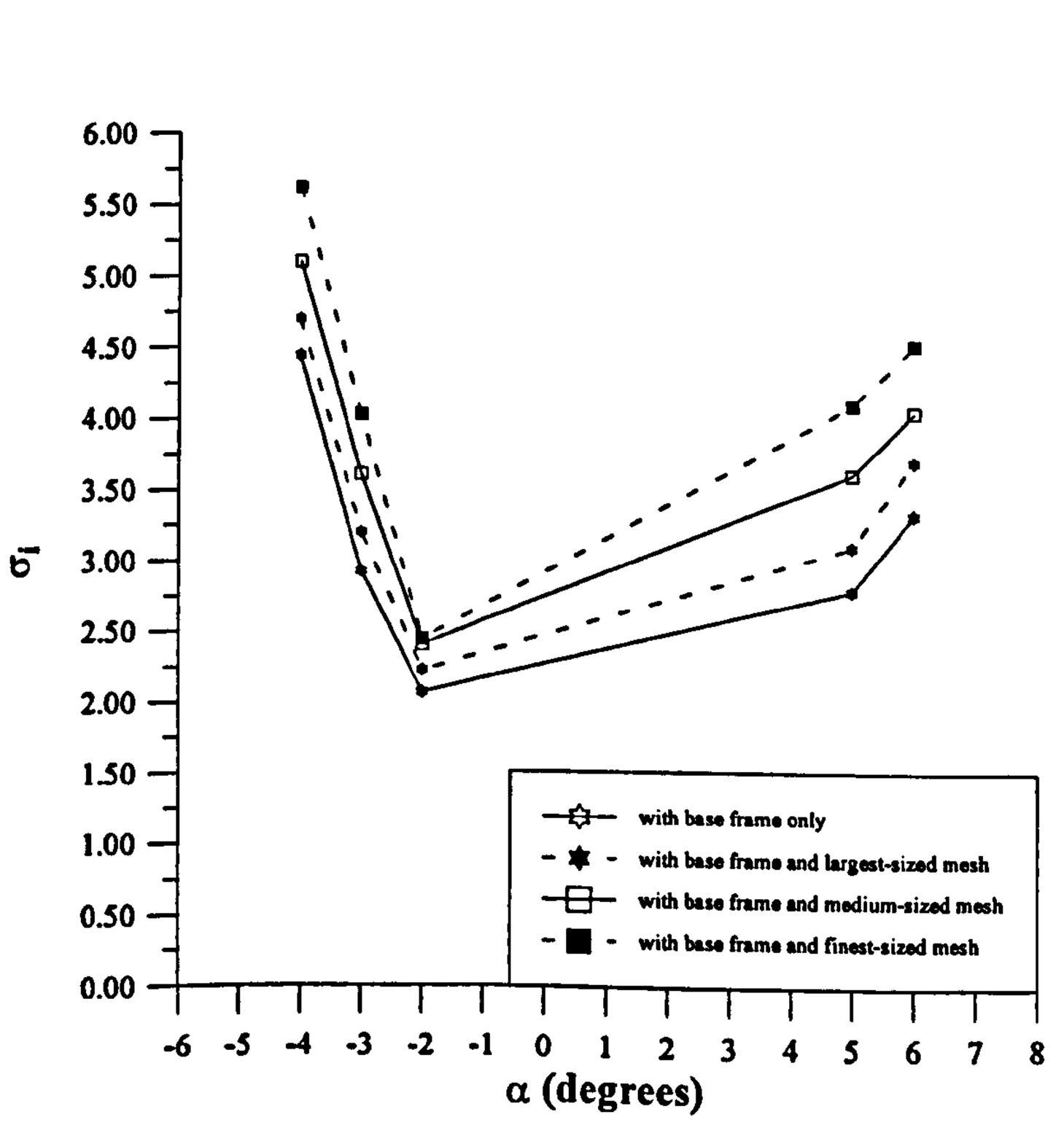

Figure 3.20 Comparison of typical cavitation numbers against varying angle of attack for varying level of free-stream turbulence at k = 60μm

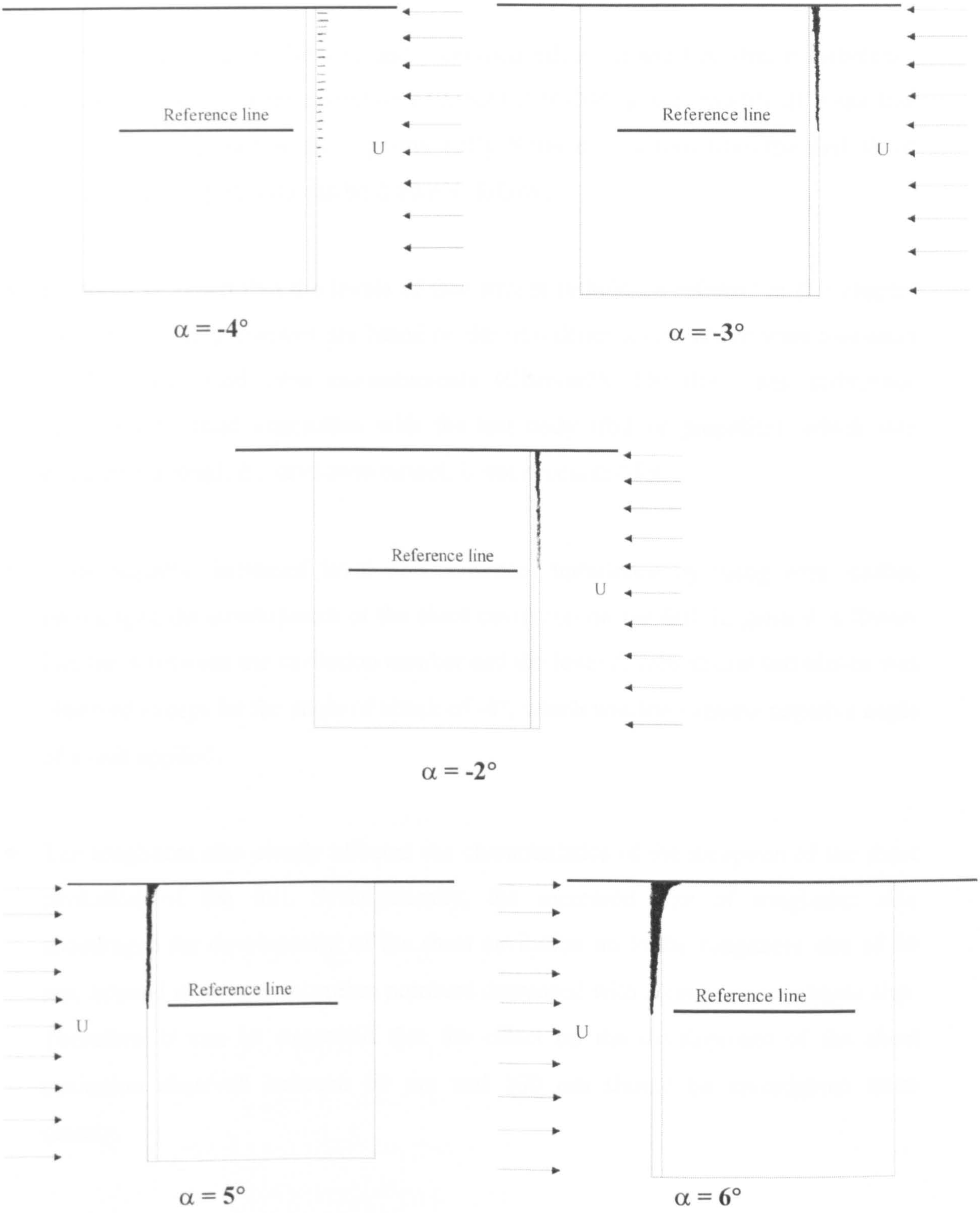

Figure 3.21 Cavitation pattern observed at each angle of attack tested

3.5 CONCLUSIONS

The investigation into the isolated and combined effects of the free-stream turbulence and roughness on the sheet cavitation of a NACA66-004, a=0.8 (modified) mean line foil section has been performed experimentally. Some conclusions from the analysis of the results of the experiment can be drawn as follows:

- It should be noted that the levels of free-stream turbulence referred in this chapter and the following chapters are based on the turbulence levels which were measured in the background flow measurements (Chapter2). Therefore, any turbulence generated by fluid interaction with the test body (foil or propeller), which was circulated through the cavitation tunnel, is not accounted for.

- Systematically, increased level of free-stream turbulence by using wire meshes encouraged the development of the sheet cavitation on the foil. In general, a linear-like trend between the cavitation number and the level of free-stream turbulence was observed except for the angle of attack of -4°, which was the extreme negative angle of attack applied.

- The roughness also clearly affected the characteristics of the inception of the sheet cavitation of the foil. Systematically, the increased size of roughness also encouraged the development of the sheet cavitation up to the roughness size of 60 μm, beyond which the inception numbers decreased with increasing roughness size. Therefore, it can be suggested that the effect on the development of the sheet cavitation observed between 60 μm and 100 μm should be investigated more closely.

- The effect of free-stream turbulence in combination with varying size of roughness showed the same trend for the sheet cavitation, indicating that the free-stream turbulence and roughness can also induce the sheet cavitation of the foil in the

combined case, and the roughness size of 100 μm may not be useful for the sheet cavitation to trip the boundary layer.

- The level of the free-stream turbulence and the roughness affected the boundary layer development and the wire meshes themselves may generate some nuclei to stimulate the cavitation process.

- The increase in the angle of attack (in either direction positive or negative) will result in increase in the inception of cavitation regardless of the level of the free-stream turbulence or roughness or both mechanisms in combination.

- The pattern of the sheet cavitation of the foil varied depending upon the angle of attack, hence whether it was a face or back cavitation. While the face cavitation appeared as flashes and streak type along the span, the back cavitation developed gradually from the top of the span and appeared as wedge shape.

- Because of the physical limitations, the foil was tested in vertical position. This restricted the investigations into the sheet cavitation only. However, if a complex system could be developed and the foil could be positioned horizontally an investigation into the tip vortex cavitation as well as into the noise characteristics could be carried out, provided that the speed and vacuum condition of the tunnel was sufficient. Therefore, the investigations on the tip vortex cavitation and noise were thought to be appropriate for the model propeller.

- The similar trend in the inception of cavitation with the varying levels of free-stream turbulence and roughness up to 60 μm may suggest that although the nature of the two mechanisms may be different, there could be interesting correlation in terms of their effects on the inception of cavitation which should be explored.

CHAPTER 4 MEASUREMENTS OF THE INCEPTION OF CAVITATION WITH ECT103 MODEL PROPELLER

4.1 INTRODUCTION

Following the tests with the foil section described in Chapter 3, the next stage of the research work was to perform the similar measurements with a model propeller in the cavitation tunnel. However, this time the scope of the investigation was much wider including two types of cavitation patterns, which were tip vortex and sheet cavitation, as well as the effect of the dissolved gas content. The investigation into the tip vortex and the effects of the dissolved gas content could not be included in the foil measurements due to the physical restrictions discussed in the earlier chapter.

Therefore, the main objective of this chapter was to explore the effects of the free-stream turbulence, roughness and dissolved gas content on the inception of cavitation of a propeller as well as quantifying these effects. As stated earlier in the layout of the research (Section 1.3.3), the information obtained from these measurements will be used to derive a semi-empirical relationship to predict the inception of cavitation, based upon a theoretical analysis to be carried out in Chapter 6.

In this chapter, the measurements of the inception of cavitation of a Meridian type model propeller were performed for the phases of cavitation from tip vortex to sheet cavitation at varying levels of dissolved gas content in four groups:

- The first group was the inception measurements with the propeller in the free flow.
- The second group was to explore the effect of free-stream turbulence on the inception of cavitation by using the earlier described turbulence generator.

- The third group involved the measurements of the inception of cavitation of the propeller with varying level of blade roughness in the free flow.
- The fourth and last group of the experiments was to explore the combined effects of the free-stream turbulence and roughness on the cavitation, which also involved the measurements of the inception by combining the former two groups of the experiments.

The remaining part of this chapter describes the details of the model propeller used, test conditions and experimental set-up, measurements, presentation of the results, analyses and conclusions. Although full information on these tests can be found in (Korkut, 1997b), appropriate details of the experiments are presented in this chapter.

4.2 CHARACTERISTICS OF MODEL PROPELLER ECT103

The model propeller used in the experiments of inception of cavitation was a 5 bladed, right-handed Meridian type of propeller made from Manganese-Bronze, ECT103. The reason for selecting this propeller was that it was already available in the cavitation tunnel and represented a current state-of-the-art commercial ship propeller. The propeller had moderately-skewed blades. A general view of the propeller is shown in Figure 4.1. Table 4.1 shows the main particulars of the propeller while Figure 4.2, Tables 4.2 and 4.3 show the definition of the main parameters of a blade section, radial details and offset data of a blade respectively.

Table 4.1 Main particulars of test propeller

Main Particulars	
Diameter, D, (mm)	240.00
Mean pitch, P_m, (mm)	220.00
Expanded surface area, A_E, (m^2)	0.0325
Blade area ratio, B.A.R.	0.73
Pitch to diameter ratio, P/D	0.91
Maximum chord length, c_{max}, (mm)	79.00
Number of blades, Z	5
Direction of rotation	Right hand
Material	Manganese Bronze

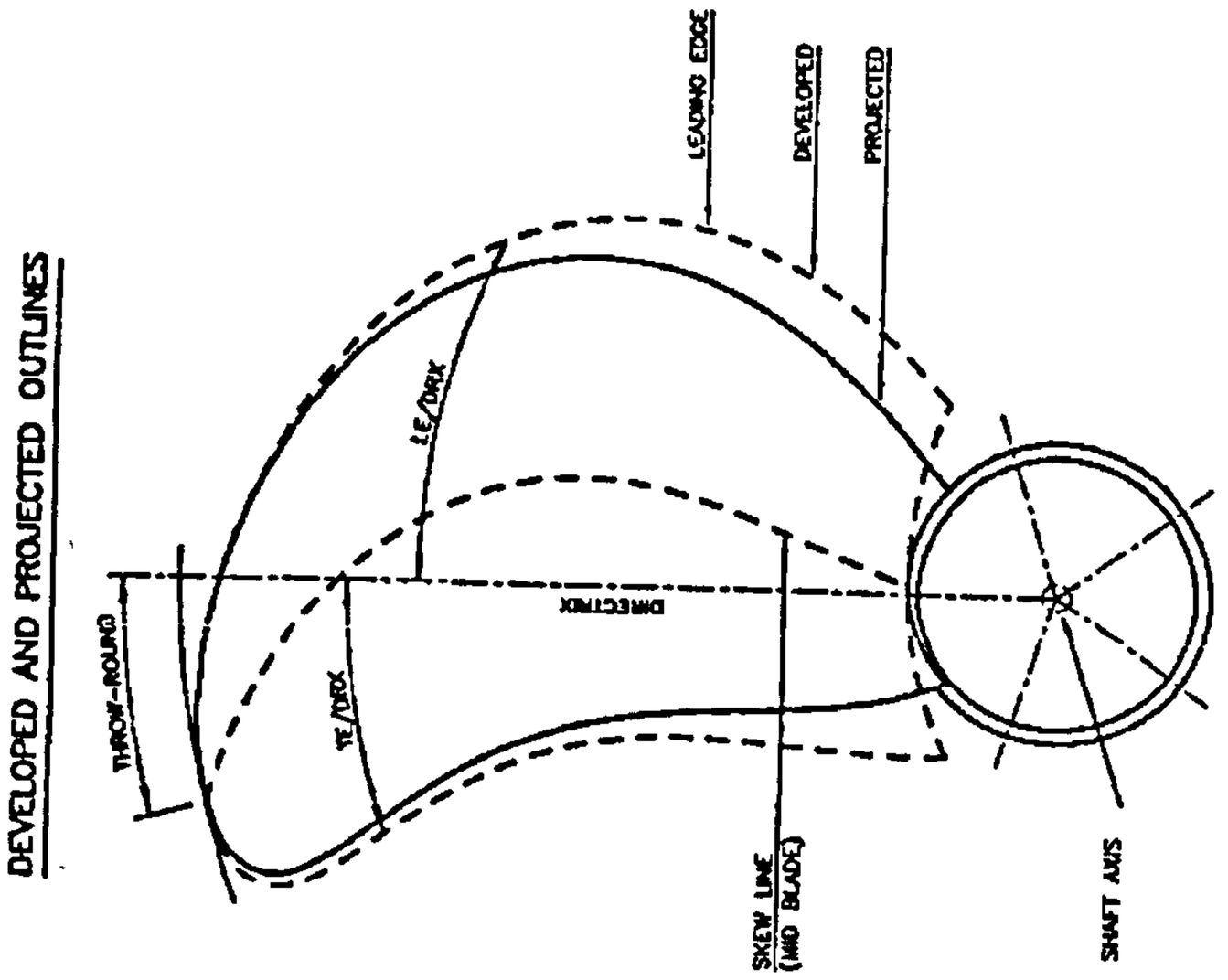

Figure 4.1 General view of propeller

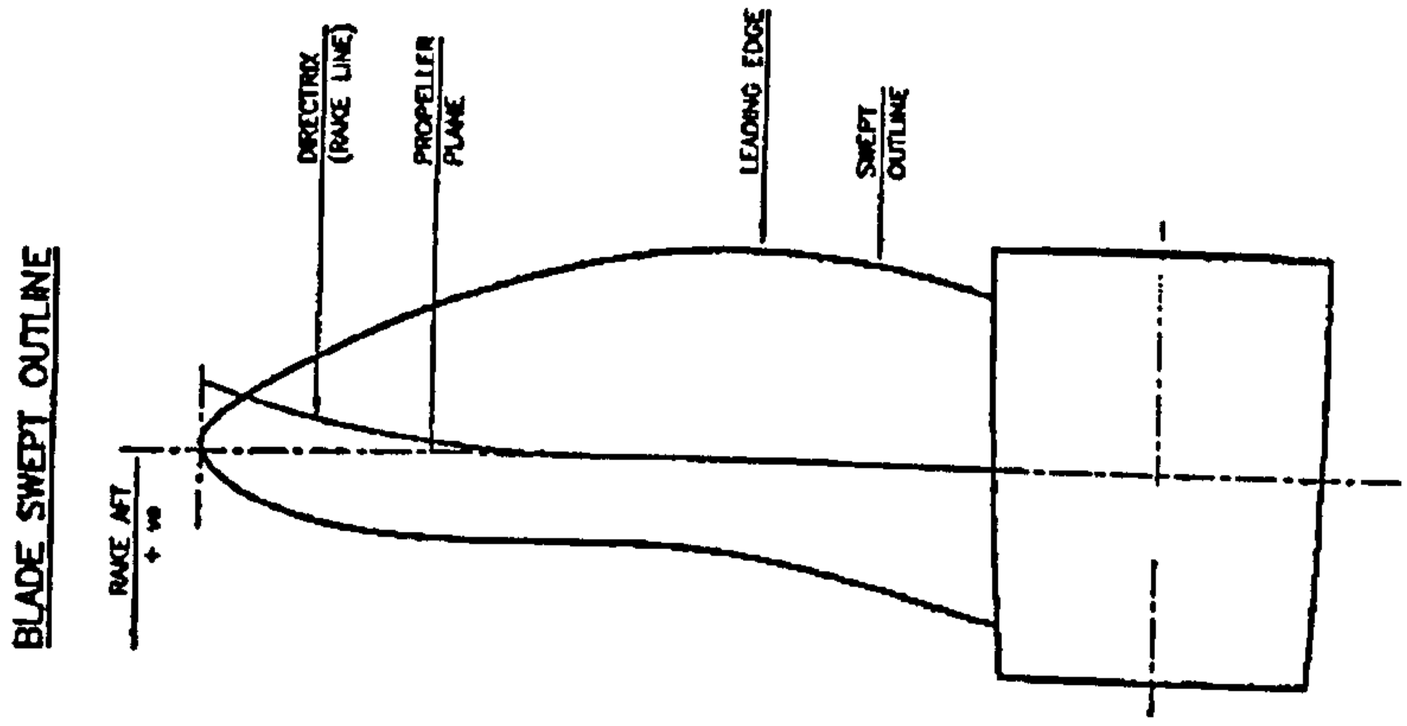

Table 4.2 Radial details of a blade of model propeller

Non-Dim. Radius	Radius (mm)	Pitch (mm)	Pitch Angle (deg)	TE/ DRX (mm)	LE/ DRX (mm)	Total Width (mm)	TE/ MaxT (mm)	Mid-Blade/ Max T (mm)	DRX/ Max T (mm)	Basic Max T (mm)	Actual T (mm)	Design Rake (mm)	Rake from Origin (mm)	Skew-Back (mm)	Skew Angle (deg)
1.0000	120.00	186.68	13.91	32.36	-32.36	0.00	0.00	0.00	32.36	0.48	0.33	-8.73	-8.73	32.36	15.00
0.9875	118.50	190.94	14.39	41.34	-17.42	23.92	11.96	0.00	29.38	0.57	0.49	-8.23	-8.23	29.38	13.76
0.9750	117.00	194.50	14.82	43.31	-9.75	33.56	16.78	0.00	26.53	0.66	0.63	-7.69	-7.69	26.53	12.56
0.9500	114.00	201.62	15.72	44.37	2.10	46.47	23.24	0.00	21.14	0.85	0.85	-6.67	-6.67	21.14	10.23
0.9250	111.00	207.74	16.59	43.93	11.53	55.46	27.73	0.00	16.20	1.05	1.05	-5.73	-5.73	16.20	8.01
0.9000	108.00	212.69	17.40	42.75	19.42	62.17	31.08	0.00	11.66	1.25	1.25	-4.87	-4.87	11.66	5.91
0.8000	96.00	226.36	20.57	35.67	40.54	76.21	38.10	0.00	-2.43	2.14	2.14	-2.14	-2.14	-2.43	-1.36
0.7000	84.00	232.47	23.77	28.73	50.39	79.12	39.56	0.00	-10.83	3.12	3.12	-0.53	-0.53	-10.83	-6.76
0.6000	72.00	232.39	27.19	23.92	52.90	76.82	38.41	0.00	-14.49	4.22	4.22	0.00	0.00	-14.49	-10.26
0.5000	60.00	226.90	31.04	21.71	50.54	72.25	36.13	0.00	-14.41	5.40	5.40	0.00	0.00	-14.41	-11.79
0.4000	48.00	215.52	35.55	21.78	45.06	66.84	33.87	0.45	-12.09	6.68	6.68	0.00	0.00	-11.64	-11.30
0.3000	36.00	200.85	41.61	23.07	37.66	60.73	31.99	1.62	-8.92	8.04	8.23	0.00	0.00	-7.30	-8.69
0.2500	30.00	193.00	45.68	23.67	33.47	57.14	30.96	2.38	-7.28	8.75	9.27	0.00	0.00	-4.90	-6.54
0.2000	24.00	184.63	50.76	23.96	28.98	52.94	29.65	3.17	-5.69	9.48	10.50	0.00	0.00	-2.51	-3.79

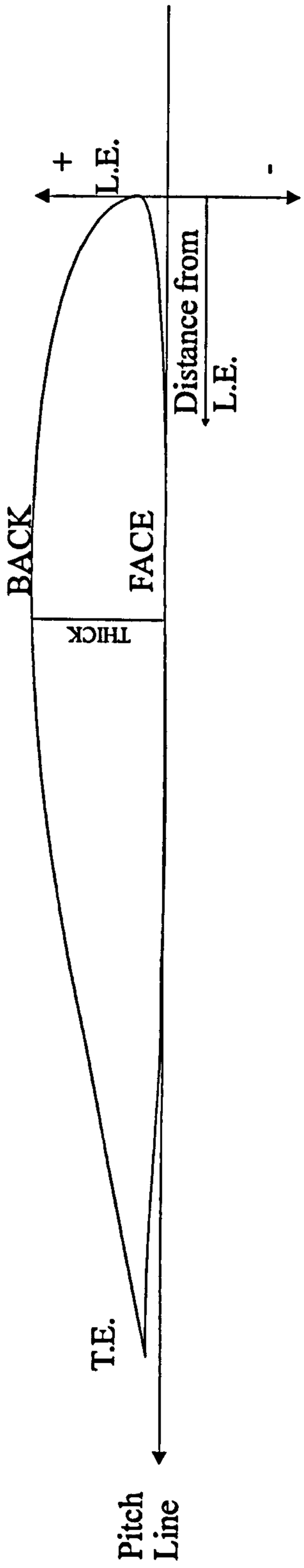

Figure 4.2 Definition of main parameters of a typical blade section of model propeller

Table 4.3 Offset data of a blade of model propeller

Radius (mm) (Non-Dim.)		L.E.	Percentage Distance from Leading Edge											T.E.
		0.00	2.50	5.00	10.00	20.00	30.00	40.00	50.00	60.00	70.00	80.00	90.00	95.00	100.00
120.00	Face	0.000	0.000	0.000	0.000	0.000	0.000	0.000	0.000	0.000	0.000	0.000	0.000	0.000	0.000
	Thick	0.329	0.329	0.329	0.329	0.329	0.329	0.329	0.329	0.329	0.329	0.329	0.329	0.329	0.329
(1.0000)	Back	0.329	0.329	0.329	0.329	0.329	0.329	0.329	0.329	0.329	0.329	0.329	0.329	0.329	0.329
118.50	Face	0.000	0.008	0.015	0.031	0.058	0.077	0.089	0.097	0.093	0.085	0.066	0.039	0.023	0.000
	Thick	0.329	0.344	0.360	0.387	0.437	0.472	0.484	0.488	0.484	0.461	0.434	0.387	0.360	0.333
(0.9875)	Back	0.329	0.352	0.375	0.418	0.495	0.550	0.573	0.584	0.577	0.546	0.499	0.426	0.383	0.333
117.00	Face	0.000	0.012	0.027	0.050	0.101	0.139	0.163	0.174	0.170	0.151	0.120	0.070	0.035	0.000
	Thick	0.329	0.364	0.391	0.441	0.515	0.573	0.615	0.627	0.615	0.581	0.523	0.441	0.395	0.341
(0.9750)	Back	0.329	0.375	0.418	0.492	0.615	0.712	0.778	0.801	0.786	0.732	0.643	0.511	0.430	0.341
114.00	Face	0.000	0.019	0.042	0.081	0.163	0.224	0.267	0.286	0.283	0.252	0.197	0.116	0.062	0.000
	Thick	0.329	0.368	0.410	0.492	0.635	0.751	0.824	0.852	0.828	0.759	0.650	0.519	0.441	0.356
(0.9500)	Back	0.329	0.387	0.453	0.573	0.797	0.975	1.092	1.138	1.111	1.010	0.848	0.635	0.503	0.356
111.00	Face	0.000	0.023	0.046	0.089	0.182	0.259	0.314	0.341	0.337	0.298	0.232	0.135	0.070	0.000
	Thick	0.329	0.379	0.441	0.557	0.759	0.913	1.010	1.045	1.014	0.921	0.778	0.592	0.484	0.375
(0.9250)	Back	0.329	0.403	0.488	0.646	0.941	1.173	1.324	1.386	1.351	1.219	1.010	0.728	0.554	0.375
108.00	Face	0.000	0.019	0.039	0.085	0.178	0.263	0.325	0.356	0.356	0.317	0.248	0.143	0.074	0.000
	Thick	0.329	0.414	0.495	0.646	0.902	1.092	1.212	1.250	1.212	1.099	0.921	0.685	0.546	0.395
(0.9000)	Back	0.329	0.434	0.534	0.732	1.080	1.355	1.537	1.606	1.568	1.417	1.169	0.828	0.619	0.395
96.00	Face	0.000	0.000	0.008	0.031	0.112	0.209	0.294	0.352	0.372	0.341	0.271	0.155	0.085	0.000
	Thick	0.372	0.550	0.719	1.026	1.525	1.870	2.071	2.137	2.063	1.854	1.509	1.041	0.763	0.457
(0.8000)	Back	0.372	0.550	0.728	1.057	1.637	2.079	2.365	2.489	2.435	2.195	1.780	1.196	0.848	0.457
84.00	Face	0.070	0.039	0.019	0.000	0.031	0.112	0.201	0.275	0.306	0.294	0.240	0.139	0.074	0.000
	Thick	0.441	0.728	0.991	1.471	2.229	2.744	3.031	3.124	3.015	2.690	2.164	1.432	0.995	0.507
(0.7000)	Back	0.511	0.766	1.010	1.471	2.260	2.857	3.232	3.398	3.321	2.984	2.404	1.571	1.068	0.507
72.00	Face	0.263	0.194	0.135	0.054	0.000	0.039	0.116	0.182	0.221	0.221	0.178	0.105	0.058	0.000
	Thick	0.554	0.956	1.328	1.997	3.038	3.724	4.103	4.219	4.068	3.623	2.884	1.854	1.235	0.542
(0.6000)	Back	0.817	1.150	1.463	2.051	3.038	3.762	4.219	4.401	4.289	3.844	3.062	1.959	1.293	0.542
60.00	Face	0.550	0.434	0.333	0.178	0.023	0.004	0.046	0.093	0.120	0.124	0.100	0.058	0.031	0.000
	Thick	0.701	1.223	1.707	2.574	3.913	4.788	5.260	5.403	5.210	4.629	3.662	2.306	1.486	0.565
(0.5000)	Back	1.250	1.657	2.039	2.752	3.936	4.792	5.307	5.496	5.330	4.753	3.762	2.365	1.517	0.565
48.00	Face	0.913	0.751	0.608	0.379	0.112	0.012	0.004	0.019	0.031	0.035	0.027	0.012	0.004	0.000
	Thick	0.859	1.498	2.094	3.162	4.822	5.918	6.514	6.681	6.418	5.682	4.467	2.768	1.734	0.577
(0.400)	Back	1.773	2.249	2.702	3.542	4.935	5.930	6.518	6.700	6.448	5.717	4.494	2.779	1.738	0.577

Table 4.3 (continued)

Radius (mm) (Non-Dim.)		L.E.	Percentage Distance from Leading Edge											T.E.
		0.00	2.50	5.00	10.00	20.00	30.00	40.00	50.00	60.00	70.00	80.00	90.00	95.00	100.00
36.00	Face	1.324	1.122	0.941	0.631	0.213	0.000	-0.081	-0.085	-0.066	-0.058	-0.046	-0.035	-0.023	-0.008
	Thick	1.049	1.808	2.528	3.824	5.899	7.304	8.066	8.206	7.803	6.859	5.349	3.271	2.009	0.592
(0.3000)	Back	2.373	2.930	3.468	4.455	6.112	7.304	7.985	8.121	7.737	6.801	5.303	3.236	1.986	0.584
30.00	Face	1.498	1.270	1.061	0.701	0.182	-0.120	-0.252	-0.236	-0.201	-0.173	-0.139	-0.089	-0.058	-0.015
	Thick	1.177	2.009	2.795	4.246	6.615	8.256	9.127	9.220	8.705	7.614	5.910	3.588	2.183	0.615
(0.2500)	Back	2.675	3.278	3.855	4.947	6.797	8.136	8.875	8.984	8.504	7.443	5.771	3.450	2.125	0.600
24.00	Face	1.630	1.378	1.146	0.720	0.070	-0.341	-0.503	-0.453	-0.383	-0.321	-0.252	-0.159	-0.101	-0.031
	Thick	1.328	2.241	3.120	4.761	7.509	9.437	10.412	10.397	9.742	8.469	6.545	3.948	2.384	0.643
(0.2000)	Back	2.957	3.619	4.265	5.481	7.579	9.097	9.909	9.944	9.359	8.148	6.294	3.789	2.284	0.612

4.3 TEST CONDITIONS AND EXPERIMENTAL SET-UP

Experiments were carried out in the Emerson Cavitation Tunnel and involved four groups of measurements of the inception of cavitation with the earlier defined model propeller at two different levels of dissolved gas content.

- The first group was the inception measurements with the model propeller in the free flow.
- The second group was the inception measurements with the model propeller behind the turbulence generator of various sizes of the wire mesh screens, which was described in Chapter 2.
- The third group consisted of the measurements of the inception of cavitation with the same propeller having varying levels of roughness on the leading edge of its blades.
- The fourth and last group was involved the inception measurements under the combined effects of the free-stream turbulence and roughness.

The results of the first and second group tests were reported by the Author in (Korkut et al., 1998). A summary of the test conditions is given in Table 4.4.

Table 4.4 Summary of the conditions of cavitation inception tests

Test No	Test Condition	Test Condition Details
1	In the free flow	Test with base frame only for 4 phases of cavitation at two levels of dissolved gas content
2	In the presence of turbulence generator	Test with base frame and largest-sized mesh for 4 phases of cavitation at two levels of dissolved gas content
3		Test with base frame and medium-sized mesh for 4 phases of cavitation at two levels of dissolved gas content
4		Test with base frame and finest-sized mesh for 4 phases of cavitation at two levels of dissolved gas content
5	In the presence of blade roughness	Test with base frame and 35 μm roughness for 4 phases of cavitation at two levels of dissolved gas content
6		Test with base frame and 60 μm roughness for 4 phases of cavitation at two levels of dissolved gas content
7		Test with base frame and 100 μm roughness for 4 phases of cavitation at two levels of dissolved gas content
8	In the presence of turbulence generator and blade roughness	Test with base frame, 35 μm roughness and largest-sized mesh for 4 phases of cavitation at two levels of dissolved gas content
9		Test with base frame, 35 μm roughness and finest-sized mesh for 4 phases of cavitation at two levels of dissolved gas content
10		Test with base frame, 60 μm roughness and largest-sized mesh for 4 phases of cavitation at two levels of dissolved gas content
11		Test with base frame, 60 μm roughness and finest-sized mesh for 4 phases of cavitation at two levels of dissolved gas content

The model propeller was driven by Kempf & Remmers H33 propeller dynamometer with the boat-house being in the downstream of the propeller. During the tests, the same base frame was used, as shown in Figure 2.1 of Chapter 2. The frame was placed at a distance of 0.827 m, which was approximately 3.45 times the diameter of propeller, at the upstream of the propeller to mount the wire mesh screens. The mesh area, which was 0.350 m by 0.380 m (BxH), covered the entire working area of the propeller with a comfortable margin. The cell sizes of the meshes are given in Table 2.1 of Chapter 2.

In order to investigate the effect of roughness, carborundum was used as a roughness element. The roughness was glued over an area with a length which was equal to 4 percentage of the maximum chord length of the each blade from the leading edge on both face and back sides of the blades by an adhesive resin. The adhesive used was AY103 Araldite Epoxy Resin with HY956 Hardener, in the ratio of 100 parts araldite to 18 parts hardener. The application procedure of the roughness to the propeller blades was the same as to the foil, which was described in Chapter 3. However, this time the propeller was placed in an oven at 100 °C for approximately 1-2 hours to dry the cure

resin. The sizes of roughness heights used were also the same as for the foil, which are given in Table 3.4 of Chapter 3.

The procedure for the inception tests was such that the tunnel flow velocity, U, was always kept at U = 4 m/s while the tunnel static pressure was adjusted to a required constant value at each test condition. Then the rotational speed of the propeller was initially increased until a visual appearance of the tip vortex cavitation was observed. The rotational speed was then decreased until the tip vortex cavitation was just flushing at the tip of the propeller. This point was accepted as the onset of

- **"unattached tip vortex cavitation".**

In addition to the above described cavitation phase, three more phases of the cavitation were observed and corresponding inception numbers were recorded. These were identified as:

- the tip vortex cavitation was **"attached to the one blade only"**
- the tip vortex cavitation was **"fully attached to all blades"**
- the **"sheet cavitation"** was allowed to spread up to 0.8R from the tip of the blade.

The former two cases were associated with the stage for the transition from the unattached tip vortex cavitation to the sheet cavitation while the third case was associated with the stage for the sheet cavitation. For the extent of the sheet cavitation, a laser pointer was attached to the observation window at side to mark 0.8R position on the top blade precisely. The observations were made by eye and three readings for each inception point were taken and averaged to improve the accuracy of the inception results. The propeller was illuminated by two stroboscope lights to freeze the image of the cavitation developed on the rotating propeller. The above defined phases of the cavitation are described by the sketches as shown in Figures 4.3 through 4.6.

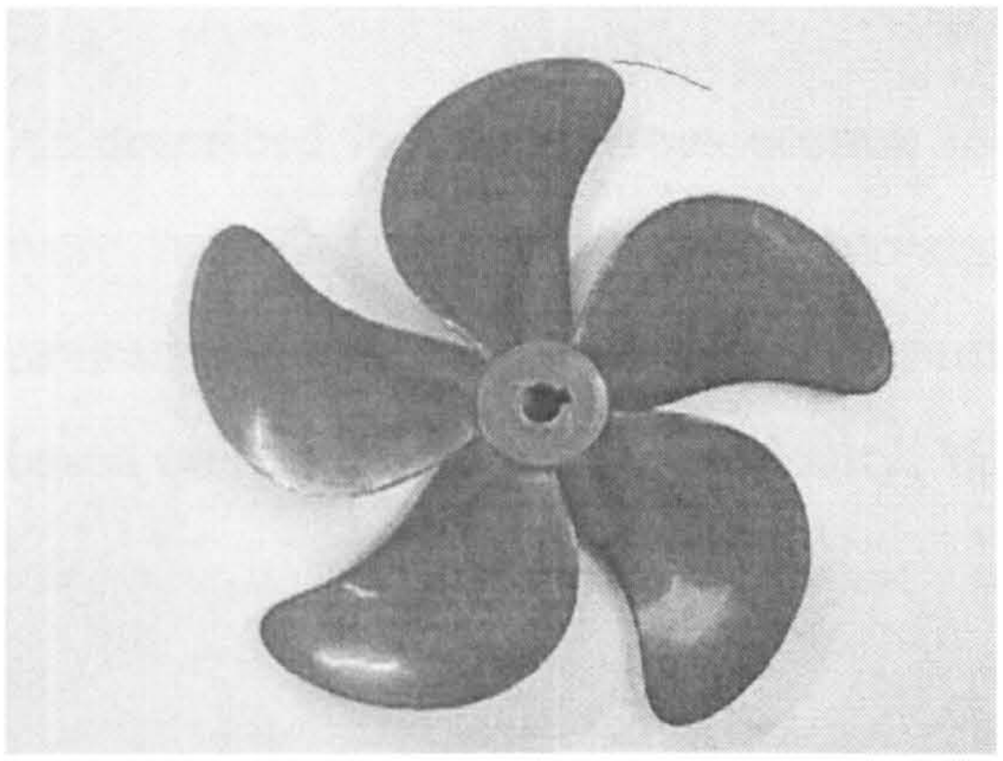

Figure 4.3 Typical unattached tip vortex cavitation

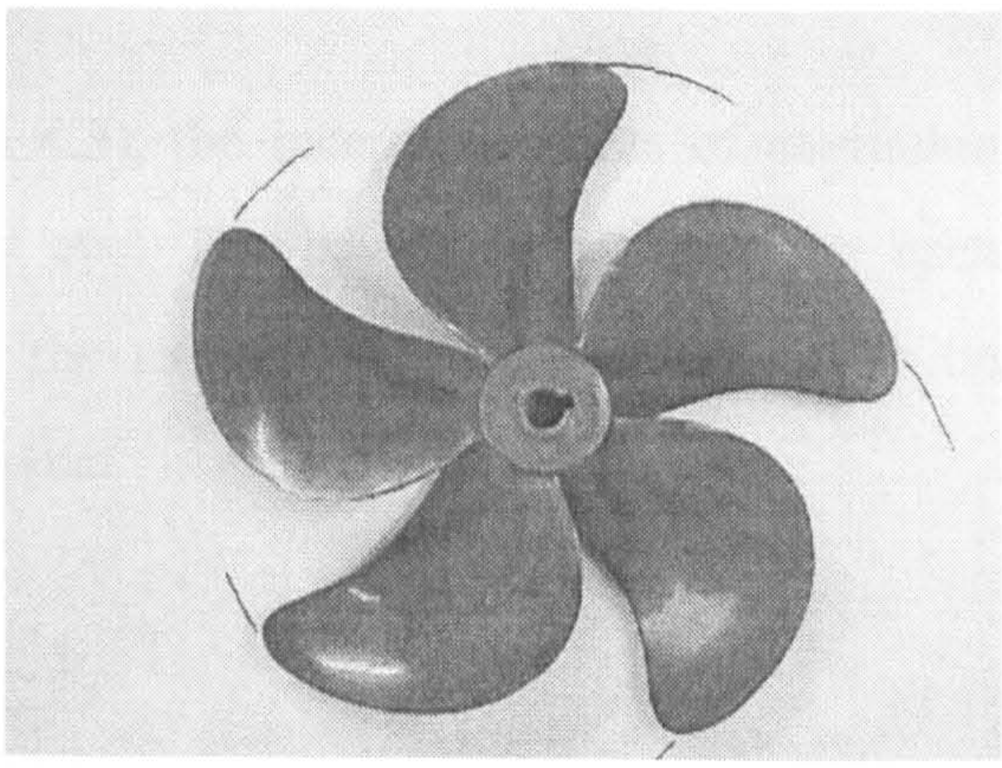

Figure 4.4 Typical tip vortex cavitation attached to one blade only

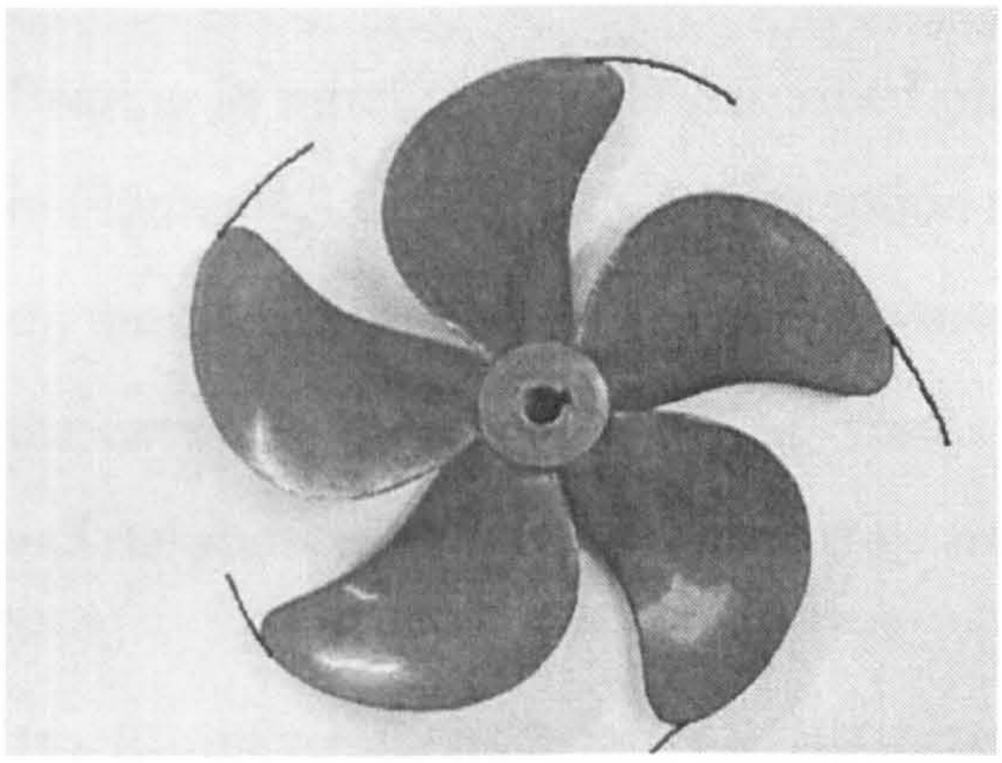

Figure 4.5 Typical tip vortex cavitation fully attached to all blades

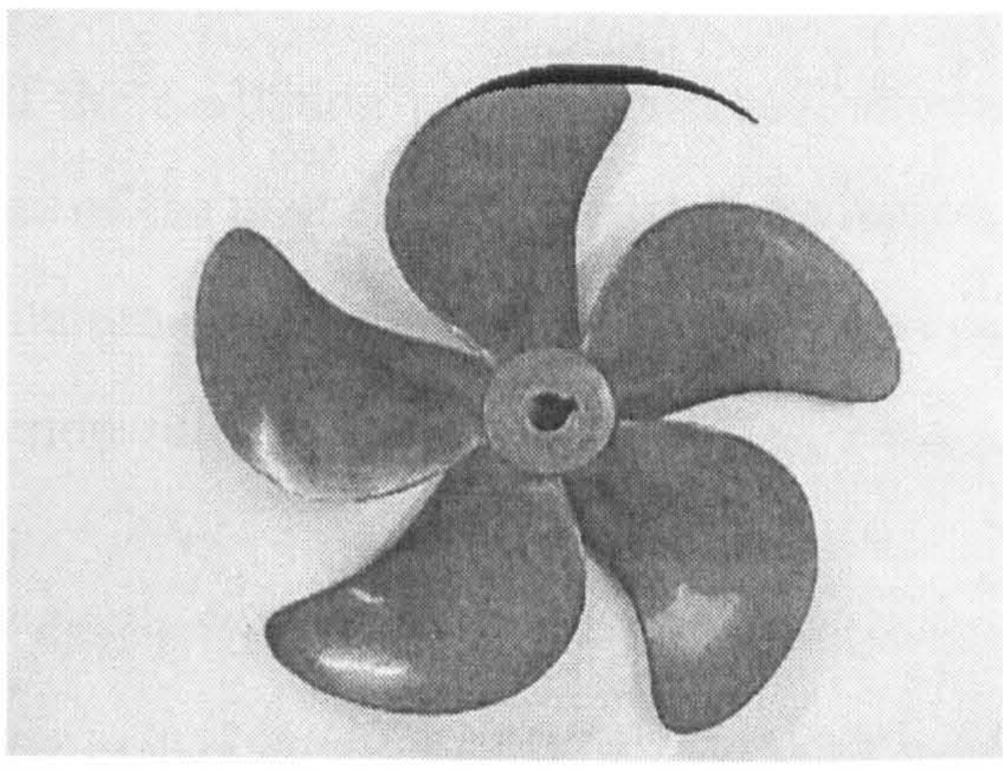

Figure 4.6 Typical sheet cavitation from tip to 0.8R at top blade

The dissolved gas content of the water was measured by using a Jenway DO_2 meter 9071 apparatus. Two different values were chosen by considering the limit of clear visibility of the cavitation patterns through the tunnel. These were 20% and 44% representing the low and high values of dissolved gas content respectively.

4.4 ANALYSIS AND PRESENTATION OF RESULTS

As described in the previous section (Section 4.3), the inception points of cavitation were recorded based on the observations by eye. The cavitation number for each cavitation phase was calculated according to the mean cavitation number definition based on resultant or relative velocity, V_R, such that

$$\sigma_i = \frac{P_{st} - P_v}{\frac{1}{2}\rho V_R^2} \tag{4.1}$$

where:

- $V_R = \sqrt{U^2 + (0.7\pi ND)^2}$

Bearing in mind the earlier described phases of the cavitation pattern observed, shown in Figures 4.3 through 4.6, the inception numbers of the unattached tip vortex cavitation, σ_i, the cavitation numbers of the tip vortex cavitation attached to one blade only, σ_{TV1B}, the cavitation numbers of the tip vortex cavitation fully attached to all blades, σ_{TVAB}, and the sheet cavitation numbers, σ_{SC}, are used.

The results of the inception measurements of the earlier mentioned four groups of tests are presented in Section 4.5 through:

- Figures 4.7 to 4.10 for the effect of the free-stream turbulence
- Figures 4.11 to 4.14 for the effect of the roughness
- Figures 4.15 to 4.18 for the combined case.

In these figures,

- x-axis presents varying levels of turbulence intensity (TI) in the free flow in percentage or varying roughness heights (k) in μm
- y-axis represents the inception of cavitation numbers described above depending upon the cavitation phase.

α_D/α_S denotes the dissolved gas content ratio where:

- α_D is the dissolved gas content at the static pressure applied
- α_S is the dissolved gas content of saturated water at 760 mmHg.

The intensities of the free-stream turbulence were obtained from the background flow measurements by using 2-D Laser Doppler Anemometry, which have already been presented in Table 3.6 of Chapter 3.

During the tests, some images of the propeller cavitation were recorded and analysed by using a digital video camera and image analysis software, PC_Image. The video camera, which was connected to a PC, was also used to monitor the cavitation events. The desired images were captured by using the grabbing facility in the software (PC_Image Version 2.2.01, 1996) and some of the appropriate images are presented in Pictures 4.1 through 4.14 in the following section.

In these pictures,

- σ_u denotes the propeller cavitation number based on the tunnel water (free-stream) velocity, U, given by:

$$\sigma_u = \frac{P_{st} - P_v}{\frac{1}{2}\rho U^2} \tag{4.2}$$

- While J denotes the advance coefficient of the propeller defined as:

$$J = \frac{U_A}{ND} \tag{4.3}$$

where:

- U_A denotes the advance velocity of the propeller, which was equal to the tunnel axial flow velocity, U, since the experiments were carried out in uniform flow.

4.5 DISCUSSION OF RESULTS

Comparisons of the inception numbers of three stages of the tip vortex and sheet cavitation for varying levels of free-stream turbulence are presented in Figures 4.7 through 4.10 at two different levels of dissolved gas content. As far as the effect of the level of the free-stream turbulence is concerned, there seems to be a linear trend for the unattached tip vortex cavitation at both levels of the dissolved gas contents, as shown in Figure 4.7. As the level of free-stream turbulence is increased, the inception number also increases, indicating that the increase in the level of free-stream turbulence results in earlier inception of cavitation.

For the stages towards the sheet cavitation, as shown in Figures 4.8 through 4.10, the results do not demonstrate the same trend as observed in the stage for the unattached tip vortex cavitation. As the level of the free-stream turbulence is increased, the cavitation number appears to increase until a critical value of the free-stream turbulence level, beyond which the cavitation number seems to be insensitive to the change in the level of turbulence. These findings are observed at the low level of the dissolved gas content. The difference in the trends between the inception characteristics of the unattached tip vortex cavitation and the other stages may be explained by the development of bubble, such that the bubble at the stage of the unattached tip vortex cavitation shows different characteristics than at the growth and collapse stages of the bubble (the stages towards the sheet cavitation). Therefore, cavitation process should be investigated separately at each stage due to the different behaviour of the bubble at each stage.

One may notice that there is a big difference in the inception results at the lowest level of the free-stream turbulence (base frame present only) between the low and high levels of dissolved gas content, as shown in Figure 4.10. This difference may be due to an observation error made for the low level of dissolved gas content.

The test results have also shown the effect of the dissolved gas content on the cavitation process. As the level of dissolved gas content is increased, the cavitation number considerably increases at each level of the free-stream turbulence for the unattached tip

vortex cavitation. However, for the stages towards the sheet cavitation this trend is not observed at some levels of the turbulence, due to the different behaviour of the bubble at the high level of the dissolved gas content. As far as the effect of the free-stream turbulence in the presence of varying levels of the dissolved gas content is concerned, the effect varies depending upon the level of the dissolved gas content and the type of cavitation investigated, indicating the importance of the combined investigation into the effect of the free-stream turbulence and dissolved gas content.

Although the characteristics of boundary layer of the propeller blades and the size and distribution of the nuclei in the tunnel water were not measured, one may suggest that the level of the free-stream turbulence affects the development of the boundary layer. As the level of the free-stream turbulence is increased, the boundary layer becomes more turbulent by moving the transition region to the leading edge of the propeller blade, as stated by Gates and Acosta (1979). The other conclusion may be that the wire meshes generate not only the free-stream turbulence, but also some nuclei in the water to stimulate the cavitation process. Therefore, the contribution of the fluctuating velocities to the development of the cavitation is crucial in earlier inception of cavitation or delay of inception as well as the contribution of nuclei effects.

In Figures 4.11 through 4.14, the comparisons of cavitation numbers of three stages of the tip vortex and sheet cavitation for varying levels of roughness (cases of roughness only) are presented at two different levels of dissolved gas content. The effect of varying sizes of roughness heights displays similar trend to that of the varying levels of free-stream turbulence for the unattached tip vortex cavitation at both levels of dissolved gas content, as shown in Figure 4.11. As the roughness height is increased, the cavitation numbers increase, demonstrating that the roughness can induce cavitation as similar to the effect of free-stream turbulence.

As far as the stages towards the sheet cavitation are concerned, in Figures 4.12 through 4.14, the results also demonstrate the similar effects on the cavitation numbers, as observed in the case of varying levels of the free-stream turbulence. As the roughness height is increased, the cavitation number increases until a critical value of roughness height, beyond which the cavitation number seems to be insensitive to the change in the

roughness height, indicating the importance of the bubble dynamics for the stages towards the sheet cavitation. The observation error mentioned for the lowest level of free-stream turbulence is also observed in Figure 4.14. Because the case of zero roughness height is the same for the case of the lowest level of free-stream turbulence.

The dissolved gas content also influences the inception of cavitation. As the level of dissolved gas content is increased, the inception of the unattached tip vortex cavitation considerably increases at each roughness height. However, the trend is somehow different at the roughness height of 35 μm for the stages towards the sheet cavitation (e.g. Figures 4.12, 4.13 and 4.14). Therefore, as far as the effect of roughness in the presence of varying levels of dissolved gas content is concerned, the trend varies depending upon the level of the dissolved gas content and the type of cavitation, as similar to the effect of varying levels of the free-stream turbulence.

During the tests, it was observed that sometimes a vortex type cavitation first occurred on the face side of the propeller blades, as shown in Picture 4.2, which was attached to the surface of a propeller blade, before the unattached tip vortex cavitation was observed on the back side of the propeller blades. This face cavitation disappeared later before the unattached tip vortex cavitation on the back of the blade was developed, but it was difficult to observe when the face cavitation started. This phenomenon, which is known as **"Premature Cavitation"**, may be caused by unequal amount of roughness applied on the face and back sides of a blade as mentioned by Holl and Billet (1986).

It was also noticed that the observations of clear inceptions with the roughened propeller were difficult due to the presence of the roughness element, which made the visibility cloudy, especially around the tips of the blades. During the tests, another difficulty that the roughness element tended to peel off in some areas near the leading edge. In this case, the tests were stopped, a new roughness layer was applied to these areas and the tests were resumed from the beginning of each particular series.

Figures 4.15 through 4.18 present the inception results of the propeller with roughened blades tested behind the turbulence generator at two different levels of dissolved gas content. Because of the excessive number of runs required, two different levels of

roughness (35 and 60 μm) and two different levels of the free-stream turbulence (largest and finest-sized meshes) were applied. The reason behind these tests was further confirmation of the effect of the free-stream turbulence and roughness. As far as the effect of the free-stream turbulence is concerned, the trend is very clear such that the inception number increases with increasing the level of the free-stream turbulence. One should note that the magnitude of the inception number in the combined case is much higher than that of the effect of the inception number recorded in the presence of the turbulence generator only (e.g. compare Figure 4.15 with Figure 4.7 for the unattached tip vortex cavitation). This confirms the additive effect of free-stream turbulence on the inception phenomena in the combined case, although it may not be linearly so.

On the other hand, as far as the roughness height is concerned, the inception numbers increase at the low level of the dissolved gas content. Similar to the previous case the magnitude of the inception numbers in this combined case is much higher than that of the inception number obtained in the presence of the effect of the roughness only (e.g. compare Figure 4.15 with Figure 4.11 for the unattached tip vortex cavitation). The trend in the effect of roughness at the high level of the dissolved gas content is not so clear because of the complex bubble effect. Indeed one would like to carry out more tests to identify if there would be any useful trend, which would require more time and cost. Because of the confirmatory nature of this investigation no further tests were carried out. However, the limited amount of combined tests clearly indicated the effectiveness of both mechanisms particularly the effect of the free-stream turbulence.

Typical stages of the cavitation pattern observed for varying levels of the free-stream turbulence and roughness heights are shown in Pictures 4.1 through 4.14 for different cavitation numbers at two levels of dissolved gas content. Picture 4.1 shows the tip vortex cavitation fully attached to the all blades with 35 μm roughness and behind the finest-sized wire mesh, while Picture 4.2 presents the **"Premature"** face cavitation.

There appears to be a distinct effect of the cavitation number on the development of tip vortex cavitation, as shown in Pictures 4.3 and 4.4. The effect of the dissolved gas content on the cavitation process can be clearly seen in Pictures 4.5 and 4.6. As the level of the gas content is increased, the extent of cavitation is increased, indicating that

increased level of the gas content encourages the development of cavitation. While Picture 4.7 and 4.8 show the effect of the advance coefficient on the development of cavitation, displaying that the extent of cavitation is increased as the advance coefficient is decreased.

In Pictures 4.9 through 4.11, the effect of the levels of the free-stream turbulence is shown for the same operational conditions. One can see that as the level of the free-stream turbulence is increased the extent of the cavitation is increased, displaying the fact that increased level of the free-stream turbulence encourages more developed cavitation, as discussed earlier. On the other hand, as the roughness height is increased, the same effect is also observed in the case of roughness, as shown in Pictures 4.12 through 4.14.

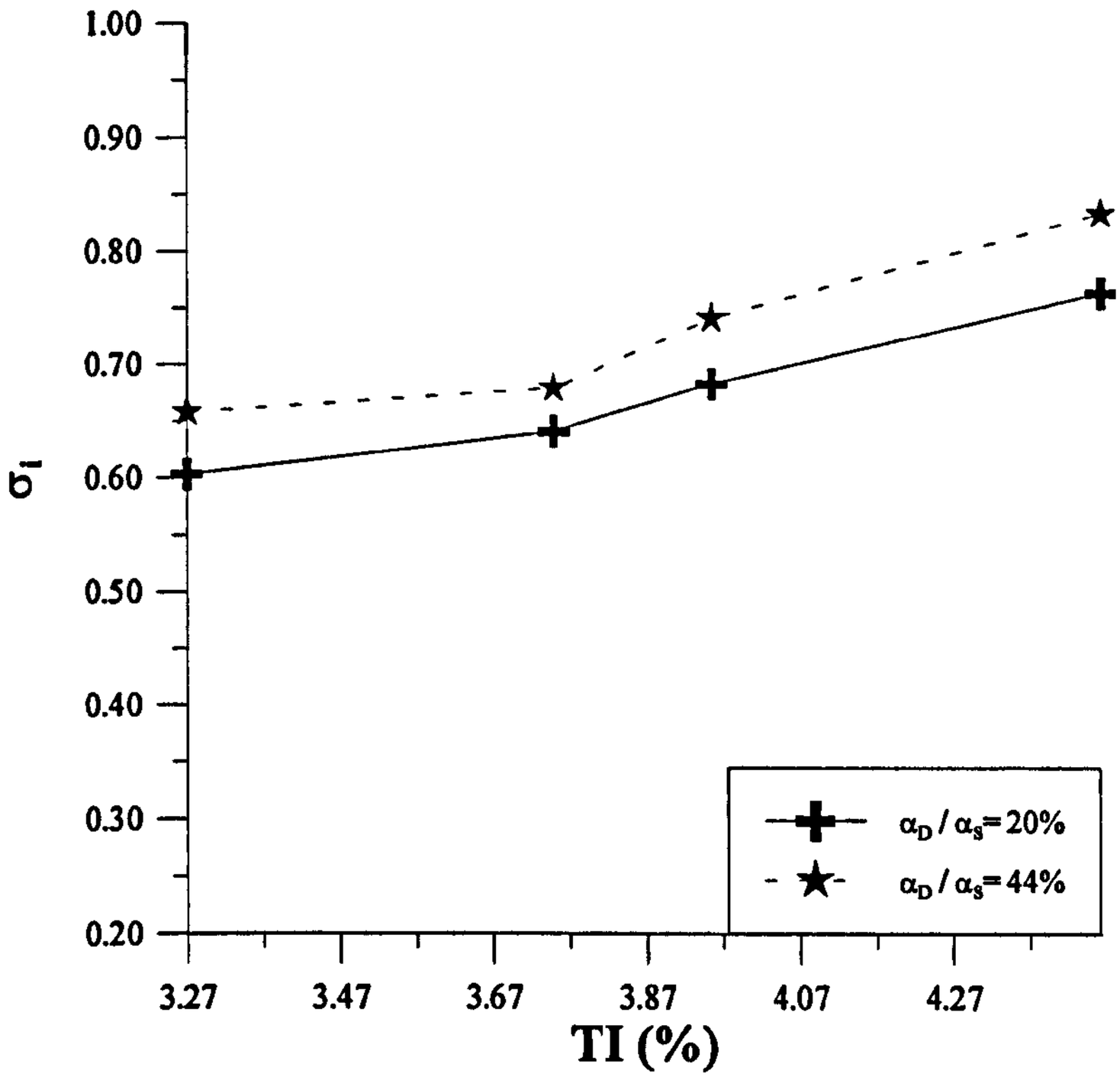

Figure 4.7 Comparison of the inception numbers of unattached tip vortex cavitation against level of free-stream turbulence in the presence of meshes only

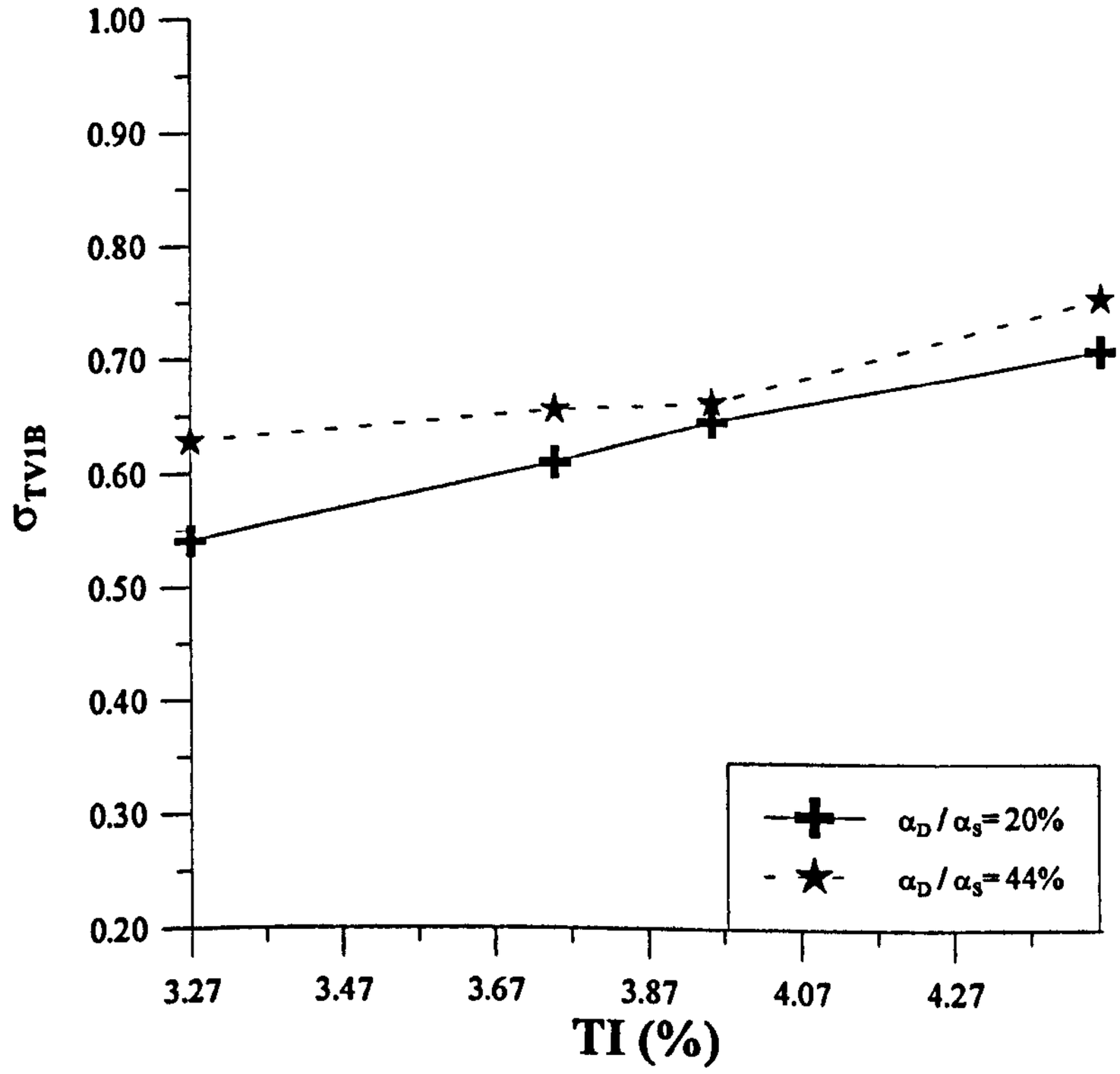

Figure 4.8 Comparison of cavitation numbers of tip vortex attached to one blade only against level of free-stream turbulence in the presence of meshes only

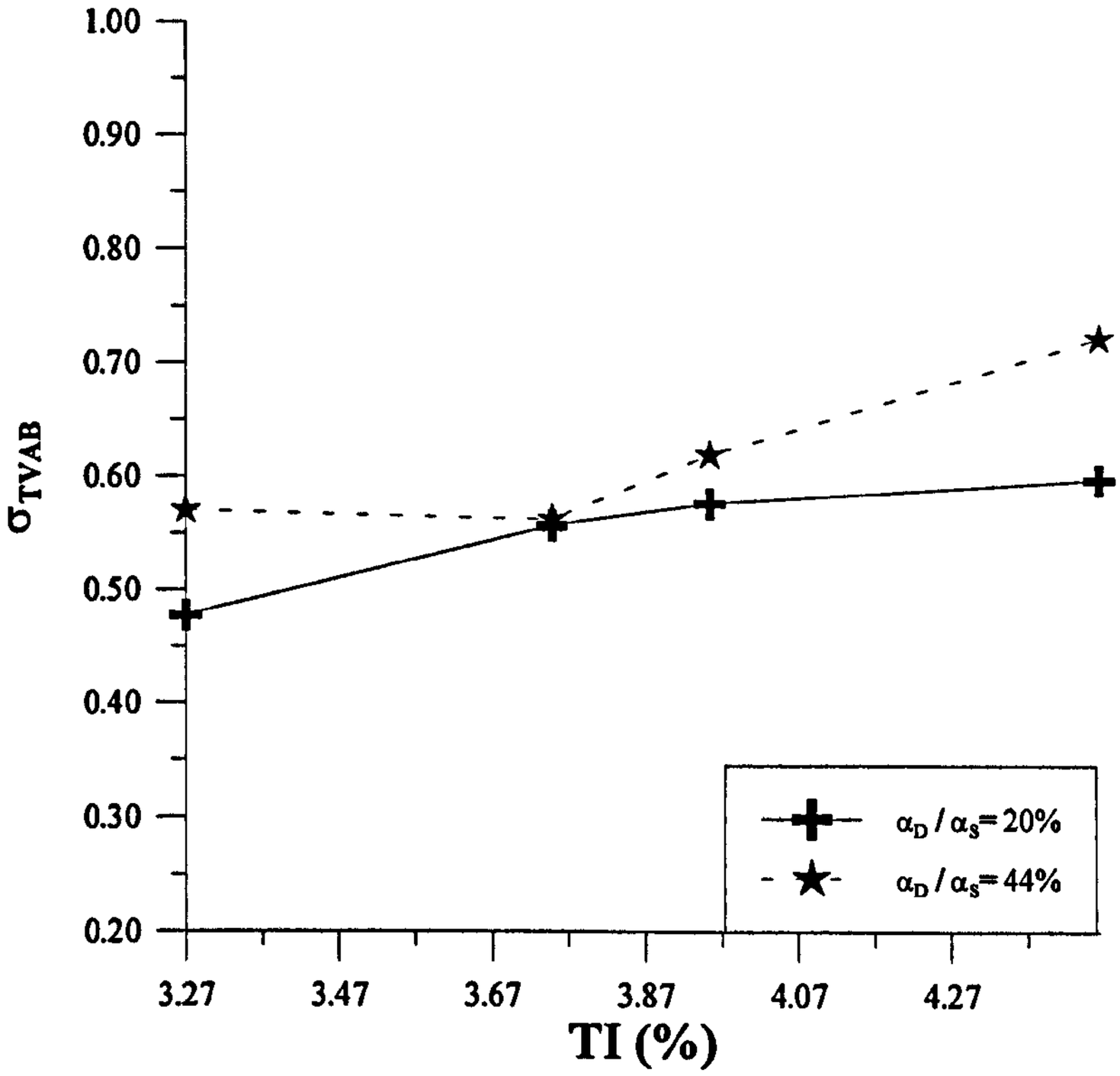

Figure 4.9 Comparison of cavitation numbers of tip vortex fully attached to all blades against level of free-stream turbulence in the presence of meshes only

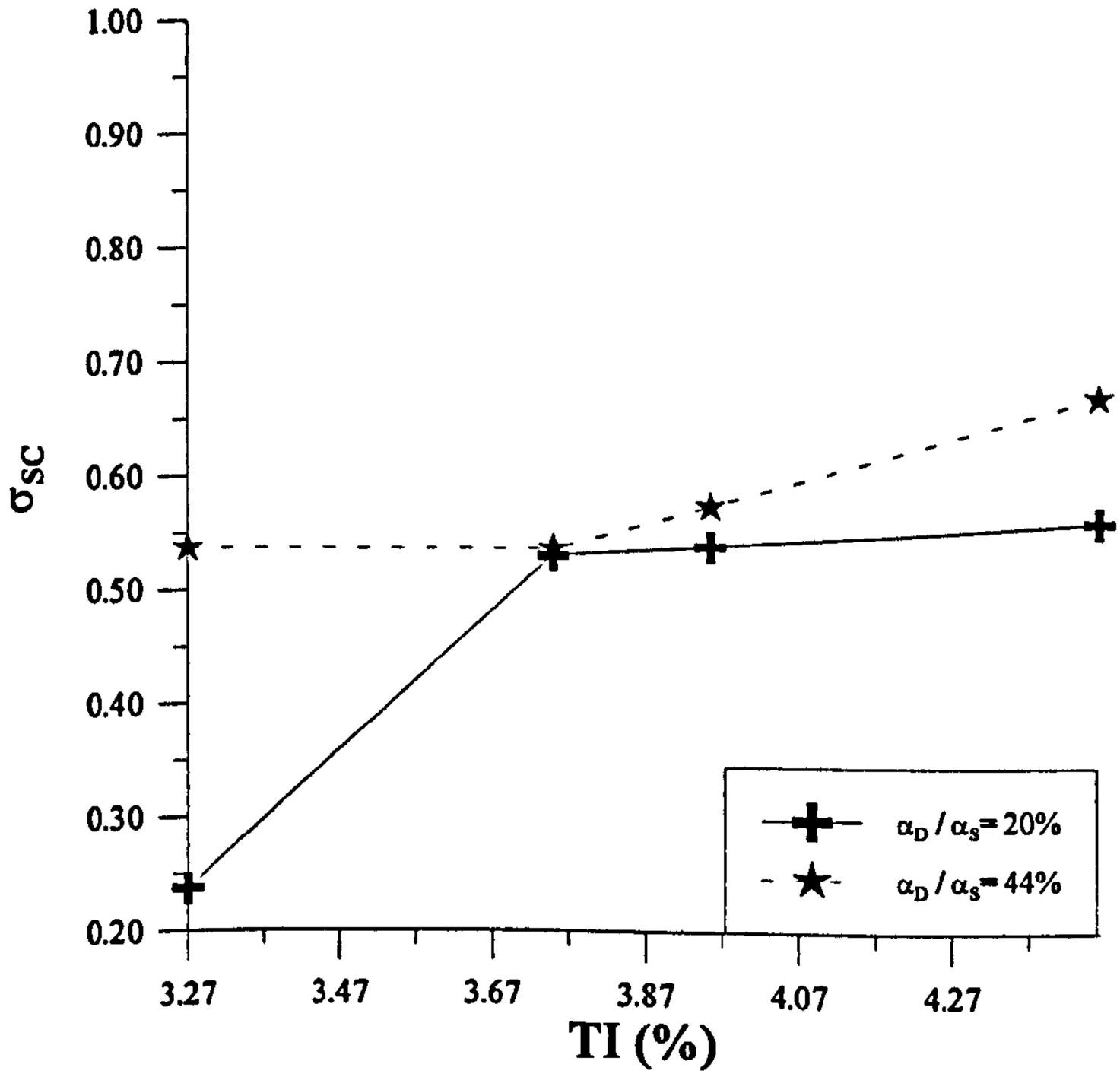

Figure 4.10 Comparison of cavitation numbers of sheet cavitation against level of free-stream turbulence in the presence of meshes only

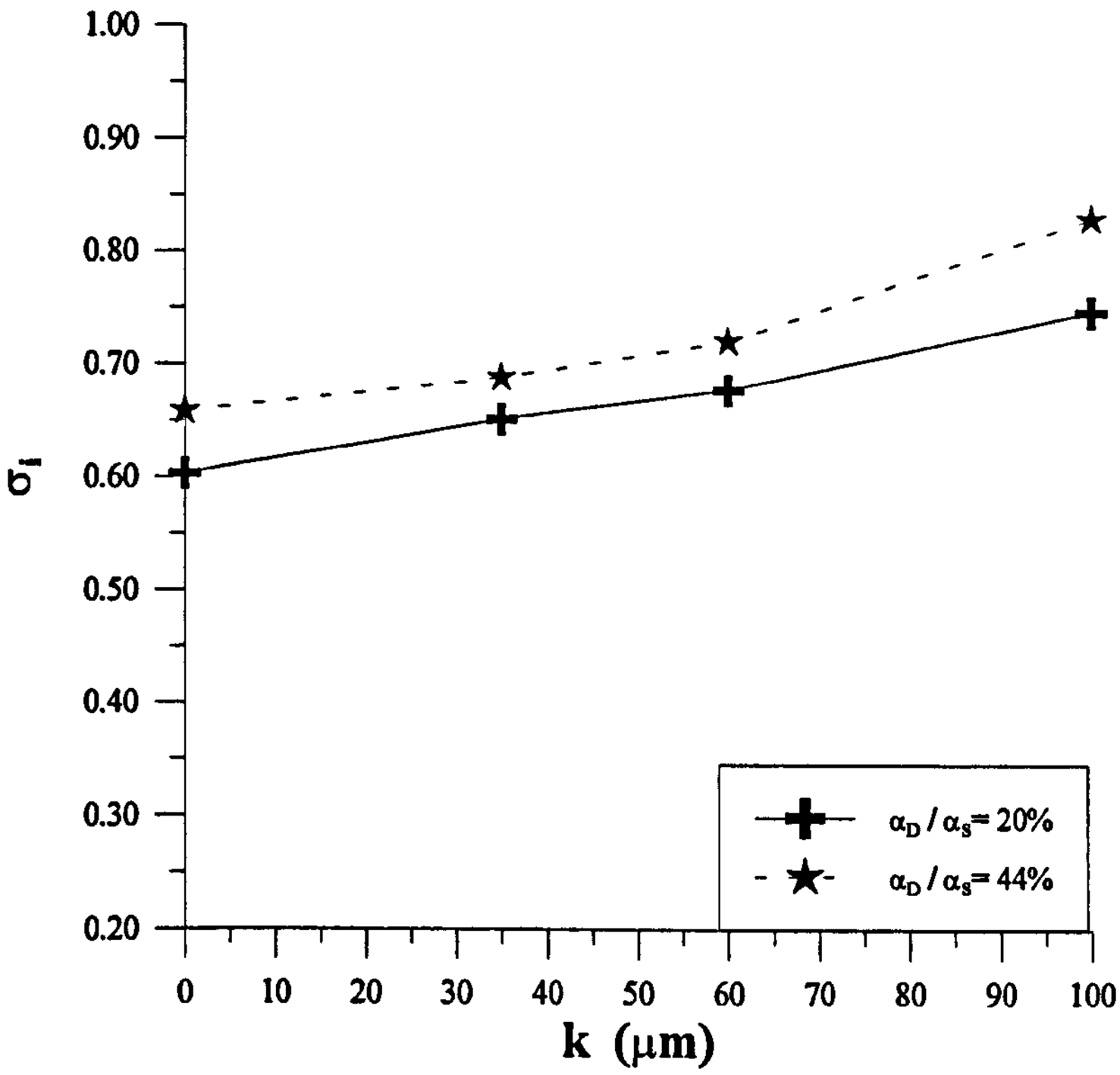

Figure 4.11 Comparison of the inception numbers of unattached tip vortex cavitation against roughness height in the presence of roughness only

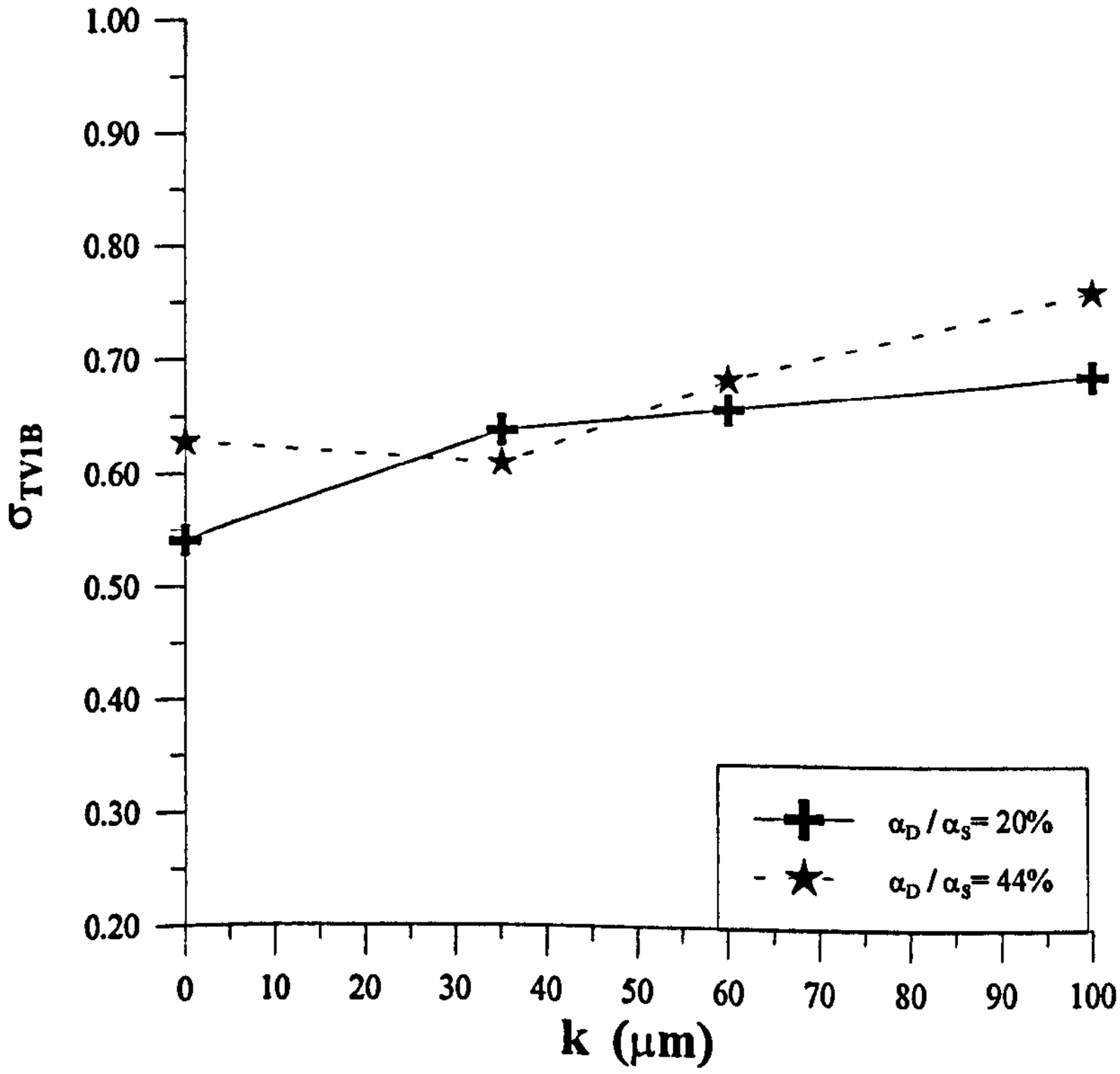

Figure 4.12 Comparison of cavitation numbers of tip vortex attached to one blade only against roughness height in the presence of roughness only

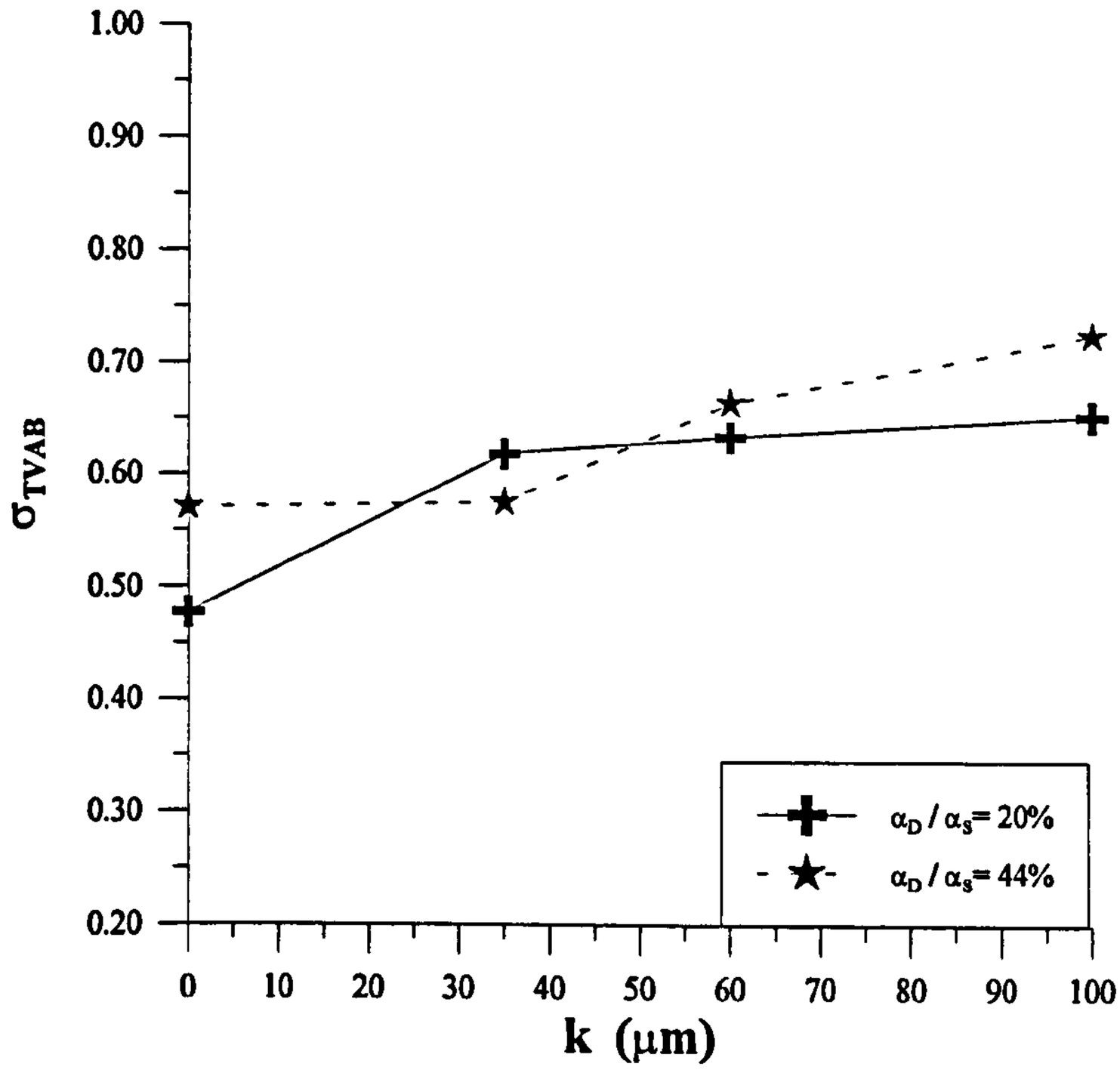

Figure 4.13 Comparison of cavitation numbers of tip vortex fully attached to all blades against roughness height in the presence of roughness only

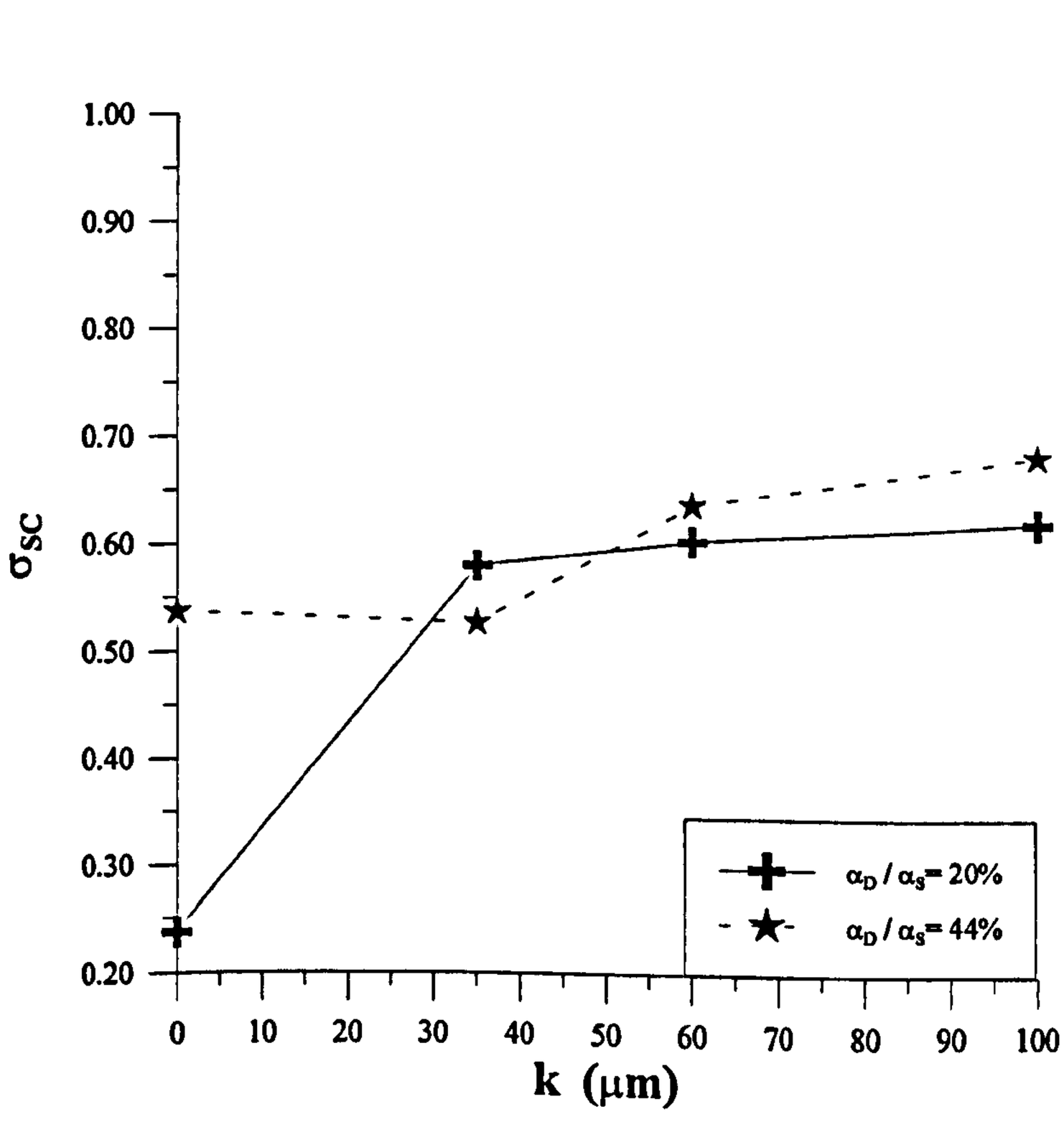

Figure 4.14 Comparison of cavitation numbers of sheet cavitation against roughness height in the presence of roughness only

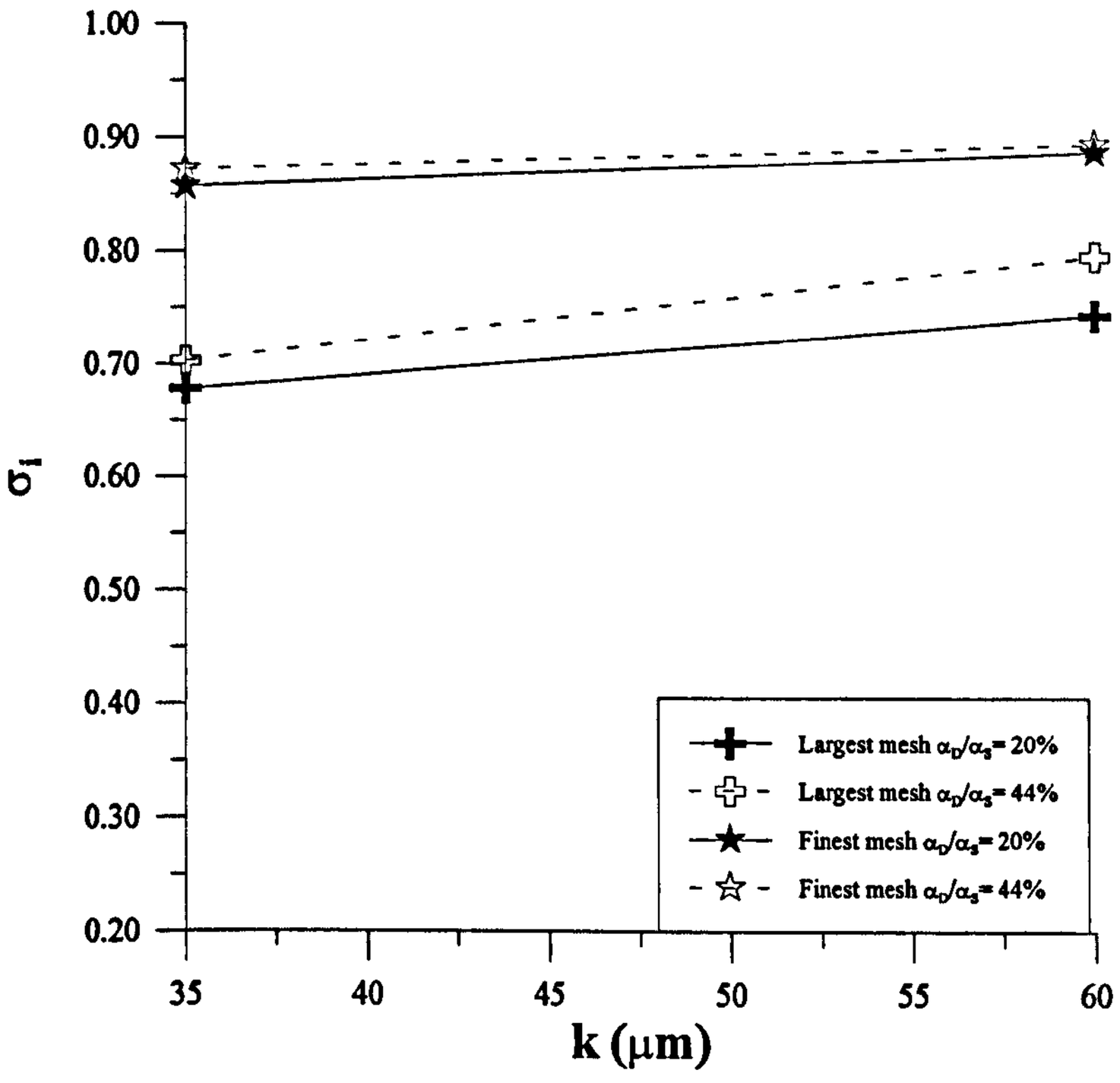

Figure 4.15 Comparison of the inception numbers of unattached tip vortex cavitation against roughness height in combined cases

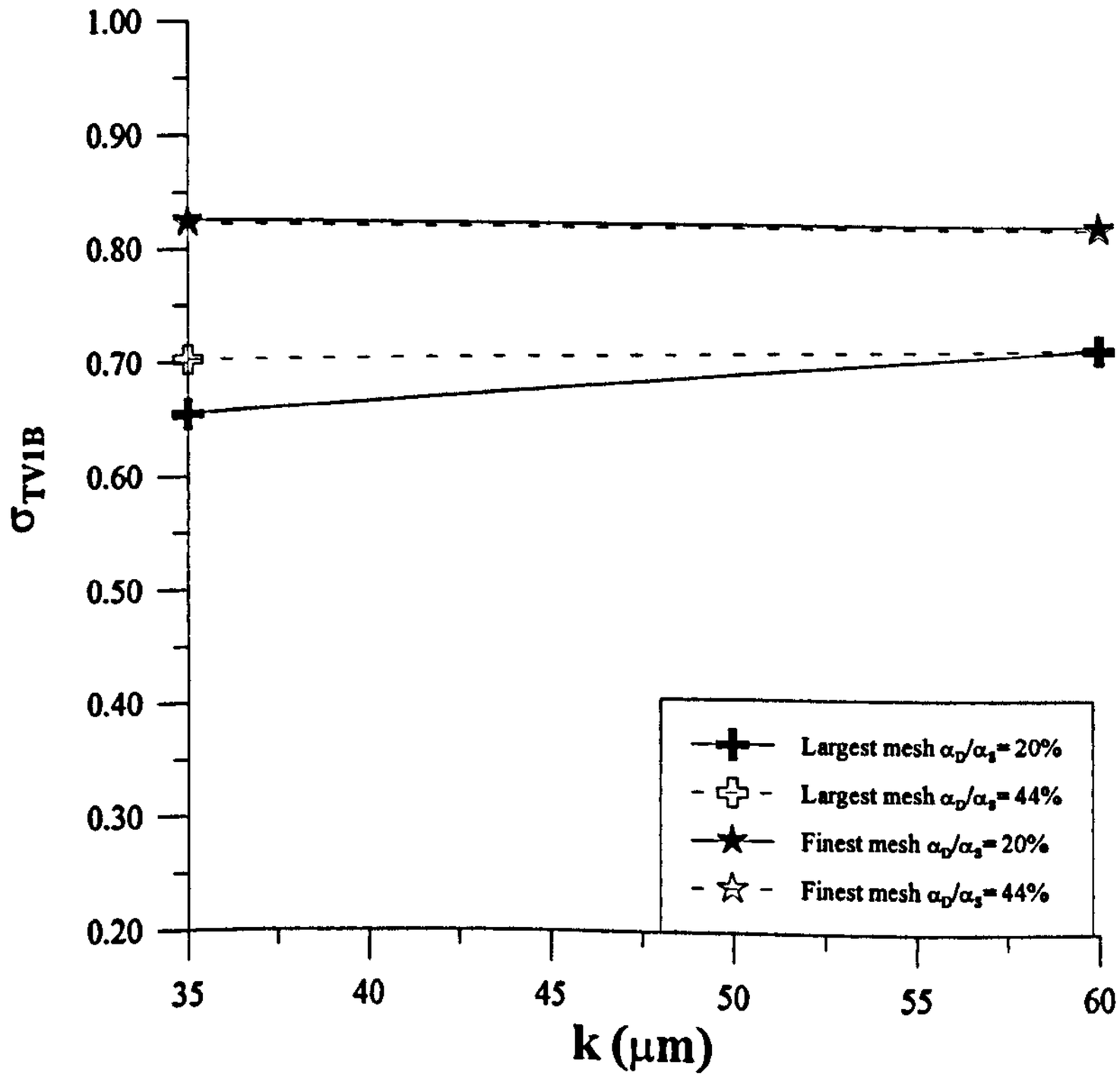

Figure 4.16 Comparison of cavitation numbers of tip vortex attached to one blade only against roughness height in combined cases

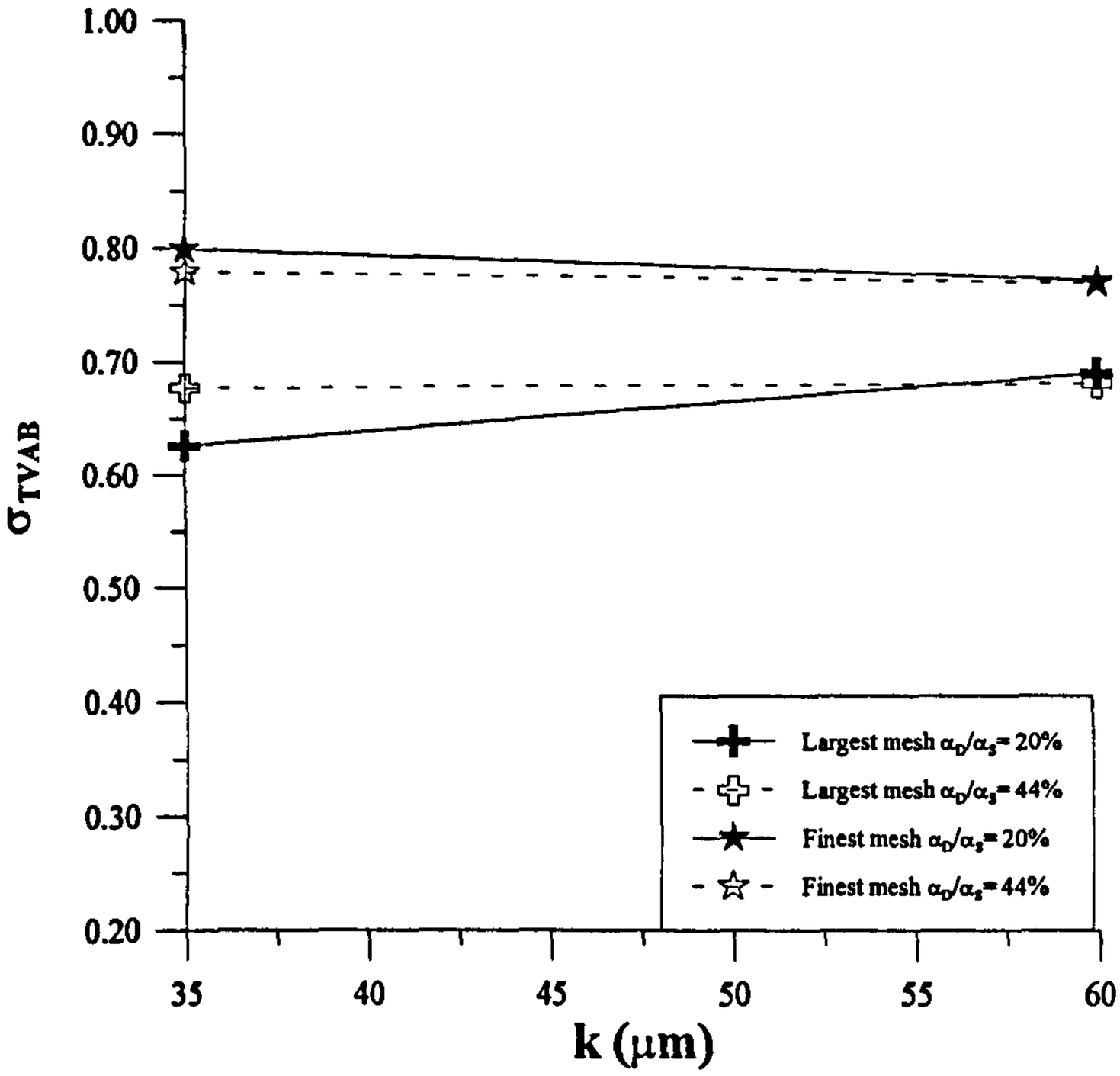

Figure 4.17 Comparison of cavitation numbers of tip vortex fully attached to all blades against roughness height in combined cases

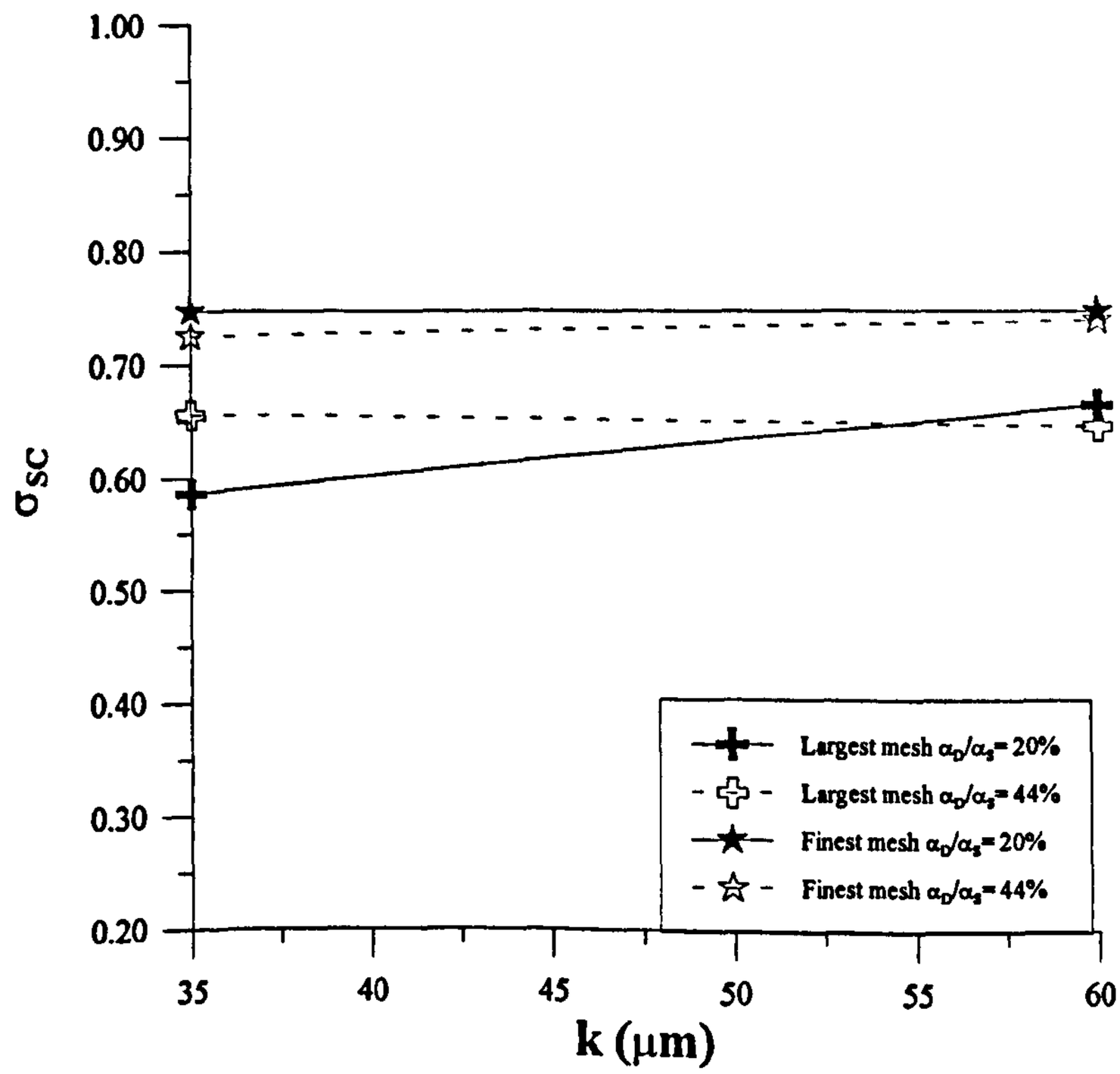

Figure 4.18 Comparison of cavitation numbers of sheet cavitation against roughness height in combined cases

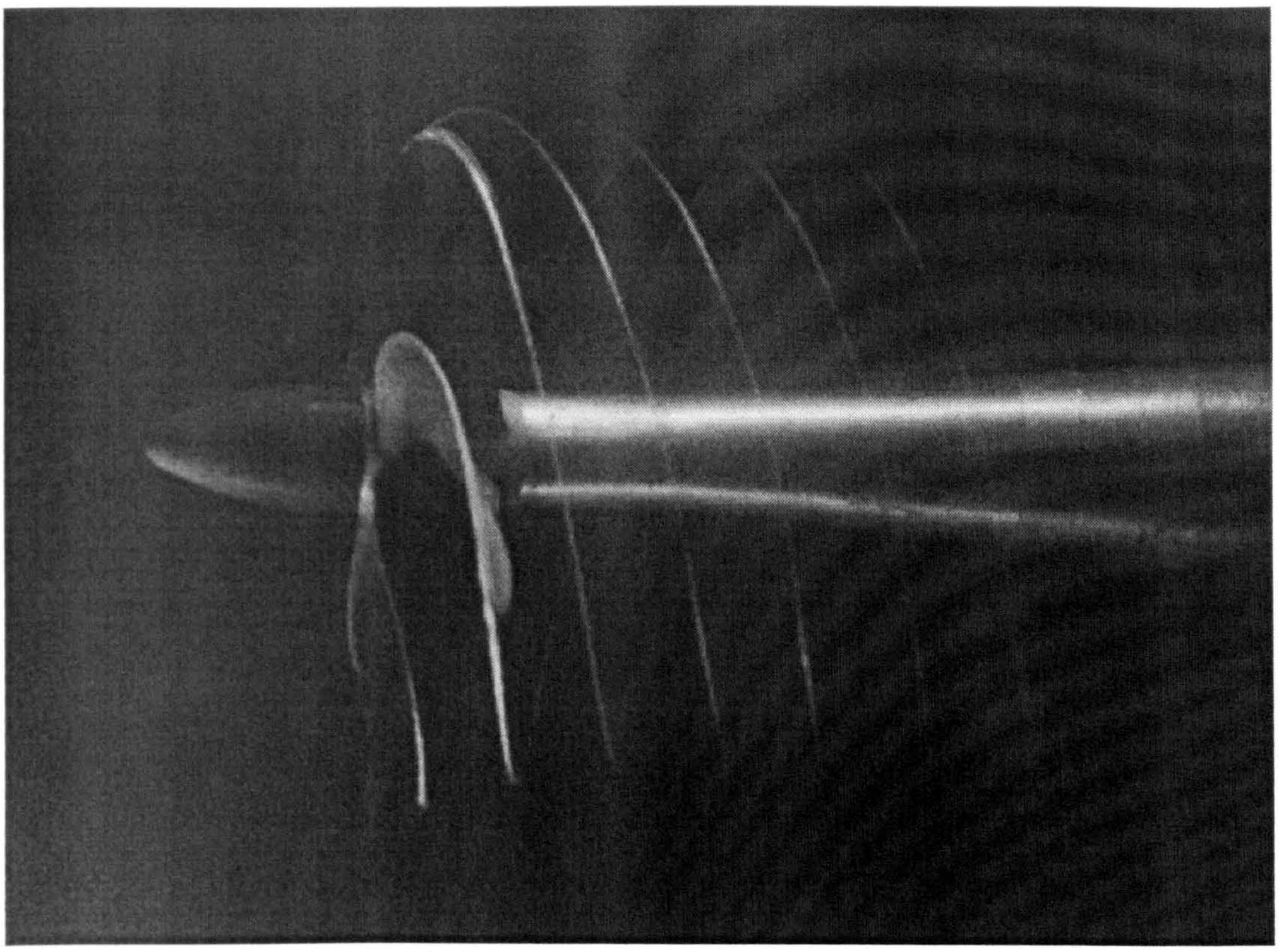

Picture 4.1 Development of tip vortex cavitation fully attached to all blades with 35 μm roughness and behind finest-sized mesh

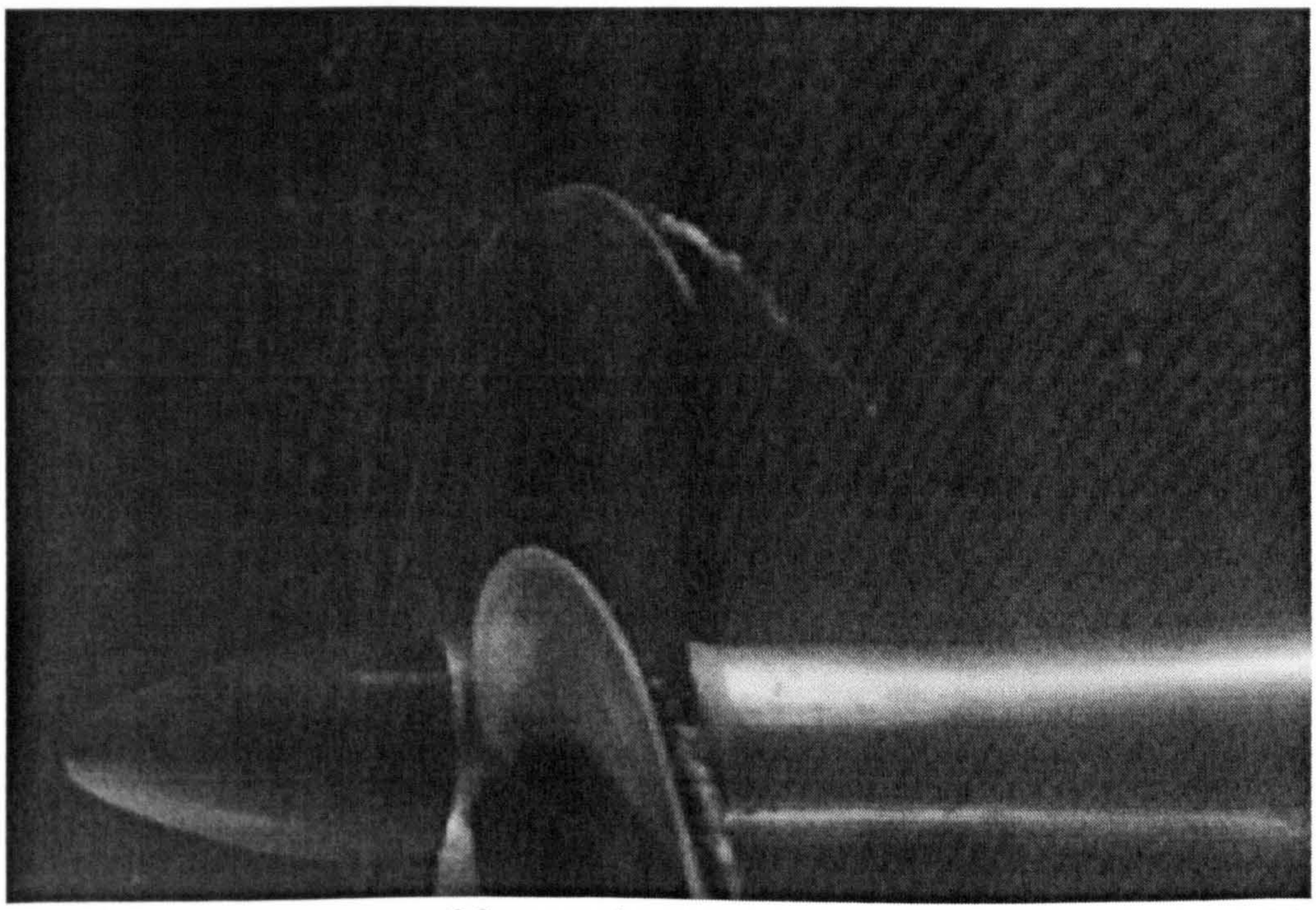

Picture 4.2 Development of face cavitation with 35 μm roughness and behind largest-sized mesh

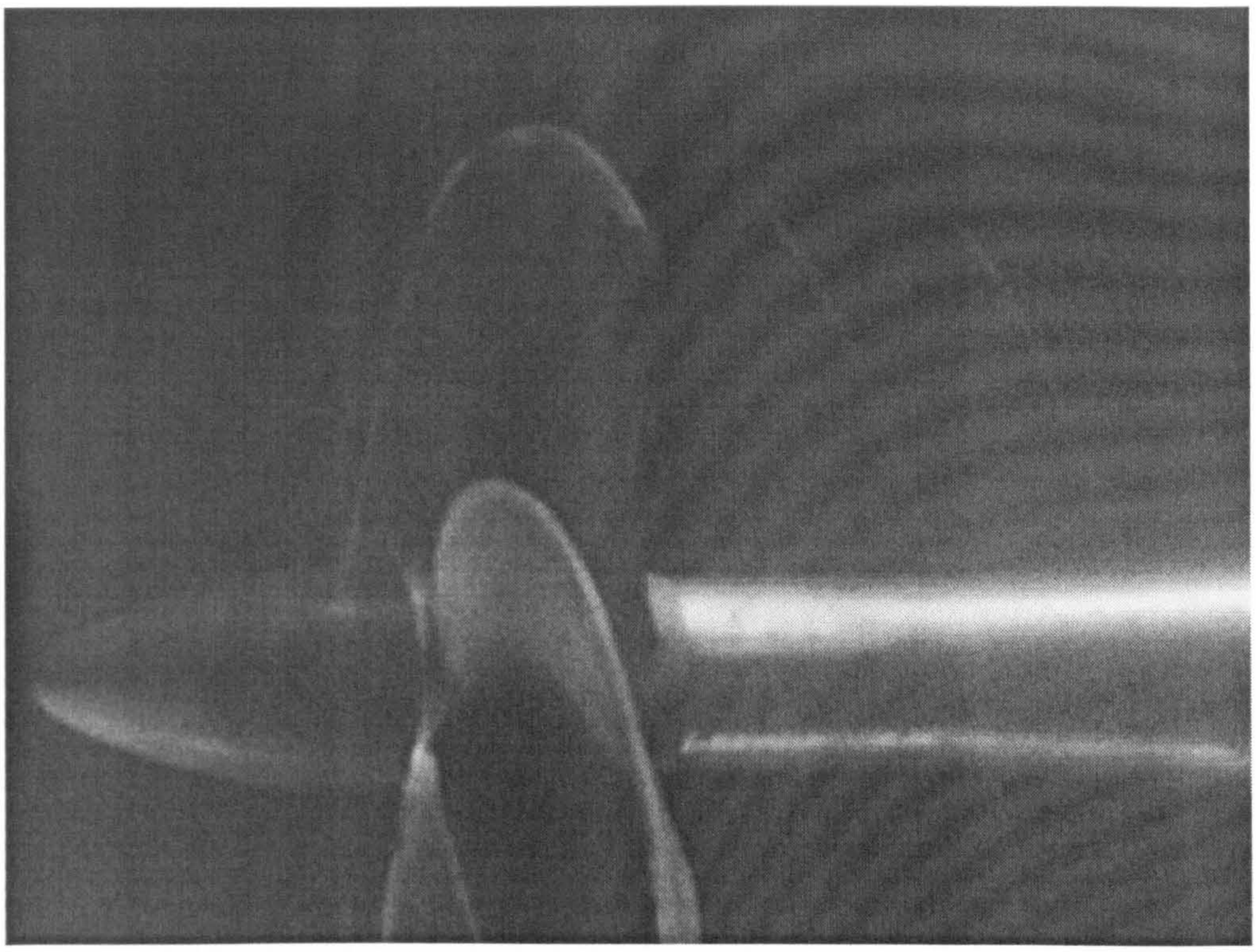

Picture 4.3 Effect of cavitation number on the development of cavitation at J=0.6, α_D/α_S=20% and σ_u=Atm.(with 35 μm roughness and behind finest-sized mesh)

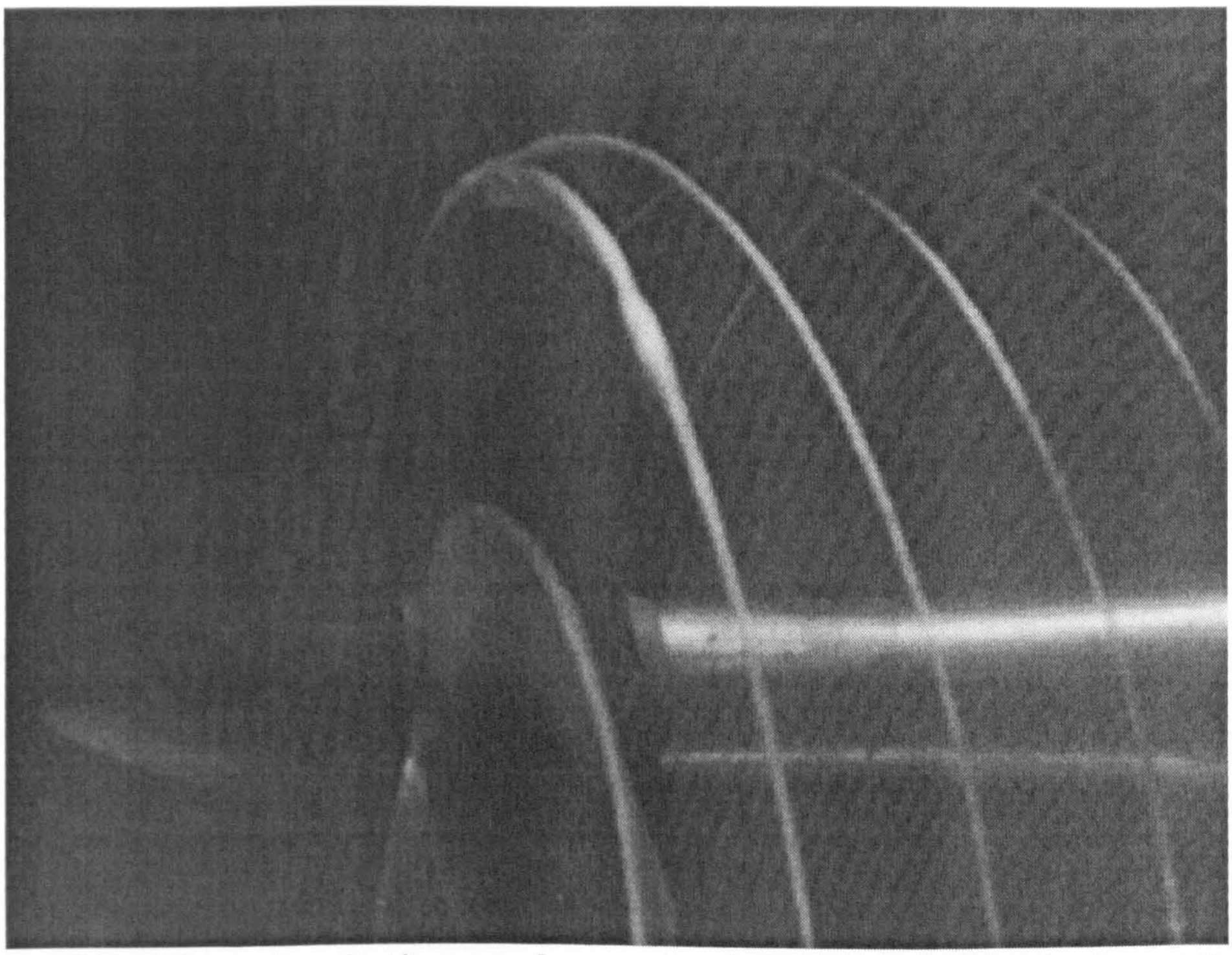

Picture 4.4 Effect of cavitation number on the development of cavitation at J=0.6, α_D/α_S=20% and σ_u=5.56(with 35 μm roughness and behind finest-sized mesh)

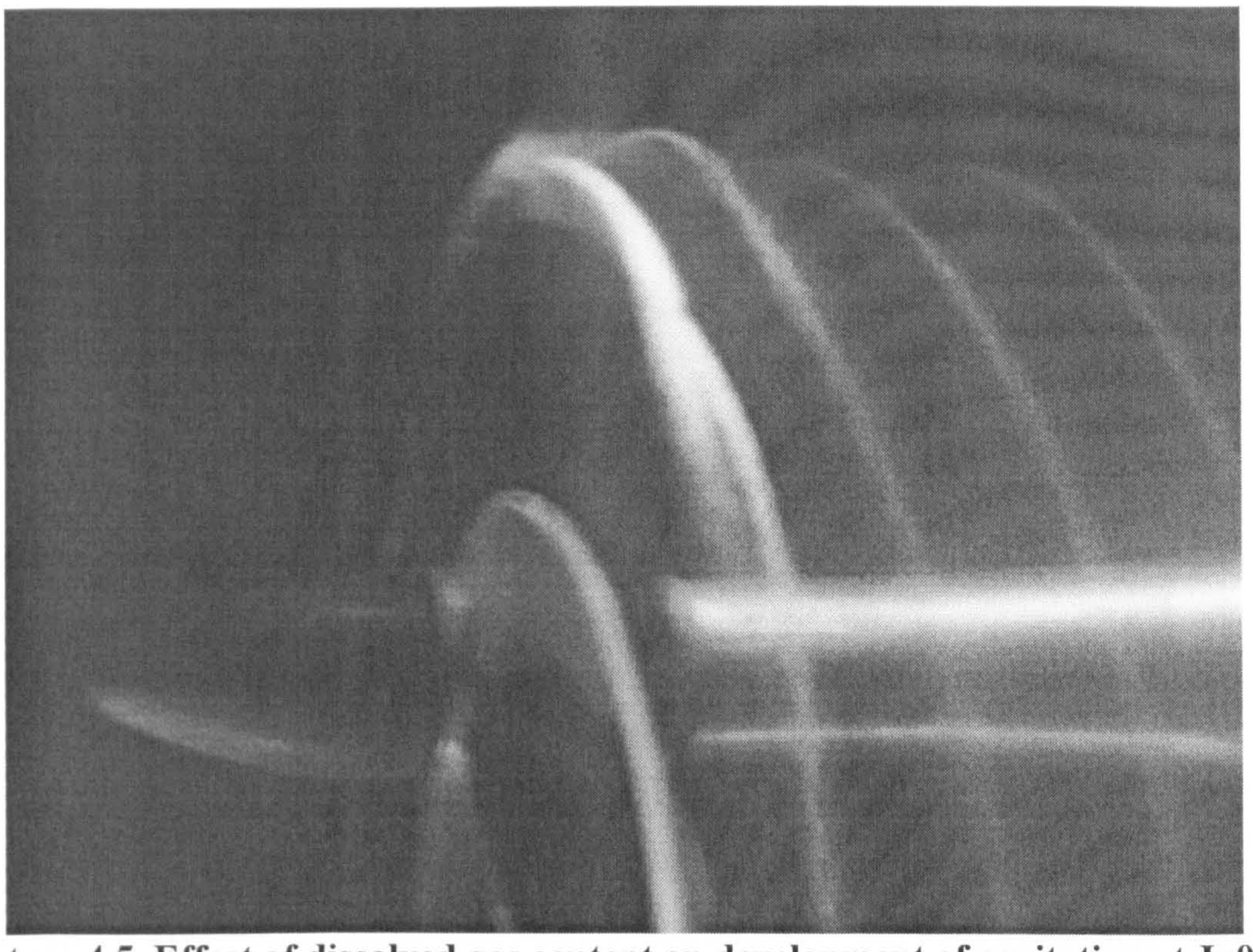

Picture 4.5 Effect of dissolved gas content on development of cavitation at J=0.4, σ_u=Atm. and α_D/α_S=20% (with 35 μm roughness and behind largest-sized mesh)

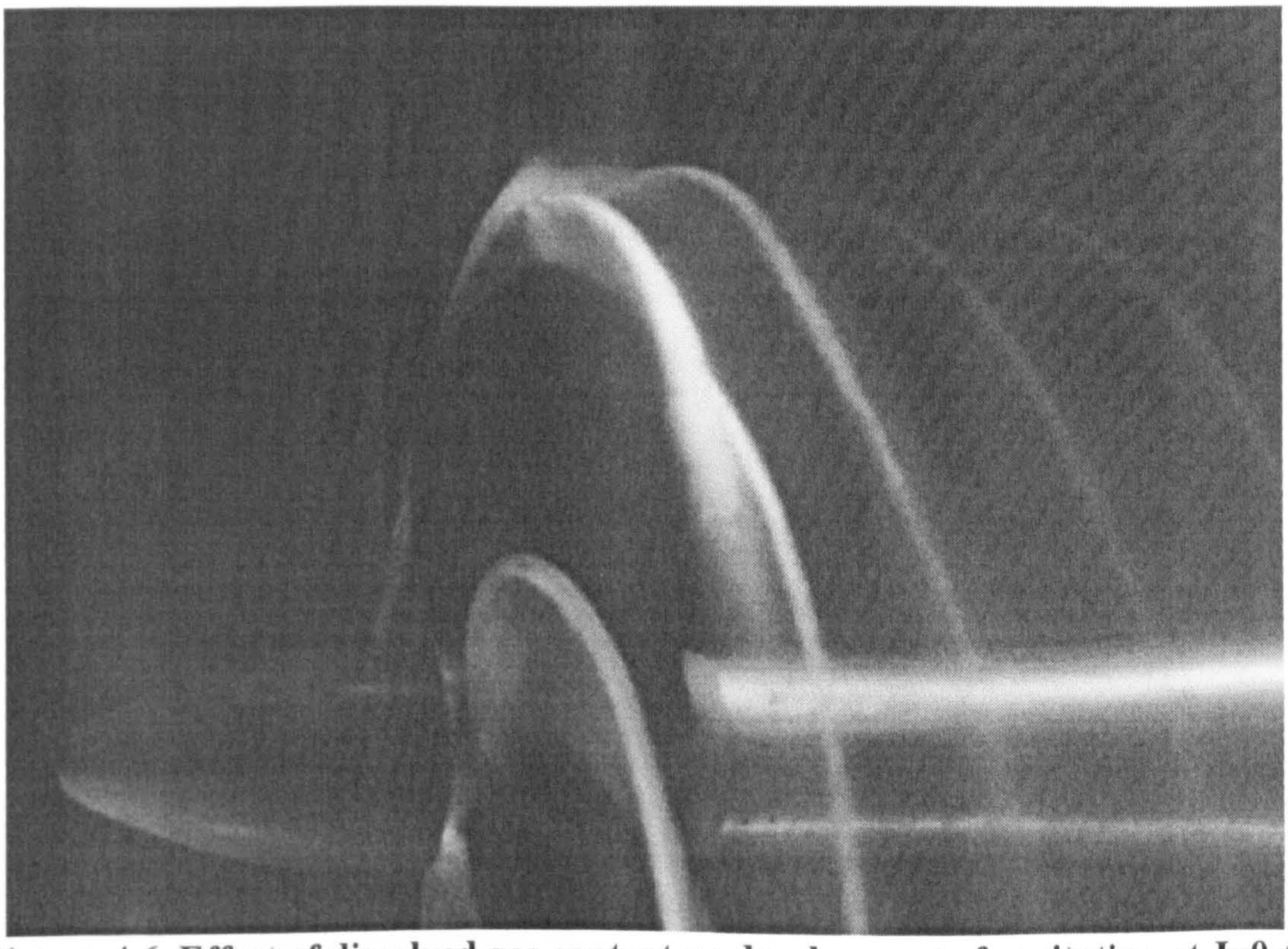

Picture 4.6 Effect of dissolved gas content on development of cavitation at J=0.4, σ_u=Atm. and α_D/α_S=44% (with 35 μm roughness and behind largest-sized mesh)

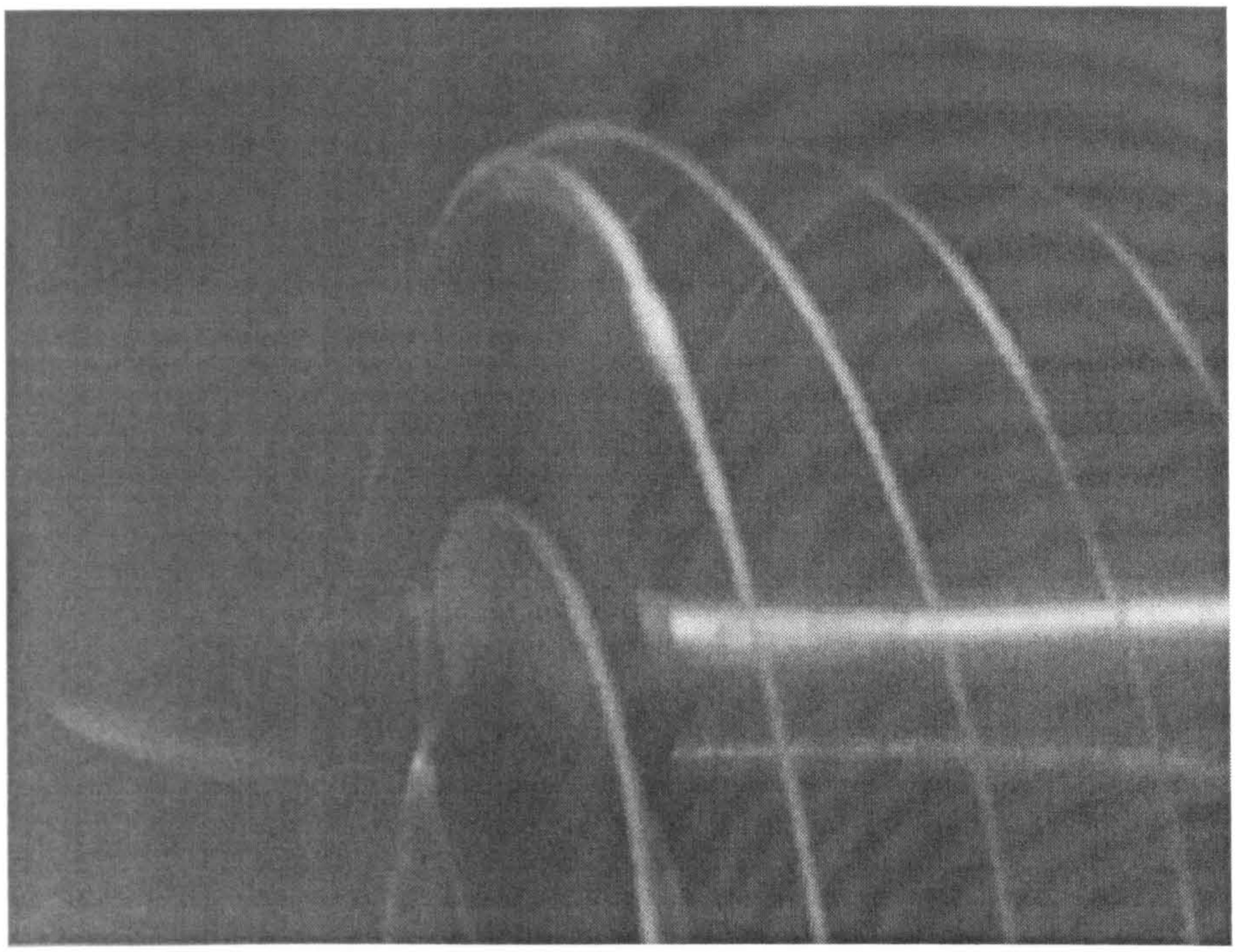

Picture 4.7 Effect of advance coefficient of propeller on the development of cavitation at σ_u=5.56, α_D/α_s=20% and J=0.6 (with 35 μm roughness and behind finest-sized mesh)

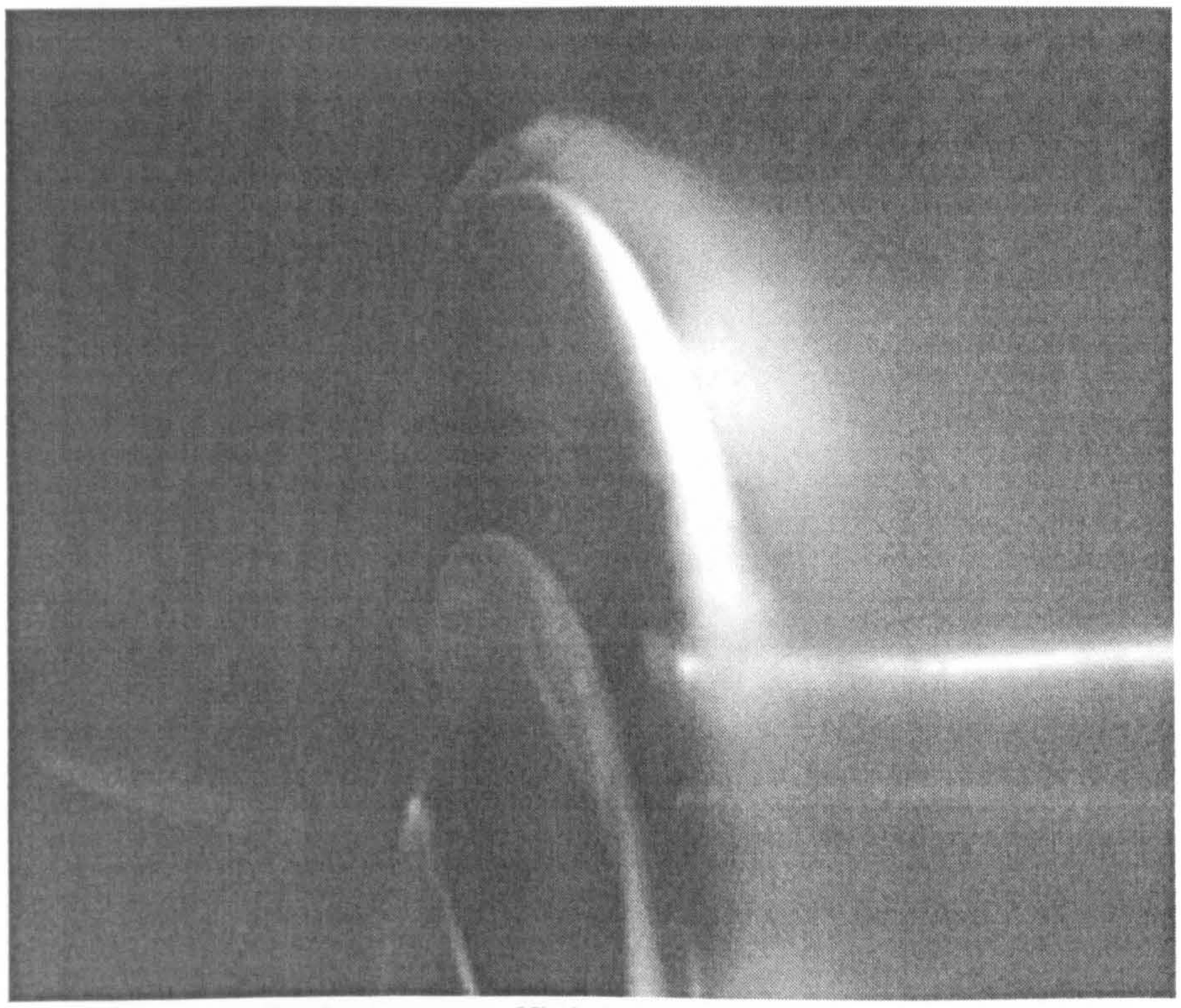

Picture 4.8 Effect of advance coefficient of propeller on the development of cavitation at σ_u=5.56, α_D/α_s=20% and J=0.4 (with 35 μm roughness and behind finest-sized mesh)

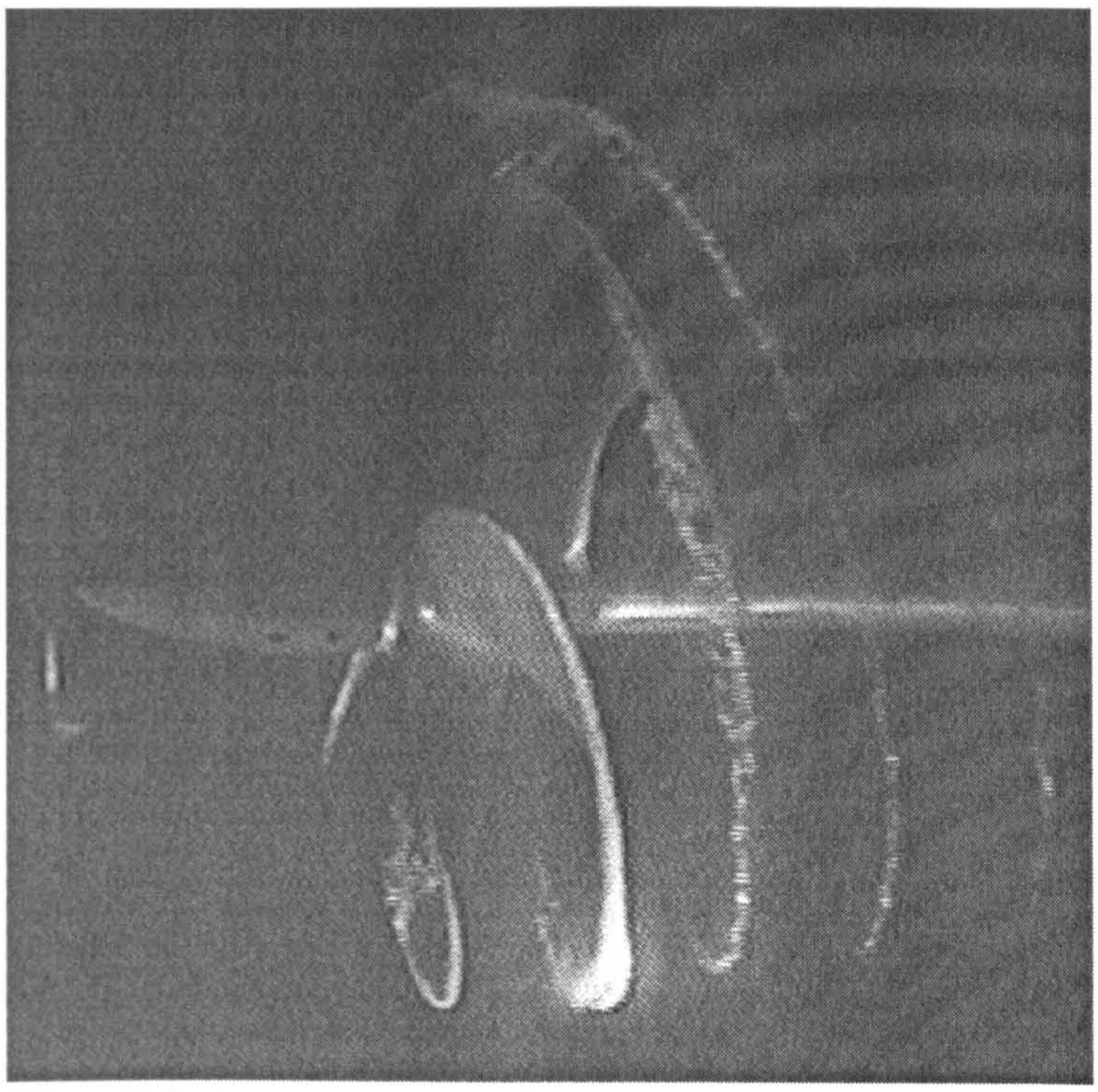

Picture 4.9 Effect of free-stream turbulence on the cavitation behind base frame only at σ_u=5.56, α_D/α_S=44% and J=0.4

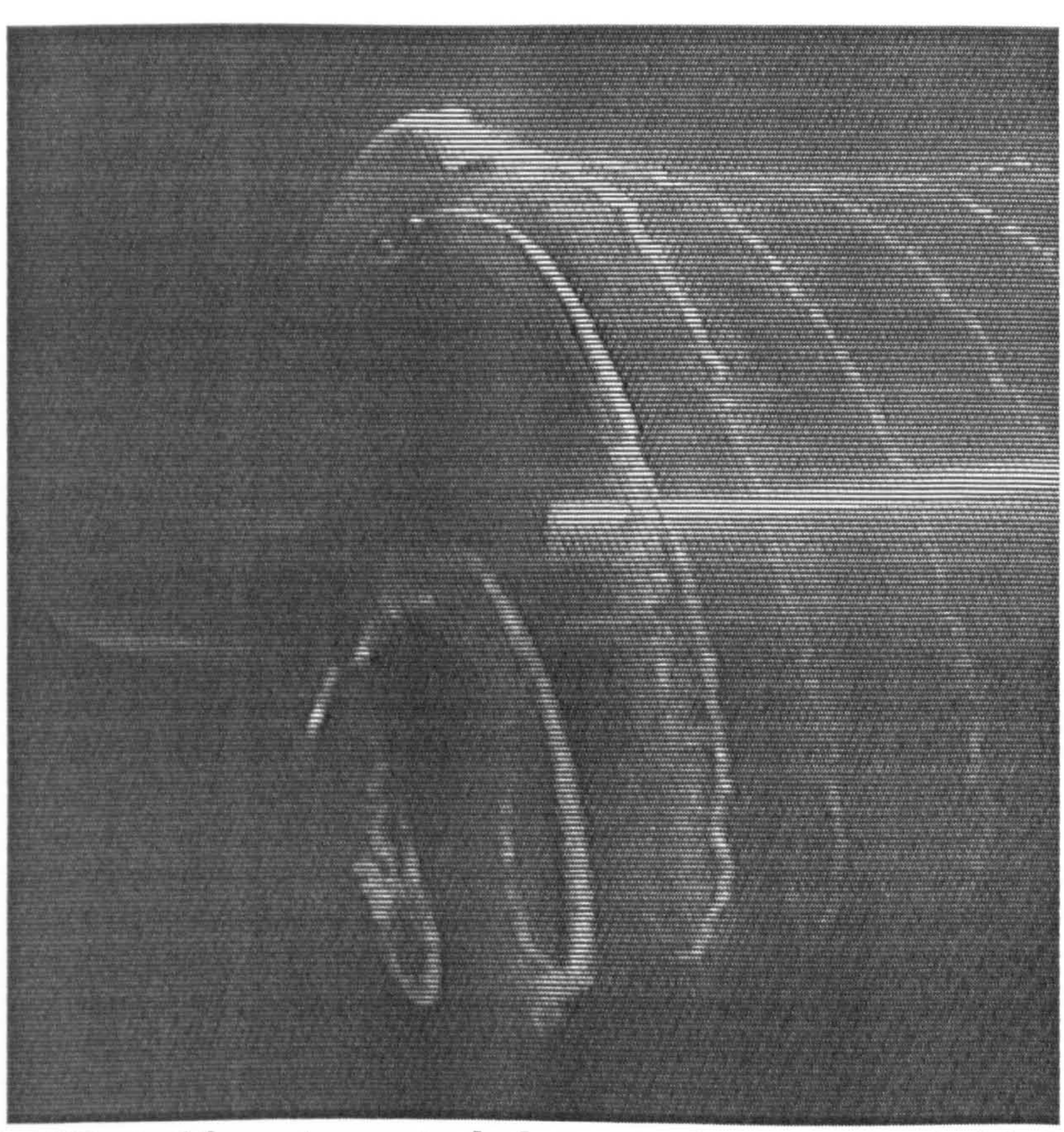

Picture 4.10 Effect of free-stream turbulence on the cavitation behind base frame and largest-sized mesh at σ_u=5.56, α_D/α_S=44% and J=0.4

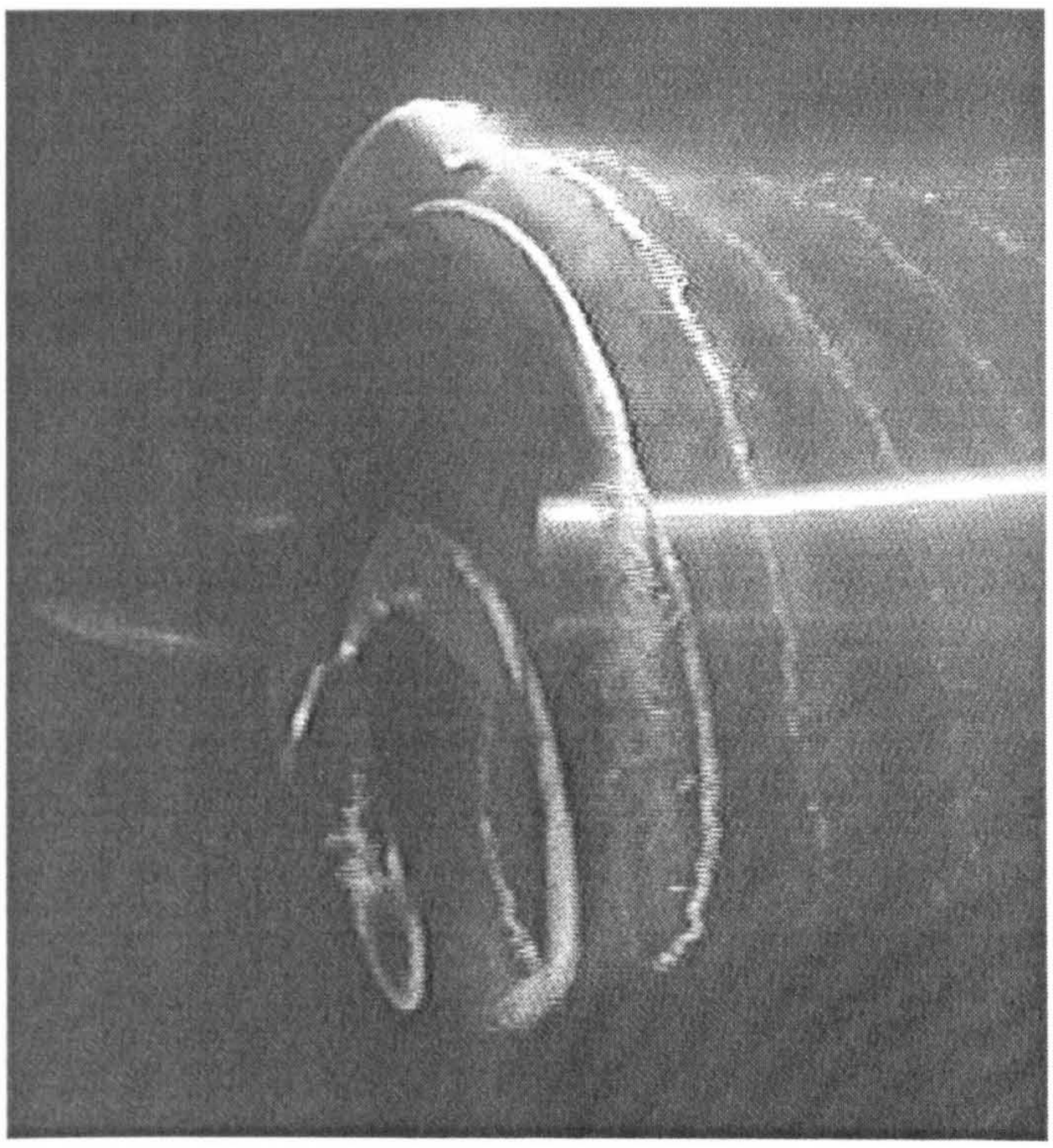

Picture 4.11 Effect of free-stream turbulence on the development of cavitation behind base frame and finest-sized mesh at σ_u=5.56, α_D/α_S=44% and J=0.4

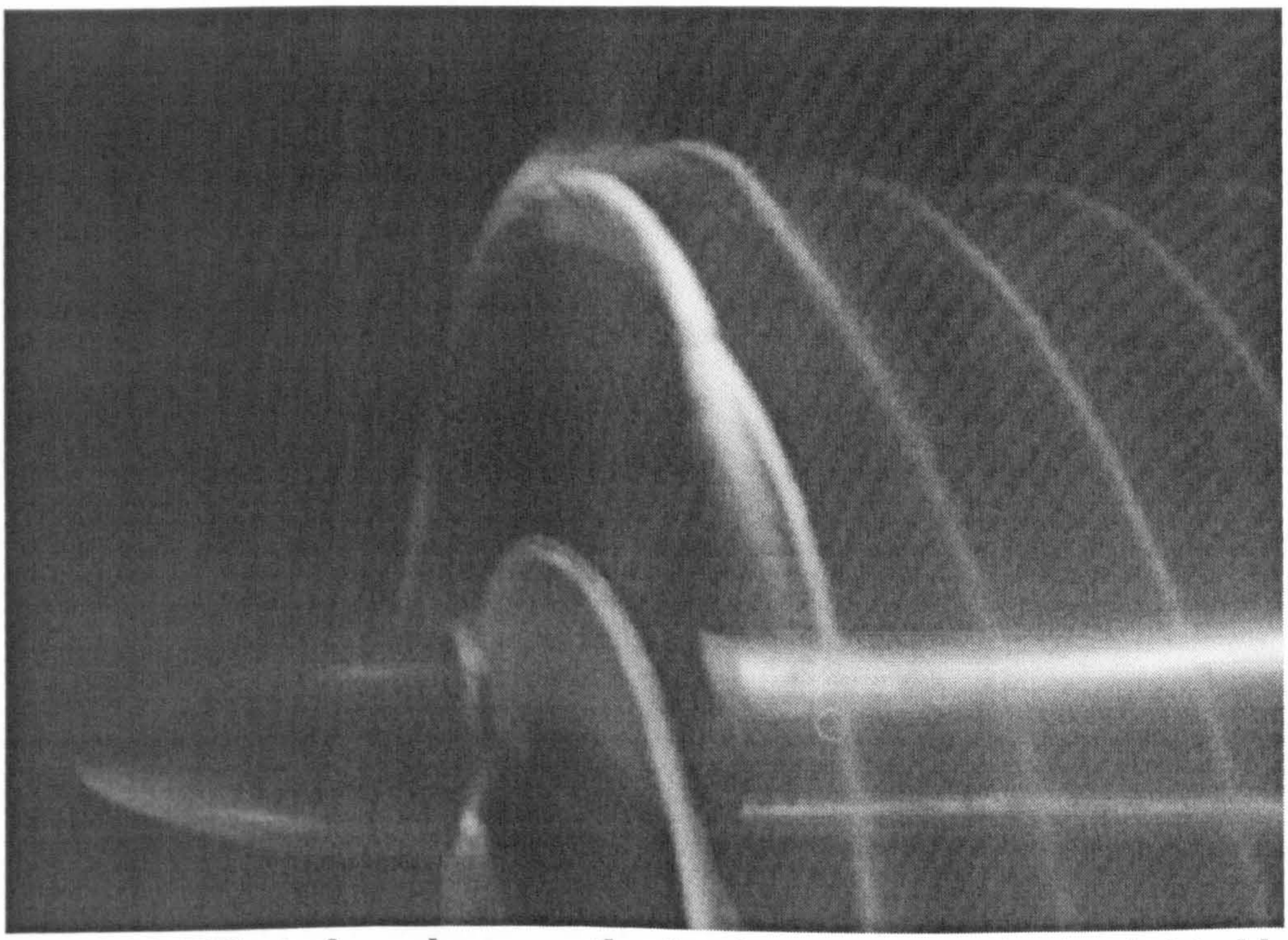

Picture 4.12 Effect of roughness on the development of cavitation behind base frame and 35 μm roughness at σ_u=Atm, α_D/α_S=20% and J=0.4

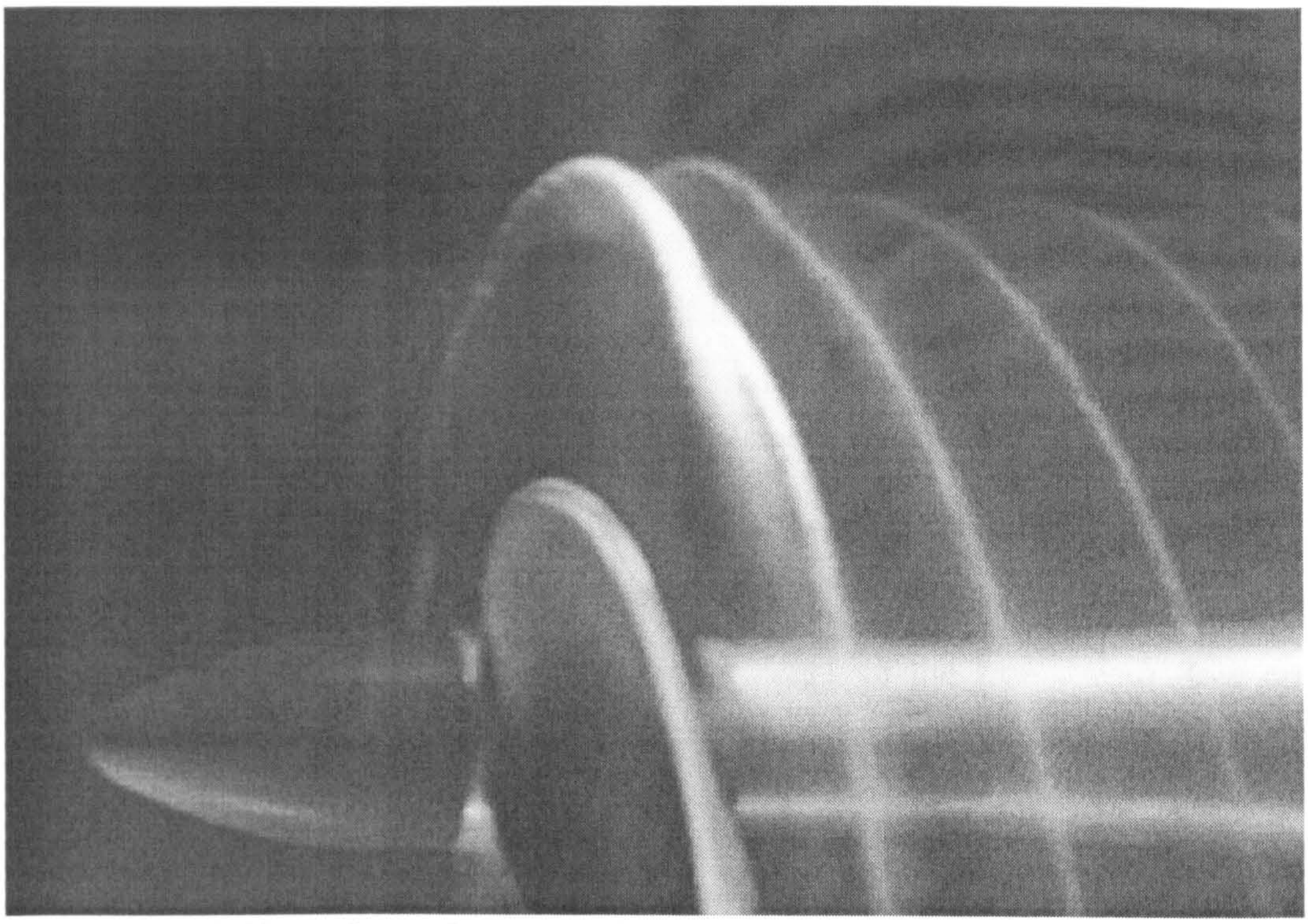

Picture 4.13 Effect of roughness on the development of cavitation behind base frame and 60 μm roughness at σ_u=Atm, α_D/α_S=20% and J=0.4

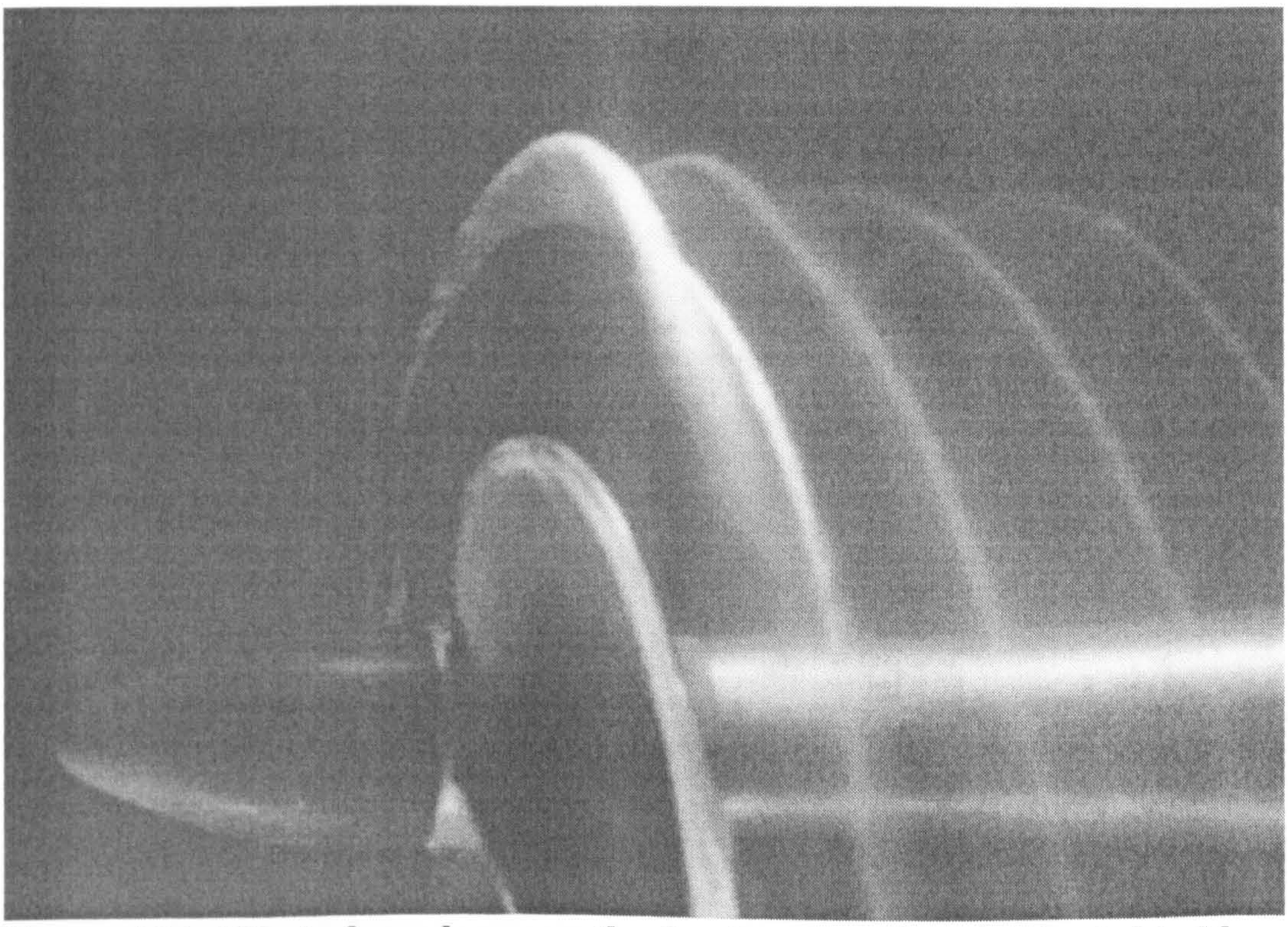

Picture 4.14 Effect of roughness on the development of cavitation behind base frame and 100 μm roughness at σ_u=Atm, α_D/α_S=20% and J=0.4

4.6 CONCLUSIONS

Systematic measurements were taken with a 5 bladed model propeller to explore the effects of the free-stream turbulence and the blade roughness on the characteristics of cavitation inception. The measurements were involved the inception values of various phases of the tip vortex and sheet cavitation under two different levels of the dissolved gas content. Based upon the analysis of the measurements, it can be concluded that:

- There was a clear effect of the level of turbulence of the free-stream flow on the inception of cavitation for the unattached tip vortex of a propeller. The systematic measurements indicated that the increased turbulence level by using wire mesh type turbulence generator encouraged the development of the unattached tip vortex cavitation. The trend between the inception number of cavitation and level of turbulence appeared to be linear at different levels of dissolved gas content.

- At low level of the dissolved gas content, the cavitation number appeared insensitive to the change in the level of turbulence beyond a critical level of the free-stream turbulence for the stages towards sheet cavitation, indicating the importance of bubble dynamics in these stages.

- The roughness also clearly affected the characteristics of the cavitation inception of the propeller. The systematic investigation on the effect of roughness has shown that the increased level of roughness also encouraged the development of the unattached tip vortex cavitation. It was also observed that the roughness can induce the cavitation as similar to the effect of the free-stream turbulence.

- At low level of the dissolved gas content, similar to the effect of the varying levels of the free-stream turbulence, the cavitation number appeared insensitive to the change in the roughness size beyond a critical roughness value for the stages towards sheet cavitation.

- The confirmatory tests to investigate the effect of the free-stream turbulence and roughness in combination confirmed that the dominating effect of the free-stream turbulence as well as the effect of roughness made higher level of the inception numbers of cavitation compared to the inception levels recorded under the effect of the turbulence generator or roughness in isolation.

- It can be conjectured that the level of the free-stream turbulence and the roughness affect the development of the boundary layer and the wire meshes may generate some nuclei to stimulate the process of cavitation.

- As far as the effect of free-stream turbulence or roughness in combination with the dissolved gas content is concerned, the effect varied depending upon the level of dissolved gas content and the type of cavitation investigated, which requires a thorough systematic investigation into the bubble dynamics.

- As observed in the propeller tests as well as in the foil tests, there seemed to be a similarity in the trends on the effects of the varying levels of the free-stream turbulence and the roughness height. This may suggest that one can establish a correspondence between the varying levels of the free-stream turbulence and roughness for the same inception effect.

- More reliable trend for the unattached tip vortex cavitation can also suggest that a semi-empirical approach can be established based upon the analysis of the results for the inception of this effect into the prediction of the inception of cavitation based upon the model test results.

- The technique in applying the roughness material (carborundum) by using glue is critical as well as in the removing procedure. Impurities occurred during the gluing process may cause premature cavitation and this process should be carried out carefully. It must also be avoided that damage to the blades may occur in the removing procedure.

CHAPTER 5 MEASUREMENTS OF NOISE WITH ECT103 MODEL PROPELLER

5.1 INTRODUCTION

Cavitation is one of the main sources of the propeller noise. In the case of special interest to the noise, it is most appropriate to combine its investigation with the cavitation. Because of this interdependency, it is expected that the main parameters contributing to the viscous scale effects in the inception of cavitation should be involved in the noise scaling too.

Therefore, the main objectives of the noise tests were similar to those of the cavitation inception tests. This involved the systematic exploration of the effects of the free-stream turbulence, roughness and the dissolved gas content on the noise characteristics of the test propeller. It is hoped that the systematic nature of the data to be produced will provide a basis for the prediction of the scale effect in combination with appropriate theoretical work to be carried out.

Similar to the cavitation inception tests described in Chapter 4, the measurements of the noise of the same model propeller for varying cavitation numbers and advance coefficients of the propeller were taken at two different values of the dissolved gas content in four groups.

- The first group was the measurements of the noise with the propeller in the free flow.
- The second group was the measurements at varying levels of the free-stream turbulence by using the same turbulence generator facility, described in Chapter 2.
- The third group was to investigate the effect of the roughness on the noise.

- The fourth group involved the noise measurements of the propeller subjected to the combined effects of varying levels of the free-stream turbulence and blade roughness.

In the following sections of this chapter, the details of the test conditions and experimental set-up, measurements, presentation of the results, analyses and conclusions of this experimental investigation are presented. Because of the volume of the measured data and the confirmatory nature of the fourth group of the measurements, only the results of the first, second and third groups of the measurements are included in the thesis

5.2 TEST CONDITIONS AND EXPERIMENTAL SET-UP

Measurements of noise were also carried out in the Emerson Cavitation Tunnel following each group of the cavitation inception tests. The experimental set-up was similar to the set-up for the inception tests in terms of the drive of the propeller, turbulence generation and application of the roughness, which were described in Chapter 4, therefore it will not be repeated here.

In order to simulate the design operational condition in full-scale, the cavitation number, σ_n, based on the rotational speed of the propeller was selected as $\sigma_n = 2.0$ at the design advance coefficient, J =0.6 (Wang, 1995). Where σ_n is defined as:

$$\sigma_n = \frac{P_{st} - P_v}{\frac{1}{2}\rho(ND)^2} \tag{5.1}$$

In order to study the effect of varying operational conditions in terms of the cavitation number and advance coefficient, an additional test condition of σ_n = Atmospheric and J=0.4 was included in the investigation. Thus, two test conditions, which corresponded to the design cavitation number $\sigma_n = 2.0$ and atmospheric cavitation number σ_n = Atm, at two different values of advance coefficient, J=0.6 and 0.4 were applied, respectively.

During the tests, it was appropriate to express the cavitation number based on axial velocity of the tunnel, U, which was kept constant at U = 4 m/s. Therefore, σ_u is defined as:

$$\sigma_u = \frac{P_{st} - P_v}{\frac{1}{2}\rho U^2} \tag{5.2}$$

However, cavitation number, σ_n, is based on the rotational speed of the propeller and this will change as the rotational speed is changed for two different advance coefficients at the constant axial speed. In this case the necessary vacuum to achieve the desired σ_n

values (i.e. σ_n = 2.0 and σ_n = Atmospheric) were calculated and imposed on the tunnel which yielded σ_u = 5.56 and σ_u = 14.0 respectively.

Similar to the cavitation inception tests, the dissolved gas content of water was measured by using a Jenway DO_2 meter 9071 apparatus and two different values were chosen as 20% and 44% representing the low and high levels of the gas content respectively.

A summary of the test parameters used in the noise tests is given in Table 5.1.

Table 5.1 Summary of parameters applied in noise tests

Parameter								
Dissolved gas content, α_D/α_S	**20%**				**44%**			
Cavitation number based on tunnel axial velocity, σ_u	5.56		Atm (~14.0)		5.56		Atm (~14.0)	
Advance coefficient, J	0.6	0.4	0.6	0.4	0.6	0.4	0.6	0.4
Tunnel axial velocity, U (m/s)	4	4	4	4	4	4	4	4
Rotational speed of propeller, N (rps)	27.77	41.66	27.77	41.66	27.77	41.66	27.77	41.66

5.2.1 EQUIPMENT FOR NOISE MEASUREMENT

The equipment used for the noise measurements consisted of a hydrophone placed on the tunnel lid, a charge amplifier, a measuring amplifier and a 1/3 Octave band pass filter, which are illustrated in Figure 5.1. The picture of the test equipment is also shown in Picture 5.1. The hydrophone was placed at the tunnel lid above the propeller in a small box filled with water and situated in the same vertical plane with the propeller at a vertical distance of 405 mm from the shaft centre line of the tunnel, as shown in Figure 5.1. The hydrophone, Brüel & Kjaer (B&K) type 8103, was basically an underwater microphone, which had a frequency range extended up to 200 kHz (Brüel & Kjaer, 1986). The normal range of a typical propeller noise in the cavitation tunnel varies from 2 Hz to 160 kHz.

When a hydrophone is used as a signal receiver like in the ECT, a pre-amplifier or charge amplifier or conditioning amplifier is required to receive high impedance output signals from the hydrophone. Therefore, a B&K type 2635 charge amplifier was used.

The charge amplifier passes only high-level signals directly to the measuring amplifier, B&K type 2610. The measuring amplifier indicates the measurement mode, range, gain, and input and output overload. Its frequency range is from 1 Hz to 200 kHz. It also has interchangeable meter scales for sound, vibration and voltage measurements (Brüel & Kjear, 1980). It was connected to a 1/3 octave band pass filter to make frequency analysis. The 1/3 octave band pass filter, B&K type 1617, has a frequency range 2 Hz to 160 kHz (Leathard, 1985).

The noise signals measured should be analysed in 1/3 Octave bands recommended by 15th ITTC (1978). The use of 1/3 Octave band frequency analysis averages modal effects in test facilities where many reflections occur. Therefore, the analysed data at each frequency by 1/3 Octave band pass filter were read from the measuring amplifier and recorded.

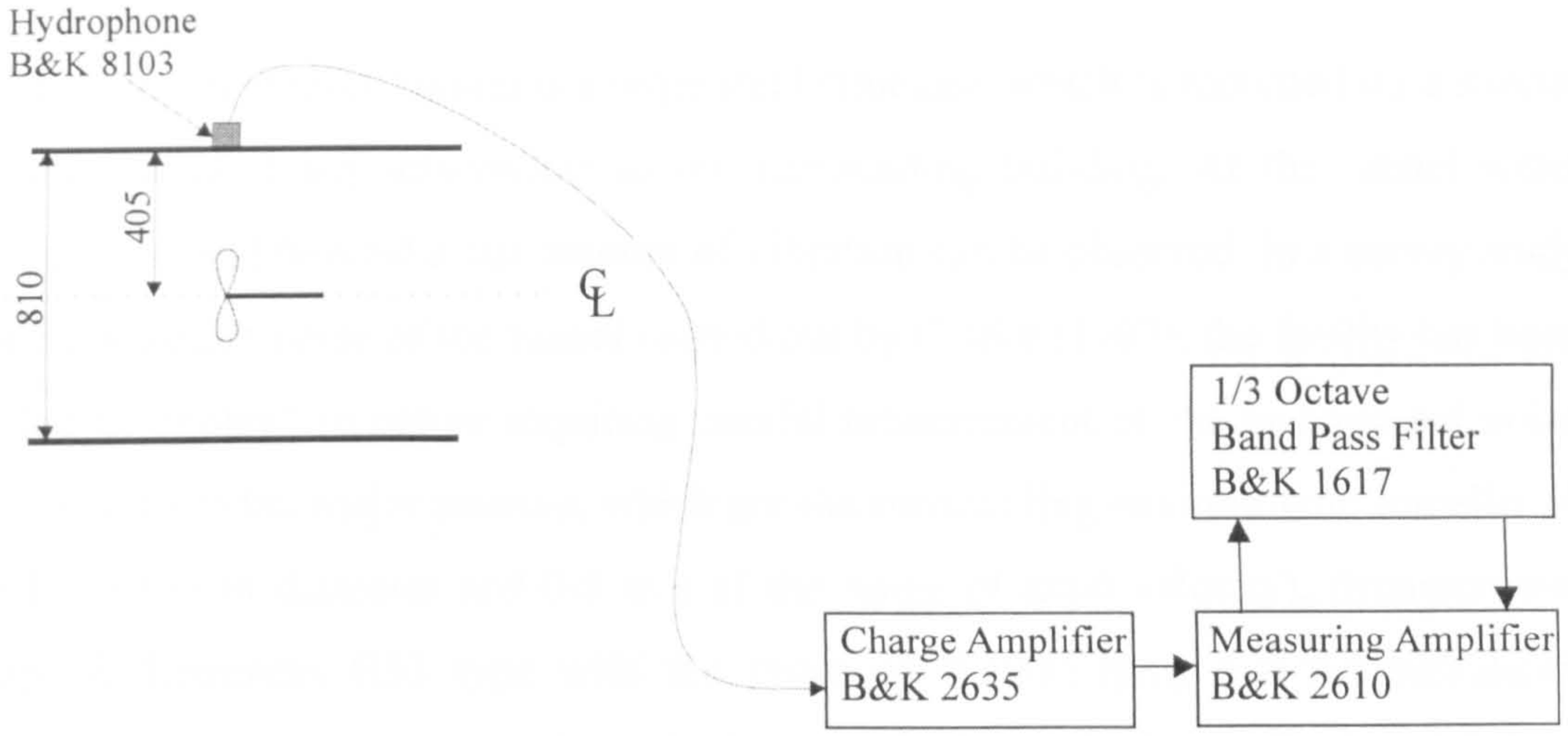

Figure 5.1 Layout of noise measurement equipment

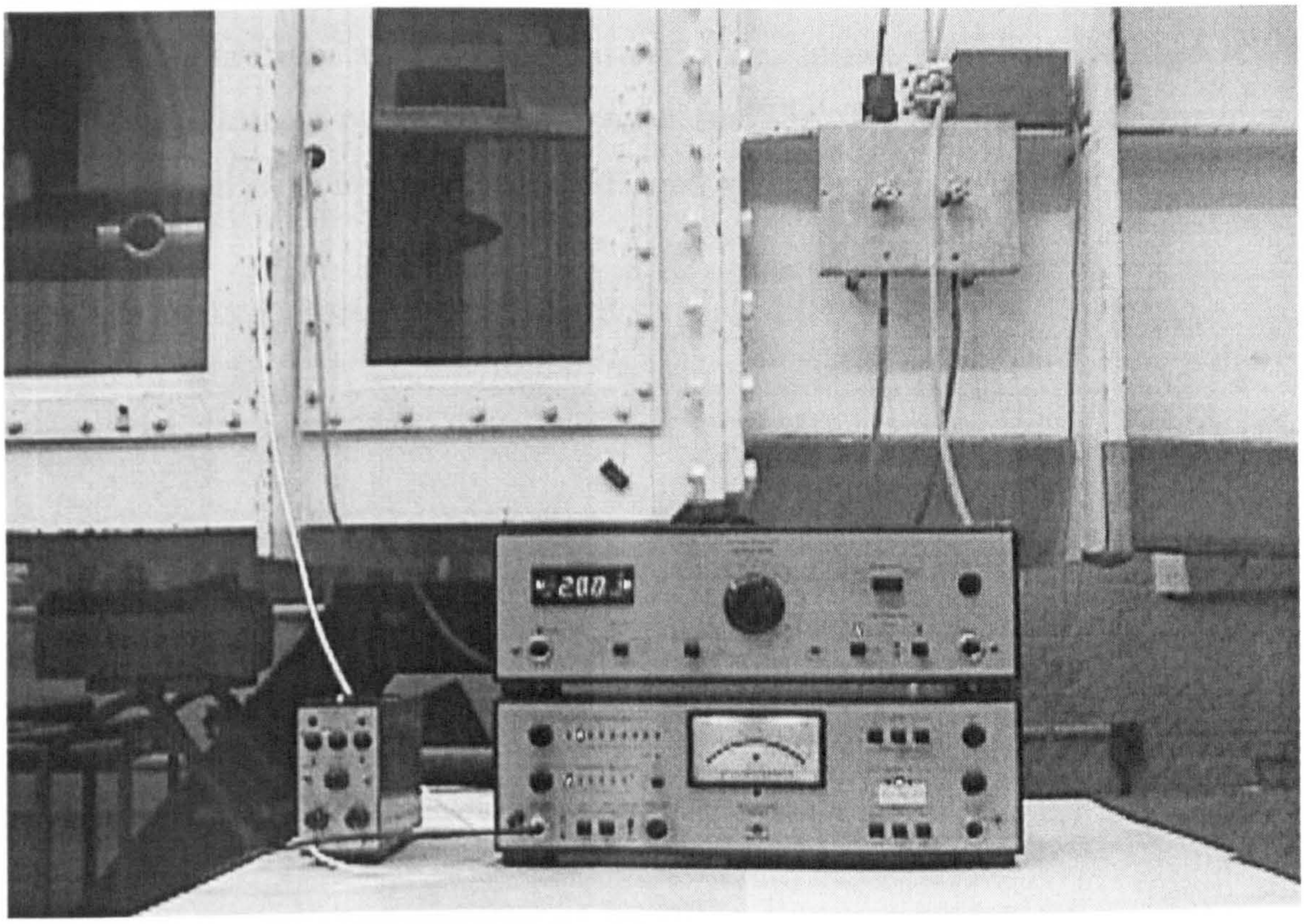

Picture 5.1 Noise test equipment in use in tunnel

5.2.2 MEASUREMENT PROCEDURE

The Emerson Cavitation Tunnel is a large steel structure, which is mounted on a special foundation without any attachment to the surrounding building. At the tunnel water speed of 5 m/s and beyond a fair amount of vibration can be observed. In a survey study on the background noise of the tunnel carried out by Clarke (1987), the facility has been specified as **"noisy"** in nature requiring careful measurement of the background noise contributed from the major sources, which are the surrounding environment, impeller (4 bladed, 1.39 m in diameter and 0-8 m/s of the range of axial velocity), dynamometer (Kempf & Remmers H33 type with the range of 0-3000 rpm) and the turbulence generator. Therefore, prior to each cavitation test the individual contributions of these sources were measured and recorded following the frequency analysis by B&K band pass filter.

For each run, the time allowed to settle down was 10 minutes before readings were taken. It was paid considerable attention to keep the environment as quiet as possible for the condition specified as **"nothing running"** in the tunnel. Since this condition could be strongly influenced by the environmental noise. While the impeller and dynamometer are in operation the noise levels are not affected by the environmental sources.

Table 5.2 shows a summary of the conditions applied for the noise measurements.

Table 5.2 Summary of conditions for noise tests

Test No	Test Condition	Test Condition Details
1	Background noise with base frame only	Nothing running in the tunnel
2		Only impeller running at U = 4 m/s
3		Only dynamometer running at N=27.77 rps and N=41.66 rps
4		Impeller and dynamometer in operation at U=4 m/s and N=27.77 rps
5		Impeller and dynamometer in operation at U=4 m/s and N=41.66 rps
6	Background noise with base frame and largest-sized mesh	U= 4 m/s and N=27.77 rps
7		U= 4 m/s and N=41.66 rps
8	Background noise with base frame and medium-sized mesh	U= 4 m/s and N=27.77 rps
9		U= 4 m/s and N=41.66 rps
10	Background noise with base frame and finest-sized mesh	U= 4 m/s and N=27.77 rps
11		U= 4 m/s and N=41.66 rps
12	Propeller noise with base frame and largest-sized mesh	U= 4 m/s and N=27.77 rps
13		U= 4 m/s and N=41.66 rps
14	Propeller noise with base frame and medium-sized mesh	U= 4 m/s and N=27.77 rps
15		U= 4 m/s and N=41.66 rps
16	Propeller noise with base frame and finest-sized mesh	U= 4 m/s and N=27.77 rps
17		U= 4 m/s and N=41.66 rps
18	Propeller noise with base frame and 35 μm roughness	U= 4 m/s and N=27.77 rps
19		U= 4 m/s and N=41.66 rps
20	Propeller noise with base frame and 60 μm roughness	U= 4 m/s and N=27.77 rps
21		U= 4 m/s and N=41.66 rps
22	Propeller noise with base frame and 100 μm roughness	U= 4 m/s and N=27.77 rps
23		U= 4 m/s and N=41.66 rps
24	Propeller noise with base frame, largest-sized mesh and 35 μm roughness	U= 4 m/s and N=27.77 rps
25		U= 4 m/s and N=41.66 rps
26	Propeller noise with base frame, largest-sized mesh and 60 μm roughness	U= 4 m/s and N=27.77 rps
27		U= 4 m/s and N=41.66 rps
28	Propeller noise with base frame, finest-sized mesh and 35 μm roughness	U= 4 m/s and N=27.77 rps
29		U= 4 m/s and N=41.66 rps
30	Propeller noise with base frame, finest-sized mesh and 60 μm roughness	U= 4 m/s and N=27.77 rps
31		U= 4 m/s and N=41.66 rps

5.3 ANALYSIS AND PRESENTATION OF RESULTS

Sound pressure level at each centre frequency ranging from 50 Hz to 160 kHz was recorded from the measuring amplifier showing the analysed data by the 1/3 Octave band filter, described in Section 5.2.1. In order to be able to compare and to average the values obtained using different filter widths, the concept of equivalent spectrum was used. This is defined as the level that would have been measured using an ideal 1 Hz filter. The measured sound pressure level in each 1/3 Octave band was reduced to an equivalent 1 Hz bandwidth by the following formula recommended by 15th ITTC (1978):

$$SPL = SPL_m - 10\log\Delta f \tag{5.3}$$

where:

- SPL is the reduced sound pressure level to 1 Hz bandwidth
- SPL_m is the measured sound pressure level in the bandwidth
- Δf is a filter bandwidth.

Level of net sound pressure at each centre frequency, SPL_N, was calculated by subtracting corresponding background noise, SPL_B, from the total (i.e. propeller plus background) noise level, SPL_T, by using the following logarithmic subtraction formula (Ross, 1976):

$$SPL_N = 10\log[10^{(SPL_T/10)} - 10^{(SPL_B/10)}] \tag{5.4}$$

The results of the analysed measurements are presented in Figures 5.3 through 5.42. In each graph:

- the logarithmic-scaled x-axis represents the centre frequencies in Hz
- while the linear-scaled y-axis represents the sound pressure levels in dB re 1 μPa (standard reference pressure for water), 1 Hz.

In the figure captions:

- α_D/α_S denotes the dissolved gas content ratio where:
    - α_D is the dissolved gas content at the static pressure applied
    - while α_S is the dissolved gas content of saturated water at 760 mmHg.

Amongst these figures,

- Figures 5.3 and 5.4 present the breakdown of the background noise of the tunnel with reference to its contributing sources at two levels of the dissolved gas content.
- Figures 5.5 through 5.12 present the contribution of the varying size of wire meshes on the background noise characteristic of the tunnel at the two different levels of gas content. The results are presented at two different operating conditions as specified earlier.
- Figures 5.13 through 5.20 show the effect of the free-stream turbulence on the net propeller noise
- while Figures 5.21 through 5.28 present the effect of roughness for the two operating conditions and two levels of gas content.

In order to display the effect of the dissolved gas content on the net propeller noise, Figures 5.29 through 5.42 are included, which are associated with only σ_u = Atm, due to the volume of the measured data. In this group:

- Figures 5.29 and 5.30 show the effect of gas content when the propeller was operating in the free-flow
- while the effect of the gas content behind the three different levels of the mesh is presented in Figures 5.31 through 5.36.
- Finally, the effect of the gas content on the net propeller noise for the three different levels of blade roughness is shown in Figures 5.37 through 5.42

In some of the following figures presenting the noise analyses, one may notice that the noise data were removed at certain figures. This was because that the levels of background noise at that range of frequencies were higher than the level of the propeller noise resulting in negative logarithmic values according to Equation (5.4), which did not make sense to present.

5.4 DISCUSSION OF RESULTS

Prior to the discussion of the analysed results, some points concerning undesirable signals, which could affect the results, should be considered. In general, the electrical signal from a hydrophone mounted in the tunnel consists of a variety of components (Bryden and Webb, 1986), which include:

- Water Borne Noise: This consists of the genuine propeller and cavitation noise.
- Vibration Pickup: Hydrophones are sensitive to vibration as well as acoustic noise.

The latter is particularly a serious problem as the dynamometer produces structural vibrations at frequencies, which may be confused with acoustic signals.

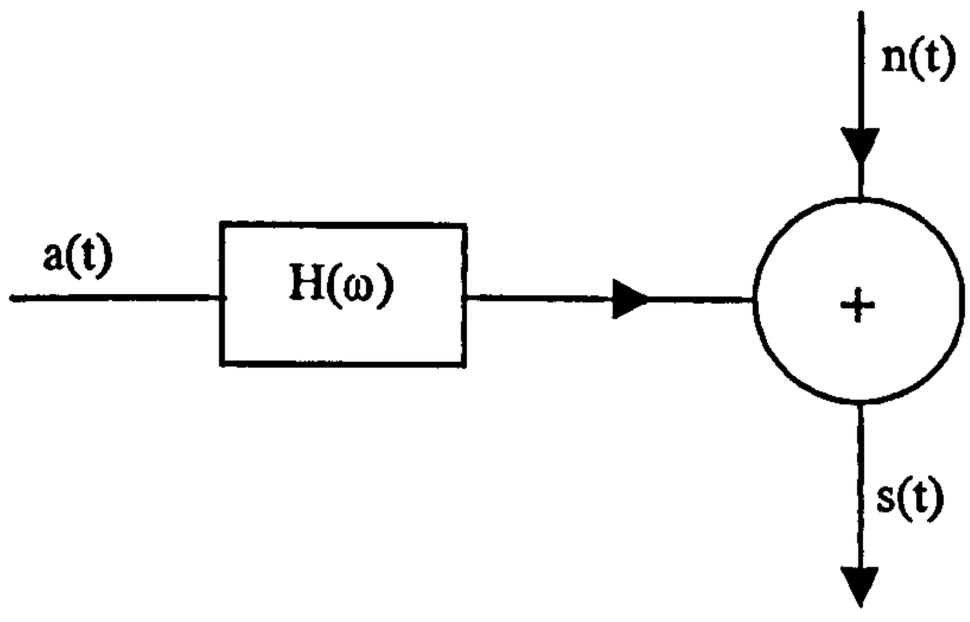

Figure 5.2 Vibration pickup with extraneous noise

As shown in Figure 5.2, the process of vibration pickup by a hydrophone can be effectively treated as a two input, single output system. Where:

- a(t) is the vibration expressed as a function of time, t
- n(t) is the waterborne noise
- s(t) is the hydrophone output
- H(ω) is the transfer function as a function of angular frequency ω, governing the vibration pickup of the hydrophone.

Therefore, the process of vibration pickup should be carried out during the noise measurements to obtain the genuine propeller noise. Unfortunately this process was not performed in the noise measurements of the propeller and has been left for the future work.

Figures 5.3 and 5.4 show the comparisons of the levels of the background noise of the tunnel in the presence of the base frame for varying levels of the dissolved gas content. It is clear that the dynamometer is the major source contributing to the total level of the background noise. As shown in these figures, when the tunnel's impeller is in operation alone, the level of noise is also considerable. As soon as the dynamometer is switched on, the combined noise level of the two sources is similar to the dynamometer's noise level alone, indicating the dominating effect of the dynamometer on the level of background noise. These findings are observed at both levels of dissolved gas content.

In Figures 5.5 through 5.12, the effect of the free-stream turbulence, which was generated by different sizes of the wire meshes, on the background noise level is shown for the two operating conditions and two different levels of gas content. In the frequency range of 50 Hz to 1000 Hz, the noise signals do not show any distinct trend for the turbulence effect. However, in the high frequency region above the centre frequency of 1000 Hz, the noise signals under the atmospheric condition clearly display that the medium-sized mesh is the noisiest and the largest and finest-sizes meshes come next contributing to the background noise level of the tunnel, as shown in Figures 5.6, 5.7 and 5.8. The above trend changes for the cavitation number, σ_u=5.56, such that the largest-sized mesh becomes the noisiest whilst the finest-sized mesh is the quietest of the three, as shown in Figures 5.9 through 5.12.

During the noise tests, it was noticed that the all meshes under the atmospheric condition (at J = 0.6) were whistling. Therefore, the levels of noise of all the meshes under the atmospheric condition at high frequency band between 1000 Hz and 160 kHz are greater than those under the vacuum condition, indicating that cavitation number has a considerable effect on the background noise signals in the high frequency region.

It is well known that noise characteristics of a propeller usually display a general trend as shown in Figure 1.4 of Chapter 1 (Lovik, 1981). The similar trend was also observed in the noise characteristics of the model propeller tested. Bearing this trend in mind, in the following, the discussion of the net propeller noise is presented.

Figures 5.13 through 5.20 show the influence of varying levels of the free-stream turbulence on the net propeller noise for the two operating conditions and two levels of gas content. By looking into these figures, to establish any trend particularly in the low frequency region is very difficult. The low frequency region, which ranges from 50 Hz to approximately 1000 Hz, contains the effect of the blade rate frequency (BRF) of the propeller (i.e. BRF= 139 and 208 Hz for N=27.77 rps and 41.66 rps, respectively) and its harmonics, as indicated in Figure 1.4 of Chapter 1. On the other hand, the vibration survey of the tunnel carried out by Clarke (1987) showed that the frequencies of the structural vibration generated by the dynamometer and impeller were also found to be effective in this low frequency region. Therefore, it is most likely that the noise levels due to the blade rate frequency and its harmonics as well as those due to the structural vibration must be effective in this frequency region.

During the noise tests, the cavitation was always observed when cavitation number is equal to $\sigma_u = 5.56$, and at this condition noise signals have different characteristics at each level of the gas content (i.e. Figures 5.17 through 5.20) due to the presence of cavitation. In contrast to the cavitating case, under the atmospheric condition, the levels of the propeller noise were quite steady (i.e. Figures 5.13 through 5.16), displaying a trend that as the level of free-stream turbulence is increased, the level of the propeller noise is slightly increased.

Figures 5.21 through 5.28 show the effect of varying levels of roughness on the net propeller noise for the two operating conditions and two levels of gas content. It seems that the roughness has a distinct influence on the level of the propeller noise in the high frequency region (1000 Hz and beyond) at atmospheric condition, for both levels of dissolved gas content. As shown in Figures 5.21 through 5.24, as the level of roughness is increased, the net propeller noise is reduced. On the other hand, for the cavitation number, $\sigma_u = 5.56$, the trend varies depending upon the advance coefficient and the

level of the dissolved gas content, indicating that the bubble dynamics is more important on the noise signals due to presence of the cavitation, as shown in Figures 5.25 through 5.28.

In Figures 5.29 through 5.42, the effect of dissolved gas content on the net propeller noise is shown for varying levels of free-stream turbulence and roughness heights at two different advance coefficients. As far as the free-stream turbulence series are concerned, it appears that the effect of the dissolved gas content on the levels of noise is very small, particularly in the high frequency region. However, at the high level of gas content, the propeller noise at each level of the free-stream turbulence is reduced slightly, as shown in Figures 5.29 through 5.34, demonstrating the fact that the high level of the dissolved gas content has a cushioning effect in the collapse stage of bubble which reduces the noise level as stated by Ross (1976) and 18th ITTC (1987). Nevertheless, this trend is not observed with the case of base frame and finest-sized mesh, as shown in Figures 5.35 and 5.36.

Figures 5.37 through 5.42 show the effect of dissolved gas content on the net propeller noise for varying levels of the blade roughness at two different advance coefficients. One can see in these figures that as the level of the dissolved gas content is increased, the propeller noise is also reduced slightly at each level of the roughness except at the roughness height of 100 μm.

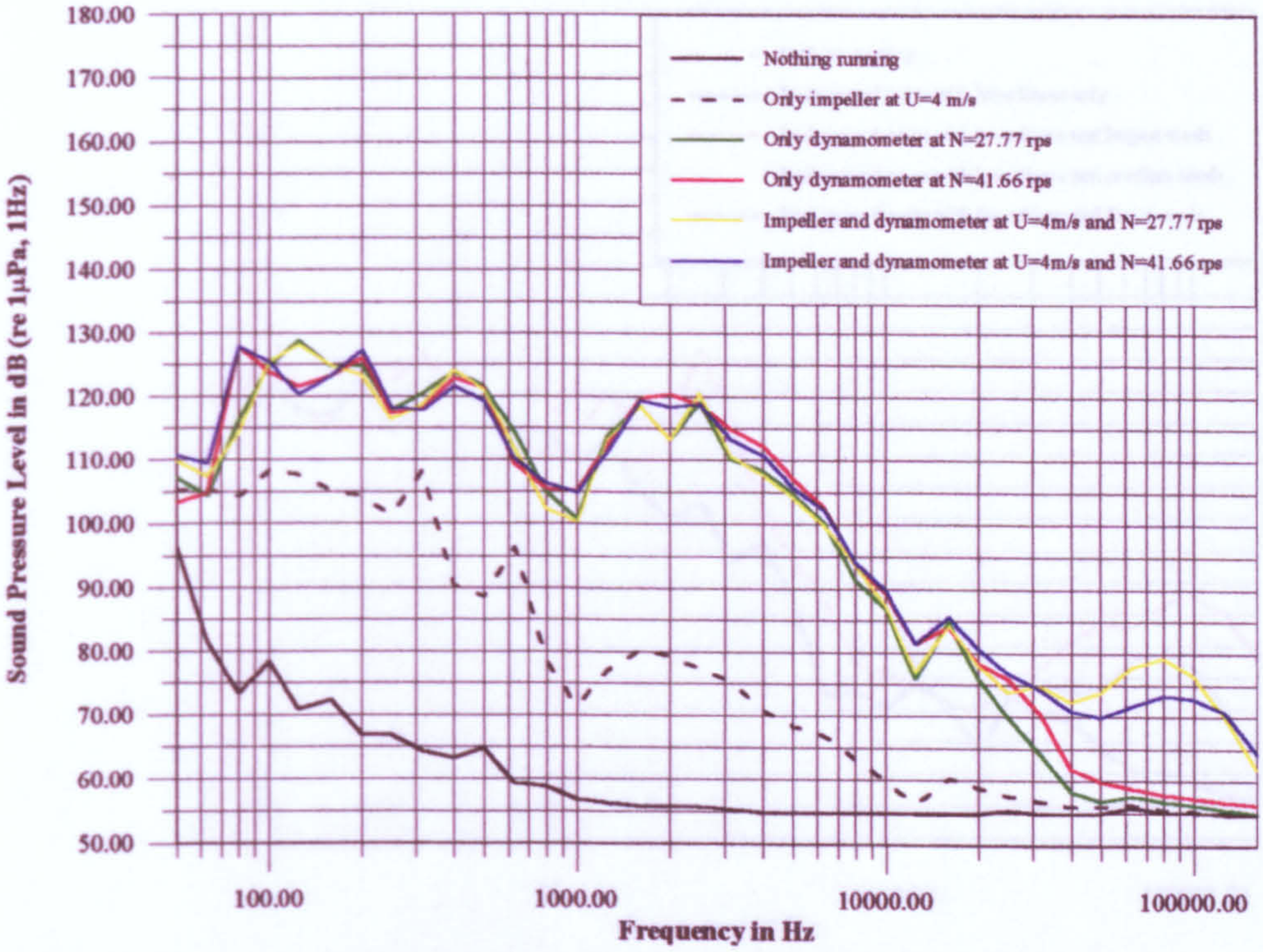

Figure 5.3 Breakdown of sources contributing to the level of background noise at α_D/α_S=20%

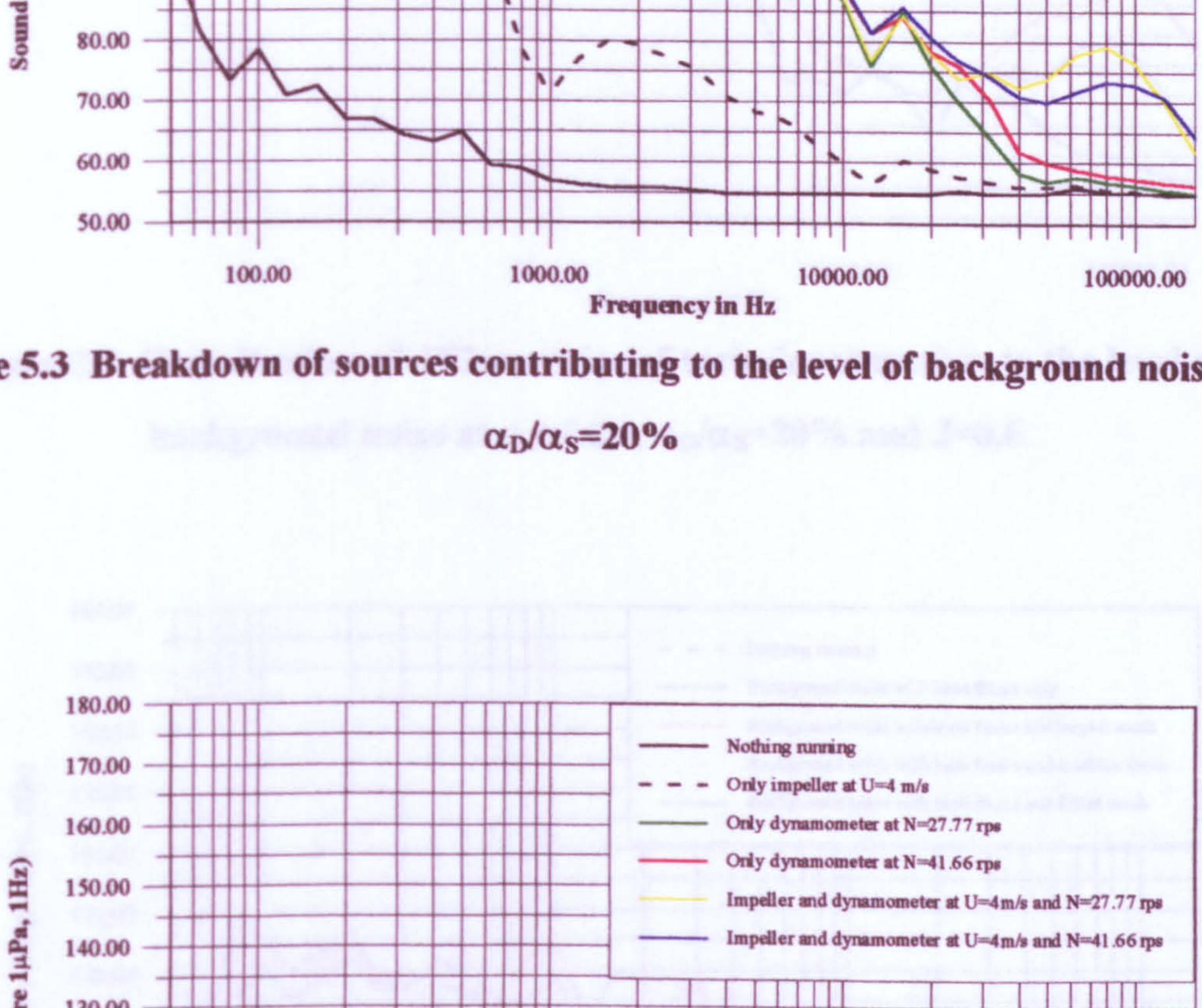

Figure 5.4 Breakdown of sources contributing to the level of background noise at α_D/α_S=44%

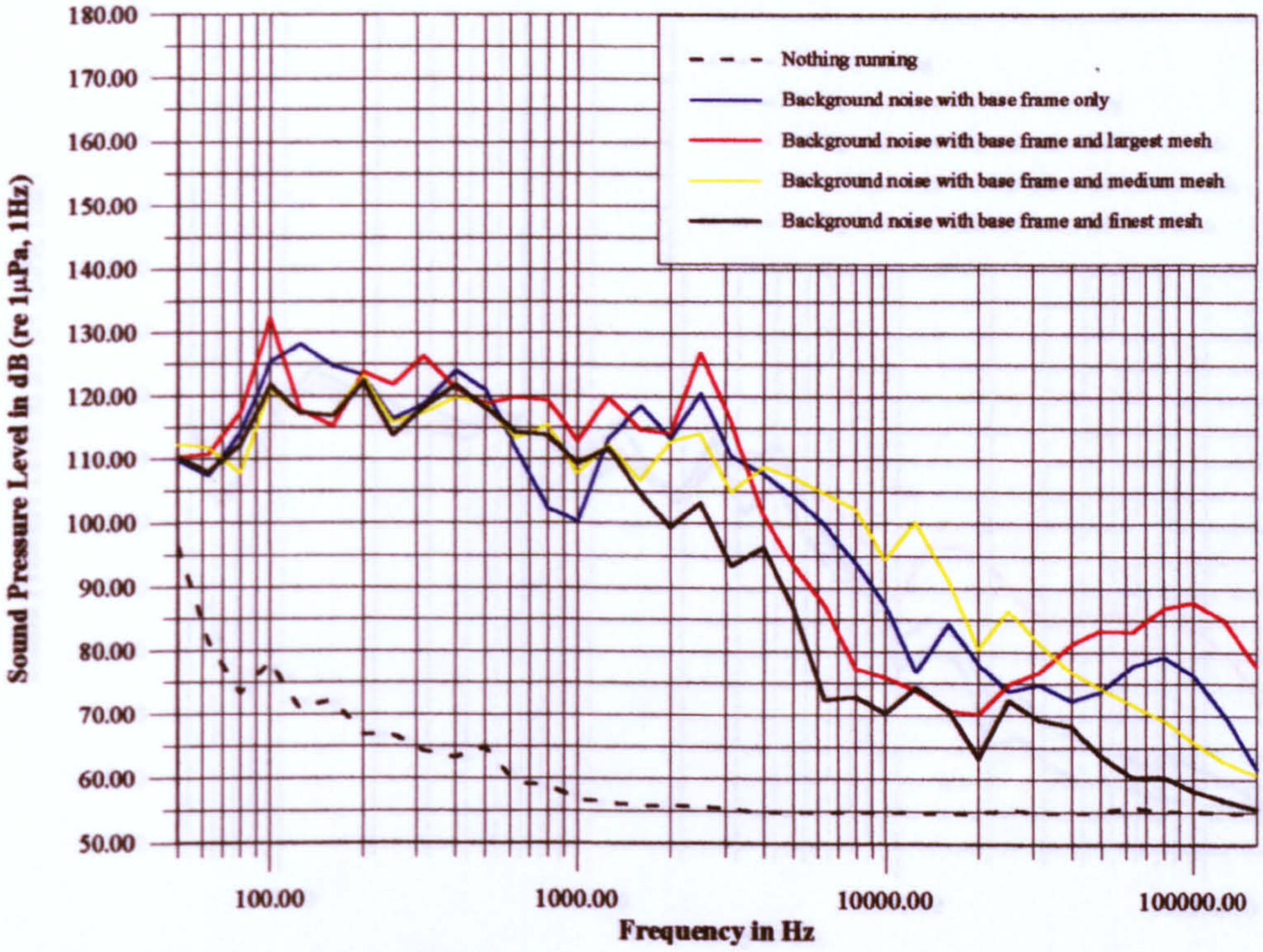

Figure 5.5 Contribution of different size of turbulence meshes to the level of background noise at σ_u=Atm, α_D/α_S=20% and J=0.6

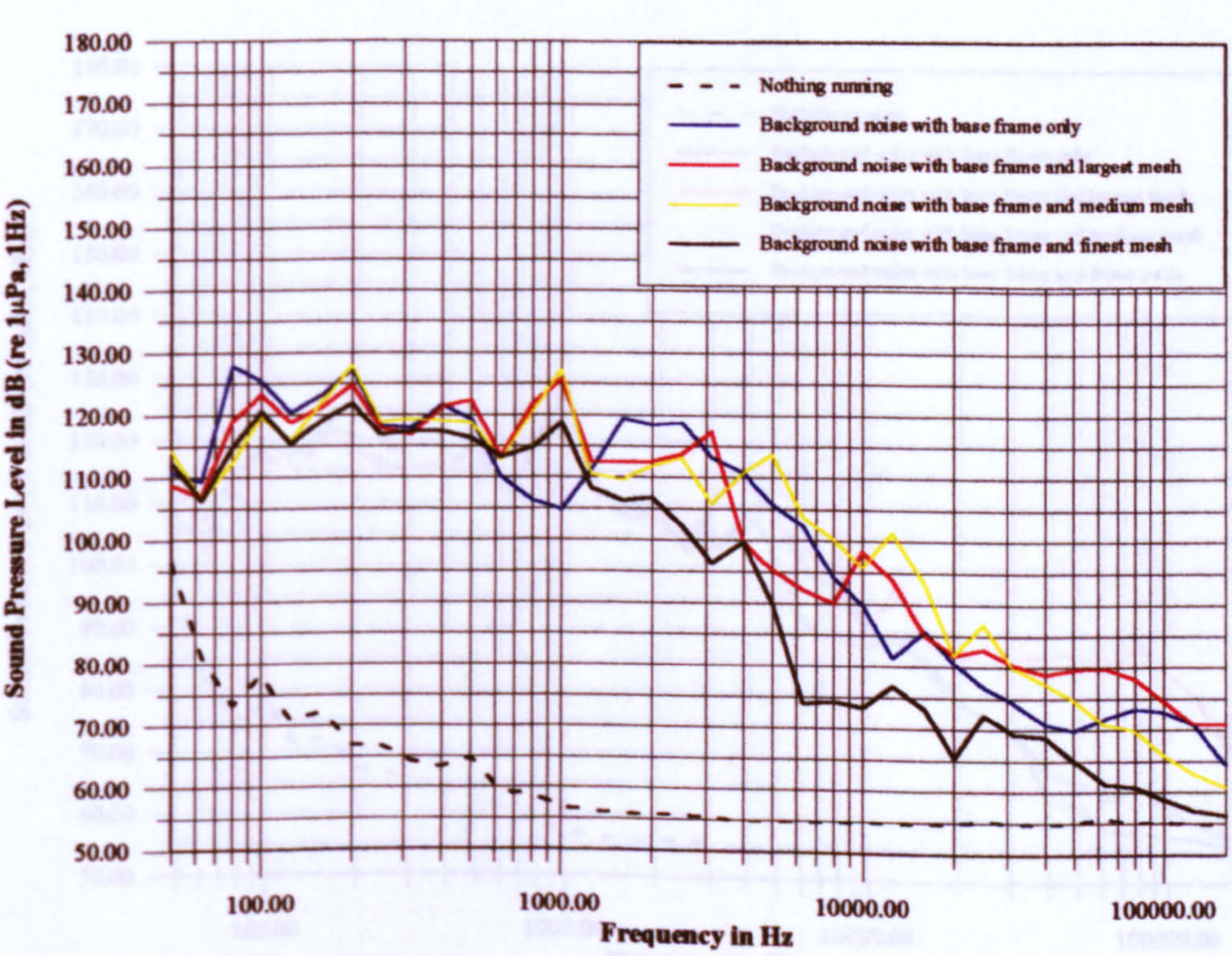

Figure 5.6 Contribution of different size of turbulence meshes to the level of background noise at σ_u=Atm, α_D/α_S=20% and J=0.4

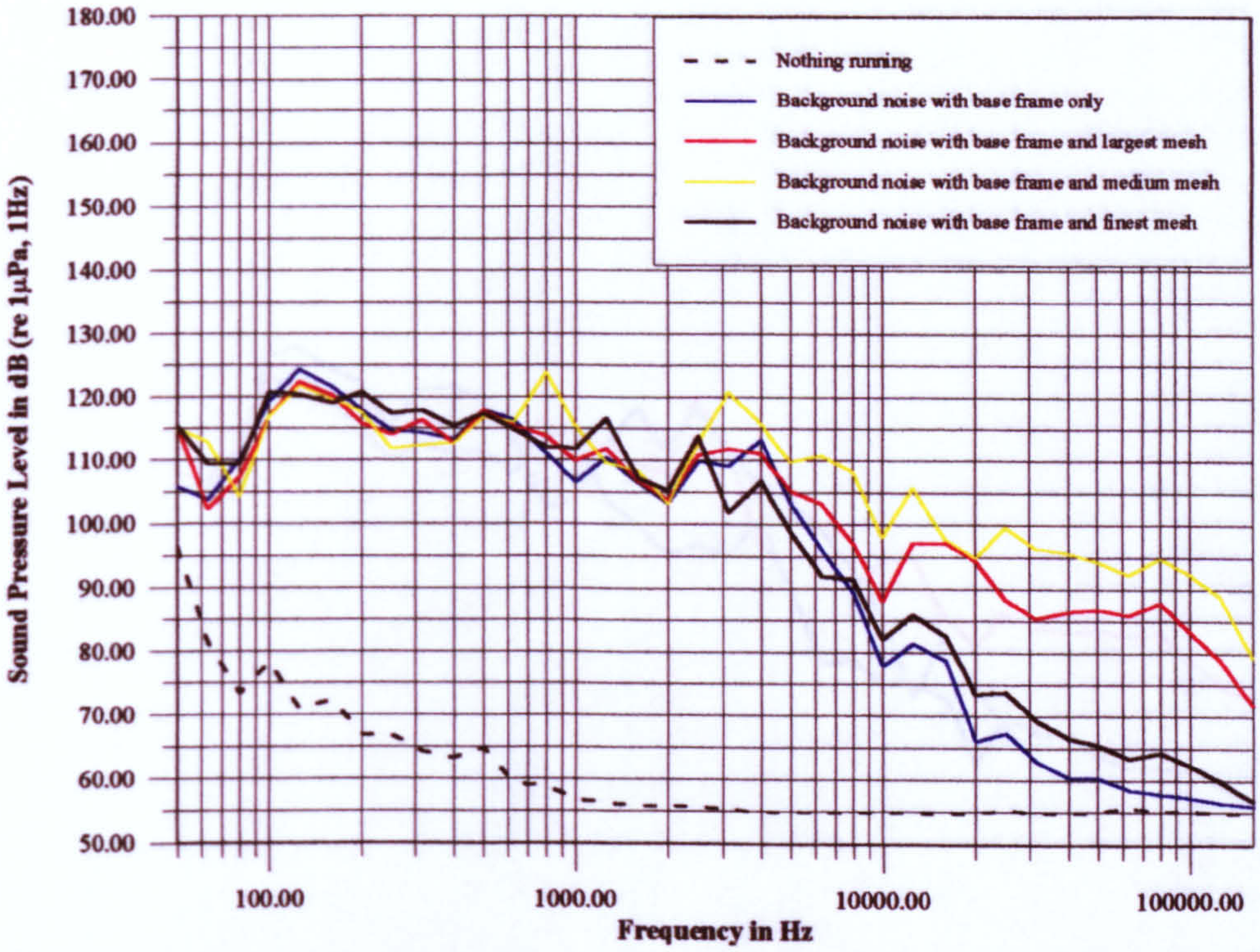

Figure 5.7 Contribution of different size of turbulence meshes to the level of background noise at σ_u=Atm, α_D/α_S=44% and J=0.6

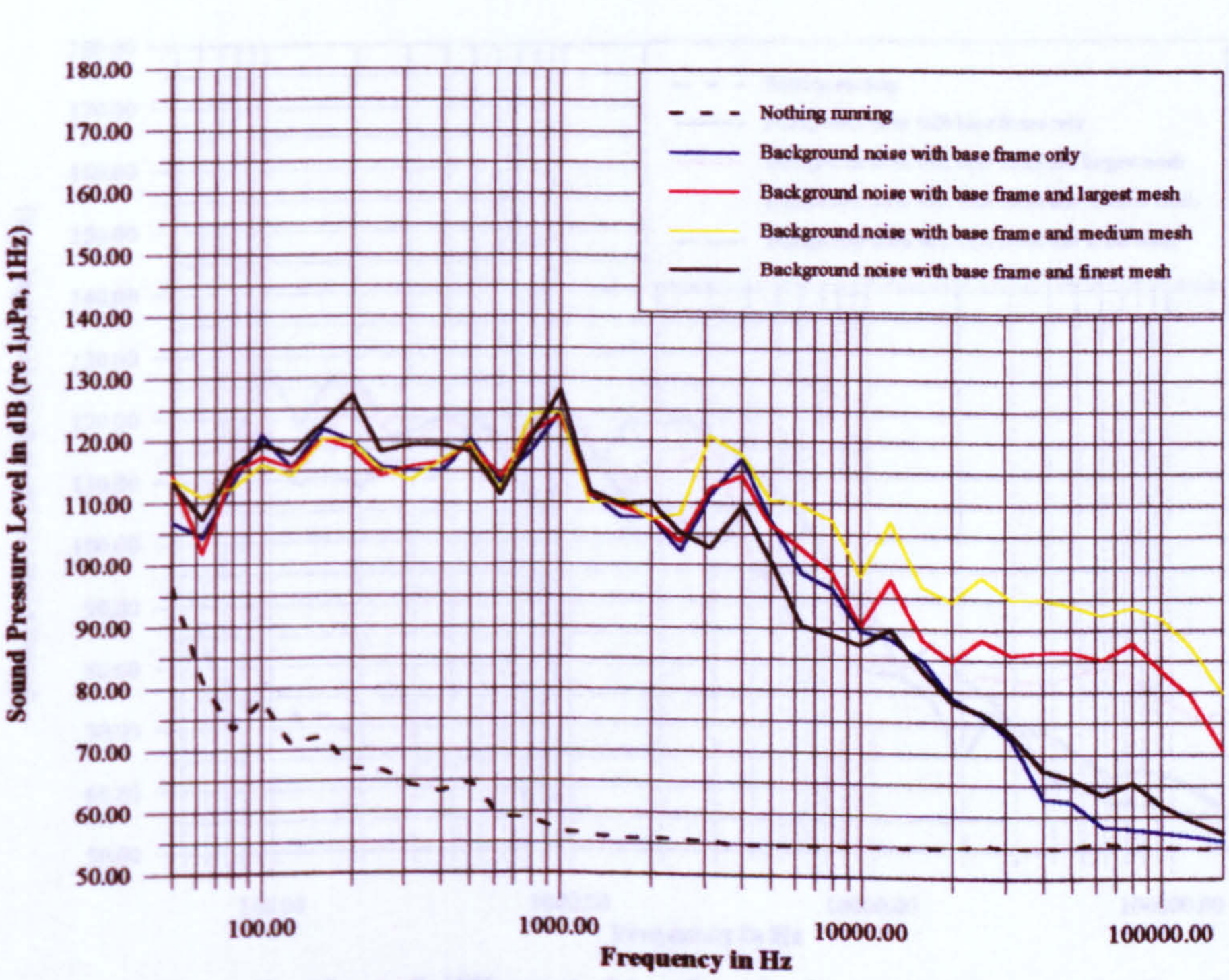

Figure 5.8 Contribution of different size of turbulence meshes to the level of background noise at σ_u=Atm, α_D/α_S=44% and J=0.4

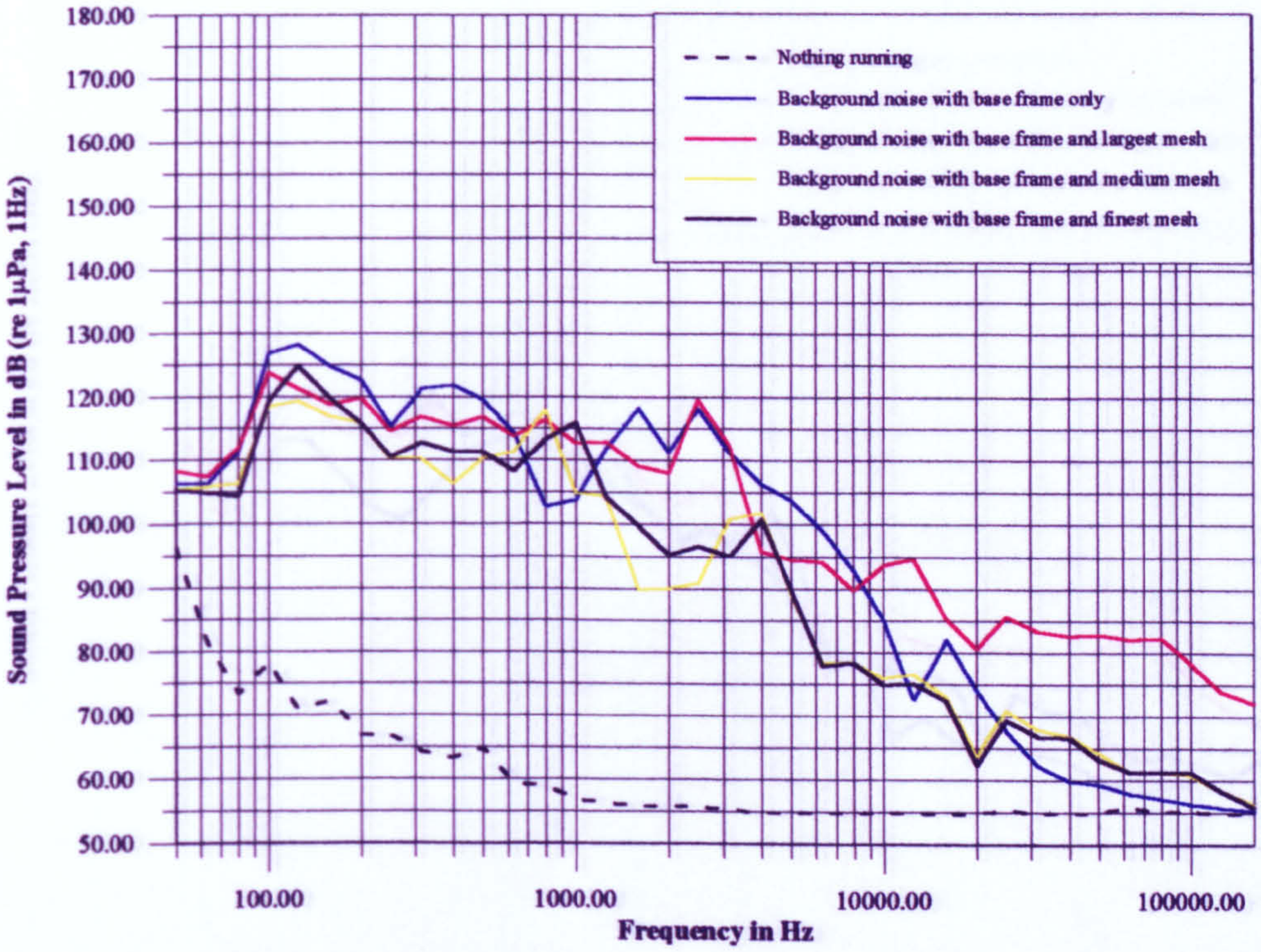

Figure 5.9 Contribution of different size of turbulence meshes to the level of background noise at σ_u=5.56, α_D/α_S=20% and J=0.6

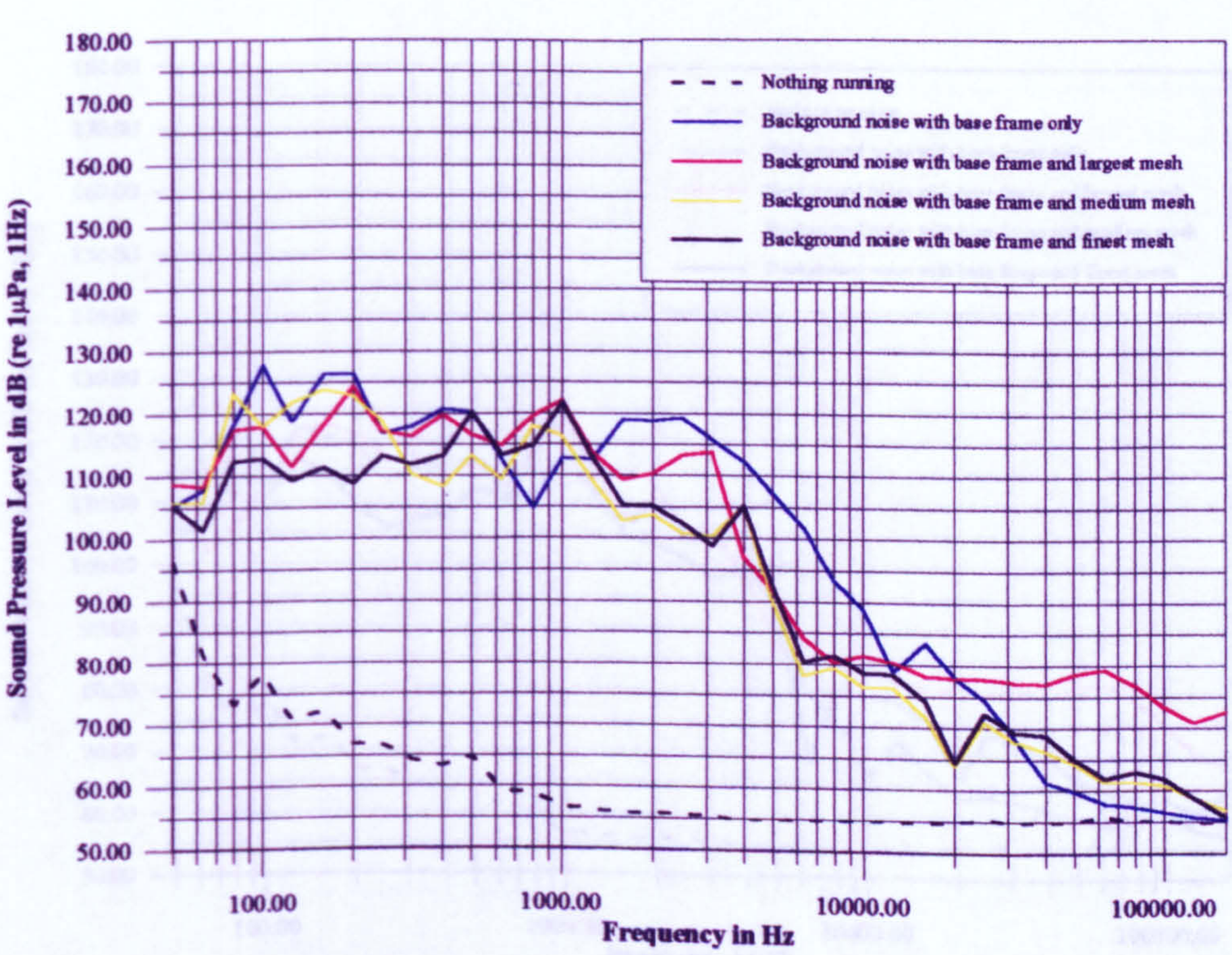

Figure 5.10 Contribution of different size of turbulence meshes to the level of background noise at σ_u=5.56, α_D/α_S=20% and J=0.4

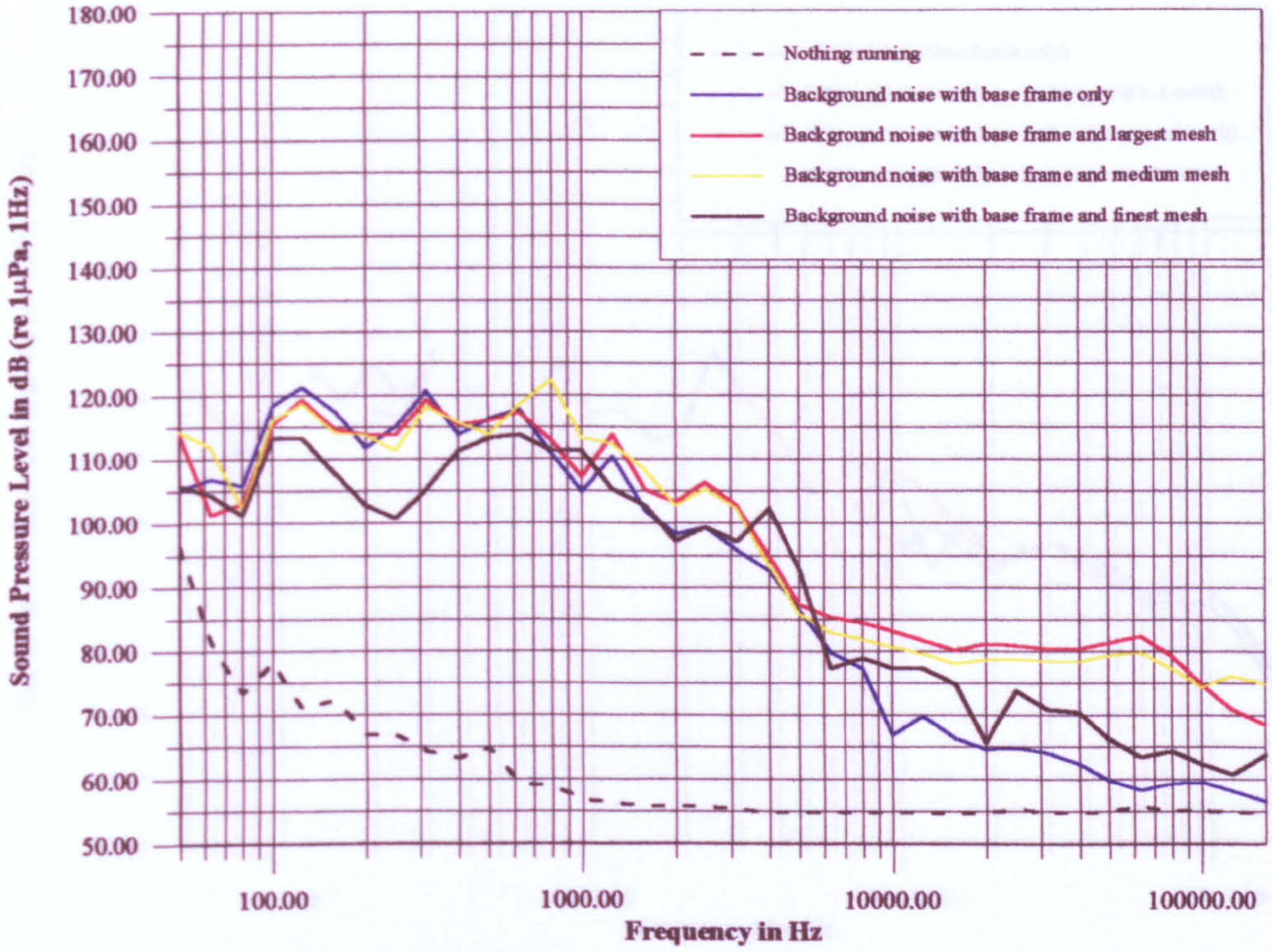

Figure 5.11 Contribution of different size of turbulence meshes to the level of background noise at σ_u=5.56, α_D/α_S=44% and J=0.6

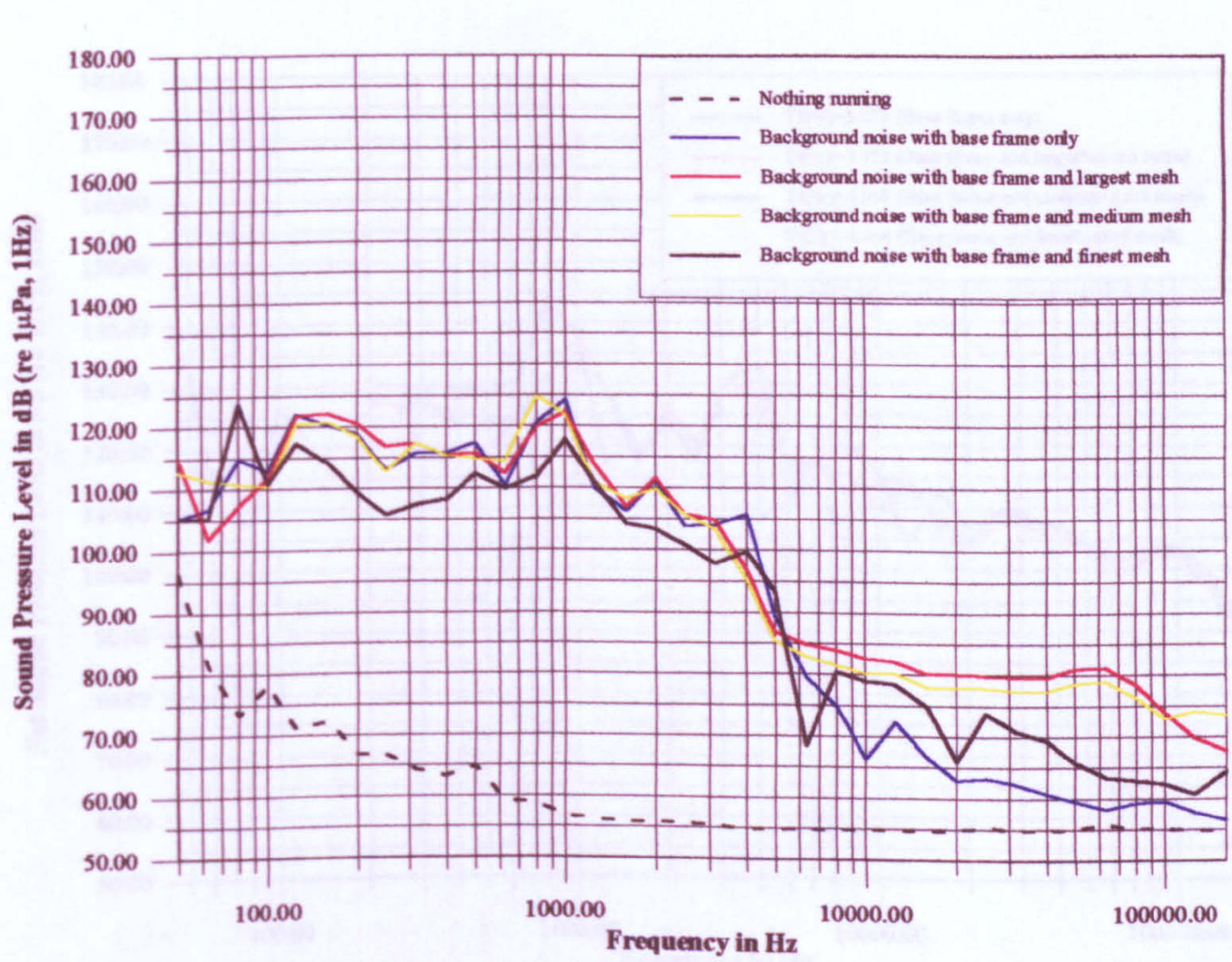

Figure 5.12 Contribution of different size of turbulence to the level of background noise at σ_u=5.56, α_D/α_S=44% and J=0.4

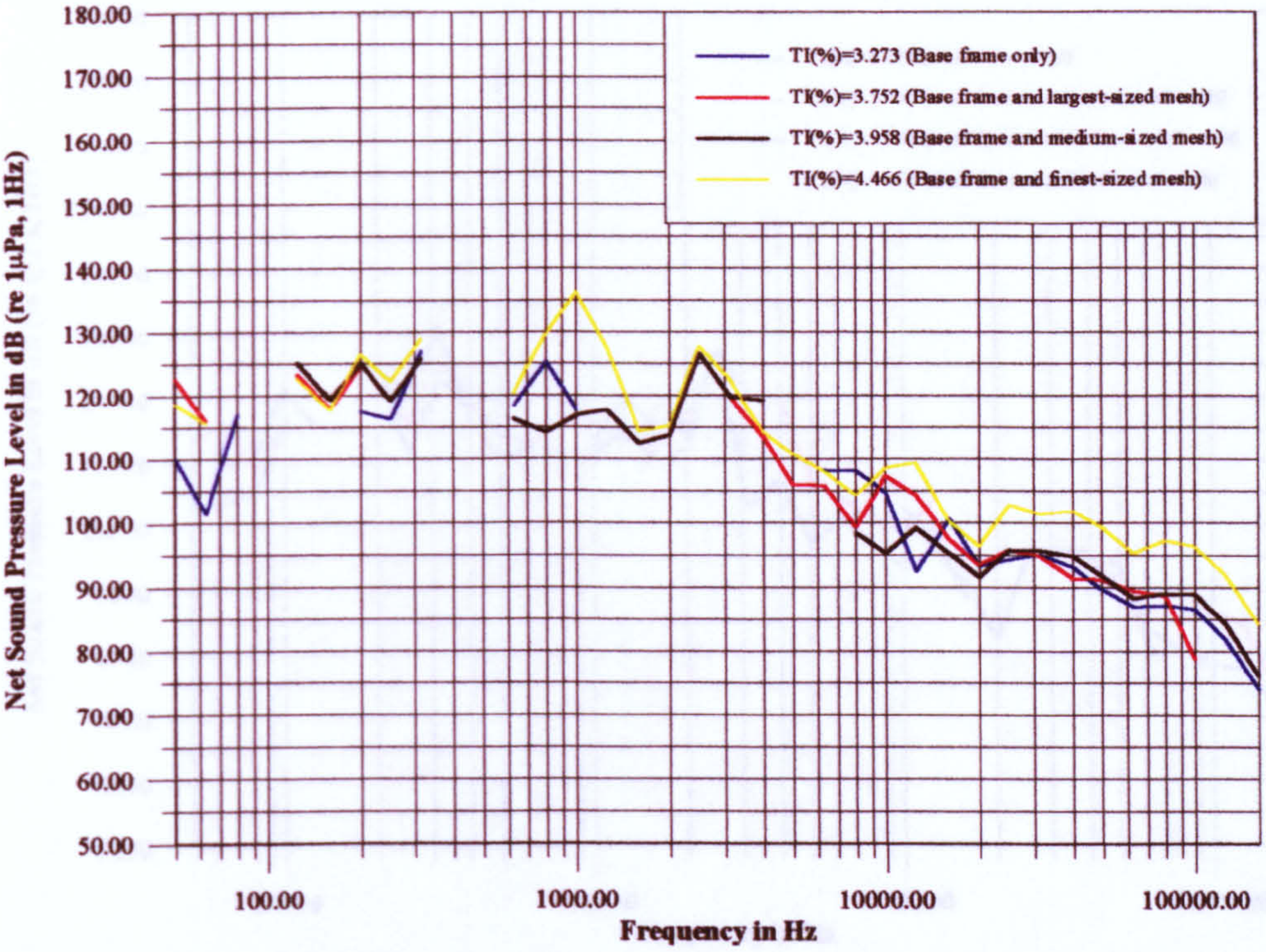

Figure 5.13 Effect of free-stream turbulence on the level of net propeller noise at σ_u=Atm, α_D/α_S=20% and J=0.6

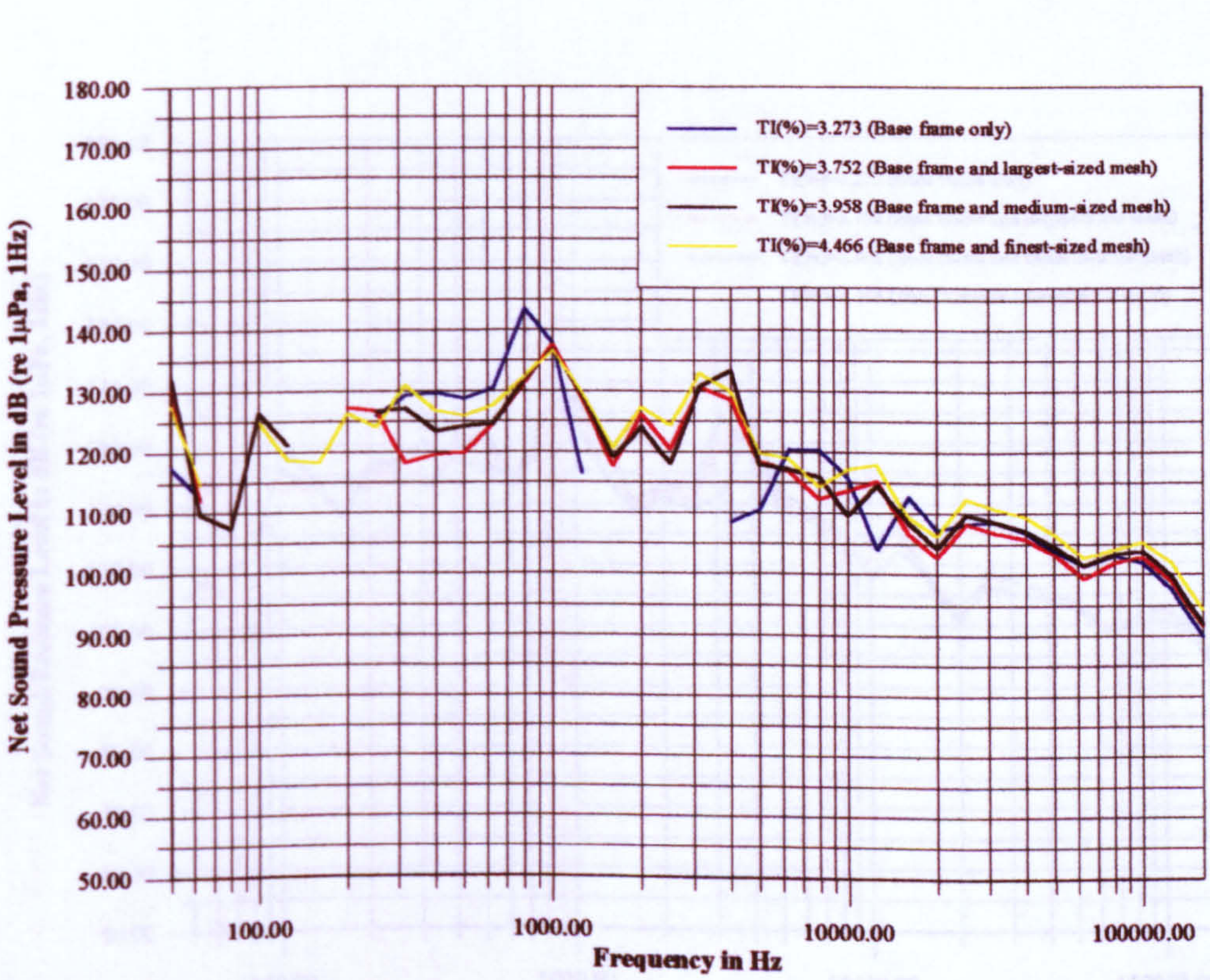

Figure 5.14 Effect of free-stream turbulence on the level of net propeller noise at σ_u=Atm, α_D/α_S=20% and J=0.4

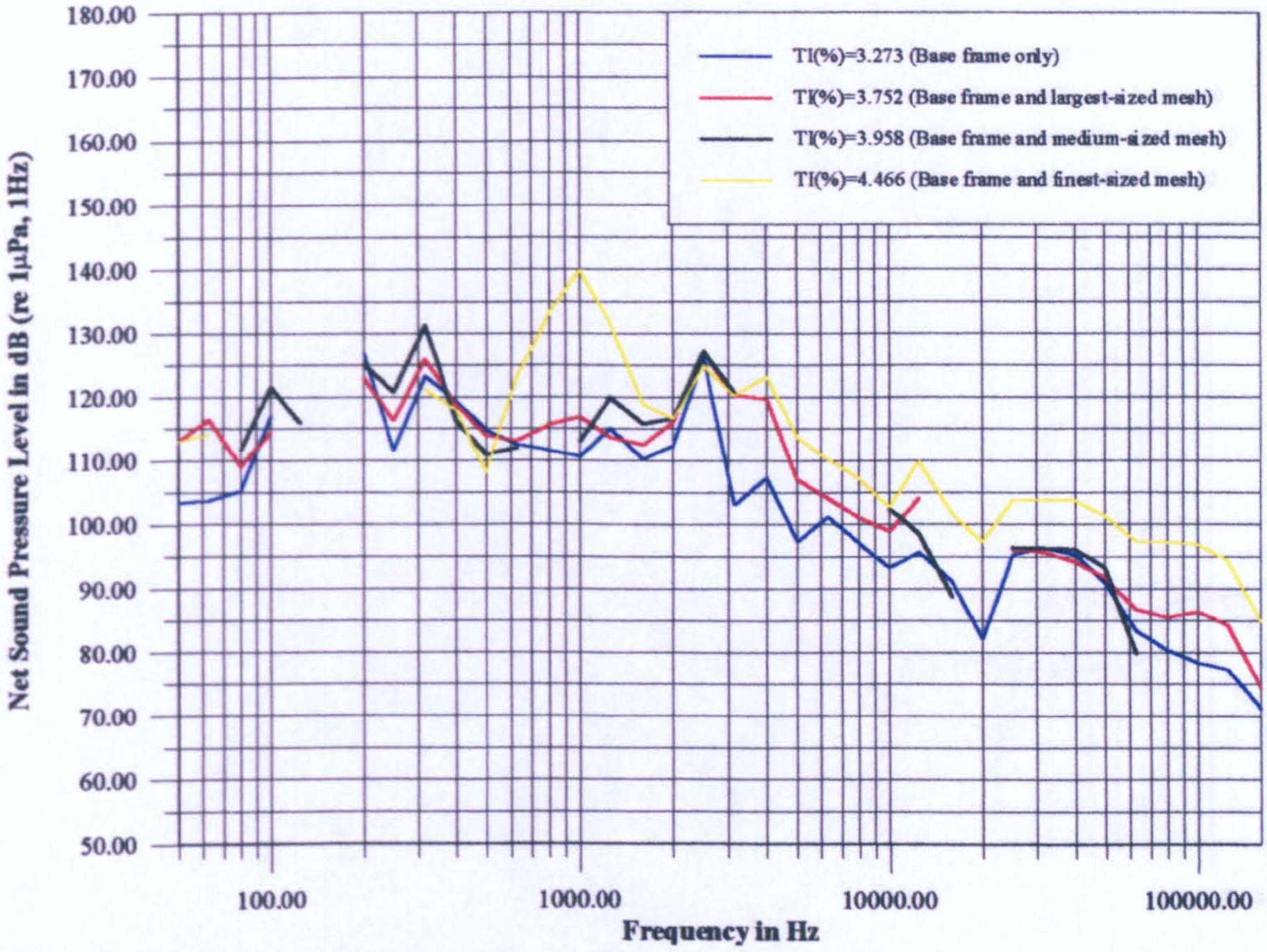

Figure 5.15 Effect of free-stream turbulence on the level of net propeller noise at σ_u=Atm, α_D/α_S=44% and J=0.6

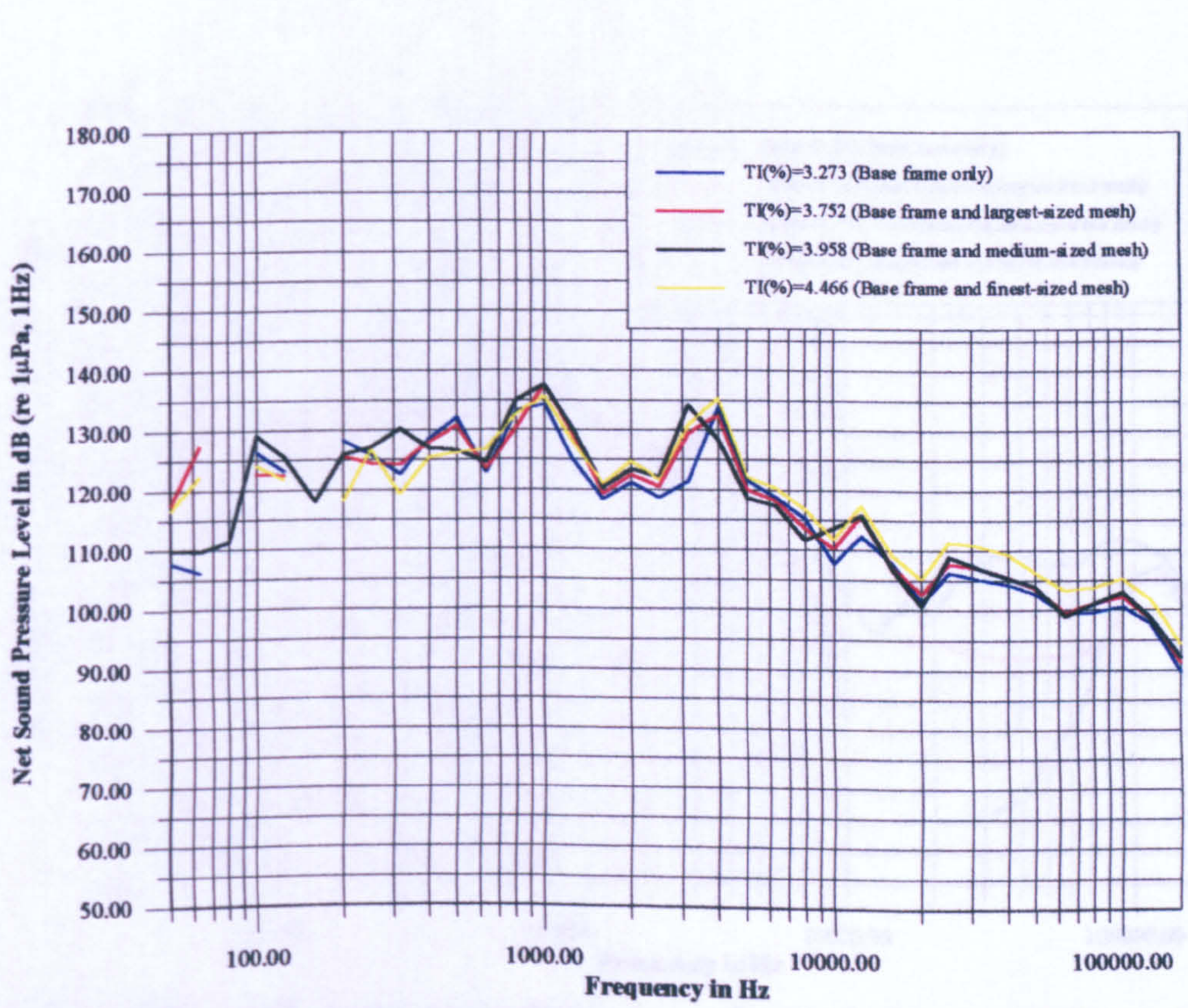

Figure 5.16 Effect of free-stream turbulence on the level of net propeller noise at σ_u=Atm, α_D/α_S=44% and J=0.4

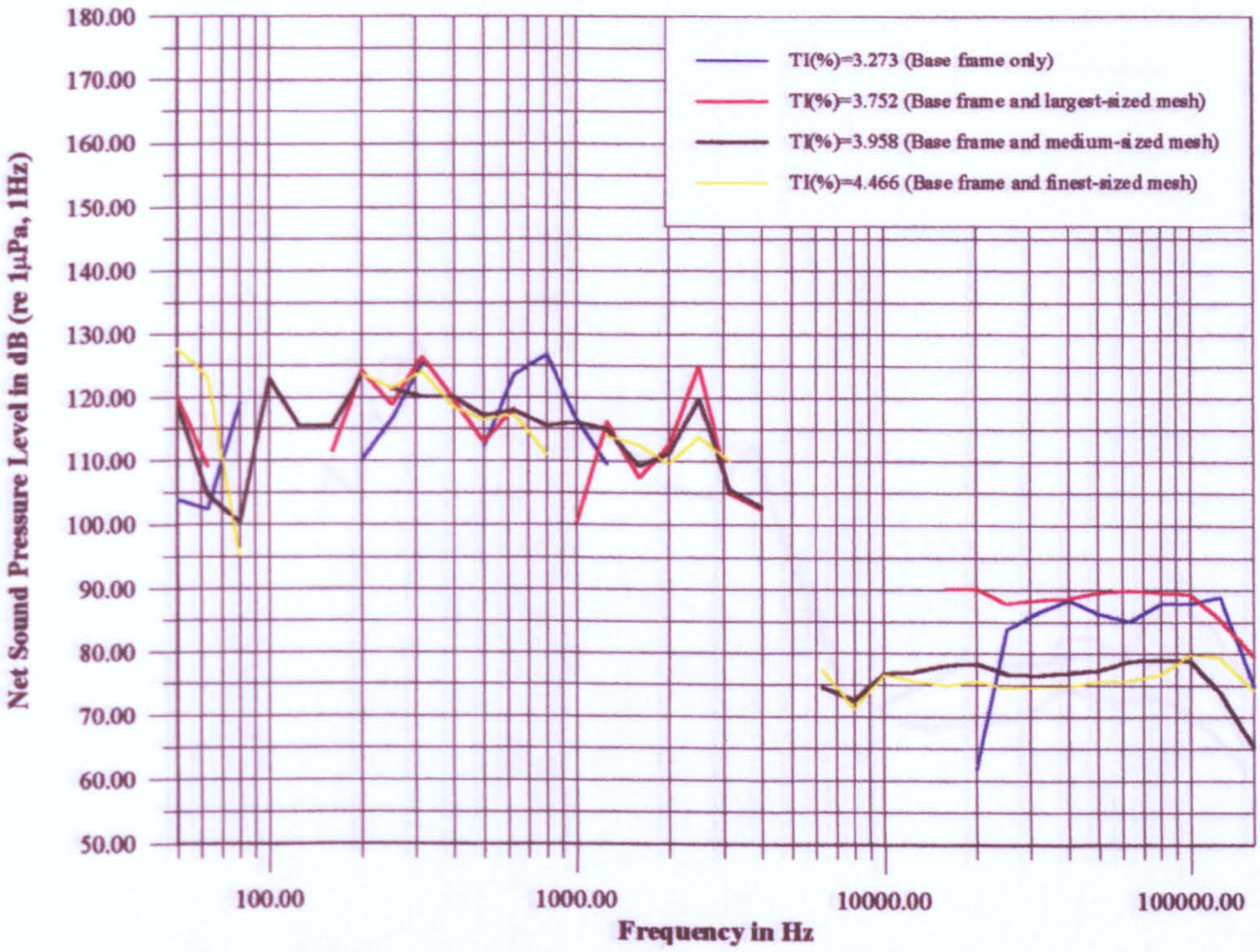

Figure 5.17 Effect of free-stream turbulence on the level of net propeller noise at σ_u=5.56, α_D/α_S=20% and J=0.6

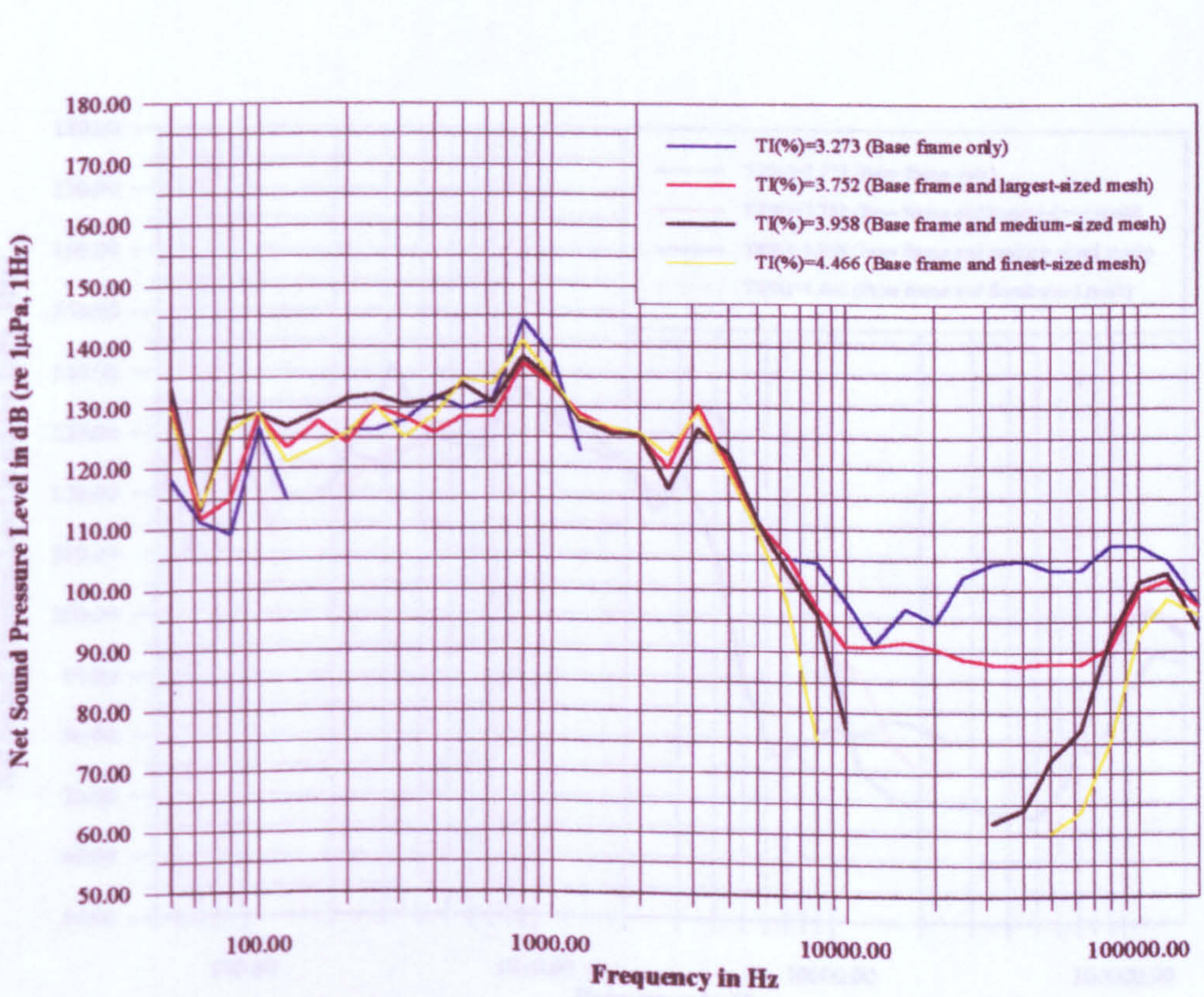

Figure 5.18 Effect of free-stream turbulence on the level of net propeller noise at σ_u=5.56, α_D/α_S=20% and J=0.4

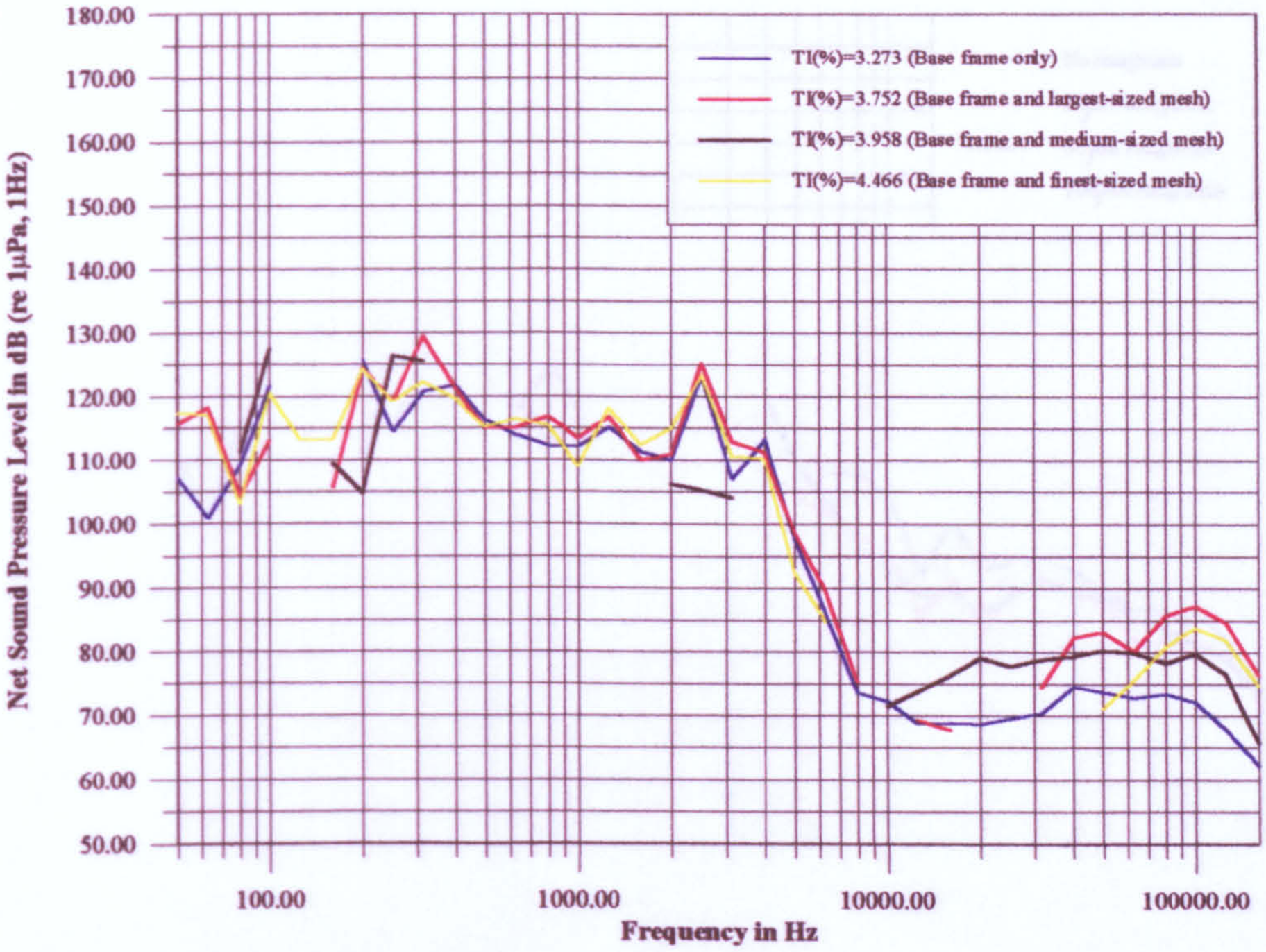

Figure 5.19 Effect of free-stream turbulence on the level of net propeller noise at σ_u=5.56, α_D/α_S=44% and J=0.6

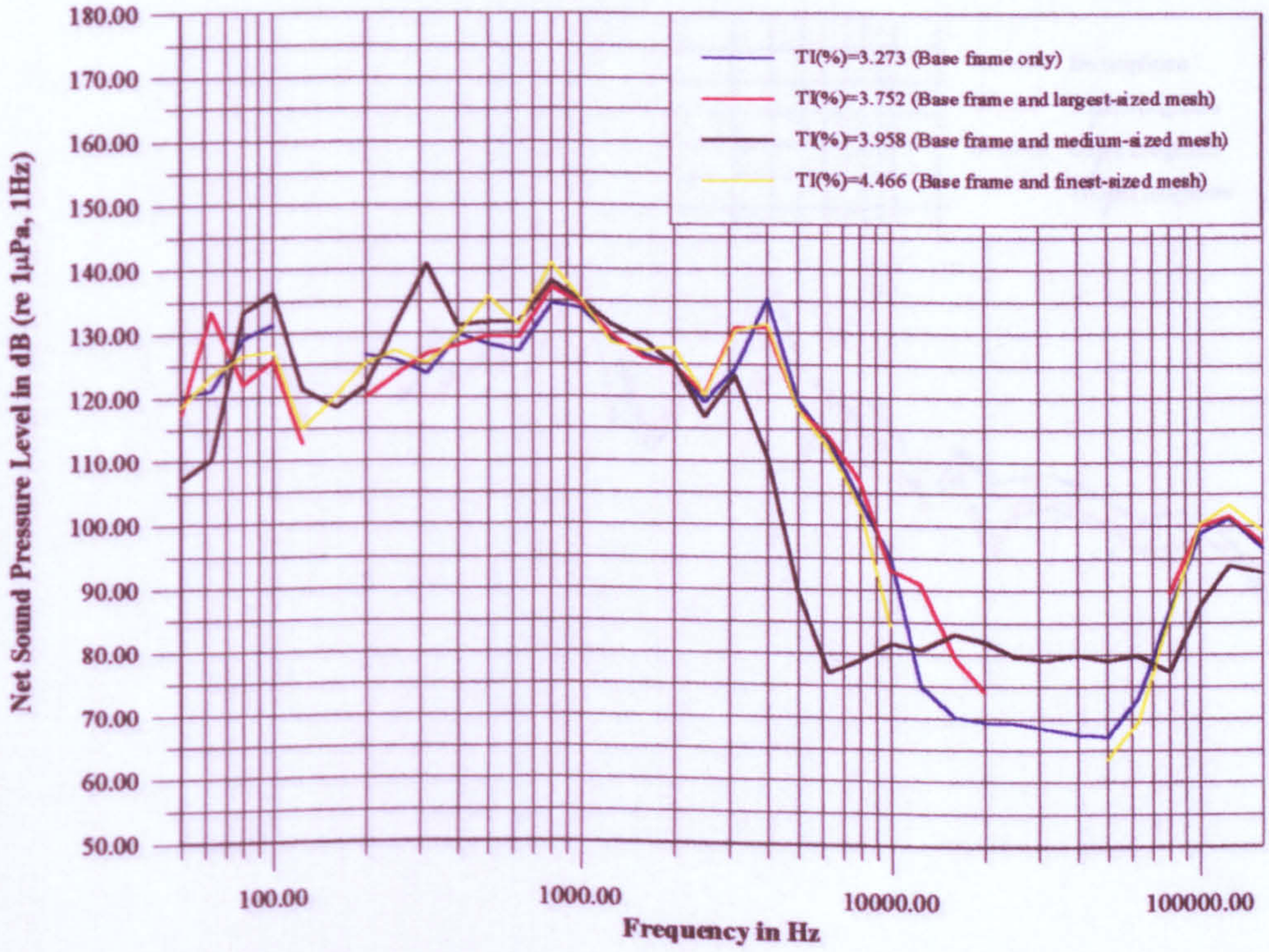

Figure 5.20 Effect of free-stream turbulence on the level of net propeller noise at σ_u=5.56, α_D/α_S=44% and J=0.4

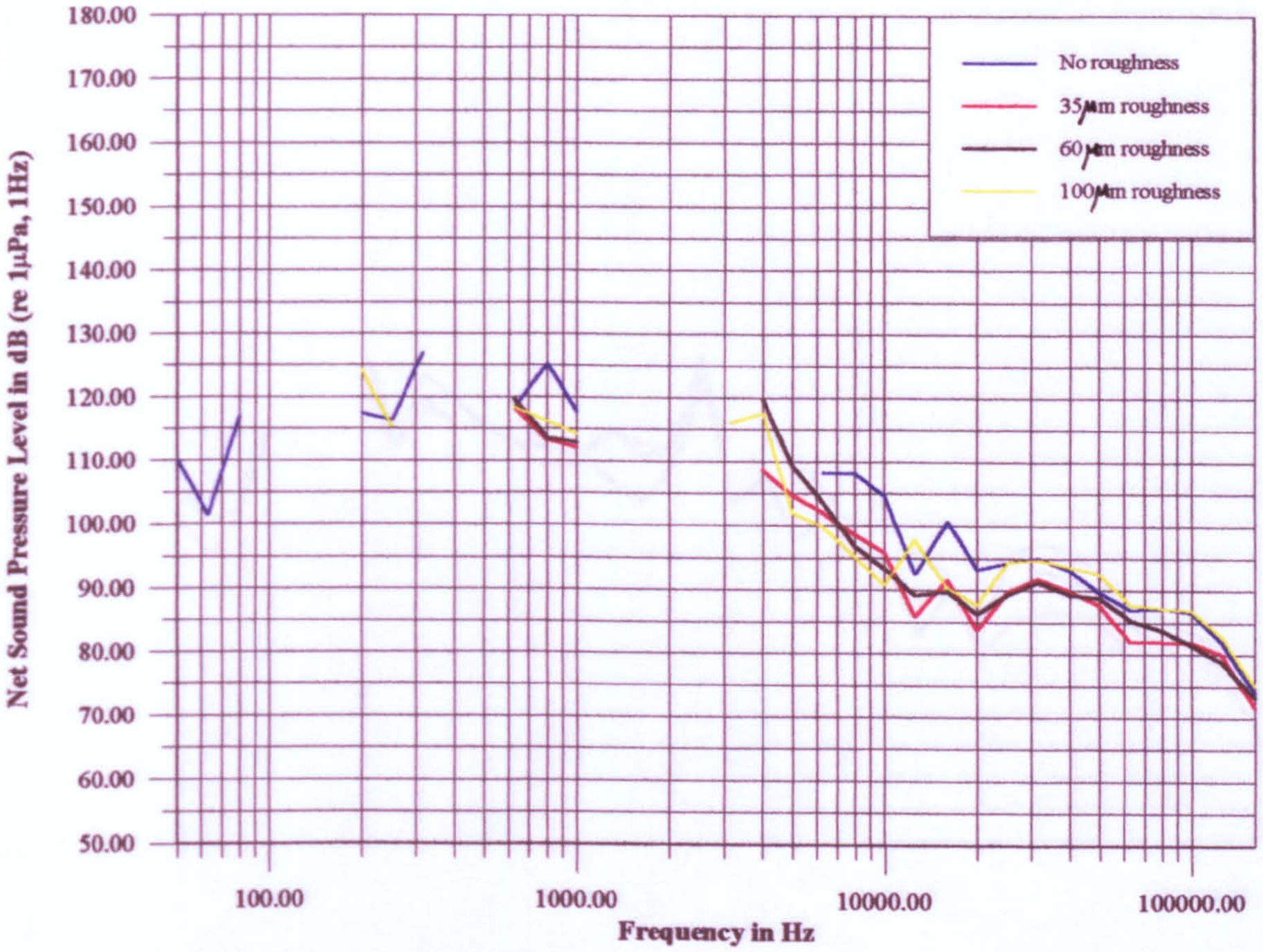

Figure 5.21 Effect of blade roughness on the level of net propeller noise at σ_u=Atm, α_D/α_S=20% and J=0.6

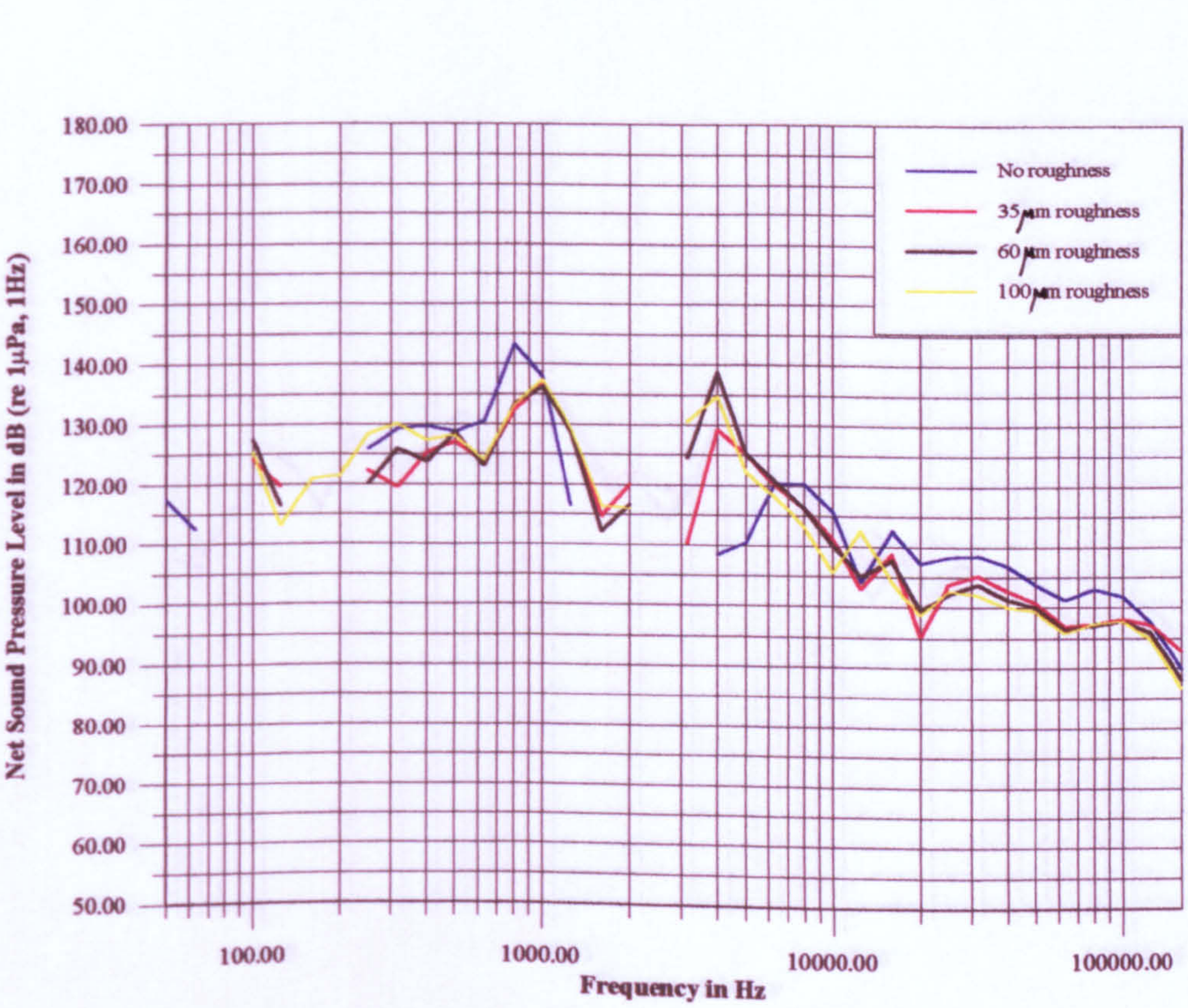

Figure 5.22 Effect of blade roughness on the level of net propeller noise at σ_u=Atm, α_D/α_S=20% and J=0.4

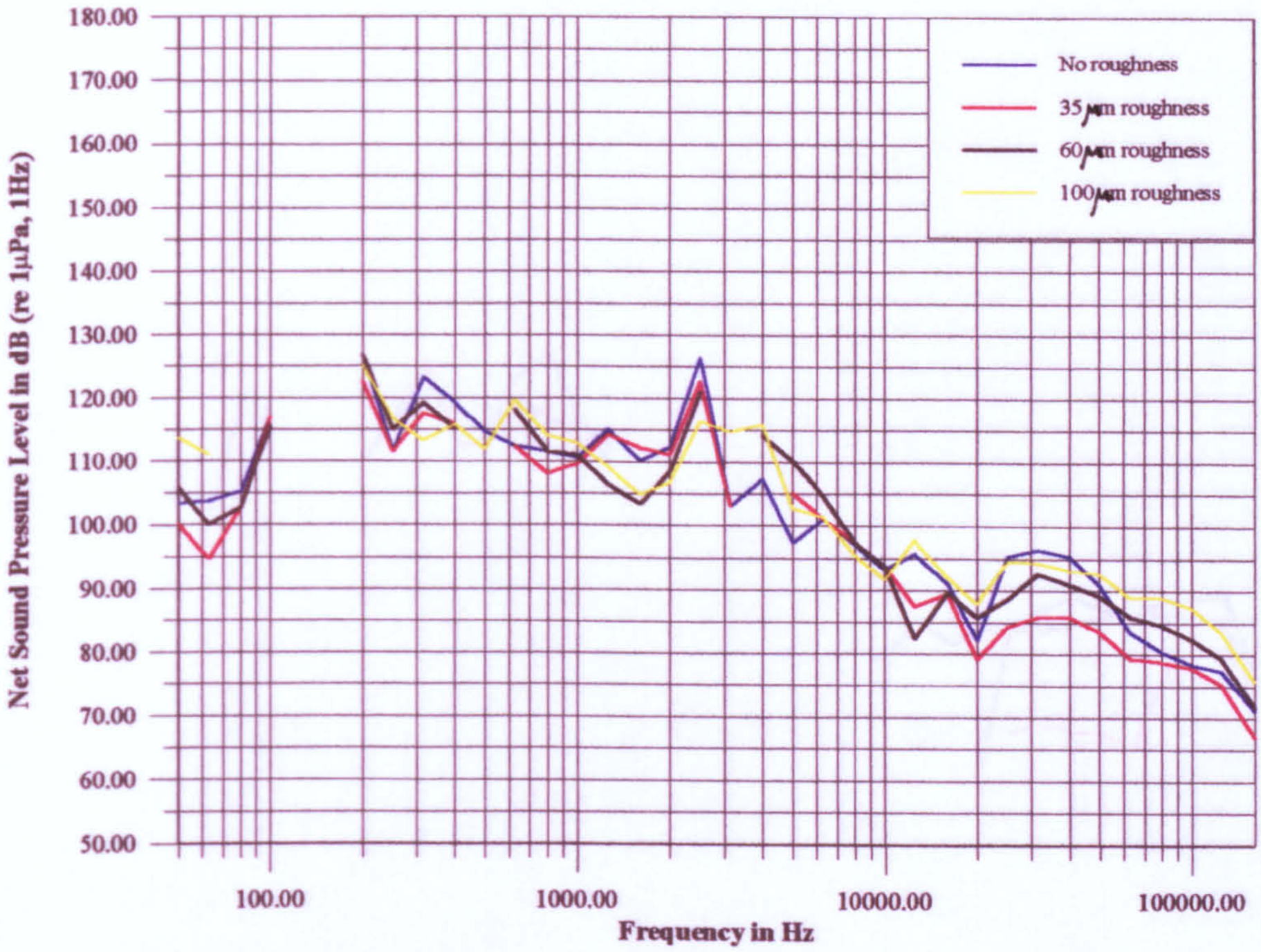

Figure 5.23 Effect of blade roughness on the level of net propeller noise at σ_u=Atm, α_D/α_S=44% and J=0.6

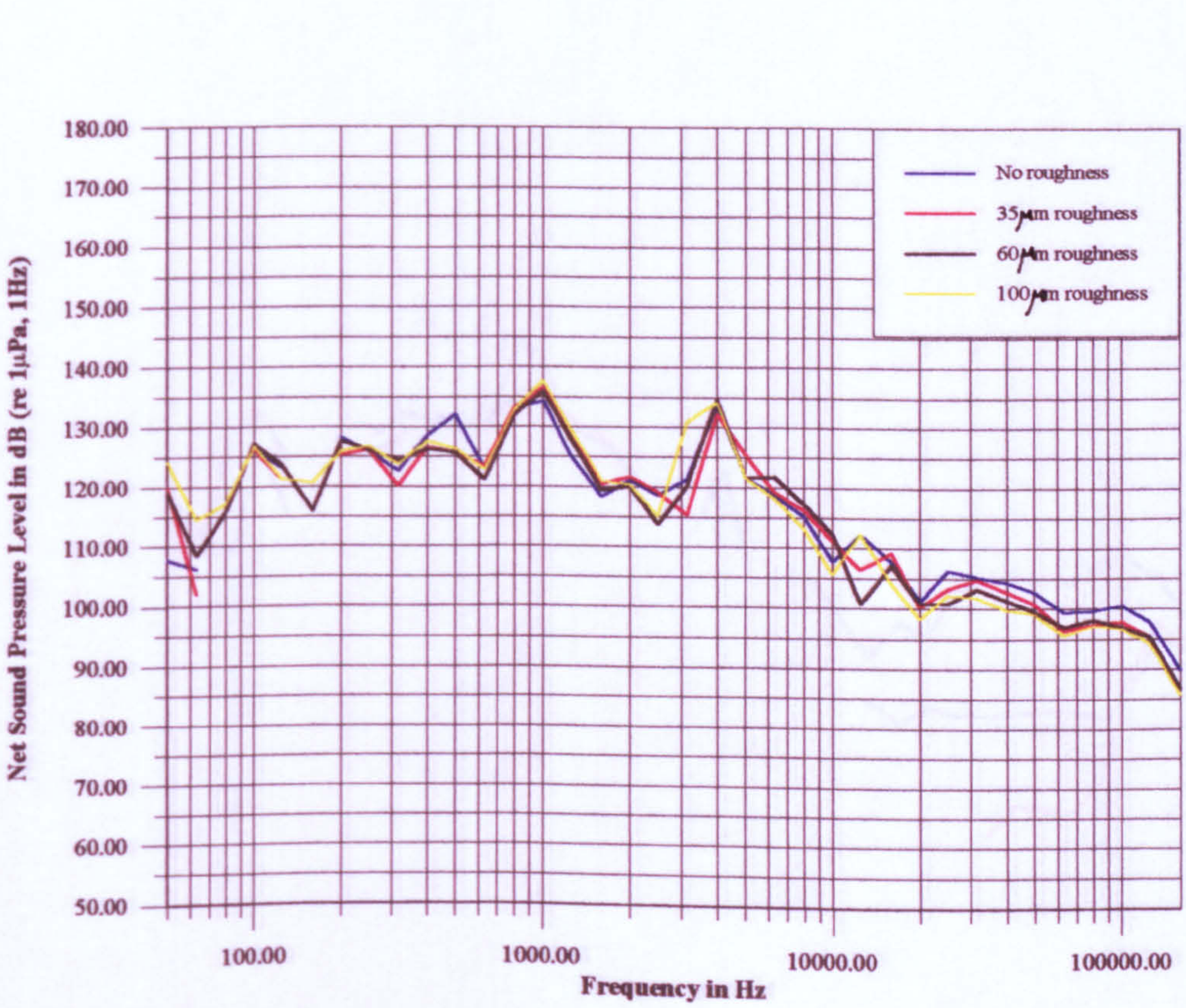

Figure 5.24 Effect of blade roughness on the level of net propeller noise at σ_u=Atm, α_D/α_S=44% and J=0.4

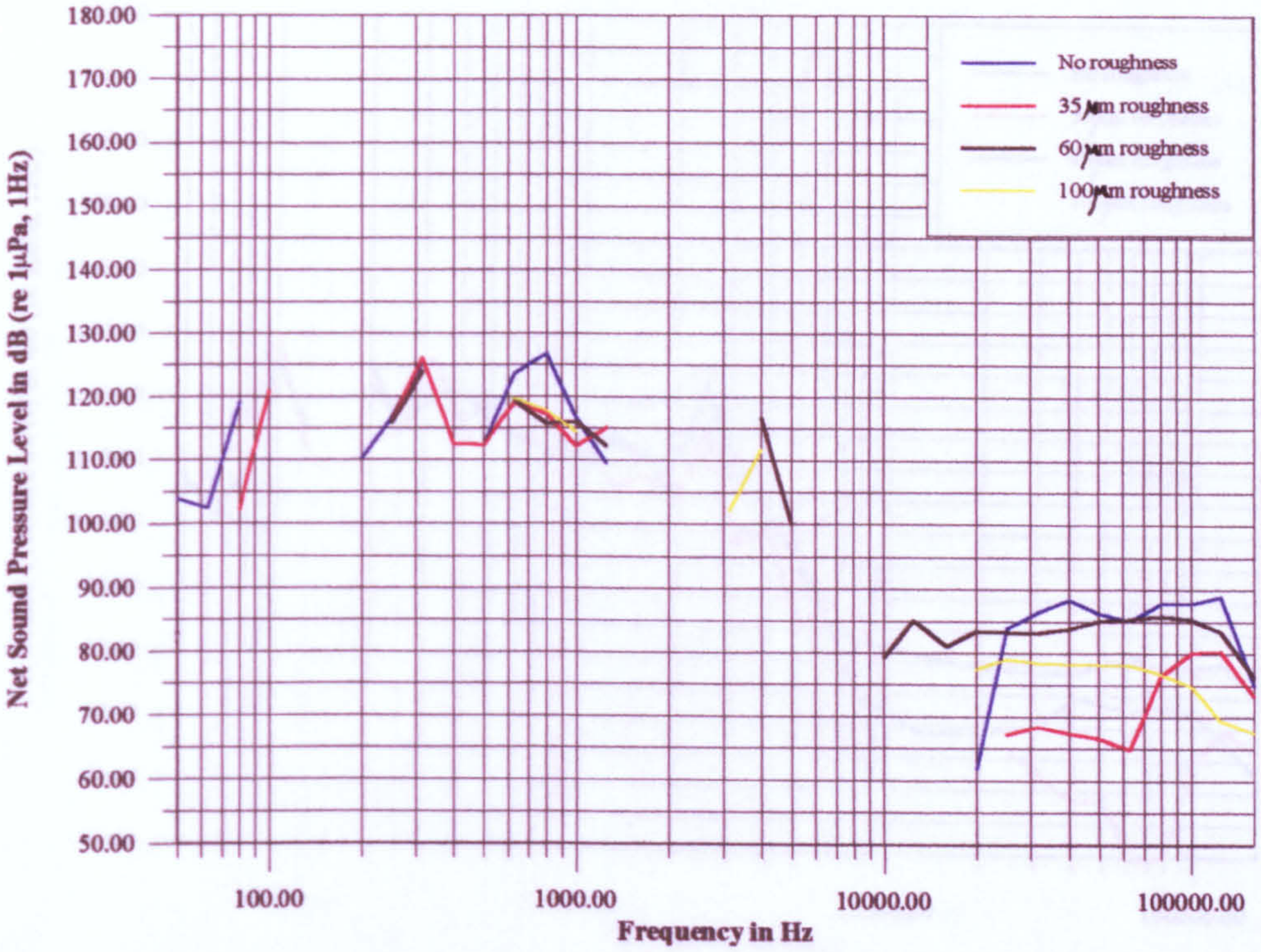

Figure 5.25 Effect of blade roughness on the level of net propeller noise at σ_u=5.56, α_D/α_S=20% and J=0.6

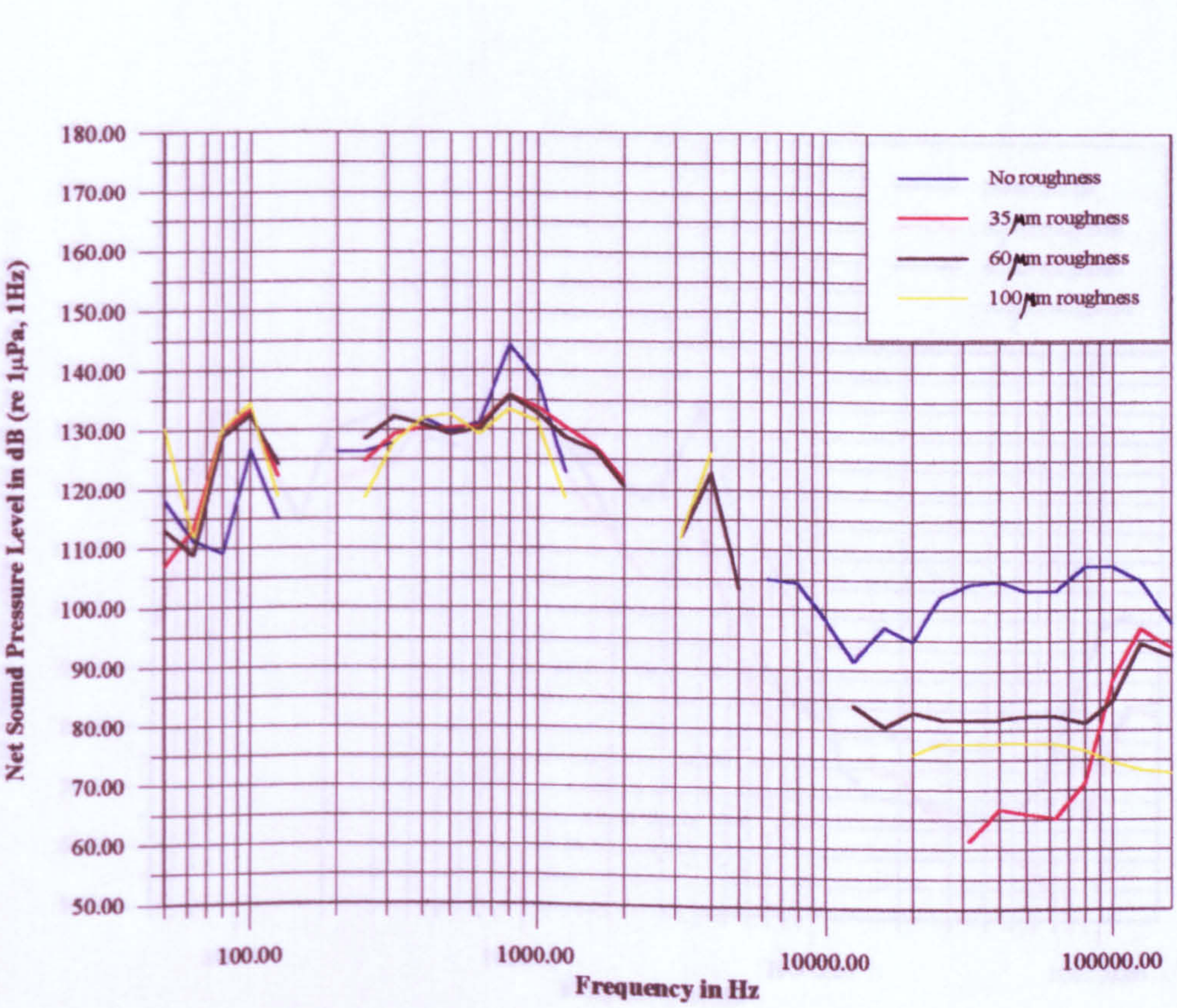

Figure 5.26 Effect of blade roughness on the level of net propeller noise at σ_u=5.56, α_D/α_S=20% and J=0.4

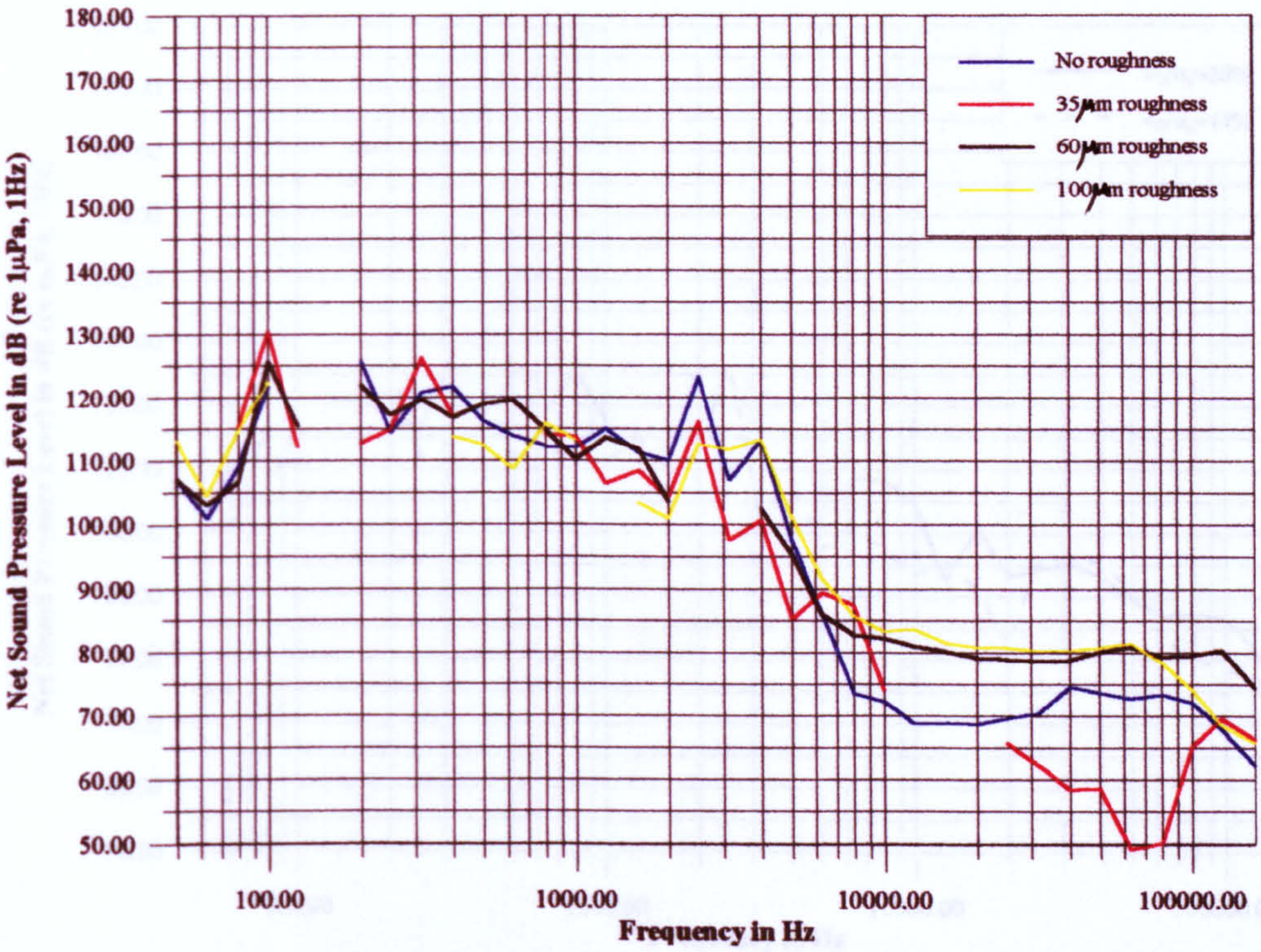

Figure 5.27 Effect of blade roughness on the level of net propeller noise at σ_u=5.56, α_D/α_S=44% and J=0.6

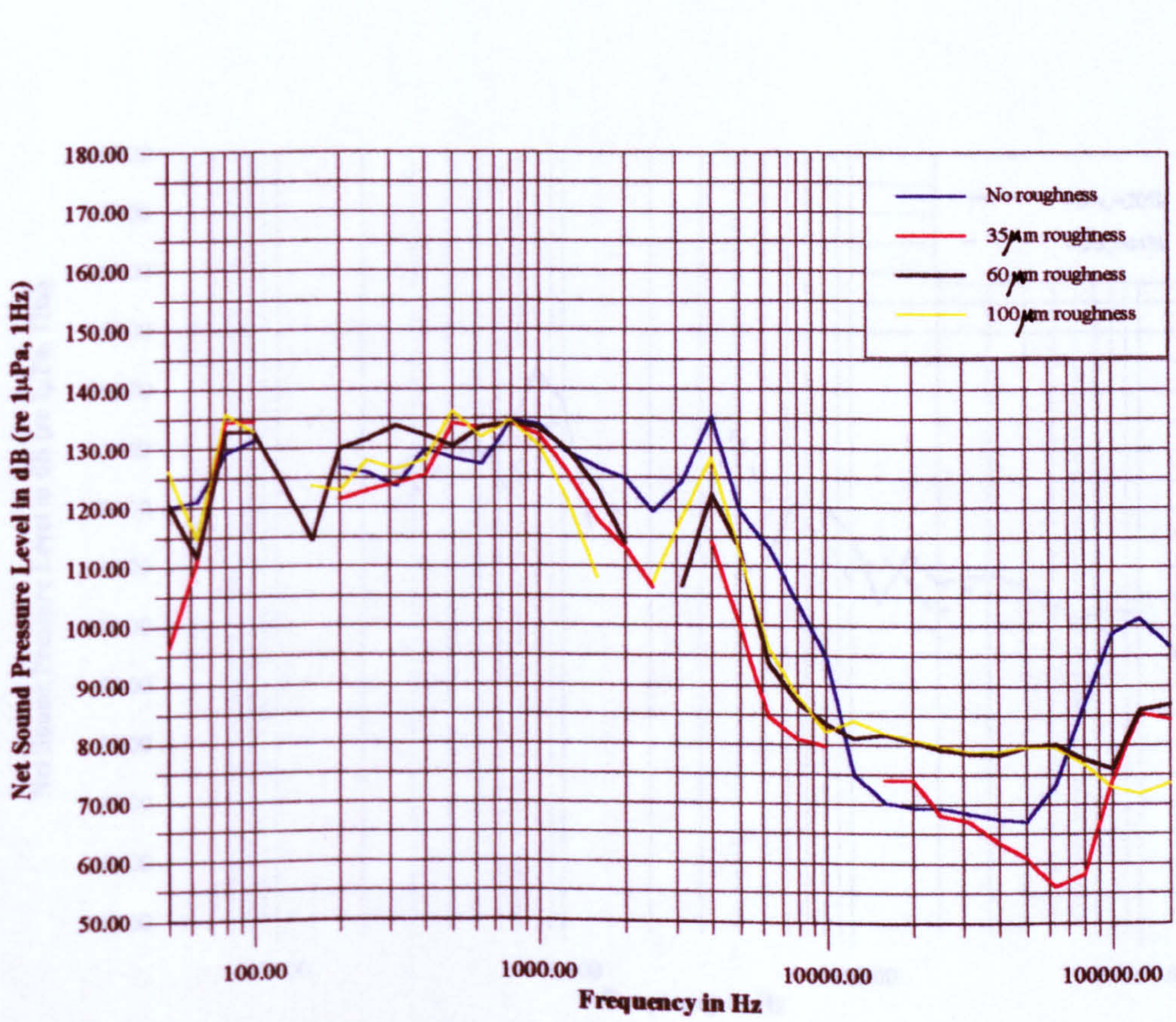

Figure 5.28 Effect of blade roughness on the level of net propeller noise at σ_u=5.56, α_D/α_S=44% and J=0.4

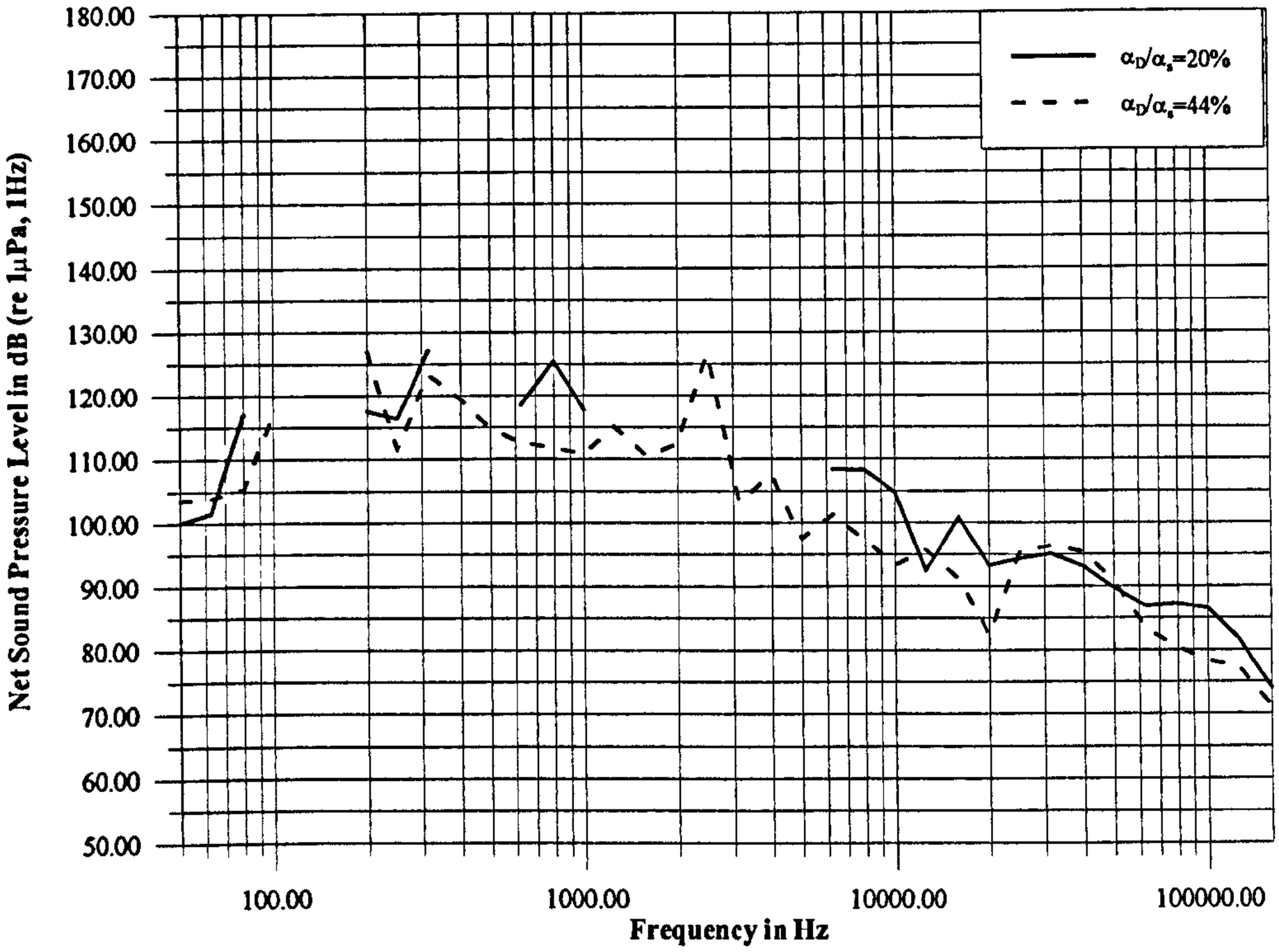

Figure 5.29 Effect of dissolved gas content on the level of net propeller noise at TI(%)=3.273 (Base frame), σ_u=Atm and J=0.6

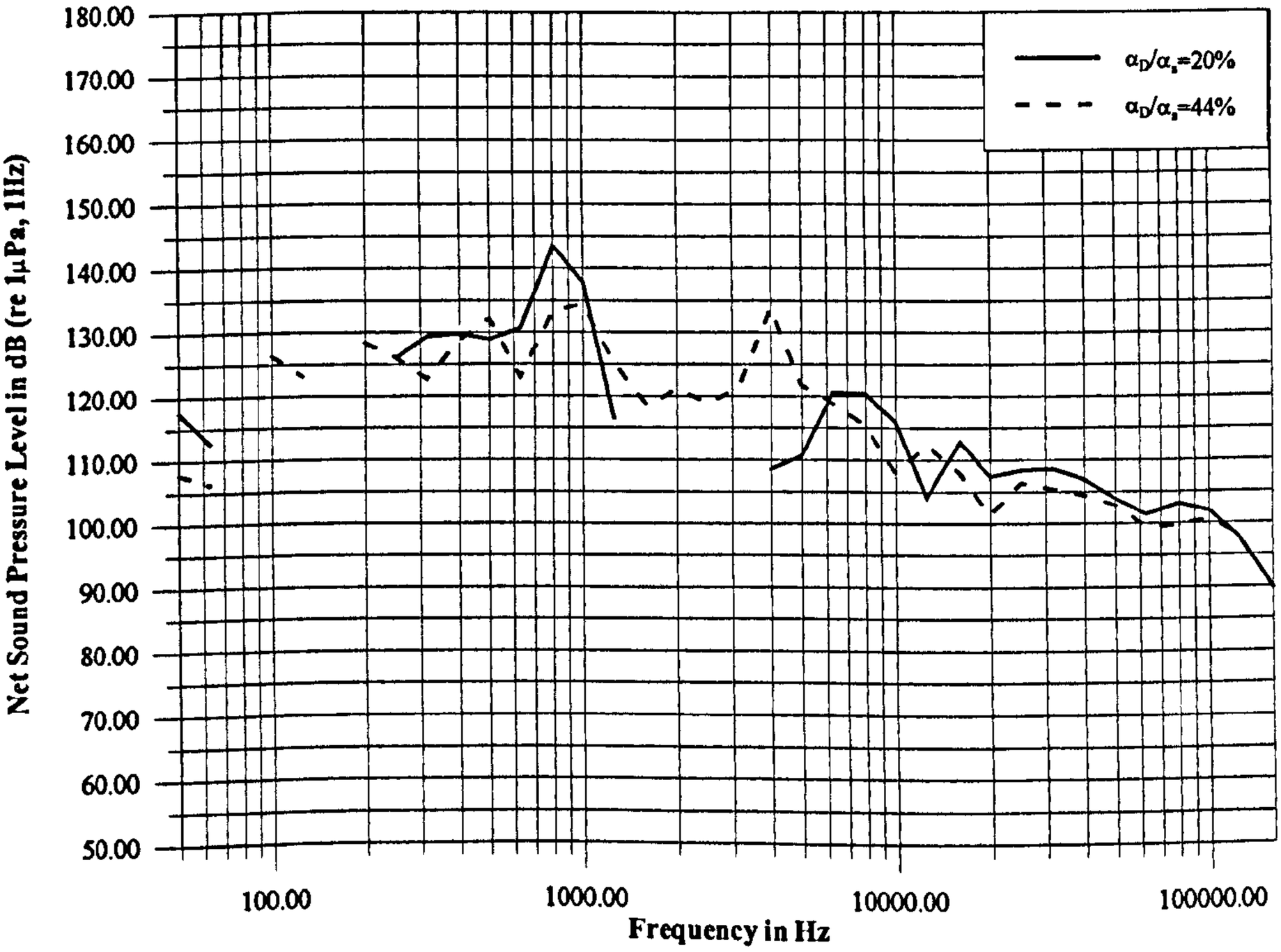

Figure 5.30 Effect of dissolved gas content on the level of net propeller noise at TI(%)=3.273 (Base frame), σ_u=Atm and J=0.4

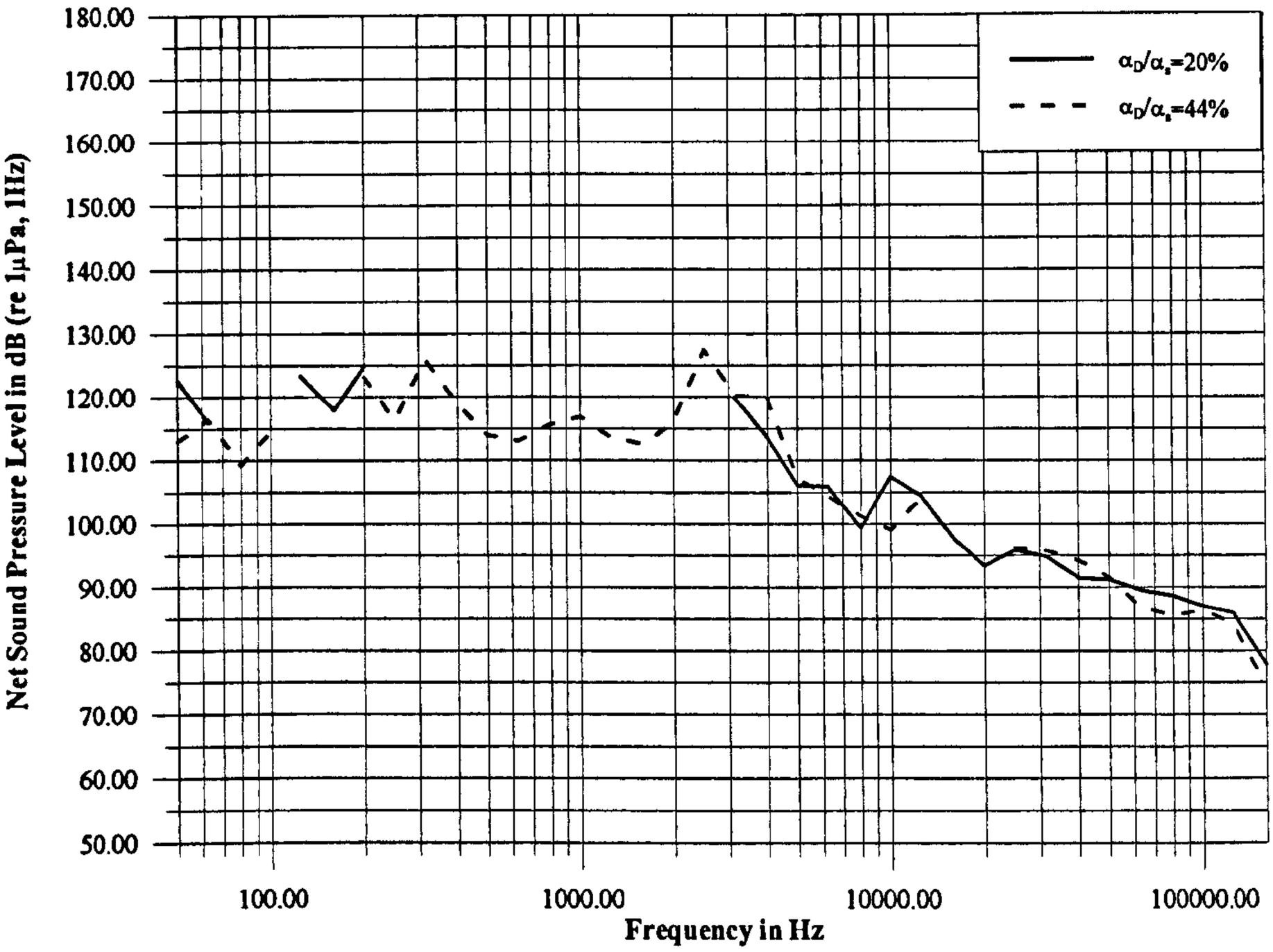

Figure 5.31 Effect of dissolved gas content on the level of net propeller noise at TI(%)=3.752 (Largest-sized mesh), σ_u=Atm and J=0.6

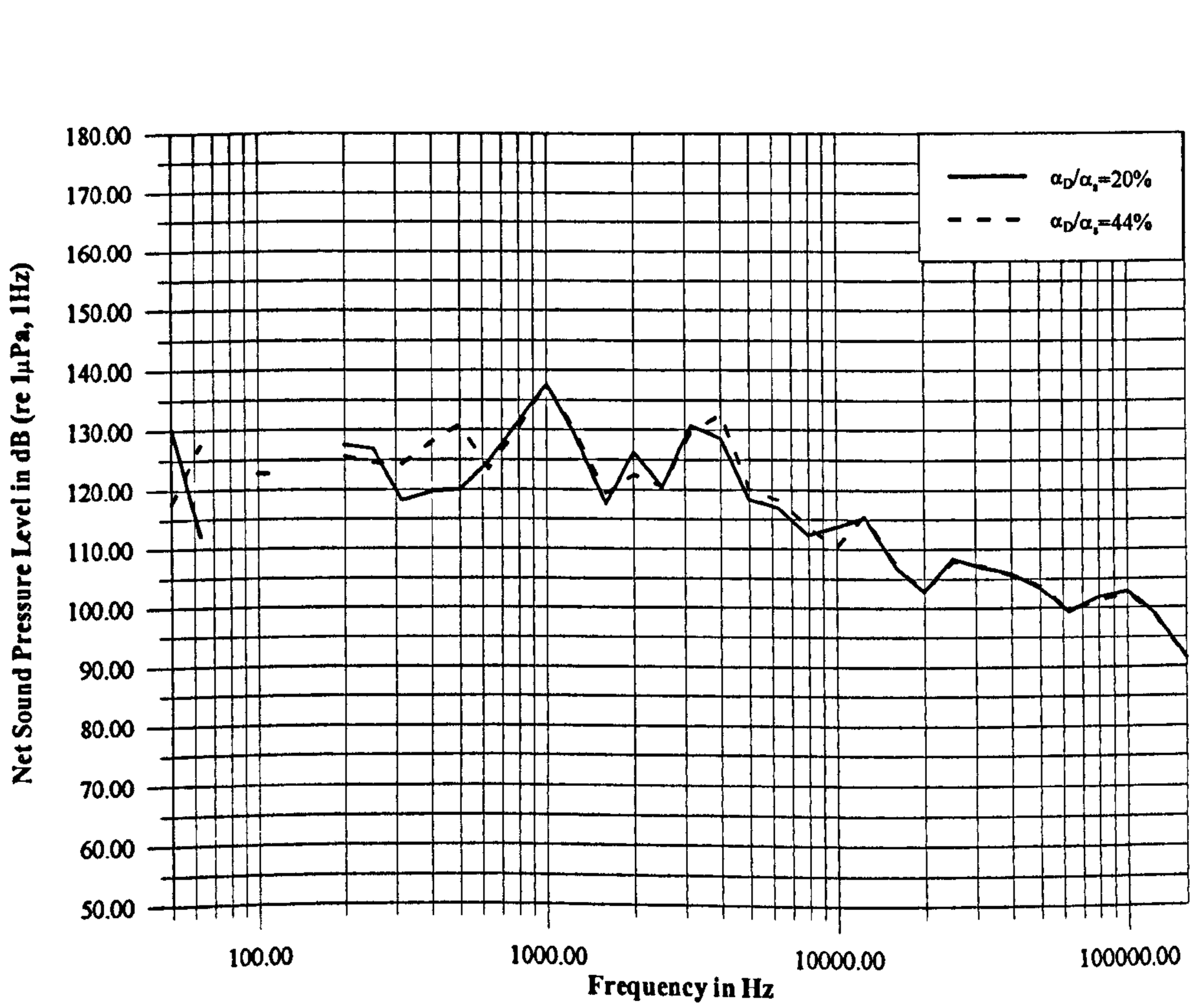

Figure 5.32 Effect of dissolved gas content on the level of net propeller noise at TI(%)=3.752 (Largest-sized mesh), σ_u=Atm and J=0.4

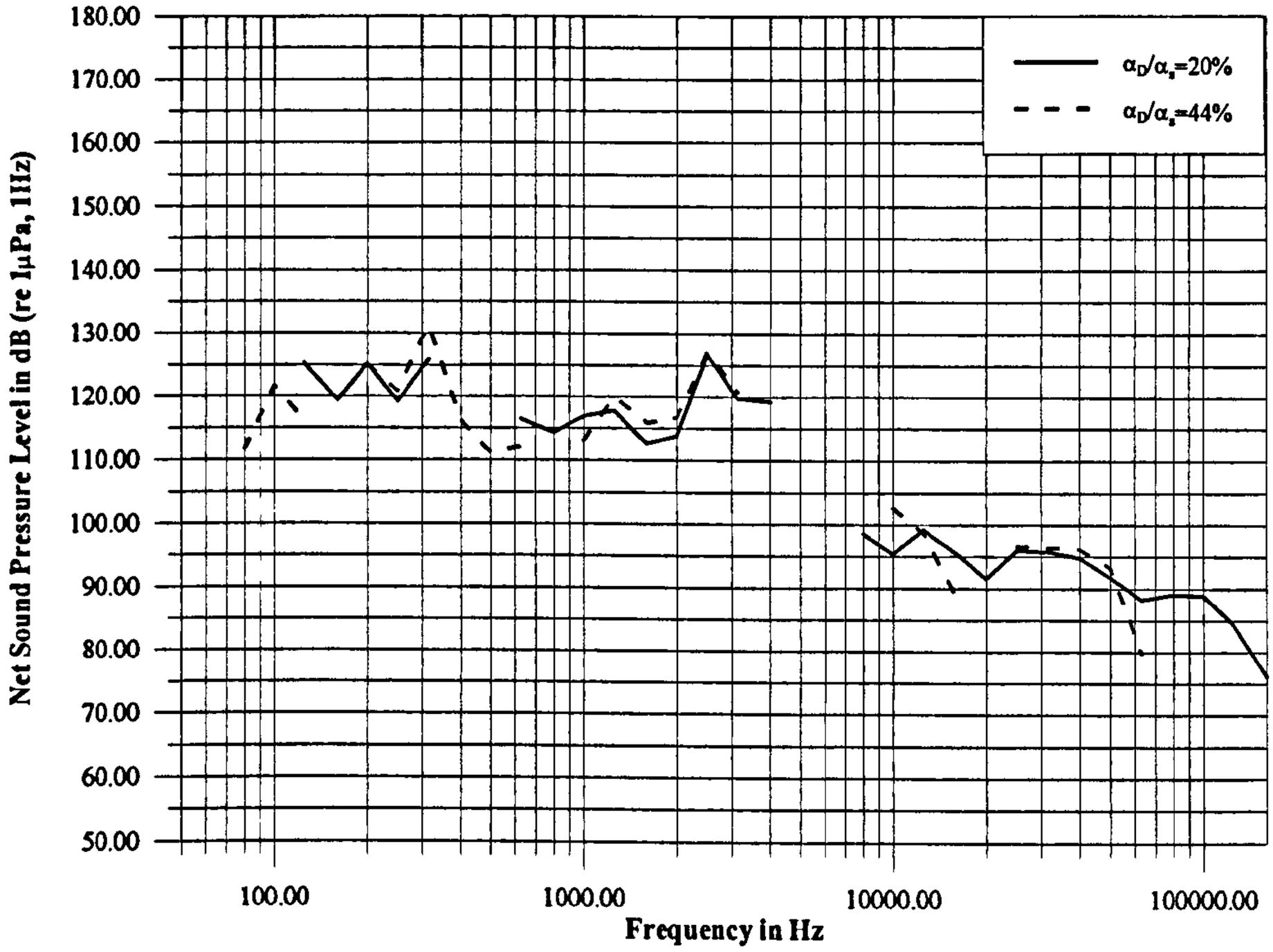

Figure 5.33 Effect of dissolved gas content on the level of net propeller noise at TI(%)=3.958 (Medium-sized mesh), σ_u=Atm and J=0.6

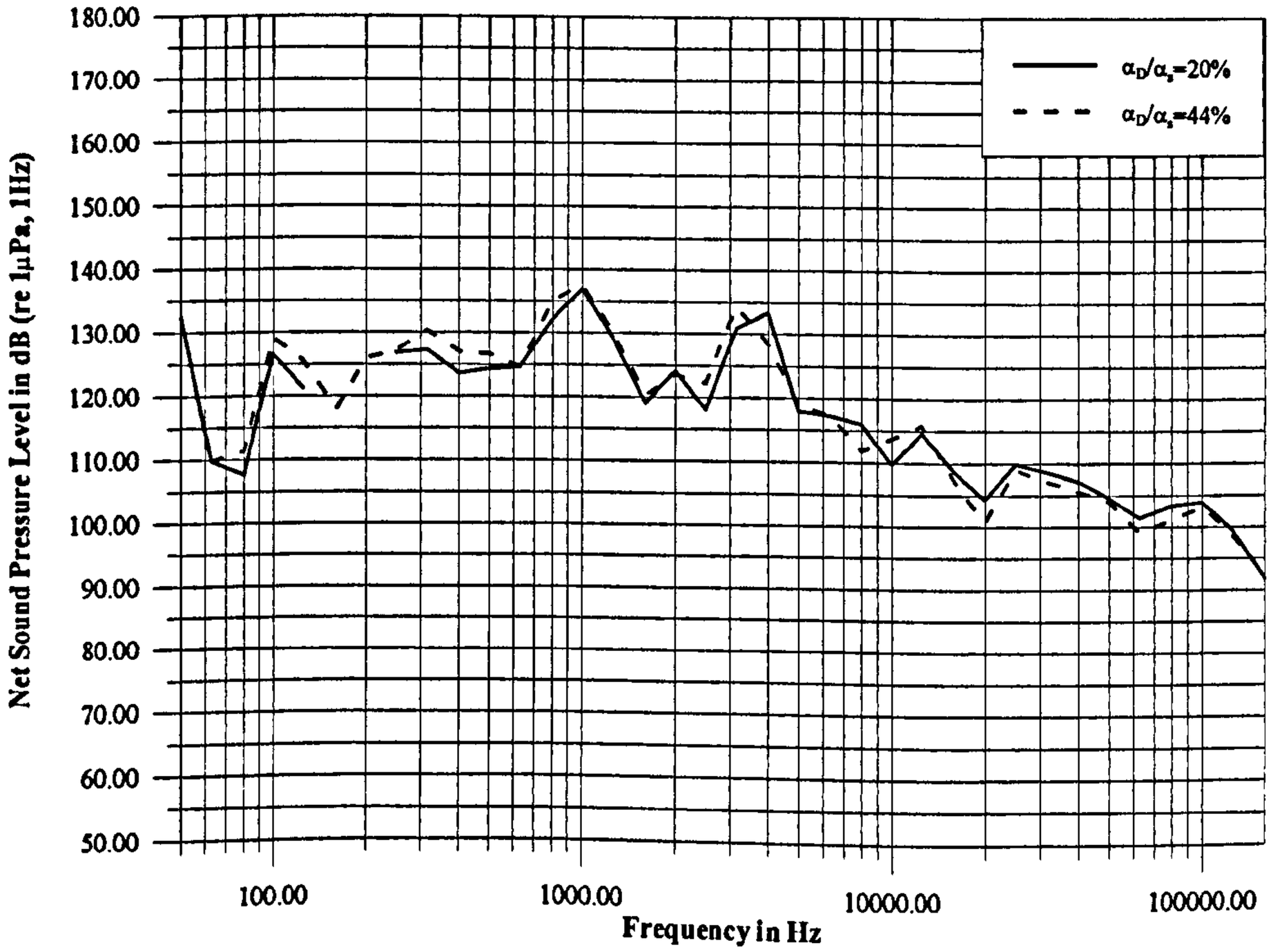

Figure 5.34 Effect of dissolved gas content on the level of net propeller noise at TI(%)=3.958 (Medium-sized mesh), σ_u=Atm and J=0.4

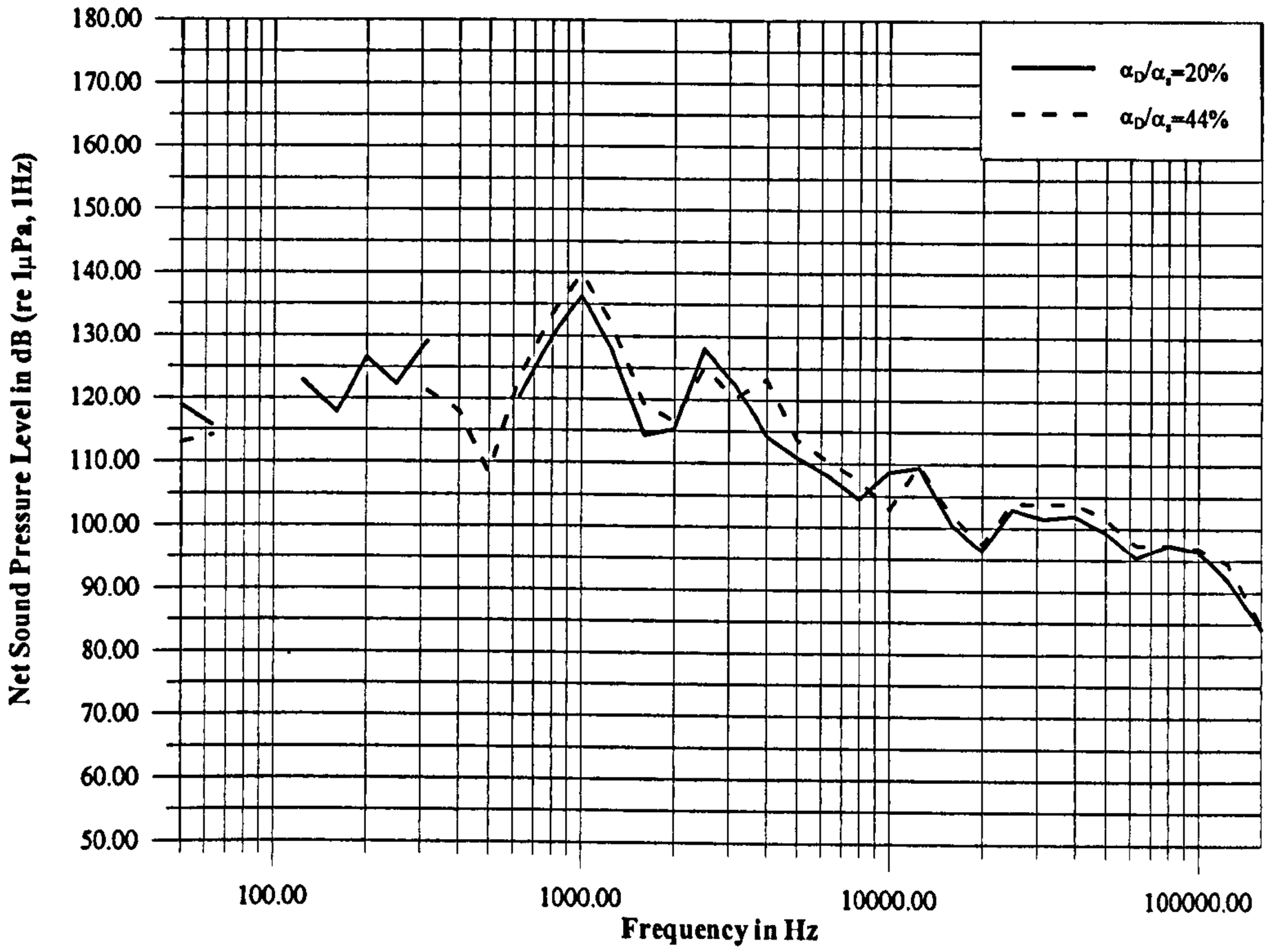

Figure 5.35 Effect of dissolved gas content on the level of net propeller noise at TI(%)=4.466 (Finest-sized mesh), σ_u=Atm and J=0.6

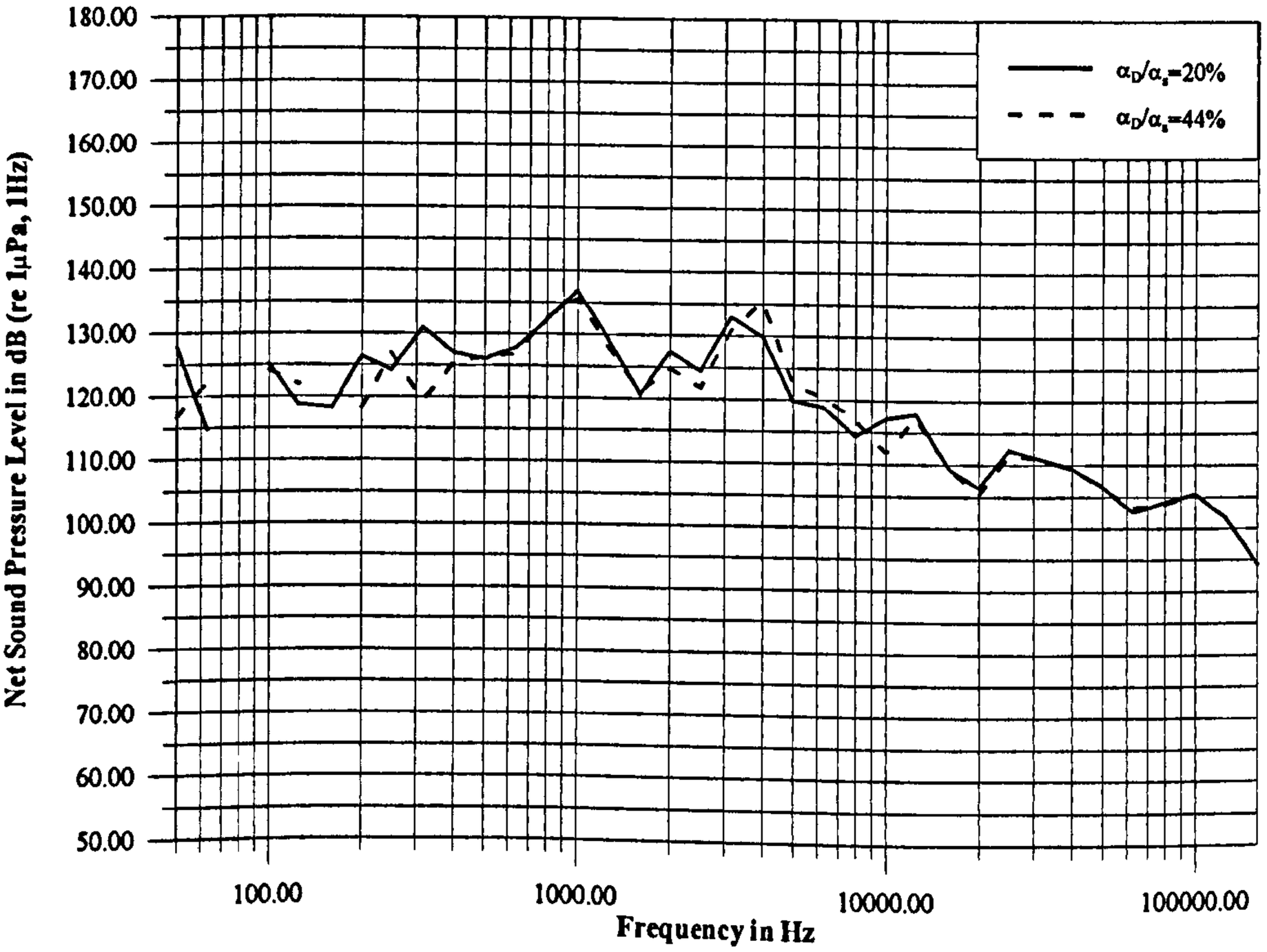

Figure 5.36 Effect of dissolved gas content on the level of net propeller noise at TI(%)=4.466 (Finest-sized mesh), σ_u=Atm and J=0.4

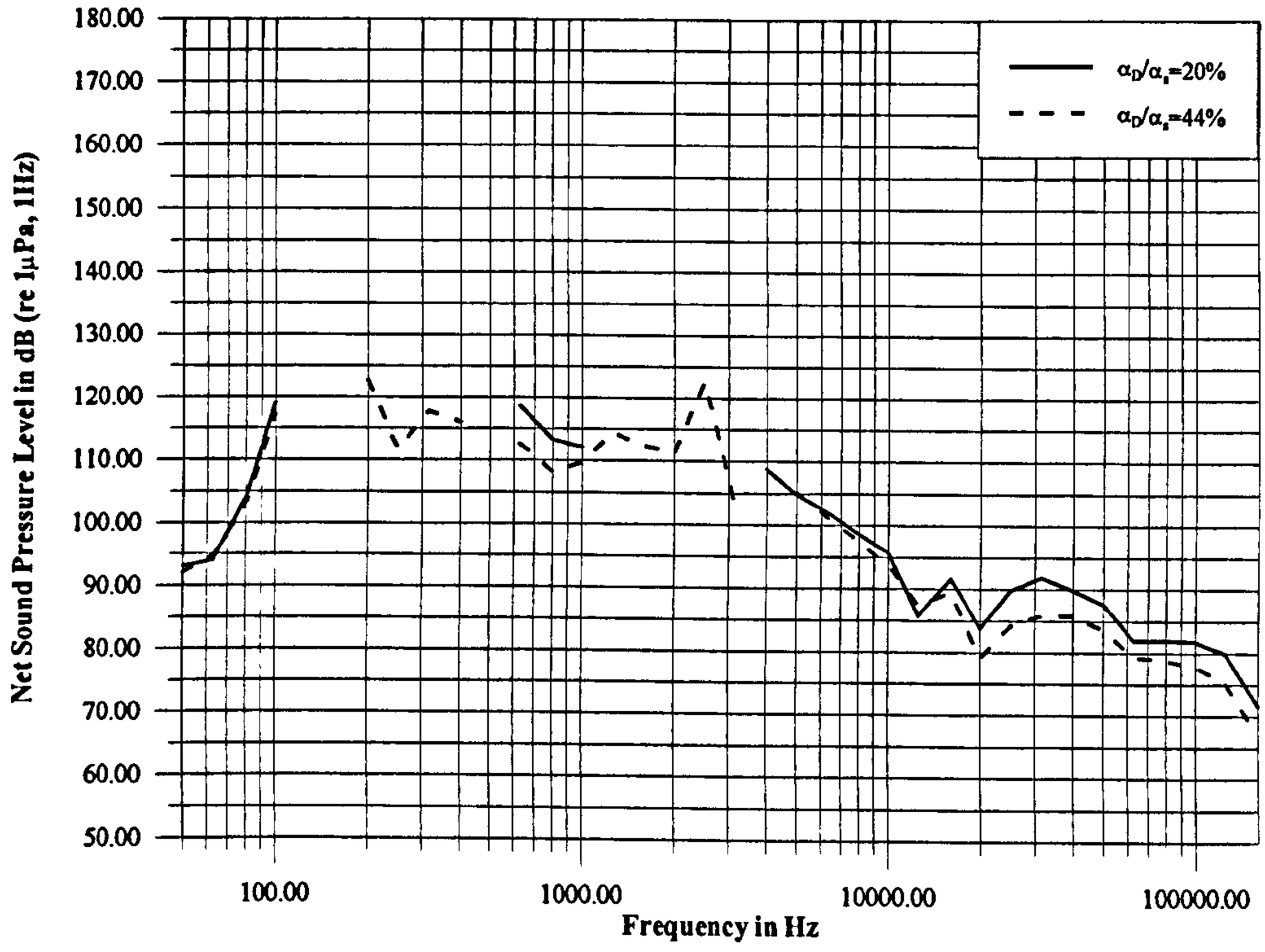

Figure 5.37 Effect of dissolved gas content on the level of net propeller noise for blade roughness level, k=35 μm, at σ_u=Atm and J=0.6

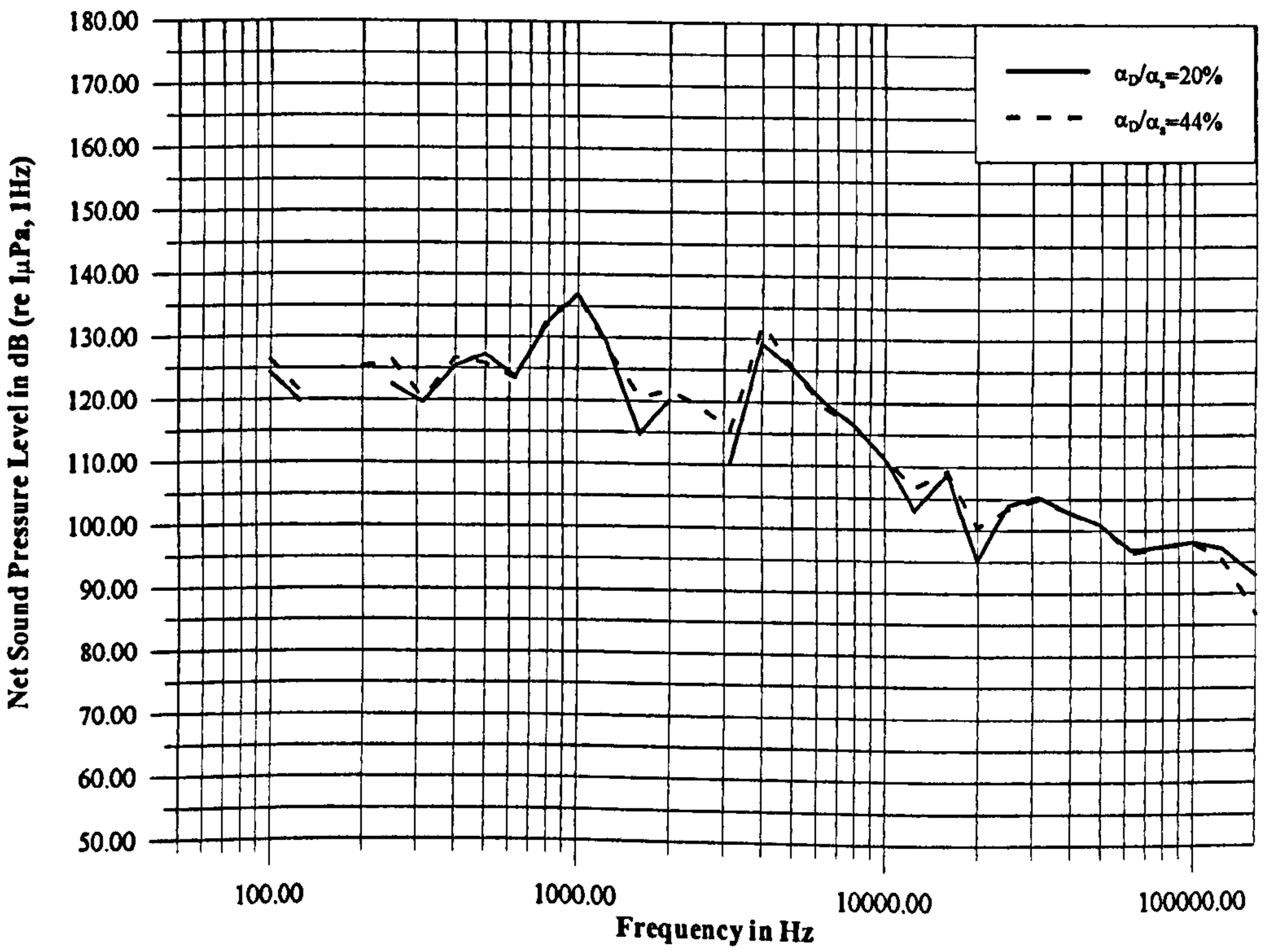

Figure 5.38 Effect of dissolved gas content on the level of net propeller noise for blade roughness level, k=35 μm, at σ_u=Atm and J=0.4

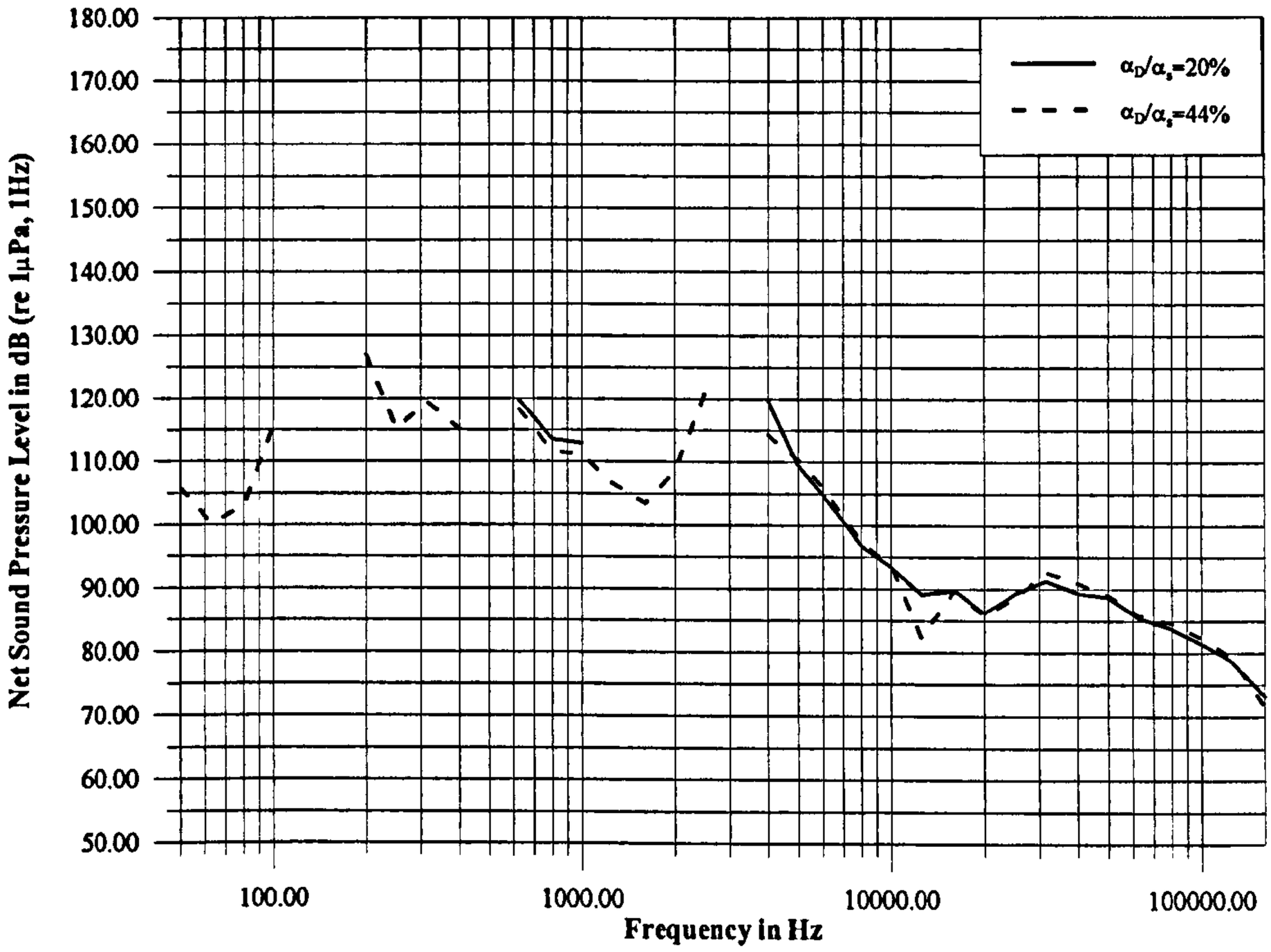

Figure 5.39 Effect of dissolved gas content on the level of net propeller noise for blade roughness level, k=60 μm, at σ_u=Atm and J=0.6

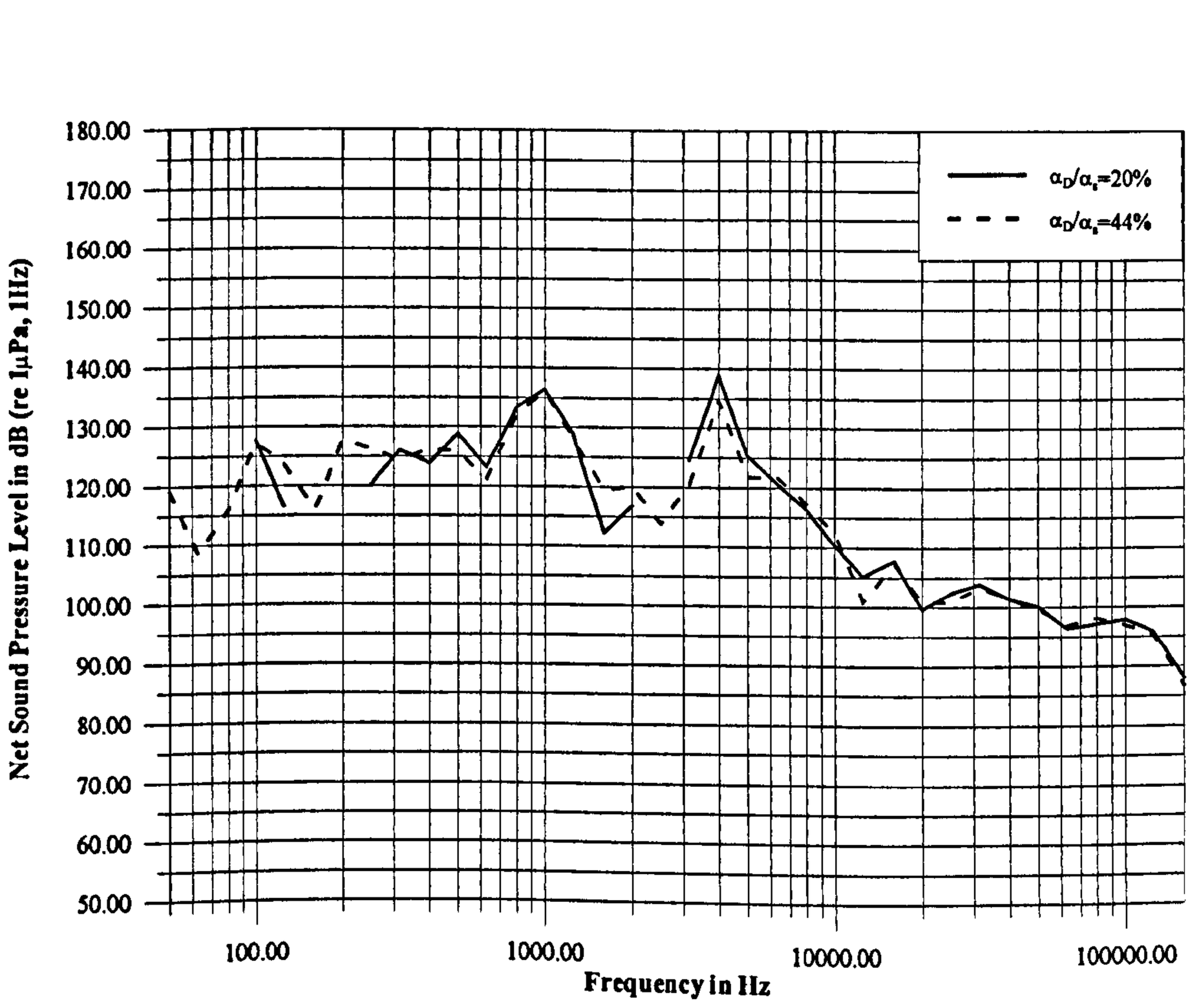

Figure 5.40 Effect of dissolved gas content on the level of net propeller noise for blade roughness level, k=60 μm, at σ_u=Atm and J=0.4

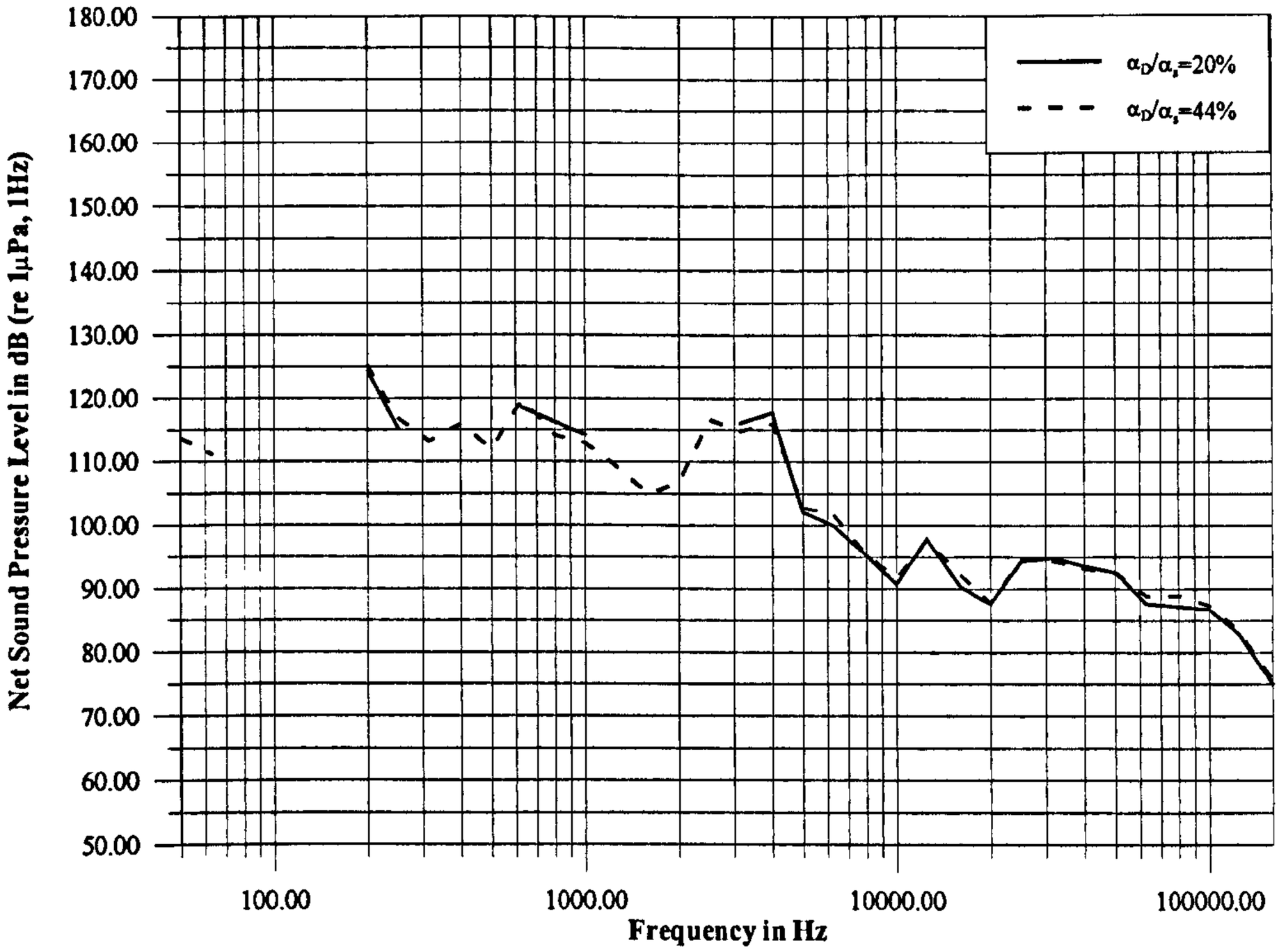

Figure 5.41 Effect of dissolved gas content on the level of net propeller noise for blade roughness level, k=100 μm, at σ_u=Atm and J=0.6

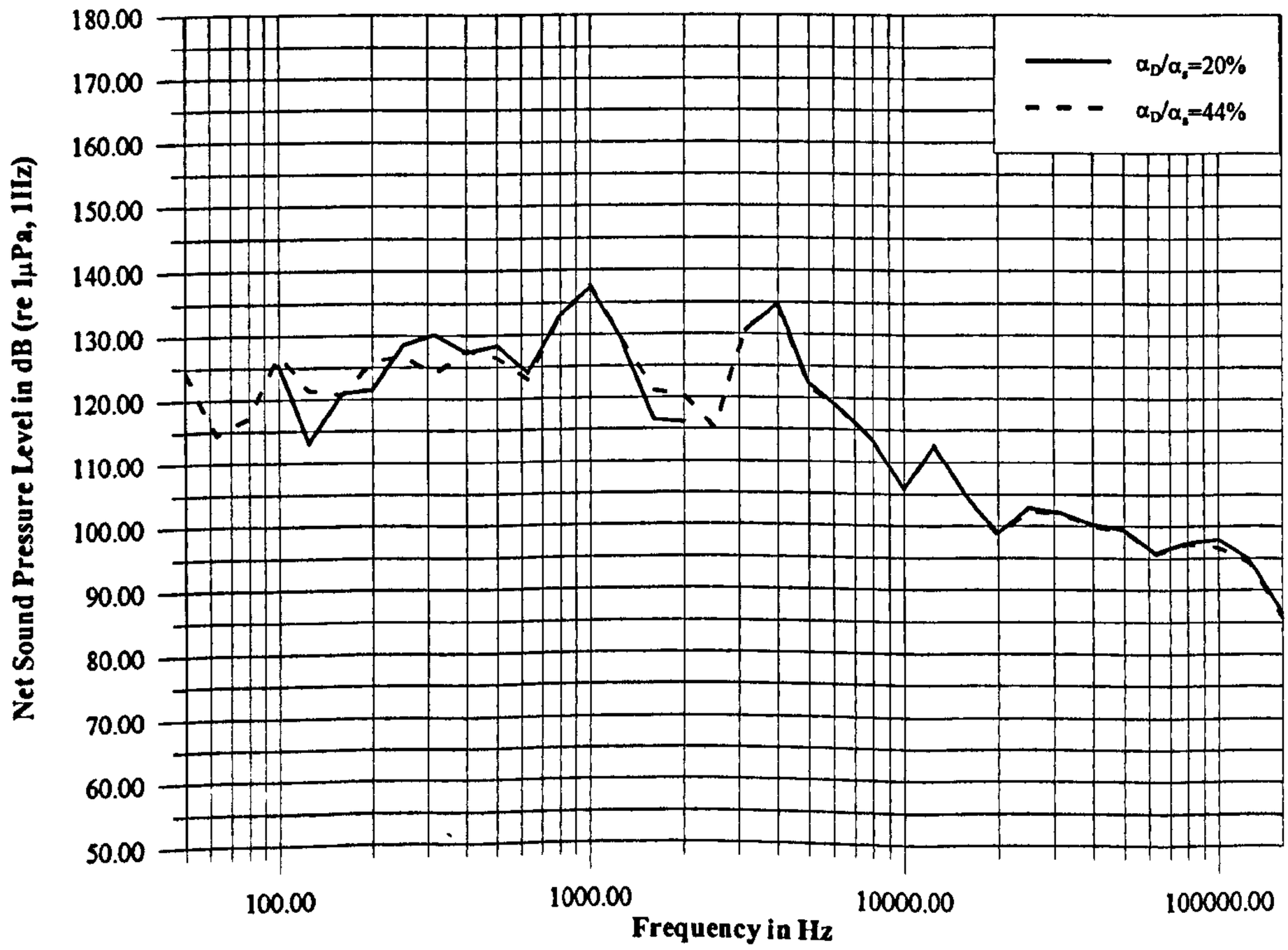

Figure 5.42 Effect of dissolved gas content on the level of net propeller noise for blade roughness level, k=100 μm, at σ_u=Atm and J=0.4

5.5 CONCLUSIONS

In order to explore the effects of the free-stream turbulence, the blade roughness and the dissolved gas content on the noise characteristics of a propeller, systematic noise measurements were taken with a 5 bladed model propeller for varying cavitation numbers and advance coefficients at two different levels of the dissolved gas content. The analysis of the measurements indicated that:

- The analyses of the sources contributing to the tunnel's background noise indicated that the dynamometer was the major source regardless of operational conditions. However, the contribution of the wire meshes to the background noise level varied depending upon the operational conditions.

- The analyses of the net propeller noise for the effect of the free-stream turbulence and roughness displayed extremely complex trends which were difficult to interpret particularly for the low frequency region between 50 Hz and 1000 Hz.

- It is conjectured that the above complex behaviour in the low frequency region was mainly caused by the frequencies of the structural vibration of the tunnel in combination with the blade rate frequency of the propeller and its harmonics.

- In the high frequency region, which is beyond 1000 Hz, the effect of the free-stream turbulence on the net propeller noise depended upon the operating conditions and displayed a complicated trend with the development of the cavitation (at σ_u=5.56). However, the levels of noise were increased with increasing levels of the free-stream turbulence for the non-cavitating case (at σ_u=Atm).

- In the low frequency region, similar to the effect of the free-stream turbulence it was impossible to observe any distinct trend for the effect of the blade roughness. However, in the high frequency region and at atmospheric condition, the levels of the propeller noise were increased with decreasing the level of roughness while this trend disappeared and became complex when cavitation was present (at σ_u=5.56).

- Although the effect of the free-stream turbulence on the inception of cavitation has been found similar to that of the blade roughness (Chapter 4), it is difficult to say that these two mechanisms had the same effect on the noise level of the propeller. In contrast to the case in the cavitation inception tests, the blade roughness reduced the noise level of the propeller while the increasing free-stream turbulence increased the noise similar to the case for the inception tests. This may be because of the different behaviour of the bubble dynamics affected by these mechanisms.

- As the dissolved gas content was increased, the propeller noise was reduced slightly in the high frequency region, displaying a cushioning effect on the noise characteristics of the propeller.

CHAPTER 6 A SEMI-EMPIRICAL APPROACH AND ANALYSIS OF SIMILARITY CRITERIA TO PREDICT THE INCEPTION OF CAVITATION

6.1 INTRODUCTION

The literature survey given in Chapter 1 has indicated that there has been no systematic investigation reported in the open literature exploring the effect of free-stream turbulence on the inception of cavitation of propellers. On the other hand, the analyses of the results of the inception measurements of cavitation with the NACA foil (Chapter 3) and the model propeller ECT103 (Chapter 4) have concluded that the increased level of free-stream turbulence encourages the inception of cavitation with reasonably clear trends. Similar trends have also been observed by the analyses of the measurements with varying levels of roughness. Therefore, it would be most appropriate to seek a semi-empirical procedure to relate the effect of the free-stream turbulence to the inception of cavitation and based upon the similarity of the trends between the effects of roughness and the free-stream turbulence, it would be worthwhile to establish a correspondence between these two effects in terms of the similar inception of cavitation. Moreover, the inclusion of the effect of the free-stream turbulence into the predicting of the inception of cavitation based on model tests may require a close look into the current similarity criteria.

Within the above context, the main objective of this chapter was to develop a semi-empirical model including the effect of the free-stream turbulence to predict the inception of cavitation of a propeller based on a reference inception of cavitation, which will be obtained with its scaled-down geometric model tested in a cavitation tunnel. The developed model will be explored to form a basis for an extrapolator to predict the

inception in full-scale. Another objective of the chapter was to establish a relationship, if there was any meaningful correspondence between the effect of the free-stream turbulence and that of the blade roughness, with an effort to improve the current cavitation model testing techniques. Finally, an attempt was made to include the effect of the free-stream turbulence in the criteria to improve the extrapolation technique for full-scale.

In achieving the above objectives, in the following sections of this chapter, a semi-empirical model, which includes the effect of the free-stream turbulence, is presented to predict the inception of cavitation of a model propeller. The semi-empirical model is based on a linear expression for more accurate prediction of the pressure distribution around the leading edge of a 2-D foil section, which is known as **"Lighthill's Leading Edge Correction"**. This expression has been modified in terms of the fluctuating angle of attack and applied to the propeller flow based on a number of simplifications made to predict the inception pressure at the blade tip region.

The developed model is then applied to predict the inception of cavitation for the model propeller tested in Chapter 4 at varying levels of the free-stream turbulence and the predicted results are compared with the test data.

The chapter continues with the analysis of the inception test data in Chapter 4 in terms of the effects of the free-stream turbulence and roughness, and establishes correspondence between these effects for the same inception numbers. Based upon this correspondence and using the semi-empirical model, further prediction and comparison are made with the test data for varying levels of the blade roughness.

Finally, Dimensional Analysis technique is applied to include the effect of the free-stream turbulence in the traditional similarity criteria for a more sound modelling of the turbulence effect.

6.2 DEVELOPMENT OF A SEMI-EMPIRICAL MATHEMATICAL MODEL TO PREDICT THE INCEPTION OF CAVITATION

As stated earlier in Section 1.1.1.1.1, Hinze (1975) describes turbulence as an irregular condition of flow in which the various quantities show a random variation with time and space co-ordinates, so that statistically distinct average values can be obtained. Therefore, an instantaneous value of the velocity at a point is given by:

$$U_i = \overline{U}_i + u_{fi} \tag{6.1}$$

where:

- $\overline{U}_i$ is the mean value of the velocity
- u_{fi} is the fluctuating component of the velocity.

The inception number of cavitation at a reference point on a propeller can be defined as:

$$\sigma_i = \frac{P_{st} - P_v}{\frac{1}{2}\rho V_R^2} \tag{6.2}$$

where:

- V_R is the resultant velocity expressed by $V_R = \sqrt{\overline{U}_A^2 + (0.7\pi ND)^2}$
- $\overline{U}_A$ is the mean value of the advance velocity of the propeller.

The pressure coefficient at any reference point on the propeller can also be described as:

$$C_p = \frac{P - P_{st}}{\frac{1}{2}\rho V_R^2} \tag{6.3}$$

where:

- P is the local pressure at the reference point on the propeller.

In ideal conditions, cavitation is assumed to occur when the local pressure around propeller is reduced to a minimum value, P_{min}, which is equal to the vapour pressure of water. That is

$$P_{min} = P_v \tag{6.4}$$

and

$$\sigma_i = -C_{p\,min} \tag{6.5}$$

where:

$$C_{p\,min} = \frac{P_{min} - P_{st}}{\frac{1}{2}\rho V_R^2} \tag{6.6}$$

In reality, however, the minimum pressure at inception stage is usually different from the vapour pressure and the pressure, at which cavitation occurs, is called **"Inception or Critical Pressure"**, P_{crit}. The deviations of the inception or critical pressure from the vapour pressure cause scale effect phenomena on the inception of cavitation. Therefore, it is more meaningful to define the inception number of cavitation in terms of the critical pressure rather than the vapour pressure as:

$$\sigma_i = \frac{P_{st} - P_{crit}}{\frac{1}{2}\rho V_R^2} \tag{6.7}$$

Then, the inception number of cavitation can be written as:

$$\sigma_i = \frac{P_{st} - P_v + P_v - P_{crit}}{\frac{1}{2}\rho V_R^2} = \frac{P_{st} - P_v}{\frac{1}{2}\rho V_R^2} + \frac{P_v - P_{crit}}{\frac{1}{2}\rho V_R^2} = \sigma_{iR} + \frac{P_v - P_{crit}}{\frac{1}{2}\rho V_R^2} = \sigma_{iR} + \Delta\sigma_i \quad (6.8)$$

where:

- σ_{iR} is defined as a reference inception number corresponding to an assumed or known level of free-stream turbulence and reference roughness, and distribution of nuclei (in terms of size, content and number) in the flow.
- $\Delta\sigma_i$ is the effects of viscosity and nuclei on the reference inception number.

In order to relate the inception of cavitation to each section taken along the span of a propeller blade, a typical velocity diagram of a propeller blade section is shown in Figure 6.1.

In this figure:

- θ is the geometric pitch angle of the propeller
- α_G is the geometric angle of attack
- α_E is the effective angle of attack
- β_i is the hydrodynamic pitch angle
- β is the advance angle
- x_r is the non-dimensional radius
- u_{ia} and u_{it} are the axial and tangential components of the induced velocity of the propeller, respectively.

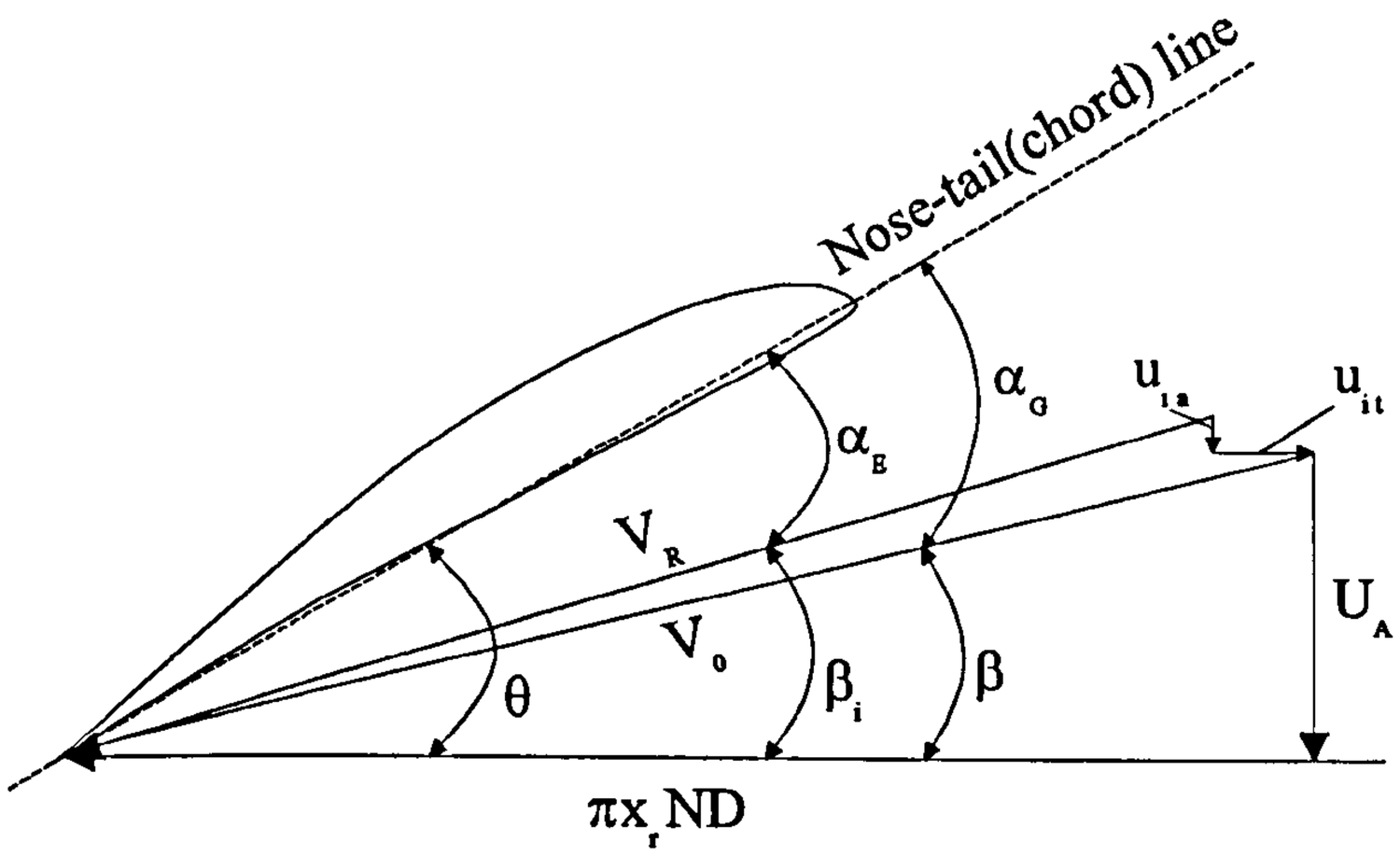

Figure 6.1 A typical velocity diagram of a propeller blade section at radius (x_rR)

For the time being, let us assume that the induced velocity components are small and negligible compared to the advance and circumferential velocity components. Thus,

$$\begin{aligned} \beta_i &\approx \beta \\ \theta &\approx \beta + \alpha_E \\ \alpha_E &\approx \theta - \beta \end{aligned} \tag{6.9}$$

The author is aware that the above assumption is open to question, but it has been made for the sake of simplicity. Indeed, the inclusion of the induced velocities is a straight forward process in the formulation. Furthermore, angle of attack α, can be represented by:

$$\alpha = \theta - \beta \tag{6.10}$$

By definition, it follows that:

$$\theta = \tan^{-1}\left(\frac{P_{xr}}{\pi x_r D}\right)$$
$$\beta = \tan^{-1}\left(\frac{U_A}{\pi x_r N D}\right) \quad (6.11)$$

where:

- P_{xr} is the pitch of the propeller at that radius

The angle of attack will then be:

$$\alpha = \tan^{-1}\left(\frac{P_{xr}}{\pi x_r D}\right) - \tan^{-1}\left(\frac{U_A}{\pi x_r N D}\right) \quad (6.12)$$

In the presence of a ship hull, the advance velocity is defined as $U_A = U(1 - w_m)$ where

- U is the free-stream velocity
- w_m is the mean wake fraction at the corresponding radius due to the ship hull.

Assuming that the propeller is operating in open water, the effect of the wake disappears, hence $U_A = U$.

On the other hand, instantaneous free-stream velocity including the effects of the turbulence can be written as:

$$\bar{U} = \overline{U} + u_f \quad (6.13)$$

where:

- $\overline{U}$ is the mean value of the free-stream velocity
- u_f is the fluctuations of the free-stream velocity due to the turbulence.

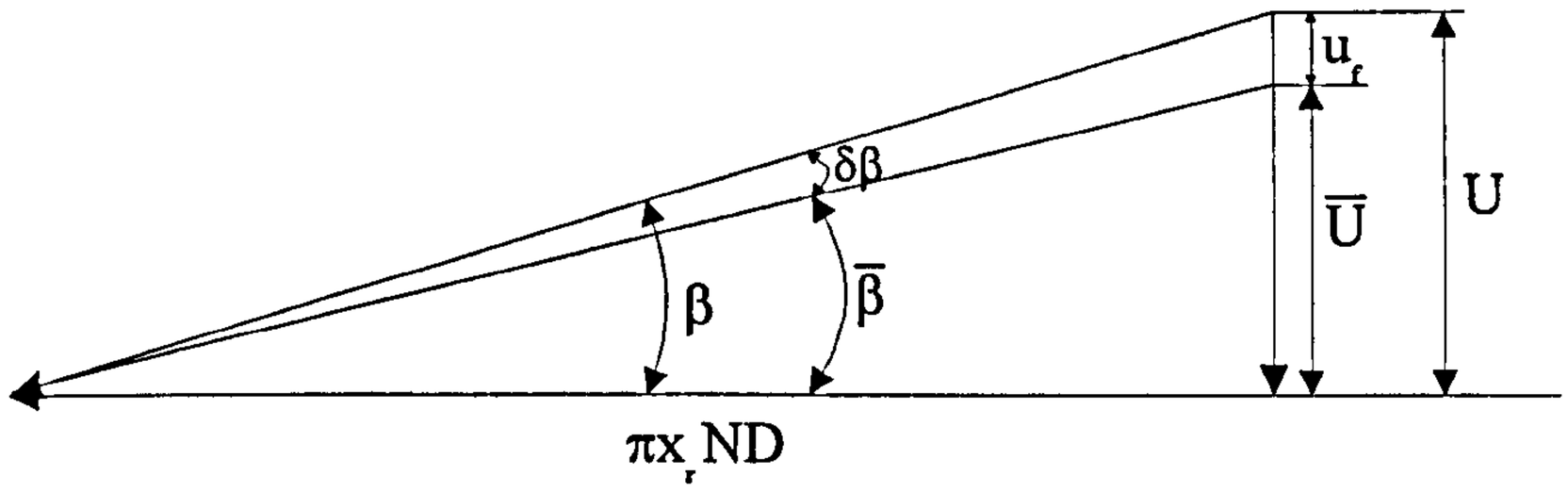

Figure 6.2 Velocity diagram of a propeller blade section at x_r including effect of free-stream turbulence only

As it is shown in Figure 6.2, the effect of the fluctuations due to the free-stream turbulence in the advance angle, β, and angle of attack,α, can be expressed as:

$$\begin{aligned} \beta &= \overline{\beta} + \delta\beta \\ \alpha &= \overline{\alpha} + \delta\alpha \end{aligned} \tag{6.14}$$

where:

- $\overline{\beta}$ and $\overline{\alpha}$ are the mean values
- $\delta\beta$ and $\delta\alpha$ are the associated fluctuating terms in the advance angle and angle of attack due to the turbulence, respectively.

By noting that θ is constant and the mean angle of attack, $\overline{\alpha}$, which is given in Equation (6.10), can also be represented as:

$$\overline{\alpha} = \theta - \overline{\beta} \tag{6.15}$$

Equations (6.14) and (6.15) are then substituted into Equations (6.10), (6.11) and (6.12) as:

$$\beta = \bar{\beta} + \delta\beta = \tan^{-1}\left(\frac{\bar{U} + u_f}{\pi x_r N D}\right)$$

$$\alpha = \bar{\alpha} + \delta\alpha = \tan^{-1}\left(\frac{P_{xr}}{\pi x_r D}\right) - \tan^{-1}\left(\frac{\bar{U} + u_f}{\pi x_r N D}\right) \tag{6.16}$$

where:

- $\bar{\beta} = \tan^{-1}\left(\frac{\bar{U}}{\pi x_r N D}\right)$ and $\bar{\alpha} = \tan^{-1}\left(\frac{P_{xr}}{\pi x_r D}\right) - \tan^{-1}\left(\frac{\bar{U}}{\pi x_r N D}\right)$

From Equation (6.16) one can see that:

$$\begin{aligned} \delta\beta &= \beta - \bar{\beta} \\ \delta\alpha &= \alpha - \bar{\alpha} \end{aligned} \tag{6.17}$$

The fluctuation of angle of attack can be obtained by substituting Equations (6.10) and (6.15) into Equation (6.17) as:

$$\delta\alpha = -\delta\beta \tag{6.18}$$

In accordance with standard definition of the turbulence, by introducing the definitions of the root-mean-square to the above fluctuations, it follows that:

$$\begin{aligned} \delta\alpha' &= \sqrt{\overline{(\delta\alpha)^2}} \\ \delta\beta' &= \sqrt{\overline{(\delta\beta)^2}} \end{aligned} \tag{6.19}$$

where:

- $\overline{(\delta\alpha)^2}$ and $\overline{(\delta\beta)^2}$ are the mean squares of fluctuations of the angle of attack and advance angle respectively.

Then, by using Equations (6.16) and (6.17) the root-mean-square of fluctuations of the angle of attack will be:

$$\delta\alpha' = \delta\beta' = \beta - \bar{\beta} = \tan^{-1}\left(\frac{\bar{U} + u_f}{\pi x_r N D}\right) - \tan^{-1}\left(\frac{\bar{U}}{\pi x_r N D}\right) \tag{6.20}$$

As cavitation usually starts near the leading edge of foils, it is a problem to predict the pressure distribution near the leading edge of the foil by the theoretical models. The existing theoretical models, such as thin aerofoil theory or other boundary element methods present singular solutions near the leading edge region. In this context, Lighthill introduced his well-known leading edge correction for the distribution of surface velocity on a two-dimensional foil to overcome the singularity near the leading edge (Lighthill, 1951). In the presence of a no reliable procedure, it is thought to be appropriate to use his approach to predict the inception pressures at the leading edge.

Lighthill's approach is based on a two-dimensional, irrotational and incompressible flow, which is the simplest form of the problem correcting the theory of thin aerofoil near a rounded leading edge. He carried out an analysis to second order in powers of a small parameter, ε. The camber, thickness, velocity components and angle of attack are taken to be of order ε.

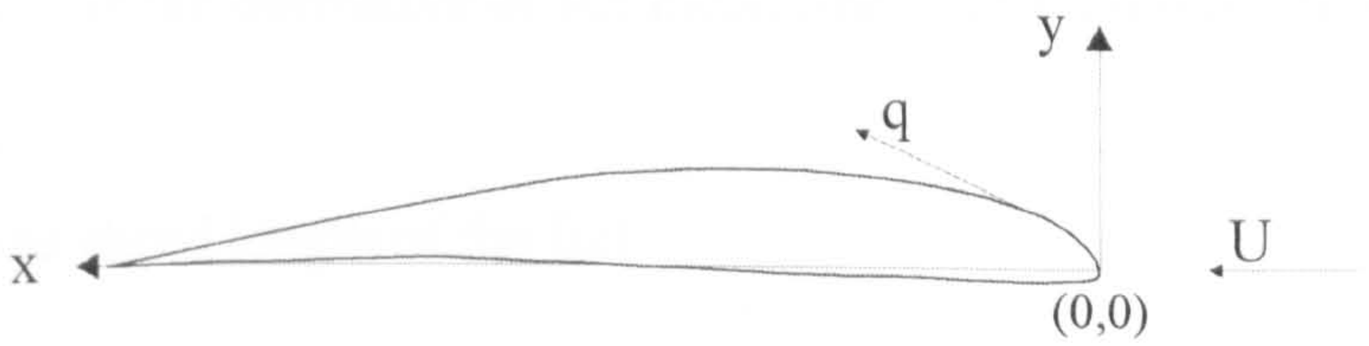

Figure 6.3 Flow approaches to a two-dimensional foil section

Two-dimensional, incompressible and potential flow past a thin foil of moderate camber at a moderate angle of attack, as shown in Figure 6.3, is treated by expanding the velocity field in a power series in powers of a parameter ε defining the size of disturbance. The singularity near the leading edge can be removed by straining the co-

ordinate system inside the foil. This shift was defined as half the leading edge radius of the foil. This radius is also itself a multiple of the square of the disturbances of the parameter, ε, (Lighthill, 1951).

Considering up to the first order of ε terms in the Lighthill's leading edge correction, his expression for the velocity distribution can be given by (Lighthill, 1951):

$$\frac{q}{U}=\left(\frac{x}{x+\frac{1}{2}r_L}\right)^{1/2}\left\{1+\frac{1}{\pi}\int_0^c\frac{F'(x_1)}{x-x_1}dx_1\pm\left(\frac{c-x}{x}\right)^{1/2}\left[\alpha+\frac{1}{\pi}\int_0^c\frac{C'(x_1)}{x-x_1}\left(\frac{x_1}{c-x_1}\right)^{1/2}dx_1\right]\right\} \quad (6.21)$$

where:

- q is the velocity distribution, which is equal to $q=\left(u^2+v^2\right)^{1/2}$
- U is the free-stream velocity
- x is the distance along the foil from the leading edge, where the velocity distribution is calculated
- r_L is the leading edge radius of the foil
- x_1 is a variable
- $F'(x_1)$ is the derivative of the thickness distribution of the symmetrical section with respect to x_1
- $C'(x_1)$ is the derivative of the mean line distribution of the foil with respect to x_1
- c is the chord length of the foil.

The upper sign applies to the suction (back) side and lower sign applies to the pressure (face) side of the foil.

When the effect of the turbulence term on the angle of attack, $\delta\alpha'$, is introduced into this expression by the earlier adopted notation $\alpha = \bar{\alpha} + \delta\alpha'$, the velocity expression becomes as:

$$\frac{q}{U} = \left(\frac{x}{x+\frac{1}{2}r_L}\right)^{1/2} \left\{1+\frac{1}{\pi}\int_0^c \frac{F'(x_1)}{x-x_1}dx_1 \pm\left(\frac{c-x}{x}\right)^{1/2}\left[\left(\bar{\alpha}+\delta\alpha'\right)+\frac{1}{\pi}\int_0^c \frac{C'(x_1)}{x-x_1}\left(\frac{x_1}{c-x_1}\right)^{1/2}dx_1\right]\right\} \tag{6.22}$$

Usually pressure coefficient of a foil is expressed by means of the linearised Bernoulli Equation as:

$$C_p = 1-\left(\frac{q}{U}\right)^2 \tag{6.23}$$

By substituting Equation (6.22) into Equation (6.23) results in:

$$C_p = 1-\left(\frac{x}{x+\frac{1}{2}r_L}\right)\left\{1+\frac{1}{\pi}\int_0^c \frac{F'(x_1)}{x-x_1}dx_1 \pm\left(\frac{c-x}{x}\right)^{1/2}\left[\left(\bar{\alpha}+\delta\alpha'\right)+\frac{1}{\pi}\int_0^c \frac{C'(x_1)}{x-x_1}\left(\frac{x_1}{c-x_1}\right)^{1/2}dx_1\right]\right\}^2 \tag{6.24}$$

Accordingly, the pressure coefficient, C_p, can also be written in terms of mean, $\bar{C}_p$, and fluctuating component, ΔCp, due to the turbulence as:

$$C_p = \bar{C}_p + \Delta C_p \tag{6.25}$$

The mean value of the pressure coefficient, $\overline{C}_p$, by disregarding $\delta\alpha'$ term in Equation (6.24), can be written as:

$$\overline{C}_p = 1 - \left(\frac{x}{x + \frac{1}{2}r_L}\right)\left\{1 + \frac{1}{\pi}\int_0^c \frac{F'(x_1)}{x - x_1}dx_1 \pm \left(\frac{c-x}{x}\right)^{1/2}\left[\overline{\alpha} + \frac{1}{\pi}\int_0^c \frac{C'(x_1)}{x - x_1}\left(\frac{x_1}{c - x_1}\right)^{1/2} dx_1\right]\right\}^2 \quad (6.26)$$

While the fluctuating component, ΔC_p, can, then, be obtained by subtracting Equation (6.26) from Equation (6.24) and ignoring the second order terms of $\delta\alpha'$, which are assumed to be negligible compared to the first order of $\delta\alpha'$, as:

$$\Delta C_p = 2\delta\alpha'\left(\frac{x}{x + \frac{1}{2}r_L}\right)\left(\frac{c-x}{x}\right)^{1/2}\left\{\left(\mp 1 + \frac{1}{\pi}\int_0^c \frac{F'(x_1)}{x - x_1}dx_1\right) - \left(\frac{c-x}{x}\right)^{1/2}\left[\overline{\alpha} + \frac{1}{\pi}\int_0^c \frac{C'(x_1)}{x - x_1}\left(\frac{x_1}{c - x_1}\right)^{1/2} dx_1\right]\right\} \quad (6.27)$$

Let us assume that x_m is the position of the minimum pressure from the leading edge. Then,

$$\Delta C_{pmin} = 2\delta\alpha'\left(\frac{x_m}{x_m + \frac{1}{2}r_L}\right)\left(\frac{c-x_m}{x_m}\right)^{1/2}\left\{\left(\mp 1 + \frac{1}{\pi}\int_0^c \frac{F'(x_1)}{x_m - x_1}dx_1\right) - \left(\frac{c-x_m}{x_m}\right)^{1/2}\left[\overline{\alpha} + \frac{1}{\pi}\int_0^c \frac{C'(x_1)}{x_m - x_1}\left(\frac{x_1}{c - x_1}\right)^{1/2} dx_1\right]\right\} \quad (6.28)$$

where:

- x_m can be calculated by differentiating Equation (6.23) with respect to x and by setting the derivative to zero, which can be found as (Breslin and Andersen, 1994):

$$x_m = \frac{1}{4c}\left(\frac{r_L}{\bar{\alpha} - \alpha_i}\right)^2 \tag{6.29}$$

where:

- α_i is the ideal angle of attack.

In applying Equation (6.28) to the blade section of a propeller, if one considers the case that the cavitation is usually observed on the suction side of the blade, the appropriate sign in Equation (6.28) will be (-). Thus, the minimum pressure equation for the back cavitation becomes:

$$\Delta C_{pmin} = 2\delta\alpha'\left(\frac{x_m}{x_m + \frac{1}{2}r_L}\right)\left(\frac{c - x_m}{x_m}\right)^{1/2}\left\{\left(-1 + \frac{1}{\pi}\int_0^c \frac{F'(x_1)}{x_m - x_1}dx_1\right)\right. \tag{6.30}$$
$$\left. -\left(\frac{c - x_m}{x_m}\right)^{1/2}\left[\frac{\bar{\alpha}}{\alpha} + \frac{1}{\pi}\int_0^c \frac{C'(x_1)}{x_m - x_1}\left(\frac{x_1}{c - x_1}\right)^{1/2}dx_1\right]\right\}$$

In summary, based upon Equations (6.8), (6.5) and (6.30) inception number,σ_i, on a propeller blade can be written as:

$$\sigma_i = \sigma_{iR} + \Delta\sigma_i = \sigma_{iR} - \Delta C_{pmin} \tag{6.31}$$

The above relationship indicates that the inception of cavitation of a propeller can be predicted based upon a reference inception number, σ_{iR}, which can be obtained from model tests and fluctuating pressure component, ΔC_{pmin}, which is given in Equation (6.30) based on the Lighthill's modified leading edge correction.

However, to be strictly consistent in Equation (6.31), the reference inception (σ_{iR}) should occur at a corresponding reference free-stream turbulence level, $\Delta\sigma_{iR}$ or reference minimum pressure, ($-\Delta C_{pminR}$). By considering this argument, Equation (6.31) becomes:

$$\sigma_{calc} = \sigma_{iR} - (\Delta C_{pmin} - \Delta C_{pminR}) \tag{6.32}$$

6.3 APPLICATION OF THE SEMI-EMPIRICAL MODEL TO PREDICT THE INCEPTION OF CAVITATION AT VARYING LEVELS OF FREE-STREAM TURBULENCE

In this section, the semi-empirical model derived earlier and expressed by Equation (6.32) will be applied to ECT103 model propeller, which has been tested behind the turbulence generator, to compare the predictions with the inception test data presented in Chapter 4.

Prior to this application, one should bear in mind that the experimental data analysed in Chapter 4 displayed a different trend for the different levels of dissolved gas content, particularly, towards the sheet cavitation. This effect has not been taken into account in the simple model proposed here and therefore, the following discussions and associated amendments are thought to be appropriate.

As demonstrated in Chapter 4 (see Figures 4.8 through 4.10), the analyses of the experiments indicated that as the level of the free-stream turbulence was increased, the inception numbers of cavitation were also increased until a critical value of the free-stream turbulence, beyond which the inception numbers appeared to be insensitive to change in the level of turbulence for the stages of cavitation towards the sheet type. This trend was observed at the low level of dissolved gas content. On the other hand, at the high level of dissolved gas content, the trend was completely different, indicating the important effect of the bubble dynamics on the development of cavitation, although this effect has been neglected in this study due to the time and constraints on the effect of the bubble dynamics.

In order to build a mechanism for this trend in the semi-empirical model, there is a need to specify the above mentioned critical level of the turbulence. This can be achieved by analysing the experimental inception data, which can be presented as $(\sigma_i/\delta\alpha')$ versus $\delta\alpha'$ or $(\sigma_i/\delta\alpha')$ against u_f. As it will be re-called, $\delta\alpha'$ is the fluctuating angle of attack due to the free-stream turbulence and u_f is corresponding fluctuating component of the free-

stream velocity. If one fits polynomials to these two sets of data, takes the derivative of the polynomial functions with respect to $\delta\alpha'$ or u_f and equates them to zero this will provide the critical values for $\delta\alpha'$ and u_f. Having specified the critical value of u_f ($u_{fcritical}$) by this procedure, $u_{fcritical}$ will be substituted in Equation (6.20) to find the corresponding $\delta\alpha'_{critical}$ or alternatively $\delta\alpha'_{critical}$ can be obtained directly from the derivation procedure. This critical angle will be substituted in Equation (6.32) to compare the data of the tip vortex cavitation fully attached to all blades and the sheet cavitation at the low level of the dissolved gas content, as discussed in Chapter 4.

Typical plots associated with the application of the above procedure for the critical level of the free-stream turbulence are shown in Figures 6.4 and 6.5. As one can see in Figure 6.4, the minimum or maximum level of the fluctuating advance angle or the fluctuating component of the free-stream velocity cannot be obtained for the unattached tip vortex cavitation due to linear trends in these lines. However, for the sheet cavitation, as shown in Figure 6.5, the critical levels are observed and the associated values are obtained by the above mentioned procedure to be used in the following section for the comparisons.

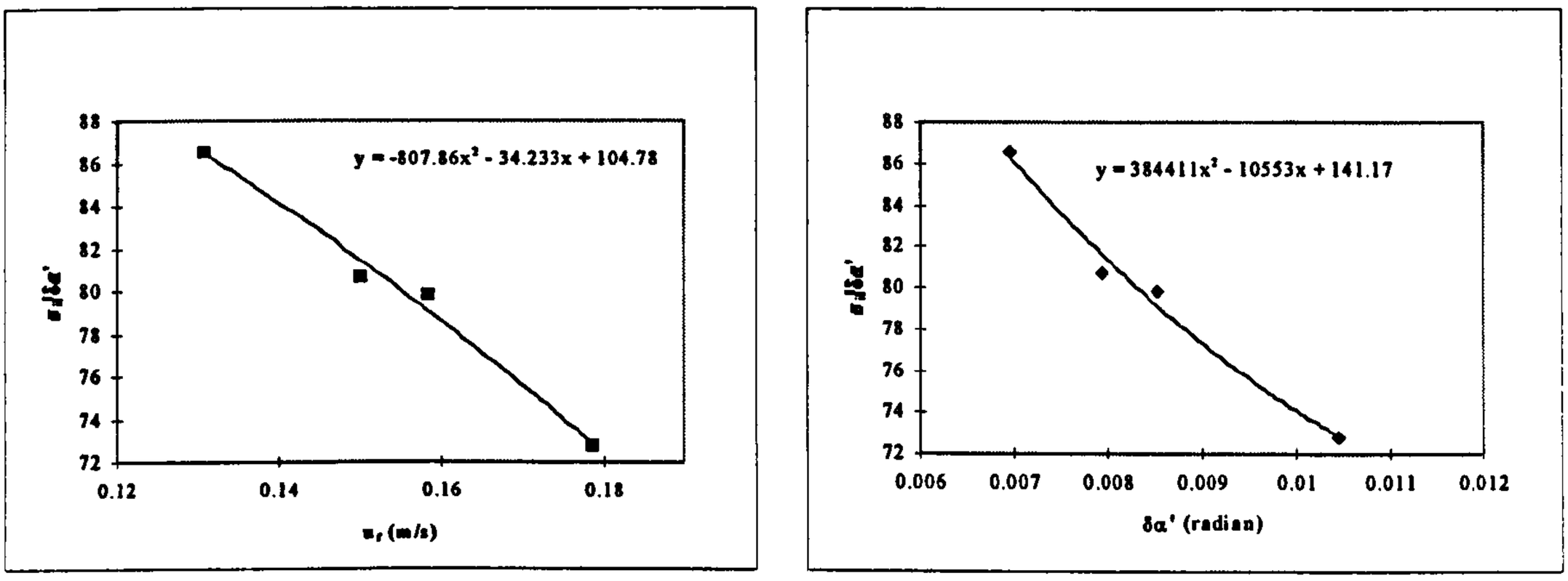

Figure 6.4 Plots of $\sigma_i/\delta\alpha'$ against u_f and $\delta\alpha'$ for unattached tip vortex cavitation in cases of mesh at low level of dissolved gas content, $\alpha_D/\alpha_S = 20\%$

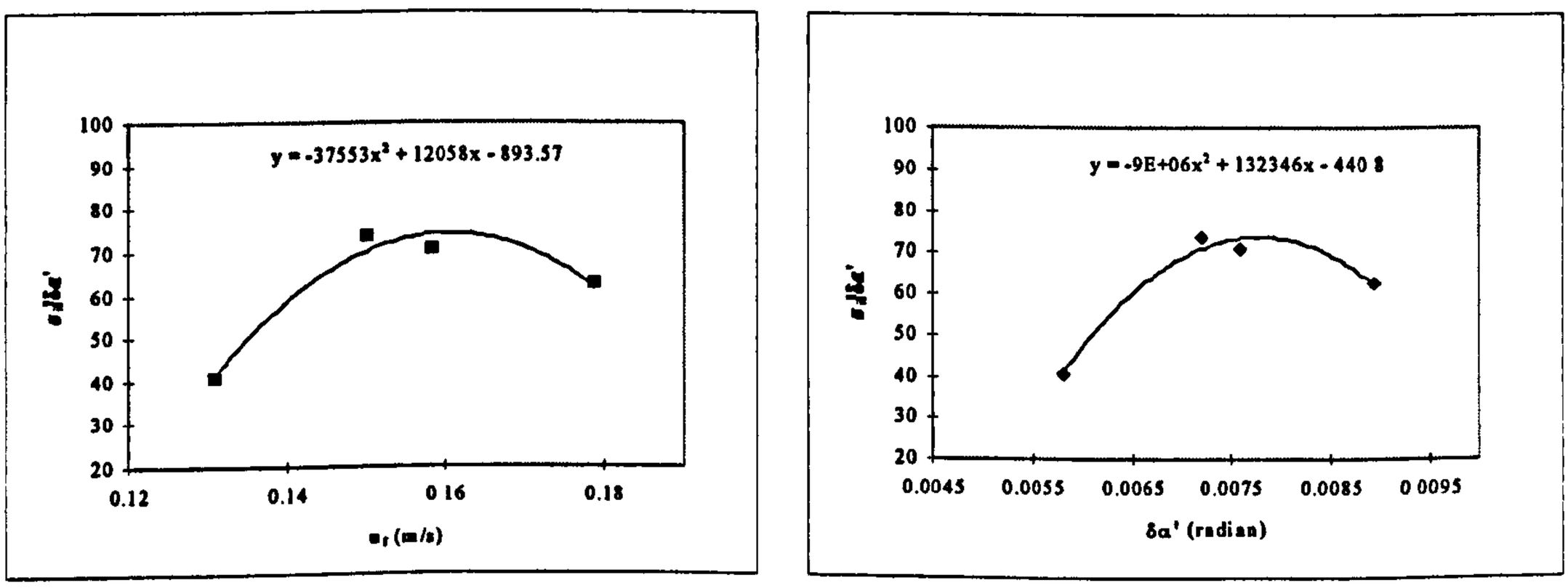

Figure 6.5 Plots of $\sigma_i/\delta\alpha'$ against u_f and $\delta\alpha'$ for sheet cavitation in cases of mesh at low level of dissolved gas content, $\alpha_D/\alpha_S = 20\%$

Returning back to the application of Equation (6.32), the values of the reference inception number, σ_{iR}, are obtained from the test data with no turbulence mesh and the corresponding values of the reference fluctuating pressure, ΔC_{pminR}, are calculated at the reference level of free-stream turbulence based on Equation (6.30). Then, the ΔC_{pmin} values are also calculated at varying levels of the free-stream turbulence based on Equation (6.30) where the integral terms associated with the symmetrical section and the camber line distribution are evaluated numerically and these calculations are performed at $x_r = 0.9875R$ radius of the propeller.

The application results are presented in Figures 6.6 through 6.9 for two different levels of dissolved gas content. In these figures:

- x axis presents the level of free-stream turbulence intensity, TI,
- while y axis presents the inception values of cavitation obtained straight forward from the tests as well as predicted from Equation (6.32).

As one can see in Figure 6.6, the predictions of varying levels of the free-stream turbulence are in good agreement with the experiments for the unattached tip vortex cavitation. The discrepancy increases as the cavitation is transformed towards the sheet type especially at the high level of dissolved gas content, as shown in Figures 6.7 through 6.9.

As shown in Figure 6.7, the correlation between the predictions and the experiments for the tip vortex cavitation attached to one blade only is as good as the correlation for the unattached tip vortex cavitation at the low level of dissolved gas content. However, the theoretical model overestimates the inception numbers of cavitation at the high level of dissolved gas content.

For the stage of the tip vortex cavitation fully attached to all blades (see Figure 6.8), one can see that the assumption of the critical level of the free-stream turbulence may work well at the low level of dissolved gas content, indicating good correlation between the predictions and experiments. The discrepancies between the experiments and

predictions become more at the high level of dissolved gas content compared to the previous stages of the cavitation.

One may notice that there is a big difference for the sheet cavitation at the low level of dissolved gas content, as shown in Figure 6.9. The gross difference can be explained by an observation error made for the reference cavitation number, which resulted in underestimated values of the inception. At the high level of dissolved gas content, the weak correlation is also observed, indicating the importance of the bubble dynamics.

In spite of the increasing discrepancy between the experiments and the predictions towards the sheet cavitation, the proposed semi-empirical model appears to be working to include the effect of the free-stream turbulence on the inception values at least for the unattached tip vortex cavitation at both levels of dissolved gas content and the tip vortex cavitation attached to one blade only at the low level of dissolved gas content.

Having developed and demonstrated the effectiveness of the proposed model, one needs to describe its practical use and contribution to the current-state-of-the-art cavitation prediction techniques and test procedure, which are discussed in the following:

There is no doubt that forming an extrapolator to predict the inception of cavitation in full-scale based on the model test measurements is the most challenging and complex task since such an extrapolator should include so many factors involved in the scaling phenomena. Bearing in mind this reality, if one considers the fact that the effect of the free-stream turbulence is one of the most important factors contributing to the inception phenomena, e.g. Equation (6.32) can form a basis for an extrapolator to include this important effect.

In essence, Equation (6.32) requires the reference inception number (σ_{iR}) and the associated turbulence velocities (u_f) as the input, and then it predicts the inception value for any required condition based on the required level of turbulence. In a cavitation tunnel facility thorough systematic investigations and correlation with the measurements simple extrapolators (i.e. σ_i versus TI), as shown in Figures 6.6 through 6.9, for a particular propeller can be developed. In the most plausible case, concentrating on the

effect of the free-stream turbulence only, it will be theoretically possible to predict the inception of cavitation in the full-scale based on the reference inception level obtained in model tests and the levels of turbulence expected at the full-scale which are to be input to the inception equation.

Other practical use of such extrapolators is to save the testing time in a cavitation tunnel facility. This can be materialised if the background flow turbulence characteristics are established systematically for varying levels of turbulence, it will be possible to estimate the inception of cavitation of a model propeller in various conditions, provided that the reference inception values (i.e. σ_{iR}) are known. In other words, the tunnel will perform a set of measurements for the reference inception values of a particular propeller and it will be possible to predict the inception value for any other condition required by using Equation (6.32). This will save considerable amount of testing time once the confidence in the extrapolator is established.

It is obvious that the establishment of confidence in such extrapolators would require systematic correlation of the predictions including the full-scale measurements, which are scarce world-wide. Beside this major requirement the strength of Equation (6.32) is proportional with the accurate modelling of ΔC_{pmin} and reliable reference input values. The present theoretical model for ΔC_{pmin}, which is based on a number of simplifications and heuristic assumptions, is a pioneering model.

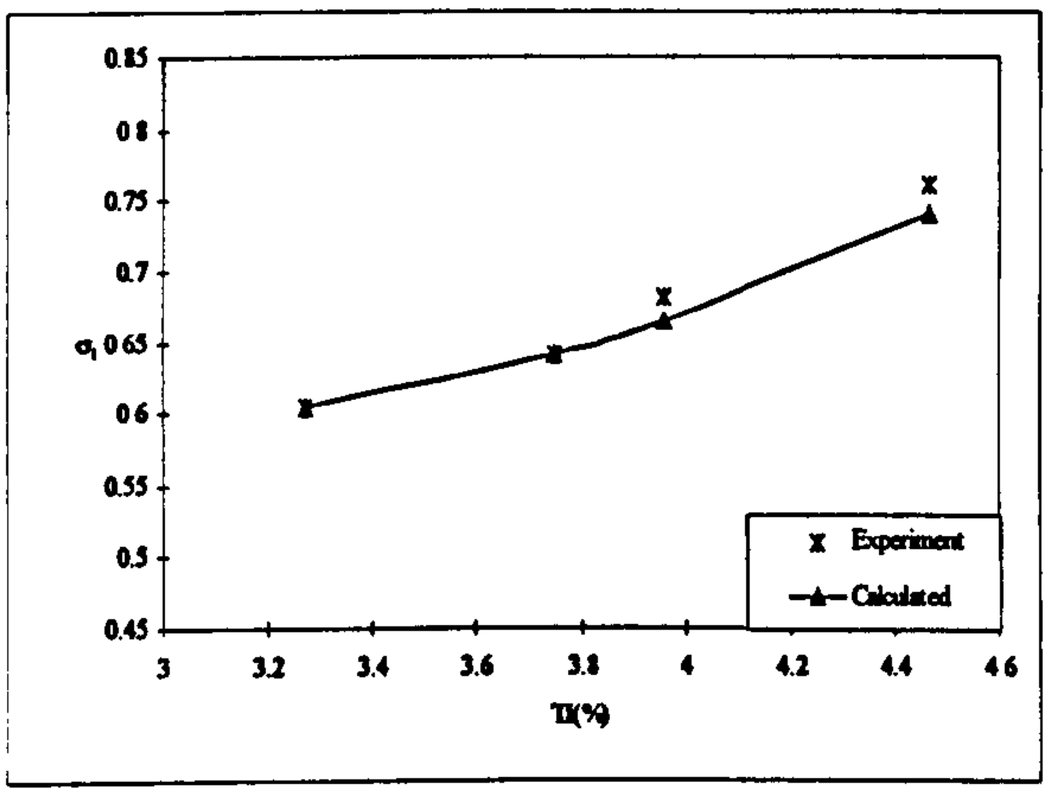

$\alpha_D/\alpha_S = 20\%$

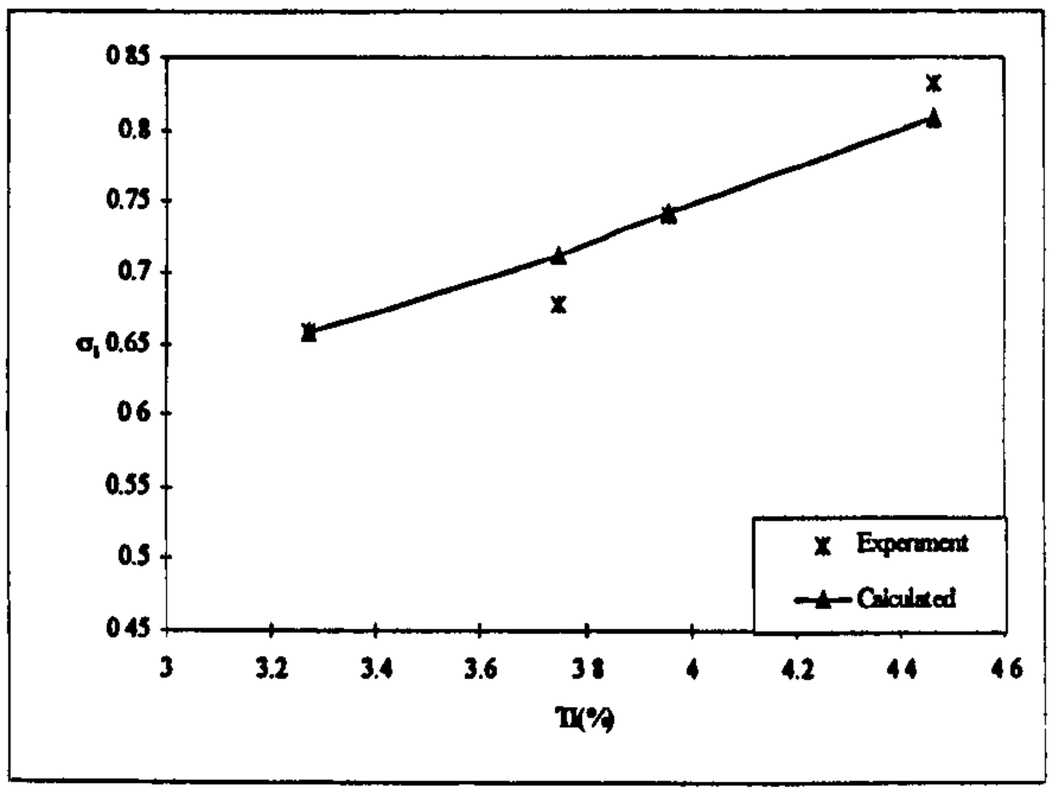

$\alpha_D/\alpha_S = 44\%$

Figure 6.6 Comparison of calculated inception numbers of unattached tip vortex cavitation with experimental results against level of free-stream turbulence in cases of mesh

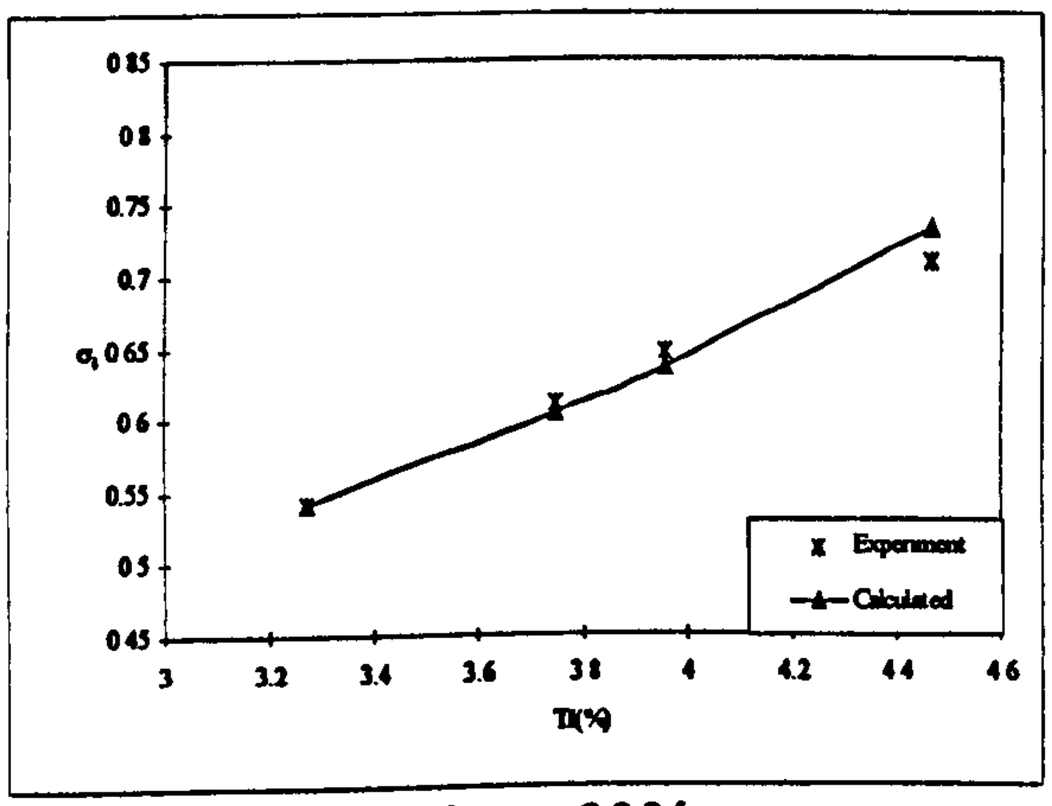

$\alpha_D/\alpha_S = 20\%$

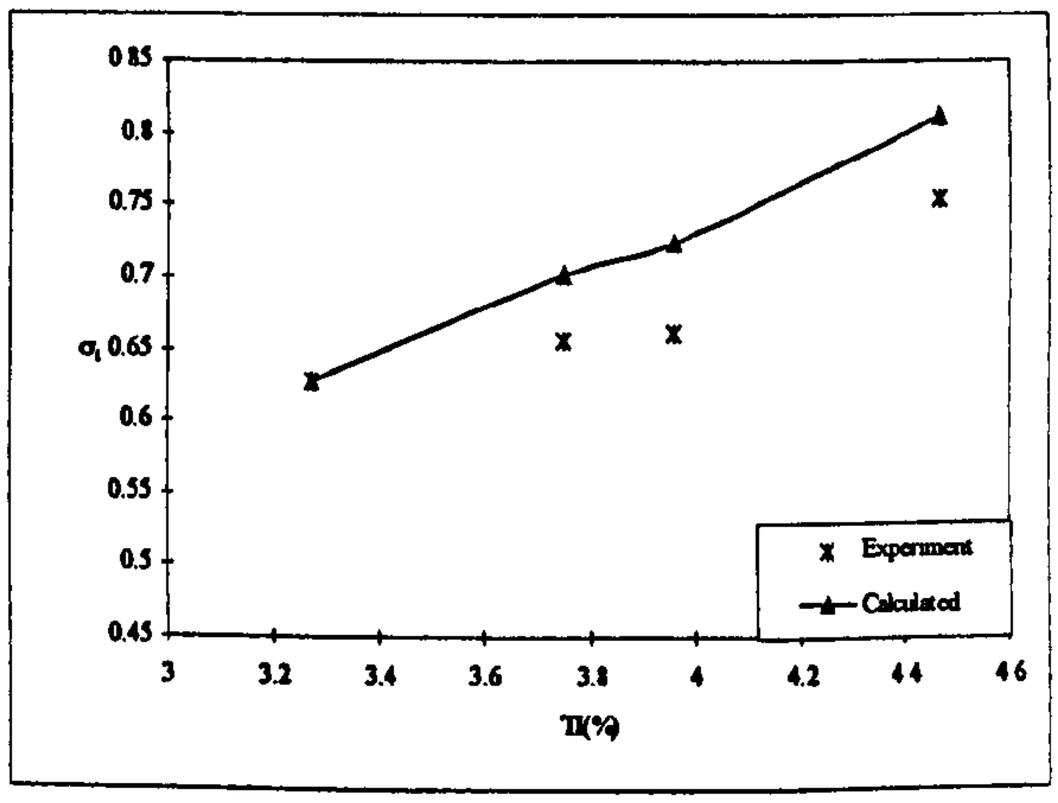

$\alpha_D/\alpha_S = 44\%$

Figure 6.7 Comparison of calculated inception numbers of tip vortex cavitation attached to one blade only with experimental results against level of free-stream turbulence in cases of mesh

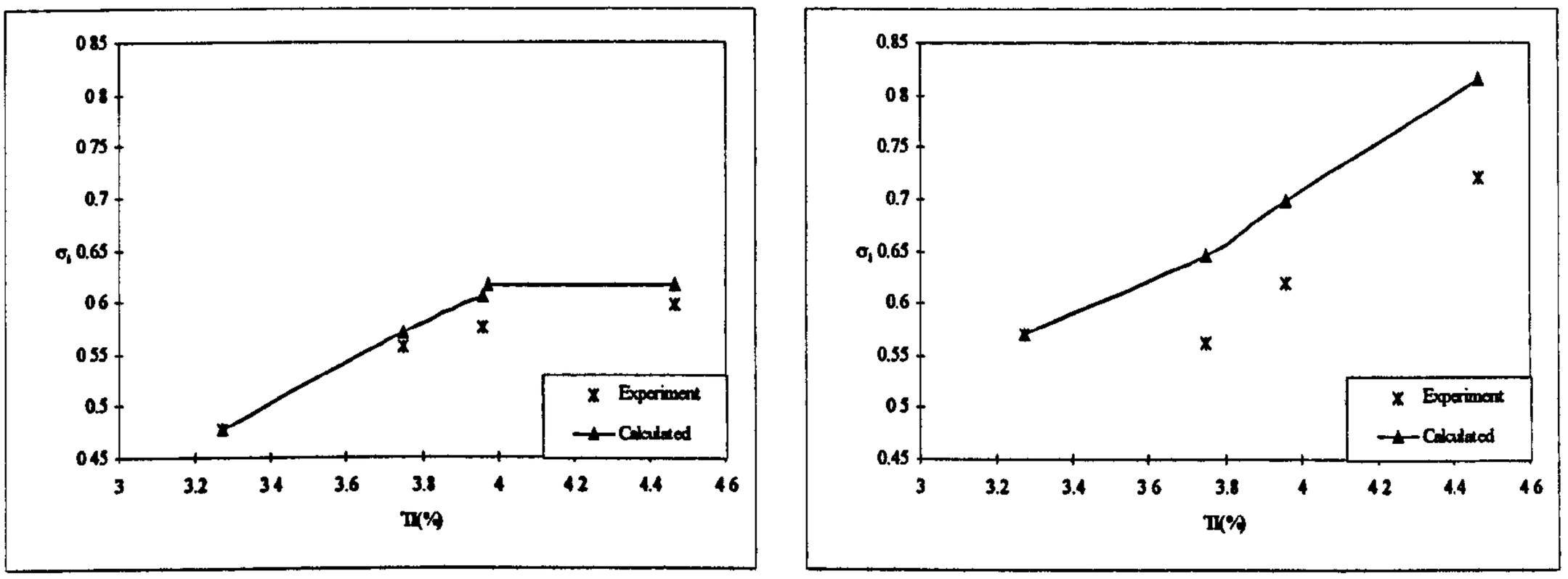

$\alpha_D/\alpha_S = 20\%$ $\alpha_D/\alpha_S = 44\%$

Figure 6.8 Comparison of calculated inception numbers of tip vortex cavitation fully attached to all blades with experimental results against level of free-stream turbulence in cases of mesh

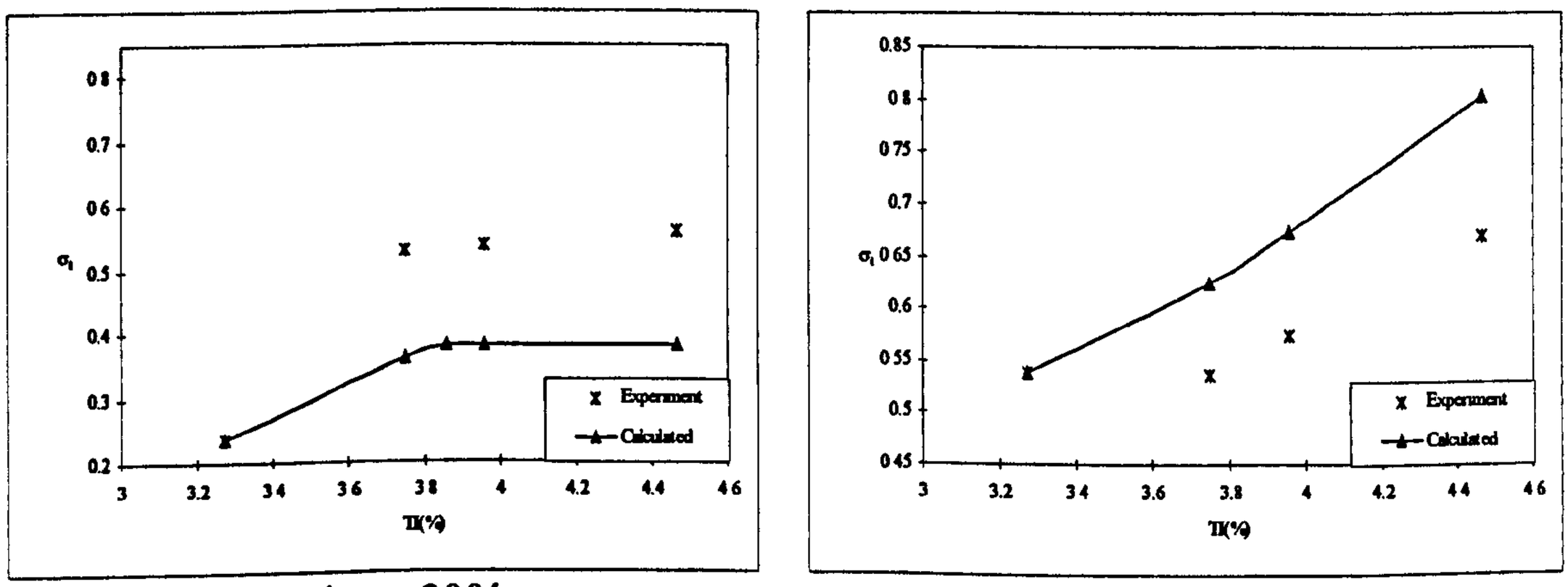

$\alpha_D/\alpha_S = 20\%$ $\alpha_D/\alpha_S = 44\%$

Figure 6.9 Comparison of calculated inception numbers of sheet cavitation with experimental results against level of free-stream turbulence in cases of mesh

6.4 ESTABLISHMENT OF RELATIONSHIP BETWEEN INTEGRAL LENGTH SCALE AND ROUGHNESS HEIGHT

The cavitation inception tests described in Chapter 4 have indicated that the level of free-stream and blade roughness clearly affected the inception of cavitation. Moreover, some useful trends have been observed between the measured values of the inception of cavitation and the levels of the free-stream turbulence and roughness height. Therefore, it will be practically useful to look to see if there is any correspondence, which can be expressed semi-empirically, between the level of the free-stream turbulence and that of the blade roughness height for the similar values of the inception of cavitation measured. The establishment of such a relationship could be extremely attractive providing flexibility for a more sound and practical approach for the turbulence stimulation instead of using cumbersome leading edge roughness technique.

As defined earlier in Chapter 2, the integral length scale, Λ_g, characterises the large eddy structure of the turbulence. Therefore, it would be appropriate to present the relationship between the level of turbulence and the roughness height in terms of the integral length scale, Λ_g, and the roughness height, k.

However, as discussed in the previous section for the reference inception condition, there is a need for the description of a reference level of the free-stream turbulence (or reference integral length scale, Λ_{gR}), that induces the reference inception of cavitation, σ_{iR}. Provided that Λ_{gR} is known, any other Λ_g to be considered can be related to the reference value.

Thus, if $\Delta\Lambda_g$ is the integral length scale relative to the above described reference integral length scale, it can be defined as:

$$\Delta\Lambda_g = \Lambda_g - \Lambda_{gR} \tag{6.33}$$

where:

- Λ_g is the integral length scale considered (or measured)
- Λ_{gR} is the reference integral length scale corresponding to the reference inception of cavitation.

Similarly, if Δk is the roughness height applied on the blade relative to a defined reference roughness height, k_R, one can write:

$$\Delta k = k - k_R \tag{6.34}$$

where:

- k is the roughness height considered
- k_R is the reference roughness height, which induces the reference inception of cavitation.

In order to demonstrate the trend for a meaningful correspondence between the integral length scale and roughness, the inception data produced in Chapter 4 with varying levels of the free-stream turbulence and blade roughness were further analysed and presented in Figures 6.10 through 6.13. In these figures:

- x axis presents the relative integral length scale, $\Delta\Lambda_g$ obtained from Equation (6.33)
- while y axis presents the relative roughness height, Δk obtained from Equation (6.34).

The construction of these figures are described as follows:

- Firstly, the inception values, σ_i, obtained from the cavitation tests with varying values of free-stream turbulence were plotted against $\Delta\Lambda_g$ values and best curves were fitted to these data.
- Secondly, the similar exercise was carried out for the inception data plotted against Δk values.
- Using these two sets of plotting, the values of $\Delta\Lambda_g$ and Δk, which induce the same inception numbers were plotted against each other in Figures 6.10 through 6.13 for various stages of the cavitation at two different levels of dissolved gas content.

As shown in Figure 6.10, the trend between the two main parameters for the unattached tip vortex cavitation appears to be fairly linear trend at both levels of the dissolved gas content. However, this trend appears to be gradually changing from the linear to non-linear in nature towards the sheet cavitation (i.e. compare Figure 6.10 with Figure 6.13) although the pattern of the curves are reasonably well behaved.

Once again, the effect of the gas content appears to be the major parameter affecting the pattern of these curves through complex behaviour of the bubble dynamics. Looking at these diagrams and comparing the figures at the low level of dissolved gas content with the figures, one can observe that the non-linearity at the low level of gas content is more than that of the high level. This is rather surprising but it is very difficult to make any comment without a thorough systematic investigation into the effect of the bubble dynamics.

The practical value and impact of the results of the above analyses on the current-state-of-the-art cavitation tests can be justified on the basis that somehow cumbersome technique of turbulence stimulation by using blade roughness can be replaced by more sound of technique of varying the level of turbulence in the free-stream. It is appreciated that the establishment of the correspondence diagram presented in Figures 6.10 through 6.13 would require enormous effort and time, particularly, including the systematic effect of the dissolved gas content. However, the tunnels with long history of service

can always analyse their data for the effect of roughness and relate them to the free-stream turbulence by performing only the effect of the turbulence tests.

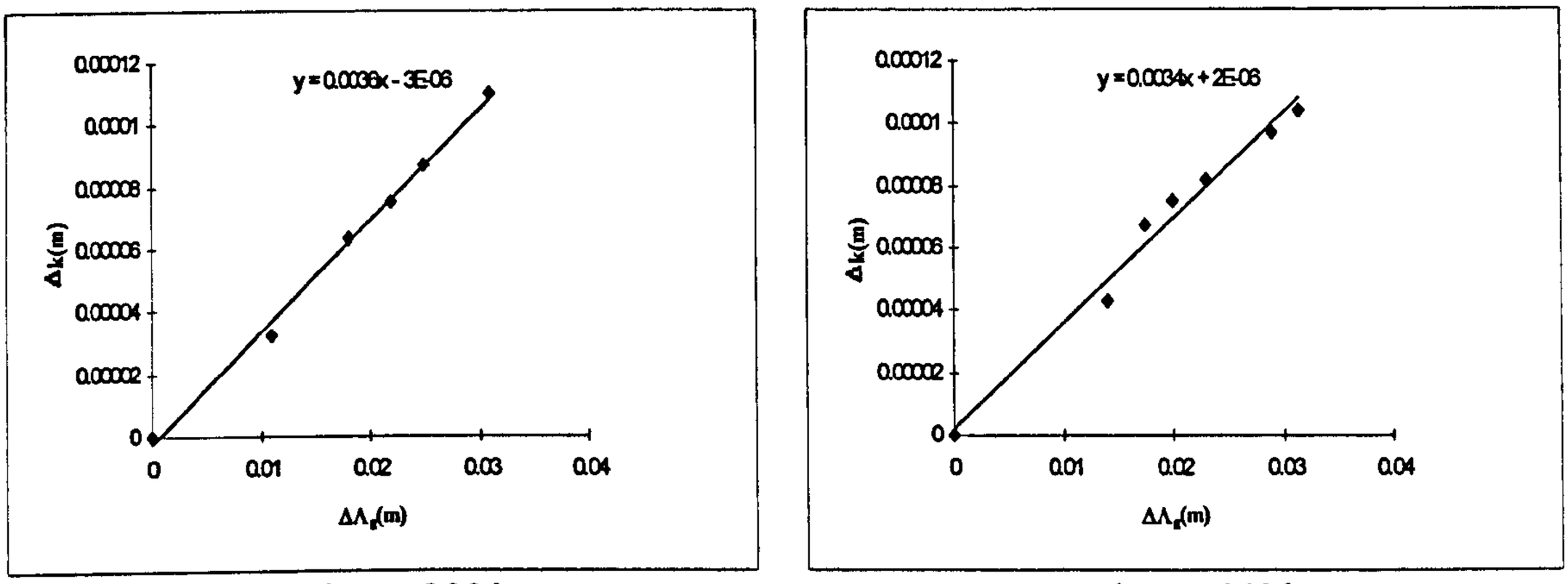

$\alpha_D/\alpha_S = 20\%$ $\alpha_D/\alpha_S = 44\%$

Figure 6.10 Plots of Δk against $\Delta\Lambda_g$ of unattached tip vortex cavitation at both level of dissolved gas content

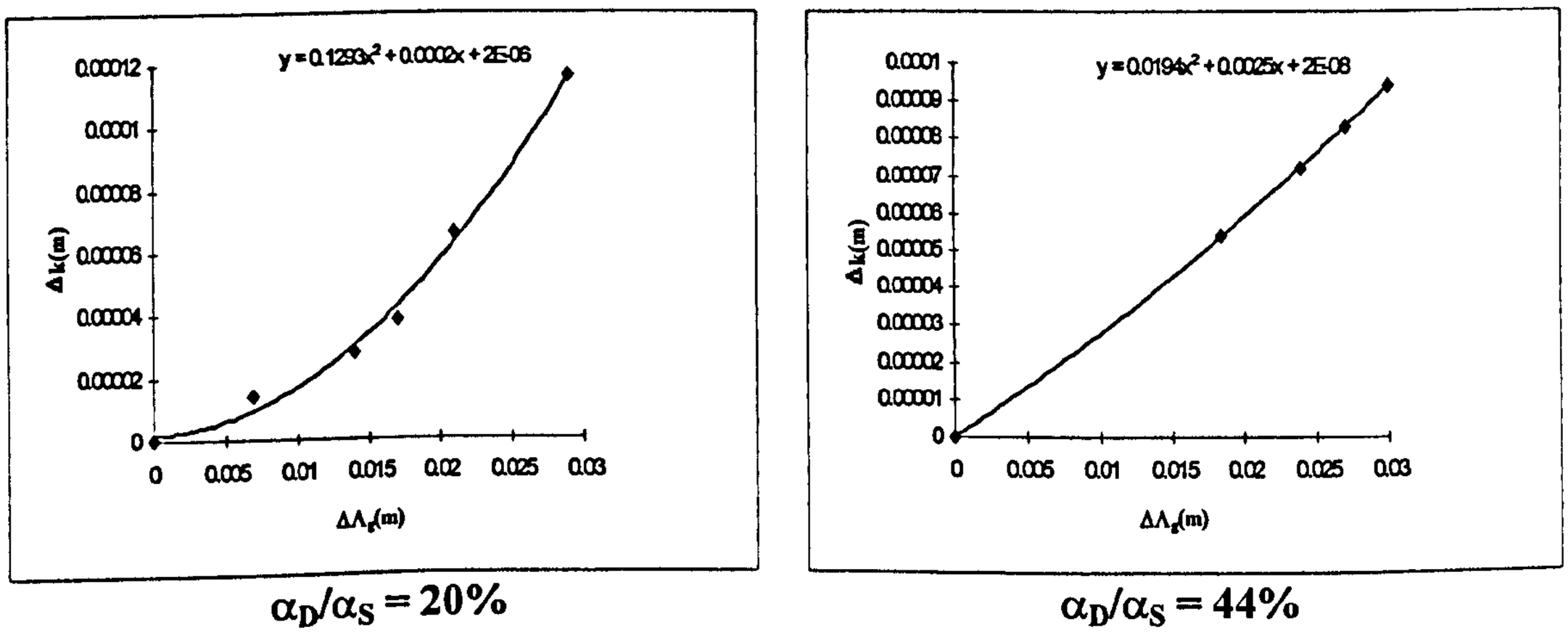

$\alpha_D/\alpha_S = 20\%$ $\alpha_D/\alpha_S = 44\%$

Figure 6.11 Plots of Δk against $\Delta\Lambda_g$ of tip vortex cavitation attached to one blade only at both level of dissolved gas content

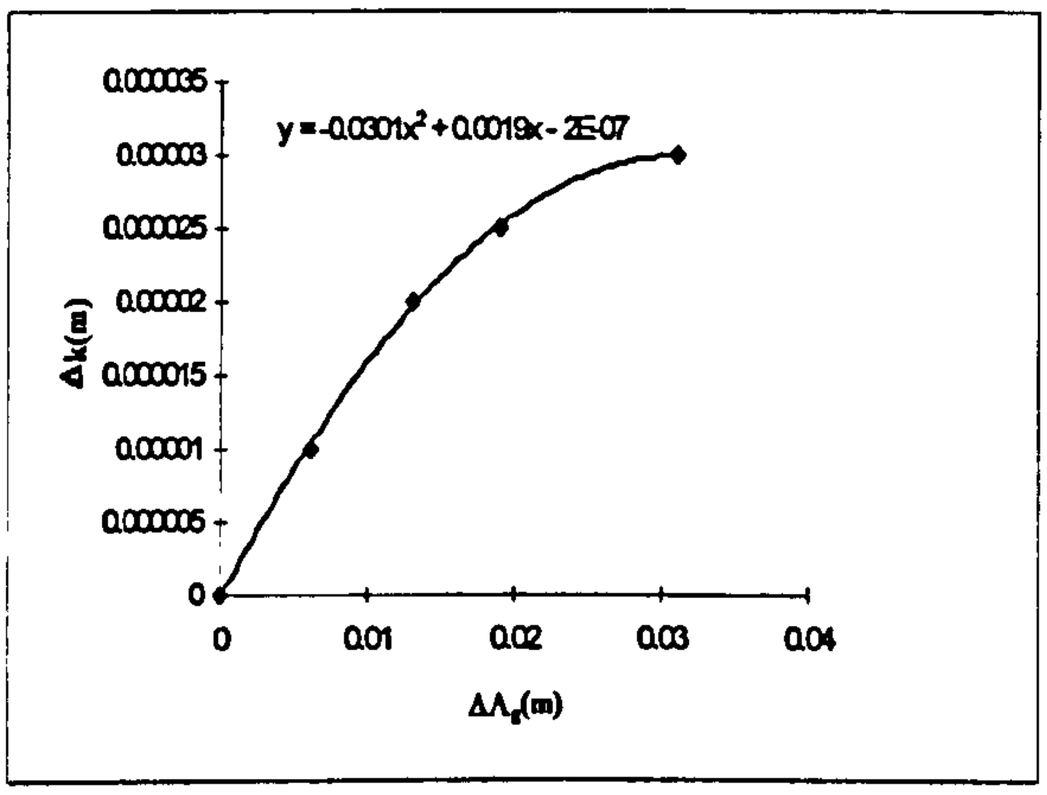

$\alpha_D/\alpha_S = 20\%$

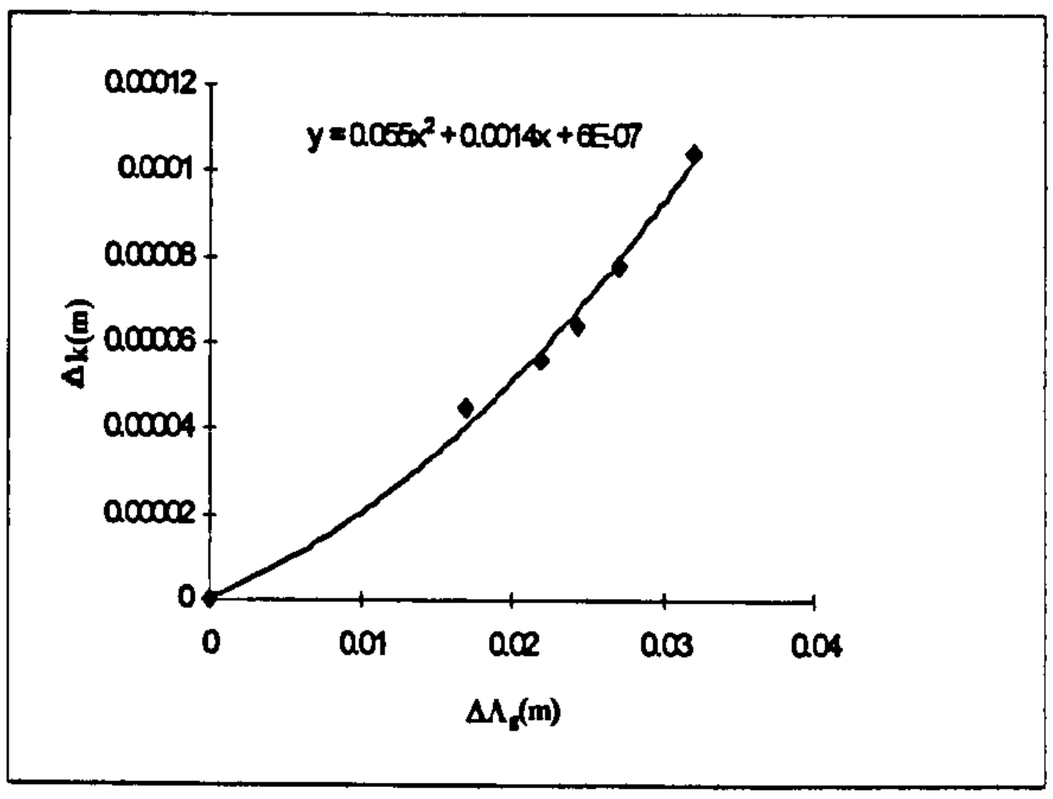

$\alpha_D/\alpha_S = 44\%$

Figure 6.12 Plots of Δk against $\Delta\Lambda_g$ of tip vortex cavitation fully attached to all blades at both level of dissolved gas content

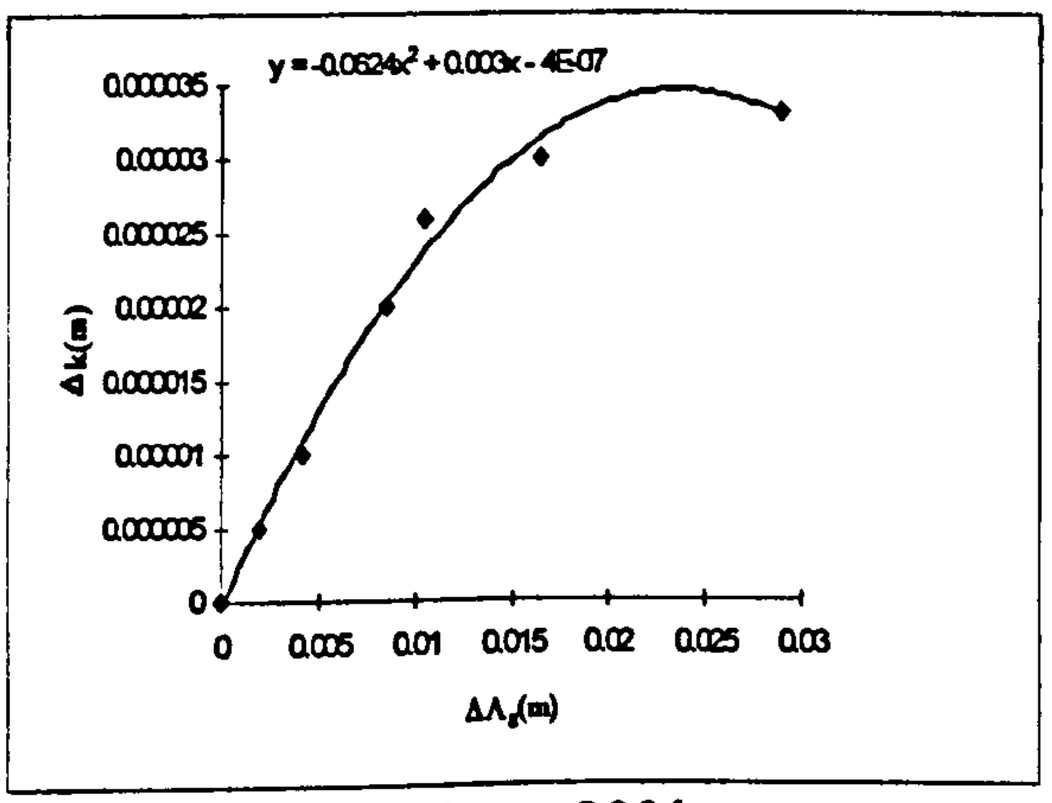

$\alpha_D/\alpha_S = 20\%$

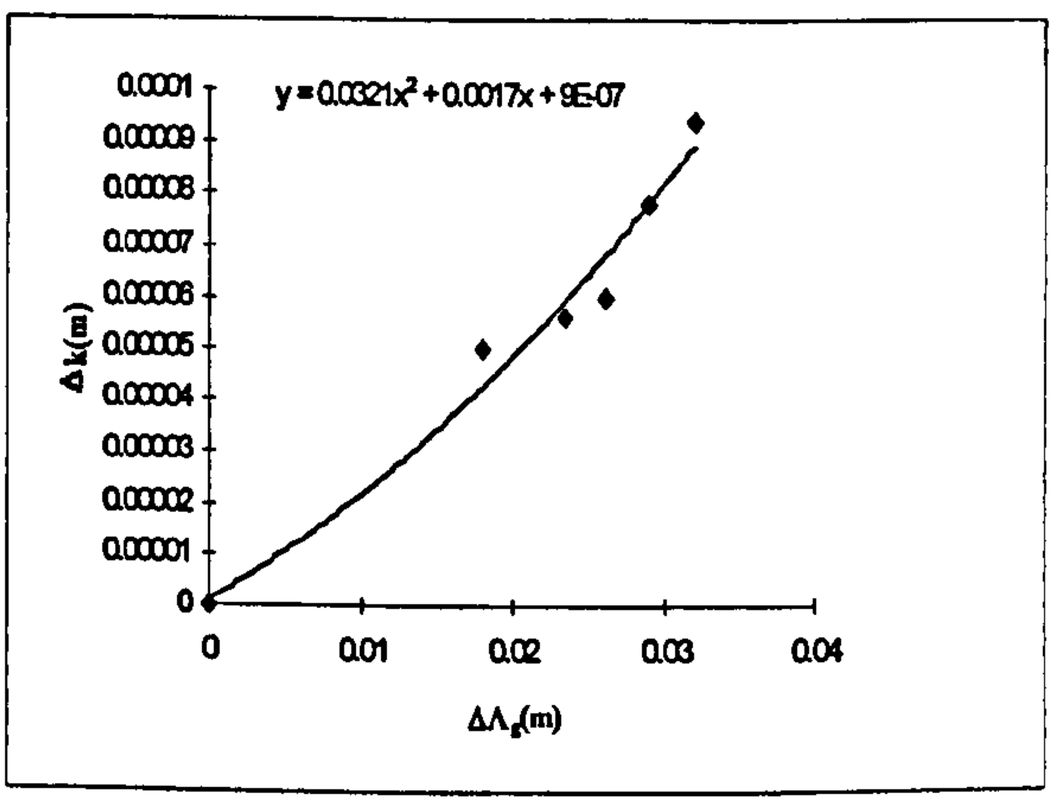

$\alpha_D/\alpha_S = 44\%$

Figure 6.13 Plots of Δk against $\Delta\Lambda_g$ of sheet cavitation at both level of dissolved gas content

6.5 APPLICATION OF THE SEMI-EMPIRICAL MODEL TO PREDICT THE INCEPTION OF CAVITATION AT VARYING LEVELS OF BLADE ROUGHNESS

In Section 6.2 of this chapter, the semi-empirical model, which takes into account the effect of the free-stream turbulence, has been presented and the predictions from this model have been compared with the cavitation test data for varying levels of free-stream turbulence in Section 6.3. On the other hand, a relationship has been established in the previous section between the level of free-stream turbulence (integral length scale) and roughness height, which induce the same inception numbers, based on the cavitation test data produced in Chapter 4. The established relationship now allows one to use the semi-empirical model to predict the inception of cavitation for varying levels of blade roughness and compare with the inception test data presented in Chapter 4.

The comparison process will be carried out in two steps:

- The first step involves the identification of the relative integral length scale ($\Delta\Lambda_g$) corresponding to a particular relative roughness values (Δk) by using the correspondence plots in the previous section for the cavitation phase concerned.
- In the second step, the $\Delta C_{pmincorresp}$ value corresponding to the relative length scale $\Delta\Lambda_g$ obtained in the first step is calculated from Equation (6.30). Then, the inception number cavitation will be eventually obtained from the following equation.

$$\sigma_{calc} = \sigma_{iR} - (\Delta C_{pmincorresp} - \Delta C_{pminR}) \tag{6.35}$$

The above formula has been applied to predict the inception values and compare with those measured for the model propeller with varying levels of blade roughness. The results of the comparison are presented in Figures 6.14 through 6.17 for various phases of the cavitation patterns at two levels of dissolved gas content. In these figures:

- x-axis presents the level of blade roughness or relative roughness height (Δk) in μm.

- while y-axis presents the cavitation inception values predicted from Equation (6.35) and the test data.

As shown in these figures, the correlation patterns are similar to the comparisons carried out with the inception tests for varying levels of free-stream turbulence (see Figures 6.4 to 6.7). While the correlation for the unattached tip vortex cavitation appears to be very good, as shown in Figure 6.14, the discrepancy between the predicted and measured inception values increases as the stages of cavitation moves towards the sheet cavitation.

The effect of the dissolved gas content on these figures can also be observed clearly. As mentioned in Section 6.3, the observation error made in the reference inception number of the sheet cavitation at the low level of dissolved gas content has made the comparison for this phase of cavitation meaningless. Therefore, the comparison has not been included for this condition.

The essence of the exercise presented here is the demonstration of the use of the semi-empirical model to predict the inceptions of cavitation at different levels of blade roughness. This will extremely be useful for the cavitation testing facilities, which have long experience with the blade roughness technique but to adopt the proposed technique with turbulence generator, to make use of their accumulated knowledge and build up confidence in using the turbulence generation technique for the future.

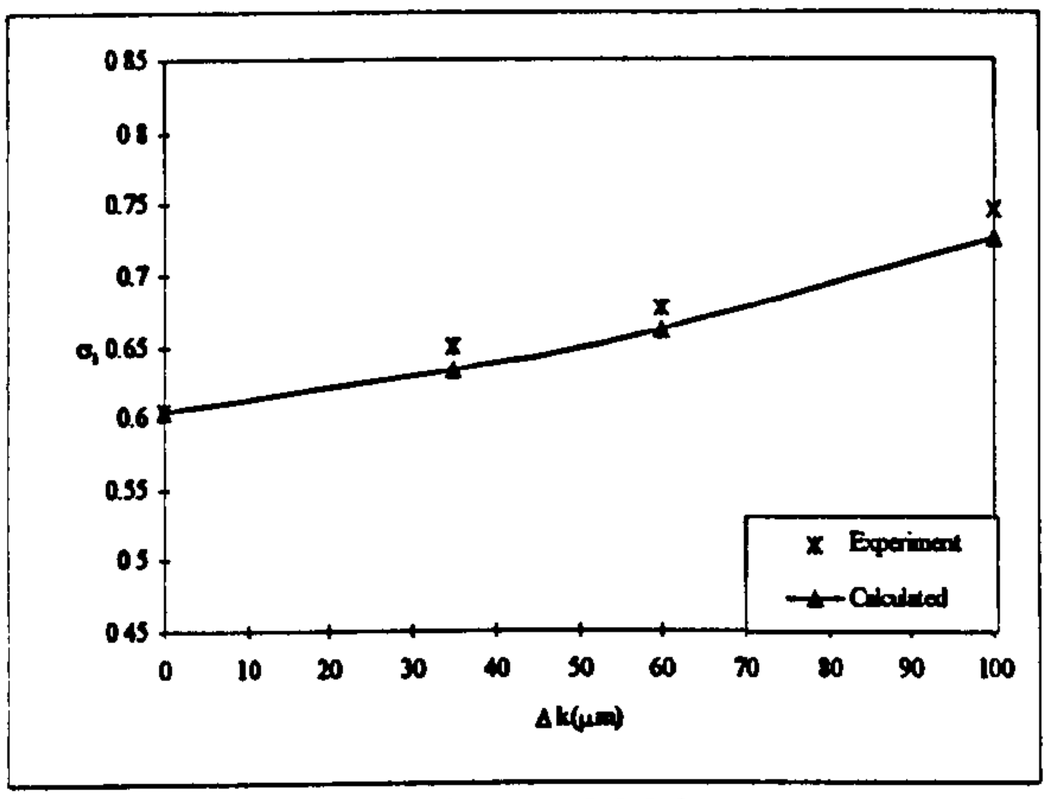

$\alpha_D/\alpha_S = 20\%$

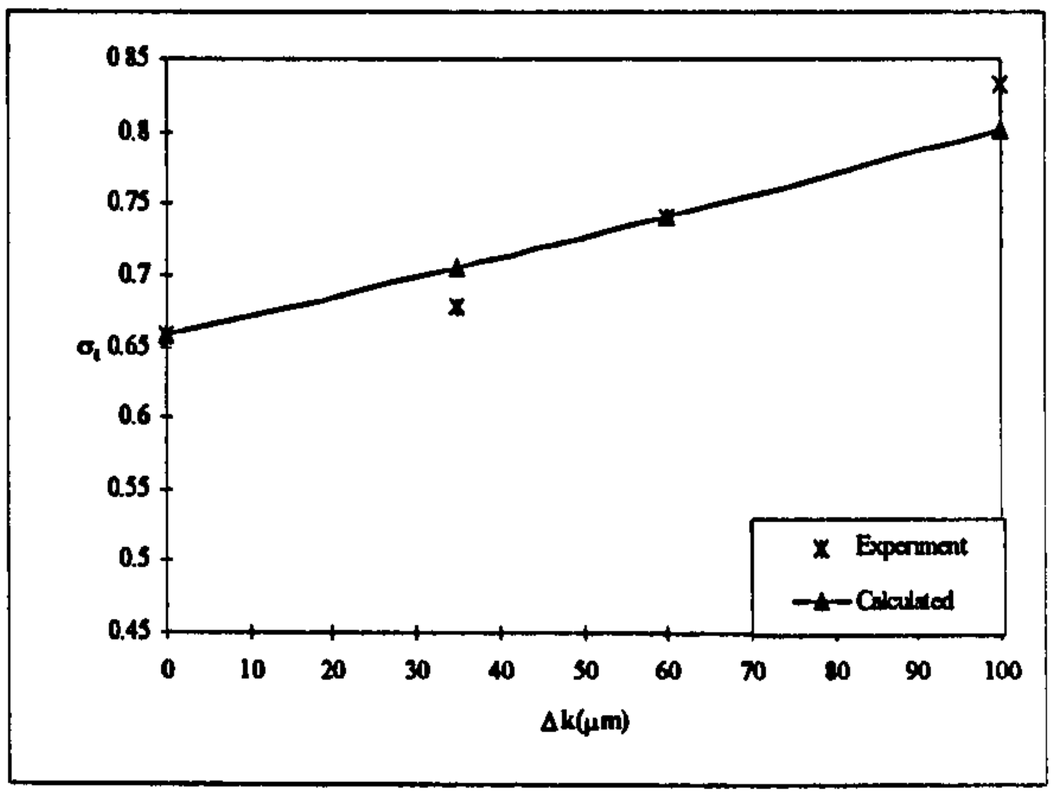

$\alpha_D/\alpha_S = 44\%$

Figure 6.14 Comparison of calculated inception numbers of unattached tip vortex cavitation with experimental results against roughness height in cases of roughness

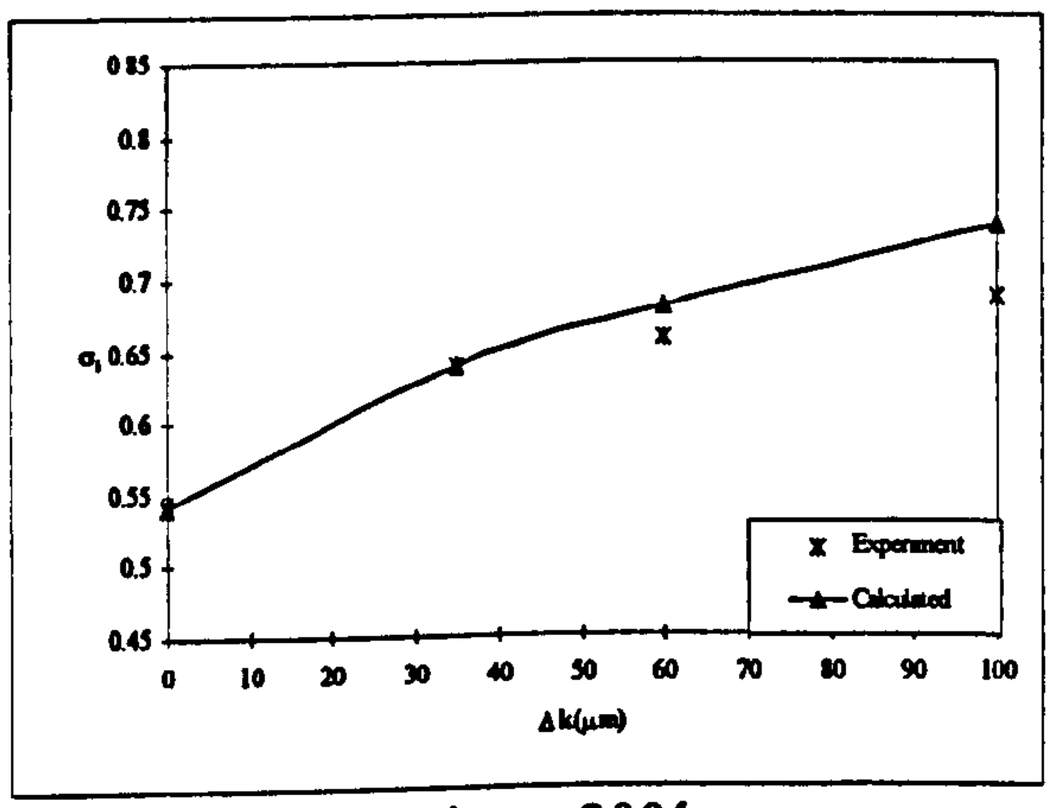

$\alpha_D/\alpha_S = 20\%$

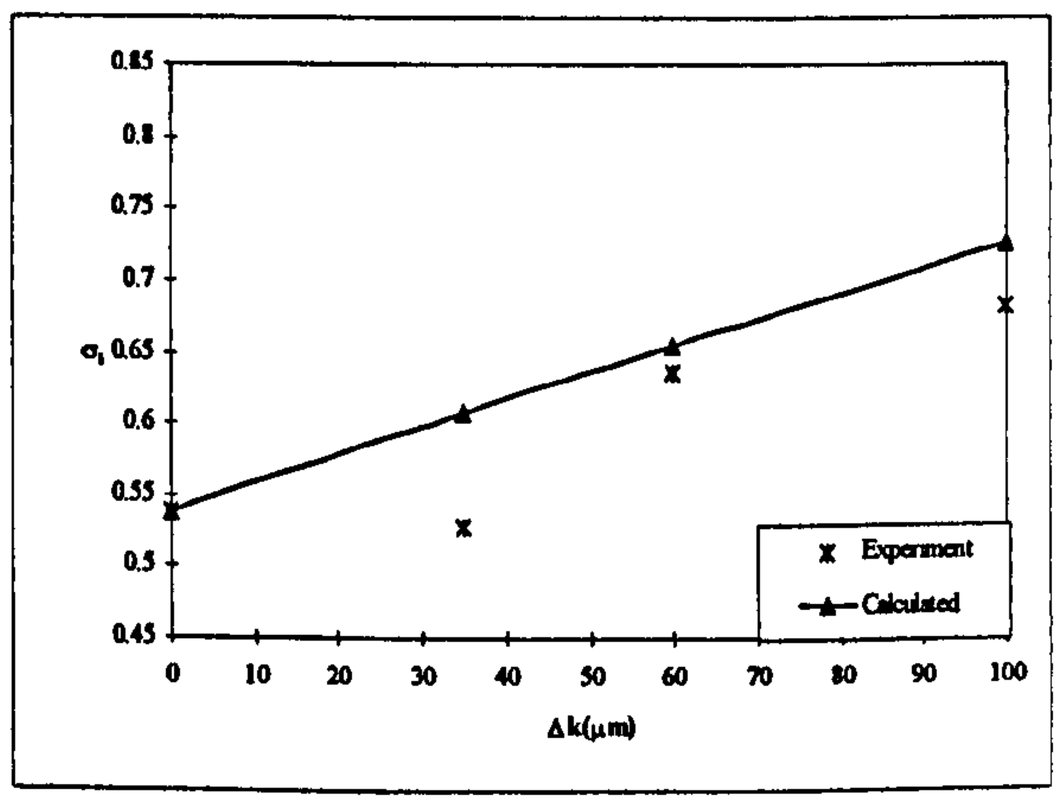

$\alpha_D/\alpha_S = 44\%$

Figure 6.15 Comparison of calculated inception numbers of tip vortex cavitation attached to one blade only with experimental results against roughness height in cases of roughness

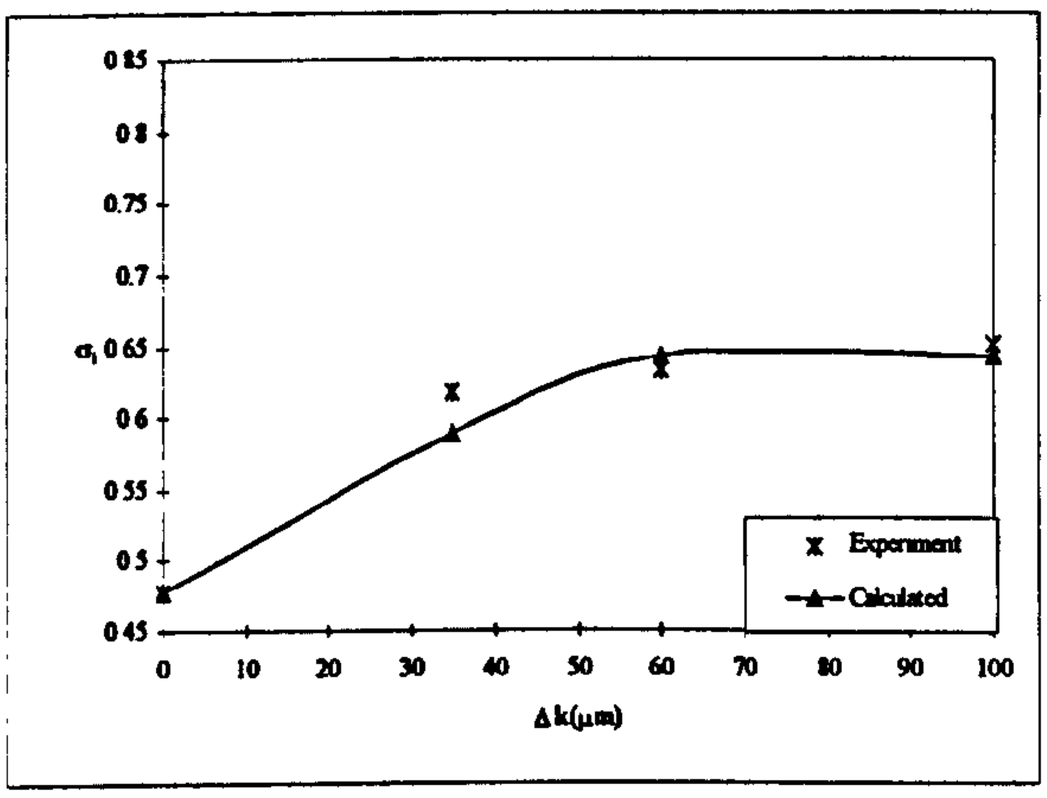

$\alpha_D/\alpha_S = 20\%$

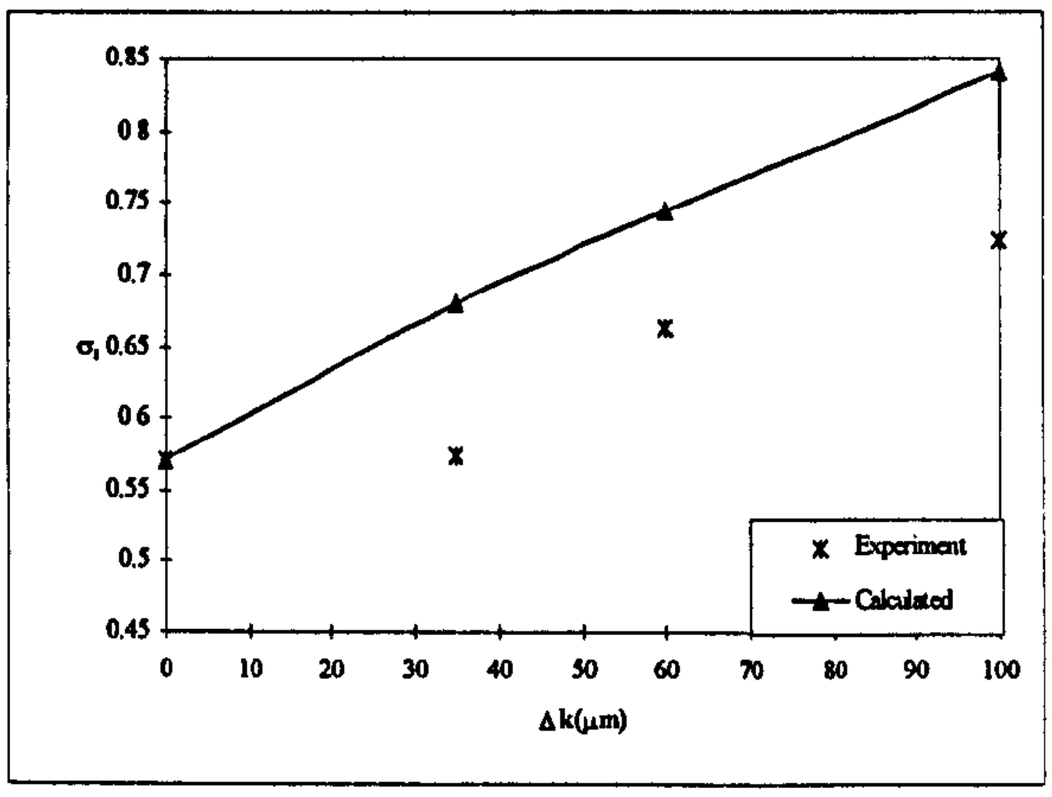

$\alpha_D/\alpha_S = 44\%$

Figure 6.16 Comparison of calculated inception numbers of tip vortex cavitation fully attached to all blades with experimental results against roughness height in cases of roughness

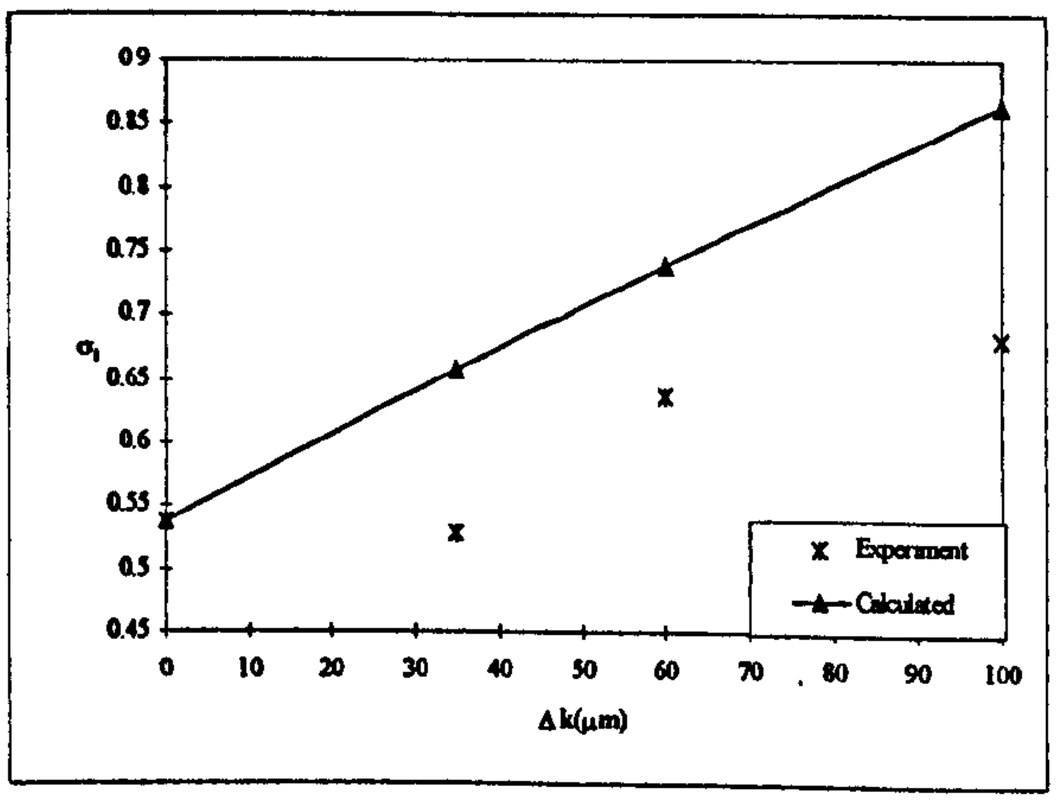

$\alpha_D/\alpha_S = 44\%$

Figure 6.17 Comparison of calculated inception numbers of sheet cavitation with experimental results against roughness height in cases of roughness

6.6 ANALYSIS OF SIMILARITY CRITERIA

In Section 6.2, the semi-empirical model has been presented to predict the inception of cavitation in model scale. In order to relate this model to the full-scale using suitable similarity criteria, one needs to find governing parameters of the inception phenomena. Traditionally, four similarity criteria, which are obtained from the method of Dimensional Analysis, are satisfied during a cavitation test in model scale (e.g. Newton, 1968 and Kuiper, 1979) and these criteria are:

- Froude number
- Reynolds number
- cavitation number
- advance coefficient of the propeller.

However, in addition to the above fundamental parameters, as observed in the results of the experiments in Chapters 3 and 4, there are other parameters, which control the inception phenomena (e.g. free-stream turbulence, roughness, bubble dynamics in terms of nuclei content, distribution etc.). Therefore, one should look for including these parameters in the present similarity criteria for more sound simulation of the flow similarity between the model and full-scale.

Within the context of the above discussion, in this section, an attempt is made to improve the traditional similarity criteria by including the effect of the free-stream turbulence.

In order to derive appropriate similarity parameters, the method of Fractional Analysis is used. This is a procedure to obtain some information about the answer to a physical problem in the absence of a complete mathematical solution. The fractional analysis always uses both physical information and mathematical analysis to obtain as much information as possible for the solution. The most commonly known and employed method for such fractional analyses is the technique known as **"Dimensional Analysis"**.

The process of dimensional analysis involves in the following procedures (Kline, 1965) and (Sedov, 1959):

- establishment of the governing parameters
- effective management of the parameters

Due to the exclusion of a systematic investigation into the effects of bubble dynamics in this study, governing parameters associated with the bubble dynamics will be excluded from the dimensional analysis for the time being. Thus, the cavitation inception number including the effect of the free-stream turbulence can be written as:

$$\sigma_i = \sigma_{iR} + \Delta\sigma_T \tag{6.37}$$

where:

- $\Delta\sigma_T$ is the effect of turbulence on inception of cavitation, which can be related to various parameters involving the physical phenomenon as follows:

$$\Delta\sigma_T = f_1(\rho, \overline{U}, u_f', \overline{U}_l, u_{fl}', \Delta P, D, \mu, \Lambda_g, N, \overline{\alpha}, \delta\alpha', P_{xr}, x_m, r_L, c) \tag{6.38}$$

where:

- u_f' is the root-mean-square of velocity fluctuations in the free-stream
- $\overline{U}_l$ is the local mean velocity at which cavitation occurs
- u_{fl}' is the root-mean-square of the fluctuations of the local velocity U_l
- ΔP is the pressure difference between the free-stream and the critical pressure
- μ is the dynamic coefficient of viscosity of the flow
- f_1 is an unspecified function.

The local velocity, U_l, can be defined as:

$$U_l = \overline{U}_l + u_{fl} \tag{6.39}$$

By definition the integral length scale, Λ_g, is a measure of the longest connection, or correlation distance, between fluctuation velocities at two points of the flow field. This parameter, which is a function of the turbulence intensity, characterises the large eddy structure of the turbulence and can be defined as (Hinze, 1975):

$$\Lambda_g = \int_0^\infty g(y)dy \tag{6.40}$$

where:

- g is the lateral velocity correlation of fluctuations in the transverse direction, y, and is defined for isotropic turbulence as:

$$g(y) = \frac{\overline{u_f(y_1)u_f(y_2)}}{u_f^2} \tag{6.41}$$

where:

- over bar denotes the mean value of the product of fluctuations
- y_1 and y_2 are two points in the transverse direction.

It can be seen in Figures 6.1 and 6.2, and obtained from the mathematical model that:

$$\bar{\alpha} = \tan^{-1}\left(\frac{P_{xr}}{\pi x_r ND}\right) - \tan^{-1}\left(\frac{\bar{U}}{\pi x_r ND}\right) = h\left(P_{xr}, N, D, \bar{U}\right)$$

$$\delta\alpha' = \tan^{-1}\left(\frac{\bar{U}+u_f}{\pi x_r ND}\right) - \tan^{-1}\left(\frac{u_f}{\pi x_r ND}\right) = i\left(\bar{U}, u_f, N, D\right) \qquad (6.42)$$

$$x_m = \frac{1}{4c}\left(\frac{r_L}{\bar{\alpha}-\alpha_i}\right)^2 = j\left(r_L, \bar{\alpha}, c\right)$$

where:

- h, i and j are the unspecified functions
- x_r is taken as 0.9875 (e.g. Noordzij, 1977 and Kuiper, 1981).

Equation (6.42) shows that P_{xr}, N, r_L are implicit in $\bar{\alpha}$, $\delta\alpha'$ and $\bar{\alpha}$ and c are implicit in x_m. Therefore, they can be dropped from the parameter list, thus Equation (6.38) becomes:

$$\Delta\sigma_T = f_1\left(\rho, \bar{U}, u_f', \bar{U}_1, u_{f1}', \Delta P, D, \mu, \Lambda_g, \delta\alpha', x_m\right) \qquad (6.43)$$

where:

- ρ, D and $\bar{U}$ are independent parameters
- whilst u_f', $\bar{U}_1$, u_{f1}', ΔP, Λ_g, μ, $\delta\alpha'$ and x_m are dependent parameters.

$\Delta\sigma_T$ can be substituted into the parameter list such that

$$f_3(\Delta\sigma_T, \rho, \bar{U}, u_f', \bar{U}_1, u_{f1}', \Delta P, D, \mu, \Lambda_g, \delta\alpha', x_m) = 0 \qquad (6.44)$$

On the other hand, in propulsory dynamics, it is customary to express the effective fluctuation as a sum of incident flow fluctuation and the additional intensity induced by the blade loading, i.e. (Odabasi, 1995):

$$\left\langle u_{fe}^2 \right\rangle^{1/2} \cong \left\langle u_f^2 \right\rangle^{1/2} + k_2 V_R \left(\frac{K_T}{BAR} \right)^{4.5} \tag{6.45}$$

where:

- $\langle u_f^2 \rangle^{1/2}$ is the root-mean-square of fluctuations in ship wake
- K_T is the propeller thrust coefficient
- BAR is the blade area ratio of the propeller and equal to $BAR = \frac{A_E}{A_0}$
- A_E is the expanded surface area of the propeller
- A_0 is the disc area of the propeller
- the constant k_2 is to be determined from experimental data.

$\left\langle u_{fe}^2 \right\rangle^{1/2} = u_{f1}^{'}$, $\left\langle u_f^2 \right\rangle^{1/2} = u_f^{'}$ and the effective fluctuation can be written as:

$$u_{f1}^{'} = u_f^{'} + k_2 V_R \left(\frac{K_T}{A_0} \right)^{4.5} \tag{6.46}$$

Equation (6.46) also shows that $u_{f1}^{'}$ is a function of $u_f^{'}$, which can be dropped from the parameter list. The parameter list becomes:

$$f_4(\Delta\sigma_T, \rho, \overline{U}, \overline{U}_1, u_{f1}^{'}, \Delta P, D, \mu, \Lambda_g, \delta\alpha', x_m) = 0 \tag{6.47}$$

To derive non-dimensional parameters the so-called π (pi)-theorem is used e.g. (Kline, 1965) and (Kuiper, 1994). According to the pi theorem, a relation is given among m parameters in the form of:

$$f_4(q_1, q_2, ...,q_m) = 0 \tag{6.48}$$

where:

- $q_1, q_2, ...,q_m$ are the parameters.

An equivalent relation can be expressed in terms of non-dimensional parameters, which can be found of the form:

$$f_5(\pi_1,\pi_2,...\pi_n) = 0 \tag{6.49}$$

where:

- π's are non-dimensional parameters and will be similar for two different systems (i.e. model and full-scale).

The theorem also states that the number of non-dimensional parameters is equal to the number of all parameters in the list minus the number of dimensions involved. Hence,

$$n = m-r \tag{6.50}$$

where:

- n is the number of parameters in non-dimensional form
- m is the number of all the parameters in the list
- r is the largest number of parameters which will not combine into any non-dimensional form or the number of dimensions concerned.

Therefore, m=11 and ρ, D and $\bar{U}$ will not form a non-dimensional form or Mass, Length and Time are the dimensions involved (Massey, 1971), hence r=3, and n=8 non-dimensional parameters are to be determined.

Furthermore, the application of pi theorem requires the following (Kline, 1965):

- the list of dimensional parameters must contain all of the parameters of physical significance including all independent parameters and one dependent parameter

- the non-dimensional pi's as finally composed should contain, at least once, each of the parameters in the original list.

- the list of dimensions used to compose the physical parameters must be independent, or else provision must be made to compensate for the redundancy.

Therefore, these non-dimensional parameters can be set as

$$\pi_1 = \Delta\sigma_T$$
$$\pi_2 = \frac{u'_{f1}}{\overline{U}}$$
$$\pi_3 = \frac{\overline{U}_1}{\overline{U}}$$
$$\pi_4 = \frac{\Delta P}{\frac{1}{2}\rho V_R^2}$$
$$\pi_5 = \frac{x_m}{D} \qquad (6.51)$$
$$\pi_6 = \frac{\Lambda_g V_{xr}}{\nu} \text{ where } V_{xr} \text{ is the resultant velocity at } x_r R$$
$$\pi_7 = \delta\alpha'$$
$$\pi_8 = \frac{\overline{U}}{ND}$$

$\Delta\sigma_T$ can be written as:

$$\Delta\sigma_T \approx f_6\left(\frac{u'_{f1}}{\overline{U}}, \frac{\overline{U}_1}{\overline{U}}, \frac{\Delta P}{0.5\rho V_R^2}, \frac{x_m}{D}, \frac{\Lambda_g V_{xr}}{\nu}, \delta\alpha', \frac{\overline{U}}{ND}\right) \qquad (6.52)$$

Seven π's remain in the list, such that:

$$\pi_1 = \frac{u'_{f1}}{\overline{U}} = \text{TI(Turbulence Intensity)}$$

$$\pi_2 = \frac{\overline{U}_1}{\overline{U}}$$

$$\pi_3 = \frac{\Delta P}{\frac{1}{2}\rho V_R^2} = \frac{P_{st} - P_{crit}}{\frac{1}{2}\rho V_R^2} = \sigma_i$$

$$\pi_4 = \frac{x_m}{D}$$

$$\pi_5 = \frac{\Lambda_g V_{xr}}{\nu} = R_{e\Lambda} \qquad (6.53)$$

$$\pi_6 = \delta\alpha'$$

$$\pi_7 = \frac{\overline{U}}{ND} = J$$

The pressure coefficient of the propeller can be written as:

$$C_p = \frac{P_1 - P_{st}}{\frac{1}{2}\rho V_R^2} = \frac{\overline{U}^2 - \overline{U}_1^2}{\frac{1}{2}\rho V_R^2} \qquad (6.54)$$

At inception stage, $P_1 = P_{crit}$, hence

$$C_p = \frac{P_{crit} - P_{st}}{\frac{1}{2}\rho V_R^2} = \frac{\overline{U}^2 - \overline{U}_1^2}{\frac{1}{2}\rho V_R^2} = -\sigma_i$$

$$\left(\frac{\overline{U}_1}{\overline{U}}\right)^2 = 1 + \sigma_i 0.5\rho\left(\frac{V_R}{\overline{U}}\right)^2 \qquad (6.55)$$

$$\left(\frac{\overline{U}_1}{\overline{U}}\right) = f(\sigma_i)$$

The integral length scale, Λ_g, is a function of the fluctuations and advance coefficient J is also a function of fluctuating angle of attack, $\delta\alpha'$, as one can see in Equations (6.40) (6.41) and (6.20) respectively. Therefore, turbulence intensity, TI, and J can be dropped from the parameter list and it follows

$$\Delta\sigma_T \approx f_7\left(\frac{x_m}{D}, \sigma_i, R_{e\Lambda}, \delta\alpha'\right) \tag{6.56}$$

where:

- σ_i is also a function of x_m/D and $R_{e\Lambda}$. Hence, the effect of turbulence on the inception of cavitation will be a function of the following non-dimensional parameters:

$$\Delta\sigma_T \approx f_8\left(\frac{x_m}{D}, R_{e\Lambda}, \delta\alpha'\right) \tag{6.56}$$

Dimensional analysis method has been applied to the scale effect phenomena to obtain new non-dimensional parameters, which reflect the better simulation of the phenomena. Bearing in mind the assumption that the effect of the bubble dynamics has been ignored for the time being, the above analysis indicates that the attempt to include the effect of the free-stream turbulence in the traditional similarity criteria brings about 3 new parameters in association with the turbulence length scale (Λ_g) and fluctuating angle of attack ($\delta\alpha'$) and the ratio of the position of the minimum pressure from the leading edge to the diameter of the propeller ($\frac{x_m}{D}$). In other words, if two systems (i.e. model and full-scale propellers) have the same x_m/D, the same Reynolds number based on Λ_g and the same root-mean-square of the fluctuating angle of attack, $\Delta\sigma_T$ will be the same for both system.

It is obvious that the establishment of the confidence to include the above terms in the existing criteria would require considerable support from the full-scale investigations, which should be correlated systematically with the model measurements

6.7 CONCLUSIONS

In this chapter, a semi-empirical model, which includes the effect of the free-stream turbulence, has been developed to predict the inception of cavitation based on model tests results and Lighthill's leading edge correction. The developed model has been correlated with the model tests results and its potential has been explored to be used as an extrapolator to predict the inception in full-scale. Furthermore, an attempt has been made to establish correspondence between the levels of the free-stream turbulence and roughness at the leading edge in terms of inducing the similar inception numbers of cavitation with an effort to improve the current model testing techniques. In order to complement the extrapolation procedure, a dimensional analysis has been applied to the inception number concentrating on the effect of the free-stream turbulence.

Based upon the above investigations, it has been concluded that:

- Bearing in mind the number of assumptions and simplifications made, the effect of the turbulence in the free-stream flow can be included in the Lighthill's leading edge correction through the fluctuating term in the angle of attack. This 2-D model, which predicts the pressure or velocity distribution at the leading edge of a propeller blade, combined with experimentally measured reference inception data can be used to predict the inception of the tip vortex and sheet cavitation on a propeller blade.

- The comparison of the predictions using the above-mentioned semi-empirical approach with the model test measurements indicated that the proposed model worked reasonably well for the unattached tip vortex cavitation. The discrepancy between the predictions and tests increased as the cavitation pattern progressed towards the sheet type, especially at the high level of dissolved gas content.

- Considering the effect of the free-stream turbulence only, the proposed semi-empirical model has the potential to save the testing time for the inception measurements of a particular propeller provided that the background flow turbulence characteristics and the reference inception numbers of the propeller are known.

- In the most plausible sense, the proposed semi-empirical model has provided a pioneering basis to establish an extrapolator to predict the inception of cavitation in full-scale. However, this will require comprehensive information on the levels of turbulence in the full-scale as well as systematic correlation with the model tests to establish confidence in using such an extrapolator.

- Based upon the analysis of the experimental measurements, it was found that there were similarities in the trends of the effect of the free-stream turbulence and that of the leading edge roughness on the inception of cavitation.

- The experimental analysis for the same cavitation inception numbers indicated a linear relationship between the level of free-stream turbulence and that of the blade roughness for the unattached tip vortex cavitation. However, this relationship became non-linear as the cavitation pattern has been transformed from the tip vortex type to the sheet cavitation.

- The previous two conclusions suggest that, it will be possible to simulate the effect of varying levels of the blade roughness on the inception of cavitation by using varying levels of the free-stream turbulence. This will provide flexibility for cavitation tunnels, which are used to the blade roughness technique, to change their code of practice for the turbulence generations instead of continuing to use somehow cumbersome leading edge roughness technique for the turbulence stimulation.

- More rigorous analysis of the similarity criteria for the inception of cavitation between the model and full-scale indicates that three parameters, which are Reynolds number based on integral length scale, $R_{e\Lambda}$, the ratio of position of minimum pressure to diameter of the propeller, $\frac{x_m}{D}$, and the fluctuating angle of attack, $\delta\alpha'$, should be similar if the effects of the free-stream turbulence are to be taken into account.

CHAPTER 7 CONCLUSIONS AND RECOMMENDATIONS FOR FUTURE WORK

7.1 CONCLUSIONS

7.1.1 REVIEW OF THESIS

Cavitation can be described as an important fluid mechanics phenomenon that occurs on marine propellers. In this phenomenon, vapour or gas-filled bubbles are formed due to the reductions in local pressures differential. There are a number of types of cavitation that occur on marine propellers, among which the tip vortex is the first type that occurs; this may develop progressively into sheet cavitation as well as other types (bubble, cloud, hub vortex, etc.). Cavitation in all its forms influences the performances of marine propellers, in terms of their useful lives, efficiencies, noise and vibration levels that they excite. In view of these deleterious effects of cavitation it is important to avoid cavitation or at least reduce its severity at the design stage of propellers, to do this it is essential to have an accurate method of predicting the inception of cavitation.

Because of the complex, multiphase nature of the flow consisting of a mixture of solid, liquid and gas as well as the inadequacy of the available empirical/semi-empirical and mathematical models, predicting the inception of cavitation is usually obtained from model tests.

The latter methods, which are based on the boundary elements (e.g. lifting surface, panel, etc.) and CFD procedures, and they have serious limitations, in terms of the accuracy of the predictions in full-scale, modelling of the viscous effects and turbulence, and requirements for the excessive computing time. Therefore, the procedures for

predicting the inception of cavitation based on the model tests still appear to be the most appropriate for the time being.

However, the use of the model test results to predict the cavitation characteristics of a full-scale propeller will suffer from discrepancies known as **"Scale Effect"** phenomena. These phenomena constitute some of the most complex research topics in experimental ship hydrodynamics. These topics become even more complicated when trying to predict the cavitation on full-scale propellers due to the multiphase nature of the physical event. It is well-known that there is an inherent interdependency between the inception of cavitation and the excitation of noise. Therefore, it would be natural to expect that the scale effects associated with the inception are also associated with the noise generated by the propeller.

Within the above general frame and limitation of the time and experimental facilities to be used, the aim of the research presented in this thesis is considered to make a further contribution to the overall understanding of the scale effect phenomena on the inception of cavitation and noise of marine propellers.

One of the important factors contributing into the above aim is the availability of the Emerson Cavitation Tunnel facility, which has a relatively large measuring section, although it has been recognised as a reverberant facility and not particularly suited to carry out research into the noise that is associated with the cavitation of marine propellers.

Given the above aim and the existing experimental facility kept in mind and in order to set the specific objectives of the research study, a state-of-the-art literature survey has been carried out on the scale effect phenomena described in Chapter 1 of this thesis. The survey indicated that the scale effects associated with the viscous nature of the flow and the bubble dynamics of cavities in the fluid dominate the scaling procedures for the inception of cavitation and noise. As far as the viscous effects are concerned, the effect of the free-stream turbulence has been reported in various studies on a limited number of test bodies, nevertheless a thorough systematic investigation using model scale marine propellers to explore its nature and quantify its contribution to the inception and

noise are found to be scarce. The effect of the bubble dynamics on the inception and noise are found to be rather complex but important. A thorough research into the effect of the bubble dynamics will require sophisticated nuclei seeding, controlling and measuring devices. From this point of view, the suitability of the Emerson Cavitation Tunnel is limited thus the objectives of the present research into the dynamics of bubbles correspondingly limited.

Bearing in mind the main conclusions (Section 1.2) of the survey and inherent limitations of the available ECT experimental facility, the main objectives of the thesis have been specified as:

- A preliminary objective is to establish a set of operational practices for using the ECT cavitation tunnel facility and testing procedures by carrying out a set of introductory tests
- to identify the inception and development of cavitation and noise of a simple foil and a propeller for varying levels of the free-stream turbulence, leading edge roughness and dissolved gas content by performing sets of systematic tests,
- to establish a semi-empirical procedure, which includes the effect of the free-stream turbulence, to predict the inception of cavitation of the tip vortex and sheet cavitation,
- and finally to develop the current similarity criteria for the prediction of the inception of cavitation by including the effect of the free-stream turbulence.

In achieving the above objectives, an experimental programme has been set up in four phases.

In the first phase of this programme the background flow measurements of the cavitation tunnel were taken using a two-dimensional Laser Doppler Anemometry facility. The maps of the main flow parameters were established for the tunnel measuring section which reflect the effects of different levels of the free-stream turbulence stimulated by using different sizes of wire mesh screens; the results are presented in Chapter 2. The information obtained from Chapter 2 has provided the basis

for analysing the measurements of the inception of cavitation and noise made in the remaining three phases of the experimental programme.

In Chapter 3 the results of the systematic tests (phase 2) to measure and record the inception of cavitation of a simple rectangular planform foil (NACA66) section for varying levels of free-stream turbulence and roughness are presented.

The third phase of the experimental programme involved systematic measurements of the inception of cavitation of a Meridian type model propeller (ECT103) for varying levels of free-stream and roughness at two different levels of dissolved gas content. The descriptions and discussions of these tests are presented in Chapter 4.

The fourth and final phase of the experimental programme was the noise measurements of the same propeller under the same test conditions used in the third phase of the test programme. The detailed records, analyses and discussions of this final group of tests are included in Chapter 5.

Based on the information obtained from the experimental test programme and the use of developed Lighthill's leading edge correction; in Chapter 6, a semi-empirical model is presented to predict the inception of the tip vortex and sheet cavitation; this model includes the effect of the free-stream turbulence.

This model was correlated with the inception measurements and its potential to be used as an extrapolator to predict the inception of cavitation on full-scale propellers is discussed. Chapter 6 also includes the result of analysing the measurements for the inception to see whether or not there was any meaningful correspondence between the level of the free-stream turbulence and blade roughness in terms of the similarity of their effects on the inception of cavitation. Chapter 6 also presents an analysis of the similarity criteria based on the use of dimensional analysis and the effect of the free-stream turbulence on the inception of cavitation to extrapolate the model test measurements so that they can be used to predict the inception of cavitation on full-scale propellers.

Finally, in the present chapter (i.e. Chapter 7), an overall review of the entire research study, main conclusions and recommendations for the future work are presented.

7.1.2 MAIN CONCLUSIONS

Within the above framework of the thesis, the main conclusions of the research study are:

- Among other factors, insufficient turbulence around model propellers causes viscous scale effects that adversely affect the usefulness of test results when predicting the inception of cavitation on full-scale propellers. In the literature the viscous scale effects have been investigated through numerous research studies mainly concentrating on the effect of roughness and turbulence of the free-stream.

- Although the effect of the free-stream turbulence on the inception of cavitation has been reported quantitatively by various investigators covering a limited number of test bodies, there has been no systematic investigation exploring its nature and quantifying its effect for the inception of cavitation of a marine propeller.

- Since the inception of cavitation and the noise generated by a propeller are inherently dependent on each other, the above conclusions also apply to the noise characteristics of marine propellers. Indeed, there is even less systematic data quantifying the effect of the free-stream turbulence as well as the blade roughness on the noise of a propeller.

- Different size of wire meshes supported with a base frame are effective in altering the level of the free-stream turbulence at the measuring plane. Except in one of the mesh cases the level of turbulence was increased linearly by reducing the net mesh area. However, it has been observed that the wire meshes can themselves be a source of generating nuclei as well as noise.

- The application of the roughness at the leading edge requires special attention, in terms of its proper size, location, gluing and procedure for removing it. The carborundum used had a range of grade varying between 35 μm and 100 μm. This was applied between 4% of the maximum chord length of the foil and propeller

blade and the leading edge roughness has displayed some practical difficulties during its application and also presented premature cavitation during the tests.

- As far as the Author is aware, the experimental information provided in this thesis is one of the most comprehensive sets of data recording the viscous scale effects on the inception of cavitation and noise, particularly for the effect of the free-stream turbulence. Excluding the introductory test runs the experimental investigation involved a total of 327 runs. These consisted of 35 for the background flow measurements, 80 for the inception of cavitation measurements of the NACA foil, 88 for the inception of cavitation measurements of the test propeller and 124 for the noise tests of the same test propeller.

- From the analyses of the measurements of the NACA foil and propeller, it has been clearly confirmed that the free-stream turbulence affects the inception of cavitation and hence will contribute to the viscous scale effects. The analyses also indicated that there were similarities in the trends of the effect of the free-stream turbulence and that of the leading edge roughness on the inception of cavitation.

- A semi-empirical model, which takes into account the effect of the free-stream turbulence, has been developed to predict the inception of cavitation. This is based on the Lighthill's rule. Bearing in mind the number of assumptions and simplifications made, the developed model has indicated reasonable correlation for the unattached tip vortex cavitation. The discrepancy between the predictions and experiments increased as the cavitation pattern developed towards the sheet type, particularly when the level of dissolved gas content was high.

- In spite of its various shortcomings, in the most plausible sense, the proposed semi-empirical procedure may form a basis for developing an extrapolator to be used to predict the inception of cavitation on full-scale propellers. However, this will require comprehensive correlation with model test measurements as well as the information on the levels of the turbulence in full-scale. Such an extrapolator could also be used to save cavitation testing time for a particular propeller model.

- The similarity in the trends of the effect of the free-stream turbulence and that of the leading edge roughness on the inception of cavitation suggests that it will be possible to replace somehow cumbersome leading edge roughness with a suitable turbulence generating technique for more efficient stimulation of turbulence.

- If the effects of the free-stream turbulence are to be taken into account then a more rigorous analysis of the similarity criteria for the inception of cavitation between the model and full-scale indicates that the Reynolds number based on integral length scale, the ratio of position of minimum pressure to diameter of the propeller and the fluctuating angle of attack should be similar.

- Analyses of the noise measurements of the test propeller also displayed the effect of the free-stream turbulence and blade roughness on the levels of net propeller noise. The interpretation of the trend in these effects was rather complex and some cases were inconclusive depending upon the range of the centre frequency tested, and the cavitation occurring.

- The complexity revealed by these trends was mainly observed in the low frequency region (50 Hz – 1000 Hz); and was mainly associated with the propeller blade rate frequency and its harmonics in combination with frequencies of the structural vibration of the tunnel. Regardless of the frequency range tested, the presence of the cavitation complicated the trends requiring a more thorough investigation in a quiet, i.e. less reverberant, environment.

- For the non-cavitating condition and over the high frequency region (1000 Hz – 160 kHz), propeller noise increased with increasing the level of the free-stream turbulence, although this trend was reversed by increasing blade roughness. In the same frequency region and condition, an increase in the level of the dissolved gas content caused a reduction in the level of noise thus indicating a cushioning effect on the noise characteristics.

7.2 RECOMMENDATIONS FOR FUTURE WORK

Various shortfalls of this research study have been identified during the course of the study as well as based on the analyses of the experimental data. These are associated with the limitations and scope set for the thesis and especially with the equipment used. Therefore, the recommended future work is:

- The turbulence measurements in this study were limited to two-dimensions due to the 2-D Laser Doppler Anemometry (LDA) equipment used. These measurements should now be performed by 3-D LDA and hence all three components of the velocity can be taken into account.

- The present investigation has concerned with the effect of free-stream turbulence, as measured in the free-flow. To gain more insight in the effect of the boundary layer on the inception of cavitation and noise these measurements should be extended to near-wall conditions, particularly near the leading edge.

- Because of the physical constraints of the Emerson Cavitation Tunnel it was necessary to mount the foil vertically. This prevented the measurement of the tip vortex cavitation and noise. Although it will require major modifications to the tunnel windows and complex fitting mechanism, this investigation can be extended by mounting the foil horizontally across the tunnel width or between the two vertical planes.

- Although the present study has excluded the effect of the bubble dynamics due to the need for more sophisticated measuring equipment, this effect should be explored in combination with the turbulence effects. Bearing in mind the safety precautions, the nuclei seeding should be performed by using a hydrogen bubble generator while the bubble details can be measured using PDA equipment.

- There is no doubt that the conclusions of this research study concerning the inception of cavitation are based on a limited number of investigations (e.g. 1 rectangular foil and 1 model propeller), various number of assumptions in heuristic nature (e.g. only two velocity components are considered, modification to the Lighthill's leading edge correction) and simplifications (e.g. effect of hull wake and induced velocities are neglected). In spite of these shortcomings, the form of the extrapolator developed in this study is novel. This will require further programmes of work in the future to develop the extrapolator further to take into account of these shortcomings as well as to correlate the systematic model test data with measurements on full-scale propellers in service.

- The current findings with the noise measurements require further detailed analytical work to establish the effects of the structural vibration and re-correlate the noise data measured in the experiments.

CHAPTER 8 REFERENCES

Arakeri, V.A. and Shanmuganathan, V., (1985), "On the Evidence for the Effect of Bubble Interference on Cavitation Noise", *Journal of Fluid Mechanics*, Vol.159, pp.131-150.

Arndt, R.E.A., (1974), "Cavitation Inception and How it Scales a Review of the Problem with a Summary of Recent Research", *Symposium on High Powered Propulsion of Large Ships*, Wageningen, The Netherlands.

Arndt, R.E.A. and George, W.K., (1979), "Pressure Fields and Cavitation in Turbulent Shear Flows", *12th Symposium on Naval Hydrodynamics*, Washington D.C, USA, pp.327-339.

Arndt, R.E.A. and Keller, A.P., (1991), "Water Quality Effects on Cavitation Inception in a Trailing Vortex", *ASME, Cavitation'91*, Portland, USA, pp.1-9.

Arndt, R.E.A. and Maines, B.H., (1998), "Nucleation and Bubble Dynamics in Vortical Flows", *Third International Symposium on Cavitation, Cavitation'98*, Grenoble, France, pp.143-148.

Atlar, M. and Korkut, E., (1997), "Emerson Cavitation Tunnel Inflow Characteristics Based on 2-D Laser Doppler Anemometry Analysis", *Report of Department of Marine Technology, University of Newcastle upon Tyne,* Report No: MT-1997-001, UK.

Baldwin, B.S. and Barth, T.J., (1990), "A One-Equation Turbulence Transport Model for High Reynolds Number Wall-Bounded Flows", *NASA TM* 102847.

Bandyopadhyay, P.R., Stead, D.J. and Ash, R.L., (1991), "Organized Nature of a Turbulent Trailing Vortex", *AIAA Journal*, Vol.29, pp.1627-1633.

Bark, G. (1982), "Prediction of Cavitation Noise from Two Alternative Propeller Designs-Model Tests and Comparisons with Full-Scale Results", *1982 ASME Summer Meeting*, Arizona, USA.

Bark, G., (1985), "Prediction of Propeller Cavitation Noise from Model Tests and its Comparison with Full Scale Data", *Transactions of the ASME, Journal of Fluids Engineering*, Vol.107, pp.112-120.

Bark, G., (1992), "On the Scaling of Propeller Cavitation Noise with Account of Scale Effects in the Cavitation Noise", *International STG-Symposium on Propulsors and Cavitation*, Hamburg, Germany.

Baur, T., Kongeter, J. and Leucker, R., (1998), "Effects of Dissolved Gas on Cavitation Inception in Free Surface Flows", *Third International Symposium on Cavitation, Cavitation'98*, Grenoble, France, pp.155-159.

Betz, A., (1933), "Behavior of Vortex Systems", *National Advisory Committee for Aeronautics Technical Memorandums,* Report No:713, USA.

Billet, M.L. and Holl, J.W., (1979), "Scale Effects on Various Type of Limited Cavitation", *ASME, International Symposium on Cavitation Inception*, New York, USA, pp.11-23.

Billet, M.L. and Gates, E.M., (1981), "A Comparison of Two Optical Techniques for Measuring Cavitation Nuclei", *Transactions of the ASME, Journal of Fluids Engineering*, Vol.109, pp.8-13.

Bjorheden, O. and Astrom, L., (1977), "Prediction of Propeller's Noise Spectra", *Hydrodynamics of Ship and Offshore Propulsion Systems*, Oslo, Sweden, pp.104-121.

Blake, W.K., Wolpert, M.J. and Geib, F.E., (1977), "Cavitation Noise and Inception as Influenced by Boundary Layer Development on a Hydrofoil", *Journal of Fluid Mechanics*, Vol.80, pp.617-640.

Blake, W.K. and Sevik, M.M., (1982), "Recent Developments in Cavitation Noise Research", *ASME, International Symposium on Cavitation Noise*, pp.1-10.

Brennen, C.E. and Ceccio, S.L., (1989), "Recent Observations on Cavitation and Cavitation Noise", *ASME, International Symposium on Cavitation Erosion and Noise*, San Francisco, USA.

Brennen, C.E., (1995), "*Cavitation and Bubble Dynamics*", Oxford Engineering Science Series 44, Oxford University Press, New York, USA.

Breslin, J.S. and Andersen, P., (1994), "*Hydrodynamics of Ship Propellers*", Cambridge Ocean Technology Series 3.

Brewer, W.H. and Kinnas, S.A., (1997), "Experimental and Computational Investigation of Sheet Cavitation on a Hydrofoil", *Journal of Ship Research*, Vol.41, pp.161-171.

Brüel & Kjear, (1980), "*Instruction Manual for Measuring Amplifier Type 2610*", Brüel & Kjaer, Naerum, Denmark.

Brüel & Kjear, (1986), "*Instruction Manual for Hydrophones Types 8101, 8103, 8104, 8105*", Brüel & Kjaer, Naerum, Denmark.

Bryden, I.G. and Webb, G.A., (1986), "Narrow Band Signal Processing and Analysis for Number Two Cavitation Tunnel", *Report of British Maritime Technology,* Report No: 14011, UK.

BSRA, (1982), "Ship Design Manual-Noise", *Report of British Ship Research Association*, UK.

Carlton, J.S., (1994), "*Marine Propellers & Propulsion*", Butterworth-Heinemann Ltd, Oxford, UK.

Chandrashekhara, N., (1976), "Analysis of Tip Vortex Cavitation Inception at Hydrofoils and Propellers", *Schiffstechnik*, Vol.23, pp.47-62.

Chesnakas, C.J. and Jessup, S.D., (1998), "Propeller Tip Vortex Measurement Using 3-Component LDV", *22nd Symposium on Naval Hydrodynamics,* Washington D.C., USA.

Clarke, M.A., "Noise Project, Newcastle University", *Report of Stone Vickers Ltd Technical Department*, Report No: H93, UK.

Dacles-Mariani, Rogers, S.E., Kwak, D., Zilliac, G. and Chow, J. (1993), "A Computational Study of Wingtip Vortex Flow field", *AIAA Paper* 93-3010.

d'Agostina, L. and Acosta, A.J., (1991), "A Cavitation Susceptibility Meter with Optical Cavitation Monitoring-Part I: Design Concepts; Part II: Experimental Apparatus and Results", *Transactions of the ASME, Journal of Fluids Engineering*, Vol.113, pp.261-277.

Daily, J.W. and Johnson, E. Jr., (1956), "Turbulence and Boundary-Layer Effects on Cavitation Inception from Gas Nuclei", *Transactions of the ASME*, pp.1695-1706.

Dantec, (1996), "*BURSTware Installation and User's Guide for Version 3.11*", Dantec Measurement Technology.

de Chizelle, Y.K., Ceccio, S.L. and Brennen, C.N., (1995), "Observations and Scaling of Travelling Bubble Cavitation", *Journal of Fluid Mechanics*, Vol.293, pp.99-126.

Farell, C. and Youssef, S., (1996), "Experiments on Turbulence Management Using Screens and Honeycombs", *Transactions of the ASME, Journal of Fluids Engineering*, Vol.118, pp.26-32.

Feng, J., Wang, L., Ahuja, V., Lee, Y.-T. and Merkle, C.L., (1998), "CFD Modelling of Tip Vortex for Open Marine Propellers", *ASME Fluids Engineering Division Summer*

Meeting: Advances in Numerical Modelling of Aerodynamics and Hydrodynamics in Turbomachinery, Paper No: FEDSM98-4873, Washington D.C., USA.

Fitzpatrick, H.M. and Strasberg, M., (1956), "Hydrodynamic Sources of Sound", *1st Symposium on Naval Hydrodynamics*, Washington D.C., USA.

Fitzpatrick, H.M., (1958), "Cavitation Noise", *2nd Symposium on Naval Hydrodynamics*, Washington D.C., USA, pp.201-205.

Franklin, R.E., McMillan, J. and Rozewicz, J., (1984), "The Stability and Concentration of Gas Micro-Bubbles in Liquids", *ASME International Symposium on Cavitation Inception*, New Orleans, USA, pp.1-8.

Friesch, J. and Johannsen, C., (1995), "Study on Tip Vortex Cavitation Inception for Navy Propellers", *International Symposium on Cavitation CAV'95*, Deauville, France, pp.101-109.

Fruman, D.H., (1995), "The Action Concertee Cavitation the Research Program and Accomplishments", *International Symposium on Cavitation CAV'95*, Deauville, France, pp.211-217.

Garen, R. and Vartdal, L., (1994), "Propeller Design and Operation on Modern Fishing Vessels", *Naval Architecture*, pp.E363-E365.

Gates, E.M. and Bacon, J., (1978), "A Note on the Determination of Cavitation Nuclei Distributions by Holography", *Journal of Ship Research*, Vol.22, pp.29-31.

Gates, E.M. and Acosta, A.J., (1979), "Some Effects of Several Free-Stream Factors on Cavitation Inception of Axisymmetric Bodies", *12th Symposium on Naval Hydrodynamics*, Washington D.C., USA, pp.86-112.

Gindroz, B. and Billet, M.L., (1993), "Influence of the Nuclei on the Cavitation Inception for Different Types of Cavitation on Ship Propeller", *ASME, Cavitation Inception -1993*, New Orleans, USA, pp.1-11.

Gindroz, B., (1995), "Propeller Cavitation Characteristics: The Practical Interest of Nuclei Measurements in Test Facilities and at Sea", *ASME*, FED-Vol.226, South Carolina, USA.

Gindroz, B., Bailo, G., Matera, F. and Elefante, M., (1996), "Influence of the Cavitation Nuclei on the Cavitation Bucket when Predicting the Full-Scale Behavior of a Marine Propeller", *21st Symposium on Naval Hydrodynamics,* Trondheim, Norway, pp.839-850.

Gowing, S. and Ling, S.C., (1980), "Measurements of Micro Bubbles in a Water Tunnel", *19th American Towing Tank Conference*, Ann Arbor, USA.

Gowing, S., Briancon-Marjollet, L., Frechou, D. and Godeffroy, V., (1995), "Dissolved Gas and Nuclei Effects on Tip Vortex Cavitation Inception and Cavitating Core Size", *International Symposium on Cavitation CAV'95*, Deauville, France, pp.173-180.

Hamilton, M.F., Thompson, D.E. and Billet, M.L., (1982), "An Experimental Study of Travelling Bubble Cavitation Noise", *ASME, International Symposium on Cavitation Noise*, pp.25-33.

Hess, J.L. and Smith, A.M.O., (1967), "Calculation of Potential Flow about Arbitrary Bodies", *Progress in Aeronautical Sciences*, Vol.8.

Higuchi, H., Arndt, R.E.A., Arakeri, V.H. and Killen, J.M., (1989), "The Structure of Tip Vortices Over a Range of Cavitation Number", *22nd American Towing Tank Conference*, St. Johns, Canada, pp.13-21.

Hinze, J.O., (1975), "*Turbulence*", Mc Graw-Hill Book Company, New York, USA.

Hoffman, J.A., (1991), "Effects of Free-Stream Turbulence on the Performance Characteristics of an Airfoil", *AIAA Journal*, Vol.29, pp.1353-1354.

Holl, J.W., (1960a), "The Inception of Cavitation on Isolated Surface Irregularities", *Transactions of the ASME, Journal of Basic Engineering*, pp.169-183.

Holl, J.W., (1960b), "An Effect of Air Content on the Occurrence of Cavitation", *Transactions of the ASME, Journal of Basic Engineering*, pp.941-946.

Holl, W.J. and Wislicenus, G.F., (1961), "Scale Effects on Cavitation", *Transactions of the ASME, Journal of Fluids Engineering*, pp.385-398.

Holl, J.W., (1970), "Nuclei and Cavitation", *Transactions of the ASME, Journal of Basic Engineering*, pp.681-688.

Holl, J.W. and Billet, M.L., (1986), "Limited Cavitation on Isolated Surface Irregularities Unsolved Problems", *International Symposium on Cavitation*, Sendai, Korea.

Hsiao, C.-T. and Pauley, L.L., (1998a), "Numerical Study of the Steady–State Tip Vortex Flow Over a Finite-Span Hydrofoil", *Transactions of the ASME, Journal of Fluids Engineering*, Vol.120, pp.345-353.

Hsiao, C.-T. and Pauley, L.L., (1998b), "Numerical Computation of Tip Vortex Flow Generated by a Marine Propeller", *ASME Fluids Engineering Division Summer Meeting: Advances in Numerical Modelling of Aerodynamics and Hydrodynamics in Turbomachinery,* Paper No: FEDSM98-4871, Washington D.C., USA.

Hsu, C. C., (1991), "Studies of Scaling of Tip Vortex Cavitation Inception on Marine Lifting Surfaces", *Trans. ASME Journal of Fluids Engineering*, Vol.113, pp.504-508.

Huang, T.T, (1986), "The Effects of Turbulence Stimulators on Cavitation Inception of Axisymmetric Headforms", *Transactions of the ASME, Journal of Fluids Engineering*, Vol.108, pp.261-268.

IMO, (1981), "*Code on Noise Levels on Board Ships*", International Maritime Organisation.

Isay, W.H. and Lederer, L., (1977), "Kavitation and Fulgelprofilen", *Schiffstecnik*, Vol.24.

ITTC, (1978), "Cavitation Committee Report", *15th International Towing Tank Conference*, The Hague, The Netherlands.

ITTC, (1987), "Cavitation Committee Report", *18th International Towing Tank Conference*, Kobe, Japan.

ITTC, (1990), "Cavitation Committee Report", *19th International Towing Tank Conference*, Madrid, Spain.

ITTC, (1993), "Cavitation Committee Report", *20th International Towing Tank Conference*, San Francisco, California, USA.

ITTC, (1996), "Cavitation Committee Report", *21st International Towing Tank Conference*, Trondheim, Norway.

Jenkins, C.I., (1988), "Optimizing Propellers for Noise", *Advances in Underwater Technology*, Vol.15, pp.107-117.

Johnsson, C-A. and Rutgersson, O., (1991), "Leading Edge Roughness-A Way to Improve Propeller Tip Vortex Cavitation", *SNAME, Propellers/Shafting'91*, Virginia, USA, pp.12(1-8).

Kamiirisa, H., (1998), "Prediction of Cavitation Noise Radiated from a Marine Screw Propeller", *Third International Symposium on Cavitation*, Grenoble, France, pp.295-299.

Keller, A.P., (1974), "Investigations Concerning Scale Effects of the Inception of Cavitation", *International Conference on Cavitation*, Edinburgh, UK, pp.109-117.

Keller, A.P., (1979), "Cavitation Inception Measurement and Flow Visualisation on Axisymmetric Bodies at Two Different Free Stream Turbulence Levels and Test Procedure", *ASME, International Symposium on Cavitation Inception*, New York, USA, pp.63-74.

Keller, A.P., (1984), "Scale Effects at Beginning Cavitation Applied to Submerged Bodies", *ASME, International Symposium on Cavitation Inception-1984*, New Orleans, USA, pp.43-47.

Keller, A.P., (1992), "Cavitation Inception-New Scaling Laws, Developed by Consideration of a Parameter of Influence Generally Blurring Experimental Results", *International Conference on Cavitation*, London, pp.171-181.

Keller, A.P., (1994), "New Scaling Laws for Hydrodynamic Cavitation Inception", *2nd International Symposium on Cavitation*, Tokyo, Japan, pp.327-334.

Kim, K.-S., Kim, K.-Y., Ahn, J.-W. and Lee, J.-T., (1995), "Effects of Reynolds Number and Leading Edge Roughness on the Cavitation Performances of a Model Propeller", *International Conference on Problems of Marine Propulsion, HYDRONAV'95*, Gdansk, Poland, pp.89-102.

Kinnas, S.A., (1990), " Fundamentals of Cavity Flows", *Supplement to the Notes on the Theory of Hydrofoils and Propellers*, Department of Ocean Engineering, Massachusetts Institute of Technology, MIT Course 13.04, USA.

Kinnas, S.A., (1992), "Leading Edge Correction to the Linear Theory of Cavitating Hydrofoils and Propellers", *2nd International Conference on Propeller and Cavitation*, Hangzhou, China, pp.319-326.

Kinnas, S.A., (1998), "The Prediction of Unsteady Sheet Cavitation", Third *International Symposium on Cavitation, Cavitation'98*, Grenoble, France, Vol.1, pp. 19-36.

Kline, S.J., (1965), "*Similitude and Approximation Theory*", McGraw-Hill Book Company, New York, USA.

Kodama, Y., Take, N., Tamiya, S. and Kato, H., (1981), "The Effect of Nuclei on the Inception of Bubble and Sheet Cavitation on Axisymmetric Bodies", *Transactions of the ASME, Journal of Fluids Engineering*, Vol.103, pp.557-563.

Korkut, E., (1995a), "The Noise Measurements of the ECT102 and ECT103 Propeller Models", *Report of Department of Marine Technology (Progress Report), University of Newcastle upon Tyne,* Report No: MT-1995-041 (EK-2), UK.

Korkut, E., (1995b), "Wake Simulation and Hull Pressure Measurements in the Emerson Cavitation Tunnel", *Report of Department of Marine Technology (Progress Report), University of Newcastle upon Tyne,* Report No: MT-1995-042 (EK-3), UK.

Korkut, E., (1997a), "Turbulence Measurements by 2-D LDA", *Report of Department of Marine Technology (Progress Report), University of Newcastle upon Tyne,* Report No: MT-1997-103 (EK-8), UK.

Korkut, E., (1997b), "Cavitation Inception and Noise Measurements of ECT103 Propeller Model", *Report of Department of Marine Technology (Progress Report), University of Newcastle upon Tyne,* Report No: MT-1997-104 (EK-9), UK.

Korkut, E., Atlar, M. and Odabasi, A.Y., (1998), "Effects of Free-Stream Turbulence on Cavitation Inception of Marine Propellers", *ASME Fluids Engineering Division Summer*

Meeting: Cavitation and Multiphase Flow Forum, Paper No: FEDSM98-5056, Washington D.C., USA.

Kuiper, G., (1978), "Cavitation Scale Effects", *International Shipbuilding Progress*, Vol.25, pp.81-90.

Kuiper, G., (1979), "Scale Effects on Propeller Cavitation Inception", *12th Symposium on Naval Hydrodynamics*, Washington D.C., USA, pp.400-429.

Kuiper, G., (1981), "Cavitation Inception on Ship Propeller Models", *Ph.D. Thesis*, Technical University of Delft, Delft, The Netherlands.

Kuiper, G., (1994), "*Resistance and Propulsion of Ships*", Course MT512, Technical University of Delft, Delft, Netherlands.

Latorre, R. and Ligneul, P., (1995), "Scaling Methods for Bubble Cavitation Noise Pulse Number", *Acustica, International Journal on Acoustics*, Vol.81, pp.58-62.

Leathard, F.I., (1985), "Cavitation Tunnel Operation Instructions", *Report of Emerson Cavitation Tunnel, Department of Marine Technology,* Report No.1/85, UK.

Lecoffre, Y. and Bonnin, J., (1979), "Cavitation Tests and Nucleation Control", *ASME, Symposium on Cavitation Inception*, New York, USA, pp.141-145.

Levkovskii, Y.L., (1968), "Modelling of Cavitation Noise", *Soviet Physics-Acoustics*, Vol.13, No.3, pp.337-339.

Lighthill, M.J., (1951), "A New Approach to Thin Aerofoil Theory", *The Aeronautical Quarterly*, Vol.3, pp.193-210.

Ling, S.C., (1984), "On Inception of Cavitation within a Thin Turbulent Boundary-Layer", *ASME, International Symposium on Cavitation Inception*, New Orleans, USA, pp.49-53.

Lovik, A., (1981), "Scaling of Propeller Cavitation Noise", *Noise Sources in Ships1: Propellers*, Nordforsk, Sweden.

Maines, B.H. and Arndt, R.E.A., (1997), "Tip Vortex Formation and Cavitation", *Transactions of the ASME, Journal of Fluids Engineering*, Vol.119, pp.413-419.

Mansour, N.N., (1984), "Numerical Simulation of the Tip Vortex of a Low-Aspect Ratio Wing at Transonic Speeds", *AIAA Paper* 84-522.

Massey, B.S., (1971), "*Units, Dimensional Analysis and Physical Similarity*", Van Nostrand Reinhold Company, London, UK.

Matsumoto, Y., (1998), "Bubble Dynamics in Cavitation", *Third International Symposium on Cavitation, Cavitation'98*, Grenoble, France, pp.3-8.

McCormick, B.W.Jr., (1962), "On Cavitation Produced by A Vortex Trailing From A Lifting Surface", *Trans. ASME, Journal of Basic Engineering*, pp.369-379

Meyer, R.S., Billet, M.L. and Holl, J.W., (1989), "Free-Stream Nuclei and Cavitation", *ASME International Symposium on Cavitation Inception*, San Francisco, USA, pp.55-62.

Murai, H., Ihara, A. and Tsurumi, Y., (1979), "Cavitation on Hydrofoils in Turbulent Shear Flow", *12th Symposium on Naval Hydrodynamics*, Washington D.C., USA, pp.385-399.

Newton, R.N., (1961), "Influence of Cavitation on Propeller Performance", *International Shipbuilding Progress*, Vol.8, pp.323-343.

Noordzij, L., (1977), "A Note on the Scaling of Tip Vortex Cavitation Inception", *International Shipbuilding Progress*, Vol.24, pp.233-236.

Odabasi, A.Y., (1987), "Cavitation Inception and Prediction of Broad-Band Noise Levels" *Report of British Maritime Technology Limited*, Report No:W1607, UK.

Odabasi, A.Y., (1995), "Turbulence Effects in Cavitation Inception and Propeller Noise", *PROPCAV'95*, Newcastle upon Tyne, UK, pp.45-58.

Oldenziel, D.M., (1982), "A New Instrument in Cavitation Research: The Cavitation Susceptibility Meter", *Transactions of the ASME, Journal of Fluids Engineering*, Vol.104, pp.136-142.

Ooi, K.K., (1985), "Scale Effects on Cavitation Inception in Submerged Water Jets: A New Look", *Journal of Fluid Mechanics*, Vol.151, pp.367-390.

Pan, S.S., Yang, Z.-M. and Hsu, P.S., (1981), "Cavitation Inception Tests on Axisymmetric Headforms", *Transactions of the ASME, Journal of Fluids Engineering*, Vol.103, pp.268-272.

Parkin, B.R. and Baker, B.B., (1986), "Bubble Dynamics and Cavitation Inception Theory", *International Symposium on Cavitation*, Sendai, Japan.

Pauchet, J. and Woillez, J., (1995), "Cavitation Inception in Turbulent Water Jets: Some Results on the Influence of Nuclei Spectra", *International Symposium on Cavitation CAV'95*, Deauville, France, pp.379-384.

Pauchet, J., (1998), "An Attempt to Predict Cavitation Level in Turbulent Jets by a Statistical Approach", *Third International Symposium on Cavitation, Cavitation'98*, Grenoble, France, pp.117-122.

PC_Image for Windows, (1996), *"User Manual of PC_Image for Windows Version 2.2.01, VGA24 Imagegrabbers"*, Foster Findlay Associates Ltd., Newcastle upon Tyne, UK.

Pham, T.M., Michel, J.M. and Lecoffre, Y., (1995), "Development of a New Type of CSM: Design Concepts and Investigation of Performance Characteristics", *International Symposium on Cavitation CAV'95*, Deauville, France, pp.305-312.

Pham, T.M., Michel, J.M. and Lecoffre, Y., (1997), "Dynamical Nuclei Measurement: On the Development and the Performance Evaluation of an Optimized Center-Body Meter", *Transactions of the ASME, Journal of Fluids Engineering*, Vol.119, pp.744-751.

Pichon, T., Fruman, D.H. and Billard, J-Y., (1995), "Effect of Tripping Laminar to Turbulent Boundary Layer Transition on Tip Vortex Cavitation", *International Symposium on Cavitation CAV'95*, Deauville, France, pp.153-161.

Pichon, T., Pauchet, A., Astolfi, A., Fruman, D.H. and Billard, J-Y., (1997), "Effect of Tripping Laminar -to-Turbulent Boundary Layer Transition on Tip Vortex Cavitation", *Journal of Ship Research*, pp.1-9.

Plesset, M.S., (1949), "The Dynamics of Cavitation Bubbles", *Journal of Applied Mechanics*, pp.278-282.

Plesset, M.S. and Gilmore, R., (1950), "Unpublished work" reported by the Cavitation Committee of the *18th International Towing Tank Conference*, Kobe, Japan.

Pollman, U., (1995), "Generalized Acoustic Similarity Parameters for the Broadband Cavitation Noise of a Five-Bladed Marine Propeller. Their Empirical Determination of Acoustic Model and Full-Scale Data", *International Symposium on Cavitation CAV'95*, Deauville, France, pp.181-200.

Rayleigh, L., (1917), "On the Pressure Developed in a Liquid During the Collapse of a Spherical Cavity", *Philosophical Magazine*, Vol.34, pp.94-98.

Rood, E.P., (1991), "Review-Mechanisms of Cavitation Inception", *Transactions of the ASME, Journal of Fluids Engineering*, Vol.113, pp.163-174.

Ross, D., (1976), "*Mechanics of Underwater Noise*", Pergamon Press, New York, USA.

Sasajima, T. and Tanibayashi, H. (1984), "Contribution to Cavitation Committee", *Proceedings of 17th International Towing Tank Conference*", Goteborg, Sweden.

Scarton, H.A. and McDonald, J.F., (1977), "A Review of the Acoustic Detection of Boiling in Nuclear Recators", *Proceedings of Noise and Fluids Engineering Symposium*, Atlanta, USA.

Schiebe, F.R. and Killer, J.M., (1971), "An Evaluation of Acoustic Technique for Measuring Gas Bubble Size and Distributions in Cavitation Research", *Report of St. Anthony Falls Hydraulic Laboratory*, University of Minnesota, Minneapolis, USA.

Sedov, L.I., (1959), "*Similarity and Dimensional Methods in Mechanics*", Academic Press, London, UK, ed. Holt, M.

Shamroth, S.J. and Briley, W.R., (1979), "A Viscous Flow Analysis of the Tip Vortex Generation Process", *AIAA Paper* 79-1546.

Shen, Y.T., (1985), "Wing Sections on Hydrofoils, Part 3- Experimental Verifications", *Journal of Ship Research*, Vol.29, pp.39-50.

Stinebring, D.R., Farrell, K.J. and Billet, M.L., (1991), "The Structure of a Three-Dimensional Tip Vortex at High Reynolds Numbers", *Transactions of the ASME, Journal of Fluids Engineering*, Vol.113, pp.496-503.

Strasberg, M., (1977), "Propeller Cavitation Noise after 35 Years of Study", *ASME, International Symposium on Noise and Fluids Engineering*, Atlanta, USA, pp.89-99.

Suhrbier, K.R. and Lecoffre, A., (1987), "Investigation of the Test Techniques Water Speed and Nuclei Seeding on the Characteristics of a High Speed Model Propeller in a Cavitation Tunnel and Correlation with Full Scale Measurements", *International Shipbuilding Progress*, Vol.34, pp.80-89.

Szantyr, J.A., (1994), "A Method for Analysis of Cavitating Marine Propellers in Non-Uniform Flow", *International Shipbuilding Progress*, Vol.41, pp.223-242.

Tanger, H. and Weitendorf, E.A., (1989), "Applicability Tests for the Phase Doppler Anemometer for Cavitation Nuclei Measurements", *Third International Symposium on Cavitation Inception*, San Francisco, USA, pp.45-53.

Tanibayashi, H., Ogura, K. and Matsuura, Y., (1998), "On the Cavitation Occurring at the Bottom of an Accelerated Circular Cylinder", *Third International Symposium on Cavitation, Cavitation'98*, Grenoble, France, pp.161-166.

Van der Kooij, J., (1986), "Sound Generation by Bubble Cavitation on Ship Propellers: The effects of Leading Edge Roughness", *ASME, 2nd International Symposium on Cavitation and Multiphase Flow*.

Van der Meulen, J.H.J. and Pei, Y., (1982), "Cavitation Inception Scaling by Roughness and Nuclei Generation", *14th Symposium on Naval Hydrodynamics*, Ann Arbor, USA, pp.507-545.

Wang, D., Atlar, M. and Korkut, E., (1995), "A Propeller Design Method Based on Cavitation Free Bucket of Blade Section", *International Conference on Problems of Marine Propulsion, HYDRONAV'95*, Gdansk, Poland, pp.217-226.

Wang, D., (1995), "The Development and Validation of Propeller Design Incorporating New Approaches to the Blade Section Design", *Ph.D. Thesis*, University of Newcastle upon Tyne, UK.

Weitendorf, E.A., (1979), "Conclusions from Full Scale and Model Investigations of the Free Air Content and of the Propeller Excited Hull Pressure Amplitudes due to Cavitation", *ASME, International Symposium on Cavitation Inception*, New York, USA, pp.207-218.

Wills, C.B., (1989), "Development of A Comparative Acoustic Testing Procedure for Model Propellers", *Transactions of RINA*, pp.307-319.

Ye, Y-P., Lu, F., Sjhi, M-G. and Qian, D-X., (1992), "Viscous Scale Effects on Propeller Tip Vortex Cavitation", *2nd International Symposium on Propeller and Cavitation*, Hangzhoui, China, pp.387-397.

Yu, P-W., Ceccio, S.L. and Tryggvason, G., (1995), "Direct Numerical Simulation of Cavitation Bubbles", *International Symposium on Cavitation CAV'95*, Deauville, France, pp.407-416.

APPENDIX I EMERSON CAVITATION TUNNEL

The general arrangement and dimensions of the Emerson Cavitation Tunnel are shown in Figure I.1 while the main details are given in Table I.1.

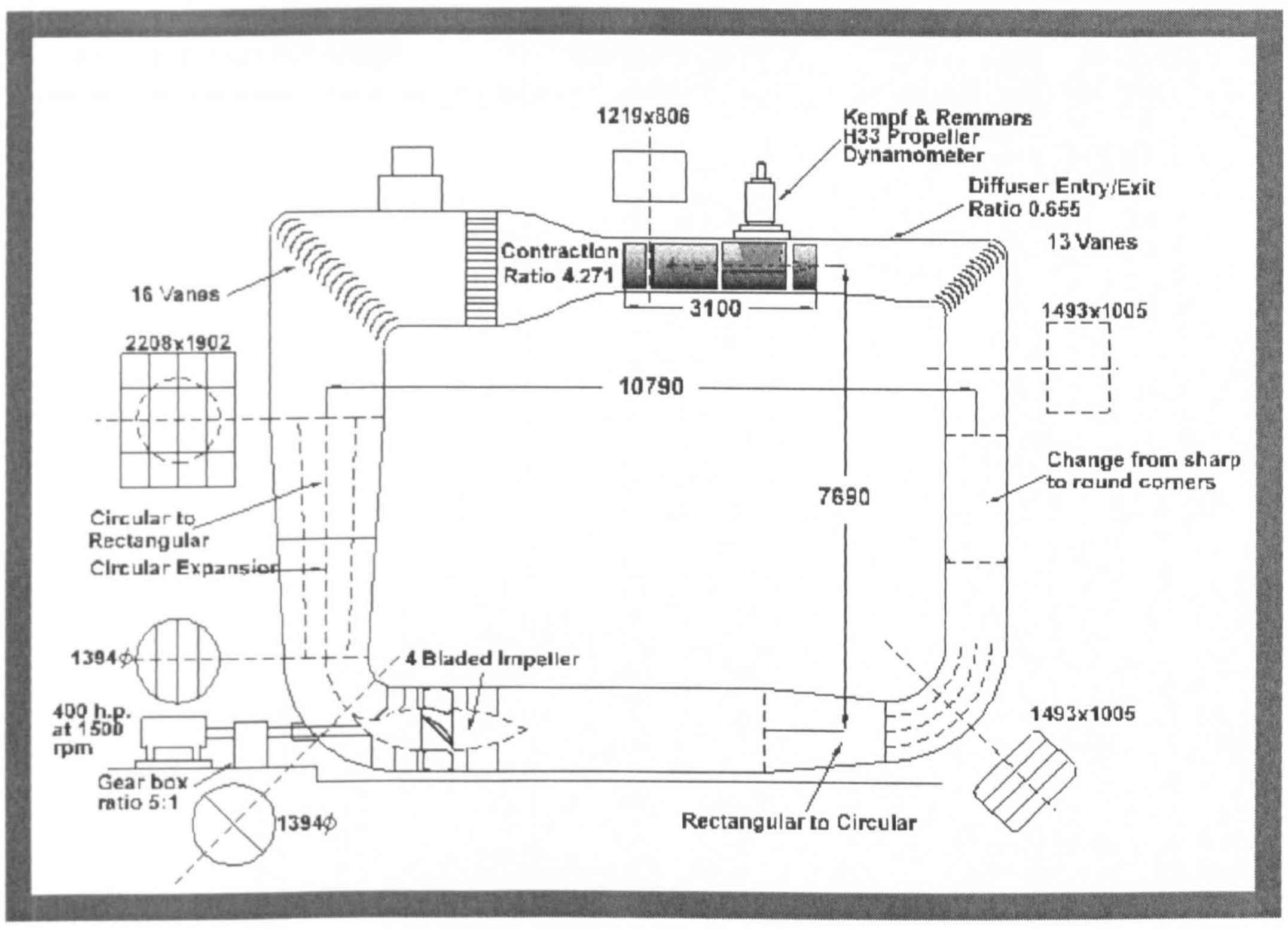

Figure I.1 General arrangement and dimensions of the Emerson Cavitation Tunnel

Table I.1 Main details of Emerson Cavitation Tunnel

Description of facility	Vertical plane, closed circulating
Test section size (LxBxH)	3.10x1.22x0.81 m
Contraction ratio	4.271
Type of drive system	4 Bladed axial flow impeller with thyristor control
Main pump power	300 kW
Main pump rotational speed	242 rpm
Impeller diameter	1.4 m
Maximum velocity	15.5 knots (8 m/s)
Absolute pressure range	7.6 kN/m^2 (min) to 106 kN/m^2 (max)
Cavitation number range	0.5 (min) to 23 (max)

APPENDIX II LASER DOPPLER ANEMOMETRY (LDA)

Laser Doppler Anemometry (LDA) is an efficient and non-intrusive flow measurement technique where a laser system is used to measure velocity of a liquid or a gaseous flow. The system is based on Doppler principal such that:

When two laser beams cross each other as shown in Figure II.1 the intersection of these beams defines the measuring control volume and the flow particles passing the measuring control volume scatter the laser light. The frequency of the scattered light is different from the transmitted light. This discrepancy is known as Doppler effect, which gives the velocity component at the measuring point. A typical Doppler signal is shown in Figure II.2.

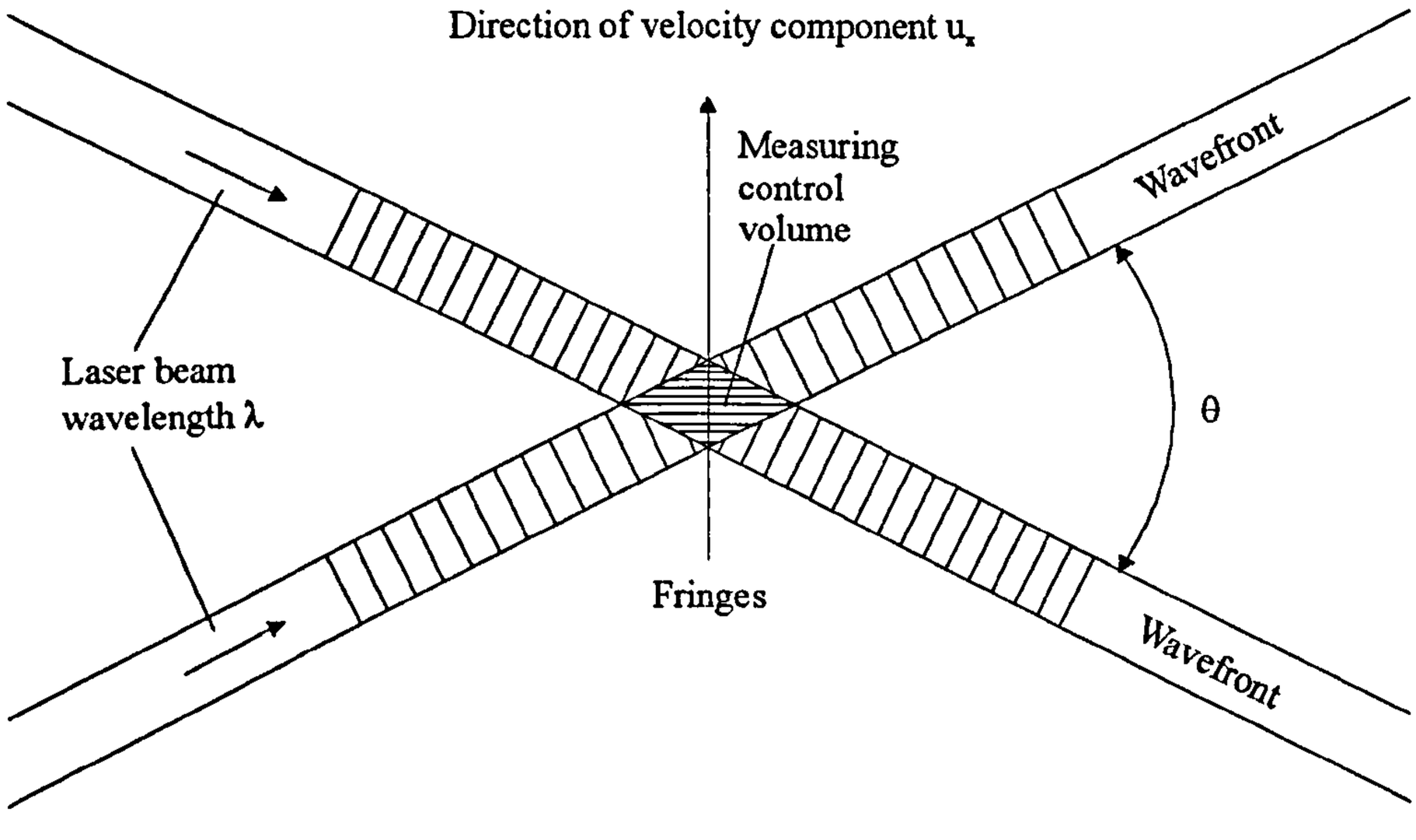

Figure II.1 Two laser beams crossing

The Doppler frequency shift is defined as:

$$f_D = f_S - f_I \tag{II.1}$$

where f_S is the frequency of the scattered light and f_I is the frequency of the incident light.

The relationship between the Doppler frequency, f_D, and the velocity component of the particle, u_x, is given by:

$$u_x = f_D \frac{\lambda / 2}{\sin(\theta / 2)} \tag{II.2}$$

where λ is the wavelength of the laser light and θ is the intersection angle of the laser beams.

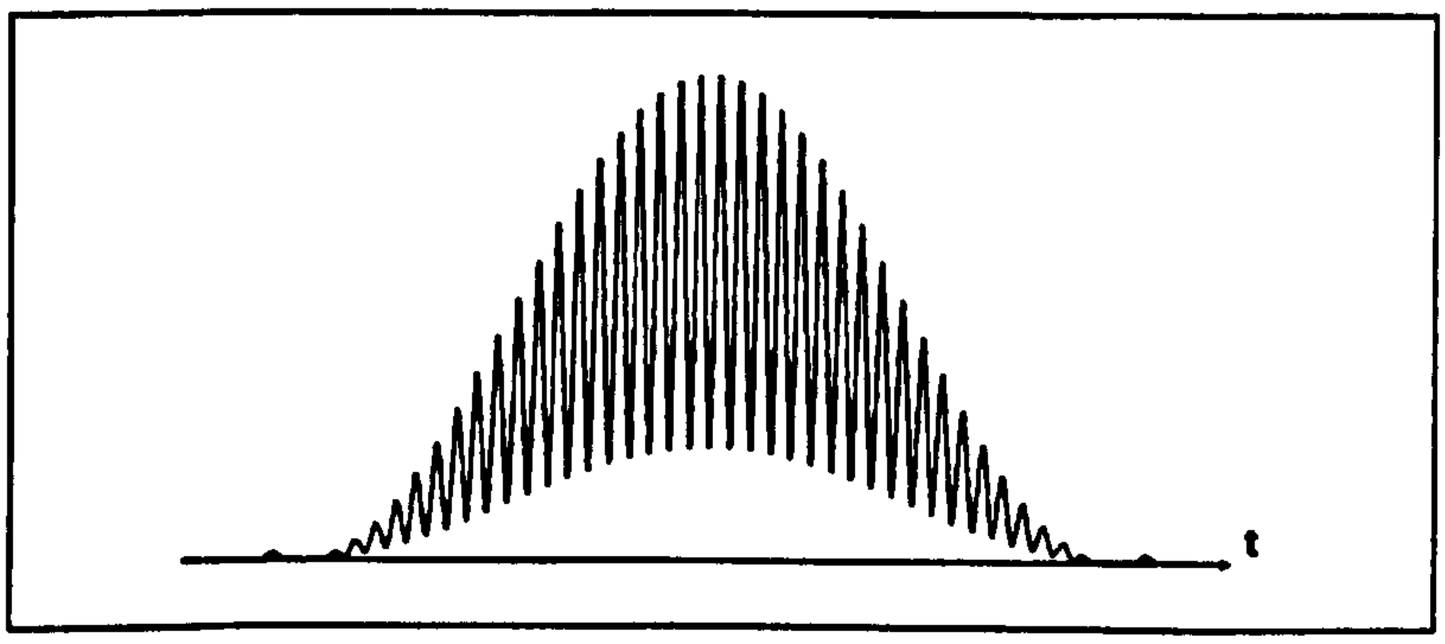

Figure II.2 Typical Doppler burst (signal)

There are mainly three scatter systems for the arrangements of optics, such as forward, side and back-scatter. General arrangements for three cases are shown in Figure II.3. As it can be seen in Figure II.3 that the back-scatter system has some physical advantages compared to the others. Thus, it has a single optical access, which can be used in very size and access limited areas. On the other hand, the forward scatter is the best system, in terms of scattered light and signal quality. This results in higher data rates and better

time resolution of the flow velocity. However, in the forward scatter system, accesses from the bottom and the top or the left side and the right side of the tunnel were required. For the side scatter system, the receiving lens should have been on the left or right window of the tunnel with an angle to the transmitting lens. Due to the limited access and area in the tunnel, it was decided to use the back-scatter LDA system although the scattered light intensity was much weaker in the back-scatter direction. Therefore, the laser power should have been higher than in the other cases.

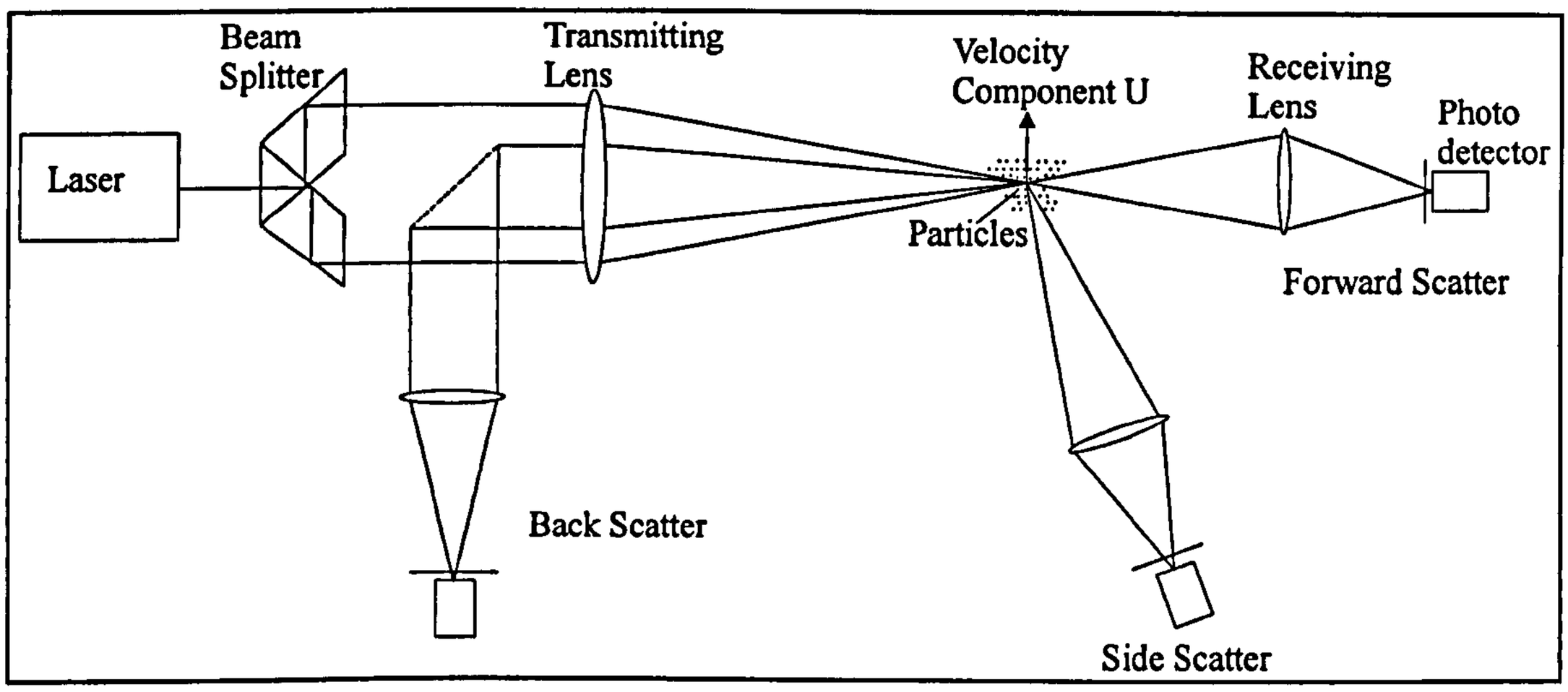

Figure II.3 Optic arrangements for three scatter systems

The system used for the velocity measurements was two-dimensional DANTEC LDA system, which mainly consisted of four discrete parts; optics, signal processors, a computer and a traverse system. The layout the system is shown in Figure II.4 and the general view of the LDA system used in the experiments is indicated in Figure II.5.

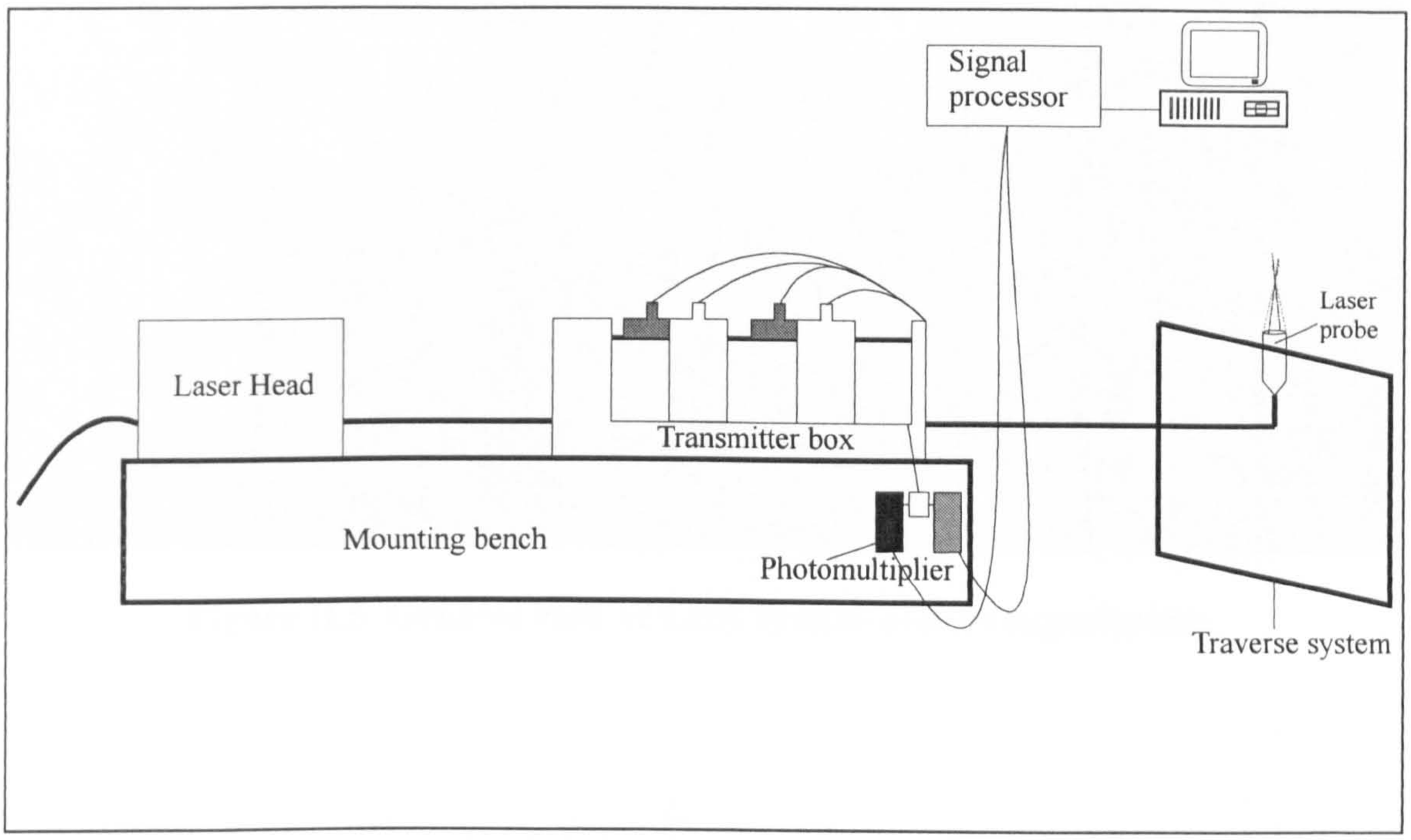

Figure II.4 Layout of LDA system

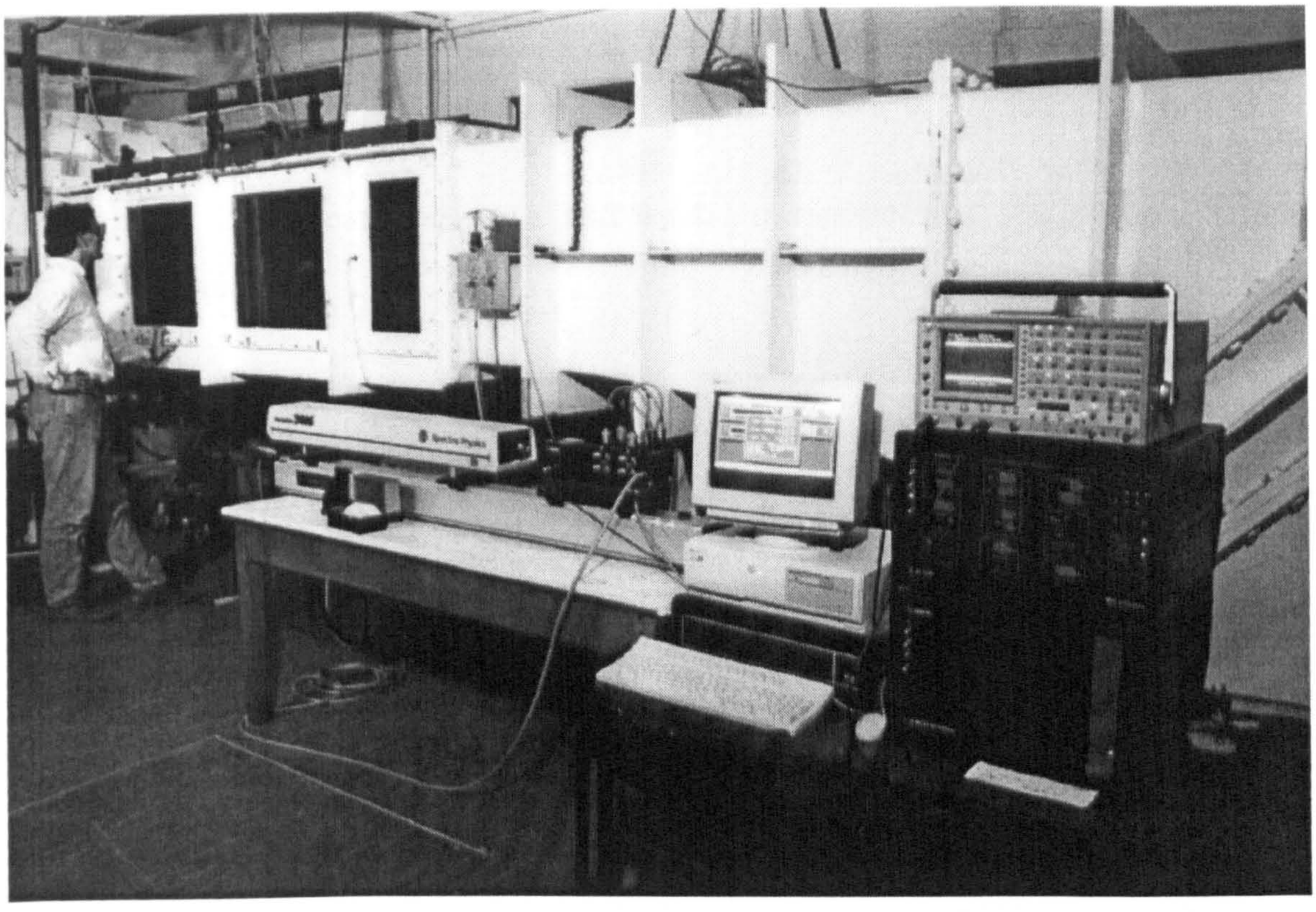

Figure II.5 General view of LDA system used in experiments

II.1 OPTICS

Optics had 5 components, such as a laser head, a transmitter box, two photomultipliers and a laser probe.

II.1.1 LASER HEAD

One of the main components of the optics was the laser head, which basically generated the laser beams and sent them to the transmitter box. The laser had was a Spectra Physics: serial number 01442258100 and type 2016, Argon-Iron, water-cooled and the three phased laser with the input power of 5 watt.

II.1.2 TRANSMITTER BOX

The main element of the 2-D system was the transmitter, which was type 60x42 and equipped with four manipulators. In the transmitter, the incoming beam from the laser head was divided into two pairs of laser beams of different colours for measurements of two velocity components, u and v. This was done by brag cells which split the laser into two pairs of beams. At the same time, a frequency shift is added to one beam of each pair to allow for measurements of reversing flow. The colours of laser beams were blue and green, which had different wavelengths. The green pair of laser beams was used to measure axial component of velocity, u, which had the wave length of 514.5 mm and the blue pair was used to measure transverse component of velocity, v, which had the wave length of 488 mm. The frequency shift was 40 MHz. The four manipulators were type 60x24 which were positioned on the transmitter. Each manipulator was used to adjust the alignment and intensity of each laser light beam precisely.

II.1.3 LASER PROBE

The incoming laser beams from the transmitter were connected to the laser probe by a fibre optic cable as sketched in Figure II.4 and shown in Figure II.6. The laser probe was two-dimensional probe with the diameter of 85 mm and the focal length of front optic of 600 mm, which contained four laser beams. The laser probe also had a type 55x12 beam expander which is usually used in conventional and fibre optics probes to reduce the size of the measuring control volume. It is recommended when measuring at very large distances. Therefore, the beam expansion improves the spatial resolution of the measurement and increases the intensity of the laser light in the measuring control volume.

II.1.4 PHOTOMULTIPLIERS

The scattered lights were detected by two photomultipliers, which were type (57x08). They converted the scattered lights into electrical energy and were connected to the two signal processors to pass the converted electrical signals.

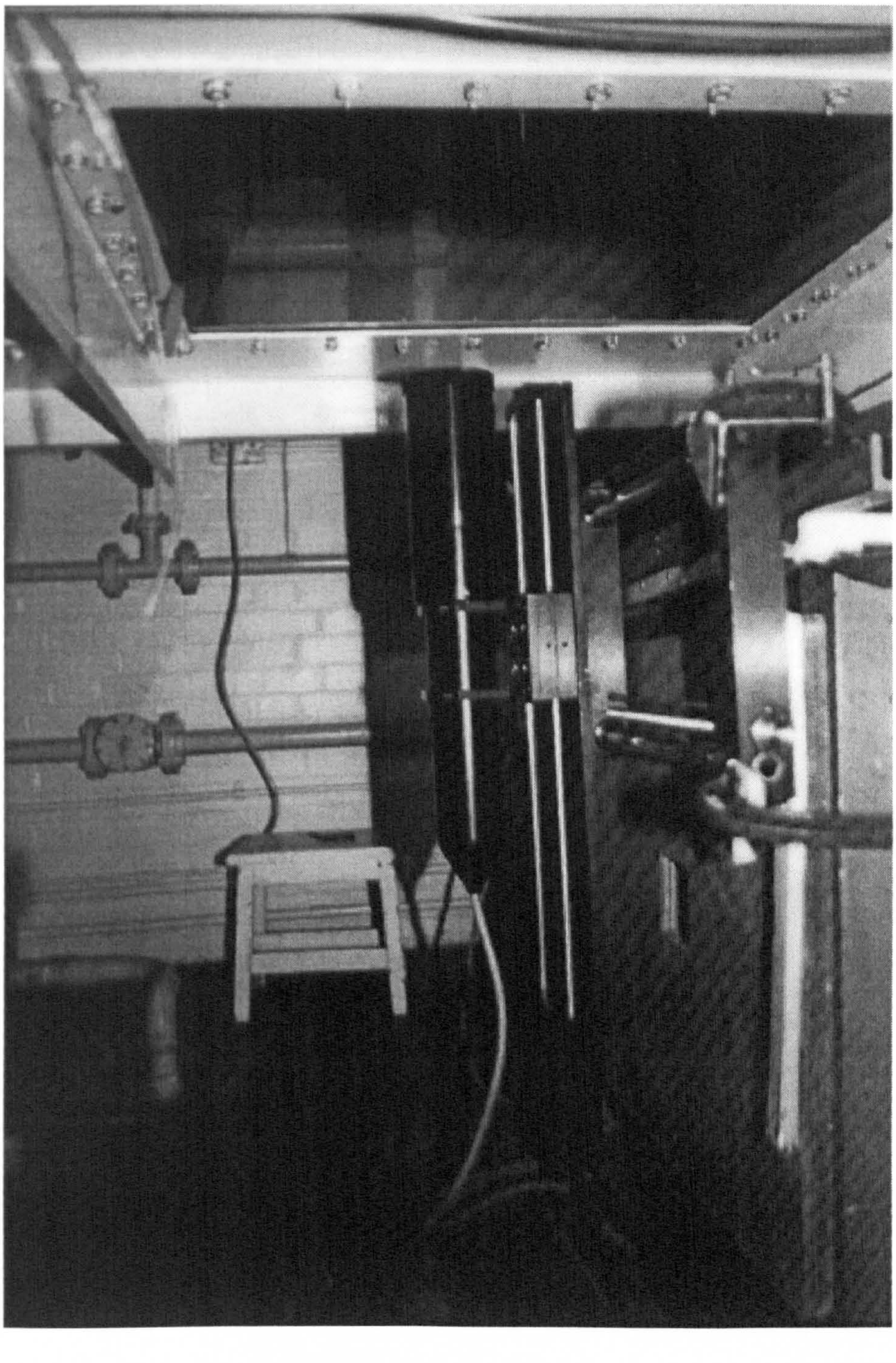

Figure II.6 Traversing mechanism and laser probe used in experiments

II.2 TRAVERSING MECHANISM

One of the main parts of the 2-D LDA system was traversing mechanism, which held the laser probe as shown in Figure II.6. The traversing mechanism was a 2-D type 57G15 system was driven by a computer, which was mounted to a bench. The system was able to operate in the size of 600 mm x 600 mm due to the size of the system, length of the laser probe and the height of the space underneath of the tunnel.

II.3 SIGNAL PROCESSORS (BURST SPECTRUM ANALYZER, BSA)

The converted electrical signals from the photomultipliers were analysed by two signal processors, Burst Spectrum Analyzer BSA1 and BSA2. The BSA1 was model 57N20 Enhanced which was used as the master processor for the axial velocity component, u, and the BSA2 was model 57N35 Enhanced which was used as the slave processor for the transverse velocity component, v.

The BSA performed a spectrum analysis of the Doppler signals based on Fast Fourier Transform (FFT) technique in order to extract the Doppler frequencies, which were converted into readable signals, e.g. voltage. There were two important components of each BSA processor, which were an FFT signal and a post processor. The FFT processor converted the Doppler signals in time histories into those in frequency domain. The post processor analysed and validated the output signals from the FFT processor and gave the correct Doppler frequency and the corresponding velocity.

The Doppler signals as shown in Figure II.2 were monitored by an oscilloscope connected to the BSA1 and the BSA2 to check, whether getting the correct signals during the experiments.

The BSA1 and BSA2 were connected to a computer. They were supported by the DANTEC analysis software BURSTWARE based on DOS system, which also drove the traversing mechanism. The BSA1 could set up from its front panel, but the BSA2 had to be operated by the computer due to the different type of front panel from the BSA1.

The BURSTWARE (Dantec, 1996) acquired the velocity data in time histories shown in Figure II.7. Velocity components at each grid point were collected in a suitable time length (e.g., 20 sec) and number of samples (e.g., 400 samples). These collected data were then averaged by using unweighted arithmetic mean defined as:

$$\overline{U}_{unweighted} = \frac{\sum_{i=1}^{N} U_i}{N} \qquad (II.3)$$

where N was the number of validated data.

By using the time history of the validated velocity data the software calculated the spectrum based on this data from which the relevant statistical quantities from the velocity spectrum, e.g. mean, rms, turbulence intensity, cross moments values, etc. could be obtained, and presented these velocity quantities graphically. It also exported the velocity data to spreadsheets and graphics packages and gave the hard copy of the velocity data.

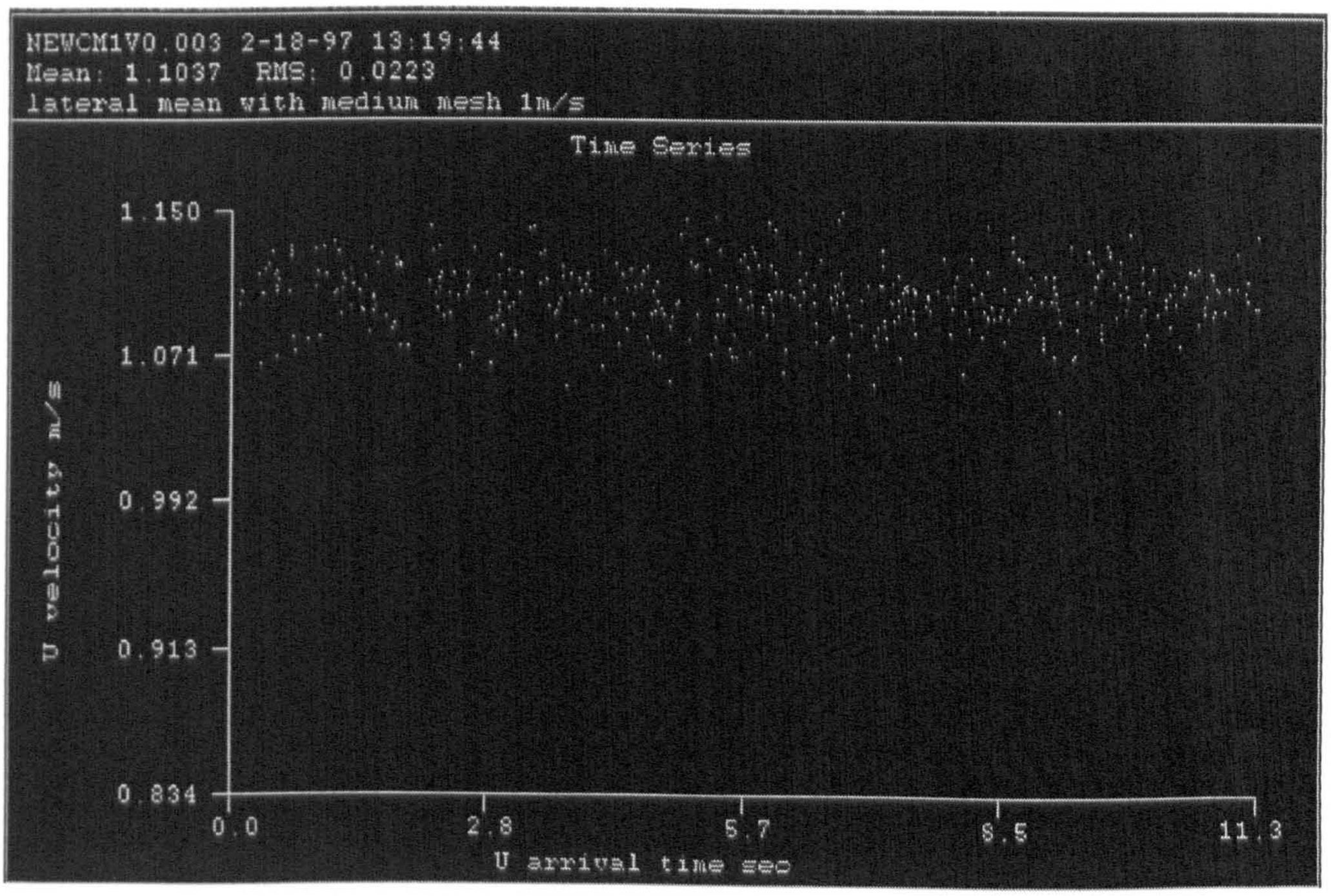

Figure II.7 Time history of a validated data at a measuring point

II.4 COMPUTER

A 486DX, 100 MHz Hewlett Packard computer was used to analyse and calculate the velocity quantities as well as controlling and driving the signal processors and the traversing mechanism.